CVD Diamond ... made simple

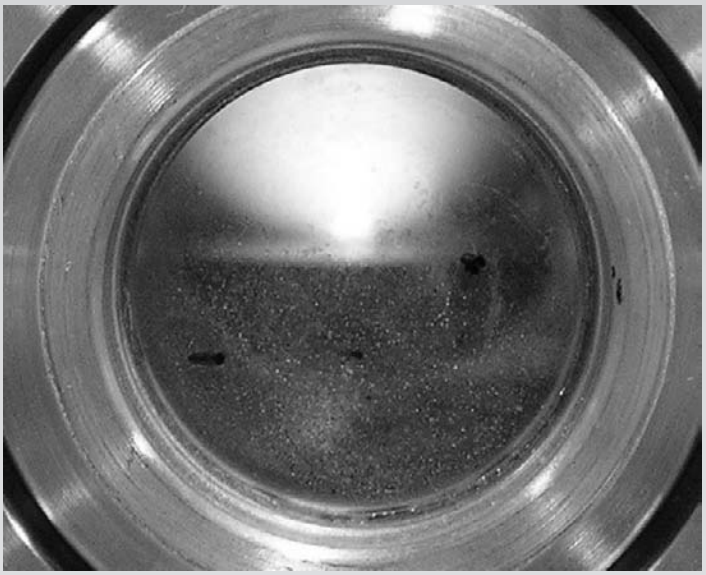

Microwave plasma CVD

High reliability and proven technology

System designs suited for R&D and production

Wide range of process applications

- Uniform films (up to 300mm wide)
- High growth rates
- Single crystal
- Electronic devices
- MEMS
- Thermal management
- CNT
- Tools/3-D coating
- ECR

Hot filament CVD

**Seki Technotron and sp3 Diamond Technologies—
bonded to your future innovations**

SEKI TECHNOTRON CORP.

sp3 diamond technologies

www.sekicvdsolutions.com

888-273-6225

2220 Martin Avenue, Santa Clara, CA

WELCOME

Dear Colleague:

It is our pleasure to extend a warm welcome to you to the 8th Applied Diamond Conference/ NanoCarbon 2005 Joint Conference. The ADC again brings together 250 of the leading researchers in industry, academia, and government laboratories from around the world, to discuss the latest advances in the fundamental and applied science of diamond and nanocarbon materials, as well as highlight products being developed by several companies in the United States, Japan, and Europe. In particular, the latest advances in the emerging area of nanocarbons, which combine different allotropes of carbon at the nanoscale into new materials with unique properties, is also well represented.

These are exciting times for the carbon and related materials community. No other area of materials research combines the excitement of major breakthroughs in fundamental research with the immediate promise of seeing those breakthroughs lead to new devices and products that have both high societal impact and high commercial potential. The elevated level of interest, the pace of new discoveries, and the number of new start-up companies founded in recent years makes having a conference of equal excitement and scope a necessity, so that our community continues to strive and flourish.

The program includes 18 invited contributions, 62 oral contributions, and 125 posters, covering topics ranging from diamond-based quantum computers, MEMS, functionalized carbon materials, nanotube electronics, hybrid nanocarbons, and the large-scale production of synthetic gems. Several presentations will also discuss the challenges of developing viable business models to further develop the fruits of basic and applied research into real technologies and products.

There's no city like Chicago, Illinois. Dubbed the "Capital of the Midwest," it's the birthplace of jazz and skyscrapers, home to more than 8 million. It's also home to many leading research universities and government laboratories, including Argonne National Laboratory. It is poised to become a major center for high-technology start-ups born of technologies developed at these institutions. Over the past several years, three R&D 100 awards have been award to local Chicago researchers for breakthrough carbon technologies.

The timing could not be better to have Argonne National Laboratory host this exciting conference. Argonne is a one of several national laboratories charged by the U.S. Department of Energy to conduct basic and applied research in physics, chemistry, materials science, and other fields. It has also been chosen to be the site of one of the major Nanoscience Research Centers, the Center for Nanoscale Materials (CNM), which will begin operations in 2006. Nanocarbon is one of six initial scientific themes upon which the CNM is founded.

We hope you enjoy your stay and we thank all of you for your valuable contributions!

Best Regards,

John A. Carlisle
Conference Chair

Organizing Committee

Chair	John A. Carlisle Argonne National Laboratory, USA
Co-Chair	Yonhua Tzeng Auburn University, USA
	James E. Butler Naval Research Laboratory, USA
	John G. Angus Case Western Reserve, USA
	Sumio Iijima Meijo University, Japan
	Erhard Kohn University of Ulm, Germany
	Orlando Auciello Argonne National Laboratory, USA

Program Committee

Chair	Jim Butler Naval Research Laboratory, USA
Co-Chair	John G. Angus Case Western Reserve, USA
Co-Chair	Sumio Iijima Meijo University, Japan
Co-Chair	Erhard Kohn University of Ulm, Germany
Co-Chair	Otto Zhou University of North Carolina, USA
Co-Chair	Yoshinori Koga National Institute of Advanced Industrial Science and Technology, Japan
Co-Chair	John W. Mintmire Oklahoma State University, USA
	Orlando Auciello
	John Carlisle
	Robert Nemanich
	Yonhua Tzeng
	Dieter Gruen
	Atsuhito Sawabe
	Lothar Schäfer
	Hiroshi Kawarada
	Kuei-Hsien Chen
	Robert J. Hamers

Local Organizing Committee

Chair	John Carlisle
Co-Chair	Orlando Auciello
	Larry Curtiss
	Millicent Firestone
	Ali Erdemir
	Jacqueline Johnson
	Joan Brunsvold
	Susan Strasser
	Amanda Barnard
	Chao Liu
	Nevin Naguib
	Peter Zapol
	Betty Waterman
Secretary	Barbara Hall

International Advisory Committee

Gehan Amaratunga	Meyya Meyyappan
Jes Asmussen	Bill Milne
Robert Carpick	Kazuhisa Miyoshi
Kuei Chen	Masao Murakawa
Jim Davidson	Robert Nemanich
Patrick Doering	Sergei Pimenov
Horacio Espinosa	Steven Prawer
Alfred Grill	John Robertson
Robert Hamers	Rodney Ruoff
Russell Hemley	Atsuhito Sawabe
Atsushi Hirata	Lothar Schäfer
Koji Kobashi	Boris Spitsyn
Yoshinori Koga	James Sung
Kunio Komaki	Ricardo Sussmann
Vitaly Konov	Greg Swain
Sir Harold Kroto	David Tomanek
Clifford Lau	Yogesh Vohra
Shuit-Tong Lee	Shuichi Watanabe
Paul May	Otto Zhou
David McKenzie	

CONTENTS

Sponsors

Exhibitors

Banquet Speaker Profile

Program

Maps

Oral Sessions Abstracts

Poster Session 1 Abstracts

Poster Session 2 Abstracts

Attendee List

SPONSORS

Argonne National Laboratory
- Center for Nanoscale Materials
- Advanced Photon Source
- Materials Science Division

U.S. Department of Energy
- Office of Basic Energy Sciences
- Office of Science

Defense Advanced Research Projects Agency (DARPA)

Naval Research Laboratory

IEEE

MRS Materials Research Society

Elsevier Science

Advanced Diamond Technologies, Inc.

EXHIBITORS

Fraunhofer/MSU Center for Coatings and Laser Applications
East Lansing, MI
http://www.ccl.fraunhofer.org/

Fraunhofer Center for Coatings and Laser Applications in partnership with Michigan State University is a nonprofit organization that provides innovative research and development services to industry and government. The Coating Technology Division specializes in plasma-assisted technologies including CVD diamond coating and synthesis, PVD amorphous carbon, and diamond-like-carbon coating. This technology can be applied to a wide variety of markets including automotive, aerospace, electronics, optical applications, MEMS, and biomedical applications.

HeatWave Labs, Inc.
Watsonville, CA
http://www.cathode.com/

HeatWave Labs specializes in the vacuum tube and vacuum equipment industries. Our expertise includes thermionic cathodes and ion emitters and guns, ion sources and ionizers, ion pumps and controllers, vacuum tube design, processing, specialized refractory materials, UHV sample heating and filament products, temperature controllers, and related products.

iplas innovative plasma systems gmbh
Troisdorf, Germany
http://www.cyrannus.com/

CYRANNUS plasma sources produce a homogeneous, stable microwave-excited plasma at vacuum to atmospheric pressure with arbitrary gases. They are appropriate for various surface processes such as etching, activation, deposition (especially diamond), and plasma chemistry. The sources are available in sizes from 2.7 to 16 inches. iplas and Argonne National Laboratory won a 2003 R&D 100 Award for their CYRANNUS-based UNCD applications.

Lambda Technologies, Inc.
Morrisville, NC
http://www.microcure.com/

Lambda Technologies is a leading supplier of advanced microwave technology, offering unique microwave solutions for a broad range of applications. Lambda’s MicroCure® Variable Frequency Microwave products are used worldwide in the semiconductor industry for the cure of polymer coatings, encapsulants, and other advanced thermal processes. Lambda has recently acquired the rights for the Plasma Disc Reactor and tunable microwave technology developed at Michigan State University (MSU), together with all associated process patents, which include proven processes, reactor, and system designs for CVD diamond and diamond-like carbon. Lambda is packaging the MSU diamond process technology, originally commercialized by Wavemat, Inc., with state-of-the-art controls that take advantage of the design's efficient controlled plasma generation and incorporate all the latest configurations optimized by ongoing research at MSU.

Renishaw
Hoffman Estates, IL 60192
http://www.renishaw.com

Renishaw Raman microscopes provide chemical information confocally at submicron spatial resolution with auto-alignment, internal calibration, and performance validation. Renishaw Raman spectrometers are configurable to include multiple excitation sources from the ultraviolet through near-infrared with automated laser switching and alignment, quick-launch fiber-optic probes, AFM/NSOM/Raman, SEM-Raman, hot and cold cells, macrosampling, global Raman imaging, near excitation analysis, two- and three-dimensional, mapping and depth profiling.

Seki Technotron USA
Sunnyvale, CA
http://www.sekicvdsolutions.com/

Seki Technotron is the leading manufacturer of microwave CVD systems for diamond, carbon nanotubes, and advanced material R&D and production. We are also the worldwide distributor for sp3 Diamond Technologies, a manufacturer of hot-filament CVD systems for diamond coating of wafers, tools, and other substrates. Both the microwave and hot-filament CVD technologies have a wide range of R&D and production applications depending on desired substrate size, growth rate, and type of diamond film or carbon nanotube growth required. The microwave CVD systems were originally developed by ASTeX and are offered in several models with a wide range of substrate area from 100 to 300 mm, and power levels from 1.5 to 60 kW, which can be selected for growth rate and process desired. The sp3 Diamond Technologies hot-filament CVD system is designed for wide-area deposition and deposits very uniform films, for example, over a single 300-mm wafer. It can batch process mixed substrate sizes over a 300-mm-square area. Seki works closely with its customers to help select the optimum system using microwave or hot filament CVD technology best suited for the intended R&D or production use.

FEATURED BANQUET SPEAKER

Smithsonian Diamonds: Science and Lore

The speaker at the banquet will be Dr. Jeffrey Post, Curator-in-Charge, Mineral Collection, at the Smithsonian Institution. His recent research interest has been the study of mineral structures and behaviors, with a focus on environmentally significant minerals.

The National Gem and Mineral Collection at the Smithsonian Institution is well known as the home of the Hope Diamond. This great blue diamond, weighing 45.52 carats, was found in India and became part of the French Crown Jewels until it was stolen in 1792. But the National Collection also has several other notable diamonds, including the Blue Heart, Portuguese, and Victoria Transvaal Diamonds, and historic diamond jewelry pieces, such as the Napoleon Necklace and Inquisition Necklace. This talk will explore the science and lore associated with these famous diamonds, including some recent research on the Hope Diamond and also provide an overview of the many other diamonds in the National Collection.

PROGRAM

SUNDAY, MAY 15, 2005	
1:00-4:00	Nanocarbon Workshop
5:00-7:00	Registration and Welcome Reception
MONDAY, MAY 16, 2005	
Session 1: Application/Devices: General Chair: John A. Carlisle, Argonne National Laboratory	
8:00	Welcome, John A. Carlisle, Argonne National Laboratory
8:15	*VLSI Quantum Computer in Diamond*, Phil Hemmer, Texas A&M University (invited)
8:45	*Carbon Nanotube Electronics*, Y-Ming Lin (IBM Watson Laboratory) (invited)
9:15	*CVD Diamond Coating of Interior Surfaces*, L. Schäfer, M. Höfer, T. Hollstein, B. Blug, M. Herrmann, and T. Huhns (Fraunhofer Alliance Diamond-Coated Ceramics, Germany)
9:30	*Electrical Methods for Creating and Characterizing Biomolecular Arrays for DNA Hybridization and Antibody Detection at Diamond Surfaces*, W. Wang, B. Sun, S. Baker, K-Y Tse, and R.J. Hamers (University of Wisconsin-Madison); J.E. Butler and J.N. Russell, Jr. (Naval Research Laboratory)
9:45	*Diamond Electrodes for Neurodynamic Studies in Aplysia californica*, J.M. Halpern, S. Xie, G.P. Sutton, B.T. Higashikubo, C.A. Chestek, H.J. Chiel, and H.B. Martin (Case Western Reserve University)
10:00	**Break**
Session 2: Defects and Doping Chair: Robert Nemanich	
10:30	*Spectroscopic Studies of Hydrogen Complexes in Diamond*, M. Newton, R.J. Cruddace (University of Warwick); H.E. Smith (University of Oxford); Martineau and S.J. Quinn (DTC Research Centre); D.J. Twitchen (Element Six Ltd.) (invited)
11:00	*Optical and Structural Properties of Amorphous Carbon Thin Films Deposited by Microwave Surface-Wave Plasma CVD*, S. Adhikari, S. Adhikary, M. Omer, H. Uchida, and M. Umeno (Chubu University, Japan); M. Rusop and T. Sogar (Nagoya Institute of Technology, Japan)
11:15	*Inelastic Neutron Scattering Study of Carbon Nanomaterials*, A.I. Kolesnikov and C.K. Loong (Argonne National Laboratory); A.P. Moravsky and R.O. Loutfy (NER Corporation))
11:30	*Boron-Doped Nanocrystalline Diamond Films*, O.A. Williams, M. Daenen, J. D'Haen, M. Nesladek, and M. D'Olieslager (Limburgs Universitair Centrum, Belgium)
11:45	*Photoconductivity and Ambipolar Diffusion Length of Minority Carriers in S-Doped Microcrystalline and Nanocrystalline Diamond*, F. Piazza, O. Resto, G. Nery, L. Fonseca, and G. Morell, University of Puerto Rico

12:00	**Lunch**
Session 3: Application/Devices: MEMS Chair: Erhard Kohn, University of Ulm	
1:00	*Vibrating RF MEMS in Diamond Structural Material*, C. Nguyen (University of Michigan) (invited)
1:30	*Nanocrystalline Diamond Films for Surface Acoustic Wave Devices*, F. Benedic and F. SIlva (Laboratoire d'Ingenierie des Materiaux et des Hautes Pressions, France); P. Elmazria, M.B. Assouar, and M. El Hakiki (Laboratoire de Physique des Milieux Ionises et Applications, France
1:45	*Fracturing Templated Carbon Nanotubes with a MEMS Testing Stage*, S. Lu, W. Ding, and R.S. Ruoff, Northwestern University
2:00	*Materials Science and Processing Strategies for Integration of Piezoelectric and Ultrananocrystalline Diamond (UNCD) Thin Films for Piezoactuated Hybrid MEMS,* O. Auciello, W. Fan. G. Bai, and J.A. Carlisle (Argonne National Laboratory)
2:15	*Carbon-Nanotube-Based NEMS and Modeling*, C. Ke and H.D. Espinosa, Northwestern University
2:30	*Fabrication and Test of Poly-Crystalline Diamond Piezoresistive Position Sensors for Cochlear Implant Probe*, Y. Tang and D.M. Aslam (Michigan State University); J. Wang and K.D. Wise (University of Michigan)
2:45	**Break**
Session 4: Mechanical, Tribology, and Protective Applications Chair: Dieter M. Gruen, Argonne National Laboratory	
3:00	*Is There Another Way to Make/Grow Diamond?*, Rodney Ruoff (Northwestern University) (invited)
3:30	*Controlling the Nanotribology of Nanostructured Diamond Films*, R.W. Carpick, D.S. Grierson, A.V. Sumant, E.E. Flater, G. Ning, K. Sridharan (University of Wisconsin, Madison); T.A. Friedmann and J.P. Sullivan (Sandia National Laboratories); J.E. Gerbi, J. Birrell, X. Xiao, O. Auciello, and J.A. Carlisle (Argonne National Laboratory) (invited)
4:00	*Nanotribology of Self-Mated Nanocrystalline and Amorphous Carbon Interfaces*, D.S. Grierson, A.V. Sumant, K. Sridharan, E.E. Flater, and R.W. Carpick (University of Wisconsin-Madison); J.E. Gerbi (University of Illinois at Urbana-Champaign); J. Birrell (Advanced Diamond Technologies); O. Auciello and J.A. Carlisle (Argonne National Laboratory); T.A. Friedmann and J.P. Sullivan (Sandia National Laboratories)
4:15	*Fracture Strength of Multiwall Carbon Nanotubes*, W. Ding, L. Calabri, X. Chen, K. Kohlhaas, and R.S. Ruoff, Northwestern University
4:30	*Mechanics of Carbon Nanoplates*, H.W. Shim, L.G. Zhou, and H.C. Huang (Rensselaer Polytechnic Institute)
4:45	*Nano Fountain Probe for Sub-100 nm Fountain-Pen Writing*, K-H Kim, N. Moldovan, and H.D. Espinosa, Northwestern University
7:00-9:00	**Poster Session 1**

TUESDAY, MAY 17, 2005	
Session 5: Application/Devices: Electronics Chair: Hiroshi Kawarada	
8:00	*Key Issues of Electrical Application of Diamond*, N. Fujimori (National Institute of Advance Industrial Science and Technology, Diamond Research Center) (invited)
8:30	*High-Performance MISFET Using High-Mobility Substrate and Aluminum Oxide Gate Insulator*, K. Hirama, T. Toshiba, K. Yohara, H. Takayanagi, M. Satoh, H. Umezawa, and H. Kawarada (Waseda University, Japan); T. Saitoh, K. Park, and N. Fujimori (AIST NEDO, Japan)
8:45	*Carbon Nanotubes as a Cold Electron Beam Source for Pseudospark Plasma Switches and Pulsed Power Applications*, Y. Tzeng, H. Kirkici, C. Liu, C. Seymore, A-J Cheng, Y-C Chen, K. Koppisetty, and H. Kim (Auburn University)
9:00	*Nanocrystalline Diamond pn: Structure Grown by Hot-Filament CVD*, T. Zimmermann, K. Janischowsky, A. Denisenko, M. Kubovic, and E. Kohn (University of Ulm, Germany); D.M. Gruen (Argonne National Laboratory)
9:15	*Electrical Properties of Thin Nanocrystalline-Diamond-Based Structures*, M.D. Parr and D.K. Reinhard (Michigan State University)
9:30	*Formation of Junctions and Defects in Carbon Nanotubes*, F-Y Meng and S-Q Shi (Hong Kong Polytechnic University); L-G Zhou (Rensselaer Polytechnic Institute); R, Yang (Institute of Metal Research, CAS, China), Hong Kong
9:45	**Break**
Session 6: Application/Devices: Vacuum Electronics, Electron Emission, and Electronics Chairs: Sumio Ijima, Mejio University, and Yonhua Tzeng, Auburn University	
10:15	*Robust and Regenerable Carbon Nanotube Field Emitter Arrays with Integral Gates*, D.S.Y Hsu and J.L. Shaw (Naval Research Laboratory) (invited)
10:45	*Stability of Field Emission Current from Various Carbon Nanotube Films*, B. Ulmen, A. DeConinck, V.K. Kayastha, J. Wang, and Y.K. Yap (Michigan Technological University)
11:00	*Imaging Temperature-Dependent Field Emission from Carbon Nanotube Films: Single- vs. Multiwalled*, Sanju Gupta (Southwest Missouri State University); Y.Y. Wang, G.M. Garguilo, and R.J. Nemanich (North Caroline State University)
11:15	*Emission Characterization from Nitrogen-Doped Diamond with Respect to Energy Conversion*, F. Koeck, Y. Tang, and R.J. Nemanich (North Carolina State University)
11:30	*The Bright View of DEL Seen from LED*, J.C. Sung (KINIK Company, Taiwan); J-C Pu, and S-F Wang (National Taipei University of Technology, Taiwan
11:45	*Local Electron Field Emission Properties of Nanodiamond Films Measured Using Scanning Tunneling Microscopic Technique*, I-N Lin (Tamkang University, Taiwan); Y-P Chou and T.T. Chen (National Tsing-Hua University, Taiwan); H-F Cheng (National Taiwan Normal University)
12:00	**Lunch**

Session 7: Application/Devices: Sensors, Surface Properties Chair: Robert J. Hamers	
1:00	*FET-Based Diamond Biosensors,* H. Umezawa*,* K-W Song, M. Degawa, Y. Sasaki, and H. Kawarada (Waseda University) (invited)
1:30	*Diamond-Based Biochemical Sensors*, J.A. Garrido, A. Hartl, J. Hernando, M. Stutzmann, and S. Walter (Technische Universitat Munchen, Germany) (invited)
2:00	*Oxygen Effect on the Surface Conductivity of N-type Sulfur-Doped Diamond*, I. Gonzalez-Gonzalez, C.R. Cabrera, D.A. Tryk, G. Morell, and J. De Jesus (University of Puerto Rico)
2:15	*In Vitro Adenosine Detection with a Diamond-Based Sensor*, S. Xie, G. Schafer, C.G. Wilson, and H.B. Martin (Case Western Reserve University)
2:30	*Adsorbate-Induced Conductivity of Hydrogen-Terminated Diamond*, V. Chakrapani, S.E. Eaton, A.B. Anderson, and J.C. Angus (Case Western Reserve University)
2:45	**Break**
Session 8: Synthesis, Production, and Scale-Up Chair: Otto Zhou, University of North Carolina	
3:00	*Mass Production, Selective Formation, and Applications of Carbon Nanotubes*, M. Endo (Shinshu University, Japan) (invited)
3:30	*Large-Area Microwave Plasma Deposition System for UNCD Coating of SiC Pump Seals*, J.A. Libera, J. Hryn, J. Elam, J. Birrell, O. Auciello, and J.A. Carlisle (Argonne National Laboratory)
3:45	*Aspects of Scaling CVD Diamond Reactors*, J. Zimmer (sp3 Inc.) and K.V. Ravi (Intel Corporation)
4:30-10:00	**Bus Trip to Millenium Park and Downtown Chicago**
WEDNESDAY, MAY 18, 2005	
Session 9: Synthesis and Growth Mechanisms I Chair: Kuei-Hsien Chen	
8:00	*Growth Mechanism of Superlong and Aligned Single-Walled Carbon Nanotubes*, J. Liu (Duke University) (invited)
8:30	*Superconductivity in Doped Diamond*, R. J. Soulen, Jr., and M. Osofsky (Naval Research Laboratory)
8:45	*Micro- and Nanocrystalline Diamond Film Synthesis at Substrate Temperatures Below 400°C*, F. Piazza, A. Makarov, R. Velazquez, J. De Jesus, and G. Morell (University of Puerto Rico)
9:00	*Comparative Study of Nucleation Processes for the Growth of Nanocrystalline Diamond*, Y.K. Liu and P.L. Tso (National Tsing-Hua University, Taiwan); I-N Lin (Tamkang University, Taiwan); Y. Tzeng (Auburn University)
9:15	*Origin of Spiral Growth Defects During Early Stages of Homoepitaxial Diamond Growth on (100) Surfaces*, G. Bhimarassetti and M.K. Sunkara (University of Louisville); J.E. Butler (Naval Research Laboratory)

9:30	*Effects of Synthesis Parameters on Properties of Carbide-Derived Carbon Formed on SiC*, A. Lee, C. White, R. Zhu, M. McNallan, A. Erdemir, and Y. Gogotsi (University of Illinois at Chicago)
9:45	**Break**
Session 10: Synthesis and Growth Mechanisms II Chairs: Atsuhito Sawabe and Yonhua Tzeng	
10:15	*PECVD Fabrication of Carbon Cones and Helices on a Metal Tip*, X. Jiang and G. Zhang (University of Siegen, Germany) (invited)
10:45	*HPHT Treatment of Single-Crystal CVD Diamond*, P. Doering (Apollo Diamond)
11:00	*Large Single-Crystal CVD Diamonds at Rapid Growth Rates*, C-S Yan, Y-C Chen, S-S Ho, H-K Mao, and R.J. Hemley (Carnegie Institution of Washington)
11:15	*Controlling Specific and Non-Specific Binding of Proteins at Diamond Surfaces via Covalent Functionalization with Molecular Monolayers*, T.C. Lasseter, B. Clare, B.M. Nichols, N. Abbott, and R.J. Hamers (University of Wisconsin-Madison)
11:30	*Nanocrystalline Diamond on Carbon Nanotubes: Toward a New Class of Carbon Nanomaterials*, M.L. Terranova, A. Fiori, S. Orlanducci, and E. Tamburri (Universita di Roma Tor Vergata, Italy); M. Rossi (Universita di Roma La Sapenza, Italy); and A.S. Barnard (Argonne National Laboratory)
11:45	*Synthesis of Mesoporous Carbons through Inverse Replication and Self-Assembly*, M. Kruk, B. Dufour, K. Matyjaszewski, and T. Kowalewski (Carnegie Mellon University); E.B. Celer and M. Jaroniec (Kent State University)
12:00	*Synthesis of Hybrid Nanocarbon Materials by Self-Assembly*, X. Xiao, J. Elam, S. Trasobares, O. Auciello, and J.A. Carlisle (Argonne National Laboratory)
12:30-2:30	**Poster Session 2**
Session 11: Materials Integration Chair: Orlando Auciello, Argonne National Laboratory	
2:30	*Silicon-on-Diamond: An Engineered Substrate for Electronic Applications*, A. Aleksov, J.M. Gobien, X. Lie, and N. Govindaraju (North Carolina State University); J.T. Prater (Army Research Office); Z. Sitar (North Carolina State University) (invited)
3:00	*CVD Diamond Thin-Film Technology for MEMS Packaging*, X. Zhu and D.M. Aslam (Michigan State University)
3:15	*Design of Residual Stress in Nanocrystalline Diamond Films*, N. Woehrl, A. Poukhovoi, S. Reuter, and V. Buck (University of Duisburg-Essen, Germany)
3:30	*Promising Diffusion Barrier Coatings for Flexible Packaging Based on FCVA Tetrahedral Amorphous Carbon Films*, G.A. Abbas, P. Papakonstantinou, and J.A. McLaughlin (University of Ulster, UK)
3:45	**Break**
4:00	Evaluation Stress, Nanocrystallinity, Purity Crystallinity, and Useful Mass in Diamond Films Deposited on Ti6Al2Sn4Zr2Mo Alloy Using the Assisted Technique of Microwave Plasma, T.M. de Souza, J. Possato, J. de Oliveria and J.E. Bueno (UNESP-Guaratinguetá, Brazil)

4:15	*Controlled Growth of Carbon Nanotubes for 3-D Lithium-Ion Microbatteries,* V.K. Kayastha and Y.K. Yap (Michigan Technological University); C. Wang, R. Zaouk, L. Taherabadi, and M. Madou (University of California, Irvine)
4:30	*Amorphous Carbon Nitride for Use as a High-Temperature Capacitor Dielectric*, W.C. Lanter (ISSI Corporation)
4:45	*Laser-Arc Process and Technology for Deposition of Amorphous and Nanostructured Carbon Films*, H-J Schehibe, M. Leonhardt, and T. Schuelke (Michigan State University); C-F Meyer, H. Schulz, B. Schultrich, and E. Beyer (Fraunhofer Institute)
5:00	*Wurtzitic Boron Nitride on Diamond: The Ultimate Epitomical Wafer for Semiconductor on Insulator*, J.C. Sung (KINIK Company, Taiwan)
7:00	**Banquet**
THURSDAY, MAY 19, 2005	
Session 12: Electrochemistry, Supercapacitors, etc. Chair: John G. Angus, Case Western Reserve	
8:00	*High-Power-Density Supercapacitors Made from Carbon Nanofibers,* R.J. Hamers (University of Wisconsin-Madison) (invited)
8:30	*Electrochemical Characterization of Undoped Hydrogen-Terminated Diamond*, C.E. Nebel, D. Shin, B. Rezek, D. Takeuchi, and H. Watanabe (Diamond Research Center, Japan)
8:45	*Electrochemical Sensing using Nanodiamond Microprobe*, S. Basu, W.P. Kang, J.L. Davidson, B.K. Choi, A.B. Bonds, and D.E. Cliffel (Vanderbilt University)
9:00	*Boron-Doped Diamond Electrodes for Nitric Oxide Detection*, J.B. Schaeffer, D.E. Kourennyi, and H.B. Martin (Case Western Reserve University)
9:15	*Polycrystalline Boron-Doped Diamond Films as Supports for Methanol Oxidation Electrocatalysts*, I. Gonzalez, D.A. Tryk, and C.R. Cabrera (University of Puerto Rico)
9:30	*Surface Chemistry and Electrochemical Properties of Functionalized Ultrananocrystalline Diamond Thin Films*, J. Wang, N. Naguib, X. Xiao, C. Liu, L.A. Curtiss, M.A. Firestone, O. Auciello, and J.A. Carlisle (Argonne National Laboratory)
9:45	**Break**
Session 13: Theory and Modeling Chair: John W. Mintmire, Oklahoma State University	
10:15	*Theory and Modeling of Nanocarbon Phase Stability*, A. Barnard (Argonne National Laboratory) (invited)
10:45	*Multiscale Modeling of Fracture of Graphene Sheets and Carbon Nanotubes*, S. Zhang, S.L. Mielke, R. Khare, G.C. Schatz, and T. Belytschko (Northwestern University)
11:00	*Interfacial Thermal Transport in Diamond: Insights from Simulation*, T. Watanabe, and S.R. Phillpot (University of Florida); P.K. Schelling (University of Central Florida); P. Keblinski (Rensselaer Polytechnic Institute)
11:15	*Surface and Electronic Structure of Diamond Nanoparticles*, T. van Buuren, T. Willey, C. Bostedt, R. Muelenberg, J.Y. Raty, G. Galli, and L. Terminello (Lawrence Livermore Laboratory)

11:30	*A Model for Nanocrystalline Diamond Growth*, P. Zapol and M. Sternberg (Argonne National Laboratory)
11:45	*Resolution of the Diamond Problem After 200 Years*, R. Little (Florida A&M University)
12:00	**Lunch**
Session 14: Business Models and Development Chair: Lothar Schäfer	
1:00	*Legal Opportunities and Challenges Affecting Nanotechnology Research and Commercialization*, J. H. Matsuura (Dayton School of Law)
1:20	*Anatomy of a Diamond Start-Up*, N. Kane (Advanced Diamond Technologies)
1:40	*Flexible Market Approach of CYRANNUS® Plasma Technology*, R. Spitzl and H. Sung-Spitzl (iplas innovative plasma systems gmbh)
2:00	*Adamant Technologies*, Ph. Rychen, Ch. Provent, and L. Pupunat (Adamant Technologies)
2:20	*From Tools to Technology - Stories from a Diamond Survivor*, J. Herlinger and J. Zimmer (sp3 Inc.)
2:40	**Break**
Session 15: HPHT Synthesis, Treatments, Gems, and Application Chair: John A. Carlisle, Argonne National Laboratory	
3:00	*Very High Crystal Quality Diamond Studied by a Variety of Synchrotron-Generated X-Ray Techniques*, S. H. Connell, R. K. Setshedi, D. Dube, L. Mkhonza, and M Rebak (University of the Witwatersrand, South Africa), J. Härtwig and J. Hoszowska (European Synchrotron Radiation Facility, France), RC Burns and JO Hansen (Element Six, South Africa) (invited)
3:30	*Treatment of Natural Gem Diamond and Its Identification*, W. Wang, T. Moses, and M. Hall (Gemological Institute of America)
4:00	*Colour Changes in HPHT Annealed Type IA Diamond*, F. De Weerdt (Diamond High Council, Belgium) and H. Kanda (NIMS, Japan)
4:15	*Growth and Characterization of a Single-Crystal CVD Diamond Nuclear Detector*, A. Balducci, M. Marinelli, E. Milani, M.E. Morgada, G. Pucella, A. Tucciarone, G. Veronia-Rinati (Universita di Roma Tor Vergata, Italy); M. Angelone and M. Pillon (Associazione Euratrom-ENEA sulla fusione, Italy); R. Potenza and C. Tuve (Universita di Catania, Italy)
4:30	*Laser Raman Spectra of Large Diamondoid Molecules: A Route to Understanding Nanodiamond Crystals*, P.W. May, J. Filik, and J.N. Harvey (University of Bristol, UK); J.E.P. Dahl, R.M.K. Carlson, and S. Liu (ChevronTexaco Energy Technology)
4:45	*Inroad to Modification and Functionalization of the Detonation Nanodiamond*, B.V. Spitsyn (Institute of Physical Chemistry, RAS, Russia)

POSTER SESSION 1

MONDAY, MAY 16, 2005, 7:00-9:00 p.m.

	Characterization
2-1	*Mechanism of Imaging of Carbon Nanotubes by Scanning Electron Microscopy*, D.A. Dikin and R.S. Ruoff (Northwestern University)
2-3	*Irradiation Effects of 100-MeV Au+ Ions on Multiwalled Carbon Nanotubes and Encapsulated Single-Crystal Nickel Nanorods*, A. Misra, P.K. Tyagi, and D.S. Misra (Indian Institute of Technology, Bombay); J. Ghatak and P.V. Satyan (Institute of Physics Bhubanheshawr, India)
2-5	*Step Growth in Single-Crystal Diamond Grown by Microwave Plasma Chemical Vapor Deposition*, P.K. Tyagi. A. Misra, and D.S. Misra, (Indian Institute of Technology, Bombay); F. LeNormand (CNRS, France)
2-7	*Characterization of Treated Black Diamonds*, M.A. Viktorov and M.B. Kopchikov (Moscow State University, Russia)
2-9	*Electrical Conductivity of Hydrogenated and Nitrogen-Doped Nanodiamond Films*, A-J Cheng, M. Clark, Y-K Liu, Y-C Chen, and Y. Tzeng, Auburn University
2-11	*TEM and XRD Study of Nano-Graphene Layer Formation and Texturing in Carbon Films Deposited by Pulsed Nd:YAG Laser*, E. Cappelli, C. Scilletta, and P. Ascarellli (CNR-ISC sez. Montelibretti, Italy); M. Servidori, P.G. Merli, V. Morandi, and A. Migliori (CNR-IMIP sez. Potenza, Italy); and S. Orlando (CNR-IMM sez. Bologna, Italy)
2-15	*About X-Ray Amorphous-Phase Formation of Ultradispersed Diamonds*, A. Koretz and E. Mironov (State Technical University, Krasnoyarsk, Russia), E. Petrov (Russian Academy of Sciences), and A. Lyamkin (State Technical University, Krasnoyarsk, Russia)
	MEMS
3-1	*Dissipation in Tetrahedral Amorphous Carbon Oscillators*, D.A. Czaplewski, J.P. Sullivan, T.A. Friedman, D.W. Carr, B.E.N. Keeler, and J.R. Wendt (Sandia National Laboratories)
3-3	*Carbon Nanotube Electro Mechanical Oscillator*, .Y. Song and J. Choi, Wayne State University
3-5	*High-Frequency Surface Acoustic Wave Device Fabricated by Using AlN-UNCD Thin Films*, C-H Chou, Y-C Lee, J-H Huang, and S-J Lin (National Tsing-Hua University, Taiwan); I-N Lin, Tamkang University, Taiwan
3-7	*Nanocrystalline Diamond on LiNBO3 for Surface Acoustic Wave Applications*, K-H Chen (Institute of Atomic and Molecular Sciences, Academia Sinica, Taiwan); Y.C. Lin, J.P. Huang, S.T. Lin, and L.C. Chen (National Taiwan University of Science and Technology, Taiwan)
	Tribology and Interfaces
4-1	*Mechanical Properties of Ultrananocrystalline Diamond Thin Films Relevant to UNCD-MEMS*, H.D. Espinosa, G. Schatz, B. Peng, and N. Moldovan (Northwestern University); O. Auciello and J.A. Carlisle (Argonne National Laboratory)
4-3	*Fabrication of Ultrananocrystalline Diamond Atomic Force Microscope Probes*, G. Ning, A.V. Sumant, D.S. Grierson, and R.W. Carpick (University of Wisconsin-Madison); J.E. Gerbi, J. Birrell, X. Xiao, O. Auciello, and J.A. Carlisle (Argonne National Laboratory)
4-5	*X-Ray Diffraction Analyses of the CVD Diamond Film Deposited on the TI6Al4V Alloy with the Addition of CF_4 in Methane-Hydrogen Mixtur*e, T.M. de Souza, J. Possato, J. de Oliveira, and J.E. Bueno (UNESP-Guaratinguetá, Brazil)

4-7	*Scanning Electronic Microscope Analyses and X-Rays Diffraction of the CVD Diamond Film Deposited on Ti6A14V Alloy Utilizing Microwave Plasma Reactor*, T.M. de Souza, J. Possato, J. de Oliveira, and J.E. Bueno (UNESP-Guaratinguetá, Brazil)
4-9	*Ultrananocrystalline Diamond as Hermetic and Bioinert Coating for Implantable Biomedical Devices*, X. Xiao, J. Wang, J.A. Carlisle, and O. Auciello (Argonne National Laboratory); D. Guven, R. Freda, J. Weiland, and M. Humayun (University of Southern California)
4-11	*Controlling the Nanotribology of Nanostructured Diamond Films*, R.W. Carpick, D.S. Grierson, A.V. Sumant, E.E. Flater, G. Ning, and K. Sridharan (University of Wisconsin-Madison); T.A. Friedmann and J.P. Sullivan (Sandia National Laboratories); J.E. Gerbi, J. Birrell, X. Xiao, O. Auciello, J.A. Carlisle (Argonne National Laboratory)
4-13	*Low-Temperature Catalytic Synthesis of Carbon Onions and Evaluation of Its Solid Lubricant Property*, A. and S. Namiki (Tokyo Institute of Technology, Japan)
4-15	*Tribological Studies on Ultrafine Diamond Composite Coatings Deposited on Tungsten Carbide*, X.G. Jian (Tong Ji University, China); M. Chen and F.H. Sun (Shanghai Jiao Tong University); and L.D. Li (Tong Ji University, China)
4-17	*Direct Wafer Polishing with 5-nm Diamond,* J.C. Sung (KINIK Company, Taiwan) and M-F Tai (Wufeng Institute of Technology, Taiwan)
4-19	*DNA Sensor Based on the Modified Nitrogen-Doped Nanocrystalline Diamond Film*, Z. Xu, A. Kumar, M. Singh, A. Kumar, and S. Jeedigunta (University of South Florida)
	Electronic Devices
5-1	*Modeling of Single-Crystal Diamond Schottky Barrier Diodes for High-Voltage Applications*, S.J. Rashid, M. Brezeanu, T. Butler, N.L. Rupesinghe, F. Udea, and G.A.J. Amaratunga (University of Cambridge, UK); L. Coulbeck, A. Garraway, and P. Taylor (Dynex Semiconductors Ltd., UK); D.J. Twitchen, A. Tajani, and C. Wort (Element Six Ltd., UK)
5-3	*Acceptor and Donor Trapping Centers in Boron-Doped CVD Diamond*, V.I. Polyakov and A.I. Rukovishnikov (Institute of Radio Engineering and Electronics, RAS, Russia); V.P. Varnin (Institiute of Physical Chemistry, RAS, Russia); V.G. Ralchenko (General Physical Institute, RAS, Russia)
5-5	*Enhancement Mode MESFET from Free-Standing Polycrystalline Diamond Grown by High-Power DC Arc Plasma Jet CVD*, Y. Dai, R. Long, L. Yu, Z. Zhang, Z. Chang, and C. Yan (Shandong University, China)
5-7	*Seebeck Effect DVD-Diamond/Pd Gas Sensors*, A. Balducci, M. Martinelli, E. Milani, M.E. Morgada, G. Pucella, G. Rodriguez, A. Tucciarone, G. Verona-Rinati, A. D'Amico and C. Di Natali (Universita di Roma Tor Vergata, Italy)
5-9	*Semiconductor Properties of the DLC Thin Films Doped with Nitrogen*, Zh.R. Panosyan, A.S. Voskanyan, R.V. Grzaryan, and K.M. Yeghishyan (State Engineering University of Armenia): J.F. Pern and K.J. Touryan (National Renewable Energy Laboratory); V.I. Polyakov (Institute of Radio Engineering and Electronics, RAS, Russia)
5-11	*Homoepitaxial and Polycrystalline CVD Diamond pn Junctions*, K. Haenen, V. Mortet, J. D'Haen, O.A. Williams, M. Nesladek, L. De Schepper (Limburgs Universitair Centrum, Belgium); S. Koizumi (National Institute for Materials Science, Japan)
	Field Emission
6-1	*Thermionic Field Emission from UNCD-Coated Tip Structures*, J.M. Garguilo, F.A.M. Koeck, and R.J. Nemanich (North Carolina State University); X.C. Xiao, O. Auciello, and J.A. Carlisle (Argonne National Laboratory)

6-3	*Characteristics of Ultra-Nanocrystalline Diamond Films Grown on a Porous Anodic Alumina Template*, Y-C Chen, C-Y Chen, N-H Tai, Y-C Lee, and S-J Lin (National Tsing-Hua University, Taiwan); I-N Lin (Tamkang University, Taiwan)
6-5	*Field Emission Characteristics of Diamond Edge Shaped Emitters Fabricated using Nitrogen-Methane Plasma*, R.S. Takalkar, W.P. Kang, J.L. Davidson, B.K. Choi, W.H. Hofmeister, and K. Subramanian (Vanderbilt University)
6-7	*Fabrication of Aligned Convex CNT Field Emission Triode by MPCVD*, Y.M. Wong, W.P. Kang, J.L. Davidson, B.K. Choi, W.H. Hofmeister (Vanderbilt University); J.H. Huang (National Tsing-Hua University, Taiwan)
6-9	*Study of the Field Emission Properties of Carbon Nanotubes Grown on Sulfur-Doped Nanocrystalline Diamond Films*, K. Uppireddi, F. Piazza, and G. Morell (University of Puerto Rico)
6-11	*Amorphous Diamond Electron Emission Capabilities: Implications to Thermal Generators and Heat Spreaders*, J.C. Sung and K. Kan (KINIK Company, Taiwan); M. Sung (Massachusetts Institute of Technology); J-L Huang (National Cheng-Kung University, Taiwan); E. Sung (Johnson and Johnson), C-P Chen (KINIK Company, Taiwan); K-H Hsu (National Taipei University of Technology, Taiwan); M-F Tai (Wufeng Institute of Technology, Taiwan)
6-13	*Competition of Field Emission from CNT Films Produced by Five Different Techniques*, A.V. Karabutov, S.M. Pimentov, V.I. Konov, E.D. Obraztsova, V.G. Pereverzev, A.S. Pozharov, and S.V. Terekhov (General Physics Institute, Russia); P. Ya. Detkov and E.V. Shorokhov (RFNC-RITF, Russia); E.N. Loubnin (Institute of Physical Chemistry, Russia)
	Surfaces and Sensors
7-1	*Surface Conductivity as a Natural Property for Hydrogenated Diamond*, Y. Dai, B.B. Huang, and R. Long (Shandong University, China); D. Dai (North Carolina State University)
7-3	*Chemically and Biologically Functionalized Diamond Solution Gate TFT and Its Application for DNA Sensing*, B. Sun, W. yang, K-Y Tse, and R.J. Hamers (University of Wisconsin-Madison)
7-5	*Photochemical Modification of Diamond Films: A Structural and Mechanistic Study*, B.M. Nichols and R.J. Hamers (University of Wisconsin-Madison); J.E. Butler and J.N. Russell, Jr. (Naval Research Laboratory)
7-7	*Neural Cell Patterning on Thin-Film Boron-Doped Diamond Electrodes for Neurotransmitter Detection in vitro*, J. Bursee, H. Baskaran, and H.B. Martin (Case Western Reserve University)
	Growth
9-1	*Synthesis of Large-Area, Thick, Uniform, Smooth Ultrananocrystalline Diamond Films by Microwave Plasma-Assisted Chemical Vapor Deposition*, Dzung Tran and Jes Asmussen, Michigan State University
9-3	*Deposition of (U)NCD Films using Hot-Filament CVD*, Paul W. May (University of Bristol, UK)
9-5	*Enhanced Nucleation of Ultrananocrystalline Diamond using Tungsten Films*, N. Naguib, J. Wang, O. Auciello, J.A. Carlisle, and J. Elam (Argonne National Laboratory); J. Birrell (Advanced Diamond Technologies)
9-7	*Improvement on the Growth of Ultrananocrystalline Diamond by using Pre-Nucleation Technique*, Y-C Lee and S-J Lin (National Tsing-Hua University, Taiwan); I-N Lin (Tamkang University, Taiwan)

9-9	*Improving the Adhesion Properties of Nanocrystalline Diamond Films by Bias-Enhanced Nucleation*, E. Mujica, F. Piazza, and G. Morell (University of Puerto Rico); S. Wolter (Duke University)
9-11	*Formation of Diamond Whiskers by RF Plasma Etching*, C.Y. Li and A. Hatta (Kochi University of Technology, Japan)
9-13	*Liquid Carbon Sources for Deposition of Nanostructural Diamond*, T.V. Semikina, K. Gyopda, and Y. Takagi (Teikyo University of Science and Technology, Japan)
9-15	*Nanoporous Carbons Derived from Block Copolymers with Polyacrylonitrile Blocks*, C. Tang, M. Kruk, K. Matyjaszewski, and T. Kowalewski (Carnegie Mellon University); E.B. Celer and M. Jaroniec (Kent State University)
9-17	*Growth and Characterization of Aligned Carbon Nanotubes by Microwave Plasma Chemical Vapor Deposition*, A. Vaseashta (Marshall University) and J.A. Carlisle (Argonne National Laboratory)
9-19	*Synthesis and Characterization of Carbide-Derived Carbon Nanowires*, X. Chen, D.R. Cantrell, S. Stankovich, and R.S. Ruoff, Northwestern University
9-21	*Effects of NH3 Plasma Pretreatment on the Growth of Carbon Nanotubes*, S. Wang, P. Wang, and O. Zhou (University of North Carolina)
9-23	*Structure and Electronic Properties of Novel Unconventional Carbon Allotropes and BN Polymorphes*, V.V. Pokropivny and V.L. Bekenev (Frantsevich Institute for Problems of Materials Science of NASU, Ukraine)
9-25	*Direct Growth of Boron Nitride Nanotubes on Substrates*, Y.K. Yap, J. Wang, and V. Kayatha (Michigan Technological University)
9-27	*Thermodynamic Conditions of ta-C Formation at Implantation of Noble-Gas Ions in Carbon*, A.I. Kalinichenko, S.S. Perepelkin, and V.E. Strel'nitskij (National Science Center, Kharkov Institute of Physics and Technology, Ukraine)
9-29	*Action of Acoustic Effects at Ion Implantation on Kinetic Processes in Carbon Films*, A.I. Kalinichenko and V.E. Strel'nitskij (National Science Center, Kharkov Institute of Physics and Technology, Ukraine)
9-31	*Effects of Methane Gas Pressure on Optical and Electrical Properties of Nitrogenated Camphoric Carbon Thin Films Grown by Surface Wave Microwave Plasma*, M. Rusop, T. Soga, and T. Jimbo (Nagoya Institute of Technology, Japan); S. Adhikari, A.M.M. Omer, S. Adhikary, H. Uchida, and M. Umeno (Chubu University)
9-33	*Diamond Growth on an Array of Seeds: The Revolution of Diamond Production*, J.C. Sung (KINIK Company, Taiwan)
	Electrochemistry
12-1	*Probing Electrical Conductivity Homogeneity Across a Boron-Doped Nanocrystalline Diamond Film using Michigan State University Conductive Probe-Atomic Force Microscop*y, S. Wang and G.M. Swain (Michigan State University)
12-3	*Analysis of Chlorinated Phenols Pollutants using Diamond Microelectrodes*, G. W. Muna, V. Quaiserova-Mocko, and G.M. Swain (Michigan State University)
12-5	*Monitoring Arsenic (III) in Water Supplies using Anodic Stripping Voltammetry and a Diamond Electrode*, Y. Song and G.M. Swain (Michigan State University)
12-7	*Diamond Microelectrodes for the In Vitro Measurement of Norepinephrine Release from Sympathetic Nerves in Rats*, J. Park, J.J. Galligan, G.D. Fink, and G.M. Swain (Michigan State University)

12-9	*Electrochemical Tuning and Investigations on Actuator Mechanism of Single-Wall Carbon Nanotubes*, S. Gupta (Southwest Missouri State University)
	Theory
14-1	*Electronic Structure Calculations of Nitrogen and Hydrogen in Diamond Twist Grain Boundaries*, M. Sternberg, P. Zapol, and L.A. Curtiss (Argonne National Laboratory)
14-3	*Thermodynamic Stability of Nanodiamond*, H. Cui, C.X. Wang, P. Liu, and G.W. Yang (Zhongshan University, China)
14-5	*Comparison Study of Hydrogen Incorporation in Diamond: Effect of Crystalline State and Origin of Diamond*, C.J. Tang, A.J. Neves, and L. Rino (University of Aveiro, Portugal)

POSTER SESSION 2

Wednesday, May 18, 2005, 3:00-5:00 p.m.

	Characterization
2-2	*Surface Plasmon Resonance Study of Single-Walled Nanotube Polymer Film*, V.I. Chegel, (Lashkarev Institute of Physics of Semiconductors of NASU, Ukraine); L.V. Poperenko and Y.V. Chegel (T. Shevchenko National Kyiv University, Ukraine); V.V. Pokropivny (Frantsevich Institute of Problems of Materials Science of NASU, Ukraine)
2-4	*FTIR Studies of Nitrogen-Doped Carbon Nanotubes*, A. Misra, P.K. Tyagi, M.K. Singh, and D.S. Misrah (Indian Institute of Technology, Bombay)
2-6	*Characterization of Single-Crystal Diamonds Grown by High Growth Rate Chemical Vapor Deposition Methods*, Y-C Chen, C-S Yan, H-K Mao, and R.J. Hemley (Carnegie Institution of Washington); M. Origlieri (University of Arizona); S. Krasnicki (Argonne National Laboratory); Y. Tzeng (Auburn University)
2-8	*Spectroscopy Application for Characterization and Identification of Artificially Colored Diamonds*, M.A. Viktorov and M.B. Kopchikov (Moscow State University, Russia)
2-10	*Extending the 3-Omega Method to the Megahertz Range for Thermal Conductivity Measurements of Diamond Thin Films*, R. Liske, T. Wunderer, M. Leonhardt, T. Grotjohn, J. Asmussun, and T. Schuelke, Michigan State University
2-14	*Observation of Structural Changes in Carbon Films under External Influences*, Zh. R. Panosyan, A.V. Meliksetyan, A.S. Voskanyan, Y.V. Yengibaryan, A.A. Sahakyan, and A.T. Darbasyan (State Engineering University of Armenia)
	MEMS
3-2	*Polycrystalline Diamond MEMS Resonator Technology for Sensor Applications*, N. Sepulveda and D.M. Aslam (Michigan State University); D. A. Czaplewski, J.P. Sullivan, and T.A. Friedman (Sandia National Laboratories)
3-4	*Carbon Nanotube Technology for Micro Gas Chromatograph and Chemical Nanosensors*, Y. Lu and D.M. Aslam (Michigan State University); E.T. Zellers (University of Michigan)
3-6	*Growth of High-Quality AlN using Ti Buffer Layer on Diamond*, C-H Chou, Y-C Lin, J-H Huang, N-H Tai (National Tsing-Hua University, Taiwan); I-N Lin (Tamkang University, Taiwan)
	Tribology and Interfaces
4-2	*Development of a MEMS Platform for the Assessment of Reinforcement Mechanisms of Carbon Nanotubes in a Polymer Matrix*, E. Zimney, J. Chung, and R.S. Ruoff (Northwestern University)
4-4	*Silicon Carbide Samples for CVD Diamond Film Deposition with Application on Rastilho for Musical Instruments of Chord and Waves Analysis Transmitted by the Samples*, T.M. de Souza, L.N. Kawakami, S.E. Lucena, andn P.R. Alves (UNESP-Guaratinguetá, Brazil)
4-6	*Stress and Purity Crystallinity of CVD Diamond Films Growth in Hot-Filament Reactor on Ti6Al4V Alloy with Various Methane Concentration*, T.M. de Souza, J. Possato, J. de Oliveira, and J.E. Bueno (UNESP-Guaratinguetá, Brazil); V.J. Trava-Airoldi (INPE, Brazil)

4-8	*Dental Implants Recovered with CVD Diamond Film*, J. Possato and T.M. de Souza (UNESP-Guaratinguetá, Brazil)
4-10	*Human Micro-Vascular Endothelial Cells Attachment and Tube Formation on Balloon-Expanded Stainless Steel Stents Coated with DLC and Si-DLC Thin Solid Film*, T. Okpalugo, P.D. Maguire, and J. McLaughlin (University of Ulster, UK)
4-12	*Nanocarbon Thin Films: The Link between Surface Chemistry and Nanotribology*, A. Sumant, D.S. Grierson, and R.W. Carpick (University of Wisconsin-Madison); J.E. Gerbi, J. Birrell, J.A. Carlisle, and O. Auciello (Argonne National Laboratory); T. A. Friedmann and J.P. Sullivan (Sandia National Laboratories)
4-14	*In Situ Nanoindentation of Ultrananocrystalline Diamond and Amorphous Diamond Thin Film Coatings*, E.A. Stach, A.M. Minor, D. Ge, J.W. Morris, Jr., T.A. Friedmann, X. Xiao (Purdue University); O. Auciello and J.A. Carlisle (Argonne National Laboratory)
4-16	*Structural Changes during the Wear of Diamondlike Carbon Films at Low Temperature*, J.B. Woodford and J.A. Johnson (Argonne National Laboratory); G.H. Xu (University of Alaska); H. Liang (texas A&M University)
	Electronic Devices
5-2	*Analysis of P-Type CVD Diamond for High-Power and High-Temperature Applications*, S.L. Heidger (Air Force Research Laboratory)
5-4	*Neutron Transmutation of ^{10}B-Doped Diamond*, K. Jagannadham and M.L. Reed (North Carolina State University); M.J. Lance and T.R. Watkins (Oak Ridge National Laboratory); K Verghese (North Carolina State Universith); J.E. Butler (Naval Research Laboratory)
5-6	*CVD Single-Crystal Diamond for Extreme UV Photodetection*, A. Balducci, M. Marinelli, E. Milani, M.E. Morgada, C. Pucella, A. Tuccirone, and G. Verona-Rinati (Universita di Roma Tor Vergata, Italy); E. Pace and A. De Sio (Universita di Firenze, Italy)
5-8	*Tailoring the Properties of CVD Diamond for Passive and Active Radiation Applications*, P. Ascarelli, E. Cappelli, and D.M.Trucchi (CNR-ISC, Italy); G. Conte (Universita de Rome Tre, Italy)
5-10	*Morphology, Optical Properties, and Single-Electron Spectrum of "Detector-Quality" DLC Layers Prepared by MW CVD*, V. Ligatchev (Nanyang Technological University, Singapore) and B. Gan (Agilent Technologies, Singapore)
	Field Emission
6-2	*Syntheses of Boron-Doped Polycrystalline Diamond on Molybdenum Substrate for Cold Discharge Cathode*, H. Yoshida, I. Yanase, N. Sakuma, T. Ono, and T. Sakai (Toshiba Corporation, Japan)
6-4	*Effect of Granular Structure on the Electron Field Emission Properties of Nanodiamond Films*, H-F Cheng (National Taiwan Normal University, Taiwan); Y-C Lee and S-J Lin (National Tsing-Hua University, Taiwan); I-N Lin (Tamkang University, Taiwan)
6-6	*Geometrical Field Enhancement on Micropatterned Nanodiamond Film for Electron Emissions*, K. Subramanian, W.P. Kang, J.L. Davidson, W.H. Hofmeister, B.K. Choi, and M. Howell (Vanderbilt University)
6-8	*Field Emission Properties of Selected Single-Wall Carbon Nanotube Samples*, A. Fiori, S. Orlanducci, V. Sessa, E. Tamburri, and M.L. Terranova, A. Di Carlo, A. Reale, F. Brunetti, P. Regoliosi, and R. Riccitelli (Universita di Roma Tor Vergata, Italy); A. Ciorba and M. Rossi (Universita di Roma La Sapienza, Italy)

6-10	*Cold Cathodes for Applications in Poor Vacuum and Low-Pressure Gas Environments: Carbon Nanotubes versus Zinc Oxide Nanoneedles*, A-J Cheng, D. Wang, H.W. Seo, M. Park, and Y. Tzeng (Auburn University)
6-12	*Nitrogen Doping and Graphitization of Nanocrystalline Diamond Films for Enhanced Field Electron Emission*, A.V. Karabutov and V.I. Konov (General Physics Institute, Russia); E.N. Loubnin (Institute of Physical Chemistry, Russia); V.V. Pereverzev, I.I. Vlasov, E.V. Zavedeev, and S.M. Pimenov (General Physics Institute, Russia)
	Surfaces and Sensors
7-2	*Electrochemical Detection of Iodophenols at Boron-Doped Diamond Thin-Film Electrodes*, Audrey N. Martin and Greg M. Swain, Michigan State University
7-4	*Electrical Characterization and Biosensing Application of Modified Carbon Nanofibers and Nanocrystalline Diamond*, K-Y Tse, S.E. Baker, B.M. Nichols, W. Yang, and R.J. Hamers, (University of Wisconsin-Madison)
7-6	*Fabrication and Addressable Functionalization of Vertically Aligned Carbon Nanofibers*, S.E. Baker, K.Y. Tse, C-S Lee, R.J. Hamers, M.S. Marcus, and M. Eriksson (University of Wisconsin-Madison)
	Growth
9-2	*Scale-Up of Diamond Deposition with Microwave Plasma CVD*, R. Spitzl and H. Sung-Spitzl (iplas innovative plasma systems gmbh, Germany)
9-6	*Investigating the Role of Hydrogen in Ultrananocrystalline Diamond Thin-Film Growth*, J. Birrell (Advanced Diamond Technologies); J.E. Gerbi (University of Illinois at Urbana-Champaign); O. Auciello and J.A. Carlisle (Argonne National Laboratory)
9-8	*Effect of Nucleation Methods for Low Temperature Ultrananocrystalline Diamond Deposition*, L-J Chen, Y-C Lee, N-H Tai, C-Y Lee, and S-J Lin (National Tsing-Hua University, Taiwan); I-N Lin (Tamkang University, Taiwan)
9-10	*Effects of Nano- and Microcrystalline Seeds on the Growth of Nano- and Microcrystalline Diamond Thin Films*, F. Piazza, R. Velazquez, J. De Jesus, and G. Morell (University of Puerto Rico)
9-12	Deposition and Post-Processing of Polycrystalline Diamond for Freestanding Films and Substrates, S. Zuo, T. Grotjohn, D. Reinhard, J. Asmussen, R. Ziervogel (Michigan State University)
9-14	*Reactive Ion Etching of Multiphase Structures for CDC Synthesis*, P. Gupta, M. Tlustochowicz, R. Zhu, C. White, M. McNallan, A. Erdemir, B. Prorok, and Y. Gogotsi (University of Illinois at Chicago)
9-16	*Characterization of High-Temperature-Treated Nanostructured Carbons from Self-Assembled Block Copolymer Precursors*, K. Kohlhaas, X. Chen, and R.S. Ruoff (Northwestern University); M. Kruk. B. Dufour, K. Matyjaszewski, and T. Kowalewski (Carnegie Mellon University); E.B. Celer and M. Jaroniec (Kent State University)
9-18	*Synthesis of Aligned Carbon Nanotubes by Microwave Plasma Chemical Vapor Deposition*, S. Zhou, L. Zong, N. Sgriccia, M.C. Hawley, S. Zuo, and J. Asmussen (Michigan State University)
9-20	*Fe Catalyst on Copper Substrates: A Way Forward for Production of Carbon Nanotube Bundles, Ropes, and Other Self-Assembled Structures*, P.K. Tyagi. A. Mixra, M.K. Singh, P. Das, and D.S. Misra (Indian Institute of Technology, Bombay); J. Gharak, P.V. Satyam, F. Le Normand (CNRS, France)

9-22	*Purification of Nanocrystalline Ultra-Dispersed Diamond to be Employed as Nanoprobes for Cellular Imaging*, R. Acosta, J. De Jesus, F. Piazza, G. Morell, and E.R. Fachini (University of Puerto Rico)
9-24	*Fluid Synthesis and Structure of Novel Boron Nitride Polymorphe - Hyperdiamond Fulborenite HDF-B12N12 (E-Phase)*, V. Pokropivny, A. Smolyar, and A. Pokropivny (Frantsevich Institute for Problems of Materials Science of NASU, Ukraine); V. Kuts (Institute of Magnetism of NASU, Ukraine); and R. Partch (Clarkson University)
9-26	*Growth of Adhesive Cubic-Phase Boron Nitride Films without Argon Ion Bombardment*, J. Wang and Y.K. Yap (Michigan Technological University)
9-28	*Features of DC Cathodic Vacuum-Arc Plasma Sources for DLC Films Deposition*, I.I. Akesenov and V.E. Strel'nitskij (Kharkov Institute of Physics and Technology, Ukraine)
9-30	*Structural Studies of Graphite-Like CNx Films Deposited on Silicon by Chemical Vapor Deposition of 1 H-1,2,3-triazole*, Md. Nizam Uddin and M. Nagano (Saga University, Japan); M.J. Islam (Shah Jalal University of Science and Technology, Bangladesh)
9-32	*Properties of Amorphous Carbon Nitride Films Grown by Newly Developed Surface Wave Microwave Plasma CVD After Heat-Treated at Various Annealing Temperatures*, M. Rusop, T. Soga, and T. Jimbo (Nagoya Institute of Technology, Japan); S. Adhikari, A.M.M. Omer, S. Adhikary, H. Uchida, and M. Umeno (Chubu University, Japan)
9-34	*Cermet Ceramic Coating on Diamond Dresser for In Situ Dressing of Chemical Mechanical Planarization*, J.C. Sung and K. Kan (KINIK Company, Taiwan)
	Electrochemistry
12-2	*Effects of Grain-Size Reduction on the Electroanalytical Performance of Conductive Diamond Electrode Deposited in CH4/H2 Gas Mixture*, K.L. Soh, W.P. Kang, J.L. Davidson, Y.M. Wong, B.K. Choi, and D.E. Cliffel (Vanderbilt University)
12-4	*Electrochemical Detection of Nitroaromatics using the Boron-Doped Diamond Electrode*, J.C. Seegmiller, V. Quaiserova-Mocko, J.M. Stotter, and G.M. Swain (Michigan State University)
12-6	*Water Quality Monitoring on Boron-Doped Diamond Electrodes*, E.A. McGaw, P. Sonthalia, and G.M. Swain (Michigan State University)
12-8	*Diamond Nanoparticles as a Support Material for Fuel Cell Electrocatalysts*, D.A. Tryk, L. La Torre, I. Gonzalez, and C.R. Cabrera (University of Puerto Rico)
12-10	*Bentonite Carbon Composite Polyvinyl-Coated Wire Electrode for Lead Detection as an Environmental Sensor*, A. Izadyar (Shiraz University, Iran)
	Theory
14-2	*Diamond Nanowires Grown Inside Carbon Nanotubes upon Chemical Vapor Deposition: Thermodynamic and Kinetic Approach*, C.X. Wang, P. Liu, H. Cui, and G.W. Yang (Zhongshan University, China)
14-4	*Thermodynamical Predictions of Nanodiamonds Synthesized by Pulsed Laser Albation in Liquid*, P. Liu, C.X. Wang, H. Cui, and G.W. Yang (Zhongshan University, China)

THE ADVANCED PHOTON SOURCE
CONFERENCE CENTER
AT ARGONNE NATIONAL LABORATORY

BUILDINGS 401 & 402 - FIRST FLOOR

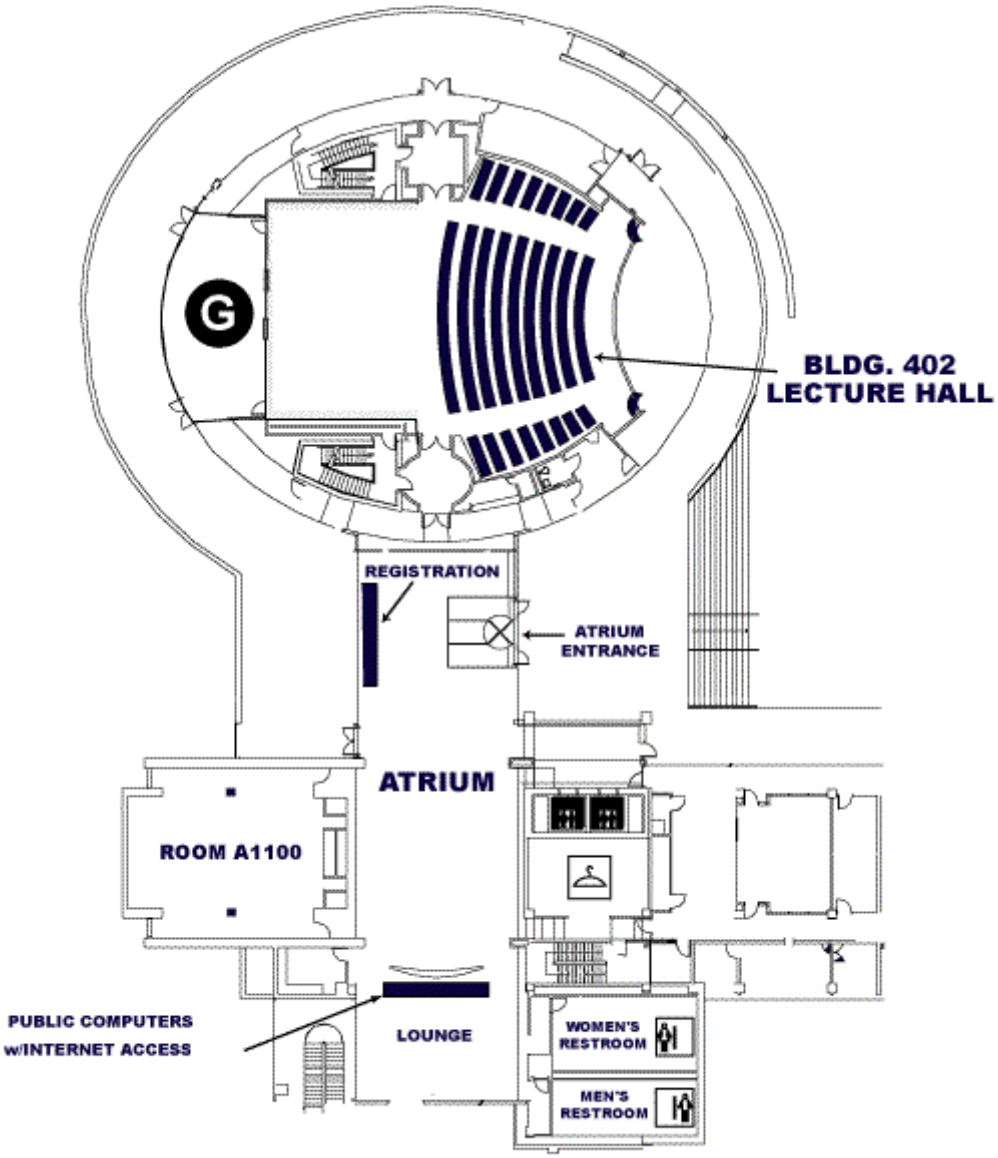

Poster/Exhibition Floor Plan

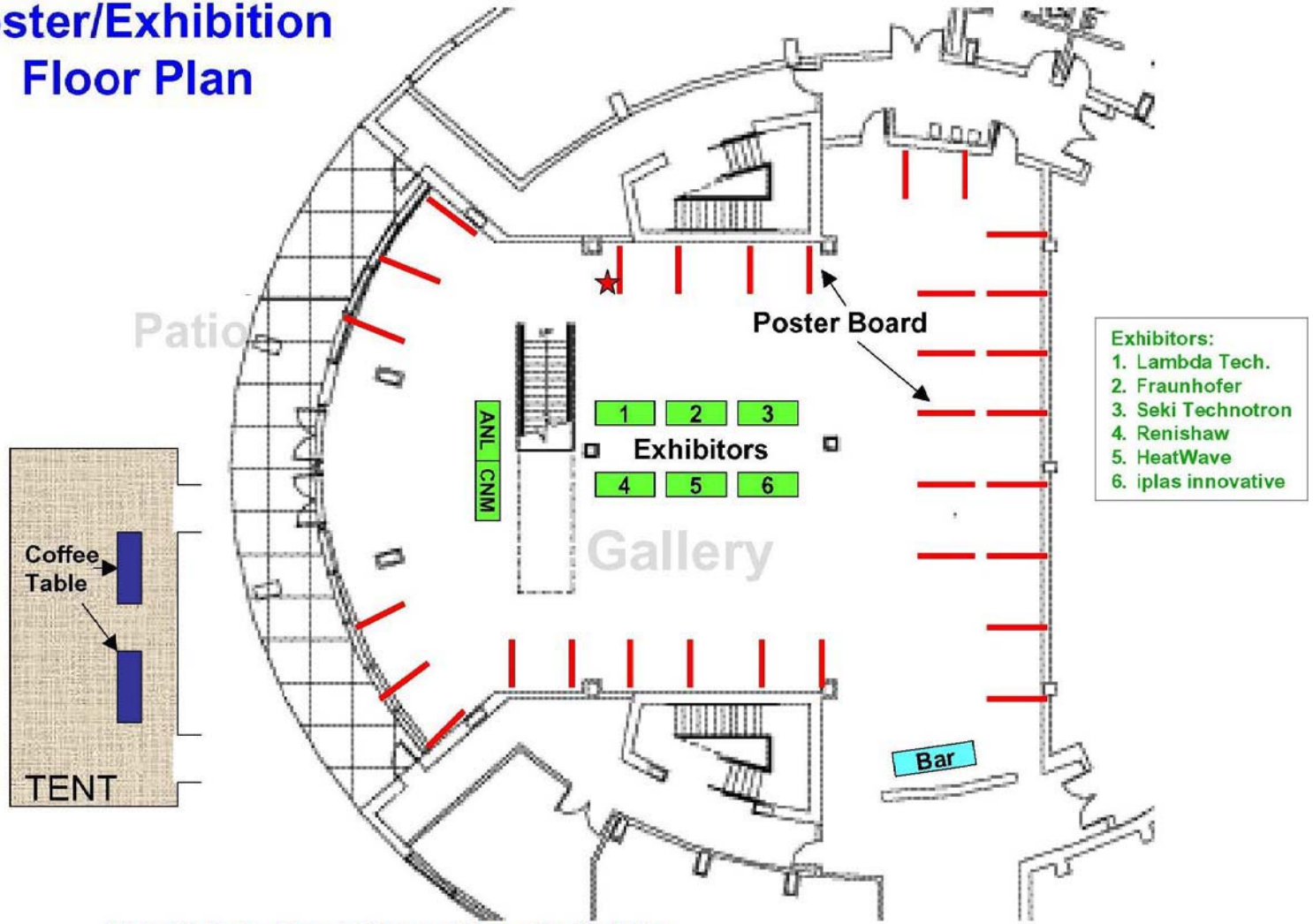

Note: 31 Poster Boards Shown. 1 Board for Back-Up.
★ : Poster 2-1 will be here. The posters are arranged clockwise according to their assigned numbers.

SESSION 1

APPLICATIONS/DEVICES: GENERAL

VLSI Quantum Computer in Diamond

Philip Hemmer
Electrical Engineering Department
Texas A&M University
3128 TAMU
College Station, TX 77843

Recently, we have been exploring the possibility developing a diamond-based VLSI quantum computer. In analogy to the VLSI quantum computer based on phosphorous in silicon, we will use nuclear spin states of nitrogen-vacancy (NV) color centers in diamond as the qubits, and we will use gate electrodes to tune qubits into and out of resonance with each other and with control fields. However in our design, the qubits will be addressed optically, and it is the optical rather than the spin transitions that will be tuned with the electrodes. I will describe current status of the program and will briefly discuss the potential for room temperature solid-state quantum computers in NV diamond.

Carbon Nanotube Electronics

Yu-Ming Lin
IBM T. J. Watson Research Center
Yorktown Heights, NY 10605

Carbon nanotubes (CNTs) are promising candidates for nanoelectronic technology because of their exceptional electrical transport properties, including ballistic 1D transport, a high Fermi velocity, and high current carrying capability. Field-effect transistors using semiconducting carbon nanotubes have been shown to possess very impressive performance comparable to or even exceeding that of state-of-the-art Si-based transistors. Carbon nanotube field-effect transistors (CNFETs), however, still have some disadvantageous issues that need to be addressed. In particular, due to the Schottky barriers formed at the metal/nanotube interface, CNFETs exhibit ambipolar behaviors upon scaling, resulting in large OFF-state currents and a shallow switching slope. I will review important factors determining the transport behavior and performance of a CNFET. I will then introduce gate structure engineering concepts in CNFETs and discuss how we can eliminate these problems by selectively doping the contact regions via electrostatic doping or chemical doping. In collaboration with: Joerg Appenzeller, Zhihong Chen, and Phaedon Avouris.

CVD DIAMOND COATING OF INTERIOR SURFACES

L. Schäfer, M. Höfer, T. Hollstein, B. Blug, M. Herrmann, T. Hühns

Fraunhofer Alliance Diamond Coated Ceramics »DiaCer«,
Bienroder Weg 54E, 38108 Braunschweig, Germany; schaefer@ist.fhg.de

Keywords: CVD diamond, coating of interior surfaces, drawing dies, wear protection, low friction.

Abstract

There are several applications where the interior surfaces of tools or parts need low friction and have to be protected against wear. Cases in point are dies for drawing wires. Top quality dies for the fabrication of wires are made of monolithic diamond or at least sintered polycrystalline diamond (PCD). Especially tools made of monolithic diamond have excellent wear resistance and low friction coefficients. These properties allow the fabrication of wires with high degree of precision of the diameter and excellent surface smoothness. In addition to that wires can be produced with high operating speed applying water suspensions as lubricant. In some cases even dry production is possible. However, especially for larger diameters high prices limit the use of diamond dies. Another limitation is the restriction to almost circular shapes. Coating of the interior walls of drawing dies with thin polycrystalline diamond films is a solution for utilizing the superior properties of diamond beyond these limitations of costs and geometries.

In a co-operation of four Fraunhofer Institutes and tool makers we investigated hot-filament chemical vapor deposition (HF-CVD) of diamond coatings on silicon-based ceramics. We have demonstrated high adhesion levels of the diamond coatings even on polished substrate surfaces [1]. Surface roughening to enhance adhesion, a typical pretreatment in the case of diamond coatings on cemented carbide, is not necessary. This is obviously due to the formation of chemical bonds between carbon atoms from the diamond and silicon atoms from the ceramic substrate at the diamond-substrate interface. Additionally, no binder material like cobalt has to be removed by laborious etching procedures which are cost effective and also influence the substrate surface roughness. Thus the surface roughness is dominated by the diamond film roughness.

In the case of drawing dies the deposition of well adherent smooth diamond coatings on polished substrate surfaces is a prerequisite to achieve the surface quality for drawn wires. To realize diamond coated drawing dies this concept has to be combined with a deposition process for interior coating.. Therefore we have investigated several versions of the HF-CVD technique to evaluate the possibilities for interior wall diamond coating. At special process conditions the deposition of diamond films is demonstrated for cylinders with inner diameters ≥ 2 mm and aspect ratios of up to 10. The film thickness distribution and morphology of the coatings was characterized by scanning electron microscopy.

Cylindrical substrates with relatively large diameters and aspect ratios can be coated by placing a hot filament for gas activation inside the substrate [2,3]. However, for typical drawing die geometries the additional expense for filament and substrate arrangement is not necessary. For drawing dies with diameters above 4 mm the diamond deposition is realized at low process pressures under diffusion controlled conditions. In this case the substrates can be coated in a deposition process which is more economic than placing the filaments inside an arrangement of dies.

For dies with diameters below 4 mm the interior coating has been realized by transporting the activated gas into the orifice of the drawing die by means of a directed gas stream (cf. figure 1). By applying this technique from both sides of the substrates, successively, almost homogeneous diamond films for aspect ratios length/depth ≥ 10 are possible. However, for drawing dies a single deposition step from one side of the drawing tool is sufficient (cf. figure 2).

In general, the diamond crystal size, which is correlated to the film roughness, decreases with increasing deposition depth. In the case of drawing dies, this effect results in smooth diamond coatings in the area of smallest diameter, which is favorable for the production of wires with high surface quality.

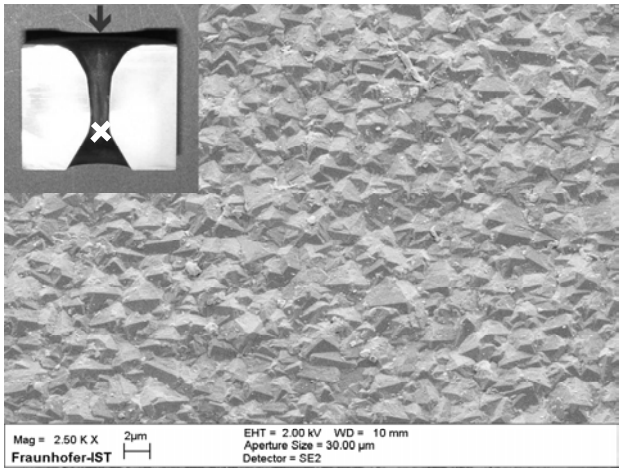

Figure 1. Diamond coated ceramic drawing die with 2 mm diameter produced by means of a directed gas stream. The small picture shows the sliced tool, the larger picture the morphology of the diamond film at the point of the lowest diameter (cross). At this point the film thickness is 6 µm compared to 10 µm at the gas inlet (arrow).

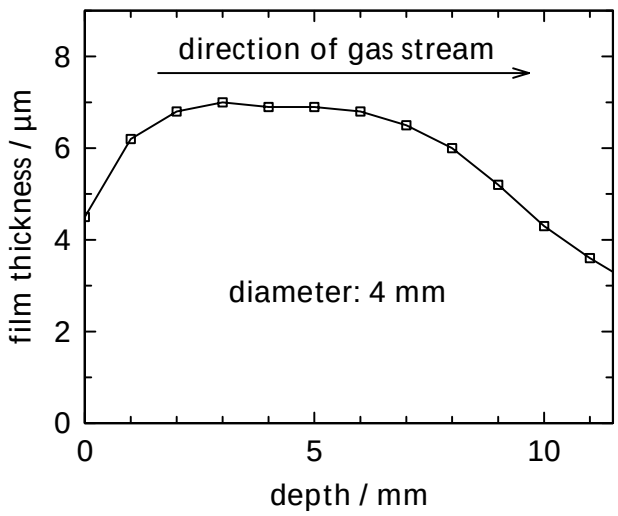

Figure 2. : Film thickness distribution in a cylindrical test geometry with 4 mm diameter. The activatd process gas is transported into the orifice by means of a directed gas stream resulting in diamond deposition on the interior surface.

REFERENCES

1. Höfer, M.; Schäfer, L.; Hollstein, T.; Blug, B.; Herrmann, M.; Brücher, M.; Hühns, T.; „Diamond Coated Ceramics »DiaCer« – a Composite Material for Extreme Industrial requirements“, Int. Conf. on New Diamond Science and Technology ICNDST-9, March 26-29, 2004, Tokyo, Japan, abstract book, pp. 77-78.
2. Patent specification DE 198 09 675, March 6, 1998.
3. Zhang, Z.M; Shen, H.S.; Sun, F.H.; He, X.C. and Wan, Y.Z.: “Fabrication and application of chemical vapor deposition diamond-coated drawing dies,” *Diamond and Related Materials*, 10, pp. 33-38 (2001).

Electrical methods for creating and characterizing biomolecular arrays for DNA hybridization and antibody detection at diamond surfaces

Wensha Yang, Bin Sun, Sarah Baker, Kiu-Yuen Tse, and Robert J. Hamers

Department of Chemistry, University of Wisconsin-Madison
1101 University Avenue
Madison, WI

James E. Butler and John N. Russell, Jr.

Gas/Surface Dynamics Section,
Chemistry Division, Naval Research Laboratory, Washington, DC 20375

Keywords: Impedance, Field-effect transistor, Bio-FET, DNA, antibodies.

Abstract

INTRODUCTION

Biologically-modified diamond presents a nearly ideal platform for integrating biological systems with microelectronics.[1-2] While most electrical biosensing schemes involve some type of amplification scheme such as the use of enzymes, in order to extend electrical biosensing to high-density arrays it is necessary to develop more general biosensing schemes in order to be able to detect a broader range of biomolecules without chemical interference between the different sensor elements. The use of the intrinsic *charge* of a biomolecule binding to a surface presents one such detection method. Since diamond is a wide-bandgap semiconductor, changes in charge distribution associated with biomolecules binding to a surface functionalized with specific, complementary biomolecular recognition elements provides a completely real-time, label free way to convert biological information into electrical control signals. We have been investigating the electrical properties of diamond surfaces modified with DNA and with antibodies,[3-5] as a basis for new types of direct electronic biosensor. Measurements have been made parallel to the interface and perpendicular to the interface in a Bio-FET geometry. We have also achieved the converse process, or using electrical control signals to induce specific molecular chemistry at the surface, as a way to perform electrically addressable preparation of diamond bioarrays without the need for microfluidics or other fluid-handling systems.[6-7] Thus, the unique electrical properties of diamond can be used both in the fabrication of bioarrays and in the direct detection of biological binding events.

ELECTRONIC BIOSENSING VIA IMPEDANCE AND BIO-FET MEASUREMENTS

Biomolecules interacting with semiconductors induce a "field effect" in which the change in local charge distribution induced by binding to the surface affects the diamond space-charge region. The impedance can be measured either perpendicular to the interface using AC impedance spectroscopy, or can be measured parallel to the surface in a field-effect-transistor geometry.[3-4] In AC impedance spectroscopy, only one electrical connection is needed to each sensing element; by choosing the AC frequency properly, one can capacitively couple across the molecular layer and achieve sensitivity to the diamond space-charge layer. Alternatively, one can place two electrical contacts directly onto the surface and measure the DC impedance changes induced in a diamond thin film.

To link biomolecules to the surface, we have developed a photochemical method that provides a very stable interface in which biomolecules of interest can be covalently linked to the diamond surface.[1] Upon hybridization, we observe a decrease in the impedance across the interface. Similar measurements made on modified silicon samples show a decrease in impedance on p-type samples and an increase in impedance on n-type samples. These results are all consistent with a field-effect, in which the negatively-charged DNA molecules induce an upward-band-bending and a corresponding decrease in resistance of the space-charge region.

` We have recently extended these measurements to true Bio-FET devices[4] in which we evaporate two contacts on top of the diamond. These contacts are then protected by evaporation of photoresist onto them (providing a hydrophobic barrier layer) while leaving the channel region open. We find that on a surface covalently

linked to the human antibody IgG, exposure to the corresponding antibody anti-IgG induces a significant decrease in drain-source current. Control experiment using a different antibody, anti-IgM, that is not expected to bind to the IgG-modified surface, shows no change in response. Thus, the diamond bio-FET responds selectively to the molecule of interest. There are many parallels between the parallel FET measurements and the perpendicular AC impedance measurements. The advantages and disadvantages of these two types of sensing will be discussed. However, both methods are useful for diamond-based biosensing arrays.

ELECTRICALLY-ADDRESSABLE FUNCTIONALIZATION OF DIAMOND FOR CREATION OF BIO-ARRAYS:

In order to create arrays of Bio-FET or other diamond-based sensing systems, it is necessary to develop methods for selectively functionalizing specific surface regions. While this has traditionally been done using mechanical "spotting" methods, we have recently developed a new method for electrically-addressable biomolecular functionalization of diamond surfaces. In this method, the diamond surfaces are first functionalized with aromatic nitro groups via a purely chemical method. The nitro groups on specific regions of the surface can then be selectively reduced to primary amines by applying a small potential of -1.5 V to the electrode of interest. These amine-functionalized surface regions can then be covalently linked to biomolecues of interest. We have used this method to functionalize diamond surfaces with specific DNA sequences in different areas without the use of microfluidics or other fluid-handling devices.

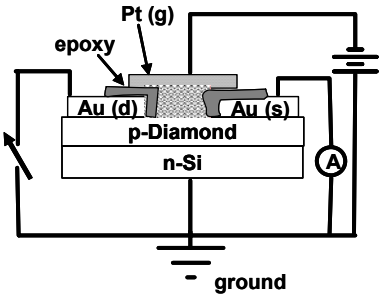

Figure 1: Diamond Bio-FET device

REFERENCES

1. Yang, W., et al. , "DNA-modified nanocrystalline diamond films as stable, biologically active substrates", *Nature Materials,* **1**, 253-257 (2002).
2. Lu, M., et al, "Invasive Cleavage Reactions on DNA-Modified Diamond Surfaces", *Biopolymers*, 73, 606-613 (2004).
3. Yang, W., et al. "Interfacial Electrical Properties of DNA-modified Diamond Thin Films: Intrinsic Response and Hybridization-Induced Field Effects", *Langmuir*, 20, 6778-6784 (2004).
4. Yang, W. and Hamers, R.J., "Detection of biological binding events using a diamond thin-film field-effect transistor", *Appl. Phys. Lett*., 85, 3626 (2004).
5. Yang, W., et al., "Electrically Addressable Biomolecular Functionalization of Conductive Nanocrystalline Diamond Thin Films", *Chemistry of Materials*, in press (Jan. 2005).
6. Lee, C.S., et al., "Electrically Addressable Biomolecular Functionalization of Carbon Nanotube and Carbon Nanofiber Electrodes", *Nano Letters*, **4,** 1713-1716 (2004)

Diamond Electrodes For Neurodynamic Studies in *Aplysia californica*

Jeffrey M. Halpern[1], Songtao Xie[1], Greg P. Sutton[2], Bryan T. Higashikubo[3], Cynthia A. Chestek[4], Hillel J. Chiel[3], and Heidi B. Martin[1]
Case Western Reserve University; [1]Dept of Chemical Engineering, [2]Dept. of Mechanical Engineering, [3]Dept. of Biology, and [4]Dept. of Electrical Engineering

Keywords: Dopamine, Serotonin, Fast Scan Cyclic Voltammetry, *Aplysia Californica*.

As part of an ongoing effort to demonstrate that diamond is a versatile electrode material for biological applications, we present our progress in development of diamond electrodes for study of neurodynamics in an animal model, *Aplysia californica*. Diamond provides a unique opportunity to integrate neural stimulation and sensing in the same implantable device. Data from several parallel studies are presented: *in vitro* measurement of dopamine and serotonin concentration, measurement of electrical activity, and neural stimulation. Using diamond microelectrodes, changes of the *Aplysia californica's* feeding patterns are being studied as a function of concentration of dopamine (acting as a neurotransmitter) or serotonin (acting as a neuromodulator).

1 Background and Motivation

We are exploring the advantages of diamond electrodes using a specific, relatively well-defined neural circuit that provides known controls for comparison and minimizes surgical challenges. At the same time, data from this newly developed diamond device may provide new insights into behavioral functions of this neural circuit. *Aplysia californica*, a marine mollusk, is a commonly used animal model for neurodynamic studies. Our focus is on the buccal mass, *i.e.*, the muscular structure for feeding, and the buccal ganglion, a collection of cells that control the feeding motor patterns of *Aplysia californica*. The somata (cell bodies) of the buccal motor neurons are large (~50-150 microns), identifiable, and readily accessible; thus, it is possible to obtain electrophysiology recordings and monitor chemical release from a single cell. In addition, neural activity can often be directly correlated with muscular response; *e.g.*, patterns of buccal nerve recordings *in vivo* (corresponding to recordings of multiple neurons firing) can distinguish between the three fundamental feeding behaviors: biting, rejecting, and swallowing (Ref. 1). *Aplysia* provides unique advantages for development of an integrated device since all three aspects – stimulation, electrical activity and neurotransmitter sensing – can be probed at the neuron cell body.

Of specific interest for these studies are the B65 neuron and the metacerebral cell (MCC). The B65 neuron is located in the collection of nerve cells controlling the feeding apparatus, the buccal ganglion; it has been shown to enhance rejection motor patterns, and is known to contain dopamine, which acts as a modulatory neurotransmitter (Ref. 2). The MCC is located in the cerebral ganglion (a more encephalized collection of nerve cells that controls higher order behavioral choice); it has multiple roles in feeding behavior that, in part, involve the release of serotonin, a neuromodulator, throughout the buccal mass. The MCC contains approximately 100 μM serotonin in the soma and 4% is released with the generation of an action potential (Ref. 3). Through use of real-time detection with diamond electrodes, we seek to determine the release site and concentration of (a) *dopamine* from the B65 neuron and (b) *serotonin* from the MCC during a normal feeding pattern.

2 Methods

Microelectrodes (~30 μm diameter) were fabricated using hot-filament-assisted CVD techniques to deposit boron-doped diamond onto a tungsten microelectrode; for details, see Ref. 4. Flow cell calibrations were used to estimate the detection limits; fast scan cyclic voltammetry (FSCV) was the detection method. **Figure 1** shows an example flow cell calibration for a diamond microelectrode; 1 nM dopamine (**Fig. 1a**) and 50 nM serotonin (**Fig. 1b**) were detected (Ref 4).

The buccal ganglion is encased in an insulating layer (sheath) that must be surgically removed (desheathed) to allow study of the chemical transmission between cells. Intracellular recordings (*i.e.*, within the cell) were conducted by inserting a sharp glass pipette (<1 micron) into the soma and recording membrane potential versus time. Extracellular measurements, *i.e.*, with the sheath still intact, are less invasive and thus more desirable for *in vivo* studies. Using extracellular suction electrodes, nerve activity was measured (*i.e.*, the combined signal representing activity in axons from various neurons). Individual neurons are distinguished by their signal amplitude on the nerve. For extracellular recordings from a single neuron with the sheath intact, a single electrode was lowered over the cell of interest and the time-varying voltage recorded (**Fig. 2a**). In all preparations, *Aplysia* saline was used. Although our ultimate interest is in the B65 and MCC neurons, the neurons B4/B5 were used for preliminary studies because they are the most surgically accessible, and our group has extensive experience in studying their function.

3 Results

We are currently using diamond electrodes for *in vitro* recordings and stimulation. Preliminary, extracellular recording and stimulation were conducted from a single neuron, B4 or B5 (two electrically coupled neighboring neurons), through the sheath (**Fig. 2**). For extracellular recording from B4/B5, a one-to-one relationship was observed on the diamond electrode, so that it was clearly recording from one neuron, whereas the suction electrode on the nerve recorded two signals, reflecting activity in both neurons (**Fig. 2b**). For extracellular stimulation, a one-to-one relationship was also observed, indicating that one neuron was stimulated without activating neighboring cells (**Fig. 2c**). Also, rejection (neural) patterns from a desheathed ganglion were obtained, and will be used to identify the B65 neuron for our dopamine studies.

We are also exploring measurement of serotonin release from the MCC. The MCC releases serotonin at the soma and throughout the buccal mass, including the I2 muscle, the primary muscle for protraction (Ref 5). Sutton *et al.* (Ref. 6) have established that exogenously added serotonin enhances I2's contractile strength, thus indicating that serotonin plays a direct role in the behavioral function of I2.

In the future, we will integrate FSCV and neural recording at the same electrode; if successful, an array will be designed to record from various sites throughout the buccal ganglion, to help map the chemical and electrical signals *in vivo* during a complete feeding behavior.

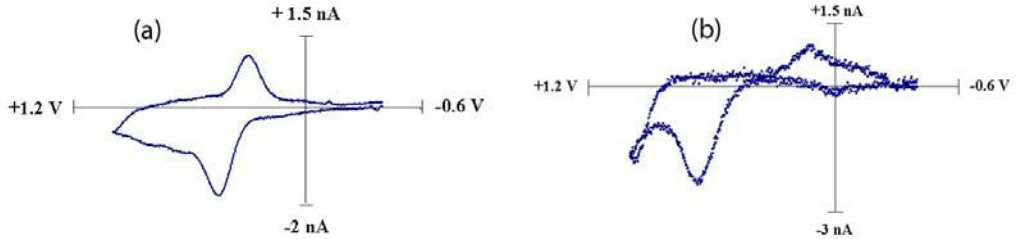

Figure 1: Cyclic voltammograms, at 300 V/s in HEPES buffer of (a) 1 nM dopamine and (b) 50 nM serotonin.

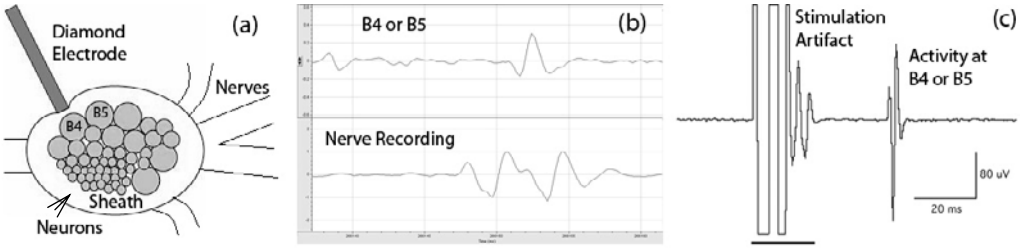

Figure 2: (a) Schematic of the extracellular stimulation/recording method, with the diamond electrode pressed into the sheath over the cells of interest for proper recording/stimulation. (b) Extracellular recording above B4 or B5. The diamond electrode (*top*) recorded single-cell activity, while a suction electrode on the nerve (*bottom)* recorded activity from both cells. (c) Extracellular stimulation at B4 or B5 produced a clear signal after stimulation.

REFERENCES

1. Morton, D. W.; Chiel, H. J.: "The timing of activity in motor neurons that produce radula movements distinguishes ingestion-like and rejection-like motor patterns in a reduced preparation of *Aplysia*," *J. Comp. Physiol. A.*, 173, 519-536 (1993).

2. Due, Michael R.; Jing, Jian; and Weiss, Klaudiusz R.: "Dopaminergic Contributions to Modulatory Functions of a Dual-Transmitter Interneuron in *Aplysia*," *Neuroscience Letters*, 358, 53-57 (2004).

3. Miao, Hai; Rubakhin, Stanislav S.; Sweedler, Jonathan V.: "Analysis of Serotonin Release from Single Neuron Soma Using Capillary Electrophoresis and Laser-Induced Fluorescence with a Pulsed Deep-UV NeCu Laser," *Anal Bioanal Chem*, 377, 1007-1013 (2003).

4. Xie, Songtao, et al.: "Boron-Doped Diamond Neurosensors and Neural Stimulating Electrodes," *Abstracts. ECS Fall annual meeting 2004*, 1808.

5. Hurwitz, I, et al.: "Activity patterns of the B31/B32 pattern initiators innervating the I2 muscle of the buccal mass during normal feeding movements in *Aplysia californica*," *J. Neurophysiol*, 75, 1309-1326 (1996).

6. Sutton, G. P., Higashikubo, B. T., and Chiel, H. J.: Unpublished data, 2004.

SESSION 2

DEFECTS & DOPING

SPECTROSCOPIC STUDIES OF HYDROGEN COMPLEXES IN DIAMOND

M E Newton and R J Cruddace

Department of Physics, University of Warwick, Coventry, UK

H E Smith

Department of Materials, University of Oxford, UK

P M Martineau and S J Quinn

DTC Research Centre, Maidenhead, UK

D J Twitchen

Element Six Ltd, Ascot, UK

Keywords: Single Crystal CVD Diamond, hydrogen, defects.

Abstract

New experimental data will be presented on hydrogen related complexes observed in as grown and annealed single crystal CVD diamond. The data has been obtained using a variety of spectroscopic techniques, but particular emphasis will be focused on the results of Infrared Absorption and Electron Paramagnetic Resonance studies, and these results will be interpreted in terms of molecular models for interstitial and substitutional hydrogen complexes in diamond. It will be shown that much of the accepted wisdom about hydrogen incorporation in diamond must be questioned.

INTRODUCTION

Hydrogen is an important impurity in silicon and III–V compound semiconductors. Particular interest has been focused on hydrogen passivation of donors or acceptors, as well as unwanted deep recombination centres. There is an ever-growing body of evidence that under appropriate conditions significant amounts of hydrogen can be incorporated in synthetic diamond grown via high temperature and pressure (HTHP) synthesis and chemical vapour deposition (CVD). Hydrogen is also a common impurity in natural diamond. Clear evidence for H-related complexes in CVD diamond comes from the passivation of boron acceptors by in-diffused deuterium [1]. It is reasonable to assume that a detailed understanding of the incorporation and properties of hydrogen in diamond will be required to ensure that single crystal CVD diamond emerges as the pre-eminent electronic material for extreme applications. Furthermore, an understanding of hydrogen incorporation should be invaluable to those modeling and perfecting synthesis, and provide insight into how hydrogen related complexes in natural diamond have evolved.

INCORPORATION OF HYDROGEN IN CVD DIAMOND

Recently attention has been focused on the structure and properties of vacancy-hydrogen and vacancy-nitrogen-hydrogen complexes in diamond detected by Electron Paramagnetic Resonance (EPR) [2,3]. Both these complexes have only been observed in CVD diamond. Fuchs and co-workers [4] observed several new absorption features in single crystal CVD diamond in the mid and near infrared spectral regions. Isotopic substitution has shown that several of these are hydrogen related, and recent work indicates that at high temperatures hydrogen is mobile in the diamond lattice and new hydrogen related complexes can be formed [5].

We will report the results of infrared absorption and EPR studies of hydrogen complexes in as grown and annealed single crystal CVD diamond. One of the defects studied in this way is the hydrogen vacancy complex, which has been shown to anneal out with an activation energy of 4.3(2) eV, which is comparable to the energy required to break a C-H bond. The consequences of this result for the diffusion of hydrogen in diamond will be discussed.

In addition to the quantitative EPR and infrared absorption measurements we have used uniaxial stress to probe the symmetry and electronic structure of hydrogen related complexes which have either or both vibrational and electronic optical absorption bands. Particular attention will be focused on the hydrogen related 3107 cm^{-1} infrared absorption band commonly detected in natural, and annealed synthetic diamond. A new model for this centre will be

presented. This assignment questions much of the accepted wisdom for hydrogen incorporation in diamond and the consequences of this identification will be discussed.

REFERENCES

1. J Chevallier, B Theys, A Lusson, C Grattepain, A Deneuville and E Gheeraert, "Hydrogen-boron interactions in p-type diamond", Phys. Rev. B **58** 7966–9 (1998)
2. C Glover, M E Newton, P M Martineau, D J Twitchen and J M Baker, " Hydrogen incorporation in diamond: The nitrogen-vacancy-hydrogen complex ", Phys. Rev. Letts., **90** (18): art. No. 185507 (2003).
3. C Glover, M E Newton, P M Martineau, S J Quinn and D J Twitchen, " Hydrogen Incorporation in Diamond: The Vacancy-Hydrogen Complex", Phys. Rev. Letts., **93** (13): art. No. 135502 (2004).
4. F. Fuchs et al , "Hydrogen induced vibrational and electronic transitions in chemical vapour deposited diamond, identified by isotopic substitution", Appl. Phys. Letts. **66**, 176-179 (1995).
5. S. J. Charles et al, "Characterization of nitrogen doped chemical vapor deposited single crystal diamond before and after high pressure, high temperature annealing", Phys. Stat. sol. (a) **201**, 2473–2485 (2004).

OPTICAL AND STRUCTURAL PROPERTIES OF AMORPHOUS CARBON THIN FILMS DEPOSITED BY MICROWAVE SURFACE-WAVE PLASMA CVD

Sudip Adhikari*, Sunil Adhikary, Ashraf M.M. Omer, Hideo Uchida and Masayoshi Umeno

Department of Electrical and Electronic Engineering, Chubu University, 1200 Matsumoto-cho, Kasugai 487-8501 Japan

Mohamad Rusop, Tetsuo Soga

Department of Environmental Technology and Urban Planning, Nagoya Institute of Technology, Gokiso-cho, showa-ku, Nagoya 466-8555 Japan

Keywords: amorphous carbon; nitrogen; microwave surface-wave plasma CVD; annealing; optical band gap.

Abstract

Nitrogen doped amorphous carbon (a-C:N) thin films were deposited on silicon and quartz substrates by microwave surface-wave plasma chemical vapor deposition technique at low temperature (< 100 ^{o}C). We used argon (Ar), camphor dissolved in alcohol and nitrogen (N) as carrier, source and dopant gases respectively. Optical band gap decreased from 4.1 eV to 2.4 eV when N_2 gas concentration increased from 0% to 4.5%. The films were annealed at different temperatures ranging from 150 to 450 ^{o}C in Ar gas environment for 30 min to investigate the optical properties of the films before and after annealing. The optical band gap remained constant (2.4 eV) until 150 ^{o}C annealing and beyond that it decreased dramatically to 1.1 eV at 400 ^{o}C annealing. The structural modification of the films leading to graphitization as a function of the annealing temperature was confirmed by the characterization of Raman spectra.

Introduction

The cost reduction of solar cell and establishment of environmentally friendly production process are very important for further spread of photovoltaic technology. Carbon (C) is a material of highly stable, cheap and non-toxic, which can be obtained from precursors those, are sufficiently available in nature. Furthermore, amorphous carbon (a-C) has been an attractive material for the fabrication of photovoltaic solar cells because of its outstanding properties such as chemical inertness, high hardness, high electrical resistivity, high thermal conductivity, high dielectric strength, infrared optical transparency and optical band gap varying over a wide range from about 5.5 eV for insulating diamond to 0.0 eV for metallic graphite [1]. Impurity doping, such as nitrogen (N), phosphorus (P) and Iodine (I) can modify optoelectronic properties of the films by increasing either the electron or hole concentration in the semiconductor device. In addition, structural properties of the films can be changed due to the effect of annealing; the ratio of hybridized bonds like trigonal (sp^2) and tetragonal (sp^3) in carbon film can be tuned by appropriate annealing temperature. In this paper, we report the optical and structural properties of N doped a-C (a-C:N) thin films deposited on silicon (Si) and quartz substrates by microwave (MW) surface-wave plasma (SWP) chemical vapor deposition (CVD), a newly developed C thin film deposition method, before and after annealing the films. Our experimental purpose is to control properties of the films suitable for solar cell application.

Results and discussion

To study the optical characteristics of both the as-deposited and the annealed films, we carried out the reflectance and transmittance measurements by UV/VIS/NIR spectrophotometer in the range of 200-2000 nm. The absorption coefficient (α) was calculated by the spectral reflectance and transmittance, and the film thickness data. The film thickness was measured by Nanopics 2100/NPX200 surface profiler. The optical band gaps were obtained by Tauc plot. The Tauc optical band gap (Eg) was obtained from the extrapolation of the linear part of the curve at α = 0 by using the Tauc equation,

$$(\alpha h\nu)^{1/2} = B(Eg - h\nu) \quad (1)$$

where B is the density of the localized state constant [2].

Fig. 1 shows that optical band gap decreased almost exponentially with increasing N_2 concentration during film deposition. The minimum optical gap is found 2.4 eV when N_2 concentration is 4.5 %. This result suggests that the doping of N_2 during film deposition can reduce the optical band gap to some extent. Chen and Robertson have also reported the qualitatively similar effect of N_2 doping on optical band gap[3]. XPS measurement gave information of chemical composition in the as-deposited film; the peak position of carbon (C) 1s, nitrogen (N) 1s and oxygen (O) 1s are at 281.1 eV, 396 eV and 529.7 eV respectively. The optical band gap (2.4 eV) of our a-C:N film is still high for solar cell application. Previous researches showed that annealing of a-C films could reduce the band gap of the films[4]. In order to examine the annealing effects in our films, the films were annealed at different temperatures (0 to 450 ^{o}C). Fig. 1 shows a plot of optical band gap versus annealing temperature. The optical band gap (2.4 eV) remained constant as of as-deposited film until 150 ^{o}C annealing, and beyond that it decreased monotonically to 1.1 eV at 400 ^{o}C. Upon annealing, the films would turn to be more graphite like in nature as sp^2 bonds start to dominate sp^3 bonds in the carbon films. Fig. 2 shows Raman spectra of the as-deposited and the annealed a-C:N films. It is clear that the broad band of the as-deposited film gradually splitted into two peaks (commonly known as D and G lines) with increasing annealing temperature. Moreover, the slight up shift of G line towards higher wave number (above 1580 cm^{-1}) indicates that the films progressively changed to graphite in nature and crystalline have a very small grain size with increasing annealing temperature [5].Our results show that it is possible to control optical band gap of a-C thin films partially by N doping during film deposition and largely by post growth annealing of the films.

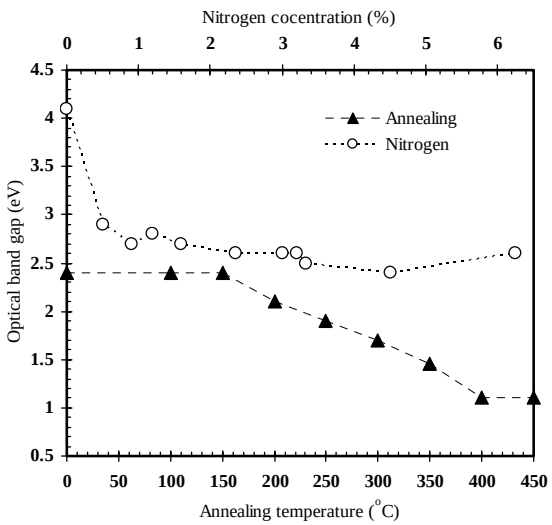

Figure* 1. *Optical band gap versus Annealing temperature and Nitrogen concentration.

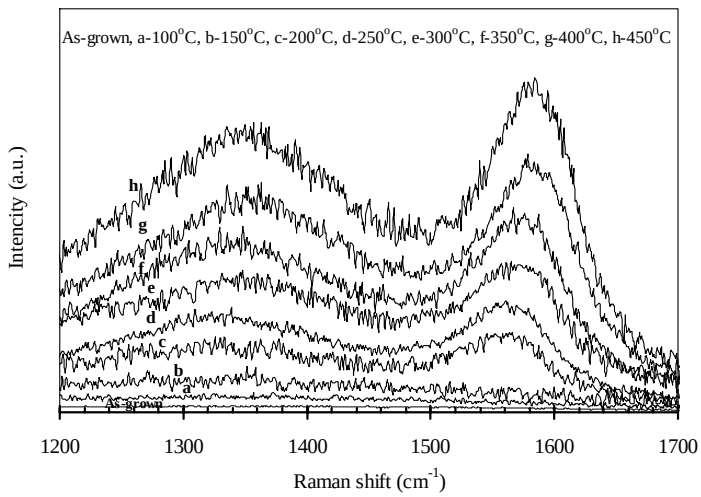

***Figure* 2. *Raman spectra of the as-deposited and the annealed a-C:N films at various temperatures*.**

REFERENCES

1. K.M. Krishna et al., "Photovoltaic solar cell from camphoric carbon A natural source", *Sol. Mater. Sol. Cells*, Vol. 48**,** 25-33 (1997).
2. J. Tauc: Amorphous and Liquid Semiconductors Plenum Press, London, New York, 1974, Chap. **4**.
3. C.W. Chen, J. Roberson, "Doping mechanism in tetrahedral amorphous carbon", *Carbon*, Vol. 37, 839-842 (1999).
4. A.M.M. Omer et al., "Effects of Iodine Doping on Optoelectronic Properties of Diamond-Like Carbon Thin-Films Deposited by Microwave Surface Wave Plasma CVD*", Diamond Relat. Mater*. Vol. 13, 2136-2139 (2004).
5. S.M. Mominuzzaman et al., "Raman spectra of ion beam sputtered amorphous carbon thin films deposited from camphoric carbon", *Carbon*, 38, 127-131 (2000).

INELASTIC NEUTRON SCATTERING STUDY OF CARBON NANO-MATERIALS

A.I. Kolesnikov and C.-K. Loong

Argonne National Laboratory, Argonne, IL 60439, USA

A.P. Moravsky and R.O. Loutfy

MER Corporation, Tucson, AZ 85706, USA

Keywords: Neutron scattering, carbon nanotubes, fullerenes.

Abstract

Vibrational spectra for single wall carbon nanotubes, double wall carbon nanotubes, single wall carbon nanohorns and C_{60}-peapods have been measured with inelastic neutron scattering in a wide range of energy transfer, 5-220 meV. A decrease in intensity around 75-100 meV and the appearance of two peaks around 120-125 meV and 150 meV in the double wall nanotubes and C_{60}-peapods spectra compared to single wall carbon nanotubes and nanohorns were observed. These findings indicate the possibility of strong interaction between the walls of the double wall carbon nanotube, and between C_{60} molecules and carbon nanotube of the peapod.

RESULTS AND DISCUSSION

Although the existence of varieties of carbon nano-materials has been known for some time, the investigation of their vibrational spectra was mainly limited to the use of optical spectroscopy. In spite of the well-recognized advantages of inelastic neutron scattering (INS) technique, namely, unrestricted by the selection rules of infrared and Raman spectroscopy and accessible to all vibrational modes in the reciprocal space, so far this method was used for the study of only fullerens (see *e.g.* review in [1]) and single-walled carbon nanotubes (SWNT) [2,3]. Here we present the INS measurements on a series of carbon nano-materials prepared by MER: SWNT (~14 Å diameter), double-walled carbon nanotubes (DWNT of ~25 Å diameter), carbon nano-horns and fullerene-C_{60} encapsulated into SWNT (so called C_{60}-peapods), aiming at the characterization of the vibrational spectra over a wide energy scale, from collective motions to localized atomic vibrations.

The spectrum of nano-horns is similar to that of SWNT (see figure 1), and the latter one agrees with the main features reported in the literature. The INS spectrum of C_{60}-peapods and DWNT are very different compared to the spectra of both pure SWNT and pristine or polymerized fullerenes. The spectral intensities of the DWNT and C_{60}-peapods show a strong reduction in the "breathing" modes (normal to surfaces of C_{60} or SWNT "molecules") over the range of 30-100 meV, and an increase at higher energies toward the "tangential" modes around 110-160 meV; exhibiting new excitations at about 120-125 and 150 meV.

A possible explanation of the observed new peaks at ~120-125 meV and ~150 meV in the spectra of generalized vibrational density of states, *G(E)*, for DWNT and C_{60}-peapods is a strong change in the C-C interaction between the inner and outer walls in DWNT and between the C_{60} and nanotube in C_{60}-peapods. Some theoretical models (see *e.g.* [4]) predict the changes of two-dimensional sp^2 bonds in cylindrical "graphene" layers in nanotubes of large diameter to three-dimensional sp^3-like bonds in nanotubes of smaller diameter. A possible change of sp^2 to $sp^{2+\delta}$ ($0<\delta<1$) hybridization in DWNT and C_{60}-peapods would result in spectral changes observed in the present work. The features at energies 120-175 meV in the *G(E)* spectrum for diamond [5] (with only sp^3 bonds) show similarities with the spectra for DWNT and C_{60}-peapods (see figure 1).

Work performed at Argonne National Laboratory is supported by the U. S. DOE-BES under contract No. W-31-109-ENG-38.

Figure* 1. *Generalized vibrational density of states, G(E), obtained from INS spectra for different carbon nano-materials: 1 – SWNH, 2 – SWNT, 3 – DWNT, 4 – C_{60}-peapods, 5 - high-pressure polymerized C_{60}, 6 - pristine C_{60}, 7 – graphite, and 8 – diamond. The spectra 1 to 4 were measured at T=8 K on the direct-geometry HRMECS spectrometer (IPNS, ANL) with different incident neutron energies, E_i=280 meV (1-4); 140 meV (1 and 2) and 50 meV (1, 2 and 4). The spectra for pristine and polymerized C_{60} [6], and graphite and diamond ([5], the data have been taken from TFXA database) are shown for comparison.

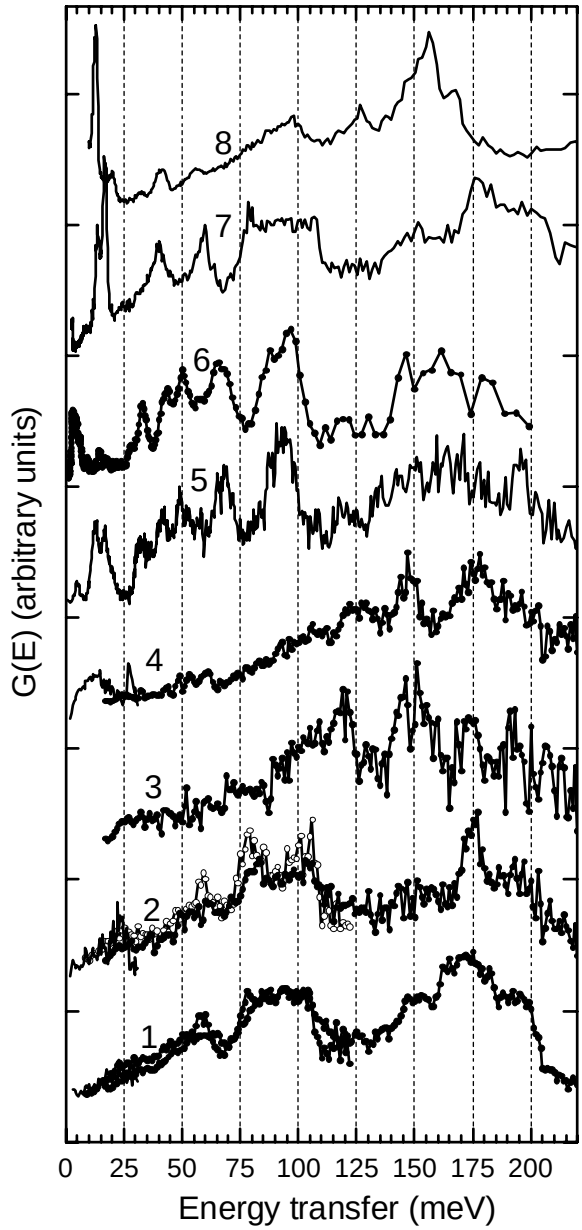

REFERENCES

1. Pintschovius, L., "Neutron Studies of Vibrations in Fullerenes," *Rep. Prog. Phys*. **57**, 473 (1996).
2. Rols, S., et al., "Phonon Density of States of Single-Wall Carbon Nanotubes," *Phys. Rev. Lett*. **85**, 5222 (2000).
3. Sauvajol, J.L., et al., "Phonons in Single Wall Carbon Nanotube Bundles," *Carbon* **40**, 1697 (2002).
4. Ding, J.W., Yan, X.H. and Cao, J.X., "Analytical Relation of Band Gaps to Both Chirality and Diameter of Single-Wall Carbon Nanotubes," *Phys. Rev*. **B66**, 073401 (2002).
5. Walters, J.K., et al., "A Spectroscopic Study of the Structure of Amorphous Hydrogenated Carbon," *J. Phys.: Condens. Matter* **7**, 10059 (1995).
6. Kolesnikov, A.I., et al., "Neutron Scattering Study of a High-Pressure Polymeric C-60 Phase," *J. Phys.: Condens. Matter* **8**, 10939 (1996).

BORON DOPED NANOCRYSTALLINE DIAMOND FILMS

O.A. Williams[1], M. Daenen[1], J. D'Haen[2], K. Haenen[1,2], M. Nesládek[1,2,3], M. D'Olieslaeger[1,2]

[1]Limburgs Universitair Centrum, Institute for Materials Research (IMO), Belgium
[2]IMEC vzw, Division IMOMEC, Belgium
[3]CEA/Saclay, LIST (CEA-Recherche Technologique)/DETECS/SSTM, France

oliver.williams@luc.ac.be

Keywords: nanocrystalline diamond, p type, boron, doping

Abstract

Nanocrystalline diamond films are of particular interest for the development of Micro/Nano-Electromechanical Systems (MEMS/NEMS), microfluidics, SAW devices, electrochemical electrodes, low friction tribological coatings etc where the high roughness of thick polycrystalline material or high cost of polished/single crystal diamond may be undesirable. In order to be useful for many of the applications listed above however, it is necessary to be able to control the conductivity of this material from near intrinsic to semi-metallic.

This work describes the current status of Boron Doping of nanocrystalline diamond films at the Institute for Materials Research, Diepenbeek, Belgium. Highly uniform nanocrystalline diamond films have been grown in an Astex 6500 15kW Microwave Plasma System over a wide range of conditions. The effect of the addition of Trimethylboron into the gas phase on the electronic properties of these films has been characterised by photothermal deflection spectroscopy (PDS), FTIR, Scanning Tunnelling Microscopy (STM), Atomic Force Microscopy (AFM) and low temperature Hall effect / conductivity measurements. Scanning Electron Microscopy has been utilised to characterise morphology, growth rate and alpha parameter as a function of temperature and trimethylboron concentration in the gas phase. Optical emission spectroscopy and interferometry were used *in-situ* to characterise the growth process.

These films show conductivity behaviour ranging from insulating to semi-metallic conductivity with increasing trimethylboron concentration in the gas phase. These films have been used for electrochemical studies. Procedures for enhancing the nucleation density of these films will be discussed.

ACKNOWLEDGEMENTS

This work was financially supported by the IWT-SBO-project No.030219 "CVD Diamond, a novel multifunctional material" and by the IUAP V programme "Quantum Size Effects in Nanostructured Materials". KH is a Postdoctoral Fellow of the Fund for Scientific Research – Flanders (Belgium) (F.W.O.-Vlaanderen).

PHOTOCONDUCTIVITY AND AMBIPOLAR DIFFUSION LENGTH OF MINORITY CARRIERS IN S-DOPED MICROCRYSTALLINE AND NANOCRYSTALLINE DIAMOND

F. Piazza, O. Resto, G. Nery and L. Fonseca

Department of Physics, University of Puerto Rico, San Juan, P.O. Box 23343, Puerto Rico 00931

G. Morell

Department of Physical Sciences, University of Puerto Rico, P.O. Box 23323, San Juan, Puerto Rico 00931

Keywords: diamond, photoconductivity, diffusion length, sulfur, photocarrier grating technique

Abstract

Diamond is a promising wide band-gap semiconductor with a strong potential for high-power high-temperature electronics. There is also great interest in reproducibly obtaining electronic-grade n-type semiconducting diamond in connection to applications requiring massive electron transport, especially those involving field electron emission and photoemission.

We recently succeeded in making n-type diamond by sulfur doping[1]. The films were grown by hot-filament chemical vapor deposition (HFCVD) from $CH_4/H_2/H_2S$ gas mixture. With increasing sulfur content in the gas phase, the room temperature conductivity[2], the room temperature electron field emission properties[3], and the thermoionic emission at 340°C[4], were enhanced.

Now we are employing the steady-state photocarrier grating technique (SSPG) to measure the photoconductivity and ambipolar diffusion length of minority carriers in S-doped microcrystalline diamond (μ-D) and nanocrystalline diamond (n-D) thin films synthesized by HFCVD from $CH_4/H_2/H_2S$ gas mixture.

In this method, two laser beams converge on a section of the sample located between two electrodes (Figure 1). If the beams are polarized parallel to each other, they interfere and produce an interference pattern. If the sample has a high resistance, the resulting conductivity is the photoconductivity due to that particular illumination condition. If the interference pattern's characteristic size, Δ_G, is akin to the diffusion length of the minority carriers, the photoconductivity varies as Δ_G is varied by changing the angle between the beams. The photoconductivity is estimated by measuring the voltage across the resistance R mounted in series with the sample (Figure 1). By measuring the voltages across the resistance R when the sample is uniformly illuminated, and when it is exposed to interference patterns characterized by different Δ_G values, the minority carriers' diffusion length at a given temperature and light intensity can be estimated[5].

The process parameters such as substrate temperature and H_2S concentration are systematically varied while the CH_4 concentration is fixed at 0.3 and 2 % for μ-D and n-D, respectively, to study the corresponding variation on the nanostructure and electronic properties. The nanostructure is analyzed using scanning electron microscopy, atomic force microscopy, X-ray diffraction analysis, X-ray photoelectron spectroscopy, Auger electron spectroscopy, and visible and UV Raman spectroscopy. The results are employed to elucidate the mechanism of n-type conductivity in these S-doped diamond films.

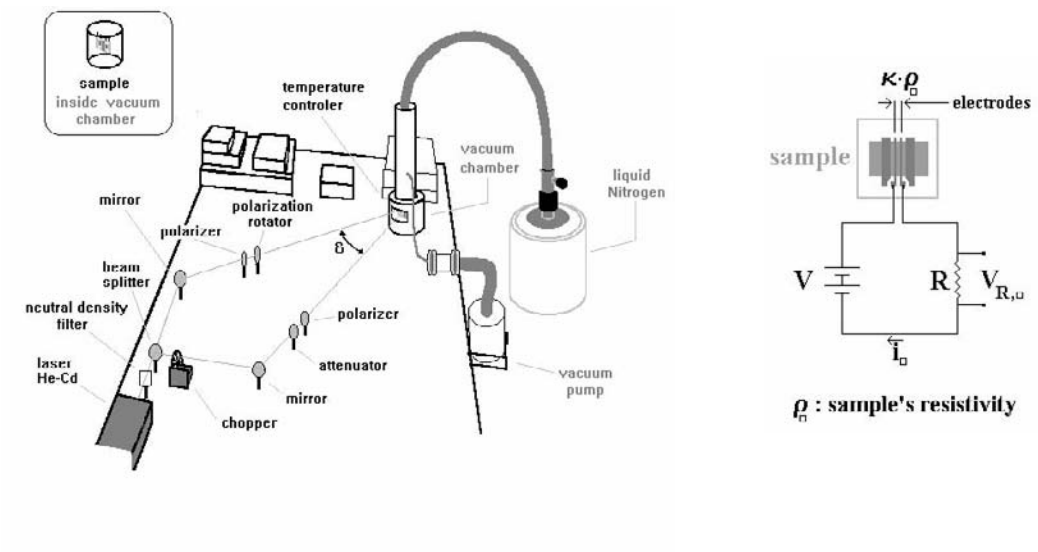

Figure 1. Steady-state photocarrier grating (left) technique setup; sample's series circuit (right).

Acknowledgements: Research supported by NASA (Grants NCC3-1034 and NGT5-40091; Cooperative Agreement NCC5-595), Department of Energy (Grant DE-FG02-01ER45868), and the UPR-Río Piedras FIPI (Grant 8-80-514).

REFERENCES

1. Gupta, S.; Weiner, B.R.; and Morell, G.: "Room-temperature electrical conductivity studies of sulfur-modified microcrystalline diamond thin films", *Appl. Phys. Lett.* 83, 491 (2003).
2. Gupta, S.; Martínez, A.; Weiner, B.R., et al.: "Electrical conductivity studies of chemical vapor deposited sulfur-incorporated nanocomposite carbon thin films", *Appl. Phys. Lett*. 81, 283 (2002).
3. Gupta, S.; Weiner, B.R. and Morell, G.: "Electron field emission properties of microcrystalline and nanocrystalline carbon thin films deposited by S-assisted hot filament CVD", *Diamond Relat. Mater.* 11, 799 (2002).
4. Köck, F.A.M.; Garguillo, J.M.; Nemanich, R.J., et al., "Spatial distribution of electron emission sites for sulfur doped and intrinsic nanocrystalline diamond films", *Diamond Relat. Mater.* 12, 474 (2003).
5. Balberg, I.: "Theory of the small photocarrier grating under the application of an electric field", *Phys. Rev. B* 44, 1628 (1991).

SESSION 3

APPLICATIONS/DEVICES: MEMS

Vibrating RF MEMS in Diamond Structural Material

Clark T.-C. Nguyen

DARPA/MTO
(On leave from the University of Michigan)
Arlington, VA 22203

Invited Paper Abstract

The increasing demand for secure, mobile, wireless communications has stimulated interest in technologies capable of reducing the size and power consumption of wireless modules, and enhancing the bandwidth efficiency of communication networks. With frequencies now in the GHz range and *Q*'s greater than 10,000, on-chip vibrating micromechanical resonators measuring only a few tens of microns on edge are now well positioned for inclusion into a number of future wireless communication sub-systems, from cellular handsets, to PDA's, to low-power networked sensors. The list of micromachinable materials used so far to implement such vibrating RF MEMS devices includes silicon (both single- and poly-crystalline), aluminum nitride, zinc oxide, silicon germanium, silicon carbide, and CVD diamond. Among this set, CVD nanocrystalline diamond shines as the material that (in combination with polysilicon support structures) presently holds the record for the highest frequency-*Q* product figure of merit (equal to 2.75×10^{13}) of any UHF resonator at room temperature [1]. Needless to say, that diamond's acoustic velocity is twice that of polysilicon is instrumental to achieving such impressive frequency-*Q* product performance.

In recent years, however, polysilicon resonators using loss-minimizing geometries (e.g., quarter-wavelength-supported extensional rings [2]) have begun to close the frequency-*Q* performance gap, to the point where diamond material is no longer needed to achieve the *Q*'s needed for the advanced communication architectures made possible by tiny high-*Q* resonators [3]. Nevertheless, CVD diamond remains a very important material for vibrating RF MEMS, mainly due to its likely amenability to fully planar, single-chip, post-CMOS integration with transistor circuits. In particular, the thermal budget required by diamond structural material might end up being much lower than that of polysilicon in post-CMOS integration processes, especially given recent examples of ultra-nanocrystalline films deposited at low temperatures, and given the likelihood that annealing will not be needed to improve material quality, as has been the case for polysilicon [4].

After giving a brief history of vibrating RF MEMS technology, its recent rapid progression, and the role that diamond material has played to date, this paper conveys some of the issues that presently plague planar MEMS/transistor integration processes and describes how the use of CVD diamond structural material might alleviate them.

References.

[1] J. Wang, J. E. Butler, T. Feygelson, and C. T.-C. Nguyen, "1.51-GHz polydiamond micromechanical disk resonator with impedance-mismatched isolating support," *Proceedings*, 17th Int. IEEE Micro Electro Mechanical Systems Conf., Maastricht, The Netherlands, Jan. 25-29, 2004, pp. 641-644.

[2] S.-S. Li, Y.-W. Lin, Y. Xie, Z. Ren, and Clark T.-C. Nguyen, "Micromechanical Hollow-Disk Ring Resonators," *Proceedings*, 17th Int. IEEE Micro Electro Mechanical Systems Conf., Maastricht, The Netherlands, Jan. 25-29, 2004, pp. 821-824.

[3] C. T.-C. Nguyen, "Vibrating RF MEMS for next generation wireless applications," *Proceedings*, 2004 IEEE Custom Integrated Circuits Conf., Orlando, Florida, Oct. 3-6, 2004, pp. 257-264.

[4] J. M. Bustillo, G. K. Fedder, C. T.-C. Nguyen, and R. T. Howe, "Process technology for the modular integration of CMOS and polysilicon microstructures," *Microsystem Technologies*, **1** (1994), pp. 30-41.

NANOCRYSTALLINE DIAMOND FILMS FOR SURFACE ACOUSTIC WAVE DEVICES

F. Bénédic, F. Silva

Laboratoire d'Ingénierie des Matériaux et des Hautes Pressions, UPR 1311 CNRS, Université Paris 13, 99 avenue J.B. Clément, 93430 Villetaneuse, France

O. Elmazria, M.B. Assouar, M. El Hakiki

Laboratoire de Physique des Milieux Ionisés et Applications, UMR 7040 CNRS, Université H. Poincaré - Nancy I, 54506 Vandoeuvre-lès-Nancy, France

Keywords: Nanocrystalline diamond; Surface acoustic wave; High frequency electronics

Abstract

Surface acoustic wave (SAW) devices are critical components in wireless communication systems. In this work, the potentialities of nanocrystalline diamond films as high velocity and low propagation losses substrates for high frequency SAW devices are investigated from an experimental and theoretical point of view.

INTRODUCTION

The high acoustic phase velocity of chemical vapor deposited (CVD) diamond makes it, when combined with piezoelectric films such as AlN or ZnO, very attractive for high frequency (GHz range) surface acoustic wave devices. However, the processed diamond based SAW devices suffer from relatively low performances mainly due to the important propagation losses in polycrystalline structures. According to previous study, the propagation losses decrease while the diamond grain size diminishes[1,2]. Therefore, the very small grain size of nanocrystalline diamond makes it an hopeful alternative to the commonly used polycrystalline diamond, as illustrated in preliminary study[3]. In the present work we investigate the structural and electrical properties of nanocrystalline diamond films and their potentiality as SAW device substrates by both experimental and theoretical approaches.

RESULTS

Very low surface roughness nanocrystalline diamond (NCD) layers were deposited on silicon substrates by microwave plasma assisted CVD (MPACVD) process. Both continuous wave (CW) and pulsed wave (PW) were employed with $Ar/H_2/CH_4$ gas mixtures in order to obtain films of different thicknesses with grain size varying between a few nanometers and a few tens of nanometers. The various characteristics of the elaborated films were principally investigated through SEM, AFM, TEM, Raman spectroscopy and XRD.

Highly oriented piezoelectric aluminum nitride films were grown by RF reactive magnetron sputtering on the NCD substrates. Aluminum inter-digital transducers (IDT) were patterned by photolithography technique on AlN films or at the AlN/NCD interface, depending on the configuration considered for the layered structure. Dispersion curves of elastic velocity and electromechanical coupling coefficient were determined for the both structures AlN/IDT/NCD/Silicon and IDT/AlN/NCD/Silicon, and for various NCD films properties, from the high frequency characterization of the SAW devices.

The phase velocity (v_φ) was determined from the peak's frequency f_i using the following equation:

$$f_i = \frac{v_\varphi}{\lambda} \quad (1)$$

where λ is the wavelength of the acoustic wave and is fixed by the spatial periodicity (P) of IDT and the order of the considered harmonic (n):

$$\lambda = \frac{P}{n} \quad (2)$$

The harmonic peak intensities are governed by the metallization ratio of IDT.

The propagation losses were determined by measuring the insertion losses (α_i) of SAW devices showing identical geometry except the propagation distance, i.e. the gap between input and output IDT. The propagation loss (p) can be then expressed in dB/λ by:

$$p = \lambda \frac{\alpha_2 - \alpha_1}{gap_2 - gap_1} \quad (3)$$

where gap_1, gap_2 and λ are expressed in µm and α_i in dB.

The experimental results are in satisfactory agreement with the theoretical predictions of a model developed for layered structures. In particular, they show that a high surface acoustic velocity, close to 10^4 m/s for some devices, may be obtained by using NCD layers. As an illustration, Fig. 1 shows the acoustic velocity estimated on IDT/AlN/NCD/Silicon layered structures as a function of kh_{NCD}, where k is the wavevector modulus and h_{NCD} is the thickness of NCD films.

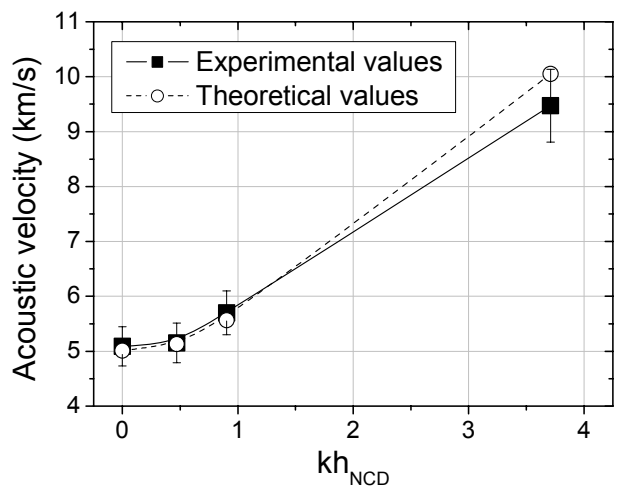

Figure 1: Experimental and theoretical values of the acoustic velocity determined for SAW devices achieved on IDT/AlN/NCD/Silicon layered structures as a function of kh_{NCD}.

REFERENCES

1. Uemura, T., et al.: "Low-loss diamond surface acoustic wave devices using small-grain poly-crystalline diamond", Jpn. J. Appl. Phys., Vol. 41, No. 5B, 3476-3479 (2002).
2. Elmazria, O., et al.: "Effect of diamond nucleation process on propagation losses of AlN/Diamond SAW filter", IEEE Trans. Ultras. Ferr. Freq. Contr., Vol. 51, No. 12, 1704-1709 (2004).
3. Bénédic, F., et al.: "Surface acoustic wave devices based on nanocrystalline diamond and aluminium nitride", Diamond Relat. Mater., Vol. 13, No. 2, 347-353 (2004).

FRACTURING TEMPLATED CARBON NANOTUBES WITH A MEMS TESTING STAGE

Shaoning Lu, Weiqiang Ding, Rodney S. Ruoff*

Department of Mechanical Engineering, Northwestern University, Evanston, IL 60208

*r-ruoff@northwestern.edu

Keywords: fracture mechanics, templated carbon nanotube, MEMS testing stage, tensile loading

Abstract

An *in-situ* mechanics study on individual templated carbon nanotubes (T-CNTs) was conducted in a scanning electron microscope (SEM, LEO1525), using a MEMS-based tensile testing system.[1] The T-CNTs were made by pyrolyzing ethylene in alumina nanopore membranes.[2] The testing system is composed of a high aspect ratio MEMS device with an integrated thermal actuator and force sensing structures. The device provides well-controlled nanoscale displacement and force for loading nanostructures. Novel approaches have been developed to align and mount[3] a T-CNT on the two opposing platforms of the testing stage (Figure 1). A fountain-pen writing technique was developed to deposit paraffin for quick clamping of the T-CNT in the SEM by electron beam induced deposition (EBID).

An increasing tensile load was applied to the T-CNT by moving the platform attached to the actuator away from the other platform. High-resolution SEM images were acquired while increasing the load on the T-CNT. The T-CNT eventually fractured without sliding. The diameter of the T-CNT was measured on the exposed fracture surface of the two fracture segments that remained attached to the platform (Figure 2). The load can be obtained from the deformation of the force-sensing beam integrated in the device. This force from the force-sensing beam is obtained through FEM modeling and further calibrated with an AFM cantilever operated by a home-built manipulator. Stress concentration due to a non-uniform diameter is speculated as being the cause of the location of fracture. The stress *vs* strain, Young's modulus, and tensile strength of several T-CNTs loaded in this way, are being characterized. The experiment suggests the potential use of this home-built testing stage for tensile loading of a variety of nanowires and nanotubes.

We appreciate the support from the ONR (grant No. N000140210870) and the NSF (CMS-0304506). This work was performed in part at the Cornell Nano-Scale Science & Technology Facility which is supported by the NSF under Grant ECS-9731293, its users, Cornell University and Industrial Affiliates.

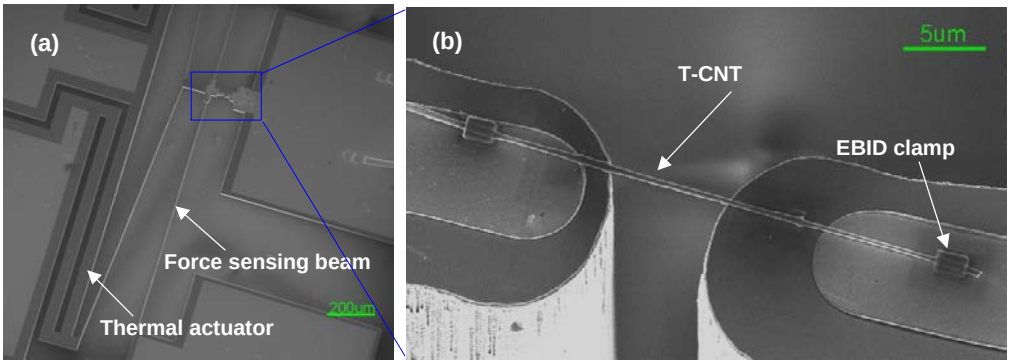

Figure 1. SEM images of: (a) MEMS testing stage; (b) a T-CNT aligned across the platforms (thus 100 μm above the bottom of the trench between the platforms) of the testing stage shown in (a), and clamped with EBID before being tensile loaded.

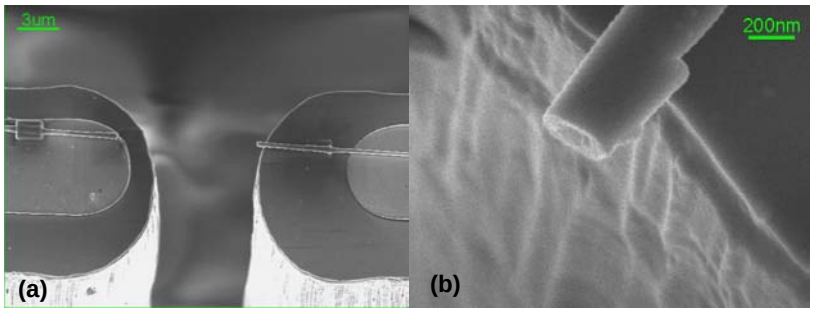

Figure 2. SEM images of: (a) the T-CNT after fracture; (b) one of the fracture surfaces of the T-CNT shown in (a).

REFERENCES

1. Lu, S, et al., "Realization of nanoscale resolution with a micromachined thermally actuated testing stage," *Review of Scientific Instruments*, 75 (6), 2154-2162, June 2004.
2. Xu, T. T., et al., "Bone-shaped Nanomaterials for Nanocomposite Applications," *Nano Letters*, **3**, 1135-1139, (2003).
3. Lu, S., Chung, J., Dikin, D., Lee, J. and Ruoff, R. S., "An integrated MEMS system for in-situ mechanical testing of nanostructures," extended abstract, *Proceedings of 3rd ASME Annual Integrated Nanosystems: Design, Synthesis & Applications Conference*, Sept. 22-24, 2004, Pasadena, CA.

MATERIALS SCIENCE AND PROCESSING STRATEGIES FOR INTEGRATION OF PIEZOELECTRIC AND ULTRANANOCRYSTALLINE DIAMOND (UNCD) THIN FILMS FOR PIEZOACTUATED HYBRID MEMS

O. Auciello , W, Fan, G. Bai, and J.A. Carlisle

Material Science Division, Argonne National Laboratory, Argonne, IL. 60439

Abstract

,
The integration of dissimilar materials and micro and nanofabrication processes need to be investigated and developed to enable a new generation of multifunctional microelectromechanical and nanoelectromechanical system (MEMS/NEMS) devices. Ultrananocrystalline diamond (UNCD) with exceptional mechanical strength, chemical inertness and tribological performance exhibits great potential as a new high-performance material for application to MEMS and NEMS. On a parallel scientific and technological path, ferroelectric/piezoelectric $Pb(Zr_xTi_{1-x})O_3$ (PZT) thin films has attracted much attention due to projected applications for intelligent MEMS based on its outstanding piezoelectric and electromechanical coupling coefficients, easy dipole reorientation and high remnant polarization. However, PZT exhibits relatively weak mechanical and tribological properties that hinder its application into MEMS/NEMS devices as a strong microstructural material. Therefore, the opportunity exists for integrating these two dissimlar materials for fabrication of piezoelectrically actuated MEMS/NEMS devices. PZT films need to be grown in O_2 at high temperatures (600-700 ˚C) on the UNCD layers to achieve the proposed integration. However, growth of PZT, at high temperature in oxygen, on UNCD layers, results in chemical etching of the diamond surface due to formation of volatile CO and or CO_2 species. Another critical challenge lies in the thermal stress between PZT and UNCD that might cause film delamination, following deposition and annealing processes. We demonstrate here that a bi-functional TiAl alloy film can be used as an oxidation barrier and adhesion layer interposed between the PZT and UNCD layers in combination of using conductive metallic or oxide electrode to achieve a successful integration of these two dissimilar materials. Low-temperature thin film growth techniques, including magnetron sputter-deposition for producing the TiAl barrier layer, and MOCVD to produce $PbZr_xTi_xO$ (PZT) layers, were used to lower the risk of diamond oxidation. Post-deposition rapid thermal annealing was used to control the crystallography orientation of the PZT layer, thus its piezoelectric properties. The UNCD films were grown by CVD using an Ar-rich CH_4/Ar plasma chemistry. First PZT-films based capacitors with excellent polarization hysteresis loops were produced on UNCD structural layers using the integration described above (see Fig. 1). This result demonstrates the viability of using piezoelectric PZT layers for actuation of UNCD-based MEMS devices. Processing for producing piezoactuated PZT/UNCD cantilevers will be discussed in view of projected applications to the fabrication of piezoelectrically actuated UNCD-based MEMS/NEMS actuators and sensors.

This work was supported by the DOE-Office of Science-Materials Science, under Contract No. W-31-109-ENG-38.

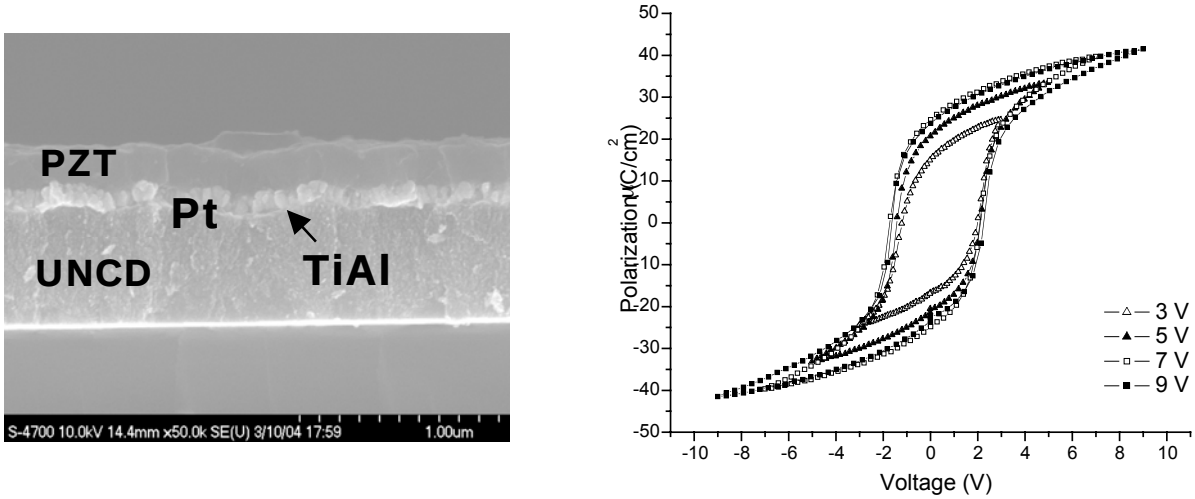

Figure 1. (a) Cross section SEM picture of integrated PZT/UNCD films with TiAl diffusion barrier layer; (b) first polarization hysteresis loop demonstrated for PZT capacitors fabricated on a diamond (UNCD) layer.

CARBON NANOTUBE BASED NEMS AND MODELING

Changhong Ke and Horacio D. Espinosa

Department of Mechanical Engineering, Northwestern University, Evanston, IL 60208

E_mail: espinosa@northwestern.edu

Keywords: Carbon nanotubes, NEMS, nanoswitches, finite kinematics

Abstract

Carbon nanotube based nanoelectromechanical systems (NEMS) are nanofabricated and tested. *In-situ* scanning electron microscopy (SEM) measurements of the deflection of the cantilever under electrostatic-actuation are reported. In particular, a cantilever nanotube suspended over an electrode (nanoswitch), from which a differential in electrical potential is imposed, is studied. The finite deformation regime here investigated is the first of its kind. An electromechanical analysis of the characteristics of the device is used to interpret the measurement. The model includes the concentration of electrical charge, at the end of the nanocantilever, finite kinematics and the van der Waals force. The results reported in this work are particularly useful in the characterization of the electro-mechanical properties of nanotubes as well as in the optimal design of nanotube based NEMS devices.

INTRODUCTION

Carbon nanotubes (CNTs) have long been considered ideal building blocks for Nanoelectromechanical systems (NEMS) due to their superior electro-mechanical properties. The CNT-based NEMS reported in the literature, such as nanotweezers,[1] and feedback-controlled nanocantilever NEMS devices,[2] can be simply modeled as CNT cantilevers hanging over an infinite conductive substrate. In order to design a functional NEMS device, its electro-mechanical characteristic should be well quantified in advance. Generally, multi-walled carbon nanotubes (MWNTs) can be modeled as homogeneous cylindrical beams and perfect conductors. In this paper, we investigate the electro-mechanical characteristics of CNT-based NEMS devices by in-situ scanning electron microscopy (SEM) measurement and electromechanical analysis. In particular, a cantilever nanotube suspended over an electrode (nanoswitch), from which a differential in electrical potential is imposed, is studied.

EXPERIMENT

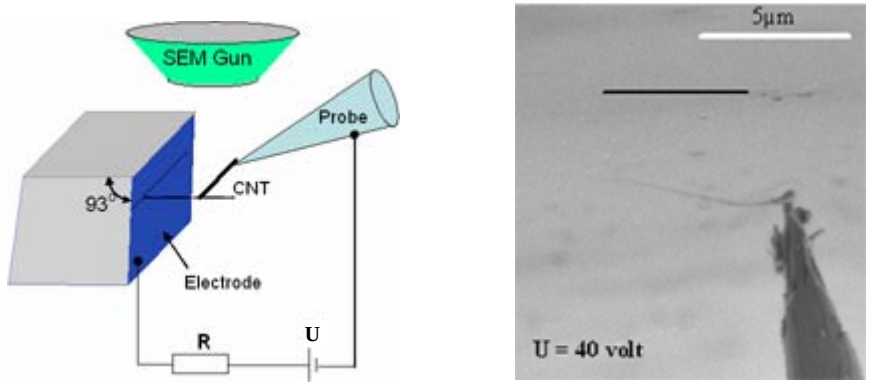

(a) (b)

Figure 1 (a) Schematic of the experimental configuration employed in the electrostatic actuation of MWNTs. (b) SEM image of the deformed carbon nanotube cantilever at biased voltage U = 40 volt.

The *in-situ* electrostatic actuation of CNT cantilever is illustrated in Fig. 1(a).[3] A MWNT with length 6.8 μm, welded to a 3D manipulator probe by nanomanipulation and electron beam induced deposition (EBID) of platinum (Pt), was placed horizontal and parallel to the electrode, which is a piece of Si wafer coated with Au film attached to a Teflon block. By focusing on the electrode surface and adjusting the working distance to be the same to that of nanotube, a feature on the electrode, which is on the same horizontal plane with the nanotube was located. Such feature is schematically marked as a line in Fig. 1 (a). The horizontal distance between the nanotube and the line was

controlled by the nanomanipulator and set to 3 µm. Because the ratio between the length of the nanotube and the gap between the nanotube and electrode is 2.3, the deflection of the nanotube under electrostatic force can be considered to be in the finite kinematics regime. With the increase of the applied voltage, the deflection of the nanotube increased and the local curvature became substantial. Fig 1 (b) shows the scanning electron images of the deflection of the carbon nanotube when applied voltages U = 40 volts. The feature on the electrode, which is in the same horizontal plane containing the cantilever nanotube, is schematically marked as a solid black line in Fig. 1(b). The deflection and local curvature of the deflected nanotube can be clearly observed. The pull-in voltage of the nanotube cantilever device was measured to be about 48 volts.

MODELING

The governing equation of the nanotube cantilever under finite kinematics (just considering bending), is

$$EI\frac{d^2}{dx^2}\left(\frac{d^2w}{dx^2}\left(1+\left(\frac{dw}{dx}\right)^2\right)^{-\frac{3}{2}}\right)=\left(q_{vdw}+q_{elec}\right)\sqrt{1+\left(\frac{dw}{dx}\right)^2} \qquad (1)$$

where E is the Young Modulus, I is the moment of the inertia of the nanotube, w is the deflection of the nanotube, x is the axis along the nanotube. q_{vdw} is the van der Waals force which can be evaluated by the method reported by Desquence, et al.,[4] q_{elec} is the electrostatic force, which can be computed by the capacitance method. The capacitance per unit length along the cantilever nanotube is approximated as[5]

$$C=C_d\left(r(x)\right)\left\{1+0.85\left[(H+R)^2R\right]^{1/3}\delta\left(x-x_{tip}\right)\right\} \qquad (2)$$

where the first term in the bracket accounts for the uniform charge along the side surface of the tube and the second term accounts for the concentrated charge at the end of the tube. $x=x_{tip}\neq L$, as a result of the finite kinematics. $\delta(x)$ is the Dirac distribution function, R=R_{ext} is the external radius of the nanotube and H is the initial distance between the low fiber of nanotube and the ground. $C_d(r)$ is the distributed capacitance along the side surface per unit length which is given by $C_d(r)=2\pi\varepsilon_0/a\,cosh(1+r/R_{ext})$, where r is the distance between the lower fiber of the nanotube and the substrate, and ε_0 is the permittivity of vacuum.

RESULT AND DISCUSSION

The comparison between experimental data and the theoretical predictions shows they are in good agreement. For the theoretical predictions, the following parameters were employed: L = 6.8 µm, H = 3 µm, R=R_{ext} = 23.5 nm, E = 1 TPa. The computed pull-in voltage is 47.8 Volts, which matches the experimentally measured value 48 Volts very well. The results from the modeling reveal that, of all the effects contributing to the deformation and pull-in of the device, the concentration of charge at the end of the cantilever was identified as the most dominant, with an error of 13.4 % when its effect is omitted. The finite kinematics effect is less pronounced, with an error of 7.0 % when neglected. These errors were computed for the geometry and material examined in our experiments.

The methodologies reported here are completely general and as such are expected to be useful in the characterization of electro-mechanical properties of nanotubes and nanowires, as well as in the optimal design of nanotube based NEMS devices.

REFERENCES

1. S. Akita, et al, *Appl. Phys. Lett.*, 79 (2001), 1691; P. Kim and C. M. Lieber, *Science*, 126 (1999), 2148.
2. C. Ke and H. D Espinosa, *Appl. Phys. Lett.*, 85 (2004), 681
3. C-H. Ke, N. Pugno, B. Peng, and H. D. Espinosa, "Analytical modelling of nanotube based NEMS devices," submitted to *J. of Mech. and Phys. Solids*, 2004.
4. Desquenes, M., Rotkin S.V. and Aluru, N. R., *Nanotechnology 13* (2002), 120.
5. C.-H. Ke, and H. D. Espinosa, "Analysis of electrostatic charge distribution in nanotubes and nanowires," submitted to *J. of Appl. Phys.*, 2004.

Fabrication and Test of Poly-Crystalline Diamond Piezoresistive Position Sensors for Cochlear Implant Probe

Yuxing Tang and Dean M. Aslam

Electrical and Computer Engineering, Michigan State University, East Lansing, MI 48824

Jianbai Wang and Kensall D. Wise

Electrical Engineering and Computer Sciences, University of Michigan, Ann Arbor, MI 48109

Key Words: Polycrystalline diamond, Piezoresistive sensor, Gauge factor, Cochlear probe

Abstract

This paper reports on the application of high-sensitivity poly-crystalline diamond (poly-C) piezoresistive position sensor in implantable cochlear probe for the first-time. The fabricated poly-C sensor, demonstrating a successful integration of diamond and silicon-based microsystems technologies, leads to a high intra-grain gauge factor (GF) of 28. The film quality, electrical properties, contact resistance and piezoresistivity of the poly-C sensors are characterized to study the dependence of GF (from 8 to 70) of poly-C on the fabrication conditions. As the reported GF values for poly-C are in the ranges of 7 – 120 [1] and 3000 – 4000 [2] for inter- and intra-grain piezoresistors, respectively, the use of poly-C sensors in microsystems is expected to lead to unprecedented applications.

POSITION SENSOR FOR COCHLEAR PROBE

Cochlear prostheses have been used as a hearing enabling technology to help over 100,000 profoundly deaf people by electrically stimulating the cochlear nerve cells with the implanted electrode. The ability to measure electrode curvature and position can greatly improve the prostheses performance by minimizing any damage to the cochlea as the probe is inserted and achieving better signal delivery [3]. While poly-Si piezoresistive sensors have been used in microsystems, poly-C sensor was explored in this study due to its high sensitivity using a 12-mask fabrication process employing surface and bulk micromachining techniques. Poly-C is an excellent sensor material especially at high temperatures and in harsh environments due to its large band gap, and its excellent physical and chemical properties. This paper reports a new application of the poly-C thin film as a high-sensitivity piezoresistive position sensor fabricated and tested for an implantable cochlear probe.

FABRICATION AND TESTING

The details of typical probe fabrication process are described elsewhere [3]. A cross-sectional diagram of the cochlear probe is shown in Fig.1 (a) to illustrate the integration of poly-C sensors using the 4th mask. Diamond-powder-loaded water (DW) was spun on top of silicon nitride dielectric layer to provide the seeding for poly-C thin film growth by microwave plasma chemical vapor deposition (MPCVD). Poly-C film was patterned using electron cyclotron resonance (ECR) assisted plasma etching process as shown in Table 1. A metal stack consisting of Ti/TiN/Al/Ti was used as the interconnect layer between poly-C sensor and poly-Si wire with a contact resistivity of 10^{-3}-10^{-5} Ω*cm^2 between poly-C and Titanium. SEM, AFM and Raman spectra were used to check the quality of poly-C and optimize the fabrication process. Fig.1(b) shows SEM pictures of the released structure with poly-C position sensors.

For testing, the probe backend was glued on a substrate and got electrically connected by gold wire bonding. Strains, applied on the probe by bending the 4 μm thick probe into different curvatures, were calculated from corresponding curvature radius and probe thickness (Fig. 2(a)). More poly-C test structures were fabricated on oxidized silicon wafers to optimize the seeding densities, sensitivities and to study the intra-grain GF. Another seeding method, diamond-power-loaded photoresist (DPR), was used to study the GF variation. Fig.2 (b) shows the dependence of poly-C film GF on resistivity and grain size. The small grain (0.2 μm) and large grain (0.6 μm) films were fabricated using DW and DPR seeding methods, respectively. The result shows that large grain size and high resistivity help improve the GF from 7 to 70, but may cause problems related to contact resistance and surface roughness. Further study of integrating intra-grain piezoresistors in the probe is expected to increase the sensitivity substantially [2].

Table 1. Poly-C fabrication & etching parameters

Poly-C deposition using MPCVD		Poly-C dry etching	
H_2/CH_4 Gas flow (sccm)	200/3	$O_2/SF_6/Ar$ Gas flow (sccm)	28/2/6
Trimethylboron doping (sccm)	0.2 - 2 x10^{-3}	Microwave power (W)	400
Microwave power (kW)	1.6 - 2.4	Pressure (mini-torr)	4
Gas pressure (torr)	22 - 45	RF power (W)	100
Substrate temperature (℃)	520 - 780	RF bias voltage (V)	-150
Deposition rate (μm/hr)	0.1 -0.3	Substrate temperature(℃)	< 50
Film thickness (μm)	0.6-1	Etch rate (nm/min)	120

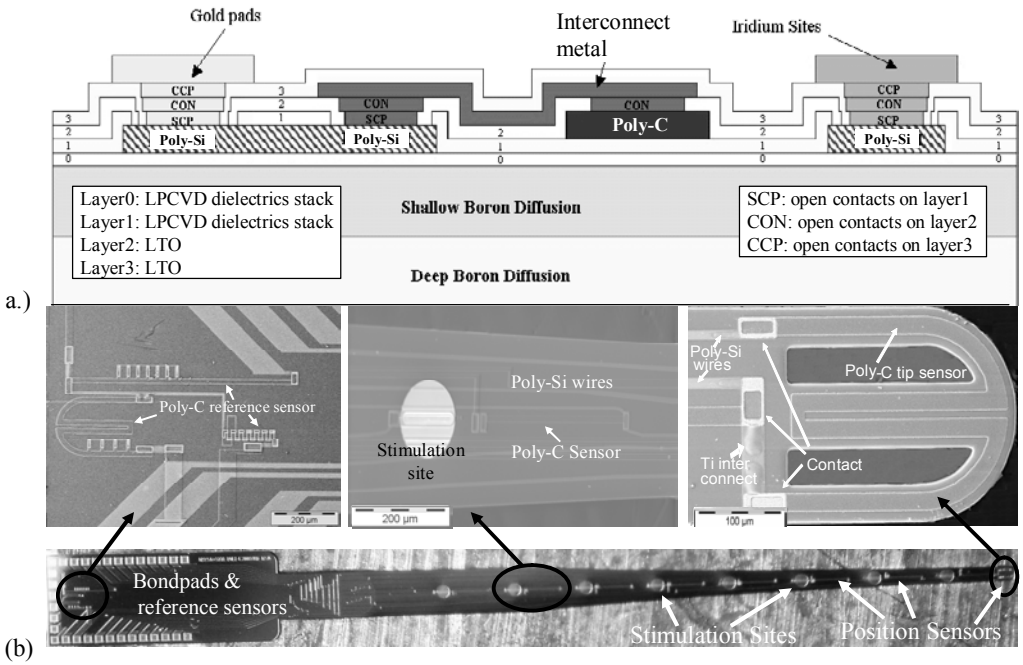

Fig.* 1 (*a) Layer description for the cochlear implant probe with poly-C strain gauges, (b) SEM of the cochlear implant probe with poly-C piezoresistive position sensors.

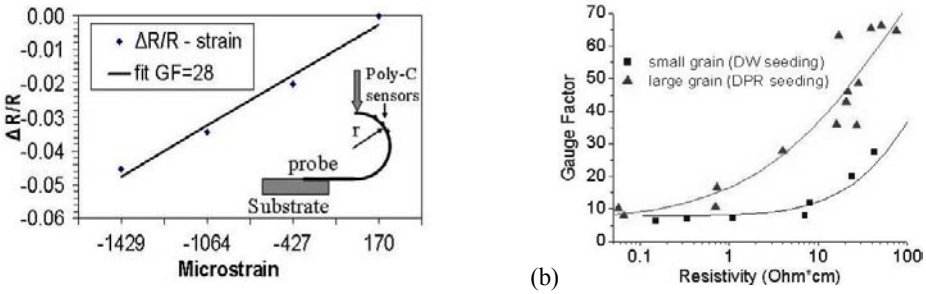

Fig.* 2 (*a) Testing structure of probe position sensing and the gauge factor result, (b) Relation between the poly-C GF and the boron doping level for DPR and DW seeded films.

REFERENCES

1. E. Kohn, M. Adamschik, P. Schmid, et al., "Diamond electro-mechanical micro devices - technology and performance", *Diamond and Related Materials*, 10, 9-10, 1684(2001).

2. S. Sahli and D. M. Aslam, "Ultra-high sensitivity intra-grain poly-diamond piezoresistors", *Sensors and Actuators a-Physical*, 71, 3, 193(1998).

3. P. T. Bhatti, B. Y. Arcand, J. Wang, et al., "A High-Density Electrode Array for A Cochlear Prosthesis", *IEEE TRANSDUCERS'03*, 1750(2003).

SESSION 4

MECHANICAL, TRIBOLOGY, & PROTECTIVE APPLICATIONS

IS THERE ANOTHER WAY TO MAKE/GROW DIAMOND?

Rodney S. Ruoff

Department of Mechanical Engineering, Northwestern University, Evanston, IL 60208

r-ruoff@northwestern.edu

Keywords: diamond nanowire, silicon carbide, VLS, vapor-liquid-solid, epitaxial

Abstract

Gogotsi et al.[1] reported the synthesis of nano- and micro-crystalline "diamond-structured" carbon films by extracting silicon from the surface region of macroscopic silicon carbide samples with chlorine-containing gases at ambient pressure and temperatures not exceeding 1,000˚C. This "carbide-derived carbon (CDC) method" has been used for the conversion of carbide to nano-crystalline diamond and graphite films on bulk pieces of SiC.[1,2] Can small diameter silicon carbide whiskers, as the precursor, yield diamond nanowires by the CDC method?

Our second approach to large-scale synthesis of single-crystal diamond NWs is to exploit the epitaxial match that diamond has with itself (thus, a diamond substrate), and also with Si and SiC,[3-7] and other materials. For brevity we provide a few examples. Small diameter and high-aspect-ratio single-crystal Si and SiC NWs with a variety of metal particles at their tips are available. Coincidentally, the same metal particles are also catalysts for decomposition of hydrocarbons and when present as individual particles, for example on a quartz substrate, they catalyze the growth of carbon nanotubes (sp^2 carbon). One may ask: as a hydrocarbon decomposes at the metal particle at the tip and carbon diffuses through it, will the "typical" situation of carbon nanotube (CNT) growth occur (sp^2 rather than sp^3 carbon)? I have hypothesized that diamond nanowire growth will occur because the growth direction of the Si and SiC NWs is such that at the Si or SiC interface with the metal particle there is a perfect epitaxial match for growth of diamond. As an analogy, "striped" Si/Ge NWs have been fabricated by alternating exposure of a metal-particle tipped NW to silane and then germane.[8]

In 1968 Deryagin[9] and colleagues claimed to have grown diamond whiskers of multi-micron diameter and millimeter lengths by thermal CVD from metal catalyst particles that had been deposited onto a single-crystal diamond surface. It was suggested that the growth occurred by the vapor-liquid-solid mechanism. A Xenon lamp was used to heat the diamond surface, which caused a previously deposited thin film of metal to break into small droplets.[9-11] Exposure of this material to various hydrocarbons led to the reported growth of diamond whiskers with multi-micron diameters and even millimeter lengths. Our experimental control and theoretical insights, as well as our abilities to analyze size, composition, and structure have, of course, advanced significantly since the 1960's. Thus, deposition of small metal particles by a variety of methods onto single-crystal diamond facets is called for. An example is provided in the figure to the right, which shows a single crystal diamond inserted into a stainless steel holder we fabricated. We propose extending these efforts to syntheses from epitaxial-matched substrates, among them Si and SiC. Should these methods yield diamond nanowires, we propose using diamond or SiC micron-scale powders, which we know from SEM analysis contain highly faceted particles. By decorating such powders with small catalytic particles, diamond NW growth may occur on those facets that are epi-matched to diamond. *Perhaps this could provide a route to production of commodity levels of diamond.*

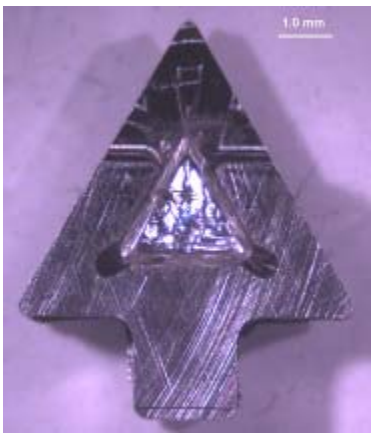

Acknowledgment

We appreciate discussions with Jim Butler.

References

1. Y. Gogotsi, S. Welz, D. A. Ersoy & M. J. McNallan. Conversion of silicon carbide to crystalline diamond-structured carbon at ambient pressure. *Nature (London, United Kingdom)* **411**, 283-7 (2001).
2. Y. G. Gogotsi, I.-D. Jeon & M. J. McNallan. Carbon coatings on silicon carbide by reaction with chlorine-containing gases. *Journal of Materials Chemistry* **7**, 1841-1848 (1997).

3. M. Schreck, R. Hessmer, S. Geier, B. Rauschenbach & B. Stritzker. Structural characterization of diamond films grown epitaxially on silicon. *Diamond and Related Materials* **3**, 510-14 (1994).
4. B. E. Williams, B. R. Stoner, D. A. Asbury & J. T. Glass. In-vacuo surface analysis of diamond nucleation and growth on silicon(111) and polycrystalline tantalum. *NATO ASI Series, Series B: Physics* **266**, 737-44 (1991).
5. K. Helming. Texture analysis of chemical vapor deposited diamond films on silicon by the component method. *Journal of Applied Physics* **77**, 4765-70 (1995).
6. B. R. Stoner & J. T. Glass. Textured diamond growth on (100) b-silicon carbide via microwave plasma chemical vapor deposition. *Applied Physics Letters* **60**, 698-700 (1992).
7. H. Kawarada. Heteroepitaxial growth of highly oriented diamond on cubic silicon carbide. *Journal of Applied Physics* **81**, 3490-3493 (1997).
8. Y. Wu, R. Fan & P. Yang. Block-by-Block Growth of Single-Crystalline Si/Si-Ge Superlattice Nanowires. *Nano Letters* **2**, 83-86 (2002).
9. B. V. Deryagin. Filamentary diamond crystals. *Journal of Crystal Growth* **2**, 380-4 (1968).
10. B. V. Deryagin. Filiform diamond crystals. *Doklady Akademii Nauk SSSR* **181**, 1094-6 (1968).
11. B. V. Deryagin. Low-pressure diamond whiskers. *New Scientist* **44**, 228-9 (1969).

CONTROLLING THE NANOTRIBOLOGY OF NANOSTRUCTURED DIAMOND FILMS

Robert W. Carpick, D. S. Grierson, A.V. Sumant, E.E. Flater, G. Ning, K. Sridharan

University of Wisconsin-Madison, Madison, WI.

T.A. Friedmann, J.P. Sullivan

Sandia National Laboratories, Albuquerque, NM.

J.E. Gerbi, J. Birrell, X. Xiao, O. Auciello, J.A. Carlisle

Materials Science Division, Argonne National Laboratory, Argonne, IL.

Keywords: Nanotribology, AFM, diamondlike carbon, ultrananocrystalline diamond, tetrahedral amorphous carbon.

Abstract

We will discuss recent studies of the nanotribological properties of carbon-based thin films, particularly nanocrystalline diamond, tetrahedral amorphous carbon, and diamond-like carbon. By using atomic force microscopy for nano-scale friction measurements and surface spectrosopy techniques for detailed chemical and structural studies, we are able to demonstrate that the carbon bonding configuration (sp2 vs sp3 hybridization) and chemical termination of the surfaces has a strong effect on nanoscale friction and adhesion. We will present these results and discuss their potential impact for nano-, micro-, and macro-scale applications.

REFERENCES

1. A.V. Sumant, D.S. Grierson, J.E. Gerbi, J. Birrell, U.D. Lanke, O. Auciello, J.A. Carlisle, and R.W. Carpick, "Toward the Ultimate Tribological Interface: Surface Chemistry and Nanotribology of Ultrananocrystalline Diamond", *Adv. Mat.*, in press (2004).

Nanotribology of Self-Mated Nanocrystalline and Amorphous Carbon Interfaces

D. S. Grierson; A.V. Sumant; K. Sridharan; E.E. Flater; R.W. Carpick

Engineering Physics, UW-Madison, Madison, WI

dsgrierson@wisc.edu

Jennifer E. Gerbi[1]; James Birrell[2]; Orlando Auciello[3,4]; John A. Carlisle[5,6]; T.A. Friedmann[5]; J.P. Sullivan[5]

1. University of Illinois at Urbana-Champaign

2. Advanced Diamond Technologies, INC

3. Materials Science Division, Argonne National Laboratory, Argonne, IL

4. Center for Nanoscale Materials, Argonne National Laboratory, Argonne, IL

5. Sandia National Laboratory, Albuquerque, NM

Keywords: nanotribology, nanocrystalline diamond, diamond-like-carbon, tetrahedral amorphous carbon, atomic force microscopy

Abstract

High performance diamond and amorphous carbon thin films are attracting interest as candidate materials to enhance the tribological characteristics of mechanical components ranging in size from the macroscale to the nanoscale. These materials have been studied extensively at the macroscale, and the resulting tribo-mechanical properties measured have been shown to be excellent. However, at the micro- and nanoscale, little is known about the tribological properties and how they are affected by the chemical environment. By studying specific forms of self-mated diamond and amorphous carbon materials at the nanoscale, we have gained fundamental insights into how differences in bonding structure, film microstructure, surface chemistry, and chemical environment produce different nanotribological behavior. We have investigated three carbon-based thin film materials: ultrananocrystalline diamond (UNCD)[1], diamond-like-carbon (DLC)[2,3], and tetrahedral amorphous carbon (ta-C)[4]. To investigate the surface properties, we have conducted extensive surface characterizations studies using surface spectroscopy and surface microscopy techniques. To understand the surface chemistry of these materials, we utilize near edge x-ray absorption fine structure (NEXAFS) spectroscopy to determine the chemical composition and the nature of the bonds at the surface. To understand the corresponding nanotribological properties, we utilize the atomic force microscope (AFM) to measure the work of adhesion and the frictional forces for self-mated interfaces of the materials of interest. This involves a significant and novel effort to create custom-made AFM tips coated or fabricated from the carbon-based materials under study. Consequently, we find that the nanotribological properties depend sensitively on the surface chemistry and bonding. In the case of UNCD, we can reach the van der Waals' limit of adhesion by terminating the surface with hydrogen, and we find that adhesion and friction are lower than for silicon self-mated interfaces. For DLC, we find that as relative humidity increases, friction increases monotonically, but the work of adhesion remains constant. We also find that dopants (specifically, fluorine and silicon) affect nanoscale friction and adhesion of DLC. The results from the ta-C studies demonstrate how bonding structure and nanotribological properties of the film can be correlated. We will discuss how our results can be used to tailor the surfaces of these carbon-based materials to optimize their tribological response.

Part of this work was funded by Sandia. Sandia is a multiprogram laboratory operated by Sandia Corporation, a Lockheed Martin Company, for the United States Department of Energy's National Nuclear Security Administration under contract DE-AC04-94AL85000. Part of this work was also supported by the US Department of Energy, BES-Materials Sciences, under Contracts DE-FG02-02ER46016 and W-13-109-ENG-38.

REFERENCES

1. A.V. Sumant, D.S. Grierson, J.E. Gerbi, J. Birrell, U.D. Lanke, O. Auciello, J.A. Carlisle, and R.W. Carpick Toward the Ultimate Tribological Interface: Surface Chemistry and Nanotribology of Ultrananocrystalline Diamond, **Adv. Mat.**, in press (2004).

2. K. Sridharan, S. Anders, M. Nastasi, K.C. Walter, A. Anders, O.R. Monteiro, and W. Ensinger, Non-Semiconductor Applications of Plasma Immersion Ion Implantation & Deposition, **Handbook of Plasma Immersion Ion Implantation & Deposition**, publisher John Wiley & Sons, New York, September 2000, pp. 553-636.

3. K. Sridharan, E.H. Wilson, D.F. Lawrence, and J.R. Jacobs, Application of Hydrocarbon Plasmas for Modifying Near-Surface Characteristics of Bearing Steel, **Applied Surface Science**, 222, 2004, p. 208.

4. T. A. Friedmann, J. P. Sullivan, J. A. Knapp, D. R. Tallant, D. M. Follstaedt, D. L. Medlin, and P. B. Mirkarimi, Thick stress-free amorphous-tetrahedral carbon films with hardness near that of diamond***, Appl. Phys. Lett***. 71, p. 3820 (1997).

FRACTURE STRENGTH OF MULTI-WALL CARBON NANOTUBES

Weiqiang Ding, Lorenzo Calabri, Xinqi Chen, Kevin Kohlhaas, Rodney S. Ruoff*

Department of Mechanical Engineering, Northwestern University, Evanston, IL 60208

Nicola Pugno

Department of Structural Engineering, Politecnico di Torino, Corso Duca degli Abruzzi 24, 10129, Italy

Keywords: tensile test, carbon nanotube, fracture mechanics

Abstract

Arc-grown multi-wall carbon nanotubes (MWCNTs) were studied with tensile loading experiments inside an scanning electron microscope (SEM) with a home-built nanomanipulator[1]. Individual MWCNT was clamped between two opposing AFM cantilever tips, and a newly developed and rapid electron beam induced deposition method[2] was used to make the clamps. An increasing tensile load was applied to the nanotube through cantilever deflection induced by the controllable bending of the piezo multi-layer bender with a DC bias. High-resolution SEM images were acquired at each loading step. Two independent methods of analysis of each image were used to obtain the corresponding tensile load. The MWCNTs eventually fractured with increasing tensile load, typically in a sword-in-sheath manner (Figure 1). The MWCNT diameters were measured by TEM after the tests (Figure 2). The stress *vs* strain, Young's modulus, and tensile strength of the MWCNTs were obtained through data analysis.

The measurements strongly suggest the presence of defects in the tested nanotubes. Assuming defects like clusters of adjacent vacancies (e.g., atomistic blunt cracks) the experimental evidence is rationalized by applying Quantized Fracture Mechanics[3].

We gratefully acknowledge the grant support from the NSF (#020079; #030450); ONR #N000140210870 (support for W. Ding), and NASA BIMat URETI # NCC-1-02037(support for X. Chen).

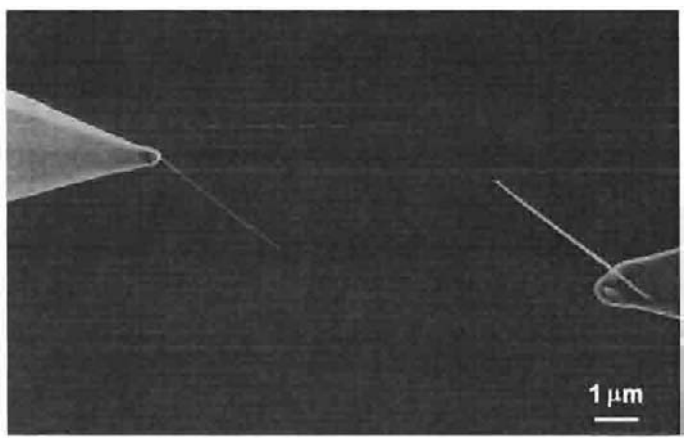

Figure 1. Sword-in-sheath failure of a MWCNT under tensile load

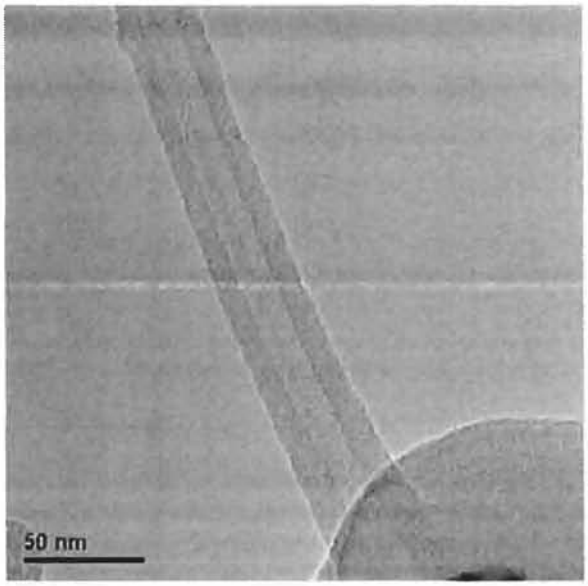

Figure 2. TEM image of a fractured MWCNTs attached to AFM tip.

REFERENCES

1. M. F. Yu, et al, "Three-dimensional manipulation of carbon nanotubes under a scanning electron microscope", *Nanotechnology,* **10,** 244-252 (1999).
2. W. Ding, et al, "Clamping nano-structures using electron beam induced deposition", *J. Appl. Phys.*, **submitted** (2004).
3. N. M. Pugno and R. S. Ruoff, "Quantized fracture mechanics",*Philosophical Magazine*, **84,** 2829-2845 (2004).

MECHANICS OF CARBON NANOPLATES

Hyun Woo Shim, L. G. Zhou, and Hanchen Huang

Department of Mechanical, Aerospace & Nuclear Engineering, Rensselaer Polytechnic Institute

110 8th Steet, Troy, NY 12180, USA

Keywords: Diamond, Surface Reconstruction, Nanoplates, Mechanical Properties

Abstract

We report the mechanics of carbon nanoplates, particularly their variable elastic constants (or moduli). Using a combination of molecular statics and density functional theory based ab initio calculations, we show that (1) the elastic moduli of carbon nanoplates vary with their thickness; (2) the variation depends on surface reconstruction; and (3) the variation depends on alignment of atomic bond chains. Through contrast and comparison with silicon nanoplates, face-centered-cubic nanoplates, body-centered-cubic nanoplates, and hexagonal-close-packed nanoplates, our studies reveal several controlling factors of the elastic moduli. They are the bond loss, the bond saturation (or electron redistribution), the surface reconstruction, and the atomic bond chain alignments on surfaces.

NANO FOUNTAIN PROBE FOR SUB-100 NM FOUNTAIN-PEN WRITING

Keun-Ho Kim, Nicolaie Moldovan and Horacio D. Espinosa

Department of Mechanical Engineering, Northwestern University, Evanston, IL 60208

Keywords: atomic force microscopy, dip pen nanolithography, fountain pen nanolithography.

Abstract

A microfluidic atomic force microscope (AFM) probe has been developed to achieve sub-100 nm patterning in a fountain-pen fashion. This probe chip, called nano fountain probe (NFP) chip, consists of a volcano like dispensing tip, integrated microchannels, and an on-chip reservoir. Features of as small as 40 nm wide have been patterned with an ink solution fed in the reservoir to experimentally demonstrate the feasibility of sub-100 nm patterning in fountain-pen mode. Direct-writing of alkane thiols as ink molecules on Au surfaces has been used to pattern self-assembled monolayers (SAM) as is used in dip pen nanolithography (DPN). Integration of alternative tip materials such as diamond or silicon carbide will be pursued to improve wear resistance of the tip for longer probe lifetime.

INTRODUCTION

Dip-pen nanolithography (DPN) is a maskless, direct-write means to transfer molecular ink coated on a tip, which is located at the free end of an AFM cantilever, to a substrate [1]. Feature sizes less than 15 nm are routinely generated by molecular self assembly of the ink on the substrate. One of the limitations in the DPN technique is the need for replenishing molecular inks if exhausted. Nano fountain probe is an AFM probe with integrated microfluidic system that allows continuous ink feeding in DPN. This probe is configured on a single chip that can be mounted in commercially available AFMs (Figure 1) [2, 3]. Ink solution is fed onto the on-chip reservoir and capillary action drives the solution through the microchannel to reach the dispensing tip (Figure 1).

EXPERIMENTS

Ink delivery from the on-chip reservoir through the microchannels was investigated by filling the reservoir with a solution containing alkane thiols, and subsequently observing the channels using a transmission microscope. Writing and imaging capabilities were also tested through patterning and imaging alkane thiol SAMs on Au surfaces.

Microfluidics: reservoir to microchannel

A solution of 16-mercaptohexadecanoic acid (MHA) in ethanol was fed to the on-chip reservoir. The optical micrograph shows that the channels are completely filled with the solution (Figure 2).

Writing and imaging

Patterns with line widths as small as 40 nm have been successfully generated using a nano fountain probe. In this experiment, the ink, a solution of MHA in ethanol at concentration of 1 mM, was supplied via the on-chip reservoir to the dispensing tip by capillary action. After the tip was brought into contact with a gold substrate, the molecules were transferred to the substrate creating features as the tip was laterally moved along a pre-programmed pattern (Figure 2b).

CONCLUSIONS

Nano fountain probes have been microfabricated for fountain-pen mode patterning. The functionality of the microchannel of the probe has been experimentally demonstrated. Writing and imaging experiments show the feasibility of sub-100 nm patterning in fountain-pen mode.

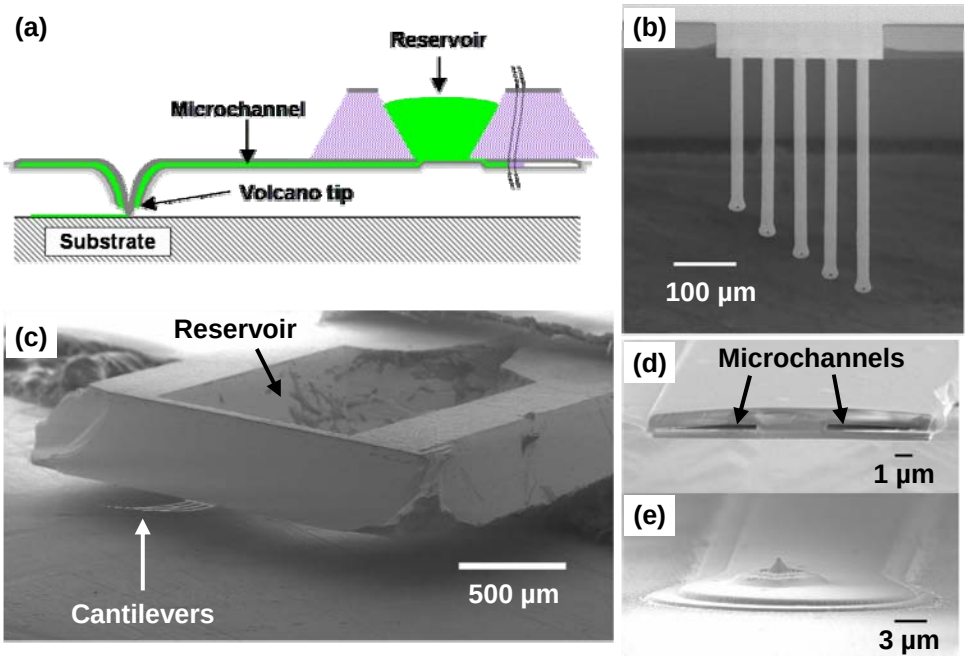

Figure 1. (a) Schematic of the device. With an ink solution placed on the reservoir, the solution fills the channel by capillary action to reach the end of the dispensing tip. Molecules are transferred by diffusion from the liquid interface to a substrate through diffusion process and water meniscus. Scanning electron micrographs of (b) five nano fountain probes on the chip, and (c) the reservoir side of the chip. Scanning electron micrographs of (d) cross-section of a cantilever showing embedded microchannels, and (e) a volcano tip at the end of the cantilever.

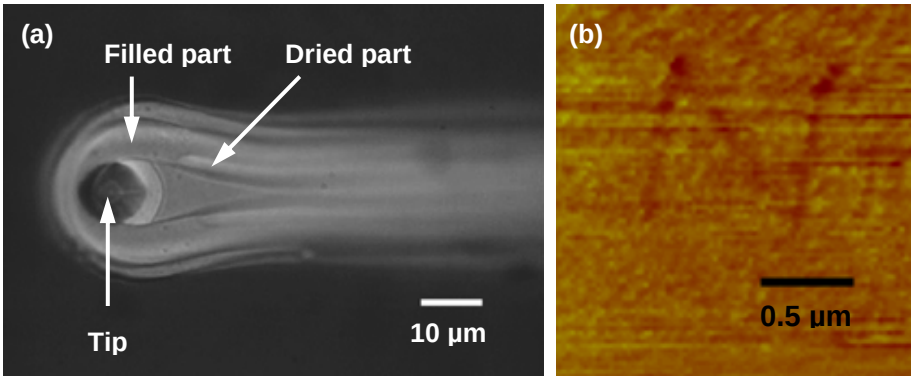

Figure 2. (a) Optical micrograph of a cantilever with a microchannel defined along the edge and a dispensing tip. The image was taken when the solution started to dry to make the filled part distinguishable. (b) Lateral force image of MHA molecules deposited onto a Au substrate by the nano fountain probe. The line width of the pattern is 80 nm. Both writing and imaging were performed with the same probe.

REFERENCES

1. Piner, R. D., et al., "Dip-Pen Nanolithography," *Science*, Vol. 283, 661-663 (1999).
2. Kim, K.-H., et al., "Massively Parallel Multi-Tip Nanoscale Writer with Fluidic Capabilities - Fountain Pen Nanolithography (FPN)," *Proc. of the 2003 SEM Annual Conference and Exposition on Experimental and Applied Mechanics*, Society of Experimental Mechanics, June 2–4, Charlotte, NC, 235-238 (2003).
3. Kim, K.-H., et al., "A Novel AFM Chip for Fountain Pen Nanolithography - Design and Microfabrication," *Materials Research Society Symposium Proceedings*, Vol. 782, Materials Research Society, December 1-5, Boston, MA, A5.56 (2003).

SESSION 5

APPLICATIONS/DEVICES: ELECTRONICS

KEY ISSUES OF ELECTRICAL APPLICATIONS OF DIAMOND

Naoji Fujimori

National Institute of Advanced Industrial Science and Technology, Diamond Research Center
AIST TC Central 2, 1-1-1 Umezono, Tsukuba 305-8568, JAPAN

Diamond has many superior characteristics, which is promising to be applied in electrical applications. However, realized products are quite few and the volume of products is still very small. It is common sense that the difficulty of realization is caused by diamond's price. hard machinability and infantile controllability of diamond itself.

Many recent research results brought us to recognize the progress of controlling diamond quality both bulk and thin film. Additionally, the controlling of diamond surface, which gives some superior characteristics of diamond, made promising the wide application of diamond such as electron emission, bio application etc. As the result of such progress, target of development for diamond products looks hopeful because the advantage of diamond may be easily confirmed.

On the other hand, issues related on production have not yet been dissolved and choosing of development target is still very difficult caused by the hard estimation of production cost. One of the most important materials for electrical application is "wafer". As the fabrication line of diamond products may not be exception, using of wafer is the necessity, hopefully larger than 3-inch wafer. Current largest single-crystalline diamond, in commercial, is 10x 10mm and the price of it is more than 10 times than other semiconducting materials. However, we can obtain poly-crystalline wafer with the size of 2 or 3 inch and their price look reasonable. Moreover, nano-crystalline diamond gives us to obtain less expensive wafer if you do not need finished surface.

Micro machining technology of diamond has progressed in these several years by using of dry etching process and the nano-scale diamond can be obtained. However, macro-scale machining, such as polishing and cutting, is still very hard and costly. Thus, the fabrication process of diamond devices looks to be incomplete.

The author will summarize current status of electrical application of diamond and will present the target of development for real production process.

HIGH PERFORMANCE MISFET USING HIGH-MOBILITY SUBSTRATE AND ALUMINUM OXIDE GATE INSULATOR

K. Hirama, T. Koshiba, K. Yohara, H. Takayanagi, M. Satoh, H. Umezawa, H. Kawarada

Waseda university, NEDO hirama@kaw.comm.waseda.ac.jp

T. Saitoh, K Park, N. Fujimori

AIST, NEDO

Keywords: B-doped diamond, naturally oxidized Al, subthreshold characteristic, gate leakage, FET

Abstract

Diamond is expected as a next generation semiconductor for high power and high frequency applications. In this study, diamond MISFETs have been fabricated on H-terminated B-doped diamond to increase the maximum drain current and transconductance. For 1-µm-gate-length MISFETs, the high I_{Dmax} of more than 230 mA/mm and the high g_m of 65 mS/mm have been obtained. Concerned influences on drainconductance and buffer leakage are not observed. Diamond MISFETs using naturally oxidized aluminum as the gate insulator have been also demonstrated. The excellent subthreshold characteristics of 95mV/dec and the low gate leakage current less than 1E-6A/mm^2 are obtained.

1. INTRODUCTION

Wide bandgap semiconductor diamond has excellent material properties such as highest thermal conductivity (22 W/cmK), high break down field (10^7 V/cm) and low dielectric constant (5.5). Figures of merit (FOM) of diamond are extremely high. For example, Johnson's FOM of diamond is much higher than that of other materials even in wide-gap materials; that is 100, 2.6, 2.5 times of Si, SiC and GaN, respectively. Therefore diamond is expected to realize high-frequency and high-power device.

The surfaces of diamond films deposited by plasma- assisted chemical vapor deposition (PACVD) are terminated by hydrogen. The hydrogen-terminated (H-terminated) surface exhibits p-type. This H-terminated surface conductive layer is suitable for the channel of field-effect transistors (FETs) because of the following excellent properties. 1) The sheet density of holes is as high as 10^{13} /cm^2. The carrier density is constant in the temperature range from 150 K to 400 K because of the low carrier activation energy of less than 50 meV. 2) The carriers are confined in a thin subsurface region of less than 10 nm thickness. 3) The H-terminated surface exhibits a low density of surface states (less than 10^{11} /cm^2), which might be due to the termination of surface dangling bonds by the hydrogen atoms.

2. MISFETS ON B-DOPED DIAMOND SUBSTRATES

Good DC and RF performances of diamond FETs on H-terminated diamond which has the resistivity of 10kΩ/sq and mobility of 100 cm^2/V· sec have been reported. Up to now, the drain current over 200mA/mm [1] and the cut-off frequency over 20GHz [1,2] have been obtained. However, the carrier density or mobility of H-terminated diamond films are difficult to control. In addition, due to the shallow channel of the surface conductive layer, the maximum current density of the FETs reaches MA/cm^2, this large current density decrease reliability of the diamond FETs. In this study, we developed the diamond MISFETs on H-terminated B-doped films to improve the transconductance and the maximum drain current by means of increase of the channel mobility and the thickness of the current flow.

Diamond MISFETs using calcium fluoride (CaF_2) as a gate insulator are fabricated on H-terminated lightly B-doped diamond films. The carrier concentration, film thickness and Hall mobility of the film are 5×10^{14} cm^{-3}, 200nm, 379 cm^2/V· sec, respectively. The DC output characteristics of a 1µm gate length MISFET is shown in Figure 1. The maximum measured drain current is I_{Dmax} = 230mA/mm at V_{GS} = -3V. The maximum g_m is 65mS/mm. Those values are relatively high for 1µm gate length MISFETs. For this device because the aspect ratio of the gate length to B-doped layer thickness is 5, which value is enough to suppress the short channel effect for GaAs devices, serious buffer leakage doesn't occur. In saturation region, high g_m/g_d ratio of 130 is obtained due to the low drainconductance of 0.5mS/mm. The cut-off frequency and the maximum frequency of oscillation of the 1µm gate length MISFET are, respectively 4GHz and 10GHz, respectively.

3. MISFETS USING NATURALLY OXIDIZED ALUMINIUM

For high power transistor application, reduction of the gate leakage current is important to improve efficiency, self-heating and reliability. High-k and stable gate insulator is needed to reduce the gate leakage current. Recently, new gate insulator materials such as aluminum or hafnium oxides are well researched for next generation CMOS application. However, these oxide insulators have generally high melting point (>1800°C) and are deposited by sputter coater or chemical vapor deposition. To prevent surface damage such as oxidation or defects, which make the resistivity of H-terminated surface high, these processes cannot be adapted diamond MISFET fabrication process. The natural oxidized aluminum is one of the promising gate insulator materials to meet the problems.

Evaporated aluminum on H-terminated undoped diamond film is oxidized in oxygen environment at room temperature. Using aluminum as a gate electrode, a 0.5µm gate length diamond FETs are fabricated. Figure 2 shows subthreshold characteristics at V_{DS} = -50mV. The minimum subthreshold factor is 95mV/dec, which value is one of the best for sub-micron gate diamond MISFETs at present. The gate leakage current is as low as 1E-6A/mm^2 without dependence on polarity of gate swings, indicating the naturally oxidized gate insulator suppress the gate current.

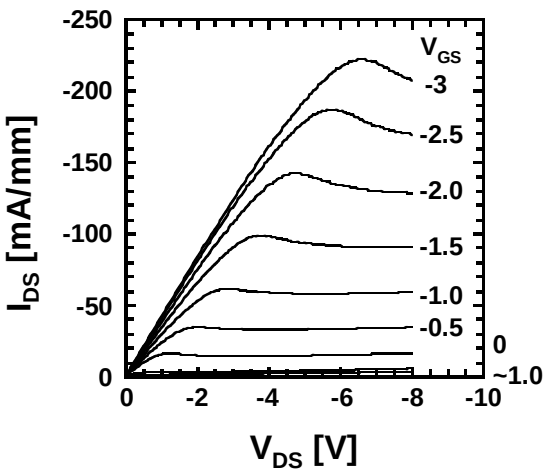

Figure 1. DC output characteristic of a 1µm gate length MISFET with 50nm CaF_2 gate insulator.

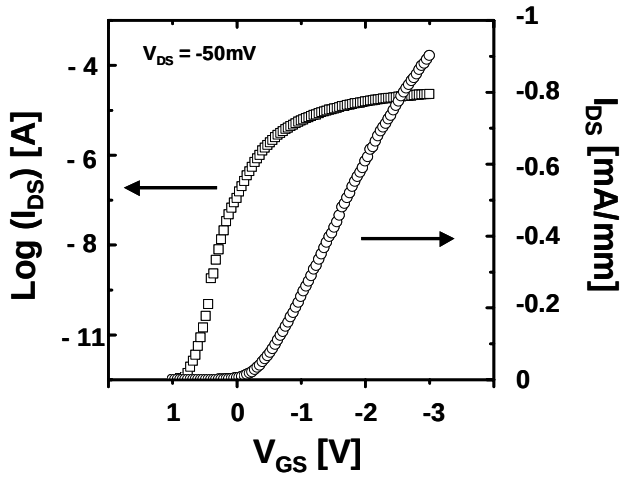

Figure 2. Subthreshold characteristics of a 0.3µm gate length MISFET with 8nm naturally oxidized Al as gate insulator.

REFERENCES

1. M. Kubovic, M. Kasu, et al, "Microwave Performance Evaluation of Diamond Surface Channel FETs" *Diamond and Related Materials*, Vol. 13, No. 4-8, pages 755-760(2004).

2. H. Umezawa, S. Miyamoto, et al, "RF Performance of Diamond Surface-Channel Field-Effect Transistors" *IEICE*, Vol. E86-C, No. 10, pages 1949(2003).

CARBON NANOTUBES AS A COLD ELECTRON BEAM SOURCE FOR PSEUDOSPARK PLASMA SWITCHES AND PULSED POWER APPLICATIONS

Yonhua Tzeng, Hulya Kirkici, Chao Liu, Chris Seymore, An-Jen Cheng, Yu-Chun Chen, Kalyan Koppisetty and Hyungwook Kim

Department of Electrical and Computer Engineering
Auburn University
Auburn, Alabama 36849 USA

Keywords: Pseudospark, Plasma Switches, Carbon nanotubes, Cold Cathodes

Electron beam generated by a carbon nanotube coated cold cathode was used to control a pseudospark plasma switch for high-voltage and high-current pulsed power applications. A pseudospark switch operating at pressures of 10-30 mTorr has been designed and tested successfully.

Pseudospark plasma switches operate at low pressure-gap distance (p-d) products on the left hand side of a Paschen curve, like a thyratron tube, but have a much simpler construction (See Figure 1). Unlike streamer electrical breakdown in high pressure arcs that can cause often severe localized electrode erosion, pseudospark causes less electrode erosion while maintaining the capability of withholding high voltage and delivering high current. A pseudospark switch consists of two conductive metal electrodes in the shape of cups with holes at the center and surrounded by a good electrical insulator. The empty areas within the device contain gas at low pressures, typically between 25 and 100 mTorr. The typical dimensions of the holes and the spacing between the electrodes are between 2-5 mm. As the pressure drops and the p-d product decreases further towards the left-hand side of a Paschen curve, the mean free path for electron collisions with gas particles increases, the probability for electron impact ionization of gas particles in the 2-5 mm gap between two electrodes decreases, and a spark does not form in the gap between the two electrodes. Instead, a discharge may occur between the inside surfaces of the two hollow cup-shaped electrodes and flows through the holes at the center of the electrodes.

In order to convert the pseudospark gap into a good electrical switch to withhold high voltage and deliver high current an effective method for precise control of the switch is needed. These methods aim at releasing as large as possible a number of electrons inside the hollow cathode or near the volume between the cathode and the anode so that these electrons can multiply rapidly by electron impact ionization of gas particles under the acceleration by a very strong electric field. Electron multiplication causes plasma to be initiated, allowing the transition of the gas from its insulating state to the conducting state so that electrical current can flow with little resistance.

To optimize the operation of a compact high-voltage and high-current switch for repetitive pulsed power generation, a high-performance switch must have (i) low statistical delay jitter so that multiple switches can operate in parallel with precise timing, (ii) low delay time for fast turn-on of the switch, (iii) high repetitive rate, and (iv) a long life for the switch.

A Pseudospark switch with a carbon nanotube coated cold cathode as an electron beam source for controlling the switch is shown in Figure 1 (a). It consists of two conductive metal cups, which serve as two electrodes of the switch, with 3 mm diameter holes drilled at the center of the cups. The dimensions of the cups are 15 mm high and 18 mm in diameter. The copper cups are surrounded by a quartz tube with bottoms of the cups facing each other and having a gap between these two electrodes about 2 mm wide. A voltage is applied between the lower cup (the anode) and the top cup (the grounded cathode). The cathode is closed up with an aluminum plate with a 1 mm diameter hole to allow the injection of electrons into the hollow cathode. The cold cathode is a piece of silicon coated with thermal CVD multi-wall carbon nanotubes which are separated from the grounded aluminum plate by glass spacers of 350μm thick. The hole in the aluminum plate can be either aligned with the holes in the metal cups along the axis of the device or off-set by a distance.

Gas was fed into the Pseudospark to establish the desired gas pressure while the carbon nanotube coated cold cathode was maintained at a lower pressure by means of differential pumping through the 1 mm diameter hole on the aluminum plate that separates the carbon-nanotube cold cathode and the hollow cathode. The setup is pumped down to a base pressure of about 1×10^{-6} Torr before gas is fed into the Pseudospark gap. The gas flow rate is varied and the gas pressure inside the Pseudospark gap changes as a result between 10 and 40 mTorr.

Shown in Figure 1 (b) are the minimum electron beam current that is required to turn on a test pseudospark filled with argon gas as a function of the voltage applied between the hollow cathode and the anode. The required electron beam current injected from a carbon nanotube cold cathode for triggering the switch is only hundreds of nano-Amperes for an applied voltage well below the typical self-breakdown voltage of a Pseudospark. This electron current decreases with increasing applied voltage. Unlike thermionic electron sources, carbon nanotube cold cathodes do not need additional heating for electron emission and allow simplified design of the switch as well as little delay time. Moreover, the electron beam source is capable of providing a large supply of initiatory electrons, which help to reduce the statistical delay time (jitter) of the switch. This is highly desirable for fast and precise control of plasma switches.

In summary, application of carbon nanotube coated cold cathodes for high-voltage, high-current, plasma switches for pulsed power applications is reported. The demonstrated cold cathode triggered Pseudospark switch is free from severe thermal management difficulties unlike switches relying on thermionic electron emission for triggering, requires only a low voltage and a low electron current emitted from carbon nanotubes for turning on a high-voltage switch, and is very compact while potentially capable of controlling a very high-voltage when gases such as hydrogen instead of argon used for this test device are used to fill the switch, e.g. 100 kV, and high-current, e.g. 100 kA, pulsed power system using a stacked and parallel connected multiple Pseudospark switch package.

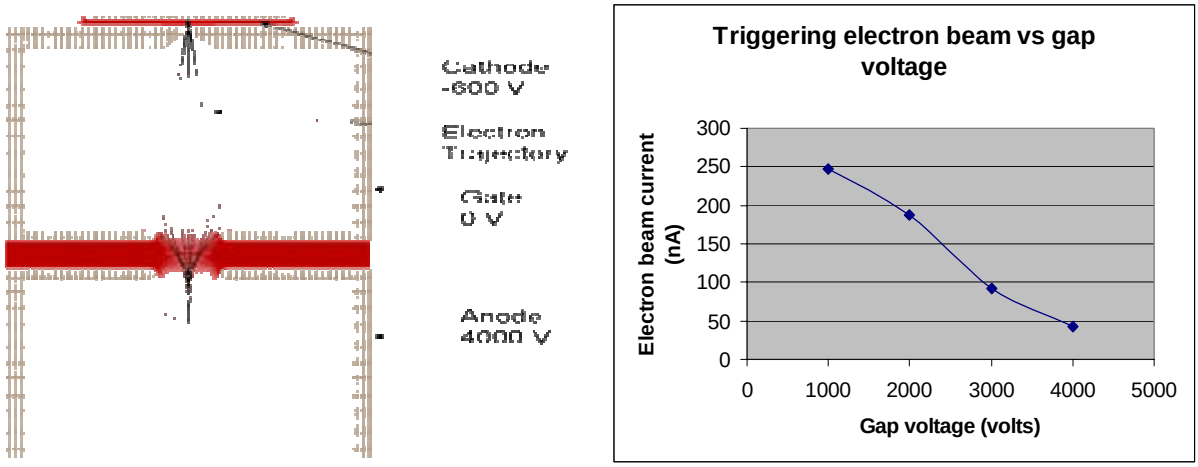

(a) (b)

Figure 1. (a) Schematic representation of a pseudospark switch and the computer simulated electron trajectories and electrical potential contours. (b) Electron beam current supplied by the carbon nanotube coated cold cathode that was required to turn on the pseudospark switch filled with argon gas at 30 mTorr at an applied voltage between 1kV and 4 kV.

Nanocrystalline Diamond pn - Structure grown by Hot-Filament CVD

T. Zimmermann*, K. Janischowsky, A. Denisenko, M. Kubovic, E. Kohn
University of Ulm, Department of Electron Devices and Circuits, Germany
*-tom.zimmermann@ebs.e-technik.uni-ulm.de

D.M. Gruen
Materials Science Division, Argonne National Laboratory, USA

Keywords: HFCVD, diamond, NCD, pn structure, diode

Abstract

Conducting diamond is generally p-type doped by boron, n-type doping still being hindered by very high activation energies. Thus, the lack of shallow donor doping has prohibited the realization of diamond bipolar structures of technical relevance. In contrast, ultra-nano-crystalline diamond (UNCD) can be n-type doped with low activation energy [1]. In the past, such n-type UNCD films have been deposited onto p-type single crystal diamond resulting in highly rectifying pn-diode characteristics [2].

The question addressed in this investigation is the following: can n-type conduction also be obtained in NCD layers with grain sizes in the order of 10 nm up to 100 nm, which is a commonly used material grown by MPCVD as well as HFCVD on large area surfaces. In contrast to UNCD, where Ar and C_2 are mostly used as precursors, NCD is normally grown by CH_4-chemistry and α-parameter engineering. Nitrogen is used in some cases, however mostly to adjust the α-parameter, not for n-type doping. If n-type doping of NCD can be obtained, this may allow in conjunction with boron doping to fabricate pn-junctions entirely in NCD.

In this study such a pn-doped structure has been grown by HFCVD (on Si). After nucleation by BEN a highly insulating NCD layer has been grown in a $H_2/CH_4/N_2$ mixture, serving as buffer layer. A p^+ contact layer was then deposited in a H_2/CH_4 mixture with boron added as trimethyborate. The active layer was created by a nominally undoped i-layer with an un-intentional boron background concentration in the order of 10^{18} cm^{-3}. This active layer has then been covered with a heavily nitrogen doped NCD layer.

Hall measurements of the heavily n-type doped NCD layer resulted in clear n-type conduction with an electron concentration of 3 x 10^{19} cm^{-3} and an electron mobility of approx. 7 cm^2/Vs, similar of what has been observed for UNCD. Hall analysis of the p^+ contact layer resulted in a hole concentration of approx. 6 x 10^{20} cm^{-3} and a hole mobility of approx. 0.6 cm^2/Vs. Thus in fact a pn-junction has been created. First diode IV-characteristics are indeed rectifying (see fig. 1). In attempt to compare these characteristics with the case of a single-crystal / nano-crystal junction [2] will be presented.

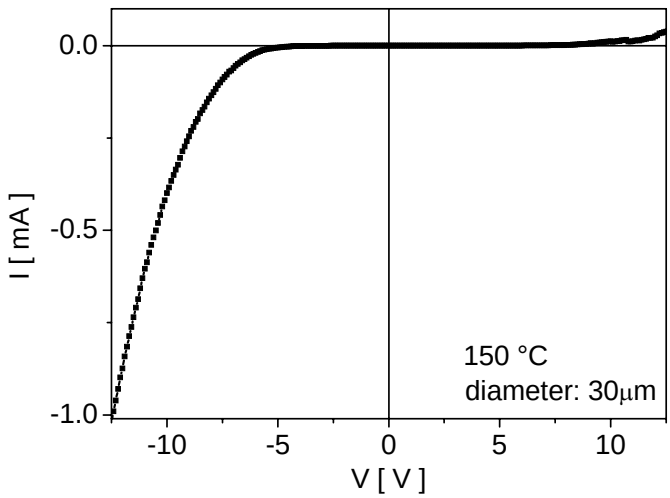

Figure 1. IV characteristics of NCD pn structure

References

1. Williams, O.A.; Curat, S.; Jackman, R.B.; Gerbi, J.E.; Gruen, D.M.: "n-type conductivity in ultrananocrystalline diamond films", *Applied Physics Letters*, vol. 85, no. 10, p. 1680-1682, 2004
2. Zimmermann, T.; Kubovic, M.; Denisenko, A.; Williams, O.A.; Gruen, D.M.; Kohn, E.: "UNCD/Diamond Heterostructure Diode", *15th European Conference on Diamond, Diamond-Like Materials, Carbon Nanotubes, Nitrides & Silicon Carbide*, 10.6, Italy, 2004

ELECTRICAL PROPERTIES OF THIN NANOCRYSTALLINE DIAMOND BASED STRUCTURES

Mitchell D. Parr and Donnie K. Reinhard

Department of Electrical and Computer Engineering and Fraunhofer Center for Coatings and Laser Applications, B100 Engineering Research Complex, Michigan State University, East Lansing, MI 48824

Keywords: nanocrystalline diamond, thin films, diodes, electrical properties.

Abstract

Electronic structures based on thin films of nanocrystalline diamond are described as well as their electrical properties. Polycrystalline diamond films with thickness between 0.25 μm and 1.0 μm and with average grain sizes of 300 nm and less are formed by microwave plasma assisted chemical vapor deposition. Electrical properties of free standing diamond films and of substrate mounted films are measured over a wide range of voltages with two-terminal electrical contacts to the growth side and nucleation side of the film. Depending on the type of electrical contacts, the rectification ratios of two-terminal structures range from 1 to 11,000.

INTRODUCTION

Thin diamond membranes and free-standing sheets are of interest for a variety of potential applications. A recent report has described methods for obtaining flexible free-standing diamond films that can be applied to a variety of substrates, and mechanical properties of such films.[1] Given the potential advantages of diamond for electronics, such diamond films may be considered as flexible materials for electronic applications. This paper describes initial experiments on the electrical properties of structures based on these films.

EXPERIMENTAL METHODS

The undoped diamond films were deposited by microwave plasma assisted chemical vapor deposition on p-type silicon wafers that had been nucleated by polishing with diamond powder. The resulting film thickness ranged from 0.25μm to 1 μm and rms surface roughness values ranged from approximately 15 nm to 25 nm. After diamond deposition, post processing was used to form 2-terminal electrical structures with one electrical contact on the growth side and the other on the nucleation side of the film.

Metallization studies in this work included indium, gold, titanium/gold, graphite based paint, zirconium, silicon, and pressure contacts against tungsten, platinum, and stainless steel. A variety of sample configurations were investigated. Metallization was performed on diamond film supported on the original silicon substrate and also on free-standing diamond. For the latter, the silicon substrate was removed by back etching and the diamond film was transferred to a different structure. An example of a two terminal structure using a free-standing diamond film is shown in Fig. 1. In this case, metallization on both sides of the film is by means of semi-transparent gold contact and the diamond film is approximately 1 μm thick.

RESULTS

The current voltage characteristics of structures such as shown in Fig. 1 are symmetrical, or nearly symmetrical for positive and negative voltages. At low electric fields the characteristics are linear with a slope corresponding to a conductivity of 1.1 x 10-^{11} (Ω-cm)$^{-1}$. At high electric fields, the conductance is electric field activated and well-modeled by the Poole-Frenkel equation as

$$\sigma = \sigma_{00} + \sigma_0 e^{\alpha E} \qquad [1]$$

with σ_{00} = 1.1 x 10^{-11} (Ω-cm)$^{-1}$ and α = 1.0 x 10^{-5} cm/V. Thus, while the structure is highly resistive at low applied bias, appreciable current can flow at higher biases.

Fig. 2 shows an example of the current-voltage characteristics for a rectifying device, in this case a structure with a Zr contact (diameter = 450 μm) on the growth surface of a 0.25 μm thick diamond film still attached to the p-type silicon substrate. With negative voltage on the Si electrode, small reverse-biased currents are observed. With

sufficient positive voltage on the Si electrode the field activated conductance is sufficient to allow appreciable forward current with a rectification ratio ($I_{FORWARD}/I_{REVERSE}$) of 1.1 x 10^4 at a bias of 80 V. The saturation at 20 mA seen in Fig. 2 is due to the current limitations of the measuring device.

SUMMARY

Two terminal electric structures that incorporate undoped nanocrystalline diamond have been investigated with symmetric and asymmetric electrodes and with free-standing films and substrate attached films. With rectifying electrodes, significant rectification ratios can be observed at high bias due to field activated conduction in the diamond.

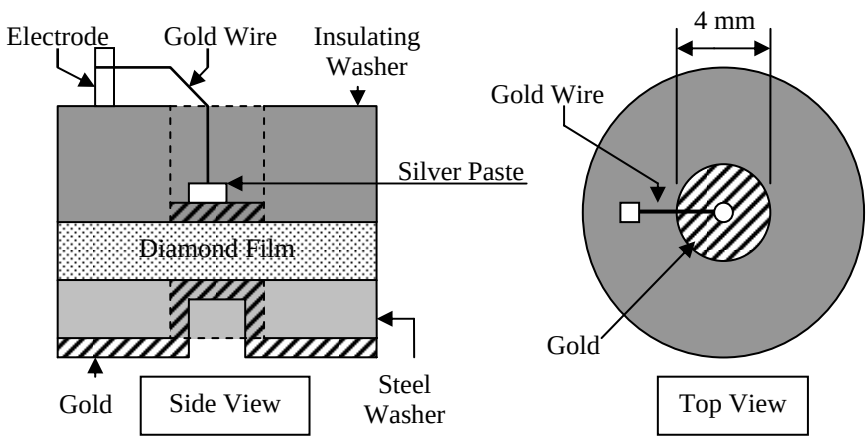

Figure 1. Example of free-standing, diamond film structure with symmetric gold contacts.

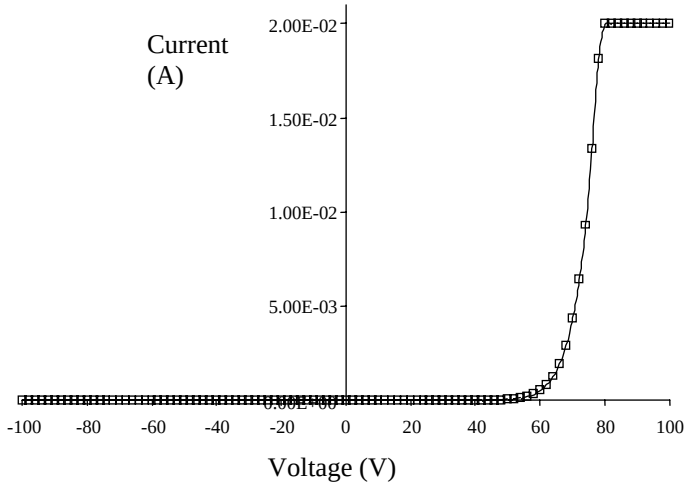

Figure 2. Example of current-voltage characteristics of a rectifying structure with asymmetric contacts consisting of Zr/diamond/Si (positive polarity relative to silicon).

REFERENCES

1. Reinhard, D. K., et al. "Fabrication and Properties of unltranano, nano, and microcrystallilne diamond membranes and sheets", *J. Vac. Sci. Tech. B*, in press.

FORMATION OF JUNCTIONS AND DEFECTS IN CARBON NANOTUBES

Fan-Yan Meng, San-Qiang Shi*

Department of Mechanical Engineering, The Hong Kong Polytechnic University
Hung Hom, Kowloon, Hong Kong

Long-Guang Zhou

Department of Mechanical, Aerospace & Nuclear Engineering, Rensselaer Polytechnic Institute
110 Eighth Street, Troy, NY 12180, USA

Rui Yang

Institute of Metal Research, Chinese Academy of Sciences
72 Wenhua Road, Shenyang, P.R. China 110016

Keywords: junctions, defects, size effect, carbon nanotubes.

Abstract

Future generation of electronic devices made by carbon nanotubes may critically depend on how the junctions between different nanotubes can be manufactured. Thin single-walled carbon nanotubes (SWNTs) could be welded together by heating to form molecular multiterminal junctions at elevated temperature without initially introducing structural defects such as vacancies and interstitials. This was demonstrated by classical molecular dynamics calculations with empirical Brenner potential to simulate the dynamic formation pathway of junctions between crossing nanotube pairs. Junctions are established through forming new intertube sp^3-like covalent bonds, followed by breaking up bonds in the original nanotubes. The final configuration of junctions depends on the diameter of SWNTs, chirality of the crossing tube pairs, initial intertube distance and temperature. The size of SWNTs also affects the minimum temperature for junction formation. The larger the diameter, the higher the welding temperature will be needed. Formation energies of X-shaped junctions have been systematically studied, which shows clearly a size effect. This size effect may be due to the strain energy of small nanotubes and the energy required for defect formation in SWNTs. For example, the formation energy of a Stone-Wales (SW) defect in SWNTs is a function of the diameter of SWNTs. This was demonstrated by a first principle calculation based on the extended Hückel method. The formation energy of SW defects was fitted to a simple formula as a function of the tube radius and the orientation of a SW defect in the tube, which provides a convenient tool for the study of thermodynamics and kinetics of SW defects in SWNTs. This work was partially supported by research grants from The Hong Kong Polytechnic University (A-PE54) and Research Grand Council of Hong Kong (PolyU 5306/03E).

*Corresponding author: mmsqshi@polyu.edu.hk

SESSION 6

APPLICATIONS/DEVICES:
VACUUM ELECTRONICS, ELECTRON EMISSION, & ELECTRONICS

ROBUST AND REGENERABLE CARBON NANOTUBE FIELD EMITTER ARRAYS WITH INTEGRAL GATES

David S.Y. Hsu and Jonathan L. Shaw

Naval Research Laboratory , Washington DC 20375-5320 E-mail: dhsu@ccs.nrl.navy.mil

Keywords: Carbon nanotubes, CVD growth, field emitter array, integral gates, field emission

Abstract

We have grown multi-walled carbon nanotubes by chemical vapor deposition on two types of gated structures, one containing a silicon post, another having an open aperture. Threshold below 20V and emission current up to 1 mA at 40V (from 0.5 mm^2 area) have been measured. Highly stable emission with a notable lack of electrical arcing have been observed. Emission was enhanced by ambient water vapor and hydrogen and was unaffected by xenon. Operation in 10^{-4} Torr hydrogen regenerated emission many folds from emitters degraded from operation in oxygen. Electron energy distributions reveal a current saturation phenomenon at energies just below the Fermi level, suggesting a limit in electron transport at the emission site. A gate current to anode current ratio of 2.5%, the lowest of any nanotube field emitter arrays (FEAs), was measured for the open aperture configuration.

INTRODUCTION

Carbon nanotubes (cNT) satisfy many demanding requirements for field emission, including stability, long lifetime, low voltage, high current-carrying capacity and mechanical strength. A key factor to their stability as field emitters is the lack of a nonvolatile surface oxide. Surface dielectrics such as oxides on conventional metal and silicon emitters could be the main cause for FEA catastrophic destruction by trapping charge which could lead to arcing [1]. Their small diameters (2-50nm) and high aspect ratios enable the high electric field enhancement for low voltage operation, despite the relatively high work function (~5.0 eV for graphite), which affords them a high degree of chemical inertness. Gating of cNT emitters has been undertaken only within the last five years, using two general approaches of patterning cNT paste or CVD growth of cNTs inside gated structures. The use of chemical vapor deposition (CVD) allows the nanotubes to be grown in much smaller micro-gated structures, thereby enabling lower operating voltages, much higher cell packing densities and total current densities.

EXPERIMENTAL

A nanotube FEA cell of our Type I configuration consists of CVD grown nanotubes on top of a gated silicon post centered in a 2.5 micron diameter gate aperture (See fig.1 of ref. 3). The growth starts with sputter deposition of a catalyst over a silicon-on-post FEA (with blunt post tips) from MCNC[2] and its preferential removal from areas except the top region of the posts. The nanotubes are grown using hot filament-assisted[3] or DC plasma CVD using C_2H_4 or C_2H_2 with NH_3. In Type II emitter cell configuration, nanotubes were grown on the sidewall of an oxide spacer lining a gated open aperture[4] with a 1.5 micron diameter (See fig.2 of ref.4). The catalyst was removed from the top surface by glancing angle ion beam sputtering prior to nanotube growth. A single gated array consisted of up to many thousands of cells for Type I emitters and only up to 40 cells for Type II emitters. Emission measurements (current-voltage, current-time, energy distribution) were carried out under UHV conditions (base pressure 10^{-10} Torr).

RESULTS AND DISCUSSION

The absence of arcing is one of the most prominent properties we have observed for these nanotube emitters, which we believe is due to the lack of a surface dielectric. This represents a major advantage over the conventional FEAs. Nanotubes can burn out but neighboring cNTs can keep on working. We observed emission at much lower voltages than those for conventional Mo and Si tip FEAs with comparable gate aperture diameters. For example, we obtained 1 mA emission at 40 volts gate voltage from a 0.5 mm^2 area of a Type I emitter array consisting of 30,000 cells. Good emission stability with few percent short term noise has been observed.[3] However, Type I emitter arrays exhibit a significant fraction of total current in gate current (leakage and interception) due to unfavorably aligned nanotubes in the cell.

We anticipate improvement by fabrication optimization such as better catalyst placement and aligned growth.

Dosing Type I emitter with H_2O vapor increased the emission up to an order of magnitude. This enhancement effect is consistent with observations by Dean and Chalamala[5] and could be attributed to the H_2O -nanotube surface dipole, which reduced the effective work function.

The effect of operating the emitter array in Xe gas ambient is of interest for Hall effect and ion thrusters for small satellites. We operated an array of our FEAs at a pressure of 10^{-5} Torr (the pressure used in thrusters) at 33 V gate voltage in DC mode for 15 hours without degradation in emission. The main contributing factor was the low voltages enabled by nanotubes, resulting in low ion energies and negligible sputtering.

Operating the emitter arrays at temperatures up to 700C has resulted in significant enhancement in emission, likely due to thermal effects on the Schottky barrier at the nanotube-silicon interface. This effect suggests that these emitters could be used for high temperature electronics applications such as switching devices in engines.

Prominent features of measured electron energy distributions include current saturation at an energy just below the Fermi level and the lack of significant shift in the leading edges as the gate potential (or current) is changed, the latter suggesting no significant potential drop in the contact (hence a good contact). During field emission, the already very low density of states near the nanotube Fermi level could become deficient of electrons because of insufficient rates of charge transport to refill them. This condition could result in the observed emission current saturation.

Emission from Type II nanotube emitters contrasts from Type I in that the gate current is only 2.5% of the anode current, the lowest observed to date for microfabricated gated nanotube emitters. We believe a contributing factor is that nanotubes in this open aperture configuration are aligned with a large directional component toward the center of the cell. Low gate current is essential for applications requiring high emission currents to prevent gate damage from heating.

Both Type I and II emitters have produce emission enhancements up to 2 orders of magnitude by operating in 10^{-4} Torr H_2. A reduction in the slopes of Fowler-Nordheim plots suggests a reduction in the effective work function due to a H-C surface dipole. Emitters degraded from overnight operation in O_2 recovered emission 340-fold by operating in H_2. These data suggest that atomic hydrogen (created by electron impact from the emitted electrons) is responsible for the large enhancement and regeneration effect by (a) removal of oxygen-containing surface species (which may act as p-type dopants and/or increase the work function), b) formation of a surface dipole (reducing the work function), and c) n-type doping by atomic hydrogen.

CONCLUSION

Microgating carbon nanotubes has effectively exploited their superior natural properties and has manifested them in the many desirable properties required for field emission devices - lack of arcing, low voltage, high current density, and ruggedness, making nanotubes premier candidates as field emitters.

REFERENCES

1. Shaw, J. L., “Effects of surface oxides on field emission from silicon,” J. Vac. Sci. Technol. B **18**, 1817-1824 (2000).
2. Temple, D., Ball, C.A., Palmer, W.D., Yadon, L.N., Vellenga, D., Mancusi, J., McGuire, G.E., and Gray, H.F., “Fabrication of column-based silicon field emitter arrays for enhanced performance and yield,” J. Vac. Sci. Technol. B **13**, 150-157 (1995).
3. Hsu, D.S.Y. and Shaw, J., “Integrally gated carbon nanotube-on-post field emitter arrays,” Appl. Phys. Lett., **80**, 118-120 (2002).
4. Hsu, D.S.Y., “”Microgating carbon nanotube field emitters by in situ growth inside open aperture arrays,” Appl. Phys. Lett., **80**, 2988-2990 (2002).
5. Dean, K. A. and Chalamala, B. R., “Current saturation mechanisms in carbon nanotube field emitters,” **76**, 375-377 (2000).

STABILITY OF FIELD EMISSION CURRENT FROM VARIOUS CARBON NANOTUBES FILMS

Benjamin Ulmen, Adam DeConinck, Vijaya Kumar Kayastha, Jiesheng Wang, Yoke Khin Yap*

Department of Physics, Michigan Technological University, Houghton, Michigan 49931

*ykyap@mtu.edu

Keywords: carbon nanotubes, electron field emission, displays, nanotechnology

Abstract

A series of emission current measurements were taken from various types of multiwalled carbon nanotubes (MWCNTs) in order to examine the short-term stability of the substrates under electron field emission (FE) conditions. According to field emission scanning electron microcopy (FESEM), these MWCNT have various tubular lengths, diameters, and growth densities. By referring to these physical properties, we have first optimized their FE properties at vacuum (~1 x 10^{-7} mbar). Then, their current stabilities are compared for samples that are having very similar emission characters i.e. threshold electric field and maximum achievable current density. We found that the MWCNTs films grown by the catalytic thermal chemical vapor deposition (CVD) method exhibited much improved emission stability as compared to MWCNT films grown using the plasma enhanced CVD method. Both types of these MWCNTs films are having a FE threshold of ~1.2 to 1.8 V/μm. As indicated by high-resolution transmission electron microscopy (HRTEM), it was found that the quality of the MWCNTs including the graphitic order and the contents of amorphous carbon, are related to the FE current stability of the MWCNTs.

INTRODUCTION

Carbon nanotubes (CNTs) are well known for their exceptional field emission properties [1, 2]. The multitude of applications for CNT field emitters, including electron microscopy, display devices, vacuum electronics, have caused this to become an exciting and promising area of research. Before this novel material can be made ready for commercial use, stability of the devices under different field emission conditions must be considered. We have studied the degradation of the emission current from multiwalled carbon nanotubes (MWCNTs) grown over a range of conditions and by the techniques of plasma-enhanced chemical vapor deposition (PECVD) and catalytic thermal chemical vapor deposition.

Our PECVD system is a dual-RF plasma system [3, 4]. The nanotubes created by this system have potential for field emission because of the natural vertical alignment caused by the electric field. According to FESEM, these nanotubes tend to be shorter (a few microns) and thick in diameters (50-200nm). We found that the catalytic thermal CVD system can produce nanotubes capable of excellent emission currents at lower voltages [5]. These nanotubes have a higher field enhancement factor caused by their slender diameter (~5 to 10 nm).

The system we have used to make our electron field emission measurements contains several features to optimize the accuracy of the measurements. We have created a "hanging" electrode design to maintain a precise spacing without the use of dielectric material in close proximity to the sample. This minimizes dielectric current leak. The gap between the sample and the electrodes has been precisely measured by a mechanical micrometer and was found to be 315 microns after subtraction of the thickness of the sample. Having a small gap allows us greater accuracy from the relatively smaller applied voltage needed from the power supply. To ensure conductivity through the sample, we have grown all our films on low resistivity (~1ohm-cm) Si substrates with a thin deposited metallic layer to act as a barrier against formation of silicides.

RESULTS AND CONCLUSIONS

We have found that the threshold current, which we have defined as 1μA/cm^2, occurs at a lower electric field for the catalytic thermal CVD grown samples than for the PECVD grown samples, i.e. ~1.2 V/μm and 1.8 V/μm, respectively. Additionally, the short-term stability in the current is much poorer for the PECVD grown samples. Ad

indicated by HRTEM, we explain this by the inferior quality of the PECVD nanotubes. The high degree of amorphous carbon accounts for the significant drop in the emission current which initial results suggest is as much as 50% of the initial value over several tens of minutes. The CNT grown by the catalytic thermal CVD method tend to exhibit higher graphitic order and thus emission current shows signs of greater stability, although still decreasing over the course of the experiment.

ACKNOWLEDGEMENT

Y.K.Y. acknowledges supports from the Michigan Tech Research Excellence Fund and the Army Research Office (W911NF-04-1-0029, through the City College of New York).

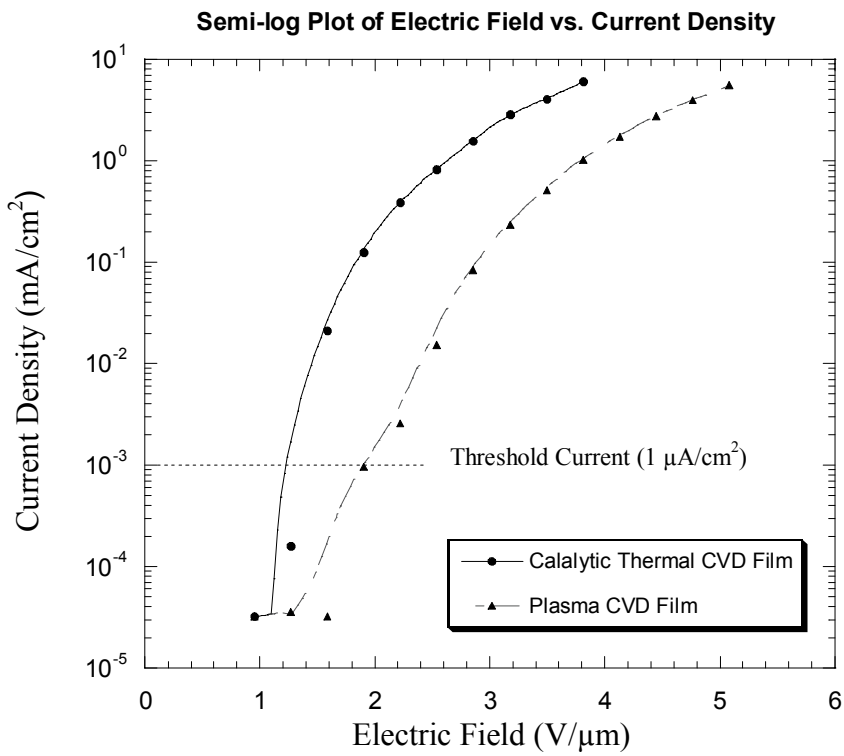

Figure 1. Catalytic thermal CVD films were found to achieve threshold currents at lower electric fields then plasma CVD films. Both types of films are capable of high emission current densities.

REFERENCES

1. de Heer, W. A.; Châtelain, A.; and Ugarte, D.: "A Carbon Nanotube Field-Emission Electron Source, " Science 270, 1179 (1995).
2. Collins, P. G.; and Zettl, A.: "A simple and robust electron beam source from carbon nanotubes, " Appl. Phys. Lett. 65, 1969 (1996).
3. Hirao, T., et al., "Formation of vertically aligned carbon nanotubes by dual-RF-plasma chemical vapor deposition," Jpn. J. Appl. Phys. 40, L631 (2001).
4. Yap, Y. K., et al., "Testing Multiwall Carbon Nanotubes on Ion Erosion for Advanced Space Propulsion," Mat. Res. Soc. Symp. Proc. Vol. 821 (2004 Materials Research Society), paper 3.7 (2004).
5. Kayastha, V., et al., "Controlling Dissociative Adsorption for Effective Growth of Carbon nanotubes," Appl. Phys. Lett. 85, 3265 (2004).

IMAGING TEMPERATURE-DEPENDENT FIELD EMISSION FROM CARBON NANOTUBEFILMS: SINGLE - *VERSUS* MULTI-WALLED

Sanju Gupta

Department of Physics and Materials Science, Missouri State University, Springfield, MO 65804-0027. E-mail address: sxg535f@smsu.edu

Y. **Y. Wang, G. M. Garguilo, R. J. Nemanich**

[2] Department of Physics, North Carolina State University, Raleigh, NC 27695-8202

Keywords: Carbon nanotubes, thermionic field emission, field emission microscopy, thermionic emission

Abstract

Fabricating small structures has almost become fashionable in the arena of both the materials science and physics of low dimensional materials. The rationale is that reducing one or more dimensions of a system below some critical length changes the systems' physical properties drastically, where nanocrystalline diamond (n-D) and carbon nanotubes (CNTs) in the class of advanced carbon materials serve model examples [1,2,3]. Emission of electrons at room temperature - cold electron emitters - are of vital importance for a variety of vacuum microelectronic devices - electron microscopes, photo multipliers, X-ray generators, lamps, flat panel displays, and microwave cathodes. Electron emitters may lead to otherwise difficult to obtain advantages in performance and/or design. This is the driving force to investigate the potential of carbon nanotubes as cold cathodes and thermionic power generators.

In this talk, field emission properties of vertically aligned single- and multi-walled carbon nanotube films at temperatures up to 1000 ^{o}C are investigated by electron emission microscopy enabling real time imaging of electron emission to provide information on emission site density, the temporal variation of the emission intensity and insight into the role of adsorbates (see Fig. 1). The nanotube films showed an emission site density of ~ 10^{4-5}/cm^2 which is compared to the areal density (from 10^{12-13}/cm^2 to 10^{8-9}/cm^2). At ambient temperature, the emission indicated temporal fluctuation (~ 6-8 %) in emission current with minimal changes in the emission pattern. At elevated temperatures, the emission site exhibited an increase in emission site intensity (see Fig.2). From the experimental observations it is proposed that the chemisorbed molecules tend to desorb presumably at high applied electric fields (*field-induced*) in combination with thermal effects (*thermal-induced*) and provide a contrasting comparison between semiconducting (single-wall) and metallic (multi-wall) nanotubes.

References

1. Gupta S., *et. al.* "Electron field-emission mechanism in nanostructured carbon films: A quest", J. Appl. Phys. **95**, 3211 (2004).

2. Gupta S., *et. al.* "Electron field emission from sulfur-incorporated nanocrystalline carbon thin films", Appl. Phys. Lett. **79**, 3446 (2001).

3. Gupta S., *et. al.* "Imaging temperature-dependent field emission from carbon nanotube films: Single - *versus* multi-walled", Appl. Phys. Lett. **86**, xx (2005).

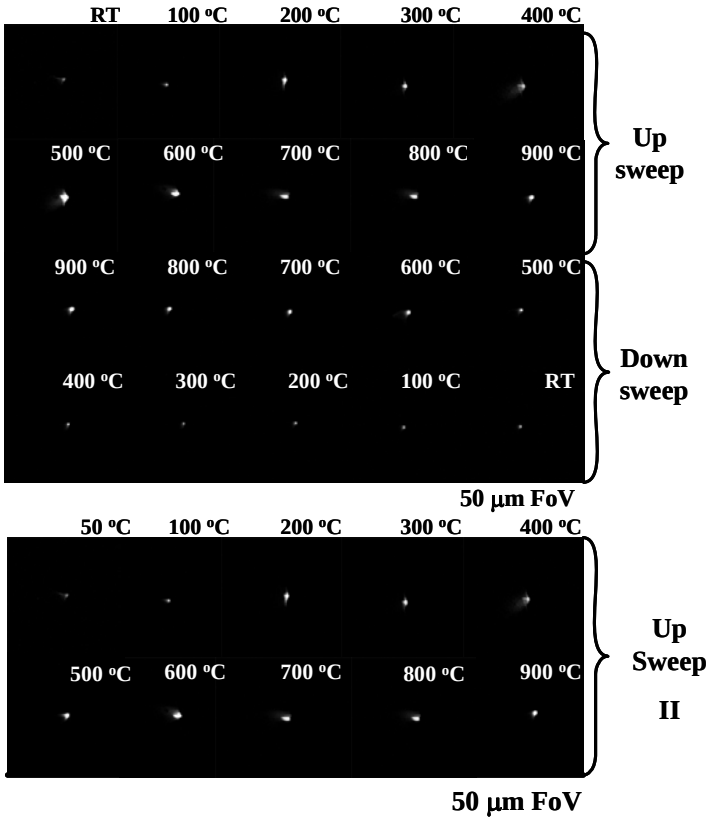

Figure 1. Temperature dependent field emission imaging for a representative multi-wall nanotube film for two warming up (Cycle I and Cycle II) and cooling down cycles. The Cycle II exhibits the thermionic field emission component in addition to field emission.

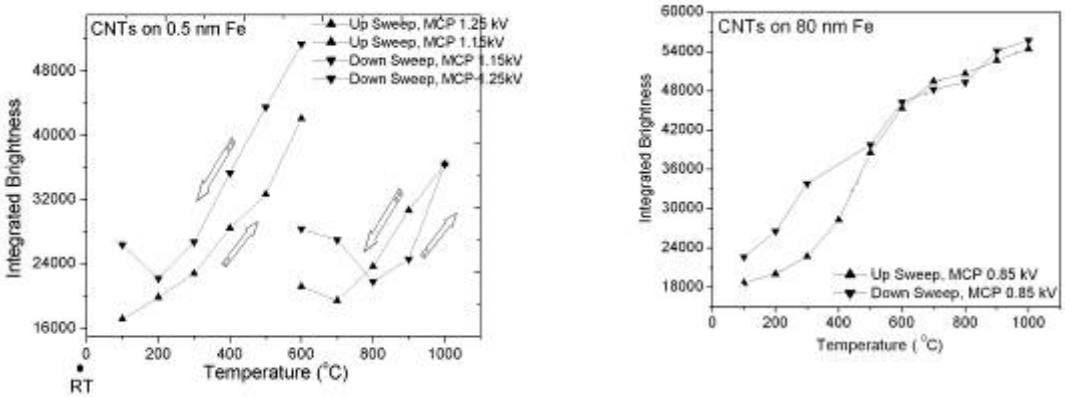

Figure 2. Variation of integrated brightness with temperature (both up and down sweep) for multi-wall nanotube films. The dotted line is used to guide eye and points at the saturation behavior.

EMISSION CHARACTERIZATION FROM NITROGEN DOPED DIAMOND WITH RESPECT TO ENERGY CONVERSION

Franz A. M. Koeck, Yingjie Tang and Robert J. Nemanich

North Carolina State University, Department of Physics, Raleigh, NC 27695

Keywords: doped diamond, thermionic emission, energy conversion

Abstract

Vacuum thermionic energy converters utilize electron emissive materials as a key component in the transformation of thermal into electrical energy.[1] A thermionic cell is comprised of an emitter held at an elevated temperature separated from a cooler collector by a vacuum gap. Energy can now be transferred from the hot to the cold side by thermionic excitation of charge carriers and an exterior electrical path allows the electrons to do work when they return to the emitter. Conventional energy converters based on flat metal surfaces were performance limited due to high operating temperatures exceeding 1500K and space charge effects. Diamond films have been subject of numerous emissivity studies where field emission was the dominant form of emission characterization.[2] Several studies on thermionic emission from nitrogen doped diamond films describe emission in terms of donor/defect states as well as the negative electron affinity (NEA) surface characteristic with emission commencing at temperatures below 1000K.[3] In fact, the observed uniformity in the emission can be attributed to the NEA characteristic which is not typical for other carbon based emitters that exhibit locally confined emission. Basically, local uniformity in thermionic emission as observed for flat metal surfaces can be described by the Richardson-Dushman equation where the emission current density follows

$$J = AT^2 e^{-\varphi/k_B T}, \qquad [1]$$

with

$$A = \frac{emk_B^2}{2\pi^2\hbar^3}. \qquad [2]$$

Two parameters dominate the emission described by this relation, the work function, φ, of the material and Richardson's constant, A. The emission barrier, i.e. the temperature at which emission commences is then determined by the work function, φ, of the emitter. While A for a metal has been described theoretically with the result a collection of fundamental constants an experimental evaluation also identifies the contribution of surface characteristics to the solution. By measuring thermionic emission from nitrogen doped diamond films with respect to the Richardson-Dushman equation an evaluation of emission critical parameters can be performed. As shown in Figure 1, emission can be detected at temperatures as low as 900K with a strong increase in emission with emitter temperature. The observed emission behavior, i.e. a stronger increase in emission with temperature than predicted by Richardson is due to a temperature dependent work function which decreases with increasing temperature. In the observed temperature range an average work function for this material of ~2.4eV and a Richardson constant of $120 A/cm^2K^2$ can be obtained with the work function the most critical fitting parameter. By increasing the electric field between emitter and collector, an increase in the emission current is observed which is due to a diminished effective work function.

FIGURES

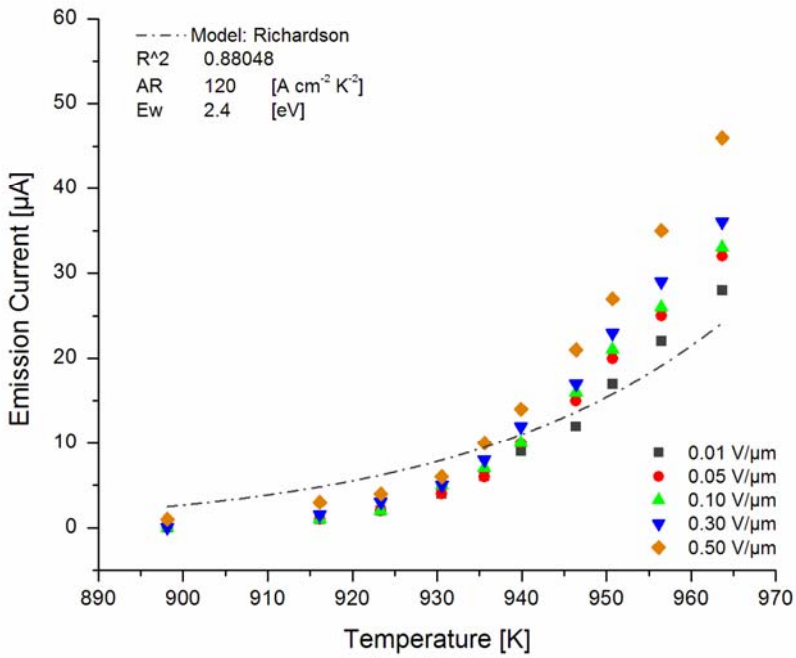

Figure 1. Thermionic electron emission from a nitrogen doped diamond film as a function of temperature and applied electric field. The dotted curve shows a fit to the Richardson-Dushman equation.

REFERENCES

1. Decher R, Direct Energy Conversion, Oxford University Press, New York, NY, 1999
2. Sowers AT, Ward BL, English SL and Nemanich RJ, Measurement of field emission from nitrogen-doped diamond films, Diamond and Rel. Mat.,9, 1569-1573, 2000
3. Koeck FAM, Garguilo JM, Brown B and Nemanich RJ, Enhanced low-temperature thermionic field emission from surface-treated N-doped diamond films, Diamond and Rel. Mat.,11, 774-779, 2002

The Bright View of DEL Seen Form LED

James C. Sung[*,1,2,3], Juen-Chen Pu[3], Sea-Fue Wang[3]

Address: KINIK Company, 64, Chung-San Rd., Ying-Kuo, Taipei Hsien 239, Taiwan, R.O.C.
Tel: 886-2-2677-5490 ext.1150
Fax: 886-2-8677-2171
e-mail: sung@kinik.com.tw

[1] KINIK Company, 64, Chung-San Rd., Ying-Kuo, Taipei Hsien 239, Taiwan, R.O.C.
[2] National Taiwan University, Taipei 106, Taiwan, R.O.C.
[3] National Taipei University of Technology, Taipei 106, Taiwan, R.O.C.

Keywords: Electroluminescence, Amorphous Diamond, Light Emitting Diode

Abstract

Light emitting diodes (LED) have a bright future as their electro-optical efficiencies are now approaching the standard fluorescence light (70 limens/watt or 10%). However, LED's costs are still prohibitive ($20/1000 lumens) in many applications so they cannot replace fluorescence light ($0.5/1000 lumens) in general. This is particularly true for the applications in back lighting that is indispensable for electronics with LCD for monitors of computer, television, scanner, PDA and the like. The backing lighting is now dominated by cold cathode fluorescence light (CCFL). For paneled lighting, the costly LEDs have other handicaps, such as their inability to diffuse light to a larger area, and their mixing colors (RGB) do not match with eye sensitivities that are tuned to more natural white light.

In terms of panel lighting, electro luminescence (EL) has intrinsical advantages. Firstly, EL is a two dimensional design that is more compatible with the panel lighting than the complicated structure of LED. Moreover, there is no semiconductor involved in emitting light so the cost is much lower. Furthermore, because the low electrical power is involved, the heat generation is minimal in the lighting device. Consequently, the electro optical efficiency for EL can be higher than LED.

Although EL has a long history tracing back to 1936 when Destriau discovered that ZnS powder dispersed in castor oil could be illuminated by applying an AC electrical field. Since then, EL has been applied to back lighting that is relatively dim. There are two major obstacles that EL has not overcome, viz., the high voltage required to trigger the illumination, and the rapid decay of the luminosity with time. These two problems are now solved with the use of amorphous diamond as the electrode and the replacement of AlN as the phosphor. Amorphous diamond can dramatically reduce the voltage required for illumination; and AlN significantly boost the stability of the phosphor.

Amorphous diamond (tetrahedral amorphous carbon or tac) contains carbon atoms with mostly in distorted diamond bonding (sp3). It has the highest atomic density (>176 nm^3 for diamond) of all materials (e.g. four times higher than most closest packed metals). Because each atom is unique in the distortion of tetrahedral bonds, there are numerous discrete energy levels for electrons to perch on. Amorphous diamond has the highest entropies of all materials in both atomic configuration and electronic configuration, as such it is uniquely capable to allow electrons to increase energy by receiving incremental energies that exceed the energy difference among various electronic states. For example, amorphous diamond can allow valence electrons to climb up the energy ladder with thermal agitation so electrons can emit in vacuum or in a dielectric material. In contrast, electrons in an insulator (e.g. diamond) will not be disturbed by weak phonons due to the wide energy gap between valence band and conduction band; whereas electrons in a conductor (e.g. graphite) cannot accumulate phonon energy due to the overlapping of conduction band and valence band.

Two ITO (indium tin oxide) coated glass of the common LCD panels were used to construct a Diamond EL or DEL. One of them is coated on the ITO with copper doped ZnS as the phosphor; and the other is coated on the ITO with amorphous diamond. The two panels are glued together by epoxy with a total gap between them of about 60 microns. It was observed that the effective turn-on voltage for the panel was reduced by coating with amorphous diamond from 80 V to 40 V. Moreover, the input voltage could be reduced to only 3V by converting the DC field into AC of 3500 Hz.

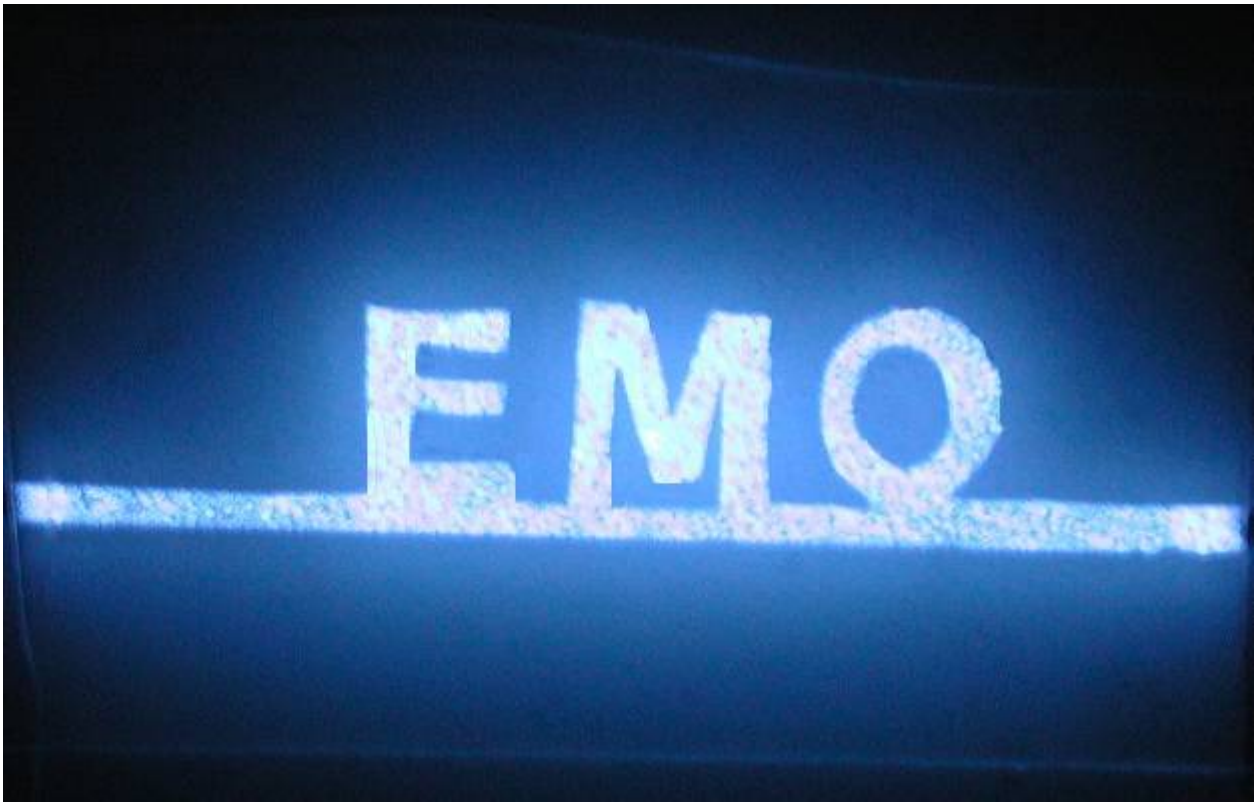

Fig.1: The DEL display with the input of 3V at 3500 Hz. EMO stands for electro-magnetic-optical research lab at Taipei University of Technology.

Although DEL may be used to generate bright light with high energy efficiency, its decay rate of luminosity must be reduced. One problem of the decay is caused by the irreversible diffusion of the activator atoms (e.g. Cu) in the phosphor layer, particularly along the grain boundaries of the carrier (e.g. ZnS) particles. This diffusion is triggered by the local heating due to the concentration of electrical current through the low resistance path. One way to overcome this problem is to disperse the electrical path by using phosphors of nano sized particles. The phosphor layer must be heat treated beforehand to assure the thermal stability of the host structure (e.g. the reduction of defect concentration by annealing) and the dopant substitutions (e.g. in the tetrahedral coordinated positions).

Another way to improve the reliability of the DEL is to use dielectric materials (e.g. PZT) to sandwich the phosphor layer. In this case, the phosphor layer is separated from the electrodes so electrons can flow more uniformly in the phosphor layer to avoid local heating.

The best method to stabilize the phosphor layer is to use AlN as the host material. AlN is with the wurtzite structure that is isostructural to ZnS. AlN is much more compact in atomic packing and it is significantly more thermally stable. During the processing of AlN (e.g. in making AlN heat spreader for laser diode), oxygen is inevitably incorporated (e.g. by adding yttrium oxide as a sintering additive). The oxygen substitution of nitrogen in AlN will give luminescence at about 380 nm and this peak position is relatively fixed when the oxygen content is higher than 0.7 wt%. Moreover, if AlN is doped with Mn (e.g. 0.1-1 wt%), a red luminescence peak is observed for Mn4+ around 600 nm; and another green one is formed with Mn++ ions in AlN. If Eu is used as the dopant, a green luminescence peak around 2.4 eV (green) is formed.

If AlN phosphor with the right dopant (e.g. Mn, Eu, Sm...) is used, the DEL can be much more thermally stable so the decay rate of luminosity can be greatly slowed down. Moreover, AlN phosphor can be combined with ZnS or oxide phosphor to produced a mixed spectrum of luminescence. These different phosphor layers may also be combined to become a composite material for multiple luminescence with different triggers such as by moving electrons, as well as UV radiation from other phosphor layers.

LOCAL ELECTRON FIELD EMISSION PROPERTIES OF THE NANODIAMOND FILMS MEASURED USING SCANNING TUNNELING MICROSCOPIC TECHNIQUE

I-Nan Lin

Department of Physics, Tamkang University, Tamsui, Taiwan 251, R.O.C.

Yi-Ping Chou, Tom T. Chen

Department of Materials Science & Engineering and [c]Department of Physics, National Tsing Hua University, Hsin-Chu, Taiwan 300, R.O.C.

Hsiu-Fung Cheng

Department of Physics, National Taiwan Normal University, Taipei, Taiwan 116, R. O. C.

Keywords: Nanodiamonds, Electron field emission properties, Scanning Tunneling microscopy

Abstract

Diamond films, which can be synthesized easily by using microwave plasma enhanced chemical vapor deposition (MPECVD) process have been extensively investigated for the applications as electron sources, since they possess very consistent and good electron field emission properties[1]. However, the electron field emission properties of the diamond films are still pronouncedly inferior to those of carbon nanotubes (CNTs). Therefore, there have wide interest in improving the electron field emission properties of diamond films recently. One of the possible routes for increasing the electron field emission capacity of diamond films is to increase the proportion of grain boundary region, as it has been proposed that the grain boundaries contain sp^2-bond and provide conduction path for electrons, facilitating the electron field emission process[2]. In this paper, we adopted the bias enhanced technique for synthesizing boron-doped nanodiamonds. The electron field emission properties of the nanodiamond films were examined using scanning tunneling microscopic (STM) technique. Current image tunneling spectroscopic (CITS) measurements reveal the direct dependence of electron tunneling/field emission behavior of the films on the proportion of grain boundaries contained in the films. Local tunneling current-voltage (I_t-V) measurements show that incorporation of boron species insignificantly alters the occupied state, but markedly modifies the empty state of the diamond films, viz. it induced the presence of impurity states for the films heavily doped with borons, resulting in smaller emission energy gap for the samples. Such a characteristic improves both the local electron field emission behavior of the diamond films measured by STM and the average electron field emission properties measured by conventional parallel plate setup. These results infer clearly that the presence of impurity states due to boron doping is a prime factor improving the field emission properties for these boron-doped nanodiamond films.

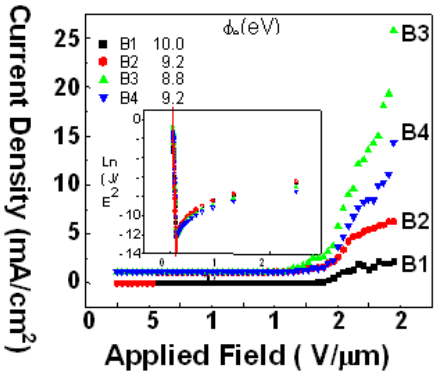

Fig. 1 Eelectron field emission properties of nano diamond films doped with 1-4 sccm $B(OCH_3)_3$ species, which were designated as B1-B4 (the inset shows Fowler-Nordheim plots of the I-V curves).

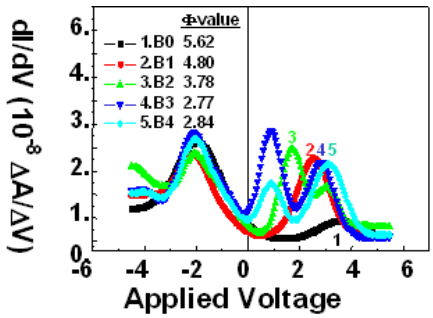

Fig. 2 The derivatives of tunneling current, dI_t/dV-V, for boron-doped nanodiamond films measured by STM techniques with tip-to-film gap set to at 1 nm.

REFERENCES

1. C. A. Spindt, I. Brodie, L. Humphrey, and E. R. Westerberg, **J. Appl. Phys. 47 (12)**, 5248 (1976).
2. F. J. Himpsel, J. A. Knapp, J. A. Van Vechten, and D. E. Eastman, **Phys. Rev. B 20 (2)**, 624 (1979).

SESSION 7

APPLICATIONS/DEVICES:
SENSORS & SURFACE PROPERTIES

FET BASED DIAMOND BIOSENSORS

Hitoshi UMEZAWA, Kwang-Soup SONG, Munenori DEGAWA, Yoshinori SASAKI and Hiroshi KAWARADA

School of Science & Engineering, Waseda University, Tokyo, Japan

Keywords: Diamond, Field-effect transistor, Biosensor, DNA, Site binding model.

Abstract

FET based diamond biosensors have been demonstrated by utilizing surface functionalizing techniques. pH sensitivity is obtained on diamond SGFETs with O or NH_2 terminated channel. The sensitivities of 50 mV/pH have been obtained on diamond SGFETs with O and NH_2 terminated channel, in contrast with the no pH sensitivity on that with H-terminated channel. FET based biosensors whose channel has functionalized by the biomolecules such as DNAs and enzymes have been realized on diamond SGFETs.

Introduction

Electrochemical sensors are suitable to environmental monitoring, clinical trials and also critical care situations, because of fast response, portability, small samples for detection and simple testing processes. Challenging researches are proceeding with development of various kinds of sensors based on electrochemical electrode or semiconductor device fabrication with micro-electromechanical technologies in wide variety of materials. Especially, diamond is attractive attentions of sensor materials due to its superior material properties. Factors such as wide electrochemical potential window, chemical and physical stability, high thermal conductivity and biocompatibility are expected to realize the low-noise and high-sensitive sensors or integrated sensor allay with high reliability.

Recently, FET type chemical and biosensors have been reported on H-terminated diamond [1-4]. Compare to Si-ISFETs, diamond solution-gated FETs (SGFETs) work without interlayer on the surface as shown in fig. 1, because the penetration of the ions in the solution are suppressed. As a result, fast response, stability of surface potential and high sensitivity are realized.

pH sensitivity on functionalized diamond FETs

Surface of the diamond deposited by chemical vapor deposition is terminated by hydrogen. This surface shows the p-type semiconductivity with high carrier density of 10^{13} cm^{-2} within 10 nm from the surface, which is easily controlled by the applied bias and suitable as the channel of FETs. In case of diamond SGFETs, the surface carriers are controlled by not only the applied bias of electrolyte solutions, but also the adsorbed specific ions, protonations or deprotonations.

Diamond SGFETs with the completely H-terminated surface channel has no sensitivity on pH change because the surface functional groups (C-H) are not protonated or deprotonated in wide variety of pH change. On the other hand, the pH sensitivity of SGFETs can be obtained by the partially NH_2-O-terminated channel with UV irradiation in ammonia solution or atmosphere, because C-O and C-NH_2 are protonated or deprotonated in the solutions. The absolute value of the gate potential preserving constant drain current of diamond SGFET decreased approximately 50 mV/pH from pH 2 to pH 10 and the gradient of that obeyed the Nernstian response as shown in fig. 2. The time response of pH sensitivity is superior to that of Si based ISFET, because penetration of ions such as K^+, Na^+ and Ca^{2+} are vanished in diamond. The hysteresis width is approximately 1 mV, which value is one order of magnitude lower than that of membranes used in Si-ISFETs (fig.3).

Diamond Biosensors

Several types of diamond biosensors such as urea, glucose and DNA sensors, have been demonstrated by means of biomolecules functionalized diamond surfaces.

Urea-sensitive diamond SGFETs operate based on the biocatalyzed decomposition of urea by urease. This decomposition changes the surrounding pH, which is occurred on the channel surface, and NH_2 functionalized surface can detect this pH change as shown in fig. 4.

The charges on DNAs are also detectable on diamond SGFETs. When the negatively charged DNAs are hybridized on the complementary single strand DNAs immobilized on diamond surface, the surface potential of the diamond SGFETs bends upward, as a result, increase of the drain current and the positive shift of the threshold voltage of diamond SGFET are observed as shown in fig 5. The difference between complementary and non-complementary target DNAs has been detected by the real time shift of the gate voltage.

REFERENCES

1. H.Kawarada et al., Phys. Status Solidi A 185 (2001) 79.
2. A.Denisenko et al., Diamond Relat. Mater., 10, (2001) 667.
3. H.Kanazawa et al., Diamond Relat. Mater., 12 (2003) 618.
4. K.S. Song, et al., Biosens. Bioelectron. 19, (2003) 137.

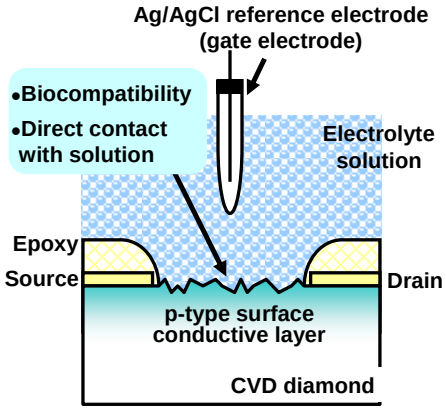

Fig.1 Diamond SGFETs

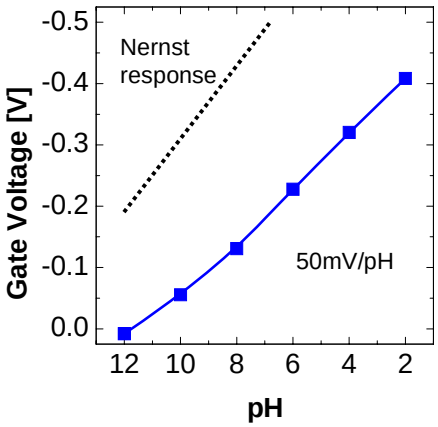

Fig.2 pH response of NH_2 terminated diamond SGFETs

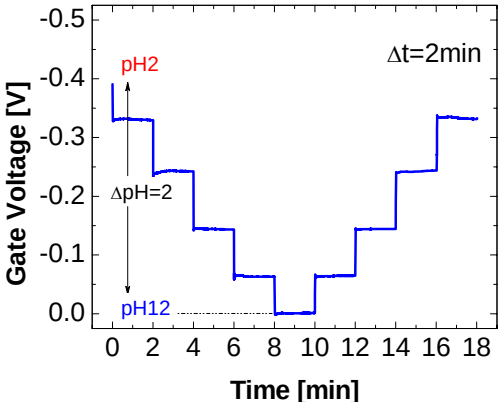

Fig.3 Hysteresis characteristics of a diamond SGFETs

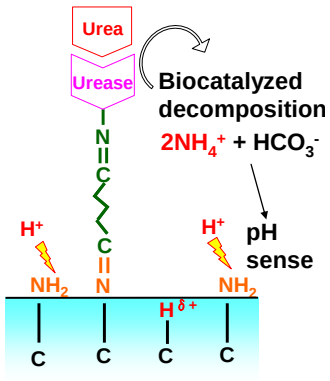

Fig.4 Urea sensing by an urease immobilized SGFET.

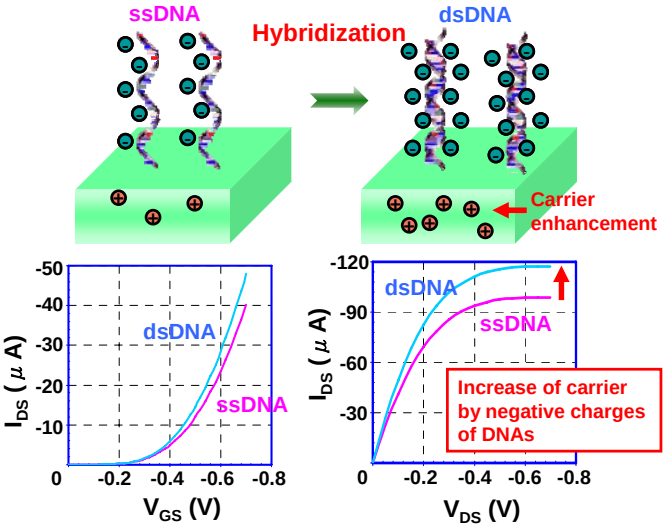

Fig.5 Hybridization of DNA sensed by diamond SGFET, where a single strad DNAs are immobilized on the diamond surface..

Diamond-based biochemical sensors

J.A. Garrido[1], A. Härtl[1], J.Hernando[1], M. Stutzmann[1], S. Walter[2]
[1]*Walter Schottky Institut, Technische Universität München, Germany.*
[2]*Institute for Organic Chemistry and Biochemistry, Technische Universität München, Germany.*
garrido@wsi.tum.de

Diamond exhibits several special properties, e.g. chemical stability, low background current, and a large electrochemical potential window, which make it particularly suitable for biofunctionalization and biosensing. In this contribution, we present the covalent attachment of enzymes to nanocrystalline diamond thin films. Although immobilized at the surface, the biomolecules are still fully functional and active. Different routes are available for the functionalization of nanocrystalline diamond surfaces depending on the surface termination, hydrogen or oxygen. Hydrogen-terminated nanocrystalline diamond films can be modified using a photochemical process to generate a surface layer of amine groups, to which proteins can be covalently bound in several following steps. For comparison, oxygen-terminated NCD films have been functionalized using different chemical methods. The enzymes catalase and horse-redish peroxidase were immobilized on the modified NCD electrodes, and the successful attachment was confirmed by measuring the enzyme activity. Impedimetric experiments were also used to study the surface modification. The enzyme-modified diamond electrodes exhibit direct electrochemical charge transfer between the enzyme redox center and the electrode. The enzyme-NCD electrodes were also used as H_2O_2 sensors. In the presence of H_2O_2, a large cathodic current is observed due to the reduction of H_2O_2 catalyzed by the enzyme modified electrode.

These results provide important steps towards the realization of diamond-based amperometric biosensors. Considering some of the unique properties of nanocrystalline diamond, such as ease of production, chemical stability, and excellent electrochemical properties, it is justified to speculate that nanocrystalline diamond can play an important role in the future of biosensors.

OXYGEN EFFECT ON THE SURFACE CONDUCTIVITY OF N-TYPE SULFUR-DOPED DIAMOND

Gonzalez-Gonzalez, I.[1] , Cabrera, C. R.[1], Tryk, D. A.[1], Morell, G.[2], De Jesús, J.[2]

University of Puerto Rico, Río Piedras Campus,
[1]Departmen[t] of Chemistry, [2]Department of Physics

Keywords: surface conductivity, sulfur-doped diamond

Recently there has been much interest in the phenomenon of surface conductivity of diamond films and the effect of various adsorbates on this conductivity. Specifically, it has been found that oxidizing conditions tend to increase the surface conductivity of boron-doped diamond films and reducing conditions tend to decrease the conductivity. Another example an oxygen saturated solution. One possible mechanism for the increased conductivity that results from the presence of an oxidant involves the transfer of electrons from the bulk of the p-type boron doped diamond to the adsorbate, which effectively increases the number of p-type charge carriers (holes). [i],[ii] This increase in conductivity can be used to as a way to sense the presence of an oxidant such as oxygen. Thus far, this phenomenon has only been reported for p-type diamond films.[iii] Recently, we have found in our laboratory that a similar phenomenon also occurs on n-type diamond films, such as sulfur-doped films. Sulfur is a deep donor in diamond.[iv], [v] In this case, however when the electron is transferred from the diamond to the oxidant, the number of n-type charge carriers (electrons) is decreased, and the surface conductivity decreases. This also results in decreases in the currents for oxygen evolution and hydrogen evolution from an aqueous solution. We have used the latter observation as a means of measuring the concentration of oxygen dissolved in aqueous solutions. There is a rough correlation between the electrochemical behavior and the sulfur doping level for a series of nanocrystalline films prepared as described previously [vi]. In particular for high doping levels, the decrease in current upon exposure of the solution to air is small, whereas for low doping levels the relative decrease is large.

[i] J. Ristein, F. Maier, M. Riedel, M. Stammer, and L. Ley, Diamond

Rel. Mater., 10, 416 (2001).

[ii] D. Takeuchi, S. Yamanaka , and H. Okushi, Diamond Rel. Mater., 11, 355–358 (2002).

[iii] V. Chakrapani, S. C. Eaton, and J. C. Angus, Extended Abstracts, Diamond Materials VIII, Spring Meeting of the Electrochemical Society (Paris), The Electrochemical Society, Pennington, N.J., U.S.A. (2003).

[iv] H. Titus, V. Albu, A. B. Anderson, and J. C. Angus, J. Electrochem. Soc., 149, E143-E147 (2002).

[v] E. Gheeraert , N. Casanova , A. Tajani , A. Deneuville , E. Bustarret , J. A. Garrido, C. E. Nebel, and M. Stutzmann, Diamond Rel. Mater., 11, 289–295 (2002).

[vi]A. Gonzalez-Berrıos , D. Huang, N. M. Medina-Emmanuelli , K. E. Kristian , O. O. Ortiz , J. A. Gonzalez , J. De Jesus , I. M. Vargas , B. R. Weiner, and G. Morell, Diamond Rel. Mater., 13, 221–225 (2004).

In vitro Adenosine Detection with a Diamond-based Sensor

Songtao Xie*, Geoffrey Shafer**,Christopher G. Wilson**, and Heidi B. Martin*
*Chemical Engineering Department;**Pediatrics Department;
Case Western Reserve University, Cleveland, OH 44106

In the central nervous system, adenosine serves as a modulator of neurotransmission and a neuroprotective agent against ischemic- and seizure-induced neuronal injury. It may be synthesized either intracellularly from degradation of adenosine monophosphate (AMP) or extracellularly by the metabolism of nucleotides. Several experimental approaches, *e.g.,* microwave irradiation or microdialysis, have been used to measure *in vitro* and *in vivo* concentrations of adenosine; a basal adenosine level was estimated at 50-200 nM[1]. However, these techniques suffer from various disadvantages, *e.g.*, inducing serious tissue damage and having low temporal resolution (minute time scale). Alternatively, adenosine is electrochemically active, and thus can be detected in real-time with electrochemical techniques including amperometry or fast-scan cyclic voltammetry (FSCV). Amperometry offers excellent temporal resolution and sensitivity, but is typically difficult to interpret for component mixtures. On the other hand, FSCV can generate a "finger print" response for each analyte, potentially allowing a distinguishable measurement in the presence of multiple components. With these methods, microelectrodes are employed, minimizing tissue damage. Recently, Brajter-Toth *et al.* used FSCV in a flow cell to detect adenosine at a carbon-fiber microelectrode, proposing a mechanism for adenosine reduction and oxidation[2]. However, the carbon-fiber electrode displayed limited sensitivity, ~10 μM. If used *in vivo* or *in vitro*, stimulation of the neuron to release substantial amount of adenosine is necessary, introducing the risk of altering the neural circuitry involved.

Boron-doped diamond electrodes are increasingly used in electroanalysis because of their exceptional electrochemical properties, including low baseline current and wide potential window of water decomposition;[3] adenosine detection provides opportunity to demonstrate both of these advantages. The diamond surface should also discourage adsorption, which likely translates into improved stability upon implantation of the device into biological systems. We are currently developing implantable, diamond-based microelectrodes to study neurotransmission in the brain and central nervous system. The diamond electrodes (**Fig.1**) mimic the needle-like geometry of widely used carbon-fiber electrodes. They are fabricated by selective CVD deposition of a diamond thin film onto a tungsten wire substrate, which is pre-sealed into quartz. With this electrodes, we have detected 10 nM adenosine using flow injection analysis.[4] With this electrode, we aim to investigate the role of adenosine in neurotransmission (ms time scale) under various physiological conditions. In this study, we focus on the PreBötzinger Complex (PreBötC) in the (rodent) brain stem, a putative site for respiratory rhythmogenesis, as a model to demonstrate the capability of a diamond-based probe as an *in vitro*, adenosine sensor.

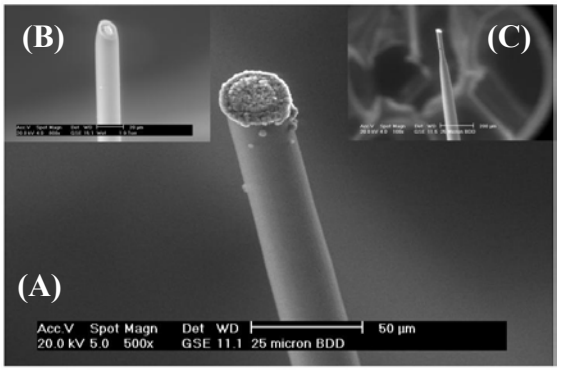

Fig. 1: *Scanning electron images of a diamond microelectrode: (A) selective diamond growth at the tip, approx. 30 μm diameter, 2~5 μm (111) crystals dominant; (B) tungsten wire substrate sealed into quartz capillary; (c) intact electrode body.*

In the PreBötC, neurons with "pacemaker" autorhythmic properties are hypothesized to generate inspiratory rhythm. The neural activity may be inhibited by the administration of adenosine or adenosine analogues during early development[5]. However, the mechanism whereby adenosine inhibits inspiratory drive is not well characterized. There are multiple adenosine receptor subtypes: A_1, A_{2A}, A_{2B}, and A_3, present in PreBötC, with different affinities for adenosine. When each receptor is activated, it can either inhibit or excite neurons. Thus, it is necessary to individually understand the effects of

these receptors on inspiratory drive. Here, we present our initial results (**Fig.2)** of *in vitro* adenosine detection from selective A_{2A} receptor activation.

A brain slice containing PreBötC was obtained from a neonatal (P1-P3) Sprague-Dawley rat. The slice was perfused with artificial cerebrospinal fluid (aCSF), saturated with 95% O_2 and 5% CO_2. Respiratory frequency and magnitude were indirectly monitored by extracellular, suction-electrode recording from hypoglossal nerve rootlets; this provides an index of inspiratory drive in young animals. The diamond microelectrode was lowered into the PreBötC, with Ag/AgCl as the reference/counter electrode. Its potential was continuously scanned between –1.0 V and +1.5 V, at 500 V/s (see **Fig. 2(A)**). After administration of CGS 21680, an adenosine analogue selective for A_{2A} receptor, several "island" features representing the occurrence of electrochemical reactions, were observed on the 3-D false-color plot (**Fig. 2(A)**). A typical cyclic voltammogram, **Fig. 2(B)**, obtained by extracting data from the color plot along the Y-axis, showed an oxidation peak near +0.8V for adenosine[2]. The peak-current for oxidation of adenosine, **Fig. 2(C)**, increased in a series of waves, whose frequencies varied between 50 and 200 seconds. After post-calibration of the diamond electrode **(Fig. 2(D))**, it was determined that the *in vitro* adenosine concentration varied between 2 to 5 µM **(Fig. 2(E))**. With respect to repiratory rhythm, the data suggest that CGS-induced adenosine release decreases the respiratory frequency and magnitude, as hypothesized (data not shown). A_{2A} activation, therefore, inhibits the inspiratory drive. Further investigation of the roles played by other receptors is in progress.

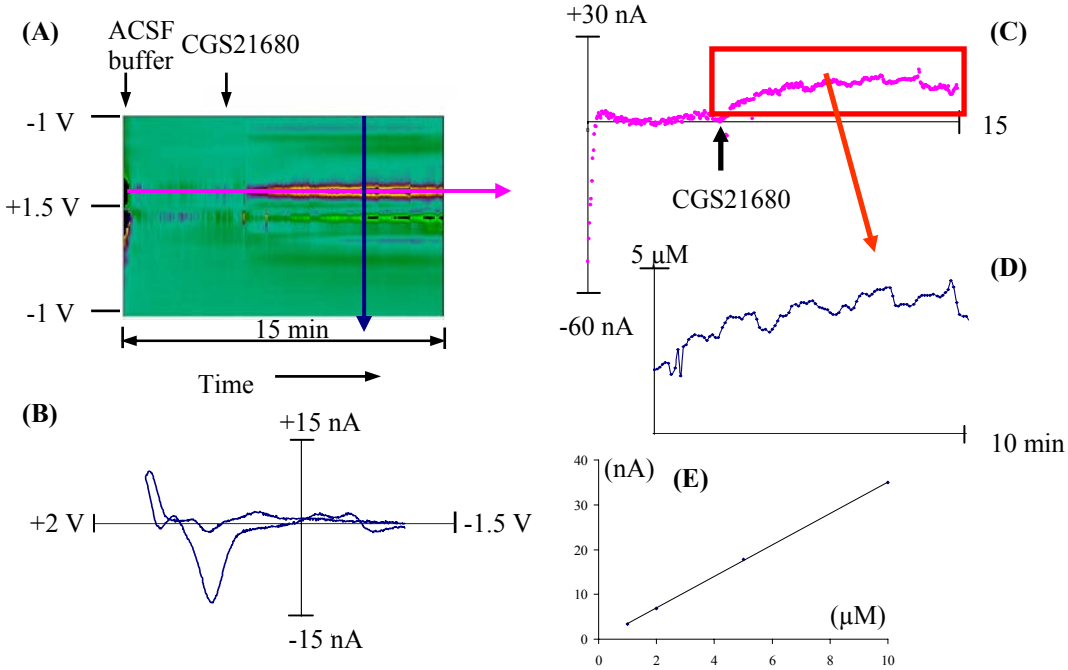

Fig. 2: *In vitro adenosine measurement; (A) 3D false color plot of released adenosine when CGS 21680 was administrated; (B) Finger print of adenosine, cyclic voltammogram; (C) Current increased after CGS 21680 treatment, which was related to the variation of adenosine concentration (D) by post calibration of electrode at flow injection system (E).*

References

1. Dunwiddie T. V. and Masino S. A., "The role and regulation of adenosine in central nervous sytem", *Annu. Rev. Neurosci* **24** (2001)31-55.
2. El-Nour K. A. and Brajter-Toth A., "Sensitivity of electrochemically nanostructured carbon fiber ultramicroelectrodes in the determination of adenosine", *Electroanalysis*, **12** (2001) 805-811.
3. Martin H. B., Argoitia A., Anderson A., Landau U. and Angus J. C., "Hydrogen and Oxygen Evolution on Boron-Doped Diamond Electrodes," *J. Electrochem. Soc.* **143** (1996) L133-L136.
4. Xie S., Blankenship B. D., Halpern J. M., Shafer G., Wilson C. G., Chiel H. and Martin H. B., "Boron-Doped Diamond Neurosensors and Neural Stimulating Electrodes", submitted to "Proceedings, Diamond Materials IX, ECS Fall Meeting, Honolulu, HI, October 2004".
5. Wilson C.G. Wilson, R. J. Martina, M. Jaber, J. Abu-Shaweesh , A. Jafri, M. A. Haxhiu, S. Zaidi, "Adenosine A(2A) receptors interact with GABAergic pathways to modulate respiration in neonatal piglets", *Respiratory Physiol. & Neurobiol.,* **141** (2004) 201-211.

ADSORBATE INDUCED CONDUCTIVITY OF HYDROGEN-TERMINATED DIAMOND

Vidhya Chakrapani,[a] Sally C. Eaton,[a] Alfred B. Anderson,[b] and John C. Angus[a]

[a] Dept of Chemical Engineering, [b] Dept of Chemistry

Case Western Reserve University

Cleveland, Ohio 44106, USA

Keywords: Hydrogen-terminated diamond, p-type conductivity, electrochemical transfer-doping model.

Abstract

The origin of the p-type surface conductivity [1, 2] of hydrogen-terminated diamond is not fully understood; however, the electrochemical transfer-doping model proposed by Maier *et al.* [3] is gaining acceptance. According to this model, a p-type accumulation layer forms in the diamond due to the relative positions of the Fermi levels of the diamond and an adsorbed water layer on the surface. The chemical potential of electrons in the water layer is fixed by an electrochemical redox couple, most likely involving dissolved oxygen in equilibrium with air.[4]

$$O_2 + 4H^+ + 4e^- = 2H_2O$$

In our previous work we have studied this effect under different chemical environments and surface terminations.[5] The conductivity increased upon exposure to acidic vapors, which lower the electron chemical potential in the water film, and decreased when exposed to basic vapors, which increase the electron chemical potential. The effect disappeared with fluorine-terminated diamond and oxidized diamond. Organic liquids that wet the hydrophobic diamond surface displace the water film and quench the surface conductivity. Furthermore, transient measurements of conductivity upon imposition of a step temperature change show an immediate increase in conductivity, followed by a decay of conductivity with a much larger time constant. All of these effects are consistent with the electrochemical transfer-doping model.

In order to obtain further insight into the electrochemical transfer-doping model the contact angle and zeta potential were measured at different pH.[6] As the pH is lowered, the model predicts an increase in the concentration of holes in the diamond and the counter-anions in the adsorbed film. At lower pH one would therefore anticipate increased electrostatic attraction between the hole accumulation layer and the negative counter ions in the water film and therefore a decreased contact angle. The increased electron transfer from the diamond to the water film at low pH should also reveal itself in a more positive zeta potential (more positive surface charge) at low pH. Furthermore, these effects should be more pronounced for hydrogen-terminated compared to oxygen-terminated diamond.

Contact angles of hydrogenated samples decreased uniformly as the pH was lowered from pH = 7 to pH = 1. Reduction of the concentration of electrochemical acceptors, *i.e.*, the dissolved oxygen, should decrease the electron transfer from the diamond and reduce the effect of pH on contact angle. Reduction of dissolved oxygen was accomplished by addition of sodium bisulfite. The effect of pH on contact angle essentially disappeared at both low and high pH after the addition of excess sodium bisulfite. Oxidized diamonds showed a decrease in contact angle as the pH was increased above 3. This latter effect is attributed to ionization of oxygen

containing functional groups on the surface. Zeta potentials of both oxygen and hydrogen-terminated diamond were measured at different pH. At high pH, both surface terminations show a negative surface charge (See Fig.1). However, the isoelectric point for hydrogen-terminated diamond occurred at approximately pH = 5.2, below which pH the surface charge is positive. In contrast, oxidized diamond did not show a positive zeta potential until the pH was reduced to 1.2.

Although the results, in general, support the electrochemical transfer-doping model, significant uncertainty remains. In particular, a greatly enhanced effect is seen with rectifying contacts compared to ohmic contacts.[5] Understanding of this effect will require detailed modeling of the diamond/contact/film interface.

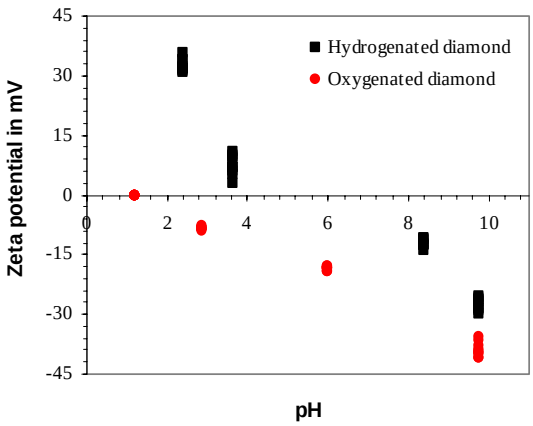

Figure 1. Zeta potential as a function of pH for both hydrogen and oxygen terminated diamond.

REFERENCES

1. Landstrass, M.I.; and Ravi, K.V.: "Resistivity of chemical vapor deposited diamond films," *Appl. Phys. Lett.*, **55,** 975-977(1988).

2. Gi, R.S., et al., "Possibility of realizing a gas sensor using surface conductive layer on diamond films," *Jap. J. Appl. Phys.*, **36**, 2057-2060 (1997).

3. Maier, F., et al., "Origin of surface conductivity in diamond," *Phys. Rev. Lett.*, **85**, 3472-3475 (2000).

4. Chakrapani, V.; Eaton, S.C.; and Angus, J.C.: **"**Studies of the conductivity of diamond surfaces," Abstract 537, The Electrochemical Society Extended Abstracts, Diamond Materials VIII, Paris, France, April 27-May 2 (2003).

5. Chakrapani, V., et al., "Studies of Adsorbate-Induced Conductance of Diamond Surfaces," *Electrochemical and Solid State Letters*, **1**, E4-E8 (2005).

6. Chakrapani, V.; Eaton, S.C.; Anderson, A.B.; Tabib-Azar, M.; and Angus, J.C.: **"**Diamond surface conductivity: effect of pH, temperature and humidity," Abstract 1819, The Electrochemical Society Extended Abstracts, Diamond Materials XI, Honolulu, Hawaii, Oct 3-Oct 8 (2004).

SESSION 8

SYNTHESIS, PRODUCTION, & SCALE-UP

MASS PRODUCTION, SELECTIVE FORMATION, AND APPLICATIONS OF CARBON NANOTUBES

Morinobu Endo

Faculty of Engineering, Shinshu University, 4-17-1 Wakasato, Nagano-shi 380-8553, Japan

Keywords: Carbon Nanotube, Selective Synthesis, Characterization, Practical Application.

Abstract

Extra-ordinary chemical and physical properties of carbon nanotubes [1, 6] and also the success of large-scale production by a catalytic chemical vapor deposition method, particularly with the use of a floating reactant technique [2-4], make them applicable in the fabrication of adsorbent, electrochemical electrode, field emitter and functional filler in composite at a possible low cost. Through judicious selection of transient metal, support materials and synthetic conditions (temperature, duration), it is possible to produce different types of carbon nanotubes such as multi-walled carbon nanotubes (MWNTs), double-walled carbon nanotubes (DWNTs) and single-walled carbon nanotubes (SWNTs) selectively. In this study, we will describe the catalytic synthesis of various carbon nanotubes from the point of synthetic conditions, and structural changes by heat treatment will be discussed in terms of structural stability, and finally their practical applications of these carbon nanotubes will be described from the industrial point of view.

It is possible to obtain various fibrous carbons which exhibit a wide range of diameters from 200 to 1 nm, different crystallinity and different angle of graphene sheet with regard to tube axis through exact control of synthetic conditions of catalytic chemical vapor deposition (CCVD) method. Recently, the development of the floating reactant technique made possible to the large-scale production of carbon nanofibers (CNFs) and MWNTs [4]. In the synthesis of SWNTs, nano-sized SiO_2 impregnated with Fe-containing compounds (seeding method) were fed into the reactor (around 1000°C) with benzene as carbon feedstock, and with hydrogen as the carrier gas [7]. In contrast to current CVD methods, this combinational technique allows high yield efficiency of the nanotubes. A detailed TEM and Raman studies revealed that there are large variations in textures (isolated and bundle) and also diameters (see Fig. 1 (a)).

The recent hot topic is the synthesis of DWNTs because these tubes are more thermally and chemically stable when compared to SWNTs; they also exhibiting the 1D character of a quantum wire. In addition, DWNTs could also be used in the fabrication of electron field emitter and nano-composites. The synthesis of DWNTs was carried out using a conditioning catalyst (Mo/Al_2O_3) on one end of the furnace, and the nanotube catalyst (Fe/MgO) in the middle part of the furnace (see supplemental information). Subsequently, a CH_4+Ar gas mixture (1:1) was fed into the reactor for 10 minutes at 875°C. When using the conditioning catalyst, preferential growth of DWNTs over SWNTs occurred, possibly due to an increased portion of active carbon species. In order to obtain a pure DWNT, a two-step purification process was applied to the synthesized products. In particular, HCl treatments were carried out in order to remove iron catalyst and the supporting material, followed by air oxidation at 500°C for 30 minutes. The latter process is used to remove amorphous carbon and chemically active SWNTs. After a filtering process, we obtained a dark and stable paper-like sheet, which is very flexible and mechanically stable (tough). Careful HRTEM (JEOL JEM-2010FEF) observations revealed an extremely high-yield of DWNTs (more than 95%) arranged in bundles. Fig. 1 (b) exhibit cross sectional image of HR-TEM images of DWNTs bundles. When heat treated at higher temperature in inert atmospheres, unusual phenomena occur in DWNTs bundles. HRTEM image of Figure 1 (c) exhibits a sequential reconstruction behaviors of DWNTs at 2100°C [9]. Two adjacent outer shells start to merge (see, (I) in Fig. 1 (c)) via a zipping process, similar to the coalescence of SWNTs under electron beam irradiation, and a large single outer shell with an oval shape is formed (see, (II) in Fig. 1(c)). The process occurs due to the coalescence and reconstruction of the outer shells of DWNTs, leaving the inner cylinders almost intact, the latter being encapsulated inside the large diameter coalesced tubule (bi-cable). We envisage this material to be useful in the fabrication of novel sensors, nanocomposites, field emission sources, nanotube bi-cables and electronic devices. On top of that, it is expected that DWNTs will replace SWNTs or MWNTs for various specific applications due to their expected superior mechanical properties, thermal conductivity and structural stability derived from their unique coaxial structure.

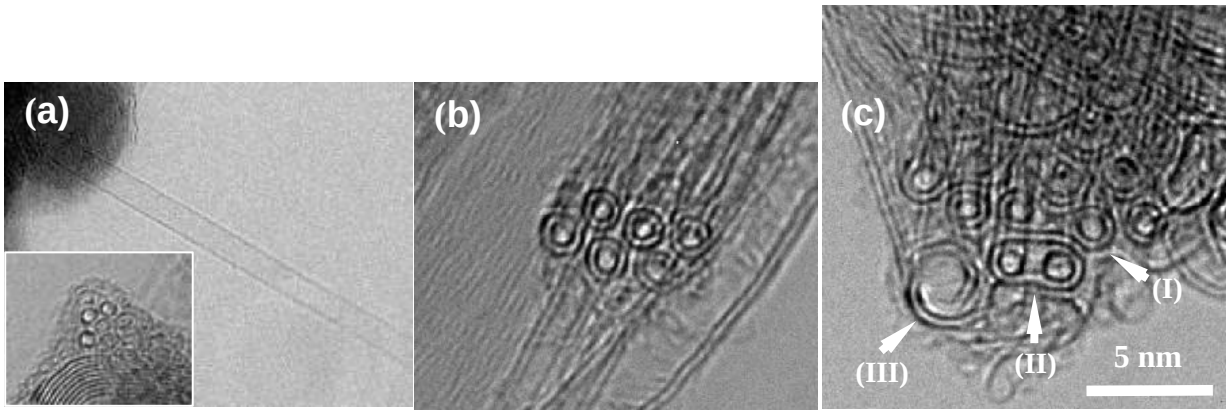

Figure 1. (a) typical HRTEM image of single wall carbon nanotubes, (b) Typical high resolution transmission electron microscopy (HRTEM) image of DWNTs in a bundle state, (c) HRTEM image of DWNTs at 2100°C. This image exhibits a sequential reconstruction process of a DWNT: (I) two outer tubes start to merge, through a zipping mechanism, (II) two outer tubes are completely combined into a single large outer tube with an oval shape containing two SWNTs, and (III) two inner SWNTs in a confined space might decompose along the inner wall of an outer shell, to form one inner single shell, like the formation of a DWNT derived from a peapod

REFERENCES

1. Dresselhaus, M. S., et al., *Science of Fullerenes and Carbon Nanotubes*, Academic Press, San Diego (1996).
2. Oberlin, A.; Endo, M.; Koyama, T.: “Filamentous Growth of Carbon through Benzene Decomposition," J. Cryst. Growth 32, 335 (1976).
3. Endo, M. et al., “The production and structure of pyrolytic carbon nanotubes (PCNTs),” J. Phys. Chem. Solids 54, 1841 (1993).
4. Endo, M. “Grow Carbon Fibers in the Vapor Phase,” Chem. Tech. (Leipzig) 18, 568 (1988).
5. Endo, M. et al., “Vapor-grown carbon fibers (VGCFs) Basic properties and battery application,” Carbon 39, 1287 (2001).
6. Iijima, S. “Helical microtubules of graphitic carbon,” Nature, 354, 56 (1991).
7. Hayashi, T. et al., “The smallest freestanding single-wall carbon nanotube,” Nanoletters 3, 887 (2003).
8. Endo, M. et al., “Buckypaper from coaxial nanotubes,” Nature 433, 476 (2005).
9. Endo, M. et al, “Coalescence of Double-walled Carbon Nanotubes: Formation of Novel Carbon Bi-cables,” Nano letters 4, 1451 (2004).

LARGE-AREA MICROWAVE PLASMA DEPOSITION SYSTEM FOR UNCD COATING OF SIC PUMP SEALS

Joseph A. Libera, John Hryn, Jeff Elam, James Birrell, Orlando Auciello, John Carlisle

Argonne National Laboratory, 9700 S. Cass Ave, Bldg. 200,. Argonne, IL 60439

Keywords: diamond film, pump seal, friction, wear, silicon carbide.

Abstract

An 11” microwave plasma Ultra-Nano-Crystalline-Diamond (UNCD) deposition system has been commissioned for the production coating of UNCD onto SiC pump seals. This work is presented along with earlier results using a similar 6” reactor where only one 2.0” diameter seal may be grown at a time, while the 11” system allows seven 2.0” diameter seals to be coated simultaneously. Seals are held in the cavities of a heated graphite “muffin tin” susceptor such that the top surface of the seals is even with the graphite presenting a flat planar surface to the plasma. The substrate heater temperature is 800-900°C while the seal growth surface temperature is up to 200°C hotter due to heating by the plasma. The plasma gas composition is primarily Ar with 1-4% CH_4 and 0-5% H_2. The plasma reactor is an 11-pole toroidal resonator cavity surrounding a vertical quartz tube reaction chamber with a aluminum top plate gas distributor. Materials to be coated are introduced into the reaction chamber from a bottom port using a cylindrical vertically-translating heated stage. Seals coated in the 6” system were tested by the manufacturer of the seals, John Crane Inc., with very satisfactory results. Preliminary results in the 11” system have successfully demonstrated growth of UNCD onto a 7-seal arrangement with a center seal and a surrounding second circle of 6 seals. Growth of high temperature UNCD on 200 mm Si wafers has also been demonstrated. The uniformity of the thickness and structural properties of the UNCD films are presented. The results presented here provide valuable information regarding the large-area deposition of UNCD diamond films.

ASPECTS OF SCALING CVD DIAMOND REACTORS

Jerry Zimmer

sp3 Inc. , 505 East Evelyn Ave., Mountain View, CA 94041

K.V. Ravi

Intel Corporation, 2200 Mission College Blvd., Santa Clara, CA 95054

Keywords: Hot filament, 300 mm wafers, uniformity, scaling

Abstract

Diamond deposition has been a functional CVD process for over a decade but little has been done to scale deposition techniques beyond the initial small areas. The basic requirements of scaling any CVD process include maintaining temperature uniformity and reactive gas composition and distribution uniformity across the entire area of deposition. The results of this control will affect growth rate uniformity, film composition uniformity and morphology control across the deposition surface. In addition, contaminants that might affect film quality or purity must be managed effectively. Each of these must be addressed to successfully scale any process. Among the several techniques available for the synthesis of diamond films the hot filament CVD approach offered some unique advantages in terms of scalability for the deposition of diamond over large area substrates. Principle among these is that filament area can be increased without sacrificing uniformity of film deposition. Power and hence the energy required to dissociate hydrocarbons and hydrogen to generate the necessary carbon specie and atomic hydrogen required for diamond deposition scales with the size of the filament array. Local power density can be made very uniform across the entire area unlike competing technologies. In addition the relatively low power density of such tools results in easier scaling from an engineering perspective when compared with other approaches used for diamond deposition. In this paper we discuss some aspects of scaling of the hot filament CVD tool up to a square deposition area of 380mm. Examples will be presented of substrate temperature uniformity, film deposition rate uniformity, film quality and purity over 300-mm silicon wafers. Figure 1 shows an example of diamond film uniformity achieved using the hot filament CVD approach on 300mm silicon wafers. This data will then be assessed to determine the degree of improvement required to meet long term objectives for several product categories as well as any issues relating to scaling to even larger areas.

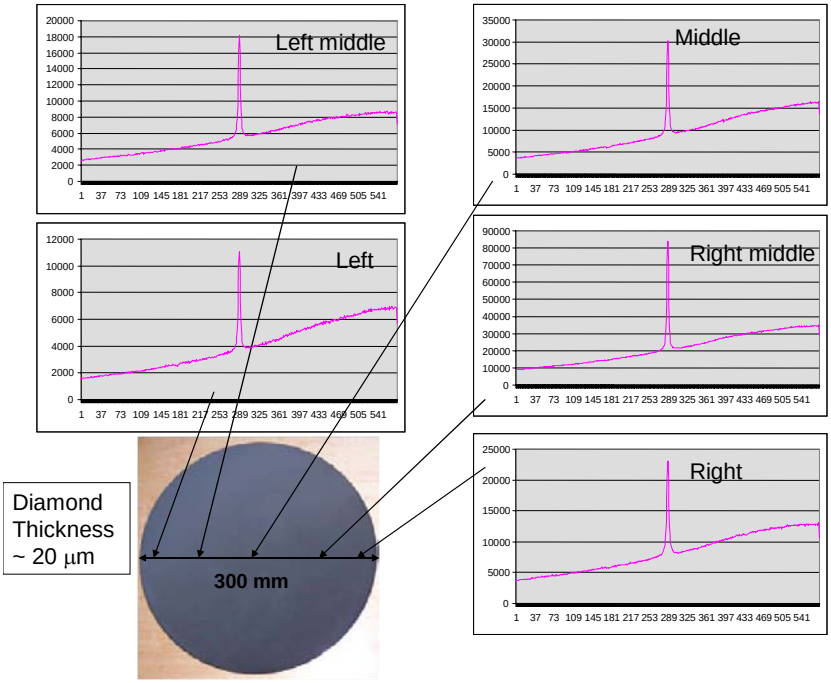

Figure1. Diamond-coated 300-mm wafer with Raman spectra at different locations of the wafer showing the film uniformity achievable with the hot filament CVD tool.

SESSION 9

SYNTHESIS & GROWTH MECHANISM I

Growth Mechanism of Super Long and Aligned Single-Walled Carbon Nanotubes

Jie Liu, Department of Chemistry, Duke University, Durham, NC 27708

Recently progress in nanotube synthesis makes it possible to grow individual single walled carbon nanotubes (SWNTs) to several centimeters long along a direction defined by the gas flow. The growth of long nanotubes and the control of the growth direction not only makes it possible to produce nanotube structures in a controller manner, it also revealed some insight of the nanotube growth mechanism in general, especially the termination mechanism for nanotube growth. The talk will provided detailed analysis of the growth mechanism of these long and aligned nanotubes.

Superconductivity in Doped Diamond

R. J. Soulen, Jr. and M. Osofsky
Naval Research Laboratory
Code 6340
Washington, DC 20375

Superconductivity has been found in boron-doped diamond by researchers in two laboratories. This dramatic result challenges models for superconductivity. We will demonstrate, however, that the phenomenon is a simple manifestation of superconductivity induced by proximity to a metal/insulator transition. We will show how the results obtained for doped diamond are quite analogous to behavior seen in several disparate classes of superconductors (disordered metals, oxide conductors-including high temperature superconductors, semiconducting materials, organic conductors and various forms of C60), whose only common feature is proximity to a metal/insulator transition (MIT), share a common phase diagram Tc(r). Here r is a coordinate characterizing the disorder and is completely defined in terms of measurable quantities. This remarkable phase diagram may be plausibly explained by explicitly incorporating an enhancement of the electron screening length, which occurs near the MIT, into the BCS equation for Tc.

Just recently we have studied Hc2 as a function of proximity to the MIT for many systems and find a similar common phase diagram for Hc2(r). Again, we find that the shape of the phase diagram for diamond is remarkably similar to that of several other systems.

MICRO-AND NANO-CRYSTALLINE DIAMOND FILM SYNTHESIS AT SUBSTRATE TEMPERATURES SUB 400°C

F. Piazza, A. Makarov, R. Velázquez and J. De Jesús

Department of Physics, University of Puerto Rico, San Juan, P.O. Box 23343, Puerto Rico 00931

G. Morell

Department of Physical Sciences, University of Puerto Rico, San Juan, P.O. Box 23323, Puerto Rico 00931

Keywords: nano-crystalline, diamond, CVD, low temperature, sulfur

Abstract

Two issues hamper the utilization of the outstanding properties of microcrystalline diamond (μ-D) in microelectronics: no electronic-grade n-type semiconducting diamond has been produced so far with good reproducibility, and most of the current growth processes are carried out at too high substrate temperature T_S, typically T_S>700°C. Electronic-grade n-type semiconducting diamond film deposition at lower substrate temperature is therefore of considerable interest.

We recently succeeded in making n-type diamond by sulfur doping[1]. The films were grown by hot-filament chemical vapor deposition (HFCVD) from $CH_4/H_2/H_2S$ gas mixture at T_S~700°C. With increasing sulfur content in the gas phase, the room temperature conductivity[2], the room temperature electron field emission properties[3], and the thermoionic emission at 340°C[4], were enhanced.

We were able to synthesize nanocrystalline diamond (n-D) at T_S~500°C by using the same technique and gas mixture[5]. The quality of n-D was shown to increase with the decrease of T_S (Figure 1). When 2.0% CH_4 was employed without H_2S, only nanocomposite carbon was grown, but the addition of 500 ppm H_2S and the reduction of T_S resulted in mixed μ-D and n-D (Figure 1). In addition, it was reported that the addition of sulfur in the gas phase induces a significant increase in the growth rate. At T_S~700°C it was possible to obtain a four-fold increase in the μ-D deposition rate, from 0.1 to 0.4 μm/h. We were then able to produce high-quality μ-D and n-D at T_S~440°C (Figure 2)[6] on molybdenum and glass.

We now report on the growth of high-quality μ-D and n-D films by sulfur-assisted HFCVD at T_S<400°C, on temperature sensitive substrates of industrial interest, such as glass. We modified the CVD system in order to attain lower substrate temperatures. The effects on diamond growth and structure of sulfur addition, substrate temperature in the presence of sulfur, and substrate nature are investigated.

The possibility of growing diamond films at such low temperature is interpreted as resulting from profound changes in the gas phase chemistry when trace amounts of sulfur in the form of H_2S are added to the diamond chemical vapor deposition reaction, as observed by laser cavity ring-down absorption spectroscopy. In particular, H_2S leads to the formation of CS in the heat-activated volume around the filament, which turns back into H_2S in the cooler region above the substrate, enhancing the transport of carbon atoms to the growing film surface to form diamond. This enables the deposition of diamond at a lower temperature and at a higher rate.

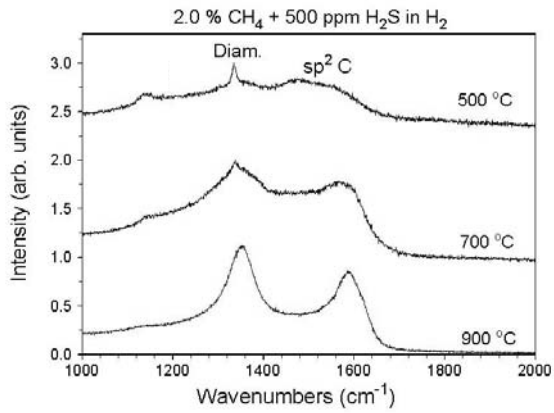

Figure 1. Visible Raman spectra of films grown with 2.0% CH_4 and 500 ppm H_2S as a function of substrate temperature. Diamond deposition is enabled at this high CH_4 concentration due to the presence of S and the lower substrate temperature.

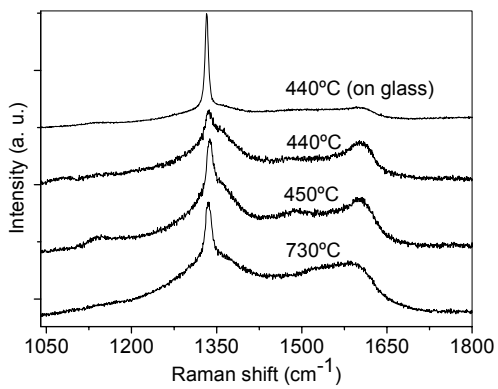

Figure 2. Visible Raman spectra showing the evolution of the diamond peak and sp^2-carbon related peaks as a function substrate temperature T_s. All substrates were Mo, except when indicated.

Acknowledgements: Research supported by NASA (Grants NCC3-1034 and NGT5-40091; Cooperative Agreement NCC5-595), Department of Energy (Grant DE-FG02-01ER45868), and the UPR-Río Piedras FIPI (Grant 8-80-514).

REFERENCES

1. Gupta, S.; Weiner, B.R.; Morell, G.: "Room-temperature electrical conductivity studies of sulfur-modified microcrystalline diamond thin films", *Appl. Phys. Lett.* 83, 491 (2003).
2. Gupta, S.; Martínez, A.; Weiner, B.R., et al.: "Electrical conductivity studies of chemical vapor deposited sulfur-incorporated nanocomposite carbon thin films", *Appl. Phys. Lett*. 81, 283 (2002).
3. Gupta,S.;Weiner, B.R.;Morell,G.:"Electron field emission properties of microcrystalline and nanocrystalline carbon thin films deposited by S-assisted hot filament CVD", *Diamond Relat. Mater.* 11, 799 (2002).
4. Köck, F.A.M.; Garguillo, J.M.; Nemanich, R.J., et al., "Spatial distribution of electron emission sites for sulfur doped and intrinsic nanocrystalline diamond films", *Diamond Relat. Mater.* 12, 474 (2003).
5. Gupta, S.; Weiner, B.R. and Morell, G.: "Synthesis and characterization of sulfur-incorporated microcrystalline diamond and nanocrystalline carbon thin films by hot filament chemical vapour deposition", *J. Mater. Res.* 18, 363 (2003).
6. Piazza, F.; González, J.A; Velázquez, R. et al., "Diamond film synthesis at low temperature", *Diamond Relat. Mater.,* submitted.

COMPARATIVE STUDY OF NUCLEATION PROCESSES FOR THE GROWTH OF NANOCRYSTALLINE DIAMOND

Y.K. Liu, and P.L. Tso

Tsing Hua University, Taiwan; d897710@oz.nthu.edu.tw

I.N. Lin

Tam Kang University, Taiwan

Y. Tzeng

Auburn University, USA

Keywords: Nanocrystalline diamond, NCD, Nucleation, MPCVD.

Abstract

Methods for seeding silicon substrates with explosion produced nanodiamond powder and the in-situ generation of diamond nuclei by the bias enhanced nucleation (BEN) method have been studied to examine their effects on the nucleation density as well as the morphology, the growth rate, and the quality of nanodiamond films. Besides the in-situ BEN process, three ex-situ diamond seeding methods were studied, i.e., (i) mechanical abrasion by diamond powder, and ultrasonication of silicon, (ii) with and (iii) without pre-treatment of the silicon substrate by a hydrocarbon plasma, in solvents with suspended nanodiamond. Although the growth of nanocrystalline diamond is predominantly controlled by the high secondary nucleation rate that is promoted by the high density C_2 radicals in a noble-gas-rich microwave plasma environment, a higher diamond seeding and nucleation density on the substrate is also found to result in a higher growth rate for nanocrystalline diamond. With an optimized diamond seeding or nucleation process, ultra-thin, smooth and homogenous nanocrystalline diamond films have been fabricated.

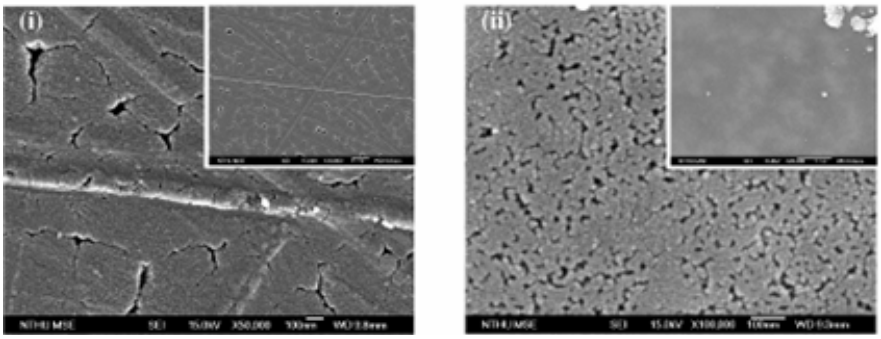

Figure 1- SEM photographs of the nucleation sides of NCD films grown using (i) diamond seeding by mechanical abrasion by diamond powder and (ii) ultrasonication of silicon in a solvent with nanodiamond powder. Silicon was pre-treated by a hydrocarbon microwave plasma.

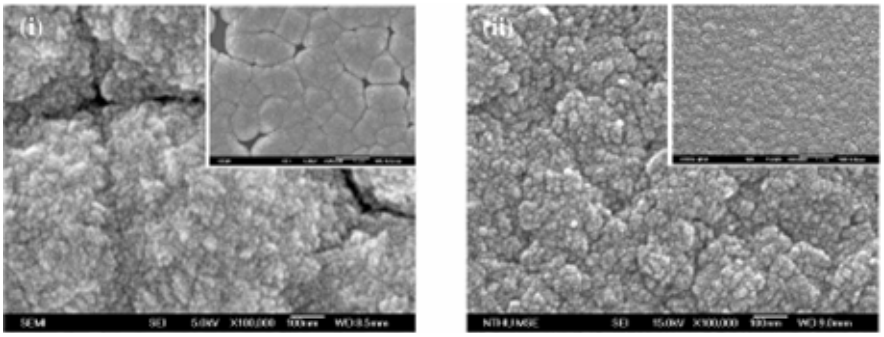

Figure 2- Morphologies of the growth surfaces of nanodiamond films that were (i) seeded by diamond by mechanical abrasion using diamond powder (left) and (ii) in-situ nucleated with diamond by means of a bias-enhanced nucleation process (right) (growth conditions: gas flow rates at CH4/Ar/N2=2/90/10sccm, microwave power of 700W, gas pressure at 125 Torr, deposition time for 1 hr.)

THE ORIGIN OF SPIRAL GROWTH DEFECTS DURING EARLY STAGES OF HOMOEPITAXIAL DIAMOND GROWTH ON (100) SURFACES

Gopinath Bhimarasetti, Mahendra K. Sunkara

Department of Chemical Engineering, University of Louisville, Louisville KY UAS 40292

James E. Butler

Gas Surface Dynamics Section (Code 6174), Naval Research Laboratory, Washington DC USA 20355

Keywords: Diamond homoepitaxy, spiral defects, polishing grooves, mis-aligned joining, lattice mis-tilts

Abstract

Interrupted growth experiments and topographical characterization using atomic force microscopy and scanning electron microscopy were used to understand the origin of defect formation during homo-epitaxial growth on well polished, diamond {100} substrates. Experimental evidence suggests that the origin of spiral growth patterns and trapezoidal growth hillocks could be traced to "mis-aligned" joining of two islands during growth on {100} substrates. The growth of mis-oriented islands on the well polished, diamond {100} surfaces occurred due to the local mis-tilts of the lattice caused by polishing in <110> direction. The results also showed that when the sub-surface damage due to polishing was removed, the defect formation was minimized and a layer by layer growth mode was observed. Further experiments are needed to further understand the reasons for observed spiral growth patterns under cases where no stresses are present, i.e., spiral growth patterns on the {100} facets of vapor phase grown cubo-octahedral shaped crystals.

Introduction

Understanding the formation and propagation of defects at the atomistic scale is the key to the development of processes for synthesis of large area, defect free diamond. Homoepitaxial growth on {100} substrates is typically used for obtaining films with smoother surfaces compared to (111) and (110) surfaces. However, homoepi growth on (100) surfaces frequently results in several characteristic defects such as: pyramidal growth hillocks, trapezoidal features and spiral growth patterns. Although, the nature of these defects is well known in terms of their geometric character, the origin of such defects is poorly understood. Several variations in growth conditions have been attempted to eliminate these defects and to obtain defect free films. These methods primarily relied on varying the growth temperature and feed gas compositions (ultra-low CH_4 concentrations) which typically result in low growth rates. Many of the studies have used topographical characterization after final stages of growth on thicker films to observe the defect formation, which cannot be used to determine the origin of defects. A better understanding of the origin of defect formation during early stages would allow one to develop "high growth rate" recipes for homoepi of diamond.

Here, we conducted a set of interrupted growth experiments followed by topographical characterization using AFM and SEM. The goal of these studies was to capture the early stages of defect formation and to follow the evolution of the same defect over a sequence of several growth runs. Such a morphological evolution sequence of defects, with respect to its local environment, is used to track the early stages of defect formation (or spiral growth pattern). However, due to the lack of large enough atomically smooth surfaces, mechanically polished (100) surfaces of HPHT type Ib diamond substrates were used.

Experimental

Growth experiments were performed in a MW plasma reactor using 0.33% CH_4/H_2 feed gases, 50 torr reactor pressure and 1100 watts microwave power. Same growth conditions were maintained throughout all the experiments. The as-received diamond substrates were mechanically polished and acid cleaned before any growth was performed on them. The mis-orientation of all the (100) surfaces used here, was maintained less than 1°. In order to capture the early stages of defect formation, growth experiments were performed for duration of a few minutes, followed by topography analysis using AFM/SEM and optical microscopy. Several such sequential growth

experiments were performed on the same substrates to obtain the morphological evolution of defects. Two different sets of substrates were used in these studies: (a) (100) substrates with <110> mechanical polishing grooves and (b) specially prepared (100) surface by removing the sub-surface damage caused by mechanical polishing.

Results

Experiments performed on substrates that were mechanically polished in the [110] direction resulted in typical defects on the surface. These defects occur primarily along the polishing grooves. Interrupted growth experiments performed in this work allowed us to determine the primary reason for defect formation. An example of the formation of a spiral defect is shown in Figure 1. The formation of the secondary crystallites, typically observed on defects on (100) surfaces, is identified to be due to the nucleation of a twined crystal on a local {111} plane appearing during the mis-aligned joining of growth islands. Homoepi growth on substrates that were treated for removing the mechanical polishing induced sub-surface damage resulted in defect free layers.

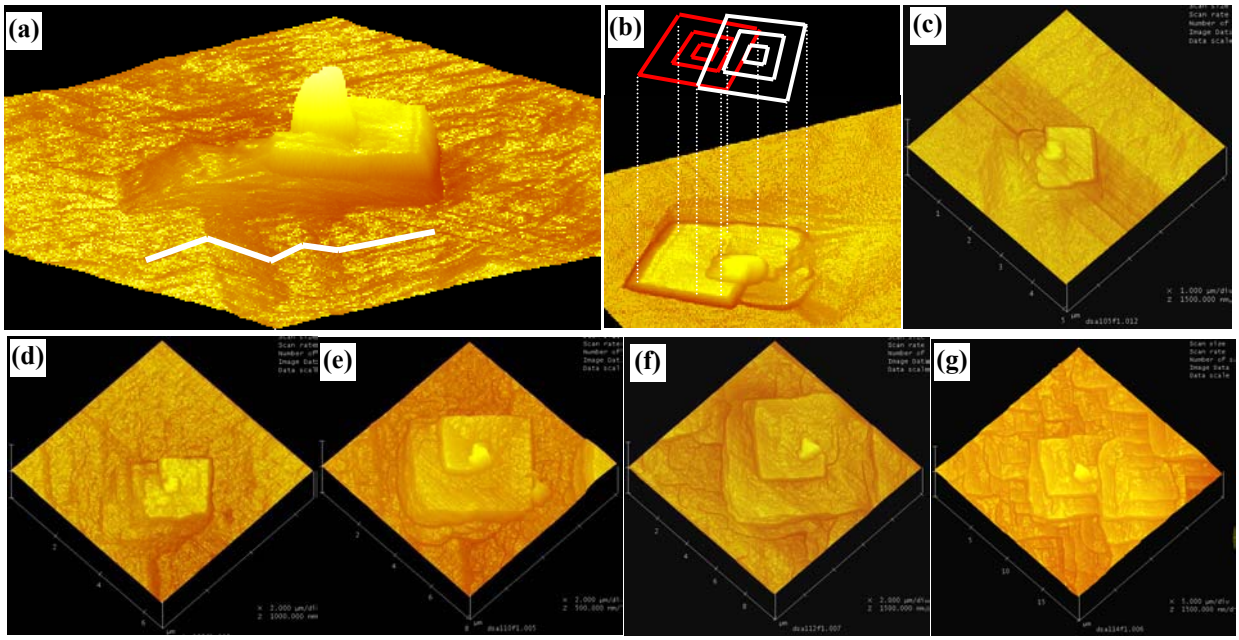

Figure 1. Formation of a spiral defect. (a) a perspective view of the defect during the early stages of growth indicating the role of polishing grooves (highlighted by white line), (b) different perspective view of the defect shown in (a) with increased z-scale and indicating the mis-aligned joining of two islands (shown in red and white and (c-g) morphological evolution sequence of the same defect shown in (a) and (b) over a sequence of 5 growth experiments, each lasting 1 hr.

The typical evolution sequence of a spiral growth pattern as shown in Figure 1 strongly suggests that the island formation on either side of the groove is favored and their joining during growth typically resulted in a mis-aligned joining as shown in Fig. 1(b). Further growth after joining led to spiraling of uneven surfaces. Earlier studies (1, 2) have revealed that mechanical polishing could generate enough stresses to cause local mis-tilts on the top surface of diamond stones. These mis-tilts in regions around polishing grooves allowed for such mis-aligned joining of islands across the grooves, causing spiral growth patterns.

References

1. Lang A.R. et al., "Optical microscopic, synchrotron X-ray topographic and reticulographic study of homoepitaxial CVD diamond," *J. Cryst. Growth*, 200, 3-4, 446-457 (1999)

2. Frank F.C.; Lawn B.R.; and Lang A.R.: "A study of strains in abraded diamond surfaces," *Proc. R. Soc. Lond. A*, 301, 1466, 239-252 (1967)

EFFECTS OF SYNTHESIS PARAMETERS ON PROPERTIES OF CARBIDE DERIVED CARBON FORMED ON SIC

A. Lee, C. White, R. Zhu, M. McNallan, A. Erdemir, Y. Gogotsi

University of Illinois at Chicago

Abstract

Carbide derived carbon (CDC) is formed when the metal component of a ceramic carbide is extracted at a temperature low enough that the residual carbon cannot relax into the equilibrium structure. CDC structures contain nanostructured amorphous carbon with substantial porosity, carbon onions and diamond structures. CDC can be produced on SiC by exposure to chlorine containing gases at temperatures in excess of 800°C so that the silicon is removed as volatile silicon chlorine compounds. The growth kinetics and properties of the CDC are influenced by the temperature of the reaction and the presence of additional gas species (particularly hydrogen) in the reactive gas mixture.

The properties of CDC formed on SiC are of particular interest because CDC layers can improve the tribological performance of SiC components in bearings and other sliding friction applications. The effects of temperature and reactive gas composition on the growth rate, hardness, friction coefficient and chlorine content of CDC layers has been investigated with the goal of identifying the processing conditions which produce the best combination of properties for sliding wear.

SESSION 10

SYNTHESIS & GROWTH MECHANISM II

PECVD Fabrication of Carbon Cones and Helices on a Metal Tip

X. Jiang and Guangyu Zhang*
Institute of Materials Engineering, University of Siegen,
Paul-Bonatz-Str. 9-11, 57076 Siegen, Germany

*Current address: Department of Chemistry, Stanford University, P.O. Box #3, Stanford, California 94305, USA

Abstract

Plasma enhanced chemical vapor deposition (PECVD) is a powerful tool for synthesis of materials such as diamond, carbon nanofibers and carbon nanotubes. Its working parameters are easily tunable thus allowing us to perform various controlled process like doping, etching etc. In addition, the plasma above a substrate surface can be modulated by the substrate's shape resulting in synthesis of amazing structures by this technique. Here we report the fabrication of carbon cones and helices on iron (or nickel) tips using the PECVD method. The cones are made of concentric cylindrical graphite sheets, which have similar structures as carbon nanotubes. The stacking sequence of inner layers prefer to a graphitic ones, that is, the chirality of each inner tubes tend to be the same. Due to their unique shapes and structures, these cones are potentially good candidates as electron emission tips and scanning probes. Other structures grown on the metal tips are the carbon nanohelices which can simply be deemed as twisted carbon ribbons. Their growth obeys a tip-growth model (catalyst particles are on the tip of the nanofibers). The field emission investigations revealed a low turn-on electric field.

HPHT Treatment of Single Crystal CVD Diamond

P. Doering
Apollo Diamond, Inc., Sherborn, MA, USA
doeringp @apollodiamond.com

Keywords: single crystal CVD diamond, stress, annealing, optical properties

Single crystal diamond grown by the CVD technique has been demonstrated to possess outstanding properties compared to single crystal diamond from other sources. Many applications of single crystal diamond (such as gem stones and optical windows) are highly sensitive to its optical properties; specifically its optical absorption and distortion at the wavelengths of interest. One technique used to manipulate diamonds optical properties is HPHT treatments. In this presentation, we will discuss our experience in using these treatments on single crystal CVD diamond.

Large Single Crystal CVD Diamonds at Rapid Growth Rates

Chih-shiue Yan, Yu-chun Chen, Shih-shian Ho,
Ho-kwang Mao and Russell J. Hemley

Geophysical Laboratory, Carnegie Institution of Washington,
5251 Broad Branch Road NW, Washington, DC 20015

The method of high growth rate single crystal CVD diamond [1] has opened new opportunities for the application of diamond. We report successful growth of large single crystal CVD diamond over 1 cm thick and 5 carat at growth rate of ~100 μm/h. Various single crystal diamonds were synthesized by MPCVD at 8-20% CH_4/H_2, 0.2-3% N_2/CH_4, 160-220 torr at various temperatures. All substrates were HPHT synthetic type Ib yellow diamonds with {100} faces on top and on the sides. Morphologies and colors of the as-grown CVD diamonds strongly depend on the deposition temperature. At temperatures over 1500 ^{o}C, black layers begin to form. Below 900 ^{o}C, black microcrystalline material is deposited. Smooth colorless CVD diamonds enlarged along three dimensions are observed at lower temperature deposition. To increase further the size of the crystals, including three dimensional enlargement, gem-quality CVD diamond are grown at the above conditions sequentially on the 6 {100} faces of the substrate. By this method, a one inch cube of single crystal diamond (~300 carat) is achievable.

1. C. S. Yan *et al*. (2002) *Proc. Natl. Acad. Sci*. **99**, 12523-12525.

Controlling specific and non-specific binding of proteins at diamond surfaces via covalent functionalization with molecular monolayers

Tami Clare Lasseter,[1] Brian Clare,[1] Beth M. Nichols,[1] Nicholas Abbott,[2] and Robert J. Hamers[1]

Department of Chemistry[1] and Dept. of Chemical and Biological Engineering[2]
University of Wisconsin-Madison
1101 University Avenue
Madison, WI 53706

Keywords: proteins, non-specific binding, diamond, covalent functionalization.

Abstract

INTRODUCTION

The non-specific binding of proteins at surfaces degrades the performance of surface-based biosensors and is also relevant for applications such as biomedical implants. Molecules containing repeated ethylene glycol

(-O-CH_2-CH_2-) units have been shown to resist the non-specific bonding of many proteins. While long EG polymers can be used in many applications, for most surface-based biosensing applications one desires to have a molecular layer that inherently resists non-specific binding, and then to embed within that layer specific molecules that have a high affinity for binding specific proteins of interest. In such applications, one desires to control the ratio of specific binding (to the target of interest) to non-specific binding (to other molecules) in a complex mixture of proteins. One way of accomplishing this is to use mixed monolayer consisting of shorter EG oligomers, mixed with specific recognition elements of interest to form a monolayer film.

Previous studies have shown that short oligomers of ethylene glycol consisting of only thee ethylene glycol units ("EG3") can be effective at reducing non-specific binding of proteins to gold surfaces. There has recently been great interest in the use of diamond as a platform for biosensing,[1-3] mandating a desire to understand how to control the specific and non-specific binding of proteins by controlling the structure and chemical composition of the diamond surface.. In this study, we have investigated how covalent functionalization of diamond surfaces with short ethylene glycol oligomers containing between 3 and 6 EG units affects the non-specific binding of four model proteins to the surface.[4-5] Studies have been performed using avidin, fibrinogen, bovine serum albumin, and casein as model proteins. We also used three different types of diamond samples: polycrystalline diamond thin films grown on silicon substrates, high-pressure high-temperature diamonds, and a natural single-crystal diamond, to help identify how surface roughness affects the non-specific binding. Finally, by mixing these EG oligomers with specific biomolecular recognition elements (such as avidin, which has a strong affinity for avidin), one can maximize the surface chemical composition to maximize the specific binding of proteins to the recognition elements of interest, while simultaneously minimize the non-specific binding of other proteins. Ultimately, our work demonstrates how to optimize the diamond surface structure and chemistry to control the specific and non-specific binding of proteins to the surface.

COVALENT MODIFICATION WITH ETHYLENE GLYCOL OLIGOMERS

We previously developed a method for covalent functionalization of diamond surfaces using molecules bearing a vinyl (C=C) group at one end of the molecule. To covalently link biomolecules such as DNA to the diamond surface, it is possible to use molecules in which one end is terminated with a vinyl group and the other end of the molecule is terminated with an amine or other suitable chemical functional group. Here, we use molecules with a vinyl group at one end and ethylene glycol oligomers at the other end.

The non-specific binding was measured in two methods. In the first method, the surfaces were exposed to fluorescently-tagged proteins of interest. After copious rinsing, the amount of residual protein on the surface was measured using a fluorescence imager. Because fluorescence quenching at surfaces can significantly affect the fluorescence intensity, this method cannot be used for quantitative measurements or to compare different substrates, such as diamond and gold, that would be expected to exhibit very different amounts of quenching. Consequently,

quantitative measurements were performed using a wash-off method in which the protein bound to a surface is removed via chemical digestion and extensive soaking in surfactant, and the fluorescence intensity of this wash-off solution is measured with a sensitive fluorometer and compared with standards of known concentration.

Since amine groups are often used for covalent attachment of biomolecules to surfaces, we compared the EG-modified surfaces with those functionalized with primary amine groups. Our experiments show that chemical modification with the short EG3 oligomer reduces non-specific binding on polycrystalline diamond samples by approximately 70% compared with the amine-terminated surface. Our data show that functionalization of diamond with EG3 is very effective at reducing non-specific binding for all four proteins investigated. However, we find additional reduction by extending the EG moiety from 3 to 6 unit, as the EG6 molecule reduces the non-specific binding of aviding by 98%, and by more than 90% for all four proteins investigated. For comparison, we have also performed experiments using dodecene, which produces a surface functionalized with simple alkyl chains. While dodecene also helps to reduce non-specific binding for some proteins, it is significantly less effective than EG3 or EG6.

By mixing EG6 with a vinyl-terminated protected amine, it is possible to fabricate mixed monolayers of controlled composition on the diamond surface. By measuring the amount of specific and non-specifically bound protein as a function of monolayer composition, we investigated how to optimize the monolayer composition to maximize the ratio of specific/non-specific binding. For the case of avidin-biotin, we find that using a mixture containing approximately 70% EG6 and 30% amine groups produces more than a factor of 12 improvement in the overall ratio of specific to non-specific binding.

Finally, we compared the reduction of non-specific binding on diamond surfaces with different microscopic morphologies. Quantitative measurements show that EG6-functionalized polycrystalline diamond samples resist non-specifically bound proteins to about the same extent as functionalized surfaces of gold self-assembled monolayers. Since gold-SAM structures are widely used, this indicates that functionalized diamond surfaces are at least as good as gold-SAM structures. However, in experiments using a (111)-cleaved natural single-crystal diamond, we find an additional significant reduction. The EG6-modified single-crystal diamond sample is significantly more effective at resisting non-specific binding than any other sample we have measurent. These results indicate that the microscopic roughness present on microcrystalline diamond samples contributes significantly to the residual non-specific binding. Thus, efforts to reduce the nanometer-scale roughness of diamond surfaces would be expected to yield further reduction in non-specific binding. For biosensing applications, this in turn leads to improvements in sensitivity and selectivity.

Our results show that the behavior of diamond films can be significantly modified using molecular monolayers consisting of short oligomers of ethylene glycol. Photochemical modification of the surface using using ethylene glycol oligomers with a terminal vinyl group provides a mean to achieve this. Diamond surfaces covalently modified in this way are highly effective at resisting protein binding, while the use of mixed monolayers provides a way to add specific biomolecular recognition elements at will. Our results demonstrate a clear pathway for producing well-defined molecular layers exhibiting precisely-tailored biological interactions.

REFERENCES

1. Yang, W., et al. , "DNA-modified nanocrystalline diamond films as stable, biologically active substrates", *Nature Materials,* **1**, 253-257 (2002).
2. Yang, W., et al. "Interfacial Electrical Properties of DNA-modified Diamond Thin Films: Intrinsic Response and Hybridization-Induced Field Effects", *Langmuir*, 20, 6778-6784 (2004).
3. Yang, W. and Hamers, R.J., "Detection of biological binding events using a diamond thin-film field-effect transistor", *Appl. Phys. Lett*., 85, 3626 (2004).
4. Lasseter, T.L., et al. ,"Covalently Modified Silicon and Diamond Surfaces: Resistance to Non-Specific Protein Adsorption and Optimization for Biosensing", *J. Am. Chem. Soc.*, 126, 10220-10221 (2004)..
5. Lasseter Clare, T.L., et al., “Improved Resistance to Protein Adsorption on Oligo(ethylene glycol) Modified Silicon and Diamond Surfaces”, *Langmuir, in preparation*.
6. Strother, T., et al., "Photochemical Functionalization of Diamond Films", *Langmuir,* 18, 968-971 (2002).

NANOCRYSTALLINE DIAMOND ON CARBON NANOTUBES: TOWARDS A NEW CLASS OF CARBON NANOMATERIALS

M.L.Terranova, A.Fiori, S.Orlanducci, V.Sessa, E.Tamburri,

Dipartimento di Scienze e Tecnologie Chimiche, Università di Roma Tor Vergata, via della Ricerca Scientifica, 00133 Roma; E-mail: **marialetizia.terranova@roma2.infn.it**

M.Rossi

Dipartimento di Energetica, Università di Roma La Sapienza, via Scarpa 16, 00162 Roma

A.S.Barnard

Center for Nanoscale Materials, Argonne National Laboratory, Argonne IL 60439

Keywords: nanotubes, nanodiamond, nucleation, modeling, CVD synthesis

Recently, carbon nanotubes and nanodiamond have emerged as the more advanced and fascinating forms of crystalline carbons. The outstanding mechanical, chemical, electronic and thermal properties of these nanomaterials suggest wide applicability in advanced technological areas. However the control of growth locations and orientation of such nanostructures and the production of well defined architectures on micro- and nano-scale is necessary for the development of high performance materials.

In this context we have focused our research activity on establishing strategies for the generation of deposits of carbon nanotubes with controlled organization in terms of alignment, orientation and density. Moreover, the development of new experimental techniques has allowed us to produce coatings of nanocrystalline diamond (grain size in the range 5-50 nm) on carbon fibers [1].

In this communication we outline a methodology for the growth of nanodiamond on bundles of single-walled carbon nanotubes (SWNT). Using a CVD-based technique, metal-catalysed reactions of carbon species with hydrogen fluxes allow us to generate the two different phases during the same run. The reactants are atomic H and carbon nanopowders (mean diameter: 40 nm) carried by an Ar stream and delivered through a nozzle across the active area of the substrate, where the C nanostructures are deposited.

The substrates (Si plates coated by a sub-micrometer dispersion of Fe particles) can be translated and positioned at controlled distance with respect to the heated filament of the CVD reactor. Several characterization techniques (FE-SEM, TEM. RHEED, Raman spectroscopy) are used to monitor the structural evolution and the growth progression of both carbon nanophases in samples with growth time ranging from 1 to 15 minutes.

The SEM analysis of samples grown for times less than 2 min shows the initial formation of randomly oriented SWNTs assembled in bundles with diameters around 120 nm. After approximately 4 min the deposits are formed by nanotube bundles which begin to align parallel each other (self-assemble). In the samples grown for 6-8 min (Fig.1 a) the graphitic walls of the SWNTs appear covered by nanocrystalline grains with the typical features of diamond (s.g Fd3m) and after 10 min the diamond coverage is complete along the whole length of the SWNT bundles. At this stage the morphological characterizations evidence arrays of tubular structures covered by well shaped crystallites with diameters in the 20-100 nm range (Fig.1 b).

The dynamic of the process is found to depend on the relative abundance of atomic H impinging on the external surface of the nanotubes. First principle calculations carried out in order to investigate the effects of H adsorbates on SWNT walls indicated that the formation of C-H bonds disrupts locally the C-C sp^2 network and promotes the creation of suitable sites for diamond nucleation [2] .

These hybrid carbon nanostructures are extremely interesting materials for nanotechnology They are likely to find applications as efficient field- and electron-emitters but can also serve in mechanics, thermal management and sensing on a nanometer scale . The functional properties of carbon nanotubes coated by nanodiamond are presently under investigation in our laboratories.

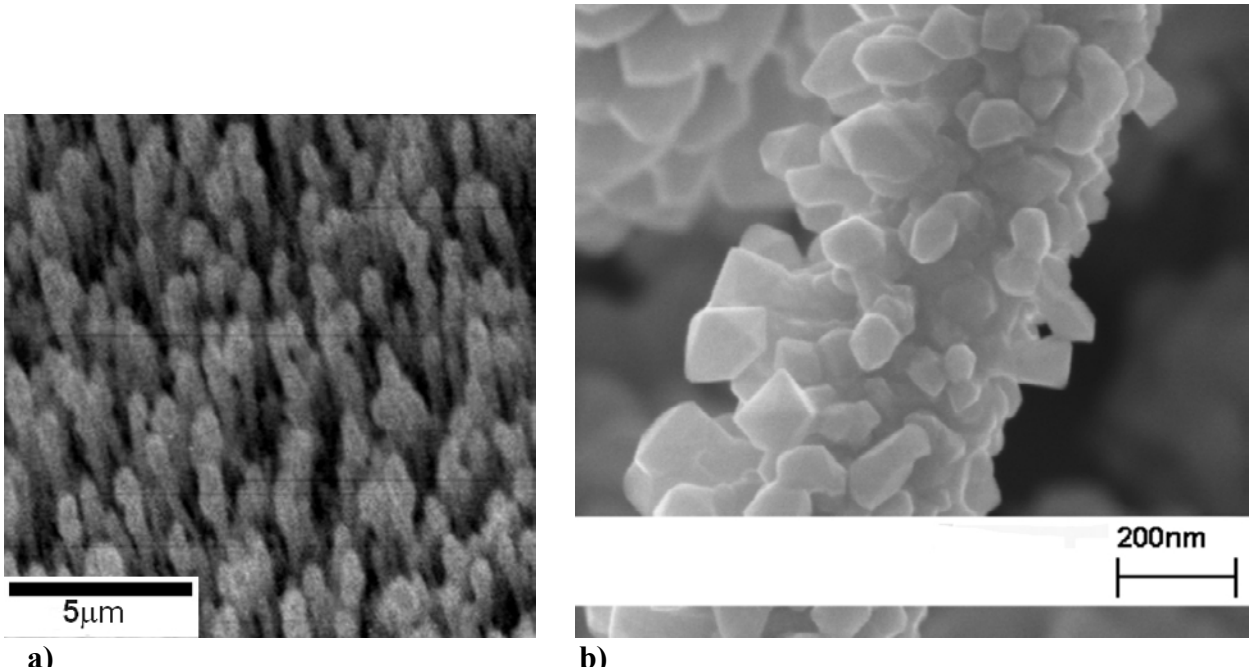

Fig.1 FE-SEM images: a) an array of nanotube bundles coated by nanodiamond; b) details of diamond nanocrystallites

REFERENCES

1. M.Rossi, M.L.Terranova, S.Piccirillo, V.Sessa and D.Manno: "Meso- and nano-scale investigation of carbon fibers coated by nano-crystalline diamond" Chem.Phys.Lett. (in press)
2. A.Barnard, M.L. Terranova and M.Rossi: "Density functional study of H-induced nucleation sites in hybrid carbon nanomaterials" Chem of Mater. (in press)

SYNTHESIS OF MESOPOROUS CARBONS THROUGH INVERSE REPLICATION AND SELF-ASSEMBLY

Michal Kruk, Bruno Dufour, Krzysztof Matyjaszewski, Tomasz Kowalewski

Department of Chemistry, Carnegie Mellon University, 4400 Fifth Avenue, Pittsburgh, Pennsylvania 15213

Ewa B. Celer, Mietek Jaroniec

Department of Chemistry, Kent State University, Kent, Ohio 44242

Keywords: polyacrylonitrile, block copolymer, mesoporous carbon

Abstract

Mesoporous carbons have recently attracted much attention, because of their usefulness as adsorbents for large molecules, components of electrochemical double-layer capacitors, catalyst supports and so forth. One of important recent achievements in this field was the synthesis of ordered mesoporous carbons through inverse replication of ordered mesoporous silica templates [1]. Herein we describe the combination of this approach with another novel route to nanostructured carbons based on the pyrolysis of nanoscale phase-separated block copolymers [2]. In the latter route, one block, e.g., polyacrylonitrile (PAN), serves as carbon precursor whereas the other block, immiscible with the first one, induces self-assembly into a variety of nanostructures and is sacrificed upon pyrolysis. Use of an organic sacrificial block, which is volatilized before carbonization of the carbon precursor block, poses the challenge in replicating and preserving of bulk nanostructure, in particular in maintaining the connectivity of mesopores. We have now designed a new system, in which sacrificial block is water soluble and is used as a template for formation of silica. Silicious phase acts as a scaffolding supporting the evolving carbon phase during the pyrolysis and is subsequently etched away, leaving behind mesoporous carbon. Appropriate copolymers were synthesized using atom transfer radical polymerization (ATRP) which provides necessary control over the polymer composition and molecular weight. Mesoporous carbons obtained from these novel precursors exhibited high specific surface area (typically 750-1000 $m^2 g^{-1}$), large pore volumes (up to 2.8 $cm^3 g^{-1}$) and pore diameters ranging from about 4 to 25 nm. In contrast with most mesoporous carbons reported to date, they exhibited very low microporosity. We also explored the synthesis of ordered nanoporous carbons from PAN via the inverse replication procedure [3]. The polymerization of acrylonitrile in the pores of ordered mesoporous silica templates was performed, followed by PAN stabilization and carbonization, and by the dissolution of the silica template. The obtained ordered mesoporous carbons exhibited high specific surface areas (700-1000 m^2g^{-1}) and large pore volumes (0.8-1.8 cm^3g^{-1}). The templates, precursors and carbons were extensively characterized using nitrogen adsorption, thermogravimetry, transmission electron microscopy, Raman spectroscopy and powder X-ray diffraction.

ACKNOWLEDGEMENTS

The support from NSF grant DMR-0304508 is gratefully acknowledged.

REFERENCES

1. Ryoo, R.; Joo, S. H.; Jun, S. “Synthesis of highly ordered carbon molecular sieves via template-mediated structural transformation”, *J. Phys. Chem. B*, 103, 37, 7743-7746 (1999).
2. Kowalewski, T.; Tsarevsky, N.V.; Matyjaszewski, K.: “Nanostructured Carbon Arrays from Block Copolymers of Polyacrylonitrile,” *J. Am. Chem. Soc.*, 124, 36, 10632-10633 (2002).
3. Kruk, M.; Dufour, B.; Celer, E. B.; Kowalewski, T.; Jaroniec, M.; Matyjaszewski, K.: “Synthesis of Mesoporous Carbons Using Ordered and Disordered Mesoporous Silica Templates and Polyacrylonitrile as Carbon Precursor”, *J. Phys. Chem. B*, submitted for publication.

SYNTHESIS OF HYBRID NANOCARBON MATERIALS BY SELF-ASSEMBLY

Xingcheng Xiao, Jeffery Elam, S. Trasobares, Orlando Auciello, John A. Carlisle

Materials Science Division, Argonne National Laboratory, 9700 S. Cass Ave. IL. 60439 USA

Keywords: Hybrid nanocarbon, ultrananocrystalline diamond, carbon nanotubes, self assembly, plasma chemistry.

Abstract

Research interest on nanocarbons has been promoted by the discovery of carbon nanotubes and the emergence of CVD nanocrystalline diamond films. The different combinations of the configurations of electronic states of carbon atoms and short/long order of the bonds lead to different form of nanocarbons and provide them with unique properties. The synergistic combination of different forms of nanocarbon in order to take advantages of their unique properties has the potential of yeielding materials with novel properties that could be used advantageously in applications such as nanoelecronics, protective coatings, and energy related technologies. In this presentation, we report our recent results on the synthesis and integration of various nanocarbon materials.

Various nanocarbons, including ultrananocrystalline diamond (UNCD) and CNTs, have been synthesized by using tailored hydrogen-poor Ar/CH_4 plasma chemistry, temperature and growth templates. The process for simultaneous growth of UNCD and CNTs was established for the first time and different configurations of integrations of UNCD and CNTs were obtained by self-assembly. Scanning and transmission electron microcopies (SEM & TEM), Raman Spectroscopy, and Near Edge X-ray Absorption Fine Structure (NEXAFS) confirmed the coexistence of ultrananocrystalline diamond (UNCD) and CNTs in the hybrid material, and also the direct covalent bonding of the two materials. Isolated diamond clusters interconnected with CNTs as well as fully-dense thin films were synthesized, and the relative proportion, nanostructure, and local order was easily controlled through adjustment of the nucleation conditions for the two phases, and can be further patterned via the straightforward application of known lithographic techniques. The capability to control the configurations and alignments of CNTs, and the success to grow CNTs and UNCD simultaneously, provides a novel approach to fabricate “self-assembly” nanostructured carbon materials. The hybrid nanocarbon materials have the potential for technololgical applications such as materials for hydrogen storage and membranes fuel cells and electrodes in supercapacitors in order to increase the energy conversion efficiency.

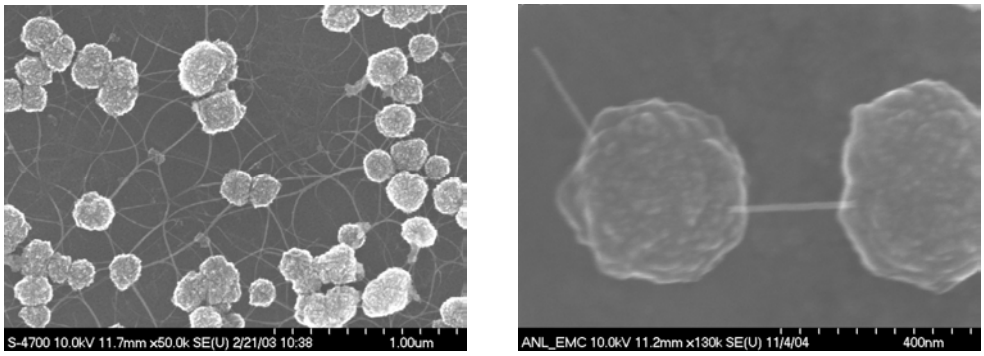

Figure 1. The simultaneous growth of ultrananocrystalline diamond and carbon nanotubes

SESSION 11

MATERIALS INTEGRATION

Silicon-on-Diamond: An Engineered Substrate for Electronic Applications

A. Aleksov[1], J. M. Gobien[1], X. Li[1], N. Govindaraju[1], J. T. Prater[2] and Z. Sitar[1]

[1)] North Carolina State University, Department of Material Science and Engineering
[2)] Army Research Office

Silicon on Diamond (SOD) is a substrate material engineered to address the major challenges of silicon-based VLSI-technology in particular thermal management and charge confinement. In the present SOD-concept, this is achieved by joining a single crystalline Si-layer (device-layer) suitable for the fabrication of IC's with a highly oriented polycrystalline diamond (HOD) layer that serves as an electrical insulator, a heat spreader and a substrate. Therefore SOD represents an alternative SOI concept, where the thermally insulating SiO_2 is replaced by highly thermally conductive diamond.

First experiments and simulations aimed at the assessments of thermal management properties of fabricated SOD wafers were made and compared to Si and SOI. Two experimental methods were used to achieve this task, direct measurements of the temperature of metallic micro-strip heaters by exploiting their thermally dependent conductivity and thermal imaging of micro-strip heaters by using an IR-CCD camera. The theoretical assessment was performed by finite element modeling (FEM) of micro-strip heaters on Si, SOI and SOD. The results of the measurements are in good agreement with the values obtained by FEM and show that SOD can sustain >15-times higher power inputs than SOI, which translates into a ~4 times higher integration density of devices on SOD.

After validating the primary benefits of SOD, namely its superior thermal management properties, the second task is to show device operation on SOD and compare the operation of these devices with respect to SOI. In addition the analysis of the interface properties between the Si-device layer and diamond is important to understand the operation of devices on SOD and their limitations. For this reason MESFETs and Schottky diodes are fabricated on the SOD and SOI wafer simultaneously, which will allow for a complete electrical analysis of the SOD concept and a direct comparison with the SOI technology. Evaluation of these first electronic devices on SOD wafers and a comparison to devices fabricated on SOI will be presented.

CVD DIAMOND THIN FILM TECHNOLOGY FOR MEMS PACKAGING

Xiangwei Zhu, Dean M. Aslam

Electrical and Computer Engineering, Michigan State University, E. Lansing, MI 48824, USA

Phone: (517)-432-5648, E-mail: zhuxiang@egr.msu.edu

Keywords: Diamond, Thin Film Package, Integrated, MEMS.

Abstract

Due to its extreme hardness, chemical and mechanical stability, large band gap and highest thermal conductivity, poly-crystalline diamond (poly-C) is expected to be an excellent packaging material for biomedical and environmental MEMS devices. Recent wafer-level MEMS packaging approaches can be characterized into two categories; integrated encapsulation process[1] and wafer bonding process[2]. To apply poly-C MEMS technology on packaging, in addition to thermal management application as heat sink[3], a fabrication technology of all-diamond packaging panel with built-in interconnects (boron-doped poly-C) was reported[4]. This paper reports, for the first time, the development of poly-C thin film packaging technology which is integrated into the post-MEMS encapsulation process. Boron-doped poly-C is studied as a material for feedthroughs, which is embedded in undoped insulating poly-C package.

DESIGN CONCEPT

A diamond thin film package for MEMS devices, depicted in Figure 1 (a), is fabricated using a 3-mask process (Figure 1 (b)). After a 1-μm-thick boron-doped poly-C film is deposited and patterned for feedthroughs, a 4-μm-thick poly-C film is deposited on 4-μm-thick sacrificial PECVD oxide. The poly-C film is patterned with fluidic access ports for the releasing of the package. These access ports are used to seal the package in final step consisting of additional poly-C growth, which will only grow on existing poly-C layers.

PACKAGE FABRICATION

A typical poly-C film fabrication involves seeding, growth and patterning. For seeding, diamond powder with an average particle size of 100 nm was applied on the sample surface using a diamond-loaded photoresist (DPR) technique[5]. Then, a poly-C thin film was grown using MPCVD system in a CH_4:H_2 (1.5 sccm : 100 sccm) gas mixture environment with 40 torr pressure at temperature of 730 °C. The Raman spectra taken on the deposited poly-C film show a sharp sp^3 peak at 1332 cm^{-1}, indicating high sp^3/sp^2 ratio. A microwave electron-cyclotron-resonance (ECR) RIE system was used to dry-etch the poly-C film using the parameters shown in Table 1. The poly-C feedthroughs were doped in-situ using tri-methyl-boron diluted in hydrogen (0.098%) as the source of boron. This doping technique leads to resistivities in the range of 0.003 – 0.31 Ω-cm[4]. The resistivity of the poly-C feedthroughs film in the test package (Figure 2) was 0.02 Ω-cm.

RESULTS AND SUMMARY

Figure 2 shows the first generation of fabricated diamond package. Fluidic access ports for etching were studied as shown in Figure. 2 (c) – (d). The poly-C thin film experienced compressive stress after release. Films with zero-strains can be fabricated by adjusting the growth conditions. During the sealing of access ports, poly-C will only grow on the areas consisting of poly-C, with typical sealing pressures of 40 torr (the poly-C growth pressure). For packages requiring lower pressures, ECR CVD diamond growth, reported at 10 mtorr[6], can be used for the final sealing step. A new set of masks is being designed which can help to optimize the releasing of the package and sealing of the package under lower pressures. The poly-C thin film packaging technology is being reported for the first time and is expected to provide new structures/concepts in the MEMS packaging.

Table 1. ECR plasma etching parameters

Gas Flow Rate (**sccm**)			Microwave Input Power (**W**)	RF Power (**W**)	DC Bias (**V**)	Chamber pressure (**mtorr**)	Typical Etch Rate (**μm/hour**)
Ar	O_2	SF_6					
8.0	28.0	2.0	400	100	-130	5	4.5

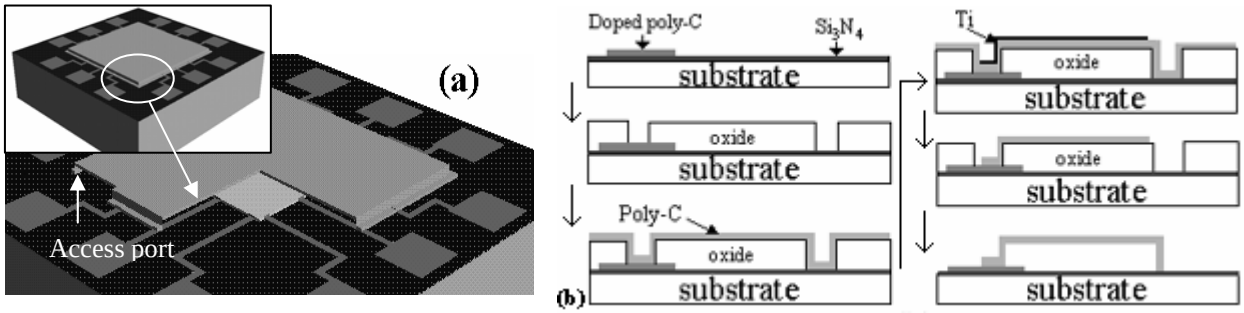

Figure 1 (a) Basic Concept and Cross-section view; (b) fabrication process.

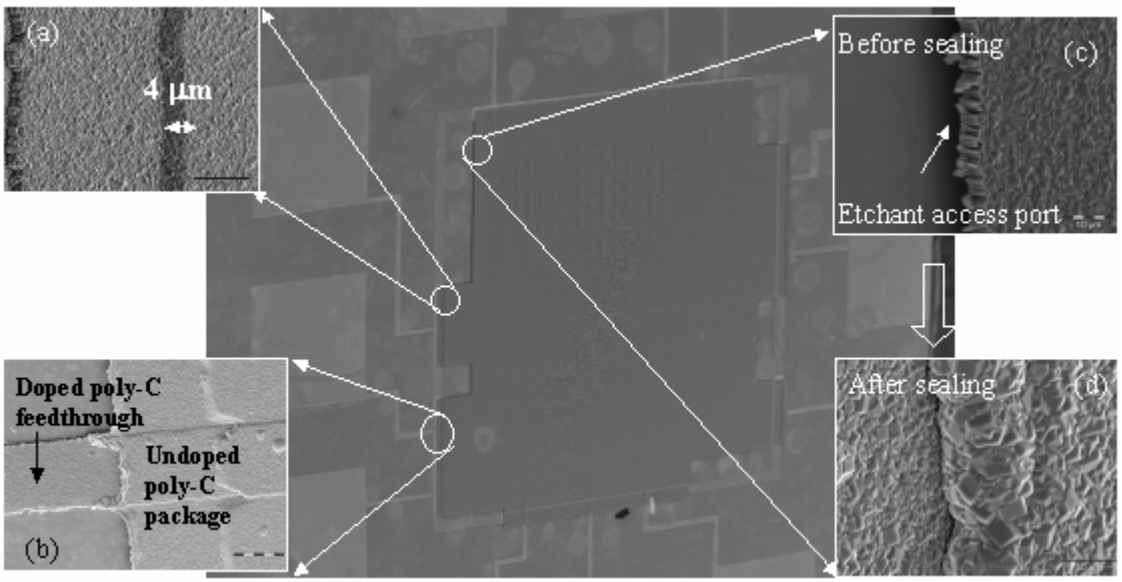

Figure 2 Fabricated poly-C thin film package; insets are close view of (a) package border, (b) poly-C feedthrough and (c) – (d) Study of etchant access port.

REFERENCES

1. Liwei Lin, R.T. Howe and A.P. Pisano, "Microelectromechanical filters for signal processing", *Journal of Microelectromechanical Systems*, Vol. **7**, pp. 286 (1998).
2. B. Stark and K. Najafi, "A low-temperature thin-film electroplated metal vacuum package", *Journal of Microelectromechanical Systems*, Vol. **13**, pp. 147 (2004).
3. K. A. Moores, and Y. K. Joshi, "High Performance Packaging Materials for Improved Thermal Management of Power Electronics", *Future Circuits International*, Issue **7**, pp. 45 (2001).
4. X. Zhu, D. M. Aslam, Y. Tang, et al., "The fabrication of all-diamond packaging panels with built-in interconnects for wireless integrated microsystems", *Journal of Microelectromechanical Systems*, Vol. **13** pp. 396 (2004).
5. G. S. Yang, M. Aslam, "Ultra-High Nucleation for Growth Smooth Diamond Films", *Appl. Phys. Lett*. **66,** pp. 311 (1995).
6. C. R. Eddy Jr., D. L. Youchison, B. D. Sartwell, K. S. Grabowski, "Deposition of diamond onto aluminum by electron cyclotron resonance microwave plasma-assisted CVD", *J. Materials Research*, Vol. **7**, No. 12 pp. 3255 (1992)

DESIGN OF RESIDUAL STRESS IN NANOCRYSTALLINE DIAMOND FILMS

Nicolas Woehrl, Alexei Poukhovoi, Stephan Reuter, Volker Buck

Thin Film Technology Group FB 7, University of Duisburg-Essen, Universitaetsstr. 3-5, 45141 Essen, Germany

Keywords: nanocrystalline diamond, residual stress

Abstract

Nanocrystalline diamond films were deposited with an IPLAS *CYRANNUS*® plasma source. The functional principle of this microwave plasma source is based on a resonator with annular antennas. This special setup allows the use of plasma from low pressure (10^{-2} mbar) to atmospheric pressure (1 bar).

The nanocrystalline films shown here were deposited in a pressure range between 200 and 300mbar from an $Ar/H_2/CH_4$ plasma. The films were characterized by two wavelength scanning micro Raman spectroscopy, SEM and AFM measurements.

Since the C_2 carbon dimers are believed to be the growth species for nanocrystalline diamond films the deposition rate was optimized using optical emission spectroscopy. The emission intensities of the C_2 dimer at 515nm from the microwave plasma correlates linearly with the absolute C_2 concentration in $Ar/H_2/CH_4$ plasma [1] and can therefore be maximized by varying the CH_4 concentration, the pressure and the gas flow. A correlation between the amount of C_2 in the plasma and the deposition rate is shown.

Residual stress is a critical parameter in thin film deposition and especially important for technical applications of nanocrystalline diamond films like tribological coatings or MEMS. High residual stress can lead to cracking or even to delamination of the film from the substrate. An ex-situ optical device (SSIOD “Surface Stress Induced Optical Deflection”) was used to measure the curvature of silicon substrates coated with nanocrystalline diamond films. With respect to Stoney’s equation one can calculate the residual stress from the curvature of the substrate. It is shown that the residual stress in the substrate can be varied in a wide range from compressive to tensile stress just by changing the gas flow of the process gas without changing the gas composition or the pressure.

Birell et al. [2] have proposed that the 1120 cm^{-1} and 1450 cm^{-1} peaks in the Raman spectra are due to carbon-hydrogen bonds in the grain boundaries of nanocrystalline films. In this work a correlation is made between the residual stress measurements and the Raman spectras of nanodiamond films. It is shown that the spectra of films with low residual stress feature clearly visible peaks at 1450 cm^{-1} and at 1120cm^{1}.

REFERENCES

1. Goyette, A.N., et al., “C_2 Swan band emission intensity as a function of C_2 density” *Plasma Sources Sci. Technol.*, Vol. 7, 149 (1998)
2. Birrell, J., et al., “Interpretation of the Raman spectra of ultrananocrystalline diamond” *Diam. Relat. Mat.*, Vol. 14, 86-92 (2005)

PROMISING DIFFUSION BARRIER COATINGS FOR FLEXIBLE BACKAGING BASED 0N FCVA TETRAHEDRAL AMORPHOUS CARBON FILMS

G.A. Abbas*, P. Papakonstantinou, J.A. McLaughlin

Nanotechnology Research Institute, School of Electrical and Mechanical Engineering, University of Ulster, Shore road, Newtownabbey, Antrim, BT 37 0QB, UK.

Gamal@nibec-s1.nibec.ulst.ac.uk

Keywords: gas barrier, FCVA, ta-C, Si-incorporation.

Abstract

In this study, surface modification of poly (ethylene terepthalate) (PET) polymeric substrates using Si-incorporated hydrogenated tetrahedral amorphous carbon (ta-C:Si:H) thin films deposited by filtered cathodic vacuum arc (FCVA) system under tetramethylsilane ($Si(CH_3)_4$ (TMS) atmosphere has been investigated. A number of characterization techniques such as high-resolution synchrotron-based x-ray reflectometry, XRR, x-ray photoemission spectroscopy, XPS, multi-wavelength Raman spectroscopies, spectroscopic ellipsometry, SE, and surface profiler have been employed to investigate the role of microstructure, composition and surface morphology on the gas barrier performance of the FCVA films. We have demonstrated that 21 at.% of silicon-incorporation into the ta-C films has caused a complete reduction of the films' intrinsic-stress (i.e. 10 GPa) and a complete disappearance of the surface micro-cracks. Stress reduction was attributed to the development of weak Si-C bonds (3.21 eV) as revealed by XPS, which played a role in releasing bond distortion of the nearby strong sp^3 C-C bonds (3.7 eV; 411 $KJmol^{-1}$). On the other hand, Si-addition significantly improved the permeation barrier performance against water vapor with a reduction factor up to 93%. In comparison with silicon-incorporated PECVD films [1] the results demonstrate that higher silicon- addition was needed for relaxing the highly stressed structure of ta-C films [10GPa]. In contrast to FCVA ta-C films, a thickness-dependence permeation study revealed that that solubility-diffusion was the main mechanism responsible for the transport of water vapor through ta-C:Si:H film/polymer composite.

INTRODUCTION

Amorphous diamond-like carbon (DLC) is becoming a new focus in the research field of flexible electronics. In addition to good impermeability to water vapor and oxygen, which is necessary for such applications, DLC's possess intrinsic flexibility, high hardness, excellent chemical and thermal stability and they are transparent in the visible spectrum. However, high-level of intrinsic-stress (especially in the un-hydrogenated form of DLC) is a major drawback of these types of coatings. We have reported earlier that highly dense ta-C thin films with density (3.3 g/cm^3) near to that of diamond (3.5 g/cm^3) have shown unexpected high water vapor transmission rate (WVTR) (1.3 g/m^3) with gas reduction factor (RF) value of 17%. This is due to the release of high residual-stress, which has affected the surface morphology with a network of deep micro-cracks. The build up of such high-level of residual stress is though to be an intrinsic property of these films caused by the subplantation process responsible on the growth of such hard films. Moreover, the transport of water vapor through surface inhomogeneties (i.e. micro-cracks) is responsible on permeation of water vapor through ta-C films/PET composite, which has resulted in poor gas barrier performance for these hard coatings [1]. However, Si-incorporated PECVD a-C:H stress-free films with lower density have shown high gas barrier performance with WVTR value of 0.03 g/m^3 with RF value of 98%.

In this study, we employed the Si-addition strategy for releasing the residual-stress in hard FCVA ta-C thin coatings deposited at varying tetramethylsilane ($Si(CH_3)_4$ (TMS) partial pressure onto PET polymeric substrates in an attempt to enhance the gas barrier performance of PET polymeric substrates.

Results and discussion

Figure 1.a displays an optical microscopy picture of PET polymer substrate coated with 130-nm-thick ta-C film where a network of cracks (wrinkles) spreads out over the whole substrate surface. AFM has revealed that these cracks have depths comparable to the film-thickness reaching down to the film/polymer interface. A similar surface morphology has been exhibited by a-C:H films on PET [1]. It is strongly believed that such a surface morphology should be attributed to the release of the residual-stress (9-13 GPa). To support the suggestion that residual-stress is the main reason for the observed surface morphology covered by a network of cracks, a series of ta-C films

deposited at different TMS partial pressures (8.0×10^{-7}-1.0×10^{-3}) has been investigated for surface morphology. For films deposited at TMS flow rate of 40 sccm (21.5 Si at.%), a new structure has been observed that has almost zero compressive stress as indicated by surface-profilometric measurments. We have to emphasize that since TMS precursor gas has been used as a source of silicon, the new structure will include also hydrogen as well as silicon. Fig.1.b. shows an optical microscope image of 300-nm layer of ta-C:Si:H film on PET substrate. As one can see, the new surface morphology is completely free of any relevant relaxation (i.e. cracks).

Fig.2. illustrates the evolution of the residual stress of the FCVA ta-C films deposited under varying TMS partial pressure on Si substrates. As one can see, the compressive stress exhibited a progressive reduction from ~ 10.5 GPa at 0.5 at.% silicon to almost 0 GPa with the increase in Si concentration up to 21.5 at.%. Since the bond strength of Si-C (320 KJ mol^{-1}) is smaller than that of the sp^3-hybridized C-C bonds (411 KJ mol^{-1}), the formation of Si-C could be responsible for the reduction in residual stress in Si-incorporated films [2]. The high level of hydrogen may have prevented SiC crystallite formation by terminating 'dangling bonds' during the film growth process, especially for films with high Si/C ratios [3]. Moreover, Si-H bonds may also participate in causing the relaxation of the three-dimensional rigid network of ta-C:Si:H structure and reduce the film stress.

The induced structural modification caused by si-addition with stress-relief has led to not only the enhancement in the surface morphology but also significantly improved the gas barrier performance of ta-C:Si:H films in comparison with ta-C films (as presented in the inset of Fig.2). The reduction in water vapor reached a value of 93 % for 400 nm-thick- ta-C:Si:H films. As a conclusion, this work demonstrated the feasibility of using modified ta-C films on soft substrates that could open a new application window for such a promising material.

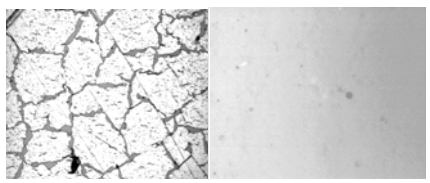

(a) **(b)**

Figure* 1. *Optical microscopy pictures of a PET substrate (magnification of X10) coated with (a) ta-C film and (b) (b) ta-C:Si:H film. The figure clearly illustrates the effect of Si- and hydrogen-addition on the surface morphology of PET coated substrate.

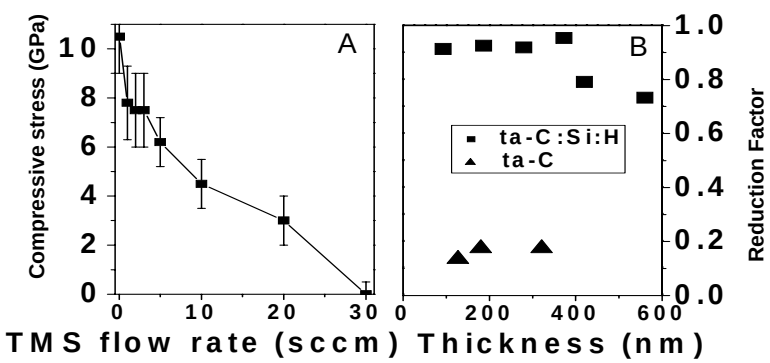

Figure* 2. (a)*Compressive residual stress (evaluated by stylus profiler) of ta-C:Si:H films deposited on Si substrate at different TMS partial pressure (flow rate).* (b)*The reduction factor, RF, of water vapor permeation through the ta-C and Si-a:C:H coated-PET as a function of coating thickness ($WVTR_{PET}$: 1.968 g/m^2 day).

REFERENCES

1- G. Abbas, Jim McLaughlin, E. Harkin-Jones, A study of ta-C, a-C:H and Si-a:C:H thin films on polymer substrates as a gas barrier, *Diamond & Rel. Mater.*,vol.13, No.4-8, pp 1342-1345 (2004).

EVALUATION STRESS, NANOCRYSTALLINITY, PURITY CRYSTALLINITY IN DIAMOND FILMS DEPOSITED ON Ti6Al2Sn4Zr2Mo ALLOY USING THE ASSISTED TECHNIQUE OF MICROWAVE PLASMA

Teófilo M. de Souza[a], Joanisa Possato[a], Joelma de Oliveira[a,b], Jomar E. Bueno[a]
a)Laboratório de Pesquisa e Desenvolvimento de Dispositivos com Diamante CVD e Novos Materiais – Unesp - Campus Guaratinguetá (teofilo@feg.unesp.br; mec03256@feg.unesp.br)
b) FAMINAS - Bairro Universitário-Muriaé-MG(joelmaoliveira@imicro.com.br)

Alix Gicquel[c]

Université Paris Nord - France

Keywords: Ti6Al2Sn4Zr2Mo, Stress, Purity Cristallinity, Diamond, Microwave Plasma

Abstract

This research looks forward to the development of new materials that could ensure the protection of titanium alloys in relation the weariness, thus increasing its usable lifetime. Deposition of CVD diamond thin films were studied on titanium alloys, aiming at further objectives such as in mechanics industry and biomedical implants. Titanium alloys are biocompatible, though not being hemocompatible, deposition of a material with exceptional organic and mechanical properties as is diamond, brings the best solution to that challenge. Another important factor is the combination between the high traction force (or compression) and the low density of the titanium alloys (between 4,37 g/cm^3 and 4,85 g/cm^3), resulting in an extremely high ratio between force and density for the alloys. This relation is practically higher than all other metals, thus allowing to be applied in many applications. Several depositions were made and the characterization of the CVD diamond films on Ti6Al2Sn4Zr2Mo alloy at 600 C. Both stress and qualitative adherence were evaluated. Films were deposited using the assisted technique of microwave plasma. Various techniques were tested in the preparation of the substrate surface before depositioning the films, promoting its modification. Data for analysis are being obtained using Raman Scattering Spectroscopy for stress and purity cristallinity calculus. Based in the singularly properties of the CVD diamond and its potential in the condition of a new material, many basic studies and consequent applications in areas such the mechanical, electronics, optical and bioimplants. The qualitative adherence and the stress calculus that the film is submitted, both are related with the parameters of growing, substrate preparation, type of substrate, film quality, roughness and grain size.

Financial support: FAPESP, FUNDUNESP, PROPP-UNESP, CNPQ.

CONTROLLED GROWTH OF CARBON NANOTUBES FOR 3D LITHIUM ION MICROBATTERIES

Vijaya Kumar Kayastha, Yoke Khin Yap, *

Michigan Technological University, Department of Physics, Houghton, MI-49931, USA

*ykyap@mtu.edu

Chunlei Wang, Rabih Zaouk, Lili Taherabadi, Marc Madou*

Department of Mechanical and Aerospace Engineering, University of California, Irvine, Irvine, CA 92697, USA.

*mmadou@uci.edu

Keywords: Carbon nanotubes, Lithium ion batteries, C-MEMS, electrochemistry

Abstract

Flat carbon plates have been used as the negative electrodes in many commercial Li-ion batteries. Their energy density is limited by the size of the cells or vice versa. These 2D batteries are not useful for applications in miniature electronic devices such as sensors, cardiac pacemakers, and hearing aids. Advanced materials and novel battery designs are desirable and will determine future advances of miniature Li ion batteries. By using carbon microelectromechanical systems (C-MEMS), we have fabricated 3D microbatteries based on arrays of carbon posts that have high aspect ratio (>10). We have demonstrated that Li ions can be charged and discharged in these carbon posts. The obtained capacity is ~220 mAh g -1, which is within the range of reversible capacities reported for coke. We have further integrated carbon nanotubes and carbon nanofibers on these 3D C-MEMS microbatteries for enhancing their storage capacity.

INTRODUCTION

Our C-MEMS fabrication process is based on the pyrolysis of photolithographically patterned photoresists [1-3]. Upon miniaturization of the active battery material in an array of posts, an increased Li capacity is important. This is very desirable so that besides increasing power density and decreasing battery charge/discharge rates, we also can maintain a high overall battery capacity. Since it has been shown that single-walled carbon nanotubes reversibly intercalate Li up to a rate of $Li_{2.7}C_6$ after applying an appropriate ball-milling treatment [4], we are now combining C-MEMS structures with CNTs and CNFs. The use of CNTs and CNFs in microbatteries has not been demonstrated. Further, the issue of the contact interface between these nanomaterials and current collectors has not been addressed.

EXPERIMENT AND RESULTS

We have fabricated 3D microbatteries based on arrays of carbon posts that have high aspect ratio (>10) as shown in Figure 1. Further, we have integrating both CNFs and CNTs into C-MEMS posts for achieving higher electrode surface areas and higher Li intercalation rates. As shown in Figure 2, CNTs can be uniformly grown on these C-MEMS posts. Furthermore, we have also been able to grow arrays of very high-density vertically-aligned multiwalled carbon nanotubes (MWNTs) by catalytic thermal chemical vapor deposition [5]. The application of these C-MEMS/CNTs, C-MEMS/CNFs, and pure CNTs arrays 3D Li ions microbatteries will be discussed in the conference.

ACKNOWLEDGEMENT

Y.K.Y. acknowledges supports from the Michigan Tech Research Excellence Fund and the Army Research Office (W911NF-04-1-0029, through the City College of New York).

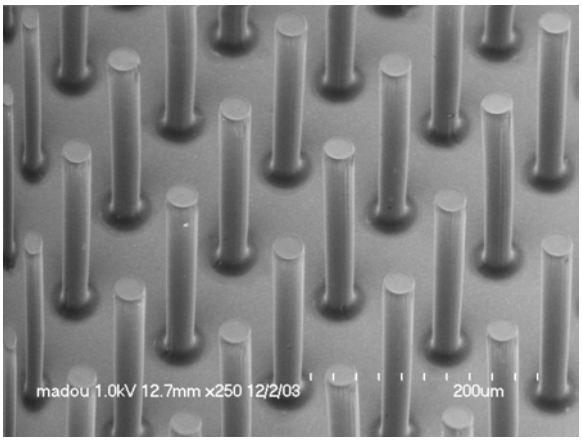

Figure 1. Arrays of carbon posts fabricated by C-MEMS technique.

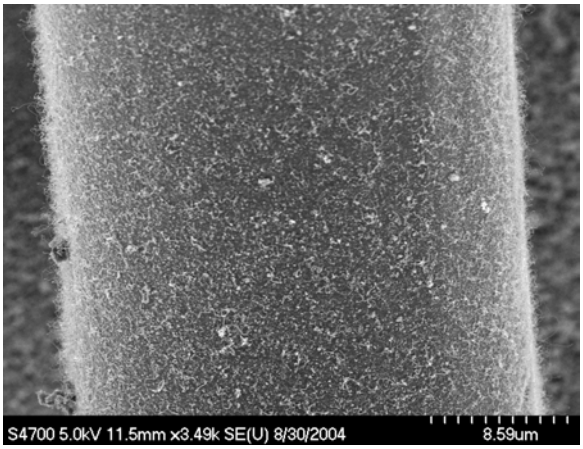

Figure 2. Growth of carbon nanotubes on arrays of the 3D C-MEMS posts.

References:

1. Kinoshita, K., et al., "Development of a carbon-based lithium microbattery, " J. Power Sources 81-82, 170 (1999).
2. Ranganathan, S., et al**.,** "Photoresist-Derived Carbon for Microelectromechanical Systems and Electrochemical Applications, " J. Eletrochem. Soc. 147, 277 (2000).
3. Wang, C., et al**.,** "C-MEMS for the Manufacture of 3D Microbatteries, " Electrochem. & Solid State Lett 7, A435 (2004).
4. Gao, B., et al., "Enhanced saturation lithium composition in ball-milled single-walled carbon nanotubes, " Chem. Phys. Lett. 327, 69 (2000).
5. Kayastha, V., et al., "Controlling Dissociative Adsorption for effective Growth of Carbon nanotubes," Appl. Phys. Lett. 85, 3265 (2004).

AMORPHOUS CARBON NITRIDE FOR USE AS A HIGH TEMPERATURE CAPACITOR DIELECTRIC

William C. Lanter

Innovative Scientific Solutions, Inc., 2766 Indian-Ripple Rd., Beavercreek, OH 45440

David C. Ingram

Condensed Matter and Surface Science Program, Department of Physics and Astronomy, Edwards Accelerator Laboratory, Ohio University, Athens, OH 45701

Charles A. DeJoseph, Jr.

Air Force Research Laboratory (AFRL/PRPE), Wright-Patterson AFB, OH 45433

Keywords: Carbon-Nitride, CN_x, Dielectric, High Temperature, Capacitor

Abstract

Amorphous carbon nitride (CN_x) thin film is being investigated for use as a high temperature dielectric for high energy density, high pulse power capacitors. It is anticipated that CN_x will display properties of high thermal conductivity, thermal stability, electrical resistance, and electrical breakdown strength. However, CN_x films containing high concentrations of hydrogen exhibit poor electrical and thermal characteristics Initial deposition techniques resulted in CN_x films with hydrogen concentrations as high as 40 at.%. Through control of the vacuum environment and deposition parameters of a dual ion-beam assisted, ion-beam sputter deposition system, CN_x films are created with hydrogen concentrations averaging less than 5 at.%. Elemental analysis using Rutherford-Backscattering Spectroscopy (RBS) and Elastic Recoil Spectroscopy (ERS) on CN_x samples annealed in 99.999% argon shows that the resulting films are thermally stable up to 500ºC. Capacitance measurements performed on CN_x films low in hydrogen concentration reveal resistivities up to 1×10^{13} Ω-cm.

LASER-ARC PROCESS AND TECHNOLOGY FOR DEPOSITION OF AMORPHOUS AND NANO-STRUCTURED CARBON FILMS

Hans-Joachim Scheibe, Michael Leonhardt, Thomas Schuelke

Fraunhofer USA Inc., Center for Coatings and Laser Applications, B100 Eng. Research Complex, Michigan State University, MI 48824-1226

Carl-Friedrich Meyer, Harald Schulz, Bernd Schultrich, E. Beyer

Fraunhofer Institute for Materials and Beam Technology, Winterbergstr. 28, D-01228 Dresden, Germany

Keywords: Pulsed Arc Deposition, Laser-induced Arc (Laser-Arc), ta-C film deposition, carbon nanostructures.

Abstract

Pulsed-laser (PLD) and vacuum arc deposition techniques (VAD) are successfully applied for thin film synthesis, especially for the preparation of super hard amorphous carbon films (ta-C) and carbon nano-structures. The main advantage of both technologies is that the evaporated material is nearly completely ionized. PLD is a well controlled process, which can be used for the deposition of nearly all materials (conducive and dielectric) with a defined nano-structure, but with a low efficiency. VAD is an industrial used technology for hard coating deposition with high deposition rate and efficiency, but limited in controlling the arc discharge. The stochastically movement of the cathode spots induces macro-particles, which will be included in the deposited films. These particles are the reason for a restricted coating quality by a high surface roughness and defect density. To deposit coatings of a high quality with VAD technologies, the arc discharge has to be better controlled and filter techniques have to be applied for removing macro-particles from the plasma.

LASER-ARC PROCESS

The Laser-Arc process is developed to combine the advantages of PLD and VAD for a controlled deposition of high quality carbon films with a defined nano-structure with a high deposition rate. In the Laser-Arc process the arc discharge is guided on the cathode surface in a highly controlled manner by positioning the igniting laser pulses. The burning time of the arc is limited to 130 µs by the high current power supply. Using a peak arc current between 1 and 1.8 kA the splitting cathode spots move from the ignition point (the laser spot) driven by intrinsic magnetic fields. The subsequent arc pulse will be ignited at a fresh position of the cathode by moving the laser beam. This way overheating and melting of the cathode surface is prevented and the particle emission is reduced. Efficient deposition rates are obtained at repetition rates of 1 kHz. To coat large areas the cathode roll is 400 mm in length. By linear scanning the laser beam and simultaneously rotating the cylindrical cathode a very regular erosion of the cathode material is achieved (Fig. 1) [1].

For industrial coating application the cathode was arranged in a separate source chamber (Laser-Arc Module/LAM), which can be combined with any conventional industrial used batch coater. The advantage of this LAM concept is that the whole equipment and all functions of the basic coater (e.g. vacuum production, sample planetary, cleaning technology, hard coating deposition and some more) can be used. Additionally, conventional coatings can be overcoated with hard ta-C, nano-structured or modified carbon top films [2].

SUPER HARD AMORPHOUS CARBON FILMS (DIAMOR®)

The plasma created by the laser controlled high current arc discharge is characterized by nearly complete ionization and high kinetic energies of the ions (e.g. 3- - 50eV for carbon). If the deposition is carried out under high vacuum ($p < 10^{-3}$ Pa) conditions at low substrate temperatures ($T < 150°C$), amorphous carbon films are obtained. Their hardness reaches values between 2,000 and 6,000 HV depending on the deposition parameters. The film micro-structure is dominated by diamond-like bonds (sp^3). Film thicknesses of 10 µm and more with an excellent adhesion to steel are achieved if a special plasma surface treatment and interlayer preparation is applied. But also other substrate materials can be coated successfully, especially Ti and Al alloys or plastics (low thermal load during the coating process). Such films are successfully tested as wear protecting coatings with a low friction coefficient in

tribological friction pairs under high mechanical loads without lubrication. Diamor coated tools are successfully applied for dry machining of Al-alloys [2].

NANO-STRUCTURED CARBON FILMS

If the carbon deposition is performed in a residual inert gas (Ar) atmosphere at pressures up to 4 Pa the film structure is dominated by graphitic bonds (sp^2). The films still exhibit a high hardness of about 4,000 HV and a corresponding Young's Modulus of more than 400 GPa. The reason of the unexpected high hardness of graphitic carbon films was found in the nanostructure by means of a high resolution transmission electron microscopy study. Fullerene-like nano-particles were found to be the reason for the high stiffness and elastic recovery properties of such films. High stiffness is not only typical for diamond but also inside the graphite layers. The easy sliding of these layers is suppressed by the curved and closed geometry of graphite nano-structures [3]. In contrast to more or less non-conducting diamond-like carbon films these nano-structured films are electrically conductive and have a similar wear resistance and low friction.

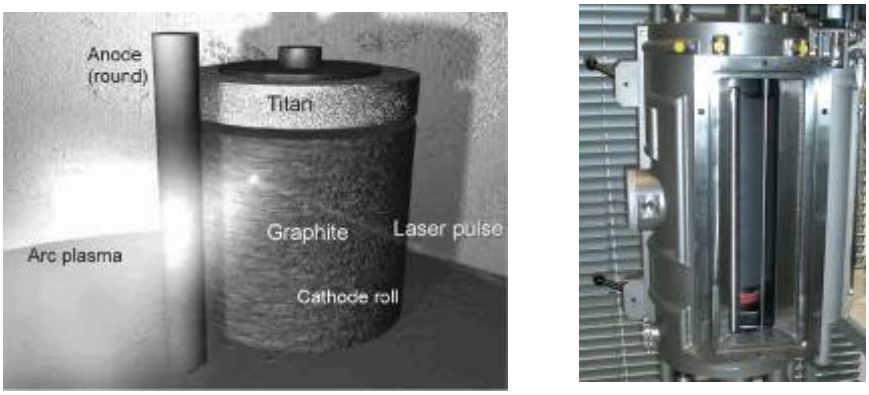

Figure1. Scheme of the Laser-Arc process and industrial used Laser-Arc-Module (LAM).

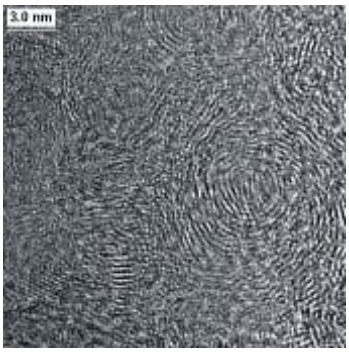

Figure 2. HRTEM image of a nano-structuredC-film (top view)

REFERENCES

1. H.-J. Scheibe and .Siemroth,"*Film deposition by laser-induced vacuum arc evaporation*, IEEE Transactions on Plasma Science **18** (6), 917-922 (1990).

2. E. Beyer, H.-J. Scheibe, B. Schultrich, V. Weihnacht, *Deposition technology, tribological properties and applications of superhard amorphous (ta-C) carbon films*, 4th International Conference "The Coatings" in Manufacturing Engineering **4**, 79-92 (2004).

3. I. Alexandrou, H.-J. Scheibe, C.J. Kiely, A.J. Papworth, G.A.J. Amaratunga, B. Schultrich, *Carbon films with an sp^2 network structure*, Physical Review B **60** (Number 15), 10 903 - 910 907 (1999).

Wurtzitic Boron Nitride On Diamond:
The Ultimate Epitomical Wafer for Semiconductor on Insulator

James C. Sung

Address: KINIK Company, 64, Chung-San Rd., Ying-Kuo, Taipei Hsien 239, Taiwan, R.O.C.
Tel: 886-2-2677-5490 ext.1150
Fax: 886-2-8677-2171
e-mail: sung@kinik.com.tw

[1] KINIK Company, 64, Chung-San Rd., Ying-Kuo, Taipei Hsien 239, Taiwan, R.O.C.
[2] National Taiwan University, Taipei 106, Taiwan, R.O.C.
[3] National Taipei University of Technology, Taipei 106, Taiwan, R.O.C.

Key Words: Diamond Film, AlN, ULSI, LED, SAW Filter

Abstract

In last four decades, the miniaturization of semiconductors devices (e.g. integrated circuitry) has been following Moore's Law with feature (e.g. transistors) density double in about every 18 months. This relentless geometrical progression would require the technological breakthroughs of many fronts such as UV photolithography with ever high frequency and nanom chemical mechanical planarization (CMP) with ever-small variations. However, with feature sizes of semiconductors entering the virus domain (10 to 100 nm), two physical barriers emerge that may not be surmountable with current wafer and substrate materials. These two barriers are stemming from the Second Law of Thermodynamics, i.e. entropy will increase along with the work performed in a closed system of semiconductor world. The entropy is the unwanted energy that may exhibit in random vibration of atoms, i.e. phonons (waste heat), and quantum fluctuation of charges, i.e. defects (intrinsic carrier).

The first barrier arises due to the accumulation of waste heat that cannot be effectively channeled out from the crystal lattice of Group IV semiconductors (e.g. Si, SiC) or III-V compound materials (e.g. GaAs, GaN). Semiconductors have thermal conductivities that are only a fraction of copper metal (about 400 W/mK) so it is now chilled by copper heat spreader. However, with the power density increasing beyond 2 watts/mm2 for the next generation chips, copper heat spreader will become a reservoir for heat accumulation rather than a river for heat transfer.

The second barrier arises due to the accumulation of charge carriers (electrons and holes) that are intrinsic to quantum fluctuation. These noisy charges will obscure the processed signal of electrical current. Moreover, the higher the temperature of the operating semiconductor, the more uncertain is the transmitted message. Eventually, the signal becomes unrecognizable or unreliable so the device will fail.

Both problems of phonon scattering and charge fluctuation can be reduced by increasing the bonding energy and by reducing its directional anisotropy of the crystal lattice. Diamond has the highest bonding energy with highest crystal symmetry of all materials. The strongest atomic structure allows diamond lattice to vibrate with the highest frequency, so it has the fastest sound speed (18 km/second) with the largest thermal conductivity (2000 W/mK). The strongest atomic structure also makes diamond lattice most stable even at high temperatures.

Consequently, diamond is the hardest and most rigid material with the lowest intrinsic carrier density. Diamond superlative structural stability is exhibited in its highest break down voltage for semiconductor applications.

The highest thermal conductivity makes diamond the ideal heat spreader. The lowest charge fluctuation makes diamond the dream barrier substrate. Hence, semiconductor on diamond (SOD) can be the best semiconductor on insulator (SOI) that is envisaged for making future ULSI, laser diodes, LED, microwave (MW) generators, and other signal processing or optic-electronic devices.

Recently breakthroughs of CVD diamond film deposition and polishing technologies have made diamond substrates engineering possibility rather than research curiosity. For example, Kinik Company is now offering diamond wafers up to four inches with a price comparable to commercial substrate materials (e.g. sapphire, silicon carbide). Moreover, the super smooth (e.g. Ra about 2 nm) polycrystalline film can be over coated with a submicron layer of hexagonal AlN that is preferentially oriented with (002) lattice plane in parallel to the interface. AlN is fully compatible with diamond in mechanical matching (e.g. thermal expansion rate) and chemical joining (e.g. covalent bonding coupling). Moreover, its (002) plane is closely similar to (111) face of diamond lattice. In essence, the oriented AlN coating has transformed polycrystalline diamond grains in volume into a single crystal plane on surface. Such an orientation transformation creates an ideal buffer layer for epitaxial deposition of Si, SiC, GaN, InN, GaAs or other semiconductors. Consequently, Kinik' DiAlN® wafers are suitable to make next generation ULSI, LD, LED, MW devices that are capable to operate with excessive power and frequency.

In addition to for making future information processing devices, the DiAlN wafer is well suited as communication message interfaces with power and frequency dwarfing the current designs. For example, AlN is piezo-electric so it can convert electromagnetic signal into sound wave, and vice versa. Consequently, DiAlN substrate can be an efficient surface acoustic wave (SAW) filters that are indispensable for receiving and transmitting wireless signals. Unlike current ceramic SAW filters (e.g. $LiTiO_3$, $LiNbO_3$) that are thermal insulator and ionic conductor that will build up heat and leak out electricity, DiAlN is thermal conductor and electrical resistor so it can handle much higher frequency (e.g. >10 GHz) and power (e.g. Kw) that can burn out instantly the current designs of ceramic filters used in cell phones and other wireless communication devices.

In summary, DiAlN wafers are a cost effective solution for epitaxial deposition of sophisticate semiconductors and for piezo-electrical transmission of electromagnetic signals. The implementation of DiAlN substrate on the commercial scale will usher our way into the next 3C (computer, communication, consumer) and 3G (third generation of design) society that is based on the efficiency of knowledge integration.

SESSION 12

ELECTROCHEMISTRY, SUPERCAPACITORS, ETC.

Electrochemical characterization of undoped hydrogen terminated diamond

C.E. Nebel*, D. Shin, B. Rezek, D. Takeuchi, H. Watanabe

Diamond Research Center, Advanced Industrial Science and Technology, 1-1-1 Umezono, Tsukuba 305-8568, Japan

Hydrogen terminated diamond shows two properties which attract significant attention and controversial discussions. The first property is the negative electron affinity (NEA) of about -1.1 to -1.3 eV which is generated by C-H dipoles at the surface [1]. The second property which can be detected in combination with H-termination is a conductive p-type surface layer, detectable on samples which are exposed to air. It is assumed that the conductive layer is generated by transfer doping where valence-band electrons diffuse into a wetting layer of appropriate pH value. Contrary to this proposal, the pH-sensitivity of such layers has been reported not to follow this prediction [2].

In this paper we discuss cyclic voltammetric experiments performed for the first time on several undoped H-terminated single crystalline diamond films, using different redox couples in electrolytes in a triode chemical reactor where the working electrode is diamond, the counter electrode is Pt and the reference electrode is saturated Calomel. The diamond substrates (Ib and IIa) have been homoepitaxially overgrown and hydrogen terminated at 800 ^{o}C in H_2 atmosphere (25 Torr) using a microwave plasma discharge (750 W). After cooling of the sample to RT, a mechanical cleaning has been applied to remove a soft carbon layer, which forms during the cooling in the plasma/H_2 atmosphere.

We applied cyclic voltammetric experiments as the chemical potentials of the electrolytes are known and can be varied by change of the redox couple/electrolyte system. The results (a typical example is shown in Fig. 1 for Ferrocyanide in Na_2SO_4) reveal: a) Undoped hydrogen terminated diamond is a perfect electrode with a chemical window in the range -2.4 V to +1.5 V. b) For voltages larger than +1.5 V oxidation takes place which can be monitored by detection of the peak currents. c) For Ferrocyanide, the peak currents are separated by about 625 mV which is a result of the electron transfer rate limiting diamond electrode. We apply the Marcus-Gerischer Model [3] to discuss these features. In addition, we have realized pH-detectors based on H-terminated diamond to measure the pH-dependence of the surface conductive channel in different electrolytes and find that the surface conductivity follows the Nernst equation nearly perfectly (56 mV/pH). The channel current of typical 10 μA is confined in a narrow energy well which shows leakage currents in the range of nano-amperes. The hole-density is photosensitive to light of 4 to 4.5 eV as detected by photocurrent experiments. In addition, for these

photon energies we also detect an onset of secondary photoelectron emission by total photoyield experiments which may be important to understand the photochemical attachment of amine groups on diamond.

Our experiments clearly reveal that a perfectly hydrogen terminated and clean diamond surface has an unpinned surface Fermi level, which gives rise to surface conductivity by transfer doping according to the Nernst equation. Our results will be discussed in detail taking into account the chemical potentials, the NEA and the specific properties of cyclic voltammetry experiments.

1) F. Maier, J. Ristein, L. Ley, Phys. Rev. B 64, 165411 (2001).

2) H. Kawarada, Y. Araki, T. Ogawa,, H. Umezawa, pys. stat. sol. A, 185, 79 (2001).

3) H. Gerischer, in „Physical Chemistry: An Advanced Treatise", Vol. 9A, H. Eyring, D. Henderson, W. Jost, Eds., Academic, New York, 1970.

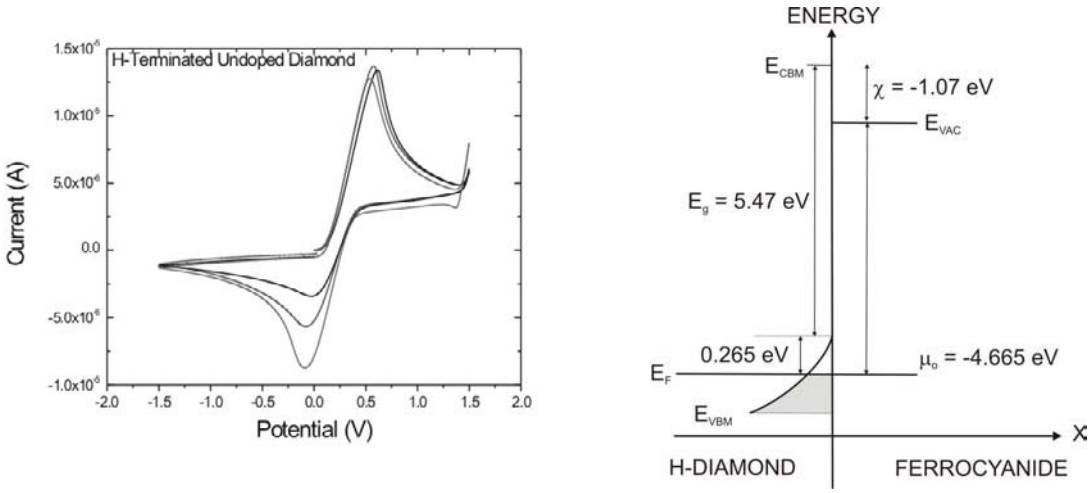

Fig. 1: Typical cyclic voltagrams, using Ferrocyanide in Na_2SO_4 and H-terminated diamond and the related energy diagram of the diamond/electrolyte-redox system.

**Corresponding author: christoph.nebel@aist.go.jp*

ELECTROCHEMICAL SENSING USING NANODIAMOND MICROPROBE

S. Basu[1], W.P. Kang[2], J.L. Davidson[2], B.K. Choi[2], A.B. Bonds[2], D.E. Cliffel[3]
[1]Interdisciplinary Material Science, Vanderbilt University, Nashville, TN 37235, USA
[2]Department of Electrical and Computer Engineering, Vanderbilt University, Nashville, TN 37235, USA
[3]Department of Chemistry, Vanderbilt University, Nashville, TN 37235, USA

Keywords: Nanodiamond, Sensing, Electroactive surface, Cyclic Voltammetry, Chronocoulometry.

Abstract

Boron doped *nanodiamond* microprobe with an excellent electrochemical sensing behavior has been developed. The microprobe was fabricated by plasma enhanced chemical vapor deposition (PECVD) of nanodiamond on a sharpened tungsten microprobe with trimethyl boron (TMB) as a doping source. Electrochemical behavior of the microprobe was characterized by chronocoulometry and cyclic voltammetry in a three-electrode cell compartment to detect $Fe(CN)6^{4-}$ with KCl as background. Excellent noise-free signals down to pico-ampere range have been achieved. The probe displays reversible kinetics and a high signal to background ratio with low background current without the need of surface pretreatment. There is no indication of adsorption of analytes at the nanodiamond surface. The characterization was also performed on different active areas of the electrode that demonstrated a stable increase in current density with scan rate. The general sigmoidal shape of the voltamogram indicates spherical diffusion (rate-limited) dominated reaction mechanism.

INTRODUCTION

Micropolycrystalline PECVD diamond with controlled conductivity, dimensional stability and chemical inertness is a promising electrode material for electrochemical analysis. A wide range of electrode impedance can be realized by varying electroactive area or doping conductivity of such diamond electrodes thereby achieving detection of in-vivo electrical signals and electrochemical analysis of chemical species. However, little research in this capacity has been reported utilizing nanocrystalline diamond [1]. This work reports the electrochemical behavior of boron doped nanodiamond coated tungsten microprobe in $Fe(CN)_6^{4-}$ with KCl as background analyte. The nanodiamond microprobes show negligible adsorption of species at the electroactive surface during electrochemical analysis. Nanodiamond microprobes with different electroactive areas have also been characterized for sensitivity in electrochemical analysis.

EXPERIMENTAL

Nanodiamond microprobes were fabricated by selective deposition of nanodiamond on a sharpened tungsten microprobe. Diamond deposition was in an Astex PECVD system at power 400 W, temperature 750 ˚C, and pressure 14.5 Torr, with methane/hydrogen flow rates 15/138 sccm. Boron doping of nanodiamond was achieved with TMB as the dopant source with flow rate 10 sccm. The electrode was then sealed in a glass capillary using insulating polymer with 50 μm of the nanodiamond tip exposed for electrochemical sensing. The nanodiamond microprobe was used as the working electrode for chronocoulometry [2] and cyclic voltammetry [3] in a three-electrode cell compartment.

RESULTS AND DISCUSSIONS

Three nanodiamond microprobes with different electroactive areas were fabricated. A typical optical microscope image of a sealed nanodiamond microprobe tip is shown in Figure 1. The electroactive areas of the electrodes were determined using two-step chronocoulometry and the slope obtained in equation (1) [2].

$$Slope = \frac{2nAFC\sqrt{D}}{\sqrt{\pi}} \quad (1)$$

where n is the number of electrons participating in a single transfer, A is the area of the active electrode, F is the Faraday constant, C is the concentration and D is the diffusion constant.

Figure 2 shows the two step chronocoulometry with nanodiamond microprobe in 3.9 mM $Fe(CN)_6^{4-/3-}$ in 0.1 M KCl. The intersection of oxidation and reduction components at zero axis (origin) shows that there is

negligible occurrence of adsorption at the nanodiamond surface. Figure 3 shows the CV for detection of various concentrations of $Fe(CN)_4^{4-/3-}$ in 0.1 M KCl at a scan rate of 10 mV s^{-1}. The curve displays high signal to background ratio and absence of any noticeable noise. The peak separation varies from 93 mV to 124 mV. The reversal peak ratio ($I_{p,red}/I_{p,ox}$), which varies from 0.95 to 0.96, satisfies the requirement for a redox couple. The sigmoidal shape of the voltamogram indicates rate-limited rather than diffusion limited reaction mechanism. Figure 4 shows the variation of oxidation current with various concentrations of $Fe(CN)_6^{4-/3-}$. The curve shows a linear variation of the current as the concentration of the analyte increases.

CONCLUSION

The nanodiamond microprobe is an excellent electrode for electrochemical analysis. It picks up current down to pico-amps range with noise-free signals. The immunity to adsorption at the nanodiamond surface and optimization for rate-limited reaction mechanisms makes it suitable for in-vivo and in-vitro analysis. Moreover, the variation of chemical reaction rate and current as the microprobe approaches targeted tissue in-vivo can be measured with SECM (Scanning Electrochemical Microscopy) facilitating reproducibility for applications such as neurological mapping. Details of SECM data will be included in the paper.

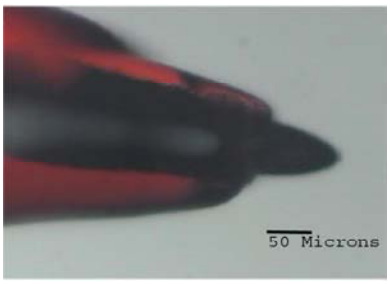

Figure 1. *View of nanodiamond microprobe in optical microscope*

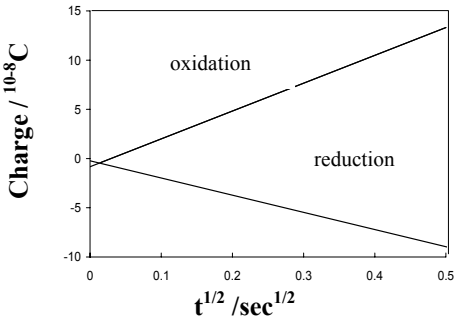

Figure 2. *Two step chronocoulometry with nanodiamond in 3.9 mM$Fe(CN)_6^{4-}$ in 0.1 M KCl.*

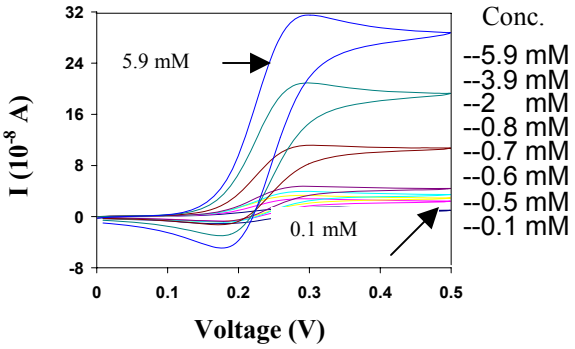

Figure 3. *Cyclic voltammogram of nanodiamond microprobe for detection of different concentrations (conc.) of $Fe(CN)_6^{4-/3-}$ in 0.1 M KCl. Scan rate = 10 mV s^{-1}*

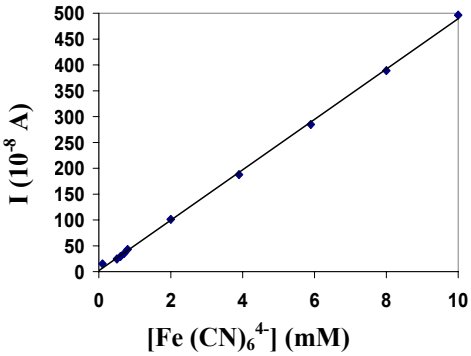

Figure 4. *The plot of oxidation current against various concentrations of $Fe(CN)_6^{4-}$ in 0.1 M KCl.*

REFERENCES

1. Soh, K.L., et al., "Diamond-derived microelectrodes array for electrochemical analysis", *Dia. and Rel. Mater.* , 13, 2009-2015 (2004)
2. Scholz, F., *Electrochem. Methods: Guide to Experiments and Applications,* Springer, NY, (2002)
3. Bond, A.M., *Broadening Electrochemical Horizons,* Oxford University Press, N.Y., (2002)

BORON-DOPED DIAMOND ELECTRODES FOR NITRIC OXIDE DETECTION

J. Ben Schaeffer[1], Dmitri E. Kourennyi[2], Heidi B. Martin[1]

[1]Dept. of Chemical Engineering; [2]Dept. of Biomedical Engineering; Case Western Reserve University

Keywords: Boron-Doped Diamond; Nitric Oxide; Microelectrodes; Fast-Scan Cyclic Voltammetry

OBJECTIVE

We intend to characterize boron-doped diamond (BDD) microelectrodes for nitric oxide (NO) detection using flow injection analysis. Our ultimate goal is to utilize our electrodes for localized, *in vitro*, real-time NO detection.

BACKGROUND & RATIONALE

Nitric oxide is a free radical signal molecule involved in many physiological functions and pathological changes in the nervous system, immune system, epithelial systems, smooth muscles and other tissues. In the retina, NO is a neurotransmitter synthesized by enzymes; it is also associated with a number of detrimental ocular conditions including uveitis and glaucoma[1]. Ability to measure NO reliably in real-time will advance the understanding of physiological and pathological processes in the retina. Typical NO detection methods, see **Ref 2,** include chemiluminescence and colorimetry, although these provide indirect NO measurement and cannot be used *in vitro* for localized, real-time sensing. Electrochemical (*e.g.*, cyclic voltammetry, amperometry) detection of NO is appealing because it may directly measure NO concentration and is inexpensive, sensitive, and relatively non-destructive to biological surroundings. The lower detection limit at typical electrodes (*e.g.*, carbon-fiber,[3,4] glassy carbon, pyrolytic graphite, and gold) for prepared NO solutions is ~1 µM; this limit varies with electrode material, surface modification scheme, and whether oxidation or reduction of NO is implemented for detection. NO's fleeting existence (seconds) and overall reactive environment in the retina make *in vitro*, real-time, selective, electrochemical detection difficult using aforementioned electrode materials.

Another major issue is that nitrite, NO_2^-, the primary interfering species for NO detection, undergoes its oxidation at a similar potential (< 100mV potential difference); thus, convolution of the response from a NO and NO_2^- mixture is necessary. Electrode surface modifications are typically used to tackle this problem; modifications,[5,6] *e.g.*, by metalloporphyrin or metalloprotein layers, to catalyze electron transfer and enhance sensor selectivity may significantly limit sensor response time. Other possible interferers in the retina include dopamine and acetylcholine.

Diamond's extreme chemical stability should provide advantage for long-term, electrochemical detection in biological media.[7] In addition, diamond has been shown[8] to slow oxygen reduction, another interfering reaction in biochemical detection. Electrochemical detection of NO on a bare, BDD macroelectrode (area, 0.07 cm^2) using slow scan cyclic voltammetry (20 mV/s) has been reported by Spataru *et al*.[9] The detection was not selective for NO over NO_2^-; the NO_2^- detection limit was <50 nM. No reports of NO detection on BDD microelectrodes are known. Using our CVD techniques, we can fabricate sufficiently small microelectrodes to enable localized, *in vitro* detection of NO.

METHODS & RESULTS

Boron-doped diamond macro- and microelectrodes were fabricated via hot-filament CVD. BDD macroelectrodes detected NO and NO_2^- oxidation, by slow scan voltammetry (scan rate, ~200 mV/s). Diamond microelectrodes were characterized for NO and NO_2^- detection in a flow cell system using fast-scan cyclic voltammetry (FSCV, scan rates, *ca.* 100 V/s) to simulate neurotransmission (ms) time scales; the effect of scan rate on current responses was studied. We believe this is the first report of FSCV for real-time NO detection; typically amperometry[3] and differential normal pulse voltammetry (DNPV)[4] have been used. Carbon-fiber microelectrodes were controls for these experiments. Diamond surface modification schemes from diazonium salt precursors (see **Ref 10**), including enzyme attachment, were used to best maintain ultrasensitivity and promote selectivity. NO detection in retinal tissue with BDD microelectrodes was also pursued.

Initial experiments using BDD macroelectrodes verified (data not shown) the ability to detect NO (nominally 10 µM) in prepared NO-containing electrolytes; BDD also appeared to display good selectivity of NO to NO_2^-. Selectivity was only observed on macroelectrodes; the source of this behavior is likely linked to surface chemistry. For FSCV flow injection, carbon-fiber microelectrodes had a NO detection limit of ~1 µM, consistent with literature

for amperometry[3] and DNPV[4]. BDD microelectrodes were more sensitive, yielding a NO detection limit of ~10 nM (See **Fig 1**); unfortunately, the sensitivity decreased over time. NO peak current was found to vary with the square root of the scan rate, in agreement with Spataru *et al*,.[9] for NO as a non-adsorbing species. Our data suggest that the initial sensitivity and stability of BDD electrodes are affected by growth conditions and surface chemistry. Progress with our ongoing surface chemistry strategies as a means to understand these relationships will be presented.

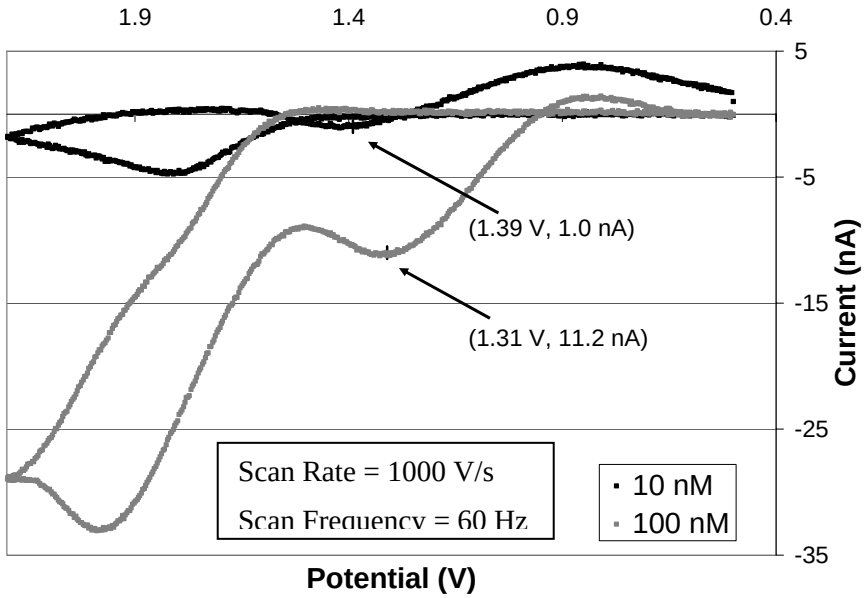

Figure* 1. *Flow injection analysis of Nitric Oxide on a Boron-Doped Diamond Microelectrode – *(NO dissolved in 0.1 M Phosphate Buffer Solution).* NO peaks in +1.3 – +1.4 V range; Peak current ratio ≈ NO concentration ratio.

REFERENCES

1. Koss, M.C., "Functional Role of Nitric Oxide in Regulation of Ocular Blood Flow," *Eur J Pharmacol*, 374, 2, 161-174 (1999).
2. Nagano, T., "Practical Methods for Detection of Nitric Oxide," *Luminescence*, 14, 6, 283-290 (1999).
3. Katrlik, J., Zalesakova, P., "Nitric Oxide Determination by Amperometric Carbon Fiber Microelectrode," *Bioelectrochemistry*, 56, 1-2, 73-76 (2002).
4. Pontie, M., et al., "Electrochemical Nitric Oxide Microsensors: Sensitivity and Selectivity Characterisation," *Anal Chim Acta*, 411, 1-2, 175-185 (2000).
5. Ciszewski, A., Grzegorz, M., "Electrochemical Detection of Nitric Oxide Using Polymer Modified Electrodes," *Talanta*, 61, 1, 11-26 (2003).
6. Nyokong, T., Vilakazi, S., "Phthalocyanines and Related Complexes as Electrocatalysts for the Detection of Nitric Oxide," *Talanta*, 61, 1, 27-35 (2003).
7. Martin, H.B., et al., "Voltammetry Studies of Single-Crystal and Polycrystalline Diamond Electrodes," *J Electrochem Soc*, 146, 8, 2959-2964 (1999).
8. Yano, T., et al., "Electrochemical behavior of highly conductive boron-doped diamond electrodes for oxygen reduction in acid solution," *J Electrochem Soc*, 146, 3, 1081-1087 (1999).
9. Spataru, N., et al., "Determination of Nitrite and Nitrogen Oxides by Anodic Voltammetry at Conductive Diamond Electrodes," *J Electrochem Soc*, 148, 3, E112-E117 (2001).
10. Bath, B.D., et al., "Dopamine Adsorption at Surface Modified Carbon-Fiber Electrodes," *Langmuir*, 17, 22, 7032-7039 (2001).

Polycrystalline boron-doped diamond films as supports for methanol oxidation electrocatalysts

I. González-González[1], D. A. Tryk[1], C. R. Cabrera[1]

[1]*University of Puerto Rico, Rio Piedras, PR*

gonzalez_ileana@yahoo.com

Keywords: Boron-doped diamond, electrocatalysts, methanol oxidation

Various studies have been done on the development of catalysts for direct methanol fuel cells.[i,ii] Various composite systems has been studied[iii,iv,v]. Electrocatalysts with nano-particles have been found to have high activity, which was found to depend on the particle size, the nature of the support as well as the method of preparation.[vi]

Boron-doped diamond films exhibit very high stability both chemical and electrochemically treatments. Other advantages of diamond over other carbon materials are a potential window of approximately three volts, and at least an order of magnitude lower background current, compared to glassy carbon. Some of these same advantages make it an excellent candidate as an analytical electrode for the examination of noble metal alloys catalyst. This excellent stability provides a rationale for the control of the bonding between the metal nanoparticles and the diamond surface. Nanoparticulate diamond may be attractive as an electrocatalyst support for fuel cells.

The electrochemical behavior of boron doped diamond (BDD) films was examined in 0.5 M H_2SO_4 using cyclic voltammetry. The morphology of low-quality diamond (LQD), high-quality diamond (HQD) and polished diamond films has studied using SEM. The boron doped diamond films were characterized using SEM/EDS, X ray diffraction analysis, XPS and Raman. Platinum, Ruthenium, and Molybdenum deposition has been done by (1) cyclic voltammetry in metal solution at 50 mV/s doing a potential sweep between 0 V and 1.5 V. Various catalyst composites, incluiding, Pt/Ru, Pt/Ru, Pt/Ru/Mo on polycrystalline boron-doped diamond will be tested for methanol oxidation. The modified diamond surfaces will be characterized by SEM/EDS, XPS, and AFM.

---

[i] Chrzanowski, W.; Kim, H.; Wieckowski, A. *Catal. Lett.* **1998** *50* 69-75.
[ii] Lin, W. F.; Zei, M. S.; Eiswirth, M.; Ertl, G; *J. Phys. Chem.* **1999** *103* 6968-6977.
[iii] Kevin, L.; Liu, R. X.; Pu, C.; Fan, Q.; Leyarovska, N.; Segre, C.; Smotkin E. S; *J. Electrochem. Soc.* **1997** *144* 1543.
[iv] E. Reddington; A. Sapienza, B; Gurau, R; Viswanathan, S; Sarangapani; E. S. Smotkin; T.E. Mallouk, *Science* **1998** *282* 1735.
[v] Zhang, H.; Wang, Y.; Fachini, E. R.; Cabrera, C. R. *Electrochem. Solid-State Lett.* **1999** 2 *9* 437-439.
[vi] Zhang Y.; Asahina S.; Yoshihara S.; Shirakashi, T. *Electrochim. Acta* **2003** *48* 741

SURFACE CHEMISTRY AND ELECTROCHEMICAL PROPERTIES OF FUNCTIONALIZED ULTRANANOCRYSTALLINE DIAMOND THIN-FILMS*

J. Wang, N. Naguib, X. Xiao, C. Liu, L. A. Curtiss, M. A. Firestone, O. Auciello, and J. A. Carlisle

Materials Science Division, Argonne National Laboratory, Argonne 60439

Keywords: Diamond; Electrochemistry; Surface Functionalization; Biosensor.

Abstract

The surface properties of ultrananocrystalline diamond (UNCD) thin-films, which include low friction coefficients, extreme chemical and biological inertness, and superb electrochemical properties, depend strongly on the UNCD surface chemical compositions. The control and manipulation of the surface chemistry of UNCD is essential in tailoring its surface properties for specific applications such as hard wear coatings, cold-cathode electron sources, biomedical implants, and chemical and biological sensors. Accordingly, we have developed different strategies for surface functionalization and interfacial engineering of UNCD thin films. Oxygen or ammonia plasma treatment allows for the introduction of oxygen or nitrogen containing functionalities to the H-terminated UNCD surfaces. Electrochemical reduction of diazonium salts is also used to introduce different aryl derivatives onto UNCD surface, which enables the control over UNCD surface charges and surface hydrophobicity. The surface morphology and chemistry of the chemically modified UNCD films were fully characterized using atomic force microscopy (AFM), X-ray photoelectron spectroscopy (XPS), and contact angle measurements. Cyclic voltammetry (CV) and ac impedance spectroscopy were employed to probe the charge transfer kinetics at the modified electrode/electrolyte interface. The attached organic adlayer also served as a linker for the subsequent coupling of a variety of biomolecules. We have demonstrated that covalent immobilization of redox active enzymes (e.g. glucose oxidase) onto UNCD surface could be achieved via the surface tethered amino or carboxyl functionalities. Fluorescence microscopy and electrochemical measurements were used to validate the biological functionalization and the enzymatic activities of the tethered biomolecules. The potential of UNCD based bio/organic-inorganic interfaces for biomedical implants and electrochemical biosensing applications will also be discussed. *This work was supported by the U.S. Department of Energy, BES-Materials Sciences, under Contract No. W-13-109-ENG-38.

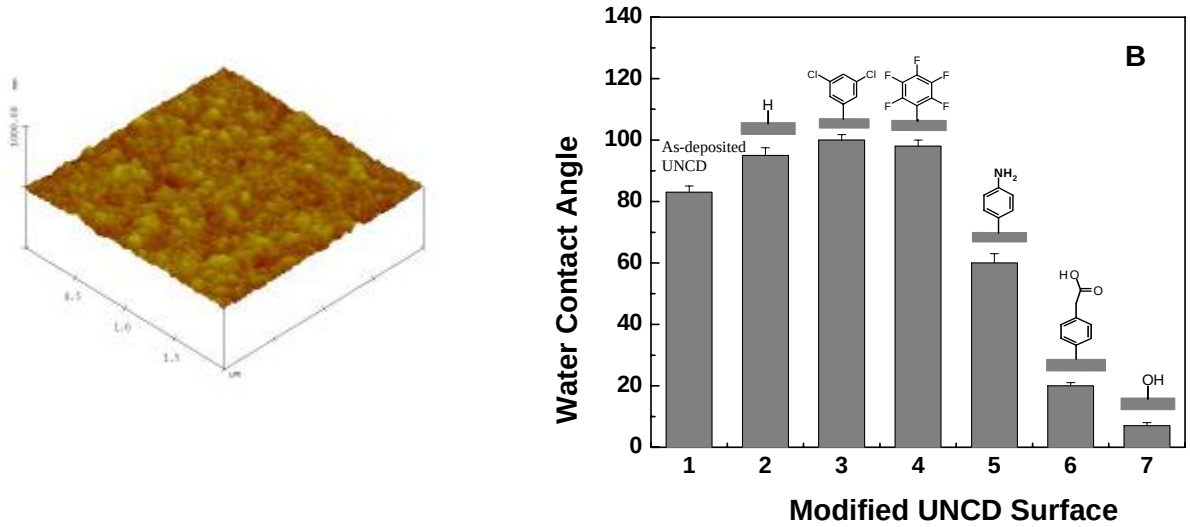

Figure 1. (A) AFM image of a dichlorophenyl-modified UNCD surface. (B) Static contact angle measurements of bare and modified UNCD surfaces.

REFERENCES

1. Wang, J., et al., “Surface Functionalization of Ultrananocrystalline Diamond Films by Electrochemical Reduction of Aryldiazonium Salts”, *Langmuir*, **20**, 11450 (2004).
2. Carlisle, J. A.; and Auciello, O., “Ultrananocrystalline Diamond: Properties and Applications in Biomedical Devices,” *Interface*, **12**, 28 (2003).
3. Yang, W., et al., “DNA-modified Nanocrystalline Diamond Thin Films as Stable, Biologically Active Substrates,” *Nature-Materials*, **1**, 253 (2002).

SESSION 13

THEORY & MODELING

THEORY AND MODELING OF NANOSCARBON PHASE STABILITY

Amanda S. Barnard

Center for Nanoscale Materials and Materials Science Division,

Argonne National Laboratory,

9700 S Cass Ave, Argonne, IL, 60439, USA

Keywords: nanodiamond, bucky-diamond, theory, simulation, phase stability.

Abstract

The transformation of nanodiamonds into carbon-onions (and vice versa) has been observed experimentally and has been modelled computationally at various levels of sophistication [1,2]. Also, several analytical theories have been derived (by a number of research groups) to describe the size, temperature and pressure dependence of this phase transition [1]. However, in most cases a pure carbon-onion or nanodiamond is not the final product. More often than not an intermediary is formed, known as a bucky-diamond, with a diamond-like core encased in an onion-like shell. This has prompted a number of studies investigating the relative stability of nanodiamonds, bucky-diamonds, carbon-onions and fullerenes, in various size regimes. Presented will be a review outlining results of numerous computational and theoretical studies examining the phase stability of carbon nanoparticles, to clarify the complicated relationship between fullerenic and diamond structures at the nanoscale [1].

REFERENCES

1. Barnard, A.S.; Russo, S.P.; and Snook, I.K., "Modeling of stability and phase transformations in 0 and 1 dimensional nanocarbon systems," in *Handbook of Theoretical and Computational Nanotechnology,* American Scientific Publishers, Stevenson Ranch, CA (2005).
2. Barnard, A.S. "Structural Properties of Diamond Nanowires: Theoretical Predications and Experimental Progress," *Rev. Adv. Mater. Sci*., 6, 94-119 (2004).

Multiscale Modeling of Fracture of Graphene Sheets and Carbon Nanotubes

Sulin Zhang[a], Steven L. Mielke [b], Roopam Khare[a], George C. Schatz[b], and Ted Belytschko[a]

[a]Department of Mechanical Engineering, Northwestern University
[b]Department of Chemistry, Northwestern University

A coupling method that bridges quantum mechanical (QM) calculations, molecular mechanics (MM) simulations, and continuum mechanics (CM) was developed, and employed to simulate the fracture of defected graphene sheets and carbon nanotubes (CNTs). Different coupling strategies are used at the QM/MM and MM/CM interfaces. Coupling between MM and CM is based on a domain decomposition scheme in which displacement compatibility conditions are imposed. Coupling between QM and MM is achieved by replacing MM calculations of the energy of defect-containing fragments by direct QM simulations. The coupling method was then verified by comparing with direct QM calculations of the energetics of uniaxial tension of defected single-walled CNTs and graphene sheets. The coupling method shows a clear advantage over direct QM calculations for its computational efficiency, while offering solutions with accuracy comparable to direct QM calculations.

Interfacial Thermal Transport in Diamond: Insights from Simulation

Taku Watanabe and Simon R. Phillpot
Department of Materials Science and Engineering, University of Florida, Gainesville, FL 32611

Patrick K. Schelling
Advanced Materials Processing and Analysis Center and Department of Physics
University of Central Florida, Orlando, FL, 32816, USA

Pawel Keblinski
Department of Materials Science and Engineering
Rensselaer Polytechnic Institute
Troy, NY 12180-3590

Diamond has the highest thermal conductivity of any known material. The effect of interfaces on the thermal conductivity is of considerable interest for applications in diamond nanostructures. We use large-scale molecular-dynamics simulations to determine the thermal conductances of a number of representative grain boundaries in diamond. We compare these with the thermal conductances in the corresponding grain boundaries in Si. We ascribe the differences between the results for diamond and silicon to the very different thermal conductivities in the bulk and to the differences in the structures of the interfaces. The implications of our results on the possibility of using nanocrystalline and ultra-nanocrystalline diamond for thermal transport applications are discussed.

Surface and electronic structure of diamond nanoparticles

T. van Buuren, T. Willey, C. Bostedt, R. Muelenburg, J.Y. Raty, G. Galli, L. Terminello
Chemistry and Material Science Department, Lawrence Livermore National Laboratory

Nanometer sized diamond is a constituent of diverse systems ranging from interstellar dusts and meteorites to carbonaceous residues of detonations. We have conducted a number of experiments tightly coupled to theory that demonstrates the impact of surfaces on the electronic and atomic structure of diamond nanoparticles produced via a detonation synthesis method. The nanodiamond K-edge absorption and emission spectra for 3-4 nm clusters show the same features as the bulk material and no blue shift is observed, contrary to previous experiments on nanocrystalline diamond films.[1] Therefore the 3nm nano-sized diamonds do not display the characteristic property of other group IV nanoparticles: a strong widening of the energy gap between the conduction and valence bands owing to quantum-confinement effects. Standard density-functional calculations on clusters in which the diamond surface bonds are terminated with hydrogen atoms, show that the bandgap begins to increase above the bulk value only for clusters smaller than 1 nm. Ab-initio calculations were preformed to investigate the effect of surface relaxation on diamond nanoparticles as well. To represent a true surface, pairs of hydrogens were removed whose interatomic distances were within 5% of the H_2 bond length and the surface atoms were allowed to relax. In this study, the surfaces spontaneously reconstructed into a fullerene-like surface but this reconstruction induced only small changes in the calculated gap values. [2] Clear signatures of these surface reconstructions were identified as pre-edge features in measured C 1s absorption spectra. The C1s core exciton feature clearly observed in the K-edge absorption edge of bulk diamond is shifted and broadening due to increased overlap of the excited electron with the core hole in the small particle. Also the depth of the second gap in the nanodiamond spectra is shallower than that of bulk diamond.

One of the weaknesses of the x-ray absorption measurement is that many particles are probed to produce the measured spectra. This is not a problem if one has a distribution of identical particles. However, with a finite size distribution or other inhomogeneity in the nanoparticle ensemble, the measured spectrum represents a combination of the spectra from all particles. To resolve and explore the electronic structure of individual quantum dots, we have employed the high spatial resolution possible from transmission electron microscopy and the electronic structure information possible with electron energy loss spectroscopy (TEM/EELS). The high spatial resolution of the TEM/EELS will allow us to; 1) make measurements of the electronic structure of the individual nanoparticles and 2) probe separately the surface and bulk structure of the nanoparticle. The TEM/EELS measurements on the diamond nanoparticles indicate that the core of the particle has similar electronic structure as bulk diamond, whereas the surface region looks much different. The EELS spectra of the surface region cannot be described by the EELS spectra from graphite or C-60 but seems to be a combination of both in agreement with our previous x-ray absorption and emission results.

The work is supported by the US-DOE, BES Material Sciences under contract W-7405-ENG-48, LLNL.

1 Y. K. Chang et al., Phys. Rev. Lett. **82**, 5377 (1999).
2 J.Y. Raty, G. Galli, C. Bostedt, T. Van Buuren, L.J. Terminello, Phys. Rev. Lett. Vol. **90**, p401 (2003).

2005 ADC meeting

Argonne, IL

A model for nanocrystalline diamond growth

Peter Zapol, Michael Sternberg

Materials Science Div., Argonne National Laboratory, Argonne, IL, USA.

Growth mechanisms for ultrananocrystalline diamond grown in hydrogen-poor argon plasmas are different from conventional CVD growth based on methyl radials. We propose a model that can account for very high renucleation rates necessary to produce diamond with grain sizes in the nanometer scale. The model is based on the calculation of stable adsorbates and transition states for reactions of C_2 with diamond surfaces calculated using electronic structure methods. The nonempirical model invokes transition state theory to calculate reaction rates from the energies and barriers. Resulting renucleation rates and grain sizes provide a mechanism for nanocrystalline diamond growth in the absence of hydrogen. The temperature dependence of renucleation rate as a function of the C_2 density in the plasma was obtained from the model. It shows that a grain size reaches its maximal value at the temperatures of about 800 °C. A comparison of the computed results with available experimental data is provided and further predictions are discussed.

* Work supported by the U.S. Department of Energy, BES-Materials Sciences, under Contract W-31-109-ENG-38.

Keywords

diamond growth, nucleation, transition state theory

The Resolution of the Diamond Problem After 200 Years

Reginald B. Little
Department of Chemistry
Florida A&M University
Tallahassee, Florida 32307

Abstract:

The diamond problem spans more than 200 years. Many technologies from electric arcs, to metal solvents to metal catalysts to electric ovens to electric resistive heating to anvil vices and presses to chemical vapor deposition (CVD) to plasma to microwaves to hot filaments to flames and now to magnets have been discovered, realized and used to resolve the diamond problem. Here the origin, definition and cause of the diamond problem are presented. The resolution of the diamond problem is then discussed. Furthermore, the partial resolutions (of high pressures and high temperatures, catalysts and atomic H vapor) for this problem within the last 50 years are reviewed and the recent complete resolution is demonstrated by use of strong magnetic fields in conjunction with these partial solutions for faster, larger single crystal diamond synthesis.

SESSION 14

BUSINESS MODELS & DEVELOPMENT

LEGAL OPPORTUNITIES AND CHALLENGES AFFECTING NANOTECHNOLOGY RESEARCH AND COMMERCIALIZATION

Jeffrey H. Matsuura

University of Dayton School of Law

Keywords: Law, Regulation, Commercialization, Public Policy

Abstract

This presentation examines the impact of law (statutes, regulations, court actions, and public policy) on nanotechnology research and development of commercial applications based on that research, and it offers suggestions to nanotechnology professionals as to how they can influence that legal impact in ways that will facilitate nanotechnology research and commercialization. The presentation concludes that a diverse range of laws significantly affect the rate and scope of nanotechnology research and commercialization of that research. Regulatory law, commercial law, and intellectual property law significantly affect nanotechnology research and the development of effective business models and commercial opportunities for the fruits of that research. Law asserts this important impact on nanotechnology research and development in both direct and indirect ways. It directly encourages or impedes nanotechnology research and it indirectly affects nanotechnology development by affecting the financial and business environment in which research and commercialization take place. As a result of the significant potential impact of law on nanotechnology research and commercialization, scientists, engineers, and other nanotechnology professionals should become familiar with the ways in which law affects nanotechnology development and use. They should also attempt to influence the legal system to promote expanded nanotechnology research and commercialization.

LAW AND NANOTECHNOLOGY

Several different forms of law have a significant impact on research involving nanotechnology and the development of commercial applications based on that research. The most significant of those legal categories affecting work involving nanotechnology are: regulatory (administrative) law, commercial law, and intellectual property law. Regulatory law affects the scope of nanotechnology research. It also affects the commercial use of nanotechnology. For example, environmental protection standards and workplace safety requirements affect the form and scope of certain nanotechnology applications involving materials and manufacturing.

Commercial law includes the law of contracts, commercial transactions (sales), and financing (including equity investments). These legal requirements are essential to the creation and operation of enterprises to conduct nanotechnology research and to develop commercial nanotechnology applications. This category of law governs the business and financial transactions and structures that provide the funding and other resources necessary for nanotechnology research and commercial development. For example, law governing securities and financial investments has a significant impact on the availability of capital to support new ventures based on nanotechnology.

Intellectual property law, particularly patent law and the law of trade secrets, plays a critical role in the conduct of nanotechnology research and the rights of access and use associated with the output of that research. Intellectual property rights provide an important incentive for financial investment in research and development. They can also provide a formidable potential barrier to innovation and refinement of prior research in nanotechnology. Those two sometimes conflicting forces associated with intellectual property must be effectively balanced.

SCOPE OF LEGAL IMPACT ON NANOTECHNOLOGY DEVELOPMENT AND BUSINESS MODELS

Law has both a direct impact on nanotechnology research and commercialization and an indirect impact. Law has a direct impact on nanotechnology research and commercialization to the extent that it encourages funding for research and commercialization efforts (e.g., the National Nanotechnology Initiative in the United States). By supporting, or potentially blocking, specific fields of nanotechnology research and commercialization, the law has a direct impact on the direction, scope, and rate of nanotechnology development.

Law can also influence nanotechnology development in indirect ways. For example, broad enforcement of intellectual property rights can provide great incentive for investment and research, but can also impede subsequent commercial development and continuing innovation. Commercial law dramatically affects the business transactions and organizations essential to effective research and commercial development involving nanotechnology.

LAW: A CRITICAL FACTOR IN NANOTECHNOLOGY RESEARCH AND COMMERCIALIZATION

Law plays a critical role in the scope of nanotechnology research, the range of commercial applications for that research, and the pace at which commercial applications based on nanotechnology develop. Law exerts this significant influence on nanotechnology development both directly (e.g., through promotion or restriction of specific fields of research or specific applications) and indirectly (e.g., through enforcement of intellectual property rights associated with nanotechnology). Law substantially affects the scope of nanotechnology research, the range and form of applications for the fruits of that research, and the financial environment available to support both research and development of commercial applications. It is, accordingly, not an overstatement to assert that law is a critical factor in the expansion of nanotechnology research and the prompt development of commercial applications for that research.

LAW AND NANOTECHNOLOGY PROFESSIONALS

As law has a significant impact on nanotechnology research and commercialization, scientists, engineers, and other nanotechnology professionals should actively monitor and influence the development and application of law in the context of nanotechnology research and commercialization. They should focus attention on both the legal initiatives that address directly nanotechnology research and development and those that influence nanotechnology development indirectly by affecting the financial and operational environment in which that research and development takes place. Nanotechnology professionals should strive to understand the range of legal issues and doctrines that affect nanotechnology research and use. In addition, they should become involved in the policy debate associated with shaping and enforcing those legal requirements. Absent such active participation by nanotechnology professionals, decisions regarding development and enforcement of legal requirements that have a profound impact on nanotechnology development will be left to the legal and business communities. Those communities, acting alone, are not in a position to ensure that an effective balance is struck between encouraging nanotechnology advances and protecting the public interest. Thus continuing advances in nanotechnology research and expansion of commercial applications for that research require effective participation by nanotechnology professionals in the legal environment that surrounds nanotechnology.

ANATOMY OF A DIAMOND STARTUP

Neil Kane, Co-founder and President

Advanced Diamond Technologies, Inc.

60 Hazelwood Drive, Suite 226

Champaign, IL 61820

Phone: 217-265-9824

Email: kane@thindiamond.com

Web: http://www.thindiamond.com

Keywords: diamond, startup, venture capital, business, formation

Abstract

Advanced Diamond Technologies, Inc. (ADT) was formed in December 2003 to commercialize the Ultrananocrystalline™ diamond (UNCD™) technology developed at Argonne National Laboratory. It took four months of a consultant's time to recommend a startup as the commercialization vehicle for UNCD, and over two years from that point until the company was formed with a license and financing. Since Argonne had never organically formed a startup before there were the usual policies and procedures that had to be followed and many more had to be created because there were no precedents.

In this talk, Neil Kane, former Co-Executive Director of the Illinois Technology Enterprise Center at Argonne, a partnership between the University of Chicago and the State of Illinois Dept. of Commerce and Economic Opportunity and co-founder of ADT, will illustrate the timelines and issues necessary to get a startup company formed from a federal laboratory or university setting. This will be a general purpose talk, using ADT as a case study, on the issues that need to be tackled to launch a startup out of an academic setting. Issues that will be addressed include:

- Allocation of founder's shares
- License terms
- Role of scientific/academic founders
- Business plan
- Conflicts of interest
- Corporate Governance issues
- Cultural issues
- Financing strategies and the role of federal contracts (SBIRs and STTRs)

Now that ADT is up and running, it hopes that it will contribute to the exciting endeavor of commercializing new technologies and enabling new products based on diamond films. It is hoped that by sharing the experience of what it took to get ADT off the ground, other efforts might be undertaken in other laboratory settings both in the U.S. and elsewhere in the world to commercialize emerging technologies.

REFERENCES

1. Kane, N.D.: "Rich of Famous: you choose," *Physics World*, March 2004.

FLEXIBLE MARKET APPROACH OF *CYRANNUS*® PLASMA TECHNOLOGY

Ralf Spitzl, Hildegard Sung-Spitzl

iplas innovative plasma systems gmbh, Langbaurghstr. 10 – 53842 Troisdorf, info@cyrannus.com

Keywords: Microwave, plasma source, plasma system, diamond deposition

Abstract

Running a high tech company successfully in the field of diamond technology does not only require highest technical performance. A carefully diversified company strategy is the best solution for a stable business development.

iplas innovative plasma systems is a young company that took the opportunity to compete against several established and low cost competitors with a fully diversified strategy. It is not only the approach into several branches, also the product spectrum is adapted to a large range of customer ship. A modular system design enables a very fast tailoring of systems to customers requirements.

Today the applications of iplas' systems are covering a range from high tech materials, optical industry, food and packages, semiconductor industry, medical implants, plastic industry, waste management, plasma chemistry, textile industry etc.. Only by looking more detailed into the field of diamond coatings the enormous range of the technology shows the specific problems in running a cross oriented company. The variety of products in different markets and applications are indicated in the chart.

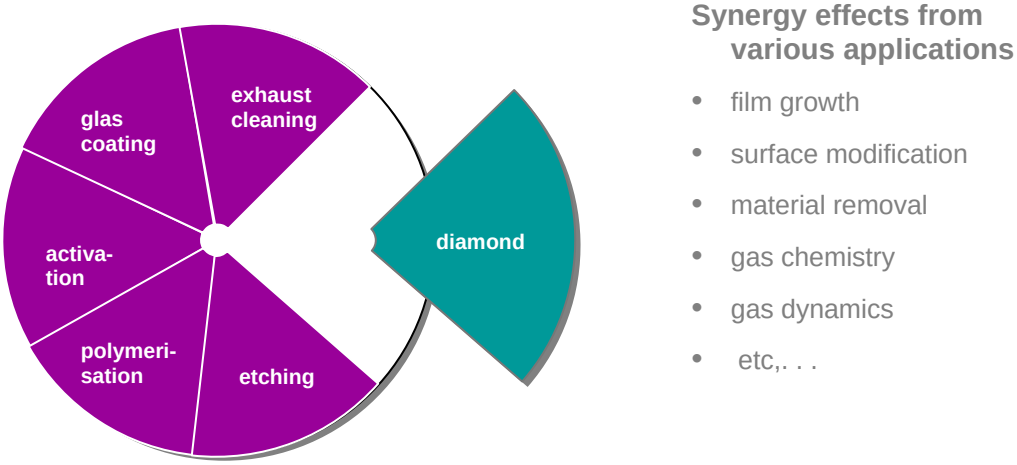

Figure* 1. *markets and applications of CYRANNUS® systems

The applications for diamond films are covering all high end applications as the production of various types of crystalline diamond (hydrogen- or also noble gas- based from single to nano crystalline diamond films). Heat sinks, SAW filter, high temperature semiconductor, corrosion protected implants, wear resistant MEM, stronger and sharper scalpels, are only few examples, the range of future products is going much further.

Balancing the diversity of processes and economic organization of company resources (human resources, R&D investments etc.) is one of the major threats. If it is working successfully the diversity comprises the advantage of very high synergy effects in production and development as well.

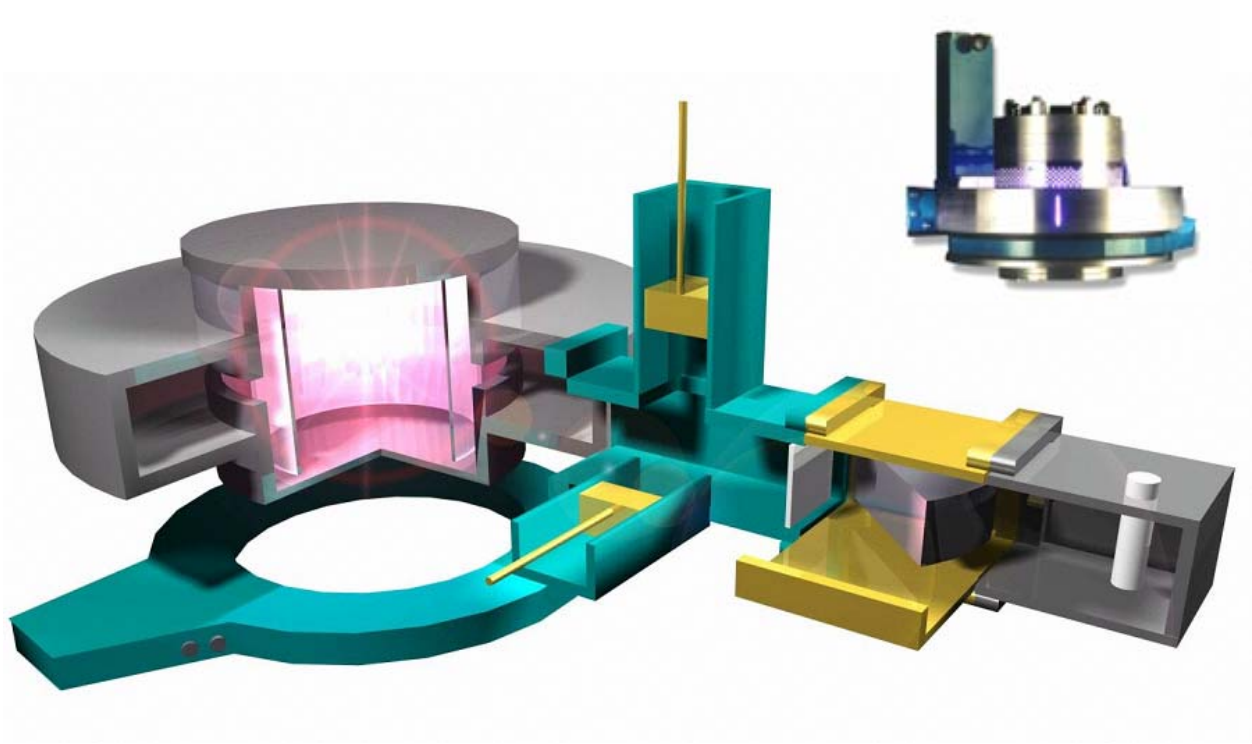

Figure 2. principle of CYRANNUS® plasma sources
(free access to plasma from top and bottom flanges, radial view through quartz tube, TM012 resonator and multi-antenna configuration for high pressure plasma operation)

iplas' intellectual property – the *CYRANNUS®* plasma sources – has several features that enable an universal design. Figure 2 shows how easily the set-up can be modified and adapted to new processes. iplas has taken the opportunity and tailored all system development around the plasma sources in the same way. The only limitation iplas accepted, was related to a control technology based fully on PLC. This decision was made to ensure highest performance and reliability for production. The result is a system with unique modularity.

Building a multi-purpose equipment on highest technical level has influence in various areas. Instead of cost optimization iplas has invested into a system architecture with perfect modularity. Higher system costs in equipment are compensated by larger advantages from production synergy effects.

To serve various markets and optimize tailored developments, iplas was able to make technology driven approach. The special configuration and performance of the *CYRANNUS®* technology is the key to the business strategy. A simple and flexible design of equipment and systems makes it possible to use the technology for various applications with unique economic advantages and performance.

ADAMANT TECHNOLOGIES

Ph. Rychen, Ch. Provent, L. Pupunat

Adamant Technologies Inc. , Jaquet Droz-1 CH- 2000 Neuchâtel, Switzerland

www.adamantec.com; info@adamantec.com

Keywords: Diamond electrodes, electrochemistry, electrolysis, water treatment

Abstract

The development of novel and innovative solutions for water treatment is focus of various research initiatives. New systems have to prove efficiency and ecofriendliness as well as their applicability for daily use and series production. CSEM Inc., Swiss Centre for Electronics and Microtechnology, and its latest spin-off company, Adamant Technologies Inc., have developed products that fulfil these conditions and are introducing new technologies for water treatment which apply electrochemical processes instead of chemicals.

In recent years, CSEM has established research activities in the field of environmental technology and developed new methods for water treatment without the use of chemicals. These new developments are based on highly efficient electrolysis technology. In December 2004, "DiaCell®" – a diamond electrode based system for water purification.

The majority of currently applied methods for water treatment use considerable quantities of chemicals to produce clean drinking and process water or for treating wastewater. The new water treatment technique DiaCell®-System needs just electricity and uses diamond coating technologies. This material is used in the electrolysis process as a self-cleaning electrode which supports the treatment of industrial wastewater by reducing pollutants and by inactivating micro-organisms of fresh water.

The new technique is based on the latest knowledge in electrochemistry, since the chemical reactions take place within the micrometric range of reactive interfaces. Thanks to the corresponding charge carrier interactions on special electrically charged surfaces, the water is split into hydroxyl radicals, with any impurities such as germs and dirt particles being destroyed. A further advantage of this technique is that the electrodes are implemented in a compact modular system, the DiaCell®, which demands little space and low energy.

The DiaCell® concept was initially developed for water disinfection i.e. in swimming pools and has later been proven to be suitable for many other applications. Legionella inactivation is a further potential for the technology, also, the systems are able to destroy organic pollutants, even non-biodegradable or so called persistant organic pollutants (POP's). This effect is mainly used in the treatment of industrial effluents. Furthermore, the DiaCell® systems allow the oxidation of inorganic pollutants such as cyanides and hypophosphites which are relevant for the regeneration or recycling of plating baths.

sp3 Inc.: From Tools to Technology - Stories from a Diamond Survivor

sp3 Inc. was founded in 1993 as a technology focused CVD Diamond company. It is still here by being in the tool business. This presentation will share lessons and insights about technology, markets and corporate survival.

SESSION 15

HPHT SYNTHESIS, TREATMENTS, GEMS, & APPLICATION

VERY HIGH CRYSTAL QUALITY DIAMOND STUDIED BY A VARIETY OF SYNCHROTRON GENERATED X-RAY TECHNIQUES

S. H. Connell, R. K. Setshedi, D. Dube, L. Mkhonza, M Rebak

Physics Department, University of the Witwatersrand, Johannesburg

J. Härtwig and J. Hoszowska

European Synchrotron Radiation Facility (ESRF), Grenoble

RC Burns, JO Hansen

Element Six, Johannesburg

Keywords: diamond, synchrotron, optic elements.

Abstract

The unique properties of diamond have identified it as one of the most attractive materials for application in a range of beam optical elements associated with modern very bright X-ray sources. This new role for diamond imposes rigorous standards of crystalline quality. The question presents itself as to whether diamond can be synthesized to adequate levels of perfection. This has motivated the present study of very high quality type IIa diamond crystals synthesised using the high pressure high temperature technique (HPHT) by Element Six in Johannesburg. The X-ray characterizations were carried out at various beam lines of the ESRF Synchrotron Facility. They included high resolution synchrotron x-ray rocking curve mapping and X-ray topography using both the white beam and plane wave methods in the Laue and Bragg geometries. These methods are sensitive to extended defects like dislocations, stacking faults, growth sector boundaries, strain fields and precipitates. The samples exhibit excellent bulk properties which improve with distance from the seed face. The rocking curve maps display essentially the Darwin line width in the central cubic growth sector, which appears essentially free of extended defects, and where the spatial variation of the lattice constant is in the $\Delta d/d \sim 10^{-8}$ range. The impurity concentration is sufficiently low that growth sectors observed by UV phosphorescence show almost no phase contrast in the topographs. The partial coherence of the beam in the modern X-ray sources is a crucial property for several applications such as coherent imaging, extreme focusing and photon correlation spectroscopy. A robust way to characterise the coherence properties of the wave front at the exit of an optical element is the Talbot effect (self-imaging of a periodic object in propagation). Coherence preservation measurements of this type using synchrotron radiation have also been made. Taken together, these results are very promising for a new role of diamond as a synchrotron beam optic element in even the most demanding of applications.

Treatment of Natural Gem Diamond and Its Identification

Wuyi Wang *, Tom Moses, Matt Hall
Gemological Institute of America, 580 Fifth Avenue, New York, NY 10036, USA

Diamond is the most important gem stone in the jewelry industry. Next to the carat weight, a diamond's color may be the most important valuation characteristic. Both colorless/near-colorless as well as highly saturated (fancy colored) diamonds are in high demand, and are of great value in the diamond market. However, only a few percent of natural diamonds are gem quality and much less show an attractive color. In fact, many gem-quality diamonds may display undesirable brown coloration with varying saturations or a diamond's inherent color may not be intense enough to qualify for the "fancy" category. Therefore, treatment techniques such as irradiation and HPHT are currently being employed to decolorize and/or enhance a diamond's color to potentially increase its value.

Artificial radiation with or without annealing has been applied to improve diamond color appearance for nearly a century, and continues to be an effective technique. The side band of the GR1 defect, which may be introduced by all types of radiation, extends into red light region and imposes additional blue coloration. For example, a light yellow diamond will show a clear green coloration after a simple irradiation. Depending upon properties of the starting material, annealing of irradiated diamonds could generate H3, H4, and N-V defects, consequently producing intense yellow, green, or pink-purple coloration. Commercial annealing of diamond under high pressure and high temperature (HPHT) started in late 90s in order to improve color appearance. This technique, for example, could turn type IIa brown diamonds into colorless/near-colorless or turn gray type IIb diamonds into intense blue. Varieties of other attractive colors (e.g., yellow, greenish yellow, orange, etc) could also be produced when type Ia diamonds are annealed under HPHT. Intense red color, which is very rare in nature, could be produced with a combination of HPHT and radiation/annealing techniques.

Currently, many attractive diamond colors are being produced in treatment laboratories and are being introduced into the gem market. Proper identification of these treated diamonds is crucial to protecting the diamond industry. In addition to many gemological properties, defects in the diamond (extended and point defects) supply essential identification criteria. Since conditions (radiation energy and intensity, pressure, temperature) applied to a diamond during laboratory treatment (radiation/annealing or HPHT annealing) are very different from those that occur in nature, it is expected that the varieties and concentrations of defects in a treated diamond differ from defects that occur in a natural diamond. Finding this difference is the basis for proper identification. Spectroscopic features of various types of natural and treated diamonds will be reviewed and some details about identification of diamond treatment will be discussed.

COLOR CHANGES IN HPHT ANNEALED TYPE IA DIAMOND

F. De Weerdt

HRD (Diamond High Council), Hoveniersstraat 22, 2018 Antwerp, Belgium

Tel: +32/3/222.06.75, fax: +32/3/222.06.05, e-mail: fdw@hrd.be

H. Kanda

NIMS, 1-1 Namiki, Tsukuba, Ibaraki 305-0044, JAPAN

Phone: +81-29-859-2000 Fax: +81-29-852-7449, e-mail: HISAO.Kanda@nims.go.jp

Keywords: HPHT annealing,

Abstract

This investigation is focussed on the color changes, which can be obtained by HPHT annealing of type Ia diamonds. The color after treatment depends strongly on the presence of nitrogen and it's aggregation state and other defects like dislocations, … Specific attention is paid to nitrogen aggregation and dissociation kinetics, which play a major role in the resulting color after HPHT annealing.

Nitrogen as single substitutional atom and as aggregates plays a crucial role in the color of a diamond. These types of diamonds are called type I diamond. A further subdivision is made depending on the aggregation state of diamond: single substitutional nitrogen gives diamonds a yellow to orangy-yellow color and these diamonds belong to the subgroup Ib. If nitrogen is aggregated, then it is called a type Ia diamond. If the nitrogen is paired up (A defect), then the diamond will be colorless. Also, groups of 4 nitrogen atoms around a vacancy (B defect) do not absorb light in visible region of the electromagnetic spectrum and thus do not color the diamond. Groups of three nitrogen atoms around a vacancy (N3 defects) give the diamond a typical yellow color, a so-called Cape Yellow color.

A systematic study of diamonds containing various types of nitrogen aggregates (type IaA, type IaB), and also diamonds containing platelets, indicate that the most stable defect is the B defect. Other defects can dissociate in its components: the A defect can dissociate in two single substitutional nitrogen atoms and the activation energy is ~ 7 eV [1].

In brown diamonds, there are other types of defects present, which can dissociate. The brown color of these diamonds is thought to originate from dislocations and these dislocations generate vacancies during HPHT annealing. It is found that the activation energy for vacancy generation in brown type Ia diamond is also equal to ~ 7 eV [2].

CL imaging, using a scanning electron microscope, can detect regions with high density of dislocations in plastically deformed diamond. A suitable region for a line scan is selected on a polished (100) surface of a natural and HPHT annealed brown type Ia diamond. A spectral region between 365 and 630 nm was selected which allows clear identification of the presence of N3 with a zero phonon line at 415 nm and H3 with a ZPL at 503 nm. In untreated brown type Ia diamond, a number of other defect can also be detected at 490.7 nm, which is thought to be related to the plastic deformation [3]. The line scans clearly indicate that the H3 and H4 and 490.7 nm defects are located close to regions with plastic deformation in the diamond. CL line scans in the HPHT treated diamond clearly indicate that the vacancies are generated close to the dislocations, which gives a larger concentration of H3 defects close to the plastically deformed diamond.

The measurements on samples, which have been subjected to multiple HPHT annealing runs, suggest that vacancy clusters decorate dislocations and act as source of vacancies during HPHT annealing. These vacancies can be trapped at various nitrogen aggregates, giving rise to a large concentration of H3 defects. This large concentration of H3 defects is typical for HPHT annealed brown diamonds.

REFERENCES

1. F. De Weerdt, A.T.Collins, "The influence of pressure on high-pressure high-temperature annealing of type Ia diamond", *Diam. Rel. Mater.*, Vol. 12, 507-5, (2003).

2. F. De Weerdt, R. Galloway, A. Anthonis, “Defect Aggregation and dissociation in type Ia diamonds by annealing at high pressure and temperature (HPHT) ", *Defect and Diffusion Forum (Annual Retrospective - Ceramics VI)*, Vol. 226-228, , p. 49-60, (2004).
3. A.T. Collins, H. Kanda, H. Kitawaki, “Colour changes produced in natural brown diamonds by high-pressure, high-temperature treatment”, Diam. Rel. Mater., Vol. 9, p. 113-122, (2000).

GROWTH AND CHARACTERIZATION OF A SINGLE CRYSTAL CVD DIAMOND NUCLEAR DETECTOR

A. Balducci, Marco Marinelli, E. Milani, M.E. Morgada, G. Pucella, A. Tucciarone, G. Verona-Rinati

Dipartimento di Ingegneria Meccanica, Università di Roma "Tor Vergata", Via del Politecnico 1, I-00133 Roma, Italy

M. Angelone, M. Pillon

Associazione EURATOM-ENEA sulla Fusione, Via E. Fermi 27, I-00044 Frascati (Roma), Italy

R. Potenza, C. Tuvè

INFN – Dipartimento di Fisica, Università di Catania, Italy

Keywords: detector, diamond, CVD, single crystal, energy resolution

Abstract

The deposition conditions and the detection properties of a homoepitaxial diamond film, grown by microwave Chemical Vapor Deposition (CVD) on a HPHT single crystal substrate are reported. The charge collection spectrum measured under irradiation with a triple ^{239}Pu ^{241}Am ^{244}Cm source, emitting 5.16 MeV, 5.48 MeV and 5.80 MeV α-particles respectively shows three clearly resolved peaks, with an energy resolution of about 1.1%. Both the charge collection efficiency and the energy resolution reach saturation values when the applied voltage exceeds 60 V, suggesting 100% collection efficiency. The detector was also tested with 14.8 MeV neutrons. The obtained collection spectrum shows a well separated $^{12}C(n,\alpha_0)^9Be$ reaction peak.

RESULTS

Diamond is known to be a suitable material for radiation detectors to be used in harsh environments. Since detector grade natural diamonds are extremely rare and expensive, and HPHT crystals contain too many defects to be used as radiation detectors, the most widely used technique to produce such devices is Chemical Vapor Deposition (CVD). However the polycrystalline nature of heteroepitaxial CVD samples severely limits the device performance, in particular energy resolution. A great effort is therefore now being devoted to the realization of homoepitaxial CVD diamond detectors. A resolution as low as 0.4% and 2.9% was reported as the best results obtained for α-particle and for neutron detection respectively[1,2], but a degradation of the device performance was observed during long time particle irradiation, due to polarization effects[2]. Moreover, the samples used are of industrial origin, so that the growth conditions are not known.

We report on the growth conditions and the α-particle and neutron detection properties of a homoepitaxial diamond film deposited by CVD in Roma "Tor Vergata" University laboratories. The film was deposited in a microwave plasma CVD tubular reactor on a low cost (100) HPHT single crystal substrate 4.0x4.0x0.3 mm^3 in size. The CVD diamond layer was deposited for 92 h, at 700 °C, in a 1% CH_4/H_2 mixture and is 110 μm thick (1.2 μm/h growth rate). Metallic contacts 2 mm in diameter and 100 nm thick were evaporated on the film in a sandwich geometry, without removing the HPHT 315 μm thick substrate. The device was connected through an Ortec 142 A charge preamplifier to a 6 μs shaping amplifier and a multichannel analyzer.

In Fig. 1 the response of the detector to irradiation from a triple ^{239}Pu ^{241}Am ^{244}Cm source, emitting 5.16 MeV, 5.48 MeV and 5.80 MeV α-particles is reported at 80 V bias voltage. A high signal to noise ratio and a very good energy resolution is observed, as shown by the clear separation of the peaks of the triple α source. The 1.1% resolution of the diamond detector is to be compared with the 0.4% value of a calibrated Si detector. Very poor detection efficiency is observed when irradiating from the substrate side, ruling out the substrate as the source of the signal. The energy resolution and the normalized charge collection efficiency were measured as a function of the applied voltage. A saturation value is reached in both cases for bias voltages exceeding +60 V. This suggests that approximately a 100% collection efficiency is achieved from the CVD diamond film, i.e. all the charges generated in the deposited layer can reach the substrate. Good stability was observed under a 4 particles/s·mm^2 α-particle flux, without any detectable polarization effect for irradiation time of the order of 1 hour.

Irradiation with 14.8 MeV neutrons was also performed using a T(d,n)^{4}He source. The diamond detector was simultaneously irradiating by an ^{241}Am α source positioned in air 4.2 mm away from the sample surface. In such a way, see Fig. 2, the α particle peak is superimposed to the neutron spectrum, allowing its energy calibration. Due to the 4.2 mm air absorbing layer, the energy of the α particles impinging on thje detector is 5.1 MeV as calculated by SRIM simulation. The measured spectrum (Fig. 2) is consistent with those reported in literature, with the ^{12}C(n,α_0)^{9}Be reaction peak well separated from the ^{12}C(n,n')3α shoulder. The FWHM of the 9.1 MeV ^{12}C(n,α_0)^{9}Be peak is about 0.5 MeV, which is thought to be compatible with the energy spread of the incident neutron. Such a value favorably compares with the values reported in literature[2], especially if the much broader neutron energy spread of the 0° detector angular position with respect to the deuteron beam is taken into account.

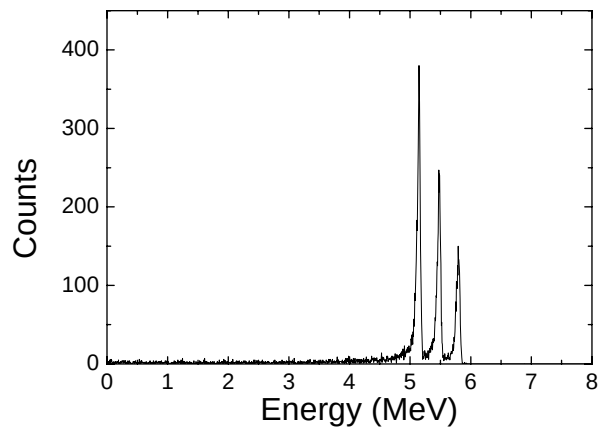

Figure 1: Detector response obtained from the triple ^{239}Pu ^{241}Am ^{244}Cm α source

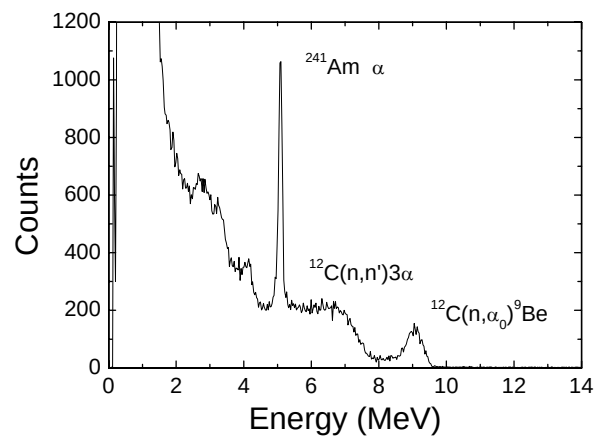

Figure 2: Neutron spectrum obtained with 14.8 MeV neutrons and ^{241}Am α-particles.

References

1. Kaneko, J.H., et al. , *Nucl. Instr. Meth. A* Vol. 505 p. 187 (2003)
2. Schmid, G.J., et al. , *Nucl. Instr. Meth. A* Vol. 527 p. 554 (2004)

THE LASER RAMAN SPECTRA OF LARGE DIAMONDOID MOLECULES: A ROUTE TO UNDERSTANDING NANODIAMOND CRYSTALS

P.W. May, J. Filik, J.N. Harvey

School of Chemistry, University of Bristol, Bristol BS8 1TS, U.K.

J.E.P. Dahl, R.M.K. Carlson and S. Liu

MolecularDiamond Technologies, ChevronTexaco Energy Technology Co.,
P.O. Box 1627, Richmond, CA 94802, USA.

Keywords: Diamondoids, nanodiamond, adamantane, laser raman spectroscopy

Abstract

Diamond is composed of tetrahedrally-bonded carbon atoms, and the simplest molecule with the diamond structure is adamantane ($C_{10}H_{16}$). Diamondoids of the adamantane series are hydrocarbons composed of fused cyclohexane rings, all in stable chair conformations, which form interlocking cage structures that can be superimposed on the diamond crystal lattice. The lower diamondoids have chemical formulas of $C_{4n+6}H_{4n+12}$, where n equals the number of diamond-cage subunits.

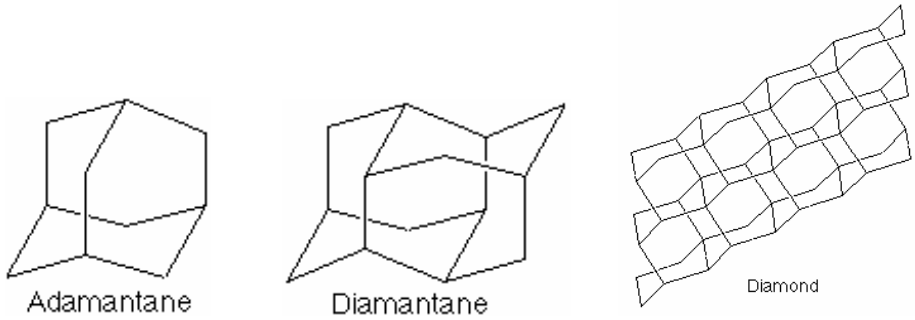

Diamondoids occur naturally in virtually all petroleum, and have been extracted by reverse phase high performance liquid chromatography (HPLC), and then isolated and recrystallised by standard organic chemistry techniques. A whole series of these diamondoid crystals from $n = 1$ (adamantane) to 10 (decamantane) have been studied by laser Raman spectroscopy using 3 laser wavelengths (325, 514 and 735 nm). The spectra have also been simulated using theoretical predictions using the Gaussian program, and this has allowed the experimental peaks to be assigned to individual vibrational motions. The larger diamondoids are similar in size to the nanodiamond grains grown during CVD of ultra-nanocrystalline diamond (UNCD) films, and so the Raman spectra of these diamondoids provides insights into the interpretation of spectra from UNCD films.

INROAD TO MODIFICATION AND FUNCTIONALIZATION OF THE DETONATION NANODIAMOND

B.V.Spitsyn

31 Leninsky pr., Institute of Physical Chemistry RAS, 119991Moscow, Russia

spitsyn@phyche.ac.ru

Keywords: Diamond, nano-diamond, modification, surface functionalization.

Abstract

Introduction. Diamond with its excellent mechanical, physical and chemical characteristics is now available from natural deposits or it can be produced both at thermodynamically stable and metastable synthesis conditions. Now widely developed detonation synthesis of nanodiamond(ND) [1-3] attracts still extended attention due to several remarkable reasons. First of all ND is one of modern nanomaterials, available from several suppliers in NIS, China, Japan and S.Korea, etc. in commercial scale achieving ton per year. Other privilege is that ND is genuine diamond, not converted to graphite phase at 1 atm and in vacuum and inert environment until 1000 ^{0}C and more. Thirdly ND have nearly spherical shape of individual particles not in wide range of dimensions 2 to 10 nm with average size close to 4.2 nm.

From the another side it reasonable to point out that actually ND is industrial semi-product due to: (1) non-diamond carbon impurities or non-carbon impurities (Fe, Cr, Ni, Al, Si, Ca, etc.) giving an ND sample a grey or dark grey appearance; (2) light elements mostly at the chemically bonded ND termination (oxygen ~ 10 wt. %, hydrogen ~1 wt. %) and nitrogen (~2 to 3 wt. %), mostly in the bulk; (3) the presence at ND surface chemical groups of C-H, C-OH, C-O-C, C=O, C=(O)H (aldehide), C=O (OH) (acid), C-NH_2, lactonic and other groups making the ND surface chemically multifunctional; (4) “ash-related” impurities (Fe, Cr, Al, Ca, Si etc.) with the total up to several wt. % occurring as free elements, oxides or carbides, both on the ND particle surface and in the bulk; (5) intrinsic impurities and those with zero- and higher dimensionality defects in the particle’s bulk, producing an appreciable excess of enthalpy (up to 25 kcal/kg); (6) one or more twin boundaries in the fractions of ND particles [6]; (7) a fairly strong agglomeration (agglutination) of individual particles which form tightly packed structures of tens, hundred or thousands of nanometers in size. Some of these characteristics do not permit considering ND as an individual nano-substance according to V.B.Aleskovsky’s definition.

Above listed reasons challenged us to efforts towards to modification and mono-functionalization of the ND.

Experimental. We have used ND sample supplied by New Technology Co. (Chelyabinsk, Russia). Before supplying the samples was finally cleaned by ozone.

Our approach include chemical interaction of the ND with hydrogen- (molecular hydrogen and ammonia) and chlorine-contained environment (carbon tetrachloride) at 1 atm and temperature in range 450 to 1100 ^{0}C.

It was established by Raman- and FTIR-spectroscopy some improvement of crystalline structure of the ND.

After 5 h interaction with hydrogen at 850 ^{0}C the heat of combustion of the ND is 1000 cal/g less relative initial ND. It suggest us about some annealing of defects after

Elaboration of the nanopowder at above condition.

FTIR-spectroscopy indicate appearance C-H, N-H and C-N groups after interaction with ammonia at 800^{0}C. Chemical analysis reveal up to 7 mass. % content of bonded chlorine after heating 1 h in CCl_4/Ar mixture at 450^{0}C. In the same time water absorbance became 10 times less in comparison wit initial powder.

Intensity of C-Cl band at 709 cm^{-1} in reflectance FTIR-spectra progressively rose with the interaction time.

Remarkable is rather modest diminishing – no more that 50 % of dangling bond content measured by ESR-spectroscopy after any of above treatment.

Finely it seems for us that there were find approach to control th behavior of community of the ND particles and systems like ND – solid substrate through intentional changing of the ND functionalization, e.g. hydrophilic/hydrophobic and/or acidic/basic. It might open more room for ND application in academic research and industrial practice.

We have suggested a simple and effective technique for vapor ND cleaning and functionalization. High temperature ND treatment allows the chemical agents to penetrate in nanoporous materials and functionalize the ND surface in a desired way. Hydrophilic/ hydrophobic or acid/base ND termination becomes feasible. We believe that this technique has a large potential in research and development projects[4]..

Acknowledgements

Great thanks devoted to P.Ya.Detkov and I.L.Petrov for ND samples of high initial purity. The author appreciate a partial support of this work through the Russian Foundation for Basic Research, grant # 04-03-32835.

REFERENCES

1. Dolmatov V. Yu., “Detonation synthesis ultra-dispersed diamond: properties and applications”, Russian Chem. Reviews 70, 607-626 (2001).
2. Vereschagin A. L., “Detonation Nanodiamonds”, Barnaul, 2001.
3. Danilenko V.V., “Synthesis and Sintering of Diamond by Detonation”, Energoatomizdat, Moscow.2003.
4. Spitsyn B.V., “Nanodiamond for science and practice”, Repts. Russian Acad. Sci., 73 (5)433-435 (2003).

POSTER SESSION 1

CHARACTERIZATION

MECHANISM OF IMAGING OF CARBON NANOTUBES BY SCANNING ELECTRON MICROSCOPY

Dmitriy A. Dikin, Rodney S. Ruoff

Department of Mechanical Engineering, Northwestern University, Evanston, IL 60208, USA

Keywords: carbon nanotube, SEM, secondary electrons.

Scanning electron microscopy (SEM) is used for imaging of nanostructures, including carbon nanotubes (CNT). Recent developments of the SEM technique[1,2] mean new capabilities for nanoscale sample analysis with potential industrial and metrological applications. This is further discussed in recent publications,[3,4] however the physics of CNT imaging is not fully understood. We have found interesting physical and chemical phenomena in our "SEM experiments", which can be used for analysis of the interaction between CNTs and neighboring material (such as a substrate). We have analysed the role of the electron beam parameters, the effect of surrounding materials and the substrate, and the influence of the properties of the CNTs on their appearance in SEM micrographs.

We use a LEO 1525 Schottky field emission SEM, which has two secondary-electron detectors. One is a phosphor scintillator detector sitting in the chamber ("side-view") and the second is in the column primary-electron beam ("in-column"). The in-column detector collects low-energy secondary electrons much more efficiently then the side-view detector, which we find at times to be a key advantage of this instrument.

We have studied CNTs grown by a variety of methods in different laboratories: chemical vapour-deposited (CVD) in the Ruoff Lab (Northwestern University), the Liu Lab (Duke University), and the Ren Lab (Boston College), and arc-discharge grown in the Chang Lab (Northwestern University).

In serious of SEM experiments, a variety of sample types have been studied: (i) CNTs in a liquid suspension were spun onto Si substrates with a range of thicknesses of the top oxide layer (2 nm – 1 μm); (ii) as grown CNTs on different substrates—that is, they are attached to the substrate at the synthesis step, and we have studied them as such; (iii) CNTs in contact with metal films. As grown, and also chemically treated, CNTs dispersed in nonconductive polymers were also imaged and their interaction with the surrounding polymer matrix was analysed.

From these imaging studies, some conclusions have been reached: (a) The chemical and physical interaction with the surrounding material and its electrical properties determine the "appearance" of the CNT (Figure 1). (b) By tuning both the primary electron energy and flux it is possible tune the "brightness" of the CNTs (Figure 2). Studies varying such parameters as in (a) and (b) can be used to understand the physics and chemistry of the CNT-surrounding interaction, and interface properties.

SEM was done at the Electron Probe Instrumentation Centre at Northwestern University. Electron beam lithography was done in the Chandrasekhar lab by Zhengfan Zhang (Dept of Physics, Northwestern University). Funding for this work has been provided by a NASA/MSFC Phase II SBIR, Contract No. NAS8-02102, through a subcontract from Lytec, LLC., and by the NSF NIRT Program, Grant No. 0304506.

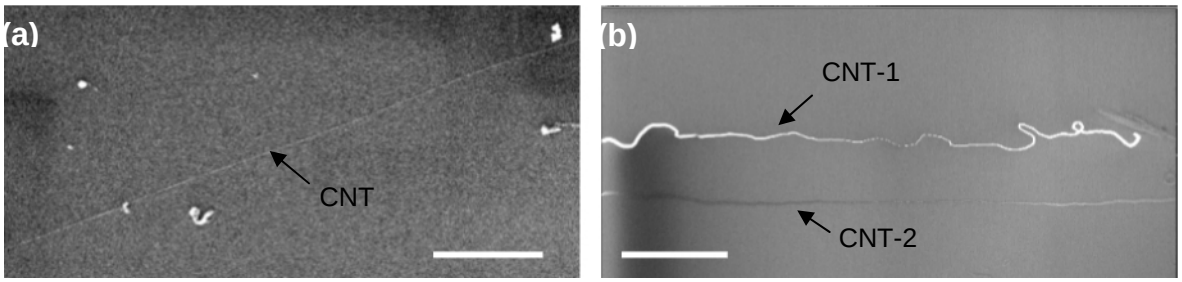

***Figure* 1.** Secondary electron images of CNTs: (a) spun on Si substrate and obtained with the *in-column* detector (3 keV incident electron energy; scale bar is 1 μm); (b) as-grown (CVD) on a Si substrate and obtained by "mixing" the *in-column* and *side-view* detectors in a 0.65:0.35 ratio (1 keV incident electron energy, scale bar is 25 μm).

Irradiation effects of 100 MeV Au^+ ions on multiwalled carbon nanotubes and encapsulated single crystal nickel nanorods

Abha Misra, Pawan K. Tyagi, D. S. Misra
Physics Department, I I T Bombay, Powai, Mumbai 400 076
Jay Ghatak and P. V. Satyam
Institute of Physics Bhubaneshawr

Abstract

Carbon nanotubes of multiwalled and single walled variety have caught the imagination of the scientists and technologists the world over. These interesting new materials are formed with the rolled graphite planes as the building blocks [1]. The nanotubes show a variety of interesting mechanical and electrical properties [2,3]. One interesting aspect of the nanotube growth is the roll of the catalyst. Nickel, cobalt, iron and several other metallic systems have been used as catalyst. In many cases, the catalyst gets filled inside the tubes enabling one to get the interesting phases of the encapsulated particles. In our case we have intentionally used a thick layer of nickel as catalyst to fabricate the nickel nanorods. In the present abstract we report the results of the irradiation of the multiwalled carbon nanotubes samples with gold ions of 100 MeV and studied the damage on the tube walls and the encapsulated Ni fillings inside using high-resolution transmission electron microscopy (HRTEM). As the nanotubes in our case are of 10-20 nm diameter, it is expected that the interaction with the tubes will be via electronic energy loss $(dE/dx)_e$ of the ion beam. The results on the damage of the tube walls, nature of the generated defects and the nickel nanorods inside the tubes will be reported. Figure 1 shows the HRTEM images of the Unirradiated and irradiated Ni filled carbon nanotubes.

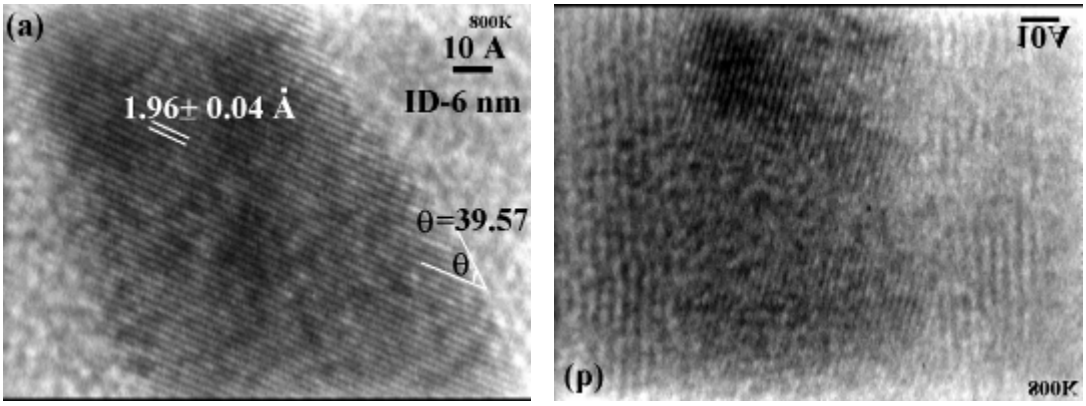

References

1. S. Iijima, Nature 354 (1991) 56
2. J.W.G. Wildoer, L.C. Venema, A.G. Rinzler, R.E. Smalley, C. Dekker, Nature 391 (1998) 59
3. T. W. Odem, J.L. Huang, P. Kim, C.M. Lieber , Nature 391 (1998) 62

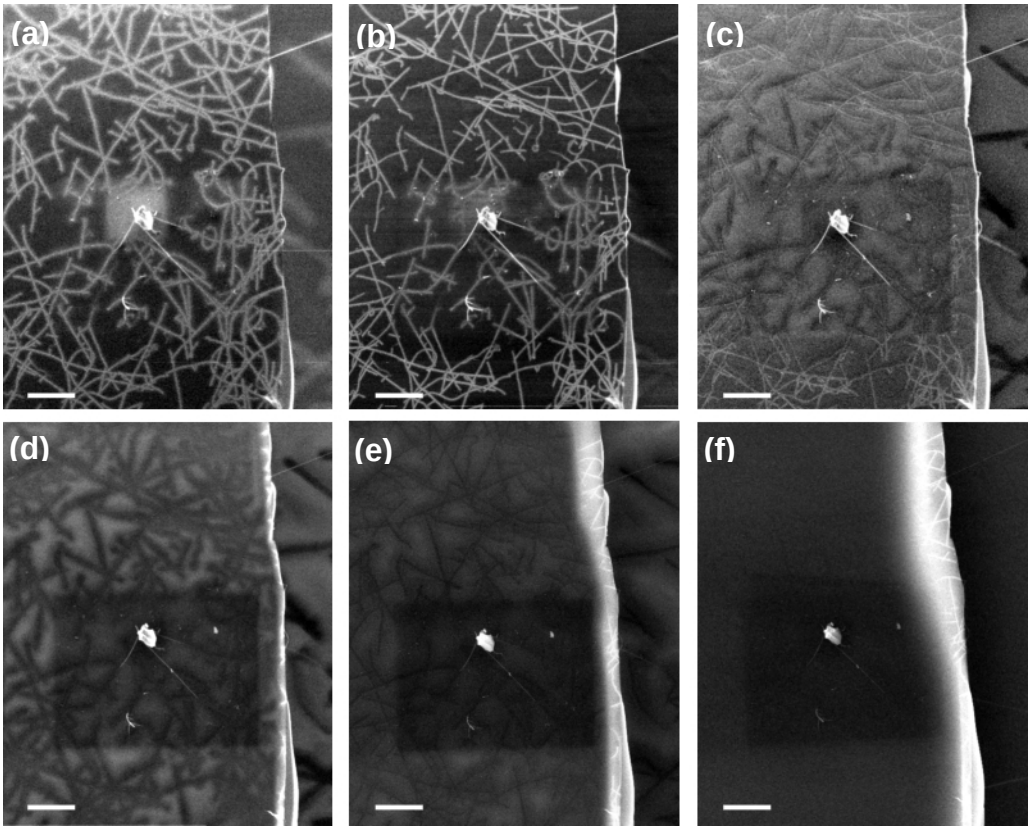

Figure 2. Secondary electron images of CVD-grown CNTs on Si obtained with the *in-column* detector at these incident beam electron energies: (a) 0.3 keV, (b) 0.6 keV, (c) 1.25 keV, (d) 2.5 keV, (e) 5.0 keV, and (f) 10 keV. Scale bar for all images 1 μm.

REFERENCES

1. Jaksch, H.; Martin, J.P.: "High-resolution, low-voltage SEM fro true surface imaging and analysis," *Fresenius J. Anal. Chem.*, **353**, 378-382 (1995).
2. Frank, L.; Zadražil, M.; Müllerova I.: "Scanning electron microscopy of nonconductive specimens at critical energies in a cathode lens system," *Scanning*, **23**, 36-50 (2001).
3. Brintlinger, T., et al., "Rapid imaging of nanotubes on insulating substrates," *Appl. Phys. Lett.*, **81**, 2454-2456 (2002).
4. Homma, Y., et al., "Mechanism of bright selective imaging of single-walled carbon nanotubes on insulators by scanning electron microscopy," *Appl. Phys. Lett.*, **84**, 1750-1752 (2004).

STEP GROWTH IN SINGLE-CRYSTAL DIAMOND GROWN BY MICROWAVE PLASMA CHEMICAL VAPOR DEPOSITION

Pawan K. Tyagi[1], Abha Misra[1], D. S. Misra[1], F. Le Normand[2]
[1]Department of Physics, Indian Institute of Technology, Bombay, Mumbai-400076, India
[2]Groupe Surfaces-Interfaces, IPCMS, UMR 7504, CNRS, BP 43, 67038, Strasbourg Cedex, France

Abstract

Diamond thin films deposited on natural single crystal diamond substrates have attracted great deal of attention recently[1]. The growth rates of single crystal diamond films are substantially high in a narrow parameter window. Diamond crystals of varying quality are deposited using microwave plasma chemical vapor deposition (MPCVD) system in our laboratory. We use a 2 kW microwave power source coupled into an optimally designed plasma chamber. Unpolished natural diamond seeds are used as substrates in the temperature (T_s) range 950-1200 ^oC. A gas mixture of methane (CH_4), hydrogen (H_2) and nitrogen (N_2) is used for the deposition of diamond. The deposition pressure varied in the range 90 to 150 torr. The films are characterized with scanning electron microscopy (SEM), X-ray diffraction (XRD) and Raman spectroscopy. The growth morphology of the films is a sensitive function of the deposition parameters. The crystalline nature of the films change from polycrystalline to single crystal as we increase T_s and for some parameters the filamentary nature of the diamond crystals can be seen. The films are polycrystalline at T_s in the range of 850 – 900 ^oC and oriented grains of diamond crystals are evident as the T_s increase. The single crystal diamond growth is observed to proceed via the step growth methods with the evidence of bunching of the steps. The study shows that the growth of single crystal diamond proceeds via the step growth process.

References:

1.C.S. Yan, Y.K. Vohra, H.K. Mao and R.J. Hemley, Very high growth rate chemical vapor deposition of single- crystal diamond. *Proc. Natl. Acad. Sci. USA* **99**,12523 (2002)

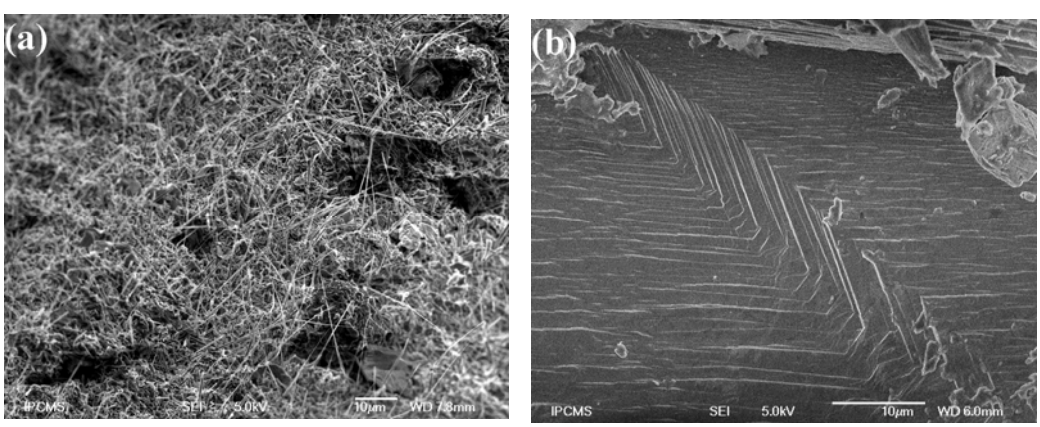

Figure 1:(a) the SEM image of the carbon filament on the surface, Fig (b) shows the step growth in single crystal diamond.

CHARACTERIZATION OF TREATED-BLACK DIAMONDS

M. A. Viktorov, M.B. Kopchikov

Moscow State University, Department of Geology, 119992 Moscow, Russia, viktorov@pisem.net

Keywords: black diamond, treatment, gemology, spectroscopy.

Abstract

In the given work samples of faceted diamonds, diamond crystals and plates which were treated to change their color to black were investigated. The technique of diamond blackening is patented in Russia however detailed research of samples that were treated in such a way was not carried out till last time. Features of this technique are not disclosed, it is only known that samples are treated at low P-T-parameters. Using of non gem (boart quality) or near gem (with numerous inclusions and cracks) diamonds for this kind of treatment gives the best result. According to the manufacturer, gem diamonds of high quality (free of inclusions) are not suitable for this blackening technology. Black color in diamonds may be produced by irradiation [1] or by heating to produce internal graphitization and by some other methods [2].

The study of the blackened diamond samples was carried out by the means of standard gemological equipment (optical microscopy, diamond&moissanite tester, UV-luminescence lamp, magnet) and laboratory research methods: absorption and reflectance spectroscopy in UV-VIS-IR-range (at room temperature), spectral cathodoluminescence (77K), color cathodoluminescence and electron microscopy.

REFERENCES

1. Collins A.T. (1982). Colour centers in diamonds. Journal of Gemmology, Vol.18, No.1, pp.37-75
2. S.V. Titkov, N.G. Zudin, A.I. Gorshkov, A.V. Sivtsov, L.O. Magazina (2003). An investigation into the cause of color in natural black diamonds from Siberia. *Gems&Gemology, Vol.39, No.3, pp.200-209*

ELECTRICAL CONDUCTIVITY OF HYDROGENATED AND NITROGEN-DOPED NANODIAMOND FILMS

An-Jen Cheng, Maurice Clark, Yen-Kang Liu, Yu-Chun Chen, and Yonhua Tzeng
Department of Electrical and Computer Engineering, Auburn University, Auburn, Alabama 36849 USA

Keywords: Conductivity, nanodiamond, hydrogenation, nitrogen doping

Electrical conductivity of undoped and nitrogen doped nanodiamonds has been characterized. Nanodiamond films were deposited on molybdenum, silicon dioxide, and silicon by means of microwave plasma assisted chemical vapor deposition in gas mixtures of methane and argon with or without hydrogen and/or nitrogen additives. Electrical conductivity of nanodiamond films was measured by either (i) directly measuring the conductivity of a metal/nanodiamond/metal sandwich test structure or (ii) applying a electrical current through two terminals of a van der Pauw test structure while measuring the voltage across the other two terminals on corners of a nanodiamond film that was deposited on the electrically insulating surface of a substrate.

Nanodiamond films with thickness of about one micrometer were deposited in gas mixtures of (2% H_2, 1% CH_4, 97% Ar) or (1% CH_4, 99% Ar) by means of microwave plasma CVD. Effects of post deposition heat treatment in air at 350°C for 30 min on electrical conductivity of these undoped nanodiamond films were analyzed by measuring the electrical conductivity of as-deposited nanodiamond films and that of the same nanodiamond films after being heat treated in air. The heat treated nanodiamond films were later exposed to a hydrogen plasma and subsequently measured for their electrical conductivities in comparison with that for the as-deposited nanodiamond films and the heat treated nanodiamond films. The as-deposited nanodiamond films with 2% hydrogen additives in the gas mixture was found to have much higher conductivities than the films without hydrogen additive by more than one order of magnitude.

After both films were heat treated in air, electrical conductivities were found to be similar in values. It is believed that the heat treatment removed hydrogen in both nanodiamond films deposited in the gas mixture with 2% hydrogen additive and the nanodiamond films deposited without hydrogen additive in the gas mixture during the growth. Nanodiamond deposited with or without 2% hydrogen additive both showed the same effects of post-heat treatment hydrogenation on increasing electrical conductivity. The electrical conductivity did not increase to the same level after the nanodiamond films were exposed to a hydrogen plasma as that for the as-deposited nanodiamond films. The increase in conductivity for heated nanodiamond after being exposed to a hydrogen plasma was much less than that for a large-grained polycrystalline diamond film because of the much smaller grain sizes and much higher density of grain boundaries for nanodiamond films (ref. 1 and ref. 2).

Examples of I-V curves measured for an as-deposited nanodiamond film deposited in a gas mixture with 2% hydrogen additive are shown in Figure 1. Conductivity of the as-deposited nanodiamond film was found to be $1.11 \times 10^{-6}\ \Omega^{-1}cm^{-1}$ (Fig. 1, curve (a)). It decreased by more than two orders of magnitude to $6.67 \times 10^{-9}\ \Omega^{-1}cm^{-1}$ after being heated in air (Fig. 1, curve (b)) and then increased to $1.33 \times 10^{-8}\ \Omega^{-1}cm^{-1}$ after being exposed to a hydrogen plasma (Fig. 1, curve (c)).

I-V curves for a nanodiamond film deposited in a gas mixture without hydrogen additive are shown in Figure 2. Conductivity for the as-deposited nanodiamond film was found to be $2.49 \times 10^{-8}\ \Omega^{-1}cm^{-1}$ (Fig. 2, curve (a)). It decreased to $6.02 \times 10^{-9}\ \Omega^{-1}cm^{-1}$ after being heated in air (Fig. 2, curve (b)) and then increased again to $1.75 \times 10^{-8}\ \Omega^{-1}cm^{-1}$ after being exposed to a hydrogen plasma (Fig. 2, curve (c)).

Nitrogen doped nanodiamond films were produced by microwave plasma CVD with up to 40% of nitrogen additive in the 1% methane-argon gas mixture. Nitrogen doping was found to increase the electrical conductivity of the nanodiamond in a way similar to what was previously reported by the research group of Argonne National Laboratory (ref. 3). However, the conductivity of 20% nitrogen doped nanodiamond deposited by our group was found to be much lower than the value reported in reference 3.

The nitrogen doped nanodiamond film, that was deposited at a gas pressure of 100 Torr and at the substrate temperature of 700°C using 800W microwave power, was measured to have a conductivity of only $2.76 \times 10^{-1}\ \Omega^{-}$

$^{1}cm^{-1}$. Nanodiamond deposited at a lower microwave power of 600W resulted in a higher conductivity of 7.76×10^{-1} $\Omega^{-1}cm^{-1}$, which was still much lower than the value reported in reference 3. Further optimization of our deposition process in an attempt to achieve the previously reported much higher electrical conductivity and the re-confirmation of the much higher conductivity reported in reference 3 are being conducted.

Details of specimen preparation processes, experimental measurement procedure, and the analysis of the effects of post-deposition heat treatment in air, hydrogenation and nitrogen doping on electrical conductivity of nanodiamond films will be reported and discussed in this presentation. High conductivity nanodiamond films are desirable for electrochemical applications.

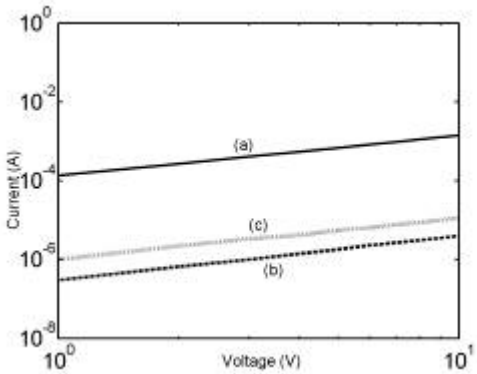

Figure 1. I-V curves for a nanodiamond film deposited in a gas mixture of 1% methane, 2% hydrogen, and 97% argon. (a) as-deposited with resistivity = 9.0×10^{5} ohm-cm; (b) after heat treatment in air with resistivity = 1.5×10^{8} ohm-cm; (c) after being exposed to a hydrogen plasma with resistivity = 7.5×10^{7} ohm-cm.

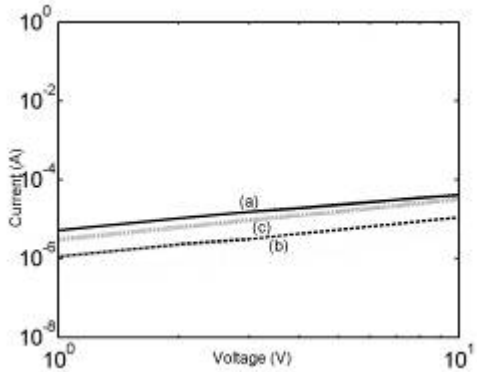

Figure 2. I-V curves for a nanodiamond film deposited in a gas mixture of 1% methane and 99% argon. (a) as-deposited with resistivity = 4.0×10^{7} ohm-cm; (b) after heat treatment in air with resistivity = 1.7×10^{8} ohm-cm; (c) after being exposed to a hydrogen plasma with resistivity = 5.7×10^{7} ohm-cm.

References:

1. Landstrass, M. I.; and Ravi, K. V., "Resistivity of chemical vapor deposited diamond films," *Applied Physics Letters*, Vol. 55, No. 10, 975-977 (1989).
2. Tzeng, Y., et al., "High electrical resistivity diamond films deposited from an oxyacetylene flame," *Applied Physics Letters*, Vol. 57, No. 8, 789-791 (1990).
3. Bhattacharyya, S., et al., "Synthesis and characterization of highly-conducting nitrogen-doped ultrananocrystalline diamond films," *Applied Physics Letters*, Vol. 79, No. 10, 1441-1443 (2001).

TEM and XRD study of nano-graphene layer formation and texturing in carbon films deposited by pulsed Nd:YAG laser

E. Cappelli[11], C. Scilletta[1] and P. Ascarelli[1]

[1] CNR-ISC sez. Montelibretti, P.O.B.10, 00016 Monterotondo, Rome, Italy.

M. Servidori[3], P.G. Merli[3], V. Morandi[3], A. Migliori[3], S. Orlando[2]

[2] CNR-IMIP sez. Potenza, P.O.B.27, 85050,Tito Scalo, Potenza, Italy.

[3] CNR-IMM sez. Bologna, via P.Gobetti 101, 40129 Bologna, Italy.

Keywords: Carbon nano-structures, grazing incidence XRD, TEM analysis, PLD deposition.

Abstract

Nano-structured carbon films are very interesting electronic material, since many electronic properties, like charge transport and low threshold field emission [1], are highly anisotropic and generally correlated to the basal plane orientation of graphene layers and to the peculiar electron energy density of states of the aromatic emission sites, associated with the π band [2]. These properties are expected to open new perspectives of technological applications.

In our work, we tried to study and model how deposition temperature can affect the aromatic particle formation and control a definite texture and growth orientation. We exploited the capability of Pulsed Laser Deposition (PLD) to deposit nano-structured carbon films, with different level of sp^2 coordination and examined the peculiar role of substrate temperature driving a preferential orientation of graphitic nano-particles with respect to Si <100> substrate.

Pulsed laser ablation of a rotating pyrolytic graphite target (Nd:YAG laser, 2nd harmonic: λ=532 nm, hν=2.33 eV, τ=7 ns, ν=10 Hz, $\Phi \approx$ 7 J/cm2), operating in vacuum (~ 10-7 mbar) at temperature ranging from RT to 900 °C has been used to prepare thin films of carbon [3]. Synchrotron X-ray diffraction, performed at grazing incidence and high resolution, established the formation of nano-sized (~7 nm) graphene structures at higher deposition temperatures (~ 900°C). These structures resulted to be formed by some parallel graphene layers (4-5), characterised by a well defined longitudinal growth (along the graphene sheets), with č axis parallel to the substrate. High resolution TEM images and selected area electron diffraction (SAED) patterns confirmed both size and orientation of these graphene nano-particles determined by X-rays.

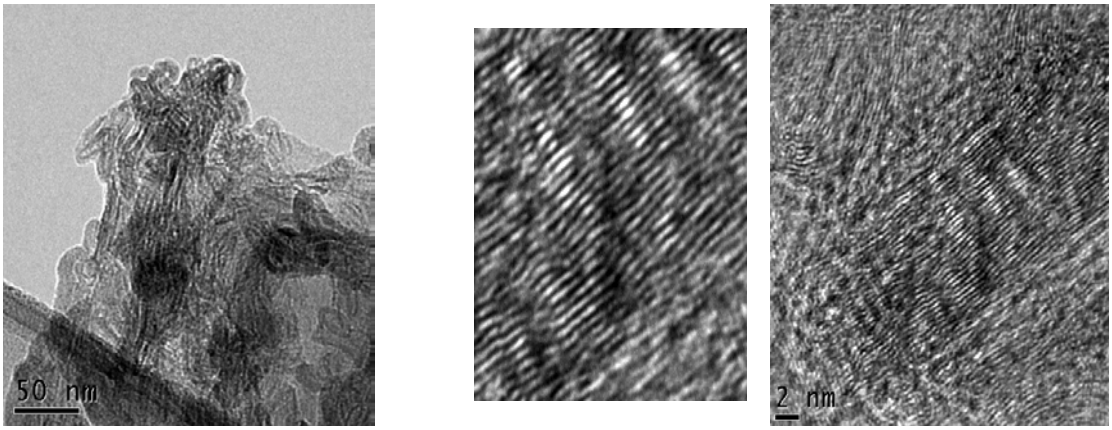

fig. 1. GRID-TEM picture of high temperature carbon nano-graphene layers taken at different magnifications

In the samples deposited at RT, taking constant the other conditions, the typical structure of random amorphous carbon material has been obtained.

[1]Corresponding author: emilia.cappelli@imip.cnr.it, tel. +390690671230,fax: +390690672238

The mass density of the deposited films, as measured by laboratory X-ray reflectivity, is also strongly dependent on the substrate temperature: films grown at room temperature show higher density than the samples deposited at high temperature.

We consider that the preferred growth direction of nano-graphene layers results from cooperating effects of thermal surface diffusion, preferential in-plane growth of graphene sheets and line source direction of the feeding activated species of the laser carbon plume.

REFERENCES

A.A. Talin, K.A. Dean, J.E. Jaskie, *Solid-State Electronics* 45 (2001) 963.

M. S. Dresselhaus, G. Dresselhaus, P.C. Eklund Eds., *Science of Fullerenes and Carbon Nanotubes*, Academic Press, London, 1996.

3. E. Cappelli[12], S. Iacobucci[1], C. Scilletta[1], R. Flammini[1], S. Orlando[2], G. Mattei and P. Ascarelli[1] "Orientation tendency of PLD carbon films as a function of substrate temperature: a NEXAFS study" *Diam Relat.Mater.* 2005 submitted

About X-Ray Amorphous Phase Formation of Ultradispersed Diamonds

A. Koretz[1,2], E. Mironov[1*], E. Petrov[3], A. Lyamkin[4]

1 - Department of Physics, State Technical University, Krasnoyarsk, Russia;
2 - Laboratory of Molecular Spectroscopy, Kirensky Physics Institute, Siberian Branch, Russian Academy of Sciences (SB RAS);
3 - Federal State Unitary Enterprise "Federal Research and Production Center "Altay " Biysk, Russia; Institute of Problems of Chemical and Energetic Technologies (Biysk), Siberian Branch, Russian Academy of Sciences (SB RAS);
4 - Department of Nano-Phase Materials, State Technical University, Krasnoyarsk

Mr. E.Mironov is a corresponding author, mir1on1@newmail.ru; prcom@kgtu.runnet.ru (for Mr.E.Mironov), Russia, 660074, Krasnoyarsk, 26 Kirensky str., Technical University, Department of Physics.

E. Petrov et al. (Lietuvos Fizikos Rinkinys, 1988, 28, N4, p.519-521, in Russian) had observed so-called "X-ray amorphous phase" of the detonation synthesis ultradispersed diamond (UDD) (right side of the fig. 1). The authors of this work connect formation of the phase with some absorption bands of 1105 and 625cm^{-1} in the infrared (IR) spectra of old UDD samples and interpret the phase from the molecular standpoint as gradual destruction of some types of UDD.

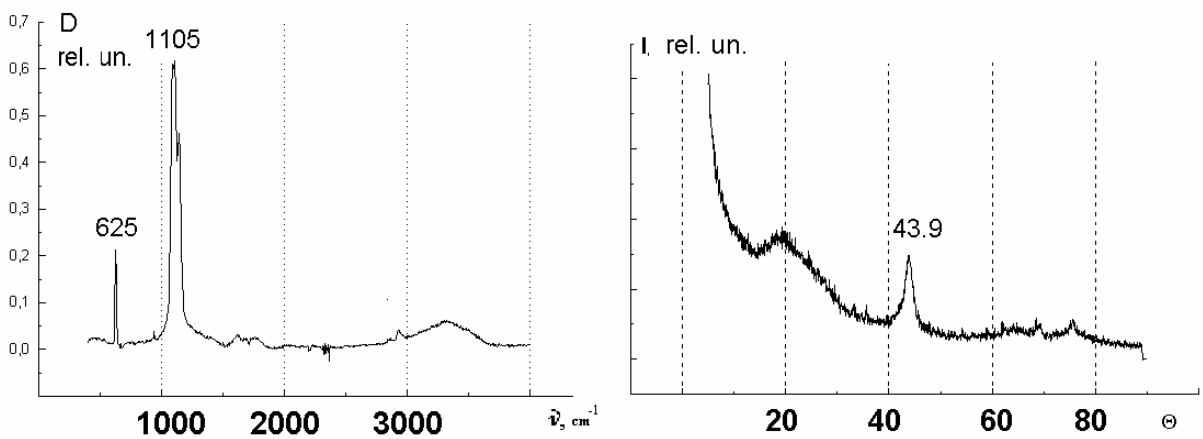

Fig.1 X-Ray amorphous phase (right), and some absorption bands (1105 and 625 cm^{-1}) of old UDD. These samples were obtained before 1984.

The discussion of the results allow to state that the important parameter characterizing the UDD structure is the nitrogen inclusions which with high probability have the high temperature origin. From the standpoint of the technological certification the authors make a conclusion that the informative parameter separating the fields of the UDD application is the nitrogen mass share in the UDD element composition (the level of 2.30 ± 0.15 mass. %). The UDD with the nitrogen content of less than 2.2% (class 1) can be applied in the fields where the principal parameter is the properties of the diamond nanograin. Class 2: the nitrogen portion is higher than 2.4%. The role of the functional groups becomes principal one and probability of the X-ray amorphous phase formation is high.

POSTER SESSION 1

MEMS

DISSIPATION IN TETRAHEDRAL AMORPHOUS CARBON OSCILLATORS

David A. Czaplewski, J. P. Sullivan, T. A. Friedmann, D. W. Carr, B. E. N. Keeler, J. R. Wendt

Sandia National Laboratories

Abstract

Tetrahedral amorphous carbon (ta-C) films have been used to fabricate micro-electromechanical systems (MEMS) with broad applications such as electronics (as clocks, filters, switches, etc.), sensors (for chemicals, biological agents, pressure, acceleration, etc.), and metrology (scanning probe microscopy). These films have superior properties to other common MEMS films such as silicon, polysilicon, silicon nitride and silicon dioxide. The Youngs' Modulus of ta-C (approximately 80% sp^3 bonding) is roughly 4 times that of the other common films, which can aide in the realization of high frequency oscillators for filter and other applications. Additionally, the ta-C films are resistant to stiction and auto-adhesion and have an abrupt surface termination, which helps prevent surface losses. Understanding surface losses and other dissipation mechanisms that limit quality factor, Q, in ta-C is essential for realization of components for electronic or sensor applications since the bandwidth for electronic components scales as Q^{-1} and the sensitivity of sensors scales as $Q^{-½}$.

We have fabricated three different oscillator structures out of ta-C: out-of-plane cantilevers, in-plane cantilevers, and free-free beam oscillators with frequencies ranging from about 1 kHz to 5 MHz. At room temperature, these structures show a consistent quality factor of approximately 3 x 10^3 over the entire frequency range, similar to that observed for other amorphous materials such as silicon dioxide. We have compared the dissipation in these oscillators with the calculated dissipation due to thermoelastic dissipation, dissipation due to phonon-mechanical vibration interaction, mechanical clamping losses, and dissipation due to defects in the material. The observed constant quality factor is only consistent with a spectrum of defects with roughly the same concentration (Fig. 1). At room temperature, the activation energies for this spectrum of defects range from 0.35 to 0.55 eV, but the atomic nature of the defect relaxation processes is not understood. In order to study a broader range of activation energies and gain insight on defect relaxation mechanisms, we performed temperature-dependent measurements on out-of-plane cantilevers having different resonant frequencies over the temperature range from 30ºC to 500ºC. From Fig 2, it can be seen that at approximately 0.8 eV the relative concentration of defects increases. These energies are approaching the activation energies for diffusional defect relaxation processes in crystalline diamond films, such as self-interstitial diffusion (1.3 eV) and vacancy self-diffusion (2.3 eV). Understanding the temperature dependence of the internal dissipation in this material is important to ensure functionality of ta-C resonators at elevated temperatures when used in filter or sensor applications.

Sandia is a multiprogram laboratory operated by Sandia Corporation, a Lockheed Martin Company, for the United States Department of Energy's National Nuclear Security Administration under contract DE-AC04-94AL85000.

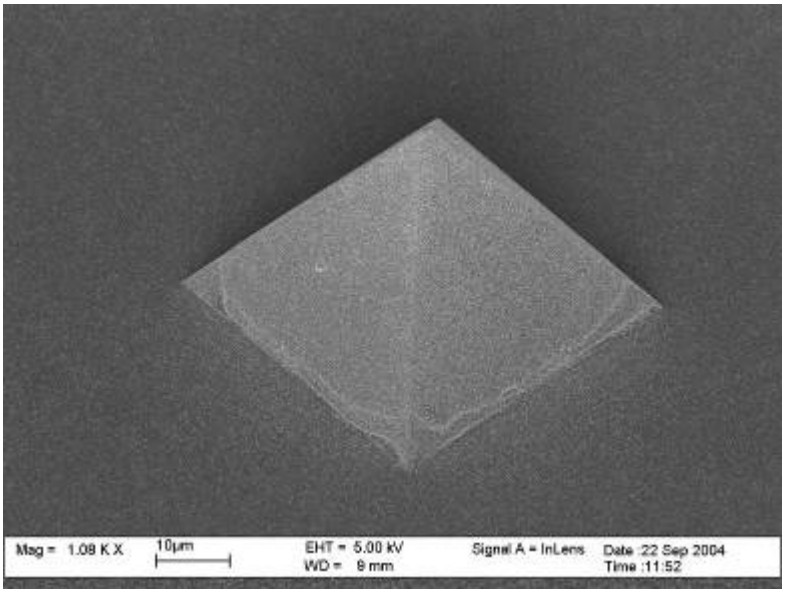

Figure2. SEM image of the UNCD tip fabricated using Si mold technique

CARBON NANOTUBE ELECTRO-MECHANICAL OSCILLATOR

Youngsik Song and Jaewu Choi

5050 Anthony Wayne Dr. #3100

Electrical and Computer Engineering

Wayne State University

Detroit, MI 48202

Keywords: Carbon Nanotube, Direct lateral growth, Electromechanicl oscillator,

Abstract

Carbon nanotube is one of the best candidates for an essential component in nanoscale electromechanical systems. Tunable nanoscale resistors, capacitors, inductors, and mechanical resonators can be implemented with carbon nanotubes. It is originated from the excellent properties of carbon nanotube such as structure dependent metallic properties, pseudo-one-dimensional transport characteristics and electronic structure, hollow structure, extremely high mechanical strength with high aspect ratio, good thermal conductivity, chemical inertness, etc. In this study, we studied carbon nanotubes as an electromechanical oscillator from suspended carbon nanotube arrays. The suspended carbon nanotube arrays are fabricated by direct lateral growth of carbon nanotubes on the multilayer electrode arrays with a field effect transistor structure by thermal chemical vapor deposition method using C_2H_2 and Ar. The characteristics of carbon nanotube electromechanical oscillator are studied using an impedance analyzer as a function of frequency and gate voltage modulation.

HIGH-FREQUENCY SURFACE ACOUSTIC WAVE DEVICE FABRICATED BY USING AlN-UNCD THIN FILMS

Cheng-Hsien Chou, Yen-Chih Lee, Jin-Hua Huang, Su-Jien Lin

Department of Material Science and Engineering, National Tsing-Hua University, Hsin-Chu 300, Taiwan, R. O. C.

I-Nan Lin

Department of Physics, Tamkang University, Tamsui 251, Taiwan, R. O. C.

Keywords: SAW, UNCD, AlN

Abstract

Surface acoustic wave (SAW) devices are important in microwave frequency communication applications due to their high degree of frequency selectivity with low insertion loss and compact in size. Operation frequency of a SAW device contain is determines by the wave length of the acoustic wave of the piezoelectric material, which in turn, is determined by the interspacity of the interdigital transducers (IDT) electrodes. Therefore, for the purpose of increasing operating frequency for the SAW devices, substrate materials having large acoustic wave velocities, such as diamond or SiC are required. However, conventional diamond films usually possess facet granular structure with large roughness, which requires large amount of polishing. Such a process is very time consuming. A diamond films, which have smooth surface is urgently needed for the development of high frequency SAW devices. Ultra-nano-crystalline diamond (UNCD) films possessing smooth surface are good candidate for high frequency SAW application. In this study, we demonstrate a SAW device using AlN/UNCD/Si as material system. UNCD films were grown in a 2.45 GHz microwave plasma enhanced chemical vapor deposition (MPECVD) system on Si (100) substrates in methane and argon (CH_4/Ar) plasma. C-axis oriented Aluminum nitride (AlN) with a thickness of 3 μm were prepared by reactive RF-sputtering technique. AlN with (002) preferred orientation were successfully obtained on UNCD films. A SAW device with good performance will be presented.. Using Network Analyzer (H.P. 8722ES) and GSG probe we can measure the acoustic properties of AlN/UNCD/Si SAW devices.

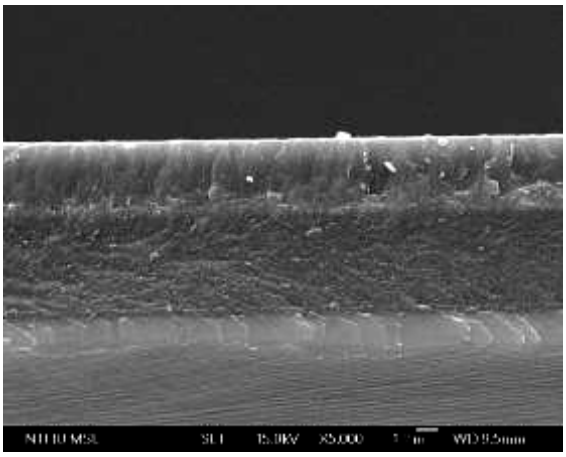

Figure 1. Cross-section SEM surface morphology of AlN/UNCD/Si structure .

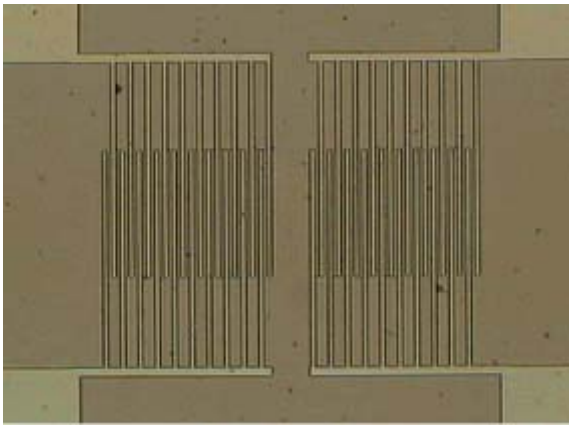

Figure* 2. *Optical Image of AlN/UNCD/Si SAW devices.

REFERENCES

1. C. Campbell, “Surface acoustic wave devices and their signal processing applications”, Academic Press, New York, 1989.
2. D. M. Gruen., A. R. Krauss, and C. D. Zuiker et al., “Characterization of nanocrystalline diamond films by core-level photoabsorption”, ***Appl. Phys. Lett.*** **68 (12)**, 1640 (1996).
3. B. Bi, W. -S. Huang, and J. Asmushen et al., “Surface acoustic waves on nanocrystalline diamond”, ***Diamond Relat. Mater.*** **11**, 677 (2002).

NANOCRYSTALLINE DIAMOND ON $LiNBO_3$ FOR SURFACE ACOUSTIC WAVE APPLICATIONS

K. H. Chen

INSTITUTE OF ATOMIC AND MOLECULAR SCIENCES, ACADEMIA SINICA, TAIPEI, TAIWAN

Y.C. Lin, J. P. Huang, S. T. Lin

Department of Mechanical Engineering, National Taiwan University of Science and Technology, Taipei, Taiwan

L. C. Chen

Center for Condensed Matter Science, National Taiwan University, Taipei, Taiwan

Keywords: NCD, LiNbO3, SAW.

Abstract

The growth of the nanocrystalline diamond (NCD) films on $LiNbO_3$ (LN) substrate using $CH_4/H_2/O_2$ in microwave plasma enhance chemical vapor deposition reactor have been investigated in this study. By varying the temperature, gas composition, and processing pressure during the growth, it is concluded that smooth NCD films on LN substrates can be obtained by MPECVD with an amorphous buffer layer. Furthermore, the nucleation density can be substantially enhanced by applying a bias voltage at the initial stage of the growth. Preliminary measurement of surface acoustic wave (SAW) characteristics on the above mentioned structure concluded that NCD/LN structure is ideal for high electromechanical coupling, which is highly desirable for SAW devices. Further study on various device architectures is proposed in this paper.

INTRODUCTION

NCD deposition using MPECVD has been demonstrated by many laboratories in the past decade. In this report, we demonstrate the growth condition for NCD on LiNbO3 substrate. An attempt to make SAW devices using NCD/LN is also demonstrated.

EXPERIMENT

The substrates were as-received LN wafers. In order to increase nucleation density, the substrates were scratched with 4-nm diamond powders to reduce surface energy and provide nucleation seeds. After that, they were subsequently cleaned ultrasonically in acetone, methanol and D.I. water in sequence and then dipped in a 10% HF aqueous solution, and dried by blowing nitrogen before the deposition. When the chamber vacuum achieves 1×10^{-3} Torr, hydrogen was inducted into the chamber to produce hydrogen plasma at 20 Torr at 1 kW microwave power. Hydrogen plasma etches oxides on substrates surface for pretreatment before deposition. Nanocrystalline diamond films were deposited using micro-wave plasma enhanced chemical vapor deposition (MWPECVD) system made by Astex Company. A schematic diagram of this system is shown in Fig. 1. Microwave generated by the generator was guided through quartz window into the chamber to to produce plasma. The substrate was put on a molybdenum holder, and a boron nitride heater provided independent substrate heating. Thermocouple placed underneath the molybdenum holder was used to monitor the substrate temperature. In order to measure the surface temperature of the substrate, a two-color pyrometer was used.

RESULTS

Fig. 1 shows the SEM image of diamond thin films that grown at 610 ℃ with smooth surface. The diamond growth rate increased with increasing temperature and as shown in Table 1. The grain size of the film grown above 610 ℃ showed no variation with increasing growth temperature. From the SEM cross-section images we can

observe that the diamond grown below 580 ℃ has columnar morphology and the diameter of the columns increase during the growth. The diamonds grown above 610 ℃ are still columnar in nature, however, the diameter of the columns stayed constant during growth. The presumable cause is because higher temperature offered enough energy to facilitate continuous secondary nucleation and restrain the grain growth.

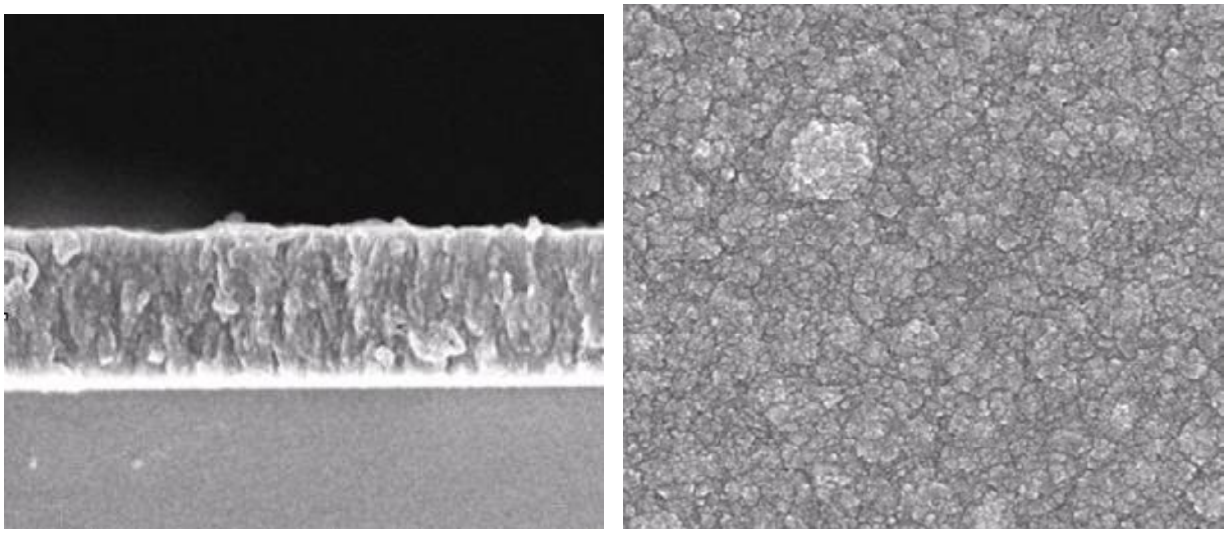

Figure* 1. *The SEM images (a) cross-section view and (b) top view images of diamond films grown at 610 ℃.

Fig. 2 shows the hardness and elastic modulus of the diamond thin films at various growth temperatures measure by nanoindentation system. Hardness and elastic modulus increased with temperature. The film grown at 750 ℃ showed the highest hardness (~49GPa) and elastic modulus (~482GPa). The hardness of nanocrystalline diamond films measured by nanoindentation was lower than the hardness of natural diamond (100GPa) [5]. The presumable cause is high proportion of non-diamond phase that exist in grain boundary surrounding the nanocrystalline diamond. Surface acoustic wave technique was also employed by Professor Peter Hess's group at Heidelberg Univresity, Germany, to measure the Young's modulus of the films. A Young's modulus and density of 746 GPa and 3.45 g/cm^3, respectively, were measured for the film grown at 610 ℃.

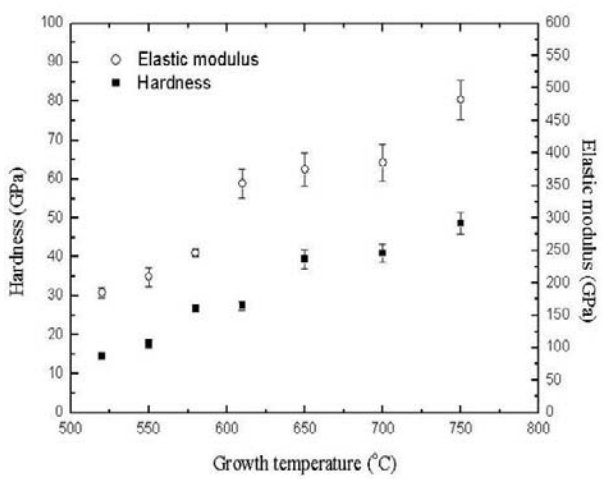

Figure* 2. *Hardness and elastic modulus of diamond thin films grown at various temperatures.

MECHANICAL PROPERTIES OF ULTRANANOCRYSTALLINE DIAMOND (UNCD) THIN FILMS RELEVANT TO UNCD-MEMS

H. D. Espinosa,[1] George Schatz[2], B. Peng,[1] N. Moldovan,[1]
Orlando Auciello[3] and J. A. Carlisle[3]
[1]Department of Mechanical Engineering, Northwestern University, Evanston, IL
[2]Department of Chemistry, Northwestern University, Evanston, IL
[3]Argonne National Laboratory, Argonne, IL

ABSTRACT

Many Si-based MEMS devices exhibit performance limitations due to the relatively poor physical, mechanical, chemical and tribological properties of Si. Diamond and diamond-like carbon offer several advantages over conventional Si and even SiC as alternate MEMS materials. However, the fabrication of diamond-MEMS components requires a synthesis method capable of producing diamond films with very smooth surface topography, high hardness and fracture strength, low coefficient of friction, and high electrical conductivity, the latter for specific MEMS devices requiring electrostatic actuation. In addition, it is desirable to use microfabrication methods from the Si-MEMS technology. A new diamond film technology developed at Argonne National Laboratory yields phase-pure, low stress ultrananocrystalline diamond (UNCD) layers with 2-5 nm grains and smooth surfaces (20-40 nm rms) that are suitable for fabrication of high-performance MEMS devices. The UNCD films are grown using an Ar-rich CH4 /Ar plasma chemistry that yields high nucleation rate for nanocrystalline diamond growth.

In this presentation, we will review work done to characterize the mechanical properties of UNCD at the MEMS scale. We will discuss studies of the mechanical properties of UNCD film-based MEMS structures fabricated with plain undoped UNCD and nitrogen-doped UNCD. Undoped UNCD films exhibit hardness and Young's modulus similar to single crystal diamond (i.e., 90 GPa and 980 Gpa, respectively), and very low friction coefficient (~ 0.02). Nitrogen-doped films that result in n-type high conductivity UNCD layers exhibit lower hardness than undoped films (reduced to ~80 GPa), but are still suitable for MEMS requiring high conductivity and mechanical strength. The mechanical and electrical properties of UNCD films with and without nitrogen incorporation will be discussed in terms of bulk defects and/or changes in grain and grain boundary structure and size induced by nitrogen incorporation. For example we have determined that the fracture strength of undoped UNCD as yielded from measurements using a membrane deflection method is about 5 GPa, which is lower than the expected intrinsic value for UNCD. Cross-section SEM studies revealed that bulk defects might be responsible for the observed relatively low value of UNCD fracture strength. In addition, nitrogen incorporation to increase UNCD electrical conductivity results in a reduction of fracture strength to about 3 GPa, which might be due to microstructural, dimensional and/or atom bond changes in grain and grain boundaries. The experimental studies will be discussed with respect to computer simulations performed by other members of the NSF NIRT program under which the work described here is being performed. Prospects for a new UNCD MEMS technology will be discussed as well.

FABRICATION OF ULTRANANOCRYSTALLINE DIAMOND ATOMIC FORCE MICROSCOPE PROBES

Guoqing Ning, A.V. Sumant, D. S. Grierson, and R. W. Carpick

Department of Engineering Physics, University of Wisconsin-Madison, Madison, WI53706

J.E.Gerbi, J. Birrell, X. Xiao, Orlando Auciello, John A. Carlisle

Materials Science Division, Argonne National Laboratory, Argonne, IL

Keywords: Atomic force microscope; Ultranonocrystalline diamond; AFM probes

Abstract

Minimizing wear on tips used in the atomic force microscope is a critical problem in scanning probe microscopy. Diamond is an ideal candidate material for such tips because of its outstanding mechanical, chemical and tribological properties. However, it is very difficult to fabricate atomically sharp diamond tips with the conventional chemical vapor deposition (CVD)-diamond technology because of the intrinsically large grain size (micrometers). Ultrananocrystalline diamond (UNCD) is an ideal candidate material for such application because of the small grain size (3-5 nm) with extremely low surface roughness (~11 nm) and the ability to form conformal ultra-thin coatings (less than 100 nm thick). Here we describe a fabrication process to batch-fabricate monolithic ultranonocrystalline diamond (UNCD) AFM probes. Detailed steps include fabricating pyramidal etch pits on the silicon wafer by anisotropic etching of Si in KOH followed by UNCD deposition (~1µm). The UNCD-coated wafer is then subjected to a series of fabrication steps including metallization, photolithography, and RIE to from monolithic UNCD cantilevers with integrated pyramidal tips. These cantilevers are finally released from the backside and then physically bonded to the holding substrate and then sawed with dicing saw to take out individually for testing. Here we present the fabrication part to demonstrate that monolithic UNCD cantilevers can be fabricated using fabrication approach we have developed in our laboratory.

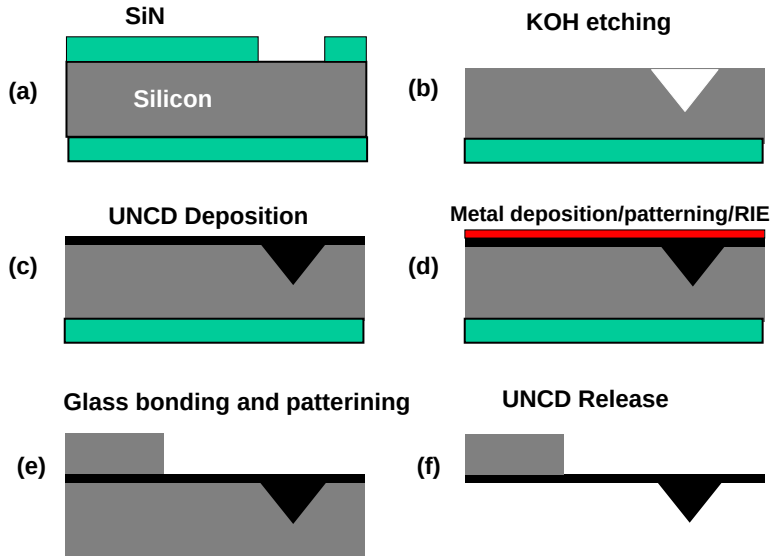

Figure1. Fabrication process flow for the UNCD probe

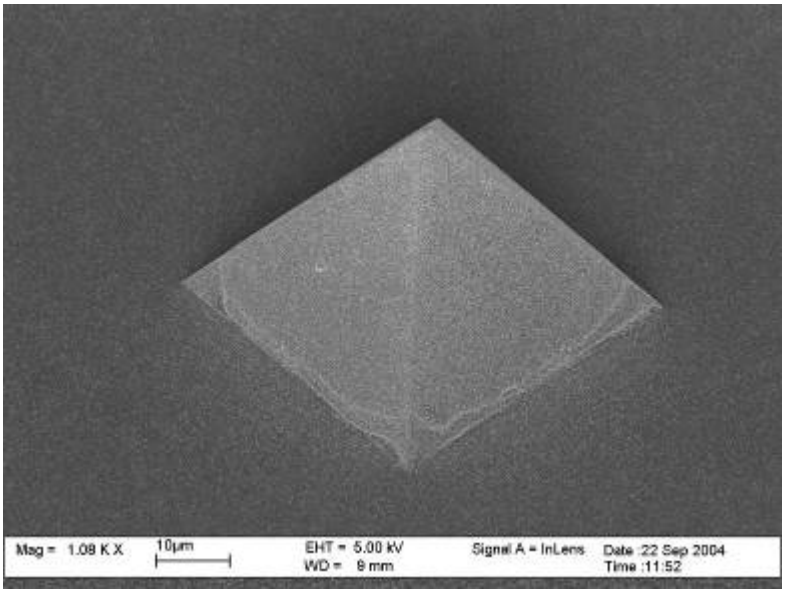

Figure2. SEM image of the UNCD tip fabricated using Si mold technique

X-RAYS DIFRACTION ANALYSES OF THE CVD DIAMOND FILM DEPOSITED ON THE TI6AL4V ALLOY WITH THE ADDITION OF CF_4 IN METHANE-HYDROGEN MIXTURE

Teófilo M. de Souza[a], Joanisa Possato[a], Joelma de Oliveira[a,b], Jomar E. Bueno[a]

a) Laboratório de Pesquisa e Desenvolvimento de Dispositivos com Diamante CVD e Novos Materiais – Unesp - Campus Guaratinguetá (teofilo@feg.unesp.br)

b) FAMINAS- Bairro Universitário-Muriaé-MG(joelmaoliveira@imicro.com.br)

Keywords: X-Rays Difraction, CF_4, Ti6Al4V

Abstract

The analyses by X-Rays difraction for the bulks with the CVD diamond film had the purpose of verify some alterations in the concentrations of carbides and of the elements Ti, Al and V, seen that the action of the fluorine in general alters the chemical composition and physics of the surface of the substrate. The difratogram with the main peaks of the titanium and of the aluminum for the diamond film deposited under the temperature of 600°C, with the time of 2 hours showed that remains a titanium peak in $2\theta = 35{,}2^o$. Also, the titanium carbide, TiC, is present in the peaks located in $2\theta = 35{,}9^o$ and 41,6º. The diamond peak also is present in 44º. The difratogram with the main peaks of the titanium and of the aluminum for the diamond film deposited under the temperature of 600 ^{o}C, with the time of 5 hours presented the titanium peak, TiC peak, and still of the a lot diamond presenting resemblance with the previous results. The difratogram with the main peaks of the titanium and of the aluminum for the diamond film deposited under the temperature of 600 ^{o}C, with the time of 7 hours presents a titanium peak in 2θ with value of $35{,}2^o$. The titanium carbide, TiC, is present in 2θ located to $35{,}9^o$ and $41{,}6^o$, where the intensity of the first peak has a value like the main one. The peak of the diamond appears in $44{,}83^o$ and $76{,}19^o$. The main peak of the diamond is bigger compared with the of orientation (220). The diamond is purer than him deposited with the mixture of methane and hidrogênio without utilization of the CF_4.

Financial support: FAPESP, FUNDUNESP, PROPP-UNESP, CNPQ.

SCANNING ELECTRONIC MICROSCOPE ANALYSES AND X-RAYS DIFRACTION OF THE CVD DIAMOND FILM DEPOSITED ON TI6Al4V ALLOY UTILIZING MICROWAVE PLASMA REACTOR

Teófilo M. de Souza[a], Joanisa Possato[a], Joelma de Oliveira[a,b], J.E.Bueno[a]

a) Laboratório de Pesquisa e Desenvolvimento de Dispositivos com Diamante CVD e Novos Materiais – Unesp - Campus Guaratinguetá (teofilo@feg.unesp.br)
b) FAMINAS- Bairro Universitário-Muriaé-MG(joelmaoliveira@imicro.com.br)

Alix Gicquel

Université Paris 13 - Paris - France.

Keywords: Microwave Plasma Reactor, X-Rays Difraction, CVD, Ti6Al4V

Abstract

The analyses by scanning electronic microscope (SEM) permitted to present to film morphology and verify itself there is some pull of the film regarding the substrate (qualitative adhesion). Through of the SEM observed himself that to film obtained presents good homogeneity, with medium size of the grains of diamond more less than 1µm in all of the cases. The handling with ultra-sound on the Ti6Al4V alloy, permitted the obtaining of a continuous film after 40 minutes of deposition, with 4% of methane in volume in the mixture hydrogen-methane, with size of grains. By X-Rays difraction[1] was possible verify the elements and composed present chemists in the sample before and after the deposition and, when possible, the crystalline orientation of the film. There is the difratogram for the Ti6Al4V alloy before of the deposition. The peak centered in the angle to the around of θ=19° corresponds to the Al. There is not presence of the V, therefore its concentration is more less than 5%. The too peaks refer to the Ti. The main peak of the is around θ=20°. The main diamond peak is around θ=22°. In the bulk surface, where the film completely, was verified the predominance of the TiC in the difratogram. Also established himself the presence of the TiC in the diverse samples analyzed after the growth of the film. The TiC forms himself, before of the deposition of the film of diamond, altering the composition of the surface.

Financial support: FAPESP, FUNDUNESP, PROPP-UNESP, CNPQ.

REFERENCES

1. Ohring, M. The Materials Science of Thin Films. Academic Press. NY, USA 1995.

ULTRANANOCRYSTALLINE DIAMOND AS HERMETIC AND BIOINTERT COATING FOR IMPLANTABLE BIOMECDICAL DEVICES

Xingcheng Xiao, Jian Wang, John A. Carlisle, Orlando Auciello

Materials Science Division, Argnonne National Laboratory, 9700 S. Cass Ave. IL 60439 USA

D. Guven, R. Freda, James Weiland and Mike Humayun

University of Southern California, Doheny Eye Institute, Los Angeles, CA 90033 USA

Keywords: Ultrananocrystalline diamond, hermetic coatings, biointerness, electrochemistry, artificial retina

Abstract

Diamond is considered as an excellent bio-inert/biocompatible material that can be used for the fabrication of implantable biomedical devices. The main form in which diamond can be applied to the fabrication of implantable biodevices is as thin films. However, the high growth temperature for conventional CVD process used for the synthesis of diamond films has limited its application as a hermetic coating for encapsulation of active implantable microchips for example, to make the Si-based CMOS device bioinert and biocompatible. We demonstrate in this presentation the application of ultrananocrystalline diamond (UNCD) as hermetic coating for encapsulation of implantable biomedical devices such as artificial retina microchips. UNCD coatings are grown in a microwave plasma enhanced chemical vapor deposition (MPECVD) system using a novel Ar-rich/CH_4 plasma chemistry, resulting in films with 3-5 nm grain size and atomically abrupt grain boundaries. The UNCD coatings discussed in this presentation were deposited at substrate temperatures in the 400 - 800 ^{o}C range and exhibited a dense and continuous texture demonstrated by cross-section SEM. The electrochemical test in 5% HF proved that these UNCD coatings possess excellent hermeticity although they exhibit a relatively high leakage current in electrochemical tests, due to the relatively high conductivity of plain UNCD films. In order to decrease the leakage current, a series of UNCD coatings were prepared with the addition of different hydrogen content in the plasma (from 1 to 20 %) and at different substrate temperatures. The electrochemical tests were carried out at wide potential range (+5/–5 V) in PBS (phosphate buffered solution). The data revealed that UNCD coatings grown with 1% hydrogen and ~ 400 ˚C substrate temperature exhibits the lowest leakage current (~ 4 x 10^{-7} A/cm^2 at the potential of +5/–5 V), which satisfies the basic requirements of the encapsulation layer for artificial retina microchips. The mechanisms responsible for increasing the electrochemical inertness of UNCD coatings will be discussed. In this respect, the data suggests that hydrogen incorporation into the grain boundaries saturates dangling bonds making the UNCD coating more insulating and resulting in lower leakage. In addition, *in vivo* tests of bioinertness of UNCD coatings were conducted via implantation of UNCD-coated Si samples into rabbit eyes. All *in vivo* and *in vitro* test results showed that UNCD coatings possess excellent biocompatibility and biostability within the physiological environment. These studies demonstrate that UNCD is a promising candidate as hermetic and bioinert coating for protection of implantable medical devices in biomedical environments .

CONTROLLING THE NANOTRIBOLOGY OF NANOSTRUCTURED DIAMOND FILMS

Robert W. Carpick, D. S. Grierson, A.V. Sumant, E.E. Flater, G. Ning, K. Sridharan

University of Wisconsin-Madison, Madison, WI.

T.A. Friedmann, J.P. Sullivan

Sandia National Laboratories, Albuquerque, NM.

J.E. Gerbi, J. Birrell, X. Xiao, O. Auciello, J.A. Carlisle

Materials Science Division, Argonne National Laboratory, Argonne, IL.

Keywords: Nanotribology, AFM, diamondlike carbon, ultrananocrystalline diamond, tetrahedral amorphous carbon.

Abstract

We will discuss recent studies of the nanotribological properties of carbon-based thin films, particularly nanocrystalline diamond, tetrahedral amorphous carbon, and diamond-like carbon. By using atomic force microscopy for nano-scale friction measurements and surface spectrosopy techniques for detailed chemical and structural studies, we are able to demonstrate that the carbon bonding configuration (sp2 vs sp3 hybridization) and chemical termination of the surfaces has a strong effect on nanoscale friction and adhesion. We will present these results and discuss their potential impact for nano-, micro-, and macro-scale applications.

REFERENCES

1. A.V. Sumant, D.S. Grierson, J.E. Gerbi, J. Birrell, U.D. Lanke, O. Auciello, J.A. Carlisle, and R.W. Carpick, "Toward the Ultimate Tribological Interface: Surface Chemistry and Nanotribology of Ultrananocrystalline Diamond", *Adv. Mat.*, in press (2004).

LOW-TEMPERATURE CATALYTIC SYNTHESIS OF CARBON ONIONS AND EVALUATION OF ITS SOLID LUBRICANT PROPERTY

Atsushi HIRATA and Shoji NAMIKI

Department of Mechanical Sciences and Engineering, Tokyo Institute of Technology

O-okayama, Meguro-ku, Tokyo 152-8550, Japan

Keywords: Carbon onion, catalysis, solid lubrication, heat treatment, diamond cluster

Abstract

Carbon onions were synthesized by heat treatment of diamond clusters at low temperatures of 800-1400°C in the presence of iron catalyst. Transmission electron microscope observations of diamond clusters before and after heating were performed. It was shown that diamond clusters have transformed their diamond structure into graphite structure after heating above 800°C. Solid lubricant properties of the carbon onions were measured by ball-on-disk type friction test using silicon wafers and stainless steel balls in air and vacuum. The carbon onions prepared at 1200°C have shown low-friction coefficients both in air and vacuum.

INTRODUCTION

Carbon onion [1] is a fullerene related carbon material having concentric graphitic shells and is expected to be an excellent solid lubricant [2] because of low interaction of carbon onions with other substances, which would be caused by dangling bond-less structure of the outermost layer of carbon onions unless defects are contained. One of the preparation processes of carbon onions is heat treatment of diamond clusters. Although this process enables us to produce milligrams order of carbon onions, higher temperature than at least 1700°C is required [3], which is usually a severe condition for building up a set-up for preparation. In order to reduce the temperature, we have experimentally investigated the employment of ferrous catalyst to the heating process.

EXPERIMENTAL

Diamond clusters produced by detonation method, of which average diameter is 5 nm, was used as a source material. For catalyst, iron was employed on the basis of its diffusion property of carbon. Diamond clusters were ultrasonically mixed in aqueous solution of $Fe(NO_3)_3 \cdot 9H_2O$ and dried in hot air. The atomic ratio of Fe/C was controlled at 1/1000. The diamond clusters containing iron catalyst was heated in argon ambience at 1.5×10^5 Pa using an infrared furnace. The heating temperature was varied 800-1400°C and kept for one minute. After heat treatment, the catalyst of iron was removed using hydrochloric acid.

The microstructure of diamond clusters before and after heat treatment was characterized by high-resolution transmission electron microscopy (HRTEM) and Raman spectroscopy. Moreover, the tribological properties of the heated sample were determined by ball-on-disk testing using SUS440C balls of 4.8 mm in diameter, (100) silicon wafers of n-type under normal applied load of 0.95 N and sliding velocity of 9.4 mm/s. Sliding testing was carried out in air at relative humidity of 35% and in vacuum at 5×10^{-3} Pa.

RESULTS AND DISCUSSIONS

The image of diamond clusters heated at 800°C taken by HRTEM is shown in Fig. 1 along with that of raw material. It is found that diamond structure of the diamond cluster disappears after heat treatment and varies to multi-layered concentric spherical structure, so that iron catalyst results in the preparation of carbon onions from diamond clusters at low heating temperature of 800°C. The variation of diamond structure to graphitic structure was also confirmed by Raman spectroscopy.

The friction property of carbon onions prepared at low heating temperature of 1200°C was determined in air and vacuum and the results are shown in Fig.2. Friction coefficients for a lubricated silicon substrate, graphite powder, diamond clusters and carbon onions prepared at 1730°C without catalyst are displayed as references. In both air and vacuum, the carbon onions prepared at 1200°C exhibits lower friction coefficients than that of graphite. The tendency to increase friction coefficients in vacuum, which is typical for graphite, is not observed for the carbon

onions in spite of the graphitic structure. This different behavior of carbon onions from graphite would be caused by their spherical closed structure of graphene sheets. However, the friction coefficients for the carbon onions prepared at 1200°C is slightly higher than that for the carbon onion prepared without catalyst at 1730°C, especially in vacuum. One of the factors to cause higher friction is the presence of defects in the outermost layer of carbon onions, and it can be considered that the carbon onions prepared at 1200°C is more defective.

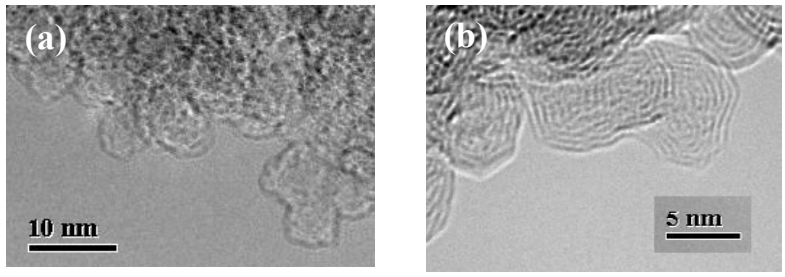

Figure 1. HRTEM observations of diamond clusters (a) before and (b) after heat treatment at 800℃

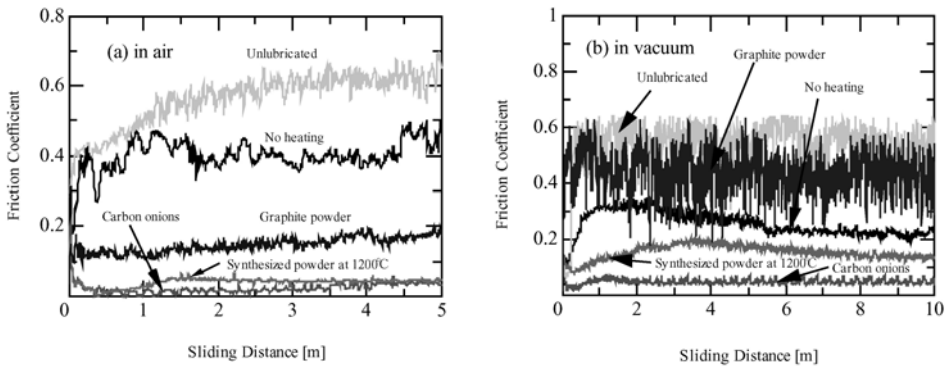

Figure 2. Variations of friction coefficients of carbon onions with other reference materials in (a) air and (b) vacuum

SUMMARY

Carbon onions have been prepared from diamond clusters by heat treatment at lower temperature using ferrous catalyst and their tribological property has been investigated. As a result of heating at 800°C, HRTEM and Raman spectroscopy have confirmed the transformation of diamond clusters to graphitic particles having concentric multilayer that is intrinsic structure for carbon onions. The carbon onions prepared at 1200°C showed low friction coefficients regardless of the ambient of air and vacuum. However, the carbon onions prepared at low temperature with the help of ferrous catalyst would be relatively defective than carbon onions prepared without catalyst so as to exhibit higher friction coefficients.

REFERENCES

1. Ugarte, D., "Curling and Closure of Graphitic Networks under Electron-beam Irradiation," *Nature*, Vol. 359, 707-709 (1992).
2. Hirata, A., Igarashi, M. and Kaito, T., "Study on Solid Lubricant Properties of Carbon Onions Produced by Heat Treatment of Diamond Clusters or Particles," *Tribology Int.*, Vol. 37, No. 11-12, 899-905 (2004).
3. Kuznetsov, V.L., et al., "Electrical Resistivity of Graphitized Ultra-disperse diamond and onion-like carbon," *Chem. Phys. Lett.*, Vol.336, pp.397-404.

TRIBOLOGICAL STUDIES ON ULTRA-FINE DIAMOND COMPOSITE COATINGS DEPOSITED ON TUNGSTEN CARBIDE

Jian X.G. [1], Chen M. [2], Sun F.H. [2], Shi L.D. [1]

1. School of Mechanical Engineering, Tong Ji University, 1239 Shi Ping Road, 200092 Shanghai, China

2. School of Mechanical Engineering, Shanghai Jiao Tong University, 1954 Hua Shan Road, 200030 Shanghai, China

Keywords: Diamond Coated Tools, Tungsten Carbide Substrates, Ultra-fine Diamond Composite Coatings, Tribological performance.

Abstract

Ultra-fine diamond composite coatings were deposited onto the Co-cemented tungsten carbide (94wt.%WC-6wt.% Co) substrates via electron aided hot filament chemical vapor deposition (EAHFCVD). These diamond coatings have been tested in dry sliding against SiC particles reinforced aluminum-matrix composites materials (15% SiC PRAMC), metal copper wire core material (Cu-1) and metal aluminum wire core material (Al-0) by tribological pin-on-disc tests under a range of test conditions to evaluate the tribological performances of these ultra-fine diamond composite coatings. It was found that the friction coefficient of ultra-fine diamond composite coatings was remarkably decreased in comparison with that of uncoated carbides and normal diamond coatings after the initial period of rising rapidly. Furthermore, the friction coefficients between ultra-fine diamond composite coatings and SiC PRAMC, Cu-1, and Al-0 were measured as 0.122, 0.143, and 0.165 respectively during the steady-state period of friction. Thus, the friction coefficients of ultra-fine diamond composite coatings under the actual cutting environment of diamond-coated tools against above three materials were measured, and these data were analyzed based on physical and chemical theory. This fundamental work will be useful to the optimization of diamond CVD process and engineering applications of diamond coated tools in machining field.

INTRODUCTION

The adhesion of diamond thin film to the tungsten carbide substrate and the surface roughness of diamond thin film are the two key factors for diamond coated tools, which are becoming the main problems to be solved in process of cutting and drawing. Therefore, it is very important to obtain high quality diamond films with high adhesive strength and low surface roughness for the diamond coated tools. However, it is very difficult to obtain such high quality diamond films by conventional CVD methods. In the previous investigation [1-3], we have solved the problem of high surface roughness of polycrystalline diamond coatings by the deposition of ultra-fine diamond composite coatings. The tribological behaviour of ultra-fine diamond composite coatings plays an important role in determining the machining quality and work-life of tools, and which were investigated in this paper, and these data were analyzed based on physical and chemical theory.

EXPERIMENTAL DETAILS

Test Materials

Tungsten carbide (K10) was used as substrates. Tungsten carbide (K10) and Ultra-fine diamond composite coatings were used as discs, and15% SiC PRAMC, Cu-1 and Al-0 were used as pins respectively.

EAHFCVD Methods and Parameters

Before the deposition process, a new surface pretreatments for the WC-Co substrates were used step by step. The deposition experiments were carried out in the EAHFCVD reactor. Ultra-fine diamond thin films were continually fabricated by adjusting CVD process parameters to enhance the secondary nucleation greatly.

Tribological Testing Procedure

The tribological tests, conducted on a classical pin-on-disc tribometer under an ambient atmospheric and non-lubricated conditions, was used to evaluate the tribological behaviour of the ultra-fine diamond composite coatings, normal diamond coatings and uncoated tungsten carbides.

RESULTS AND DISCUSSION

The surface morphology and quality of diamond coatings were characterized by SEM and Raman spectroscopy. In comparison with normal diamond coatings, diamond crystal of ultra-fine diamond composite coatings is fine and close in texture, and a layer of amorphous carbon similar to graphite was deposited on the surface of diamond crystal, which will conduce to reduce frictional coefficients of coatings against other materials. The presence of non-diamond component such as amorphous or graphitic carbon was investigated by Raman spectroscopy. The Raman shift of ultra-fine diamond composite coatings decreases in comparison with that of normal diamond coatings. Furthermore, the broad peak of sp^2-bonded carbon, which was attributed to graphite at approximately 1580 cm^{-1}, was also observed in ultra-fine diamond composite coatings. Due to the lubricating effect of graphitic debris, which can be easily sheared owing to its layered structure, and the graphitization occurs during sliding that has a lubricating effect, diamond coatings would obtain very low friction coefficients. Furthermore, the effect of the environment may be avoided by adopting the same experimental conditions including to the temperature and the relative humidity in order to investigate the friction coefficient of ultra-fine diamond composite coatings against 15 % SiC PRAMC, Cu-1 and Al-0 by tribological pin-on-disc tests. The frictional coefficients measured in tribological pin-on-disc tests for above three samples against bare WC, normal diamond coatings and Ultra-fine diamond composite coatings are shown in Fig.1. It indicates that frictional coefficients tended to be high and erratic during the initial rubbing period, and they settled down to a low and steady value afterwards. When above three samples were used to rub ultra-fine diamond composite coatings, all frictional coefficients reduced obviously due to the lubricating effect of graphitic debris of ultra-fine diamond composite coatings, which indicated ultra-fine diamond composite coatings are the more desirable tool coated materials than normal diamond coatings.

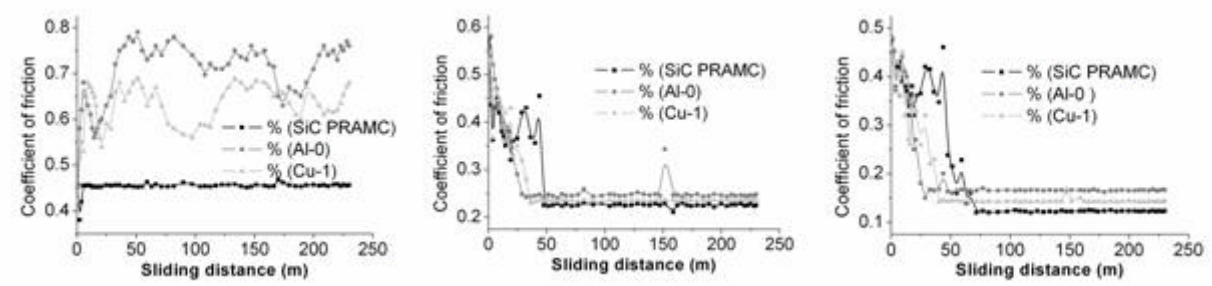

(a) (b) (c)

Fig.1 Frictional coefficients of the three samples rubbing against: (a) bare WC; (b) normal; (c) Ultra-fine;

CONCLUSIONS

Ultra-fine diamond composite coatings can drastically reduce the surface frictional coefficient during steady-state of rubbing in comparison with normal diamond coatings and bare tungsten carbides due to its especial physical and chemical performance such as the lubricating effect of graphitic debris in the machining process of 15% SiC PRAMC, Cu-1 and Al-0, as a result, which make ultra-fine diamond composite coatings become the most desirable tool coated material widely applied to the high speed machining non-ferrous difficult-to-cut materials in the field of automobiles industry, aeronautics and astronautics industry and effectively machining metal wire core material in the field of drawbench dies.

REFERENCES

1. Jian X.G., Chen M., Sun F.H., et al., "Study on the effects of substrate grain size on diamond thin film deposited on tungsten carbide substrates," *Key Engineering Materials*, Vol. 263, No.1137-1142 (2004).
2. Chen M., Jian X.G., Sun F.H., et al., " Development of diamond-coated drills and their cutting performance," *Journal of Materials Processing Technology*, Vol. 129, No.81-85 (2002).
3. Sun F.H., Zhang Z.M., Chen M, Shen H.S., et al., "Improvement of adhesive strength and surface roughness of diamond films on Co-cemented tungsten carbide tools," *Diamond And Related Materials*, Vol. 12, No.711-718 (2003).

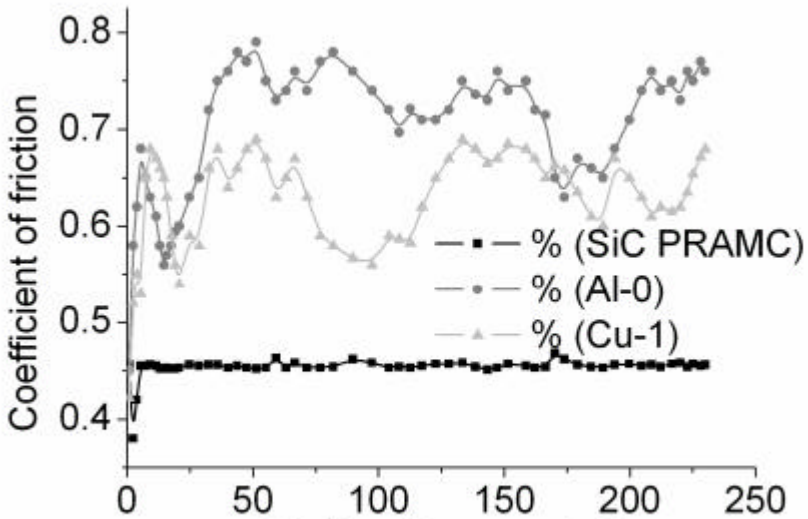

(a) bare WC;

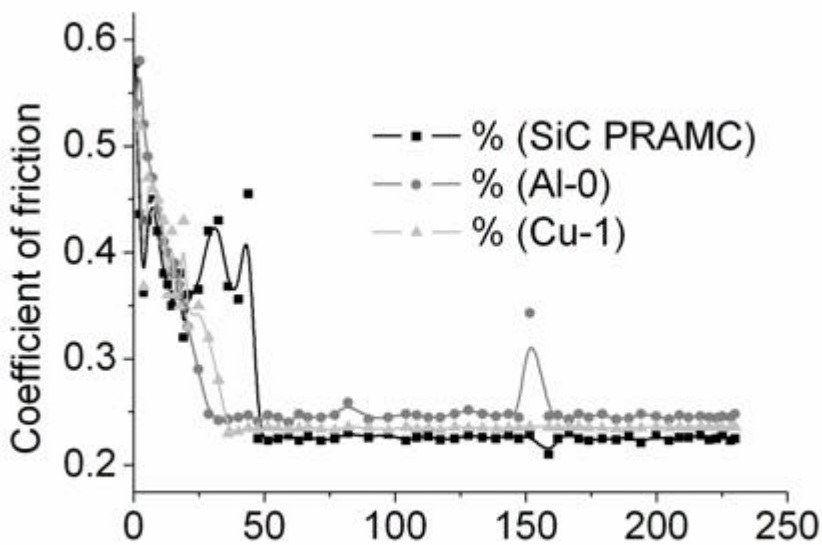

(b) normal;

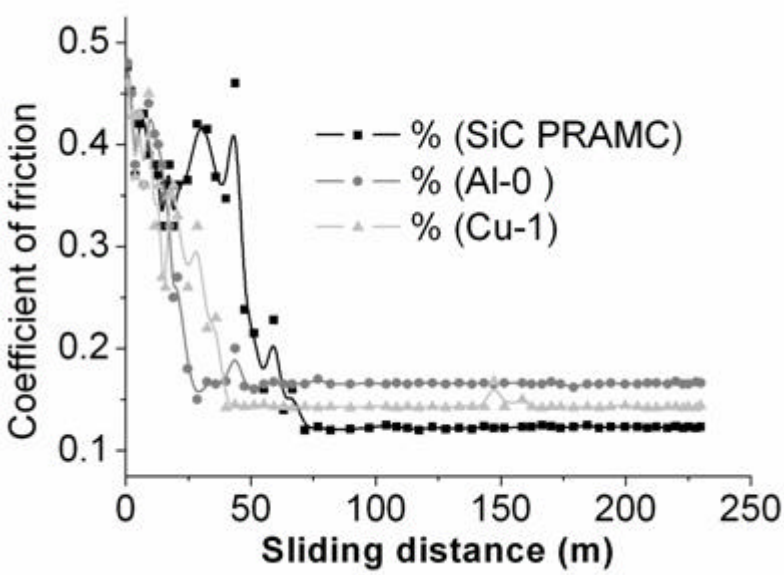

(c) Ultra-fine;

Direct Wafer Polishing with 5 nm Diamond

James C. Sung[*,1,2,3], Ming-Fong Tai[4]

Address: KINIK Company, 64, Chung-San Rd., Ying-Kuo, Taipei Hsien 239, Taiwan, R.O.C.

Tel: 886-2-2677-5490 ext.1150

Fax: 886-2-8677-2171

e-mail: sung@kinik.com.tw

[1] KINIK Company, 64, Chung-San Rd., Ying-Kuo, Taipei Hsien 239, Taiwan, R.O.C.

[2] National Taiwan University, Taipei 106, Taiwan, R.O.C.

[3] National Taipei University of Technology, Taipei 106, Taiwan, R.O.C.

[4] Department of Electronic Engineering, Wufeng Institute of Technology, Chia-yi 621, Taiwan, R.O.C.

Key Words: Nanom Diamond, CMP, ULSI, Wafer Polishing, Moore's Law

Abstract

CMP for making future semiconductor chips with nanom (nano meter) feature sizes can be accomplished by using nanom diamond particles embedded in an organic matrix (e.g. epoxy). Such nanom diamond particles are derived from the detonation of dynamite (e.g. TNR and RDX) in oxygen deficiency atmosphere. The nanom diamond particles are formed instantaneous from the residue carbon during the transient ultrahigh pressure and temperature. These nanom diamond particles are defect ridden and they are coated with a softer carbon coating (e.g. bucky balls and nano tubes). The softer carbon coating can lubricate the cutting edge in-situ during the action of nanom polishing. The nanom diamond has an intrinsic tight size distribution (4-10 nanoms) so the scratch of delicate semiconductor chip (e.g. IC with copper circuitry) is avoided. Moreover, the nanom diamond itself contains built-in defects that will allow nanom chipping so the abrasive can be self-sharpened for continual polishing with high efficiency. In addition, the nano radius of the nanom diamond can polish the wafer in the ductile domain so chipping of the polished surface is avoided. The result would be a clean and smooth surface with minimal mechanical degradation or thermal damage. The resinoid matrix that holds nanom diamond is impregnated with nanom metal particles (e.g. Ni) that can be dissolved by acidic slurry. Alternatively, the epoxy matrix may also incorporate nanom salt particles (e.g. NaCl) that can be dissolved in water. The dissolution of non-carbon nanom additives will expose new nanom diamond particles continually so the efficient polishing can be sustained.

POSTER SESSION 1

ELECTRONIC DEVICES

Modelling of Single Crystal Diamond Schottky Barrier Diodes for High Voltage Applications

S. J. Rashid, M. Brezeanu, T. Butler, N. L. Rupesinghe, F. Udrea, G. A. J. Amaratunga
Department of Engineering, University of Cambridge, Trumpington Street, Cambridge CB2 1PZ, UK
Tel: +44 1223 332766, Fax: +44 1223 332662, Email: sjr64@eng.cam.ac.uk

L. Coulbeck, A. Garraway, P. Taylor
Dynex Semiconductors Ltd., Doddington Road, Lincoln LN6 3LF, UK

D. J. Twitchen, A. Tajani, C. Wort
Element Six Ltd., King's Ride Park, Ascot, Berkshire SL5 8BP, UK

Keywords: **Diamond, Schottky Barrier Diodes, modelling**

Abstract A detailed description of transport physics in ultra high quality synthetic single-crystal (SSC) diamond layers is presented here for the first time. No numerical model detailing carrier transport in diamond devices is available as yet. This model is analysed with respect to a 10μm diamond Schottky barrier diode (SBD) in the 2D MEDICI device simulator where the numerical results obtained were compared to those obtained experimentally.

Device description and models used The diode structure comprises of a 10 μm drift region made of intrinsic *i* diamond, grown on a highly boron doped p-region, with a gold Schottky cathode (workfunction 4.9eV). This layer holds off the reverse voltage in the blocking mode and thus can be made very thin. In addition, diamond has the highest breakdown electric field, thus making it an ideal candidate for power applications, although the ultimate breakdown capability of diamond power devices is limited by their termination structures rather than the *i* layer thickness. This layer has space charge limited-like conduction across it during the on state, thus charge transport across it must be well understood to accurately model the behaviour of power devices. The *i* layer is implemented as a lowly doped N_I layer in the numerical model to aid numerical convergence as this prevents excessively low carrier count during conduction. Boron forms a deep donor in diamond, thus not fully activating all carriers at low concentrations. The model proposed incorporates these observations as well as temperature dependence, and transition to fully activated metallic conduction for concentrations > 10^{17}cm^{-3}. Concentration dependant mobility is invoked by implementing two models based on the 3800cm^2/V-s high intrinsic layer hole mobility in [1,2] and N_I^{-1} trends in [3] as shown in Fig. 1. In addition, the $T^{-1.5}$ and $T^{-3.7}$ temperature dependence of mobility for 300K < T < 380K and 400K < T < 540K respectively [2] is incorporated into the model to take into account the influence of temperature on device performance [4]. Impact ionization coefficients catering to device breakdown have yet to be described for diamond. The model proposed describes these parameters by adjustment of parameters used for SiC on the basis of the 5.45 eV band-gap of diamond [5].

On-state matching Fig. 2 shows the measured on-state characteristics of the oxygen terminated diamond SBD at 30°C. The potential barrier at the cathode was adjusted to that seen by experiment (~ 2V) due to the inability to model accurately the experimental Schottky barrier where interface traps and surface states result due to surface roughness and contaminants, leading to a change in the barrier potential. From the plot, it can be seen that by invoking the Nebel mobility trends [3] and the high hole mobility of 3800cm^2/V-s reported by Isberg [1,2], there is a good fit between the experimental and numerical data, for N_I concentrations between 10^9 and 10^{11}cm^{-3}. From Fig. 2, it can be seen that there is a mere 2% difference (at V_A = 3V) between the numerical and experimental results for the practical forward voltage range (2V + turn-on voltage) over which an SBD would be expected to operate. The experimental *I-V* curve shows more pronounced superlinear behaviour than the simulated curve at higher bias. This is due to the approximation of the intrinsic layer with a lowly doped (10^{11}cm^{-3}) layer in the simulations which cannot account for space charge limited transport. For a first attempt at modelling SSC diamond SBDs, this is a remarkable result as it verifies the 'idealness' of SSC diamond obtained by CVD. It is expected that the match shown here would be similar at higher temperatures once the model describing the mobility dependence of temperature (and doping) has been completely parameterised and optimised [6].

Reverse blocking behaviour The numerical reverse characteristics of the diode show a breakdown voltage of 2.1kV, the point of breakdown being at the quasi-*i*/p$^+$ bulk junction. The plot of electric field through the device indicates a field of 2.2MV/cm being supported by the quasi-*i* layer. The experimental breakdown voltage obtained was larger. This difference is due to the approximation made for the voltage blocking *i* layer in the device model as well as the extrapolation of impact ionization parameters from that of SiC.

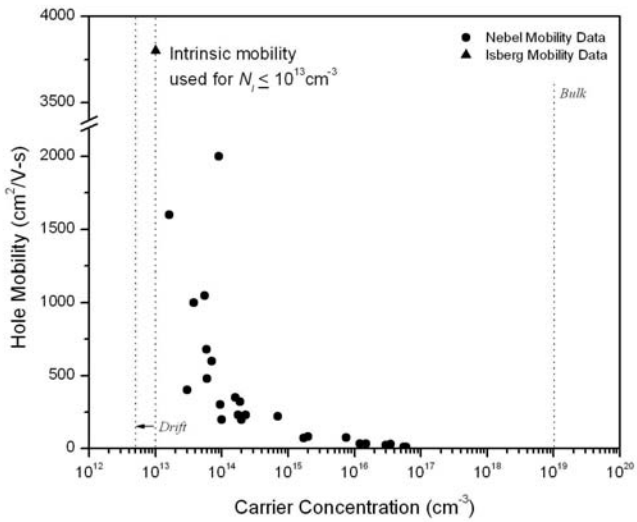

Fig. 1. Carrier concentration dependant hole mobility available in literature [1], [2]. A composite mobility model between the two was also used in the numerical investigation.

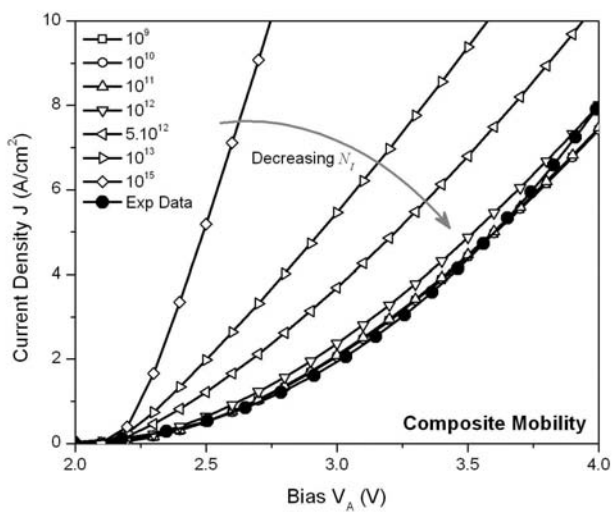

Fig. 2. Numerical and experimental forward characteristics of the i/p^+ diamond SBD. The numerical curves shown here were calculated with various N_I indicating that boron doping between 10^9 – 10^{11}cm^{-3} would be a good approximation to an *i* layer. The fit is close to perfect.

References

[1] J. Isberg, J. Hammersberg, E. Johansson, T. Wilkström, D. J. Twitchen, A. J. Whitehead, S. E. Coe, G. A. Scarsbrook, "High Carrier Mobility in Single-Crystal Plasma-Deposited Diamond", Science, pp. 1670, vol. 297, September 2002.

[2] D. J. Twitchen, A. J. Whitehead, S. E. Coe, J. Isberg, J. Hammersberg, T. Wikström and E. Johansson, "High-Voltage Single-Crystal Diamond Diodes", *IEEE Trans. Elec. Dev.*, vol. 51, no. 5, May 2004.

[3] C. E. Nebel, M. Stutzmann, "Transport properties of diamond: carrier mobility and resistivity", Handbook (Diamond and rel. Mat.), May 2000.

[4] Medici Users manual, 2000, pp. 2.19-2.20.

[5] R. Raghunathan and B. J. Baliga, "Measurement of Electron and Hole Impact Ionization Coefficients for SiC", IEEE Power Semiconductor Research Centre, pp. 173-176, 1997 (ISPSD97).

[6] K. Somogyi, "Classical approximations for ionized impurity scattering applied to diamond monocrystals", Diamond and Related Materials, vol. 11, 2002, pp. 686-691.

ACCEPTOR AND DONOR TRAPPING CENTERS IN BORON-DOPED CVD DIAMOND

V.I. Polyakov, A.I. Rukovishnikov

Institute of Radio Engineering & Electronics, RAS, 11 Mohovaya str., Moscow 103907, Russia

V.P. Varnin

Institute of Physical Chemistry, RAS, 31 Leninsky pr., Moscow 119991, Russia

V.G. Ralchenko

General Physical Institute, RAS, 38 Vavilova str., Moscow 119991, Russia

Keywords: B-doped diamond, acceptor, donor, defects, Q-DLTS.

Although donor and acceptor levels of point defects in a range of materials such as silicon, germanium and A_3B_5 materials have been extensively studied using theoretical and experimental methods, the situation is somewhat different for diamond [1]. The importance of defects as trapping centers for carriers is becoming significant now that synthetic diamond is becoming a viable electronic material. Recently was shown that boron-hydrogen complexes can act as a very shallow donor in B-doped homoepitaxially grown diamond layers [2]. However in a small number of the electrically active defects have been obtained experimentally for polycrystalline B-doped CVD diamond samples.

In the present work, the B-doped diamond films prepared by HFCVD and MPCVD technique and equipped with Ni Schottky contacts were studied by isothermal Charge-based Deep Level Transient Spectroscopy [3]. A Q-DLTS spectra for one of the sample (or functional dependence $\Delta Q(\tau m)$, where $\tau m = (t2 - t1)/\ln(t2/t1)$ is the rate window, and t1, t2 are the times from the beginning of the defect discharge upon applying a charging voltage V to the sample) are shown in Figs. 1,2. It was found, that incorporated boron atoms induce in prepared diamond samples two acceptor (A, B) and one donor (C) levels (trapping centers for holes and electrons) with activation energies of $E_A = 0.33$, $E_B = 0.26$, $E_C = 0.29$ eV, and capture cross-sections $\sigma_A = 2\times10^{-14}$, $\sigma_B = 1.5\times10^{-19}$, $\sigma_C = 2\times10^{-19}$ cm^2, respectively. For the first time the electron (donor) trapping centers in the bulk of B-doped CVD diamond was observed and investigated by Q-DLTS method. The nature of observed defects and differences between trapping centers in HFCVD and MPCVD B-doped diamond films are discussed.

This work was supported by the International Science and Technology Center (Grant ISTC No ***2503***).

Figure 1. Q-DLTS spectra of B-doped CVD diamond film. V – charging voltage. A, B– acceptor and C – donor trapping centers

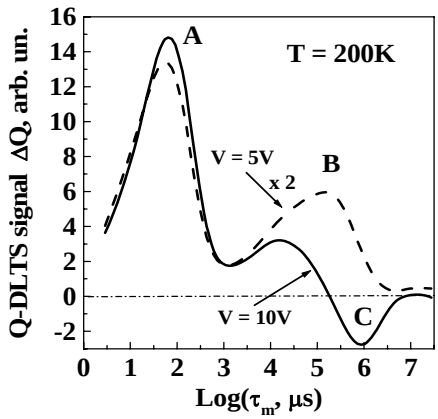

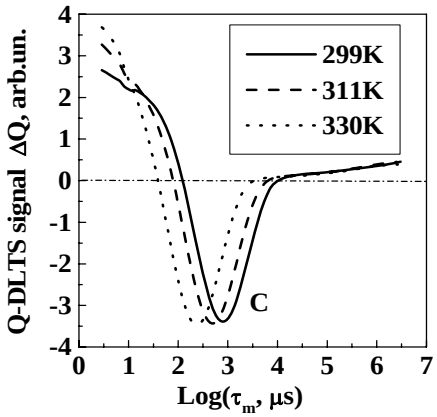

Figure 2. Q-DLTS spectra of B-doped CVD diamond film at the range of donor trapping centers overcharge. V_c = 10 V.

REFERENCES

1. J.P. Goss, P.R. Briddon, R. Jones, et al., “Donor and acceptor states in diamond,” Diamond Relat. Mater., Vol. 13, pp. 684-690, (2004).

2. C.Saguy, R. Kalish, C. Cytermann, et al., “n-type diamond with high room temperature electrical conductivity by deuteration of boron doped diamond layers,” Diamond Relat. Mater., Vol. 13, pp. 700-704, (2004).

3. V.I. Polyakov, A.I. Rukovishnikov, et al.,“Charge-based deep level transient spectroscopy of undoped and N-doped ultrananocrystalline diamond films”, Diamond Relat. Mater, Vol.12, pp. 1776-1782, (2003).

ENHANCEMENT MODE MESFET FROM FREE-STANDING POLYCRYSTALLINE DIAMOND GROWN BY HIGH POWER DC ARC PLASMA JET CVD

Ying Dai*, Run Long, Lin Yu, Zhiwei Zhang, Zhenkui Zhang,Cuixia Yan

School of Physics and Microelectronics, State Key Laboratory of Crystal Materials, Shandong University, Jinan 250100, P. R. China

Keywords: MESFET; Polycrystalline diamond

Abstract

Metal-semiconductor field-effect transistors (MESFETs) have been fabricated using the P-type layer surface conductive of undoped free-standing polycrystalline diamond grown by high power DC arc plasma jet (HPDAPJ) CVD, bring a large area and rapid deposition technique. Raman analysis revealed only the presence of a sharp peak at 1333 cm^{-1}, indicating good quality diamond.

The Au-Au I-V curve exhibits reasonably "Ohmic" characteristics and has been used for the source and drain electrode-contacts. The Al-Al measurements showed little current flow, as is typical for two back-to-back Schottky diodes. The Al-Au curve reveals strong current rectification indicating a Schottky barrier and used for the gate-electrode-contacts.

The MESFETs samples showed I-V characteristics similar to that fabricated using undoped homepitaxial diamond grown by microwave plasma-assisted CVD. A detailed discussion is given in the paper of the measured results, and it is expected that optimized forms of the MESFETs from HPDAPJ CVD diamond would appear to offer a commercially viable route to high-performance diamond-based device development.

* daiy60@sdu.edu.cn

Sustentation fund: NSFC (10374060) and Natural Science Foundation of Shandong Province (Y2003A01)

SEEBECK EFFECT CVD-DIAMOND/PD GAS SENSORS

A. Balducci, M. Marinelli, E. Milani, M.E. Morgada, G. Pucella, G. Rodriguez, A.Tucciarone, G. Verona-Rinati

INFN – Dip. di Ingegneria Meccanica, Università di Roma "Tor Vergata", Via del Politecnico 1, 00133 Roma, Italy

A. D'Amico, C. Di Natale

IMM-Sezione di Roma, CNR, via Fosso del Cavaliere 100, Roma

Dip. di Ingegneria Elettronica, Università di Roma "Tor Vergata", Via del Politecnico 1, 00133 Roma, Italy

Keywords: CVD Diamond, Seebeck Effect, Gas Sensors,

Abstract

The operation of sensors in environments characterized by high temperature, high pressure, chemical activity or nuclear radiation are increasing their relevance in several engineering applications. Thus, the development of sensors based on materials suitable for operation in harsh environment is desirable. The outstanding physical and chemical properties of Chemical Vapor Deposition diamond could then be profitably exploited in the realization of electronic devices that could work when commercial sensor fail. To this purpose, a thermochemical sensor was designed using p-type CVD-diamond films and Palladium. The sensor was tested for different temperature drops, showing values of the thermoelectric power as high as 400 ìV/°C with good stability. The catalytic properties of thin palladium films [1] allow the thermocouple to be used for gas detection. As an example the hydrogen content, within a hydrogen-nitrogen gas mixture, was measured by the changes occurred in the Seebeck output voltage, showed by the thermocouple, at constant values of the temperature drop. The sensor response was measured for hydrogen contents varying between 0.5 % and 2 %.

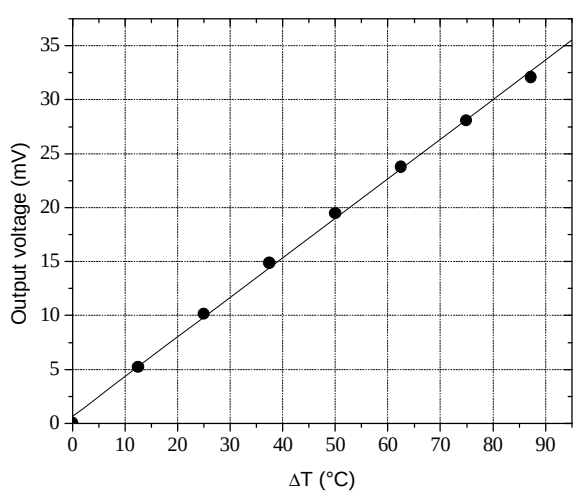

Figure 1 Thermoelectric response of the boron-doped-diamond/Pd thermocouple for a 0 °C reference temperature.

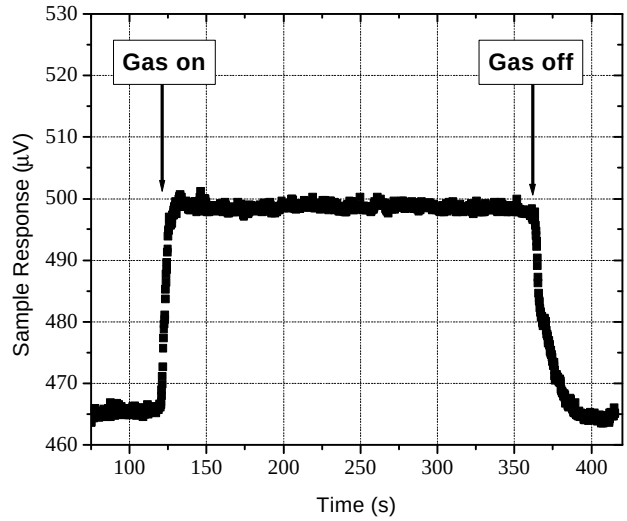

Fiure. 2 Diamond/Pd thermocouple signal when 0.5% H_2 is introduced in the test chamber.

REFERENCES

1. F.C. Thompkins, Academic Press, New York, 1978
2. Van Herwaarden, A.W., Van Duyn, D.C.; Van Oudheusden, B.W.; Sarro, P.M.. Sensors and Actuators A, 22 (1990),621-630
3. A. Bearzotti, M. Gentili, A. Lucchesini, C. Caliendo, E. Verona, A. D'Amico, Sensors and Actuators A, 21-23 (1990), 631-635.

Semiconductor Properties of the DLC Thin Films Doped with Nitrogen

Zh.R. Panosyan*, A.S. Voskanyan*, R.V. Gzraryan*, K.M. Yeghishyan*, J.F. Pern, K.J. Touryan**, V.I. Polyakov*****

***State Engineering University of Armenia, RA**

****NREL, USA**

*****Institute of Radio Engineering & Electronics, RAS. Russia**

Obtained ta–C:H:N films have been produced by the plasma enhanced chemical vapor deposition method from multi-component gas mixture of $Ar:N_2:C_7H_8$ composition. Plasma source parameters have a great impact on the structure of produced films as well as on the electro-physical and optical characteristics of the films. Properties of the obtained films were studied as depended upon the following parameters: acceleration voltage: U_{ac}=(1.5–3) kV; ion current density: J=(0.5–3.5) mA cm^{-2}; ion kinetic energy: E_k=(20–150) eV, as well as on the ratio of gas mixture and pressure in the vacuum system [1]. Three-axis rotation system in the plasma region allowed to produce homogenous films with above-given characteristics on the large-area substrates of various materials: crystalline Si and Al_2O_3, amorphous quartz, silicate and organic glass [2]. Hydrogenated tetrahedral amorphous carbon (ta-C:H:N) DLC thin films were deposited on the surface of these materials by the including of nitrogen into the gas mixture being supplied to direct current ion source.

The optimized average thickness of the produced films is ~200 nm measured by the ellipsometric (at 630 nm wavelength) and by the interference methods. The obtained films are transparent in the visible light (360–1200 nm) spectra. Optical band gap width and coefficient of absorption have been determined by the Tout's method based on the transmission spectra data.

As the investigations showed, the higher the concentration of the C_7H_8 in the gas mixture, the lesser the optical band gap width and the slope of the Tout's curve 1.0–3.5 eV.

DLC films were deposited on the surface of the crystalline n-type Si to determine the temperature dependence of electric parameters. Ni electrodes were deposited on the DLC film for carrying out both electrical and photoelectrical measurements. Ohm contacts to the Si substrate were formed with the help of arc welding of metallic In [3].

Ni/DLC/n-Si/Ni system was developed and investigated. Current-Voltage, Capacitance–Voltage dependences and Q-DLTS spectra were also determined.

It was shown that the obtained films have cluster structure [4].

The I-V characteristics of Ni/DLC/Si/Ni structure with DLC layer doped by nitrogen in different concentrations are shown on Fig.1. The obtained films are enough stable relative chemical, thermal and radiation influences, possesses by good microhardness and adhesion with various substrates. These films are successfully used in electronics, optics, as well in solar energy photovoltaic converters as protective and antireflective coatings [5].

Three samples marked as 1,2 and 3 shows that their electro physical parameters are essentially different. The conductivity determined with the help of the voltage-current characteristics analysis is changed in 9 times for different samples as it follows from Fig.1.

The temperature dependence of specific conductivity (σ) justifies the semiconductor properties of obtained DLC films Fig.2. Increasing in temperature in two times leads to σ increasing in the 5 orders. Analysis of I-V characteristics temperature dependencies evidenced hopping mechanism of charge transfer across the localized states. The sample #2 with the more density of defects possesses high conductivity. The samples 1 and 3 have low density of states and characterized by better insulate properties. The investigation of photovoltage kinetics of all samples shows that band bending in Si substrate for sample 1 is more comparing with others. The activation energies and cross-sections of defect centrums are determined.

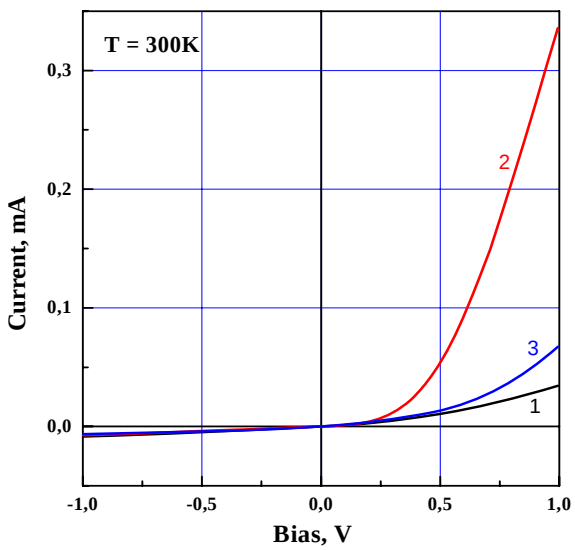

Fig.1. I-V characteristics of thesamples 1,2 and 3.

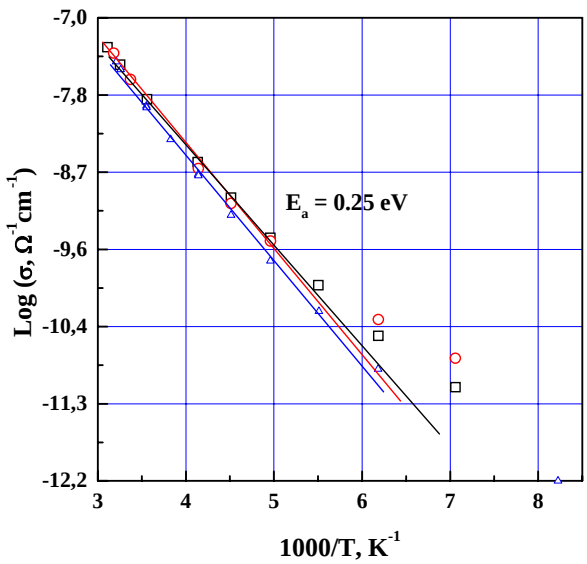

Fig.2 Arrhenius plots of the samples 1,2,3 (from I-V). E_a - the activation energy of conductivity.

References:

1. Kassabian K.G., Panosyan Zh.R. et al. Low temperature technology of obtaining the protecting layer from DLC Proceedings of the Sixth Applied Diamond Conference/Second Frontier Carbon Technology Joint Conf., Auburn, Alabama, USA, p.431-435, (2001).
2. Panosyan Zh.R et. al. DLC film growth on the substrate of monocrystalline Si and Al_2O_3 with the usage of ion source. Proceedings of the Seventh Applied Diamond Conference/Third Frontier Carbon Technology Joint Conf.,Tsukuba, Ibaraki, Japan, p.334-339, (2003)
3. Voskanyan A.S. and Panosyan Zh.R. The production and the investigation of some properties of carbon α-C:H films. Report of Nat. Acad. of Science of Armenia, Physics, v.39, N4, p. 258-261 (2004).
4. Robertson J. Diamond-like amorphous carbon. Materials Science and Engineering R37, p.129-281 (2002).
5. Panosyan Zh.R. et al. Obtaining and investigation of the thin film encapsulating DLC films of PV converters. Diamond Films and Films of Related Materials, Proceedings of 15-th Intern. “Symposium Thin Films in Optics and Electronics” Kharkov, p.213-216 (2003).

HOMOEPITAXIAL AND POLYCRYSTALLINE CVD DIAMOND PN-JUNCTIONS

K. Haenen[1,2], V. Mortet[1], J. D'Haen[2], O.A. Williams[1], M. Nesládek[1,2,3], L. De Schepper[1,2], S. Koizumi[4]

[1]Limburgs Universitair Centrum, Institute for Materials Research (IMO), Belgium
[2]IMEC vzw, Division IMOMEC, Belgium
[3]CEA/Saclay, LIST (CEA-Recherche Technologique)/DETECS/SSTM, France
[4]National Institute for Materials Science, Advanced Materials Laboratory, Japan

ken.haenen@luc.ac.be

Keywords: n-type diamond, phosphorous, pn-junctions, polycrystalline

Abstract

Up to date, in-situ phosphorous doping of CVD diamond remains the only well-established method to achieve n-type diamond films. Several research groups in the world have used the MW PE CVD technique in combination with a P-containing precursor gas, leading to the successful deposition of active P-doped films [1-3].

Most of the n-type doping efforts are focused on homoepitaxial growth using {111}-oriented HPHT Ib substrates. As {100}-oriented n-type diamond remains a problem, diamond pn-junctions are based on stacking of a n-type layer upon a {111}-oriented B-doped film, deposited on a Ib substrate. In order to improve the diode characteristics, usually a thin undoped, intrinsic CVD diamond layer is deposited between the two doped layers, creating a pin-diode. By making use of selective RIE, ohmic contacts can be deposited on both doped layers.

For this work we have deposited a set of pin-diodes under similar doping conditions, but varying the intrinsic layer thickness. We will discuss their I-V characteristics and their UV-response around the band gap.

As is known, the substrate-size is still a limiting factor in the production of n-type films and pn-junctions on larger areas. Recently, at IMO the first polycrystalline n-type films and pn-junctions were deposited making use of a polished polycrystalline CVD diamond as substrate [4,5]. Now we optimised the orientation of this substrate and looked at the morphology of the n-type layer grown on top. Using SEM, EBSD and Orientation Imaging Microscopy (OIM) images we show the relation between the grain orientation of the substrate and the grain grown on top. The novel OIM technique allows the determination of grain orientations over the complete thickness of the film. Finally, Hall-measurements on P-doped polycrystalline n-type films will show the active n-type character of these films.

REFERENCES

1. Koizumi, S., "N-type diamond growth", In: C.E. Nebel, J. Ristein (Eds.), Semiconductors and Semimetals **76** – Thin Film Diamond I, Elsevier Academic Press, Amsterdam, 239-259, 2003.
2. Kato, H., et al., "Homoepitaxial growth and characterization of phosphorus-doped diamond using tertiarybutylphosphine as a doping source", Diamond Relat. Mater. **13**/11-12, 2117-2120, 2004.
3. Nesládek, M. "Conventional n-type doping in diamond: state of the art and recent progress", Semicond. Sci. Technol. **20**, R19-R27, 2005.
4. Nesládek, M., et al., "N-type P-doped polycrystalline diamond" phys. stat. sol. (a) **199**/1, 77-81, 2003.
5. Haenen, K., et al., "The phosphorous level fine structure in homoepitaxial and polycrystalline n-type CVD diamond", Diamond Relat. Mater. **13**/11-12, 2041-2045, 2004.

ACKNOWLEDGEMENTS

This work was financially supported by the F.W.O.-Vlaanderen Research Program G.0298.02, the IWT-SBO-project No.030219 "CVD Diamond, a novel multifunctional material" and an NIMS/AML Research Fellowship (KH). KH is a Postdoctoral Fellow of the Fund for Scientific Research – Flanders (Belgium) (F.W.O.-Vlaanderen).

POSTER SESSION 1

FIELD EMISSION

THERMIONIC FIELD EMISSION FROM UNCD COATED TIP STRUCTURES

J. M. Garguilo, F. A. M. Koeck, and R. J. Nemanich

Department of Physics, North Carolina State University, Raleigh, NC 27695-8202

X. C. Xiao, O. Auciello, and J. A. Carlisle

Agronne National Labs

Keywords: UNCD, diamond, field enhancement, thermionic emission, field emission microscopy

Abstract

Current studies involving thermionic energy converters point to crystalline carbon films in combination with field enhancing properties as promising candidates for the emitting material [1]. Thermionic energy conversion is accomplished through the combination of a hot electron emitter in conjunction with a somewhat cooler electron collector. In operation, an electric potential will develop between the two surfaces that can result in a significant source of electrical energy. The system converts the thermal energy into electrical energy. Since the process is based on electron emission and collection with no mechanical motion, this source can be highly efficient and operate without maintenance for extended periods of time. A limiting phenomenon to the vacuum emission of electrons is the space charge effect in which electrons in the vacuum close to the emitter surface impede additional electron emission. A method to combat this limiting effect is the introduction of surface features which produce a field enhancement effect at the surface. The electrons emitted from the tip shaped surface features are accelerated more rapidly across the vacuum gap to the electron collector.

Ultra nanocrystalline diamond (UNCD) films have been grown on etched Silicon tip arrayed substrates. Raman spectroscopy of the films shows peaks consistent with typical UNCD films and SEM shows continuous coating of the underlying array and clear field enhancement geometry. Field emission electron microscopy (FEEM) measurements of the tip arrayed films give real time, spatially resolved images of temperature dependent electron emission. The first significant emission above room temperature emission occurs at temperatures around and below 830º C. In this regime, an intense, temperature dependence is observed from both the tip structures of the sample as well as the flat, background areas (Figure 1). Field enhancement affects the intensity of emission resulting in brighter spots at the apex of the tips. This emission reaches its strongest around 830º C, rapidly degrading for temperatures in excess of this maximum. This temperature dependent degradation in emission has been observed for other nitrogen doped crystalline CVD films and is correlated to the desorption of surface bound hydrogen and the linked loss of the film's negative electron affinity (NEA)[2]. As the temperature is further increased, intense emission is once again observed from the tips of the sample (Figure 2). This emission is stable and cyclic and present only at the tips of the array. There is no contribution from the background. In this presentation, the origin of these electron emission regimes will be examined and explained.

References

1. Koeck, F.A.M., et al., "Spatial distribution of electron emission sites for sulfur doped and intrinsic nanocrystalline diamond films," *Diam. Relat. Mater.*, Vol. 12, 474 (2003).
2. Koeck, F.A.M., et al., "Enhanced low-temperature thermionic field emission from surface-treated N-doped diamond films," *Diam. Relat. Mater.*, Vol. 11, 774 (2002).

Figures

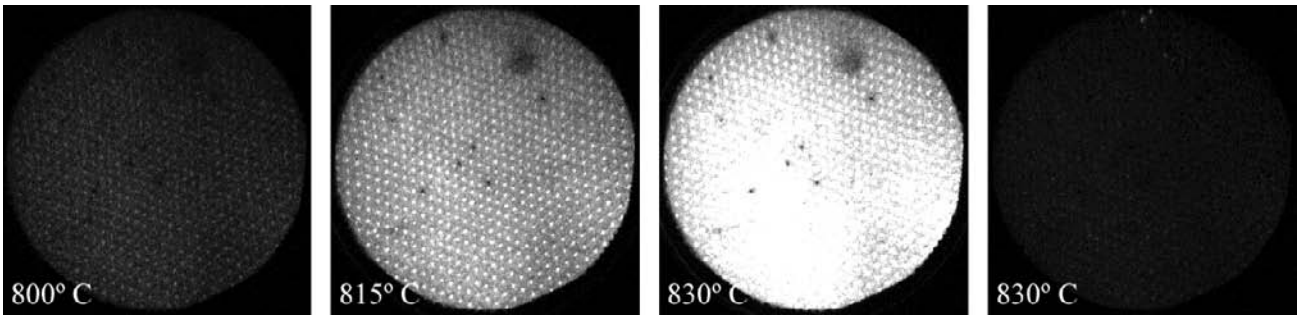

Figure 1. Temperature dependent FEEM images of the UNCD coated tip array. A steady increase in electron emission with increasing temperature is observed up to 830º C. Electron emission is detectable from both the tips and flat background of the sample. The geometric field enhancement effect results in stronger emission from the apex of the tips as compared to the background. After five minutes of exposure to the elevated temperature, the emission degrades. This corresponds to a loss in the film's NEA due to hydrogen evolution from the surface.

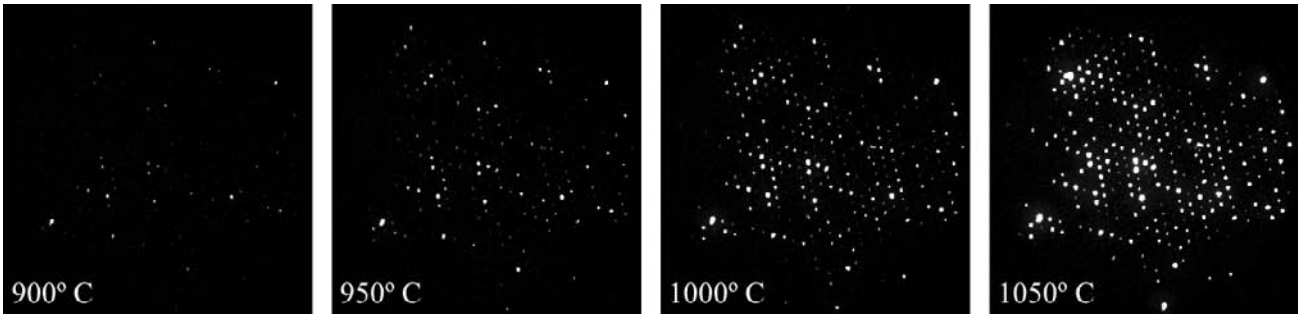

Figure 2. After the loss of the film's NEA, temperature dependent field emission continues to be present. As the sample is annealed to higher temperatures, strong electron emission is observed from the tips of the array. There is no longer detectable emission from the flat background of the sample. This emission is very stable and repeats with successive increasing and decreasing sweeps of the temperature.

CHARACTERISTICS OF ULTRA-NANO-CRYSTALLINE DIAMOND FILMS GROWN ON THE POROUS ANODIC ALUMINA TEMPLATE

Ying-Chieh Chen, Chia-Yun Chen, Nyan-Hwa Tai, Yen-Chih Lee, Su-Jien Lin

Department of Material Science and Engineering, National Tsing-Hua University, Hsin-Chu 300, Taiwan R. O. C.

I-Nan Lin

Department of Physics, Tamkang University, Tamsui 251, Taiwan R. O. C.

Keywords: UNCD, PAA, Electron Field Emission.

Abstract

Diamond films have been extensively investigated for the applications as electron sources, since diamond has negative electron affinity. The electron field emission behavior of the ultra-nano-crystalline-diamond (UNCD) films was observed to be pronouncedly superior to that of the diamond films with micron- or submicron-sized grains, due to the presence of abundant grain boundaries with sp^2-bonds. To further enhance the electron field emission capacity of diamond films, porous anodic alumina (PAA) assisted growth/etching process was used for increasing the aspect ratio of the UNCD, so as to enhance the field enhancement factor of the emission sites. Porous anodic alumina (PAA) layer was first fabricated on Si substrate, followed by the growth of UNCD. To fabricate the PAA, aluminum films were sputtered onto Si substrate, and were anodized in oxalic acid solution (0.3 M). A two step process was adopted to improve the uniformity of the PAA layer, in which, the first formed anodized layer, the prior oxide layer, was removed and the residual aluminum was then fully oxidized to produce the uniform array of hexagons. After the formation of PAA honeycomb pattern, the UNCD films were grown in a 2.45 GHz microwave plasma enhanced chemical vapor deposition (MPECVD) system, using CH_4/Ar plasma. The morphologies and bonding structures of PAA and diamond films were characterized. The electron field emission behavior of the UNCD films was measured. The correlation of the characteristics of the PAA layer with the characteristics of the UNCD films will be discussed.

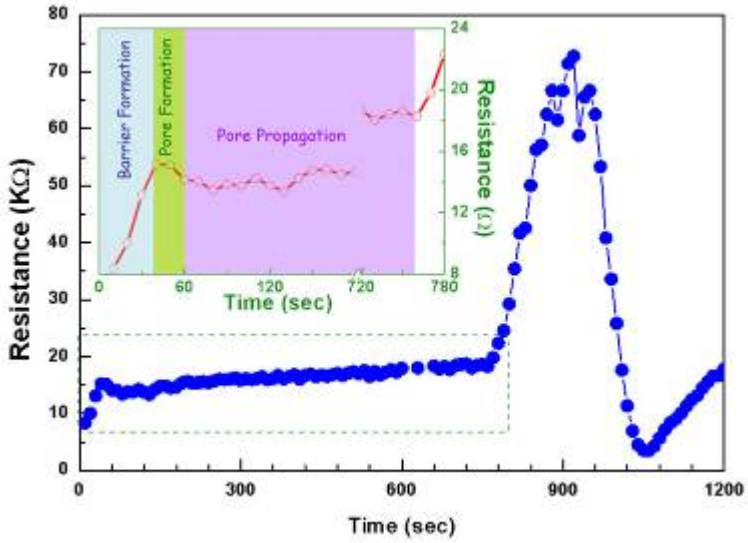

Figure *1*. Two step process for fabrication of porous anodic alumina PAA.

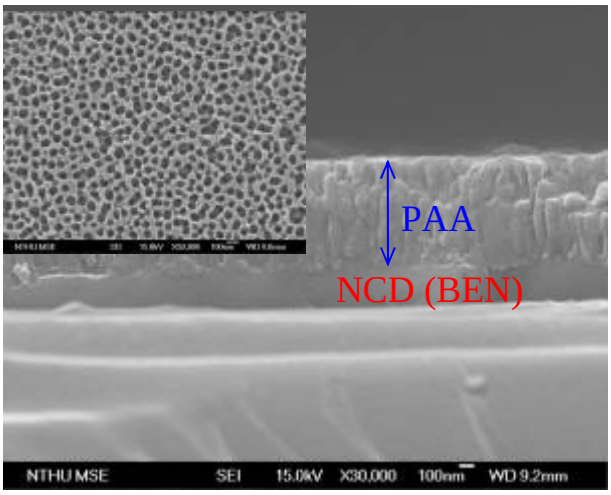

Figure *2*. Typical PAA structure and the ultrananocrystalline-diamond films.

REFERENCES

1. F. J. Himpsel, J. A. Knapp, and J. A. VanVechten, **Phys. Rev. B 20 (2)**, 624 (1979).
2. Y. C. Lee, S. J. Lin, and I. N. Lin et al., "Synthesis and electron field emission properties of nanodiamond films", ***Diamond Relat. Maert.*** **13**, 2100 (2004).
3. O. Rabin, P. R. herz, and Y. M. Lin et al., "Formation of thick porous anodic alumina films and nanowire arrays on silicon wafers and glass", ***Adv. Funct. Mater.*** **13 (8)**, 631 (2003).

FIELD EMISSION CHARACTERISTICS OF DIAMOND EDGE SHAPED EMITTERS FABRICATED USING NITROGEN-METHANE PLASMA

R. S. Takalkar[1], W. P. Kang[1], J. L. Davidson[1], B. K. Choi[1], W. H. Hofmeister[2], K. Subramanian[1]

[1]Dept. of Electrical Engineering and Computer Science, Vanderbilt University, Nashville, TN 37235, USA

[2]Dept. of Chemical Engineering, Vanderbilt University, Nashville, TN 37235, USA

Jim.Davidson@eecsmail.vuse.vanderbilt.edu

Keywords: edge-shaped Emitters, low turn-on, nitrogen-methane plasma, diamond, triode.

Abstract

A diamond based field emission device with low turn-on field and ability to produce high emission current is attractive for vacuum microelectronic applications. Recent research has suggested that nitrogen incorporated nano-crystalline diamond is advantageous for fabricating field emission devices as it is electrically conductive and exhibits low turn-on field [1]. Concurrently, an edge-shaped geometry could be better for high emission current since each edge can have multiple emission sites along the edge [2]. Thus, the utilization of edge-shaped geometry in nitrogen incorporated diamond promises an excellent field emission device. In this paper we report fabrication and field emission behavior of micro-patterned edge-shaped diamond field emission diodes fabricated using nitrogen-methane plasma.

The edge-emitter molds were fabricated from a silicon substrate utilizing silicon micropatterning and etching techniques. Further sharpening of the molds was performed by thermal oxidation of the silicon mold before diamond deposition. This oxidation process not only sharpened the edge but also served as a gate dielectric formation step for the triode device with built-in gate. Diamond was deposited into the edge molds by microwave plasma chemical vapor deposition (MPCVD) process using nitrogen-methane plasma. The deposited diamond film was characterized with energy dispersion spectroscopy (EDS), Raman spectroscopy, and scanning electron microscopy (SEM). Each diamond cathode array, consisted of 1000 edges with each edge base 15μm in width and 120μm in length, fabricated on a 1cm^2 silicon chip and bonded to molybdenum substrate by a high temperature brazing process. The cathodes were tested for emission behavior in a diode configuration. Highly doped low resistivity silicon was used as the anode and a mica spacer was used to separate the anode and cathode. The diode was considered "turned-on" when a forward emission current of 1μA was obtained.

Fig. 1(a)-(b) compares the diamond edge geometry obtained from nitrogen-methane and hydrogen-methane plasma growth processes, while holding other fabrication parameters the same. Nano-crystalline diamond with an average grain size of 5-10nm as compared to 50-100nm was obtained from nitrogen-methane plasma growth and methane-hydrogen plasma, respectively. The smaller diamond grain size obtained from nitrogen-methane plasma growth has led to a sharper edge emitter and hence a higher field enhancement factor and lower turn-on field. Nitrogen incorporation in the as grown diamond film, as seen in EDS spectrum in Fig. 1(c) and Raman spectrum in Fig. 1(d), promotes sp^2 bonding which increases the bulk conductivity of the diamond film and also improves the transport of electrons to the diamond-vacuum interface. Edge emitter diode fabricated from nitrogen-methane plasma displayed a low turn-on field of 2V/μm as compared to 5V/μm displayed by those fabricated using hydrogen-methane plasma compared in Fig. 2(a) [3]. The low turn-on cathode also displayed a high emission current of 5.3mA at 8V/μm as observed from Fig. 2(b). Lowering of turn-on field is attributed to the combination of higher bulk conductivity of deposited diamond and the ability to fabricate sharper edge emitter geometry as compared to that obtained from methane-hydrogen plasma.

In conclusion, diamond edge emitters were fabricated and their emission characteristics studied. Lowering of turn-on field was achieved by fabricating the edge emitters using nitrogen-methane plasma and emission current density of 5.3mA/cm^2 was demonstrated. We have also fabricated a self-aligned gated diamond edge triode from a silicon-on-insulator (SOI) substrate using similar fabrication techniques. Details of the field emission triode behavior will be presented in the paper.

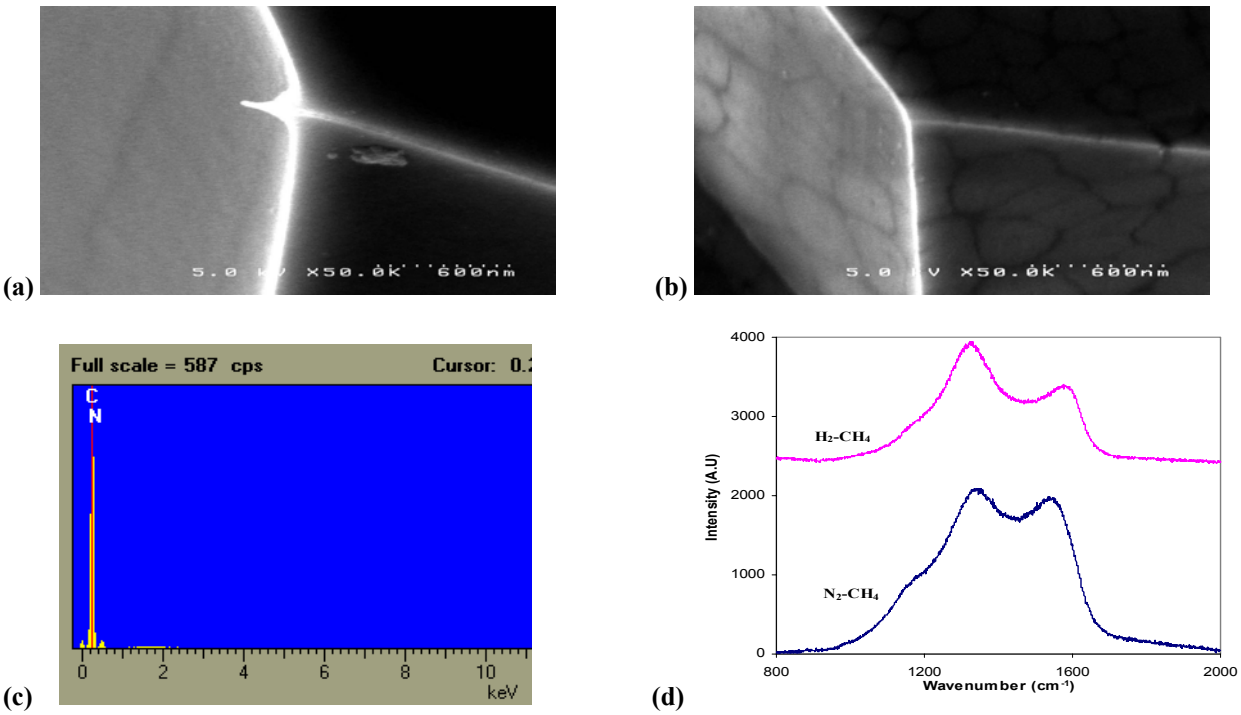

Figure 1. (a) High magnification SEM of edge emitter fabricated using nitrogen-methane plasma. (b) High magnification SEM of edge emitter fabricated using hydrogen-methane plasma. (c) Energy Dispersion Spectrum of diamond grown using nitrogen-methane plasma. (d) Comparison of Raman spectra of deposited diamond.

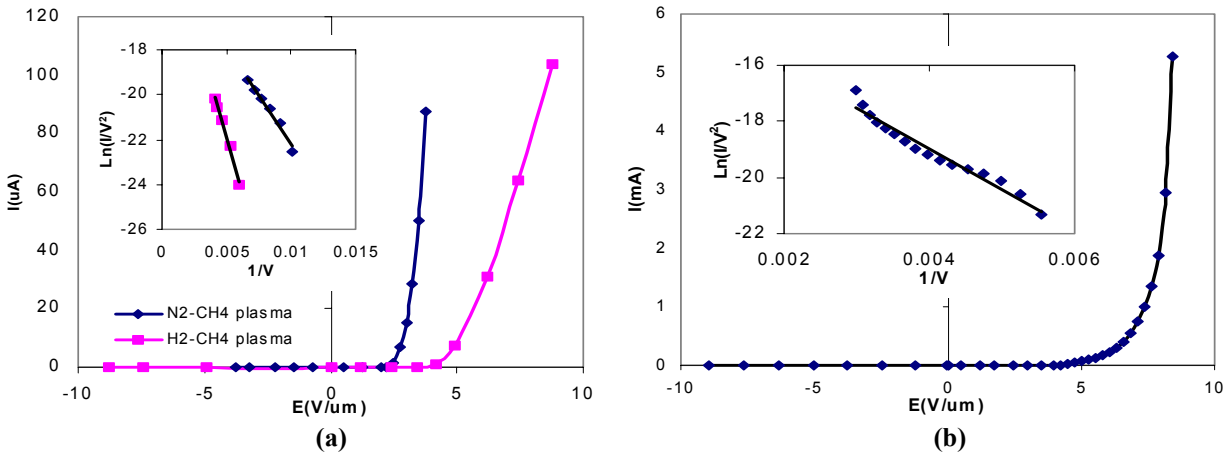

Figure 2. (a) I-E plot comparing field emission characteristics of edge-emitters fabricated using nitrogen-methane plasma and hydrogen-methane plasma. (b) High emission current characteristics of edge-emitters fabricated using nitrogen-methane plasma.

REFERENCES

1. Corrigan, T. D., Gruen, D. M., et al., "The effect of nitrogen addition to Ar/CH4 plasmas on the growth, morphology and field emission of ultrananocrystalline diamond", *Diamond and Related Materials,* 11, 43-48 (2002).

2. Bo Lee, Elliott, T. S., et al., "Knife-edge thin film field emission cathodes on (110) silicon wafers", *J. Vac. Sci. Technol. B,* 12 (2), 644- 647 (1994).

3. Takalkar, R. S., Davidson, J. L., et al., "Edge-shaped Diamond Field Emission Arrays" accepted for publication in *J. Vac. Sci. Technol. B.* (2005).

FABRICATION OF ALIGNED CONVEX CNT FIELD EMISSION TRIODE BY MPCVD

Y. M. Wong[1], W. P. Kang[1], J. L. Davidson[1], B. K. Choi[1], W. Hofmeister[2], and J. H. Huang[3]
[1]Department of Electrical Engineering and Computer Science, Vanderbilt University, Nashville, TN 37235, USA
[2]Department of Chemical Engineering, Vanderbilt University, Nashville, TN 37235, USA
[3]Dept. of Materials Science and Engineering, National Tsing Hua University, Hsinchu 300, Taiwan, ROC

wkang@vuse.vanderbilt.edu

Keywords: MPCVD, carbon nanotubes, field emission devices, triode, amplifier.

Abstract

In this work, vertically aligned carbon nanotubes (CNTs) were used to form a microcathode with a convex surface profile, being selectively synthesized from Microwave Plasma Chemical Vapor Deposition (MPCVD) with Ni or Co as catalysts. A single-mask micro-fabrication process achieved an array of 10 μm square CNT microtriodes with self-aligned gate. This convex profile is important in preventing cathode-gate leakage without resorting to more complicated fabrication processes or utilizing a gate over-etched approach. The dc characteristics of the CNT triode in a common emitter configuration were investigated, including dc parameters such as transconductance (g_m), amplification factor (μ), and anode resistance (r_a). The transconductance of a field emission triode establishes the current driving capability while the amplification factor determines the ultimate voltage gain of the amplifier. The triode device demonstrated good gate-controlled modulation of the emission current with distinct cutoff, linear and saturation regions of operation. A gate turn-on voltage as low as 25 V has been achieved. A large amplification factor of ~352 and transconductance of ~2 μS are obtained. These transistor characteristics are substantially improved compared to our previously reported results [1].

INTRODUCTION

Previously, we successfully fabricated a CNT triode with a gate turn-on voltage of ~40 V by thermal CVD [1]. Since the CNTs grown were randomly oriented, an over-etched gate structure [1] was adopted in order to avoid cathode-gate leakage problems. As a result, the large cathode-gate spacing led to high gate turn-on voltage and triode characteristics of $\mu = 10$ and $g_m = 47$ nS when configured as an amplifier. In order to overcome gate leakage which limits performance of the CNT triode, three approaches have been reported in literatures: (i) over-etched gate electrode or reduced gate overhang [1,2], (ii) sidewall protector [3,4], and (iii) post-growth processing which includes utilizing chemical mechanical polishing (CMP) technique [5], and plasma trimming of the grown CNTs [6]. In this work, an alternative approach with gated convex CNT cathodes was applied to minimize the cathode-gate leakage problems.

EXPERIMENTAL

Vertically aligned convex CNT microcathodes were synthesized selectively inside a triode mold utilizing MPCVD method. A thin layer of Ni or Co and Ti was sputter-deposited as the growth catalyst and diffusion barrier, respectively. The surplus catalyst on the polysilicon gate was removed by photoresist lift-off technique. A hydrogen plasma pretreatment of the catalysts was performed. The CNTs synthesis was at 20 Torr, microwave power 1.0 kW and substrate temperature 650°C. Methane (CH_4) diluted in hydrogen (H_2) was the carbon source. The growth time of the CNTs was ~ 60 to 90s, critical to obtain the right height of the vertically aligned CNT cathodes. In device characterization, the CNT triode was tested in common emitter amplifier configuration for dc field emission characteristics. The measurements were performed at room temperature in a vacuum chamber evacuated to a base pressure of 10^{-6} Torr. Measurements of the anode emission current, I_a as a function of the anode voltages (V_a) for different gate voltage (V_g) were collected.

RESULTS AND DISCUSSIONS

The single-mask micro-fabrication process achieved an array of 10 μm square CNT microtriode, as depicted in Figure 1. Vertically aligned CNTs with diameters ranging from 20-30 nm were grown. The H_2 plasma pretreatment of the sputtered catalysts was utilized to achieve gated CNT cathode with convex profile or shorter nanotubes on the edges, Figure 1. This convex profile is important in preventing cathode-gate leakage without resorting to complicating fabrication processes such as sidewall protector or gate over-etching that result in higher turn-on voltage. The cathode-gate spacing was ~2.0 μm. Gate turn-on voltage as low as 25 V has been achieved and the emission current follows Fowler-Nordheim electron tunneling behavior, Figure 2. When tested in a common emitter configuration, the CNT triode device demonstrated good gate-controlled modulation of the emission current with

distinct cutoff, linear and saturation regions of operation. A large dc gain or amplification factor of ~352 at I_a = 1.7 μA, and transconductance of ~2 μS at V_a = 400 V are obtained. These transistor characteristics are substantially improved compared to our previously reported results [1], where randomly oriented CNTs were grown by thermal CVD inside an over-etched gate triode mold. The improvement is attributed to the vertically aligned CNTs with convex profile, smaller cathode-gate gap and larger array size.

CONCLUSION

Vertically aligned CNT field emission triode fabricated with a single-mask process and catalyzed MPCVD, configured as an amplifier has demonstrated very good dc characteristics with high dc gain and transconductance at low operating voltages. The vertically aligned CNT triode with a convex profile performs better than the triode grown with thermal CVD method [1]. This CNT triode amplifier could be a candidate for high power, high gain and high frequency amplifier applications that requires radiation-hardness and temperature-immune capability.

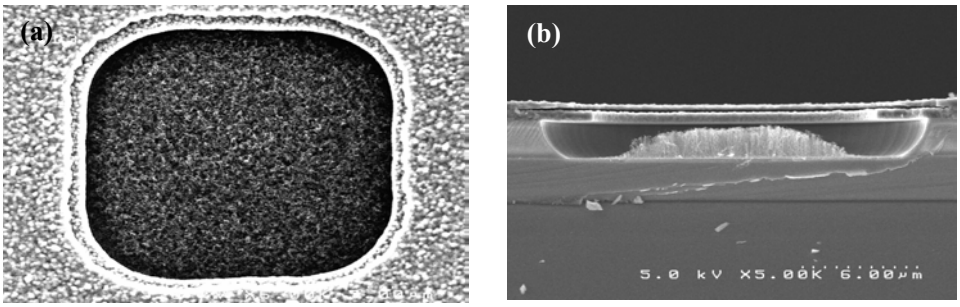

Figure 1. SEM micrograph of the aligned CNT triode (a) oblique view, and (b) cross-sectional view.

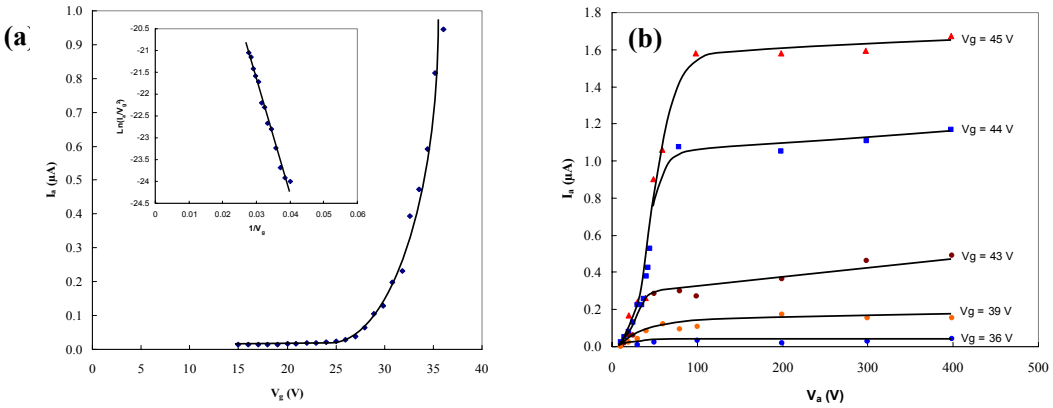

Figure 2. (a) Plot of the measured anode currents, I_a vs. the gate voltage, V_g, and (b) Plot of I_a vs. the anode voltage, V_a for different V_g of the CNT triode.

REFERENCES

1. Y. M. Wong et al., "Transistor characteristics of thermal CVD carbon nanotubes field emission triode", *International Vacuum Nanoelectronics Conference*, 282-283 (2004).
2. K. J. Chen et al., "Low turn-on voltage field emission triodes with selective growth of carbon nanotubes", *IEEE Electron Device Letters* 22, 516 – 518 (2001).
3. Y. Huh et al., "Selective growth and field emission of vertically well-aligned carbon nanotubes on hole-patterned silicon substrates", *Chem. Phys. Lett*. 375, 388-392 (2003).
4. D. S. Y. Hsu, "Microgating carbon nanotube field emitters by in situgrowth inside open aperture arrays", *Appl. Phys. Lett*. 80, 2988-2990 (2002).
5. W.J. Yu et al., "A stable high power carbon nanotube field-emitter device", *Diamond and Related Materials* 13, 1017–1021 (2004).
6. S. Kang et al., "Low temperature carbon nanotubes for field emission display", *International Vacuum Microelectronics Conference*, 51-52 (2003).

STUDY OF THE FIELD EMISSION PROPERTIES OF CARBON NANOTUBES GROWN ON SULFUR DOPED NANOCRYSTALLINE DIAMOND FILMS

Kishore Uppireddi, Fabrice Piazza

Dept of Physics, University of Puerto Rico, Puerto Rico, PR 00931, USA

Gerardo Morell

Dept of Physical Sciences, University of Puerto Rico, Puerto Rico, PR 00931, USA

Keywords: field emission, carbon nanotube, nanocrystalline carbon, sulfur doping

Abstract

The electron field emission (EFE) properties of carbon nanotubes (CNTs) grown on sulfur-doped nanocrystalline diamond (n-D:S) films were investigated. These two materials show excellent EFE properties separately. The CNTs and sulfur-doped nanocrystalline diamond films were synthesized in the same hot filament chemical vapor deposition (HFCVD) system at relatively low methane concentrations (1-2%). The effect of growth process parameters of CNTs and sulfur incorporation in the nanocrystalline diamond films on the field emission properties were studied. Their morphology and structure were characterized by SEM, energy filtered TEM and Raman spectroscopy. The dependence of EFE properties on composition and morphology is discussed.

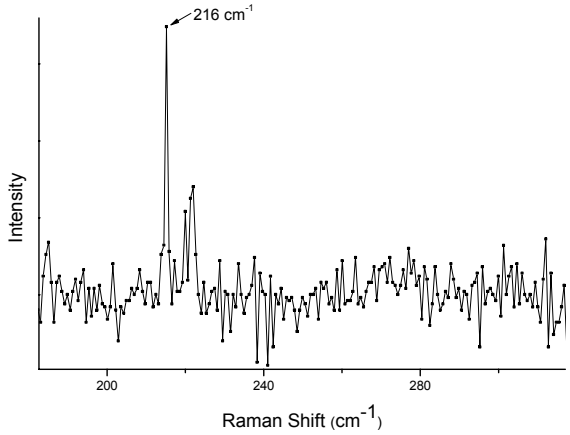

Figure 1. Radial breathing mode of multiwall CNTs measured by visible Raman Spectroscopy.

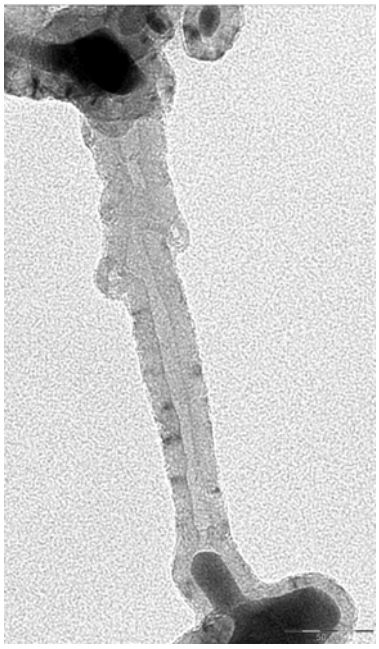

Figure 2. High resolution TEM of a multiwall CNT

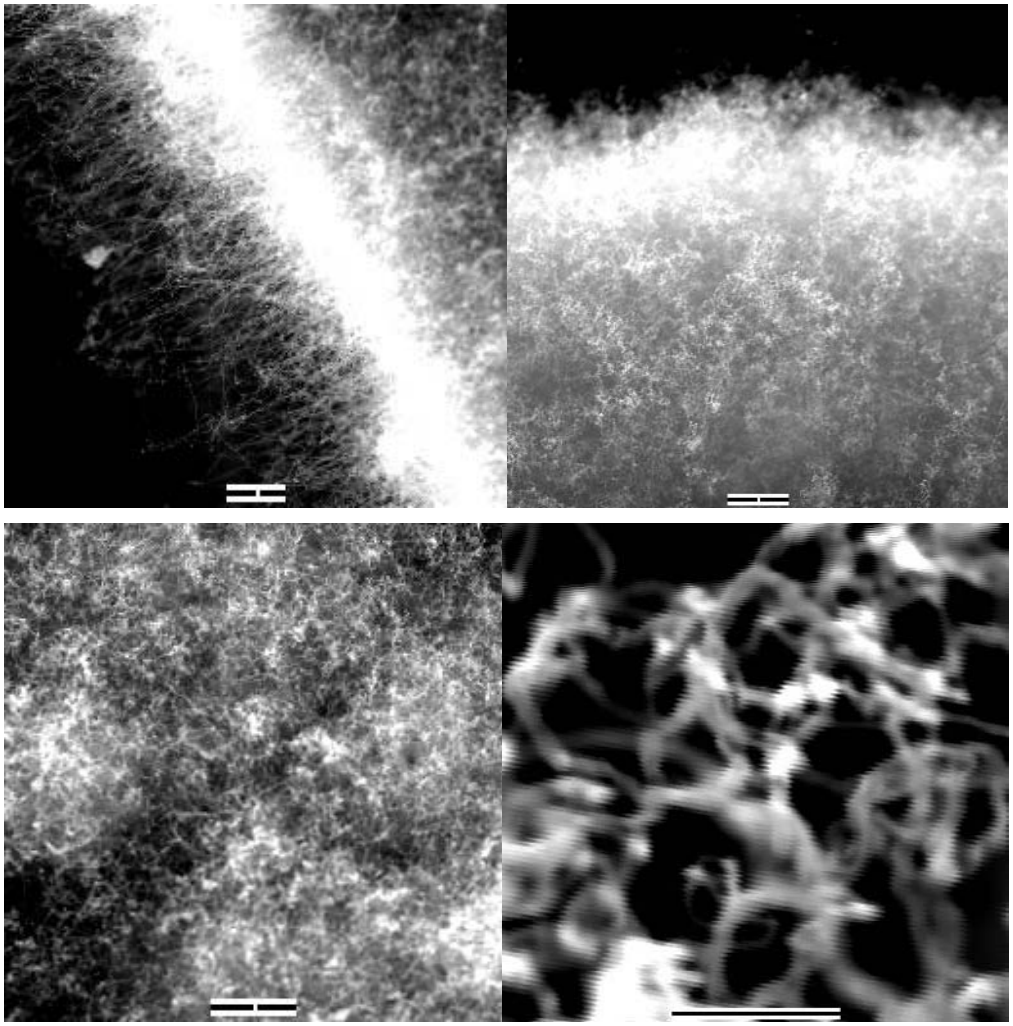

Figure 3. SEM images of CNTs grown by HFCVD: upper left - edge view; upper right – side view; lower left – top view; lower right – zooming.

Acknowledgements: Research supported by NASA (Grants NCC3-1034 and NGT5-40091; Cooperative Agreement NCC5-595), Department of Energy (Grant DE-FG02-01ER45868), and the UPR-Río Piedras FIPI (Grant 8-80-514).

References

1. Wang , S.G., et al., "Electron field emission from carbon nanotube and undoped nanodiamond," *Diamond and Related Materials*, Vol. 12, pages 8-14 (2003)
2. Sarangi, D, et al., "Growth mechanism of carbon nanotubes converted from diamond-like carbon films," *Chemical physics letters*, Vol. 397, pages 516-519(2004).
3. Koenigsfel, N, "Improved field emission at electric-discharge-conditioned sites on diamond surfaces due to the formation of carbon nanotubes," *Applied physics letters*, Vol. 82, No. 26, pages 4687 (2003).

Amorphous Diamond Electron Emission Capabilities: Implications to Thermal Generators and Heat Spreaders

James C. Sung [*,1,2,3], Kevin Kan[1], Michael Sung[5], Jow-Lay Huang[4], Emily Sung[6], Chi-Pong Chen[1], Kai-Hong Hsu[3] and Ming-Fong Tai[7]

Address: KINIK Company, 64, Chung-San Rd., Ying-Kuo, Taipei Hsien 239, Taiwan, R.O.C.

Tel: 886-2-2677-5490 ext.1150

Fax: 886-2-8677-2171

e-mail: sung@kinik.com.tw

[1] KINIK Company, 64, Chung-San Rd., Ying-Kuo, Taipei Hsien 239, Taiwan, R.O.C.
[2] National Taiwan University, Taipei 106, Taiwan, R.O.C.
[3] National Taipei University of Technology, Taipei 106, Taiwan, R.O.C.
[4] National Cheng-Kung University, Tainan, Taiwan, R.O.C
[5] Massachusetts Institute of Technology, Cambridge, Massachusetts, U.S.A.
[6] Johnson and Johnson, Freemont, California, U.S.A.
[7] Department of Electronic Engineering, Wufeng Institute of Technology, Chia-yi 621, Taiwan, R.O.C.

Key words: Amorphous Diamond, Solar Cell, Diamond Electrode, Heat Spreader

Abstract

Amorphous diamond represents a class of material of its own. It may be viewed to be a composite of metal (graphite) and insulator (diamond), but together they form a unique passage for electrons to flow through and to emit in vacuum. Amorphous diamond contains much defect so its electrical resistance is intermediate between metal and semiconductor. However, its ability to emit electrons in vacuum as cold cathode outstrips almost any class of materials. The easiness for electrons to flow through amorphous diamond and fly toward an anode across vacuum makes it an ideal material for electrical generator. In fact, the electricity generation can be so easy that amorphous diamond may become the most efficient solar cell ever invented. Moreover, by reversing the role of electricity generation, an amorphous diamond film may become an electron radiator. Such a radiator may dissipate heat much faster than the most advanced heat spreader (e.g., diamond substrate or heat pipe) currently being investigated.

Recent experimental results has confirmed that the current of electron emission in vacuum has increased two orders of magnitude when amorphous diamond is heated to 300 ^{o}C. Such a dramatic increase of current indicates that thermal energy can indeed shake off electrons in carbon atoms and accelerate them toward an anode across a vacuum. This phenomenon is consistent with the proposal that amorphous diamond can indeed be made of solar cells and/or heat spreaders.

Competition of Field Emission from CNT Films Produced by Five Different Techniques

A.V. Karabutov[1], S.M. Pimenov[1], V.I. Konov[1], E.D. Obraztsova[1], V.G. Pereverzev[1], A.S. Pozharov[1], S.V. Terekhov[1], P.Ya. Detkov[2], E.V. Shorokhov[2], E.N. Loubnin[3]

[1)] General Physics Institute, 38 Vavilova street, 119991 Moscow, Russia

[2)] RFNC-RITF, 13 Vasilieva street, 456770 Snezhinsk, Chelyabinsk region, P.O. 245, Russia

[3)] Institute of Physical Chemistry, 31 Leninsky prospect, 117915 Moscow, Russia

Carbon Nanotube (CNT) based field electron emitters are attractive for numerous applications, but there are a lot of methods to produce such emitting coatings, and a question is still open, which one is better. Here we study the field electron emission properties of CNT films produced by different techniques on Si, metal and glass substrates: (i) electrophoretic deposition of single-wall and multiwall CNT onto conducting substrates from alcohol suspensions, (ii) catalytic pyrolysis of multiwall CNT, (iii) formation of CNT films on metal substrates by gas-static pressing, (iv) explosive implantation of CNT into metal layers, (v) shock-wave compacting of various powder materials with CNT, etc. In addition we study carbon nanoparticle-based emitters produced by electrochemical codeposition of metals with nanodiamond powders or chemical vapor deposited carbon 'needle-shaped' nanostructures using a dc arc plasma activation of triple (methane-argon-nitrogen) gas mixtures.

The film microstructure was studied using AFM, SEM, Raman spectroscopy, X-ray Photoelectron Spectroscopy, Auger Electron Spectroscopy, and EELS to find correlations between the field emission and other film properties. The field electron emission was studied using both a macroscopic phosphor screen setup and a microprobe setup with tungsten probes of 10 μm in radius. Emission I-V dependences as well as emission sites distribution were measured and then analyzed depending on preparation conditions.

It was found that the CNT films produced at certain conditions emit better than other CNT films, and show better emission threshold field (1 V/μm and even lower), higher density of emission sites, and higher working limit of the emission current. Whereas in some cases of the CNT film preparation the emission is not good enough. A comparison is made with chemical vapor deposited carbon 'needle-shaped' nanostructures, which also show good emission properties. Possible field emission mechanisms are considered.

The work was supported by the ISTC Project #1400.

POSTER SESSION 1

SURFACES & SENSORS

SURFACE CONDUCTIVITY AS A NATURAL PROPERTY FOR HYDROGENATED DIAMOND

Ying Dai [a,b*], B.B.Huang[b], Run Long [a]**

a School of Physics and Microelectronics, Shandong University, Jinan 250100, P. R. China

b State Key Laboratory of Crystal Materials, Shandong University, Jinan 250100, P. R. China

Dadi Dai

Department of Chemistry, North Carolina State University, Raleigh, North Carolina, 27695-8204, USA

Keywords: hydrogenated diamond; surface conductivity; surface layer.

Abstract

The electronic structure with Milliken occupation of a series of diamond clusters with hydrogen-terminated surface has been calculated by means of density functional theory (DFT). From the obtained results it is found that the Fermi-level (E_F) of clusters lowers with the clusters-size increasing. Combining this finding with the localization character of states in the noncrystalline surface layer, we may conclude that (1) every crystalline particle is composed geometrically of two phases, one is of the surface noncrystalline layer in which the E_F is lower than that of the whole cluster and the electrons are trapped in localized states; another phase is the interior crystal in which the electron is quasi-free in delocalized states similar to that in bulk metal; (2) existence of the layer with trapped-electron at surface and free-hole-accumulation inside and near surface is the origin of surface conductivity in diamond and various impurities as well as defects at surface play the role of changing the electron distribution in the surface region, namely, they do not originally affect the surface conductivity.

* sustentation fund: NSFC (10374060) and Natural Science Foundation of Shandong Province (Y2003A01)

** bbhuang@sdu.edu.cn

A CHEMICALLY AND BIOLOGICALLY FUNCTIONALIZED DIAMOND SOLUTION GATE TFT AND ITS APPLICATION FOR DNA SENSING

Bin Sun, Wensha Yang, Kiu-Yuen Tse, and Robert J. Hamers*

Chemistry Department, University of Wisconsin-Madison

James E. Butler, Tatyana Feygelson

Chemistry Division, Naval Research Laboratory

Keywords: Diamond, Bio-FET, Fabrication, Surface functionalization.

Abstract

Diamond has been proved as a stable material and can be functionalized with DNA and other bio-molecules via covalent bond, which is stable for long time, relative harsh treatment and high temperature. Recent studies have shown that diamond thin films can be used for the fabrication of biologically-sensitive field-effect transistors (Bio-FETs), in which the change in charge distribution associated with bio-molecular binding at a diamond surface induces a change in the diamond sub-surface depletion region. This type of direct Bio-FET sensing is important because it can be easily scaled down in size, leading to potential improvements in sensitivity and the creation of arrays of bio-FETs.

While fabrication of millimeter-sized FET's can be accomplished using simple procedures, to achieve highest sensitivity, built-in controls, and develop high-density arrays, it is necessary to use more advanced processing methods. It is particularly important to protect the electrical contacts from exposure to the physiological fluids. We have used used lithographic processing methods to create small diamond FETs with channel lengths of 10 microns and have investigated how the electrical response is affected by the surface functionalization. We have compared 5 different types of surfaces, including H-terminated diamond, and diamond functionalized with molecular layers of Dodecene, TFAAD (chemically protected amine), deprotected TFAAD, and surfaces covalently linked to DNA. By characterizing the electrical response of diamond FET's modified with these different molecular layers, we gain insight into how to optimize the response for detection of chemical and biological molecules. Using this understanding, we have constructed diamond Bio-FET's functionalized with DNA and have investigated their electrical response. Our results demonstrate the ability to detect DNA hybridization and to distinguish between complementary vs. non-complementary sequences using a micron-scale diamond bio-FET.

REFERENCES

1. Yang, W. S., et al, "DNA modified nanocrystalline diamond thin film as stable, biologically active substrates",*Nature Materials* 2002, *1*, 253
2. Strother, T.,et al. "Photochemical Functionalization of Diamond Films" *Langmuir* 2002, *18*, 968.

PHOTOCHEMICAL MODIFICATION OF DIAMOND FILMS: A STRUCTURAL AND MECHANISTIC STUDY

Beth M Nichols, Robert J Hamers

Department of Chemistry, University of Wisconsin-Madison, Madison ,WI

James E. Butler, John N Russell, Jr.,

Chemistry Division, Naval Research Laboratory, Washington D.C.

Keywords: Nanocrystalline diamond, photochemistry, surface functionalization, mechanism

Abstract

Diamond and diamond films have many properties which make them attractive substrates for developing technologies in fields such as biotechnology, biological and chemical sensing, and molecular electronics. Previous work has shown that hydrogen-terminated nanocrystalline diamond films can be covalently modified with molecules bearing a terminal vinyl (C=C) group by way of a photochemical process under 254 nm light.[1] While this method has been shown to produce stable monolayer films, the reaction mechanism and film structure have not been previously investigated. The mechanism is particularly intriguing because it proceeds using sub-bandgap excitation energy. Here, we report an investigation of the structure and mechanism of the photochemical modification of diamond with functionalized terminal alkenes.

X-ray photoelectron spectroscopy experiments were performed on nanocrystalline diamond films and on single-crystal diamond samples. A comparison of the rates of photochemical modification of single crystal diamond (111) and nanocrystalline diamond films shows no significant difference in reactivity, demonstrating that the modification process is not controlled by grain-boundaries or other defects associated with the polycrystalline films. By using a molecule with a fluorine "tag" at one end, we can establish the degree to which the molecules are oriented on the surface using angle-resolved XPS measurements. These measurements show that the fluorine tag is at the exposed (vacuum) interface, thereby ruling out the possibility of polymerization onto the surface and establishing that the molecules bind to the surface via the olefin group.

To understand the mechanism of photochemical modification, we have conducted a number of experiments aimed at identifying how photoexcitation of the bulk diamond induces the surface chemical modification. Previous work has shown that hydrogen-terminated single crystal diamond exhibits negative electron affinity,[2-4] and we find that our nanocrystalline diamond samples also exhibit negative electron affinity. These results suggest that direct photoejection of electrons into the organic fluid may be responsible for the photochemical modification. Previous studies have shown that 254 nm light is sufficient to eject electrons from diamond surfaces into vacuum.[5] Since electrons are stabilized by a polarizable medium, it should also be possible to directly eject electrons from diamond into an organic liquid film. Such photoejection would alter the diamond electronic structure and would produce ions in the organic liquid. Since ions are often highly reactive, we propose that direct photoejection of electrons from diamond into the liquid induces the overall photochemical reaction. Using gas chromatography-mass spectrometry (GC-MS), we have analyzed the changes in chemical composition of 1-dodecene and trifluoroacetamide-protected 10-aminodec-1-ene after illumination with 254 nm light in contact with diamond. Our results show the formation of new chemical products in solution that are only formed when the diamond film is present, indicating that optical absorption within the diamond is necessary for the changes in solution chemical composition. The identity of these species and their use in the interpretation of the reaction mechanism will be discussed.

REFERENCES

1. Strother, T., et al., "Photochemical functionalization of diamond films," *Langmuir*, 18, 968-971 (2002).
2. Diederich, L., et al. , "Electron emission and NEA from differently terminated, doped and oriented diamond surfaces," *Diam. Relat. Mater* 8, 743-747 (1999).

3. Ley, L., et al., “Electronic properties of single crystalline diamond surface,” *Carbon*, 37, 5, 793-799 (1999).
4. Baumann, P.K., Nemanich, R.J., “Surface cleaning, electronic states and electron affinity of diamond (100), (111), and (110) surfaces” *Surf. Sci*, 409, 320-335 (1998)
5. Ristein, S., Stein, W., Ley, L., “Defect spectroscopy and determination of the electron diffusion length in single crystal diamond by total photoelectron yield spectroscopy.” *Phys. Rev. Lett.*, 78, 1803-1806 (1997)

Neural cell patterning on thin film boron doped diamond electrodes for neurotransmitter detection *in vitro*

Jeannette M. Bursee, Harihara Baskaran, and Heidi B. Martin

Department of Chemical Engineering

Case Western Reserve University, Cleveland, OH 44106

Keywords: diamond, cell patterning, neurotransmitter detection, neuron

Abstract

We present our progress in the development of an *in vitro* method to measure neurotransmitter release and electrical signals from neural cells by patterning the cells directly onto an array of diamond electrodes and by controlling the growth of neural processes in culture. The experimental model allows quantification of electrochemical communication between neural cells, and provides a more predictable system for the study of electrochemical communication between neurons than *in vivo* animal models or studies using brain slices. Using various microfabrication techniques, it is possible to achieve small feature sizes enabling observations at the cellular level. Detection with extracellular electrodes provides a non-invasive method to detect chemical and electrical signals from cells.

Cell patterning techniques provide a convenient method to control the growth of cells and for strategic placement of neurons in culture over an electrode surface to facilitate neurotransmitter detection. Self-Assembled Monolayers (SAMs) of alkanethiolates on gold substrates produced via microfabrication techniques have been used to provide a pattern of adhesive and nonadhesive regions which may be used to control cell growth over a substrate. Application of various patterns of adhesion proteins over a substrate can be achieved using microfluidic techniques or elastomer stamps. Preferential cell adhesion to these proteins can be used to create patterns of cells, and to control axon and neural process growth. [1,2] The terminal functional groups of the diamond thin film determine hydrophobicity properties and possibly cell adhesion properties; this may provide a possible avenue for cell patterning as well. Neural cells have been previously patterned over electrode arrays in order to detect electrical signals produced by these cells, *e.g.*, patterns over gold electrode contacts and commercially available microelectrode arrays. [3,4] Thus far, the technique of cell patterning to control neural process growth has not been applied to study the spatiotemporal dynamics of the release of particular neurotransmitters at the synapse between two neurons.

Diamond has gained interest as an electrode material for neurological measurements. Boron-doped diamond electrodes have been shown to have a wide potential window and low baseline current in aqueous solutions and provide long-term chemical stability. [5] Diamond electrodes potentially provide an improved sensor material for *in vivo* detection of neurotransmitters. Carbon-fiber electrodes are used widely in neurochemical sensing research, however they do not display the same long-term stability as thin film diamond electrodes; the surface becomes passivated. Protein adsorption onto the surface of carbon-fiber electrodes also decreases their functionality over time. One possible solution to this problem is to coat the electrode surface with a porous conducting layer such as Nafion, but this can limit the sensor response time.

Diamond has a simpler surface chemistry than carbon fibers, possibly enabling homogenous, surface functionalization. Diamond's surface termination can thus be more predictably modified to manipulate the electrochemical properties. The diamond surface may also discourage the adsorption of proteins, which is desired for continuous detection of biomolecules in aqueous solution. [6,7]

As the first steps to develop this diamond device to probe neural cell activity, we are developing techniques for diamond and protein patterning, as well as studying interactions of cells with these surfaces. To fabricate diamond electrode patterns, we used CVD differential growth of diamond onto a resistive silicon substrate. Prior to growth, microfluidic techniques distributed diamond seed nanoparticles into a precise pattern (minimum width of pattern ~ 200 μm, smaller microfluidic feature sizes down to ~20μm may be fabricated using current method). Initial results show that seeded regions developed nearly complete films and had smaller crystals than regions where seed particles were not deposited. Areas where no nanoparticles were applied showed incomplete film formation. The pattern of diamond film formation can be seen in Figure 1. Similarly, the conductance of the more complete diamond film in the pre-seeded regions was significantly higher than in non-seeded areas. (~55 μSiemens vs. ~2.0

µSiemens). We are currently varying the deposition time, concentration of seed particles, and the geometry of the microfluidic patterns to optimize this process.

Preliminary studies with a cancer cell line on a diamond thin film over a silicon substrate show that eukaryotic cells adhere to a diamond thin film and undergo cell division. The cells were also cultured on the diamond film pattern. The cells adhere preferentially to the more complete areas of film growth (*i.e.*, pre-seeded regions).

Coupled with our diamond patterning is development of protein patterns. In general, a culture of cells may be induced to grow in specific geometries by differential application of adhesion proteins to a substrate. [8] We are currently applying a pattern of the cellular adhesion protein, fibronectin, to the substrate using microfluidic techniques. The protein pattern is visualized by fluorescently labeling the fibronectin through a standard biotinylation process and reaction with fluorescently conjugated streptavidin. Time-lapse microscopy is then used to determine the differential time for adhesion of the cells to the protein pattern and the unpatterned substrate.

In the future, we will integrate our patterning techniques, to pattern cells from a human neuronal cell line over the diamond thin film electrode array such that release of neurotransmitters from specific groups of neural cells may be detected at an electrode surface.

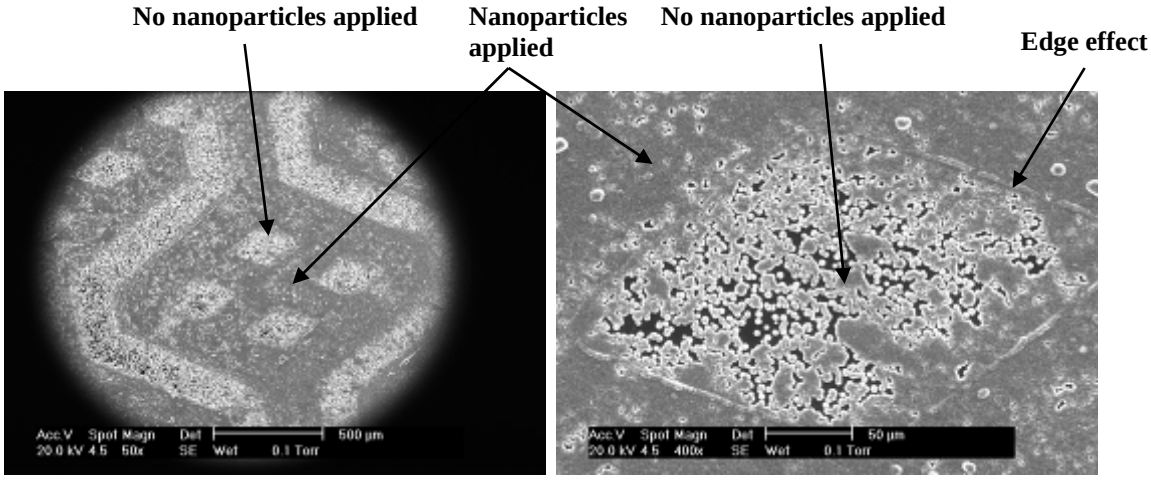

Figure 1. Diamond seed particles were applied to a resistive silicon substrate using microfluidic techniques. Areas where diamond seed nanoparticles were applied (these areas appear darker) showed nearly complete film formation and had a smaller crystal size than where seed particles were not deposited. Areas where no nanoparticles were applied showed incomplete film formation and had a larger crystal size than. The conductance of the areas where seed particle were applied was significantly higher than where seed particles were not applied. (~55 µSiemens vs. ~2.0 µSiemens). Image on left, scale bar = 500 µm, on right, scale bar = 50 µm.

References

1. C.D. James, R. Davis, M. Meyer, A. Turner, S. Turner, G. Withers, L. Kam, G. Banker, H. Craighead, M. Isaacson, J. Turner, W. Shain, IEEE Trans. Biomed. Engr., 47(1): 17-21. (2000)
2. L. Griscom, P. Degenaar, B. LePioufle, E. Tamiya, H. Fujita, Sensors and Actuators B, 83:15-21. (2002)
3. Martin, H.B., Argoitia A., Landau U., Anderson A.B., Angus J.C., J. Electrochem. Soc., 143 (6):L133-L135. (1996)
4. Tenne R., C. Levy-Clement, Isreal J. Chemistry, 38:57-73. (1998)
5. G.M. Swain, A.B. Anderson, J.C. Angus, MRS Bulletin, 23:56-60. (1998)
6. K.S. Ravi, S. Takayama, E. Ostuni, D.E. Ingber, G.M. Whitesides, Biomaterials, 20:2363-2376. (1999)
7. J.M. Corey, E.L. Feldman, Expt. Neurology, 184:S89-S99. (2003)
8. J.C. Chang, G.J. Brewer, B.C. Wheeler, Biomaterials 24:2863-2870. (2003)

POSTER SESSION 1

GROWTH

Synthesis of Large-Area, Thick, Uniform, Smooth Ultrananocrystalline Diamond Films by Microwave Plasma-Assisted Chemical Vapor Deposition

W.S. Huang, D. T. Tran, J. Asmussen[1], T.A.Grotjohn, and D.Reinhard

Michigan State University, 2120 Engineering Building, Electrical & Computer Engineering Department, East Lansing, MI 48824

[1]Fraunhofer USA, Center for Coatings and Laser Applications, B100 Engineering Research Complex, Michigan State University, East Lansing, Michigan 48826-1226

Keywords: Diamond deposition; Microwave plasma CVD; Ultrananocrystalline diamond Films; Film thickness uniformity and smoothness.

Abstract

Applications of Ultrananocrystalline (UNCD) and Nanocrystalline (NC) diamond films have been a common, recent topic of many investigations. The exceptional properties of these films, such as high hardness and chemical inertness combined with their small crystal size and smoothness and excellent mechanical properties such as high Young's modulus, fracture toughness and low coefficient of friction, have suggested application as a protective, hard coating material, a material/substrate for micromechanical systems, a SAW device substrate [1], a robust conducting coating for electrochemical electrodes, and as a freestanding film for vacuum windows or ion beam stripping foils. The commercial success of each of these applications requires the development of repeatable, CVD diamond thin film synthesis processes that are able to deposit these films on a variety of substrates. Additionally, uniform, large area, stress free, thick and thin film deposition is desirable. In this paper we report on the development of process methods and apparatus that enable the uniform and smooth deposition of both thin and thick (> 50 microns) UNCD.

UNCD films are synthesized by microwave plasma-assisted CVD using $Ar/H_2/CH_4$ (i.e. see Zhou et. al. [2]) and $He/H_2/CH_4$ input gas mixtures. The microwave plasma reactor system consists of a variable power, 6KW, and 2.45 GHz power supply, connected to a tunable, cylindrical cavity applicator in which the microwave discharge is confined inside a 12cm diameter cylindrical quartz dome located at the fixed end plate of the applicator [3]. The substrate, typically a three inch diameter silicon wafer, is placed on a stage that is adjusted to place the substrate in direct contact with the microwave discharge. The discharge assumes an intense, hemispherical shape hovering over and in direct contact with the substrate. During each deposition experiment the cavity is tuned and the plasma is adjusted for uniform species and temperature conditions across the substrate. Deposition experiments employ either a thermally floating substrate operation [4] or if desirable the substrate can also be cooled in order to vary the substrate temperature between 550- 850 C. A wide range of experimental conditions, i.e. pressures from 50-250Torr, input powers between 600-2,000 W, variable gas mixtures and flow rates, substrate placement, etc., were explored to identify the optimal conditions that enable the repeatable deposition of uniform, and smooth UNCD films over three inches.

The experimental behavior will be presented. In particular UNCD synthesis, i.e. growth rate, film uniformity and smoothness, are described versus the variables of input power (600-1500W), pressure (80-220 Torr), and input gas chemistry, i.e. H_2 (1-8%) and CH_4 (1-3%). Our experiments have demonstrated that in order to routinely synthesize high quality, smooth and uniform UNCD films the deposition process must be performed in a high purity environment. A large useful UNCD experimental deposition window (80-220Torr, 600-1500W, H_2 1-3%, CH_4 1-2%) was identified. Using 0-1% H_2, i.e. hydrogen deficient conditions, discharges were sustained in contact with the three inch substrates over a 60-200 Torr pressure regime. High quality film deposition was extended to 240 Torr when H_2 concentrations were increased to 1-3%. At a given pressure uniform deposition was achieved by optimizing substrate holder geometry, substrate position, microwave power, and gas chemistry. Film crystal sizes ranged from 3-30nm and film roughness from 11-50 nm and average film thickness over the substrate, which depends on the deposition time, ranged from a few hundred nanometers to over 50 microns. With an additional, modest post deposition mechanical polishing, a surface roughness of 3nm was obtained. Film uniformities of greater than 96% were achieved over three inch silicon wafers. Growth rate increased with increasing pressure, and hydrogen concentration. At pressures of 220 Torr and with CH_4 of 1% and H_2 of approximately 3% the average linear growth rate over the three inches wafer was approximately 1 micron per hour.

REFERENCES

1. B. Bi, et al., "Surface acoustic waves in nanocrystalline diamond," *Diamond and Related Materials*, 11, 677-708, (2002).

2. D. Zhou, et al., "Control of diamond Film microstructure by Ar additions to CH_4/H_2 microwave plasmas," J. Appl. Phys., 84, 1981- 1989, (1998).

3. K. P. Kuo and J. Asmussen, "An experimental study of high pressure synthesis of diamond films using a microwave cavity plasma reactor," *Diamond and Related Materials*, 6, 1097-1105, (1997).

4. T.A. Grotjohn and J. Asmussen, " Microwave plasma-assisted Diamond Film Deposition," *Diamond Films Handbook*, Chapter 7, pp. 211-302, edited by J. Asmussen and D. K. Reinhard, Marcel Dekker, New York, (2002).

DEPOSITION OF (U)NCD FILMS USING HOT-FILAMENT CVD

Paul W. May

School of Chemistry, University of Bristol, Bristol BS8 1TS, U.K.

Keywords: nanocrystalline diamond, hot filament CVD, $Ar/CH_4/H_2$ gas mixtures.

Abstract

$Ar/CH_4/H_2$ gas mixtures have been used in an attempt to deposit nanocrystalline and ultrananocrystalline diamond films using hot filament CVD. It was found that the standard gas mixtures of ~1%H_2 in 1%CH_4/Ar that are used successfully to grow UNCD films in microwave plasmas produce no film growth in a HF system. This is due to the carbon content of the gas being adsorbed onto the filament producing a thick graphitic covering, which rapidly reduces the efficiency of the filament inhibiting film growth. Increasing the H_2 content in the gas mixture improves the situation, but NCD was grown successfully only for H_2 concentrations above 40%, which more closely resemble the gas mixtures used for conventional microcrystalline CVD. These results will be discussed in terms of the implications for growth mechanisms of (U)NCD.

ENHANCED NUCLEATION OF ULTRANANOCRYSTALLINE DIAMOND (UNCD) USING TUNGSTEN (W) FILMS

Nevin Naguib, Jian Wang, Orlando Auciello and John A. Carlisle

Materials Science Division, Argonne National Laboratory

9700 S. Cass Ave, Argonne, IL 60439

Jeff Elam

Energy System Division, Argonne National Laboratory

9700 S. Cass Ave, Argonne, IL 60439

James Birrell

Advanced Diamond Technologies

60 Hazelwood Drive, Suite 226, Champaign, IL 61820

Keywords: Ultrananocrystalline Diamond (UNCD), Tungsten (W), Nucleation and Roughness.

Abstract

The initial nucleation density is critical in determining both the microstructure and the properties of Ultrananocrystalline Diamond (UNCD) films. Unlike hydrogen grown diamond thin films, the UNCD growth process results in a high re-nucleation rate, and thus the overall grain size is not limited by the initial nucleation density. Thus, controlling the nucleation density is critical in determining the quality of UNCD thin films, especially for facilitating the growth of low-temperature UNCD thin films and maximizing the mechanical and tribological properties of UNCD for potential MEMS applications.

Many techniques have been used to enhance the nucleation of diamond thin films. Unfortunately, most nucleation enhancement techniques have drawbacks. For instance, the "Rotter nucleation technique"[1] requires high temperatures while the bias[2] and chemical methods [3] have not been widely standardized into a common nucleation enhancement techniques.

UNCD is commonly grown on refractory metal substrates in order to integrate the growth of UNCD with a standardized process for generating a high initial nucleation density, while being compatible with low temperature growth of UNCD. In this study, we apply thin tungsten (W) films onto silicon surfaces prior to ultrasonic seeding. The thickness of the W layers varies from 36 Å to 100 Å. The influence of W on the subsequent UNCD nucleation and growth is examined. We have found that the initial UNCD nucleation density is enhanced considerably using W films from 10^{11} to $\geq 10^{12}$ sites/cm^2. Furthermore, by using W films, the initial UNCD growth rate is increased (less time is needed to grow a uniform UNCD film), while the surface roughness and interfacial void density are decreased.

In addition to using conventional RF sputtering techniques to deposit the W films, we also employ atomic layer deposition (ALD). ALD offers the flexibility for depositing W films on complex, nonplanar surfaces while maintaining monolayer thickness control. Scanning Electron Microscopy (SEM) results show considerable enhancement in nucleation density using both RF sputtered and ALD W on planar substrates as shown in Figure 1. The surface roughness of UNCD films grown on W films using the above two techniques will be compared using Atomic Force Microscopy (AFM).

This work was supported by the DOE-Office of science-Materials Science under Contract No. W-31-109-ENG-38.

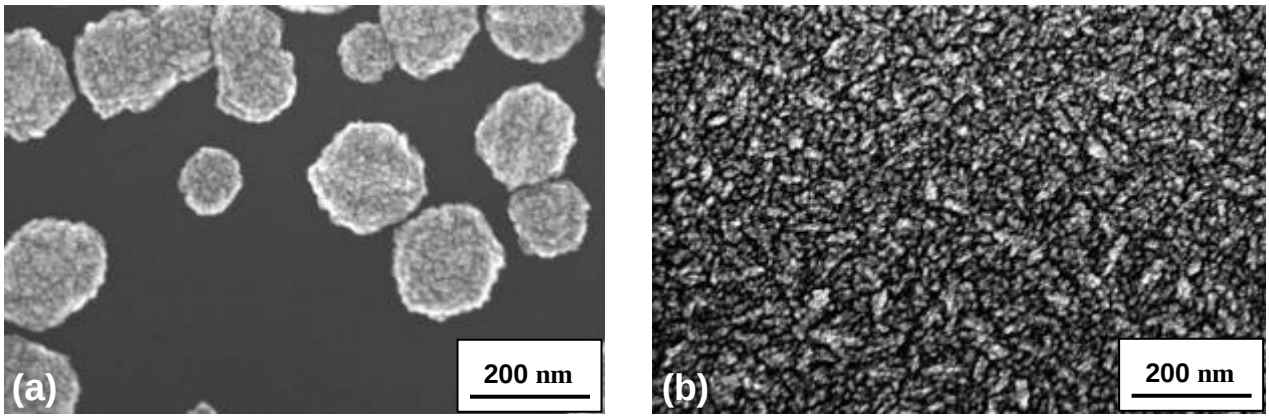

Figure 1: SEM images of UNCD films (grown at the same time under identical seeding conditions); (a) without W film added and (b) with W film (100Å thickness). The nucleation density has been dramatically increased by using the W film.

REFERENCES:

1. S. Rotter, *Proceedings of the Applied Diamond Conference/Frontier Carbon Technologies ADC/FCT '99*, edited by M. Yoshikawa, Y. Koga, Y. Tzeng, C.- P. Klages, and K. Miyoshi, ~MYU K.K., Tokyo, 25 (1999).

2. See, for example, S. Saada, S. Barrat, E. Bauer-Grosse, *Diamond & Rel. Mater.*, **10**, 300 – 305 (2001).

3. Anne Giraud, et.al , *J. Am. Chem. Soc.*, **123**, 2271 – 2274 (2001).

IMPROVEMENT ON THE GROWTH OF ULTRANANOCRYSTALLINE DIAMOND BY USING PRE-NUCLEATION TECHNIQUE

Yen-Chih Lee, Su-Jien Lin

Department of Material Science and Engineering, National Tsing-Hua University, Hsin-Chu 300, Taiwan, R. O. C.

I-Nan Lin

Department of Physics, Tamkang University, Tamsui 251, Taiwan, R. O. C.

Keywords: UNCD, high speed growth, BEN, MPECVD

Abstract

Diamond and related materials have many potential applications due to their marvelous physical and chemical properties. However, most of the applications require smooth surface. The difficulty in polishing the diamond films frequently hinders the development of device applications. Moreover, the applications such as surface acoustic wave (SAW) devices require relatively thick diamonds films, which call for a high growth rate process. In this study, ultrananocrystalline diamond (UNCD) films, which possess very smooth surface, were synthesized using CH_4/Ar plasma. The Si-substrate was pre-nucleated using bias enhanced nucleation (BEN) technique under CH_4/H_2 plasma, so that the growth of UNCD films can be markedly enhanced. The UNCD films were grown in a 2.45 GHz microwave plasma enhanced chemical vapor deposition (MPECVD) system. The growth rate of these UNCD films were observed to be correlated intimately with the deposition conditions, such as substrate temperature, microwave power, total pressure, CH_4 ratio. The nucleation process was carried out under methane and hydrogen (CH_4/H_2) plasma with negative DC bias voltage. No pretreatment on substrate was required prior to the formation of diamond nuclei. The growth kinetics of BEN induced nuclei was monitored by the evolution of the bias current to ensure the full coverage of diamond nuclei on the Si-substrate. The average grain size of BEN induced diamond nuclei is about 30 nm (Fig. 1), with the nucleation site density more than 10^{11} sites/cm^2. The thickness of BEN induced diamond nuclei layer was about 250 nm. The growth rate of UNCD is markedly enhanced due to the application of BEN induced nuclei. Moreover, the growth rate of UNCD films was more significantly affected by the substrate temperature, but was less influenced by the microwave power. All of these UNCD films showed similar morphology, i.e., with grain size less than 10 nm and surface roughness around 20 nm (Fig. 2). They also possess the same Raman spectra, i.e., the same crystallinity. However, the deposition rate can be increased from about 0.2 μm/hr to 1.0 μm/hr when substrate temperature increased from 400^0C 600^oC. How the characteristics of these UNCD correlated with their electron field emission properties will be discussed.

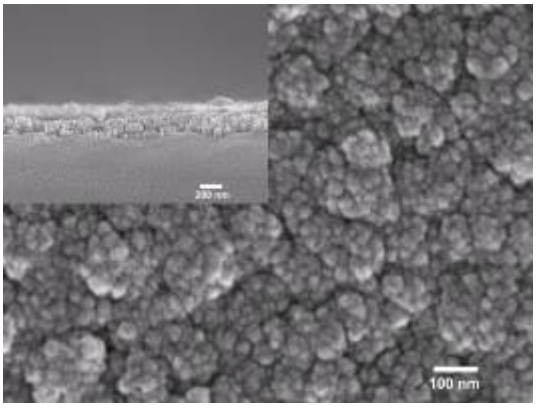

Figure 1. SEM surface morphology of BEN nanodiamond with the inset showing the cross-section.

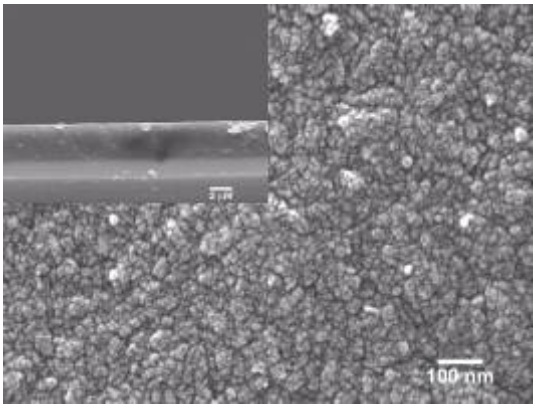

Figure* 2. *SEM surface morphology of UNCD grown under 600°C, 3 hr with the inset showing the cross-section.

REFERENCES

1. B. Bi, W. -S. Huang, and J. Asmushen et al., "Surface acoustic waves on nanocrystalline diamond", ***Diamond Relat. Mater.*** **11**, 677 (2002).
2. D. M. Gruen., A. R. Krauss, and C. D. Zuiker et al., "Characterization of nanocrystalline diamond films by core-level photoabsorption", ***Appl. Phys. Lett.*** **68 (12)**, 1640 (1996).
3. X. Xiao, J. Birrell, and J. E. Gerbi et al., "Low temperature growth of ultrananocrystalline diamond", ***J. Appl. Phys.*** **96 (4)**, 2232 (2004).
4. T. Sharda, T. Soga, T. and Jimbo et al., "Bias enhanced growth of nanocrystalline diamond films by microwave plasma chemical vapor deposition", ***Diamond Relat. Mater.*** **9**, 1331 (2000).

IMPROVING THE ADHESION PROPERTIES OF NANOCRYSTALLINE DIAMOND FILMS BY BIAS-ENHANCED NUCLEATION

Erica Mujica, Fabrice Piazza, Gerardo Morell

Dept. of Physics, University of Puerto Rico, San Juan, Puerto Rico

Scott Wolter

Electrical and Computer Engineering, Duke University, Durham, NC, USA

Keywords: diamond, nanocrystalline, bias-enhanced, chemical vapor deposition, adhesion

Abstract

Nanocrystalline diamond films (including materials referred to as tetrahedrally-bonded carbon films, ultra-nanocrystalline diamond films, and nanostructured diamond films) are highly strained materials that show a strong tendency to delaminate at relatively small thickness values around 5 microns. This situation often precludes from taking advantage of the many extreme properties of diamond that make it suitable for protective and tribological coatings (i.e. extreme hardness, radiation hardness, chemical inertness). We have employed bias-enhanced nucleation (BEN) performed in a microwave-plasma chemical vapor deposition (MWCVD) system to implant seed nanostructures in the substrate that favor the formation of strongly adherent layer at the substrate-film interface. Nanocrystalline diamond films are deposited on the BEN substrates using a hot-filament chemical vapor deposition (HFCVD) system in the continuous secondary nucleation mode that results in the deposition of nanocrystalline diamond. The observed changes in the films' structure (Fig. 1) indicates the controlling role that seeding has on film evolution. Although the films remain highly strained at the nanoscale, as evidenced from the Raman spectra (Fig. 2), they can be grown to large thickness values without compromising the substrate adhesion. Thermal shock tests evidenced the ability of these films to differentially expand and contract while remaining firmly attached to the substrate. These results are discussed in terms of the formation of a thin strong disordered carbide buffer layer at the substrate-film interface capable to adjust and accommodate dynamically any lattice mismatch. The formation of this thin carbide layer is strongly enhanced by the application of BEN to the substrates.

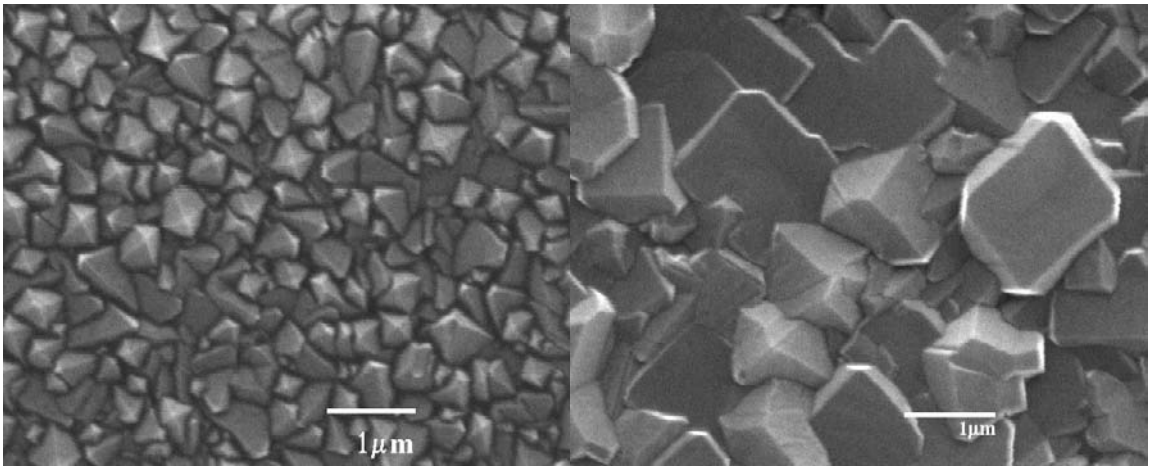

Figure 1. Substrate seeded using BEN in MWCVD (left) showing pyramidal growth habit, and diamond film grown by HFCVD on top (left) showing square growth habit.

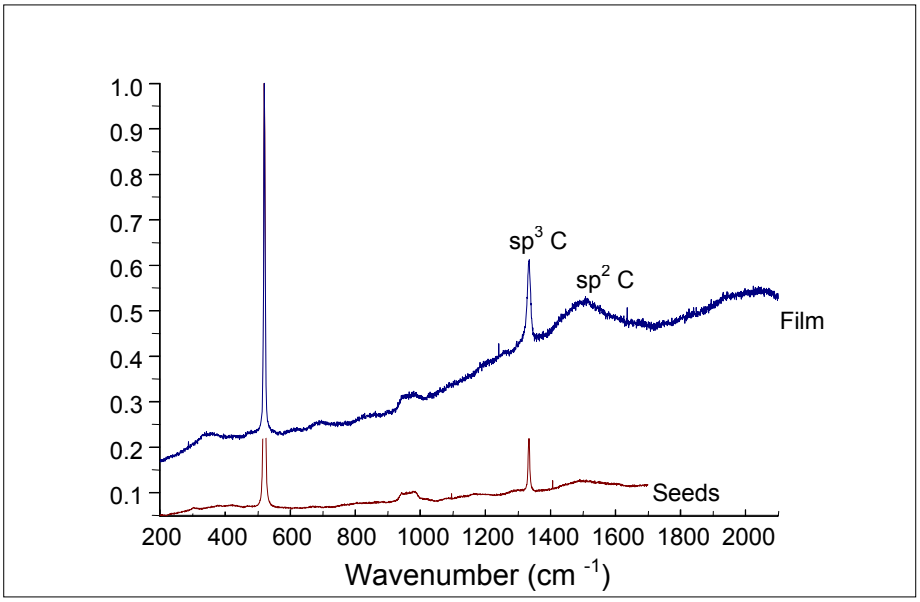

Figure 2. Microcrystalline Diamond (sp^3 C) and Graphitic Carbon (sp^2 C) Raman features of the MWCVD BEN seeds subsequent HFCVD film

Acknowledgements: Research supported by NASA (Grants NCC3-1034 and NGT5-40091; Cooperative Agreement NCC5-595), Department of Energy (Grant DE-FG02-01ER45868), and the UPR-Río Piedras FIPI (Grant 8-80-514).

REFERENCES

1. S.D. Wolter, F. Okuzumi, J.T. Prater, and Z. Sitar, AC vs. DC bias-enhanced nucleation of highly oriented diamond on silicon (100), J. Electrochem. Soc., 149, G114-117 (2002).
2. S. Gupta, B.R. Weiner, G. Morell, Synthesis and characterization of sulfur-incorporated microcrystalline diamond and nanocrystalline carbon thin films by hot filament chemical vapor deposition, Journal of Materials Research 18, 363 (2003).

FORMATION OF DIAMOND WHISKERS BY RF PLASMA ETCHING

C.Y. Li and A. Hatta

Department of Electronic and Photonic Systems Engineering, Kochi University of Technology,
185 Miyanokuchi, Tosayamada-cho, Kami-gun, Kochi 782-8502, Japan

Keywords: diamond films, whiskers, reactive ion etching, plasma

Abstract

Diamond whiskers were fabricated by means of radio frequency plasma etching. Metal particles were coated onto diamond films to serve as micro-masks before etching. Etching processing was performed using O_2/Ar plasmas, with an emphasis to elucidate the effects of reacting gas on the fabrication of diamond whiskers. The results showed that the densities and the distributions of diamond whiskers depended on the volumetric ratio of O_2 to Ar. Raman spectroscopy was carried out in order to determine the bonding structures of the whiskers. It has been found that the whiskers were still diamond after etching. X-ray photoelectron spectroscopy was carried out to investigate the components of diamond surface after etching. Field emission characteristics of the whiskers were also inspected.

I. INTRODUCTION

Diamond films are attractive to applications in cathode electron field emission devices [1]. It was reported that the electron field emission would be enhanced at the micro-tips of diamond [2]. Among the various approaches for fabrication of sharper field emission tips, reactive ion etching (RIE) in radio frequency (RF) plasmas is considered as an efficient method to sharpen diamond micro-rods [3]. In this paper, a novel method for fabrication of whiskers in O_2/Ar plasmas was reported. A comparison of the morphologies of diamond surfaces before and after etchings demonstrated that the properties of whiskers were dependent on the reacting gas, respectively.

2. EXPERIMENT DETAILS

Polycrystalline diamond films were deposited onto Si substrates using a microwave plasma chemical vapor deposition (PCVD) reactor system ASTeX (AX-6350). The deposition process was carried out under pressure of 124 torr, microwave power of 5 kW, and flow rates of 25 and 475 sccm for CH_4 and H_2, respectively. During the deposition, the substrate temperature was kept at 900-950 ℃, monitored by a spot thermometer. The diamond films were coated using metal particles after growing to 3 μm in thickness. The etching process was performed for 60 min in a self-assembled RF plasma reactor with frequency of 13.56 MHz. The chamber pressure was maintained at 22 Pa. Reacting gases were introduced through a mass flow controller. The RF power was 100 W, corresponding to a DC self-bias voltage of -510 V. In this study, the gas compositions examined were O_2 (10 sccm)/Ar (90 sccm), O_2 (20 sccm)/Ar (35 sccm), O_2 (100 sccm), and Ar (100 sccm).

3. RESULTS AND DISCUSSION

Figure 1 presented the SEM images of the diamond surfaces after etching. Whiskers were found on the surfaces of the samples. An interesting phenomenon was that the distribution of whiskers was not random. For etching in O_2/Ar plasma with 10% O_2 (vol/vol), whiskers with 150 nm diameter and 200 nm height formed only at the grain boundaries, suggesting that the whiskers might form preferentially at the grain boundaries between diamond crystals [4]. However, with increasing O_2 concentration (O_2: 36%), the whiskers extended gradually into the diamond grains. It could be noticed that the height of the whiskers remarkably increased to 900 nm. When the O_2 ratio approached to 100%, the whiskers had the highest density (40/μm^{-2}). The average diameter of the whiskers reduced to 100 nm with a height of 1 μm. In inert gas Ar (100 sccm), whiskers could not be formed on the surfaces after etching.

In general, there were two processes during the RF plasma etching [5]. Inert gas plasma only caused physical bombardment etching which could explain why whiskers could not be obtained in pure Ar. However, the etching process was different in Ar and O_2 mixture plasmas. Whiskers obtained in the latter could be ascribed to the processes of ion-enhanced chemical etching and physical bombardment etching. O_2 would dissociate into O radicals accompanied by the formation of volatile products of CO and CO_2, while Ar would contribute to bombarding the diamond surfaces. [6,7].

All of above suggested that the density and height of whiskers increased with increasing flow ratio of O_2 to Ar. It is conceivable that the formation of whiskers could be controlled by changing the concentration of O_2 in the reacting gas.

The metal masks were also critical to the erosion of diamond films. In this experiment,Al was masked on the diamond surfaces before etching, it would react with O_2 to form Al_2O_3 islands on the tops of the whiskers, inhibiting the etching underneath [8,9]. Thus, the distribution of whiskers might be controlled by masking metals on the diamond surfaces. The remains of metal particles on the tops of whiskers were examined by XPS.

In order to determine the structures of whiskers, Raman spectroscopy was performed for samples before and after etchings. In Fig.2, the Raman spectrum showed a diamond (sp^3 bonding) peak at 1331 cm^{-1} along with a low broad non-diamond (sp^2 bonding) peak at 1580 cm^{-1}. The presence of a weak graphite peak might be attributed to a small amount of local transformation from sp^3 to sp^2. Most of the bonding structures were kept on sp^3 diamond structures during etching process. Therefore, we could conclude that the whiskers were still diamond after etching.

Samples after etching were treated in hydrogen plasma for 8 min before field emission measurement. A turn-on field of 10 V/μm was obtained for the whiskers etched in pure O_2 plasma.

4. CONCLUSION

Reactive ion etching in RF plasmas is an effective method to obtain diamond whiskers. The densities and the distributions of whiskers could be controlled by adjusting the volumetric ratio of O_2 to Ar and by means of appropriate metal masks. There were few changes in the bonding structures of the whiskers, and the diamond structures remained unchanged after etching. The turn-on field of the whiskers was as low as 10 V/μm. Therefore, it is possible to use whiskers to cathode emission devices.

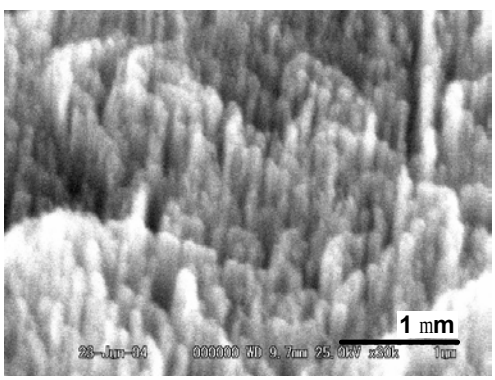

Fig.1. SEM images of diamond whiskers obtained from etching in O_2 (100 sccm).

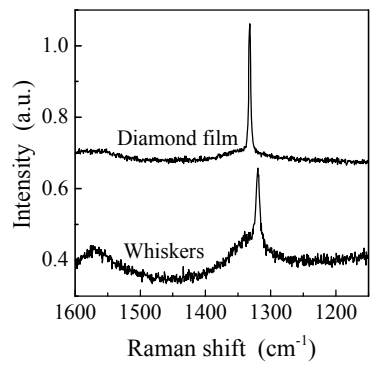

Fig.2. Raman spectra for the diamond film and the whiskers (Al coated, O_2 100 sccm, etched 60 min).

REFERENCES

1. M.Y. Teng, K.S. Liu, H.F. Cheng, I.N. Lin, Diamond and Relat. Mater, **12**, 450 (2003).
2. T. Tyler, V. V. Zhinov, A. V. Kvit, D. Kang, and J. J. Hren, Appl. Phys. Lett., **82**, 2904 (2003).
3. A. S. Barnard, S. P. Russo, and I. K. Snook, Phys. Rev., B **68**, 235407 (2003).
4. T. Tyler, V. V. Zhirnor, A. V. Kvit, D. Kang, and J. J. Hren, Appl. Phys. Lett., **82**, 2901 (2003).
5. E. S. Baik and Y. J. Baik, J. Mater. Res., **15**, 924 (2000).
6. P. W. Leech, G. K. Reeves, A. Hollolland, J. Mater. Sci., **36**, 3453-3459 (2001).
7. M. Berrnard, A. Deneuville, L. Ortega, K. Ayadi, P. Muret, Diamond and Relat. Mater, **13**, 290 (2004).
8. S. W. Lee, Appl. Surface Sci., **215**, 267 (2003).
9. Y. Ando, Y. Nishibayashi, K. Kobashi, T. Hirao, K. Oura, Diamond Relat. Mater, **11,** 824 (2002).

LIQUID CARBON SOURCES FOR DEPOSITION OF NANOSTRUCTURAL DIAMOND

T. V. Semikina, K. Gyoda, Y. Takagi

Teikyo University of Science and Technology, Japan

takagi@ntu.ac.jp

Keywords: Nanostructural diamond, hot filament CVD, liquid carbon source.

Abstract

Nanostructural diamond particles were obtained by hot filament CVD methods from vapor of liquid carbon sources and hydrogen-rich atmosphere on Si and Al_2O_3 ceramics substrates with different reaction times. During the studying the relation of gases and total pressure was changed. SEM and Raman spectrum demonstrated the diamond nature of obtained "cauliflower-like" particles.

NUCLEATION AND GROWTH, EXPERIMENTAL

In this work it is reported about nanostructural diamond deposition by hot filament chemical-vapor deposition method. The vapor of liquid acetone, butyl alcohol and ethanol were used as carbon sources. Nanostructural diamond was deposited on substrates of silicon and Al_2O_3 ceramics. Technological parameters of deposition are presented in Table 1. The influence of liquid carbon sources, substrates, reaction times, pressure ratios of hydrogen and vapor of carbon source, and total pressure on the results of deposition was studied in this work.

Table 1. Technological conditions nanodiamond deposition.

Substrate type	Al_2O_3	Si	Si	Si	Si	Si	Si
Distance filament-substrate, mm	2	2.5	2.5	2.5	2.5	2.5	2.5
Reaction time, min	30	7; 10	10	15	7	7	5; 7; 10; 30
Filament temperature, ^{0}C	2300	2300	2300	2300	2300	2300	2300
Substrate temperature, ^{0}C	700	780	780	780	780	780	780
Hydrogen pressure, Torr	294	595	597	600	472	531	590
Acetone pressure, Torr	6	-	-	-	8	9	10
Butyl alcohol pressure, Torr	-	5	3	-	-	-	-
Ethanol pressure, Torr	-	-	-	10	-	-	-
Total pressure, Torr	300	600	600	610	480	540	600

The diamond particles were characterized with field-emission scanning electron microscopy (SEM) and micro-Raman spectroscopy. The results of some samples are presented on the figure 1, and figure 2. Raman spectrum exhibits a first-order diamond peak centered at 1330-1332 cm^{-1}. For all samples it was observed the wide signals in the range at 1400-1600 cm^{-1} that certify graphite presence during the deposition process. SEM images of obtained diamond particles are similar the results reported in work [1, 2, 3] and by the same way can be characterized as "Cauliflower-like". Our cauliflower-like diamond particles were deposited for both substrate types and from all carbon liquid sources. From SEM it is seen that size of diamond particles formed cauliflower particles varies from 70 nm to 1.4 μm for process running 30 min. But during experiment it was found that reaction time has the big influence on the size of grown particles even for our case when the longest deposition time makes up only 30 min. It means that size of diamond particles deposited under shorter time was smaller and we observe the nanodiamond with size of 30-50 nm. We don't observe the dependence of shape of cauliflower-like particles from type of carbon liquid source.

The dependence of nanostructural diamond particle size on total pressure indicates that decreasing of total pressure leads to reduction of cauliflower-like diamond size and consequently to decreasing of size of particle formed it. It is difficult also to make a clear conclusion about influence of pressure relation between hydrogen and vapor of liquid carbon source, because their variation was not in wide area. One from the most interesting result obtained in this investigation is that nanostructural diamond was deposited in hydrogen-rich atmosphere without argon whose huge role was reported in many reports [1,4,5].

Thus it was found on present research that technological conditions allowed depositing nanostructural diamond from liquid carbon sources of different types on Si and Al_2O_3 substrates in hydrogen-rich atmosphere without Ar. This is a new result enhanced our knowledge about posibility of nanomaterial synthesis.

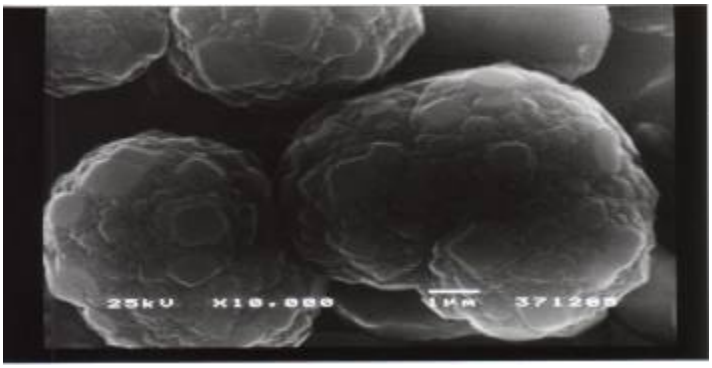

Figure1. SEM image of nanostructural diamond deposited on Al_2O_3 substrate for 30 min from acetone.

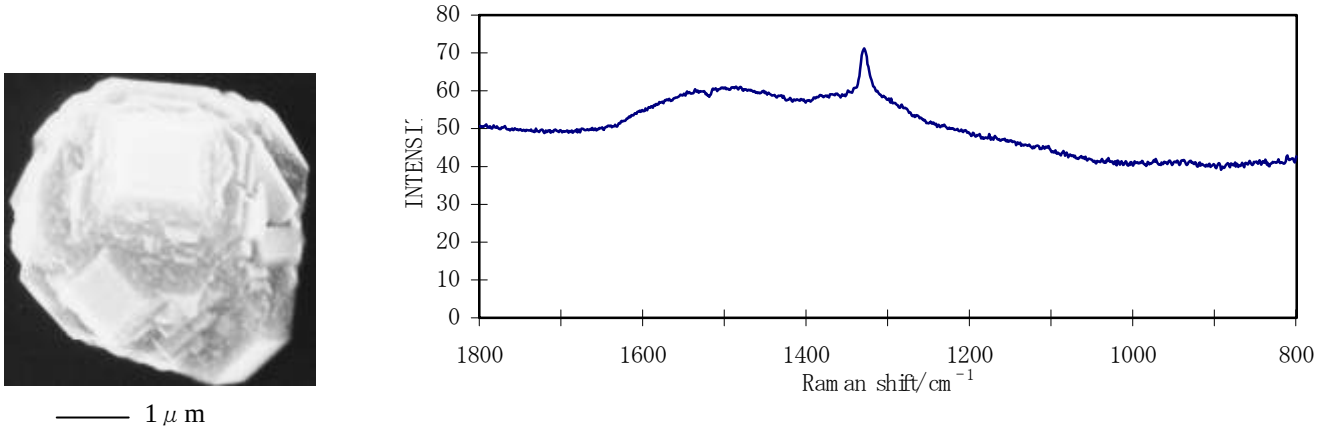

Figure 2. SEM and Raman for nanostructural diamond deposited on Si substrate for 10 min from acetone.

REFERENCES

1. Ferreira N.G., Beloto A.F., Amarai M., et al., "Nanodiamond films growth on porous silicon substrate for electrochemical application", *Abstract Book*, Elsevier, 15 th European Conference on Diamond, Diamond-like Materials, Carbon Nanotubes, Nitrides and Silicon Carbide "Diamond 2004", 12-17 Sept, 2004, Italy.
2. Subramanian K., Kang W.P., Davidson J.L., et al., "The effect of growth rate control on the morphology of nanocrystalline diamond", *Abstract Book*, Elsevier, 15 th European Conference on Diamond, Diamond-like Materials, Carbon Nanotubes, Nitrides and Silicon Carbide "Diamond 2004", 12-17 Sept, 2004, Italy.
3. Birell J., Gerbi J.E., Auciello O., et al., "Interpretation of the Raman spectra of ultrananocrystalline diamond", *Diamond and Related Materials*, Elsevier, 2004, article in press.
4. May P.V., Crichton E., Sage R., et al., "Experimental investigation and computer simulation on the growth mechanism for UNCD films", *Abstract Book*, Elsevier, 15 th European Conference on Diamond, Diamond-like Materials, Carbon Nanotubes, Nitrides and Silicon Carbide "Diamond 2004", 12-17 Sept, 2004, Italy.
5. Gruen D.M. "Nanocrystalline diamonds films", *Annu. Rev. Mater. Sci*, US Government, v.29, p.211-259, (1999).

NANOPOROUS CARBONS DERIVED FROM BLOCK COPOLYMERS WITH POLYACRYLONITRILE BLOCKS

Chuanbing Tang, Michal Kruk, Krzysztof Matyjaszewski, Tomasz Kowalewski

Department of Chemistry, Carnegie Mellon University, 4400 Fifth Avenue, Pittsburgh, Pennsylvania 15213

Ewa B. Celer, Mietek Jaroniec

Department of Chemistry, Kent State University, Kent, Ohio 44242

Keywords: polyacrylonitrile, block copolymer, nanoporous, atomic force microscopy

Abstract

Novel nanocarbons were synthesized from well-defined phase-separated polyacrylonitrile-poly(*n*-butyl acrylate) (PAN-*b*-PBA) diblock copolymers by pyrolysis, during which PAN domains were converted into carbon with concomitant decomposition of the PBA phase. The nanostructure of most of these materials resembled the morphology of their block copolymer precursors. Therefore, this new pathway allows for a control over nanocarbon architecture through a simple manipulation of block copolymer structure, including its composition and molecular weight. A variety of nanoscale morphologies, such as carbon (hemi)spheres, cylinders and lamellae were prepared using this route. Remarkably, this pathway opens an excellent chance to prepare thin or thick-film based carbons, which are usually difficult to be obtained by other methods, including the use of silica templates. The block copolymer precursors and corresponding nanostructured carbons were characterized by a variety of techniques, including atomic force microscopy, differential scanning calorimetry, thermogravimetry, transmission electron microscopy (TEM), X-ray diffraction, and Raman spectroscopy. Thermal behavior of PAN and PBA segments was thoroughly investigated and clarified. The carbons derived from PAN-b-PBA copolymers exhibit a certain degree of stacking of graphene sheets into semi-graphitic domains, but the degree of perfection of these structures is low. Further studies indicate that these carbon materials display nanoporosity in both bulk and film states, as determined by TEM and nitrogen adsorption. Our study of these materials is one of the earliest reports on the preparation of nanoporous carbons from block copolymers and our approach appears to be very convenient and attractive in applications requiring well-defined nanostructured carbon films.

REFERENCES

1. Kowalewski, T., Tsarevsky, N. V. and Matyjaszewski, K., "Nanostructured carbon arrays from block copolymers of polyacrylonitrile", *J. Am. Chem. Soc.*, 124, 36, 10632-10633 (2002).
2. Tang, C., Qi, K., Wooley, K., Matyjaszewski, K. and Kowalewski, T., "Well-defined Carbon Nanoparticles Prepared from Water Soluble Shell Cross-linked Micelles Containing Polyacrylonitrile Cores", *Angew. Chem. Int. Ed.*, 43, 2783-2787 (2004).
3. Tang, C., Kowalewski, T. and Matyjaszewski, K., "Preparation of Polyacrylonitrile-block-Poly(n-butyl acrylate) Copolymers Using Atom Transfer Radical Polymerization and Nitroxide Mediated Polymerization Processes", *Macromolecules*, 36, 5, 1465-1473 (2003).

Growth and Characterization of Aligned Carbon Nanotubes by Microwave Plasma Chemical Vapor Deposition

A. Vaseashta[1] and J. Carlisle[2]
[1]Materials Processing and Characterization Laboratories
Graduate Program in Physical Sciences and Department of Physics
Marshall University, Huntington, WV 25755-2570
[1,2] Argonne National Laboratory
9700 S. Cass Avenue
Argonne, IL 60439.

ABSTRACT

In this presentation, various growth aspects of aligned CNT using MPECVD are presented. Carbon nanotubes were grown in the same MPECVD system using hydrogen-methane-nitrogen gas reactants on a few nanometers thick metal catalyst layer on silicon substrates and characterized by Raman spectroscopy, high resolution scanning and transmission electron microscopy. Field emission investigation in terms of turn-on voltage, threshold voltage, and field enhancement factor will be presented and compared to the previously reported results. A low turn-on voltage and threshold voltage is desired for devices which can be employed for display and x-ray emission devices. Studies leading to emission stability, tip longevity, and triple junctions to boost emission will also be reported. A preliminary design of low power x-ray generation source will be presented. Many growth parameters are studied such as substrate temperature, microwave power, gas-pressure and different gas-ratios on the structural properties of both the materials. A correlation between the processing parameter and observed characteristics will be presented.

Keywords: MPECVD, carbon nanotubes, aligned CNTs

SYNTHESIS AND CHARACTERIZATION OF CARBIDE-DERIVED CARBON NANOWIRES

Xinqi Chen, Donald R. Cantrell, Sasha Stankovich, Rodney S. Ruoff

Department of Mechanical Engineering, Northwestern University, Evanston, IL 60208

Keywords: carbon nanowire, silicon carbide, CVD, TEM, surface area

Abstract

Carbon materials such as diamond, graphite, and amorphous carbon attract attention due to their physical and chemical properties. Gogotsi et al.[1] reported the synthesis of nano- and micro-crystalline "diamond-structured" carbon films by extracting silicon from the surface region of macroscopic silicon carbide samples with chlorine-containing gases at ambient pressure and temperatures not exceeding 1,000˚C. This "carbide-derived carbon (CDC) method" has been used for the conversion of carbide to nano-crystalline diamond and graphite films on SiC.[1,2] In this work, we have used small diameter silicon carbide whiskers as the precursor and have successfully extracted Si to create carbon nanowires by the CDC method.

The β-silicon carbide whiskers (Advanced Composite Materials Corp., South Carolina) used as the precursor in this work are of high purity (99%) with 0.45–0.65 micron diameters and 5- 80 micron lengths. Our X-ray diffraction (XRD) data of the as-received whiskers proves they are β-SiC. Silicon extraction experiments have been carried out in a home-built thermal chemical vapor deposition (CVD) apparatus. The green SiC whisker precursor material was converted to a dark black product after 8 hours of the extraction reaction at 1000°C. Transmission electron microscope (TEM) images are shown in Fig. 1(a) and (b). The high-resolution TEM image and electron diffraction data (not shown) indicate that the structure is amorphous. Energy Dispersive X-ray Analysis (EDX) has been performed on the product and the data in Fig. 1(c) show >97% carbon with the remainder being oxygen, silicon and chlorine. There was no significant variation of the composition across the specimen (by EDX analysis) for the 5 spots shown in Fig. 1(a). The fraction of sp^2-bonded atoms in the specimen is ~0.88 according to EELS analysis.

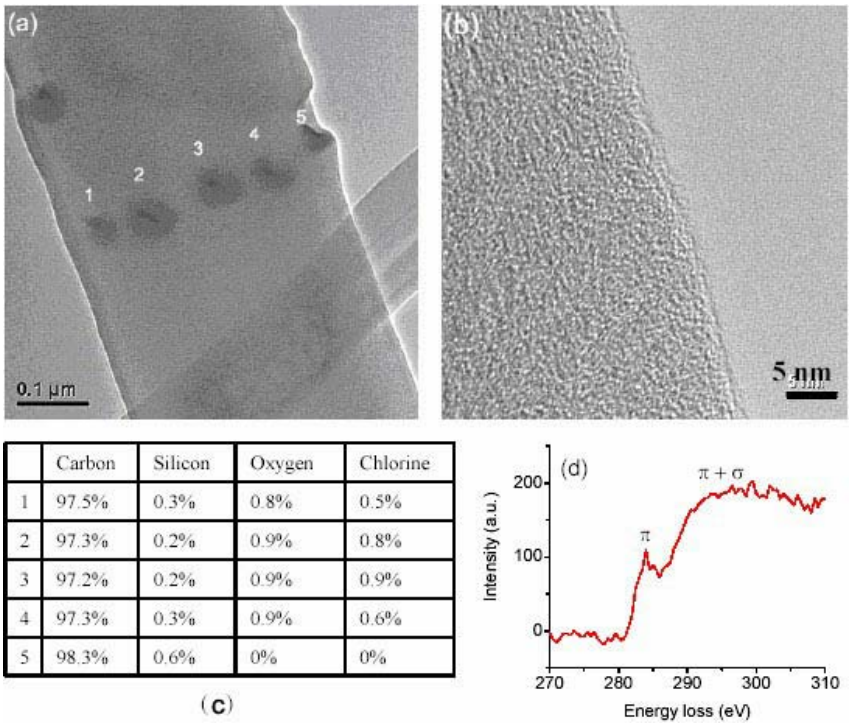

	Carbon	Silicon	Oxygen	Chlorine
1	97.5%	0.3%	0.8%	0.5%
2	97.3%	0.2%	0.9%	0.8%
3	97.2%	0.2%	0.9%	0.9%
4	97.3%	0.3%	0.9%	0.6%
5	98.3%	0.6%	0%	0%

(c)

Figure 1. (a) Low-magnification TEM image of the product nanowire; (b) High-magnification TEM image of the product nanowire; (c) atomic percentages assigned by the Hitachi HF-2000 software from the five spots in (a); (d) EELS spectrum taken with the Hitachi HF-2000 at the edge of the product nanowire.

Materials with high specific surface area and controlled pore size distribution have potential applications as molecular sieves, and for gas storage, catalysis, and use as absorbents, battery electrodes, supercapacitors, water/air filters, and medical devices. The TEM images of these carbon nanowires suggest a nanoporous structure. The surface area and pore size have been measured with a *Micromeritics ASAP 2010 Accelerated Surface Area and Porosimetry* analyzer. Isotherms of the adsorption of nitrogen were recorded at -195.8 $^{\circ}$ C. The Langmuir surface area obtained in one measurement on 100 mg of material was 1658 m^2/g and the surface area analyzed by the micropore analysis method for the same sample was 1978 m^2/g: *these two surface areas show we have synthesized a new ultra-high surface area material composed primarily of carbon and in nanowire form*. The pore size distribution was calculated by the Horvath-Kawazoe method and the median pore radius is 0.57 nm.

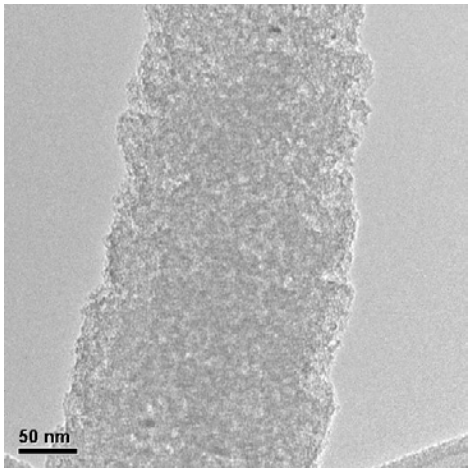

Figure 2. TEM image of porous carbon NW derived from silicon carbide.

In summary, we have converted silicon carbide whiskers to carbon nanowires by the CDC method and the analysis indicates that the carbon nanowires have very high surface area and a nano-porous structure. The EELS results show primarily sp^2 C-C bonding. We are currently trying to enhance the fraction of sp^3 bonding in an attempt to make diamond-like, or even single crystal diamond, nanowires.

Acknowledgement

RSR appreciates support from Northwestern University for this effort.

REFERENCES

1. Gogotsi, Y., et al., "Conversion of silicon carbide to crystalline diamond-structured carbon at ambient pressure", *Nature*, Vol. 411, No. 6835, 283 (2001).
2. Gogotsi, Y. G., Jeon, I.-D. & McNallan, M. J. "Carbon coatings on silicon carbide by reaction with chlorine-containing gases", *J. Mater. Chem.,* Vol. **7**, No. 9, 1841 (1997).

EFFECTS OF NH3 PLASMA PRETREATMENT ON THE GROWTH OF CARBON NANOTUBES

Shuxia Wang *,Peng Wang, Otto Zhou****

* Department of Physics, Chongqing University, Chongqing, 400044, P.R.C.

**Department of Physics and Astronomy and Curriculum in Applied and Materials Sciences, University of North Carolina, Chapel Hill, NC 27599

Keywords: Carbon Nanotube, catalyst, CVD, NH3 plasma

Abstract

Since the first discovery of carbon nanotubes (CNTs) in 1991[1], CNTs have attracted much attention. CNTs exhibit unique electronic and extraordinary mechanical properties. They have many potential applications. There are various synthetic methods for the production of CNTs[2-7]. CVD methods have many advantages. In CVD, it is believed that the catalyst on the substrate must be in the form of particles instead of smooth, continuous films and the CNT diameter tends to depend on the size of the catalyst particles. These catalysts can be deposited onto the substrate from solutions with pre-formed particles[8]or by physical techniques[9]. Physical techniques are quick, easy, and amenable to produce small patterns. The film thickness is a crucial parameter for the diameter and the density of the CNTs. The island size depends on the thickness of the initial catalyst films. Typical thin catalyst film thickness should be less than 20 nm. While the catalyst film thickness is more than 30 nm, a small grain size is not guaranteed. It is very difficult to grow thinner CNTs. Pretreatment further to break the film into desired particles should be taken.

NH3 is believed to be essential to the growth of CNTs in the CVD system[10]. The purpose of this paper is to study the pretreatment effect of NH3 plasma on CNT growth. In this paper, multi-wall carbon nanotubes have been grown on silicon substrates with NH3 plasma pretreatment to the thick catalyst films by CVD using C2H2/NH3 mixtures. The morphology and structure of carbon nanotubes were studied by scanning electron microscopy and transmission electron microscopy. Both concentric hollow and bamboo-type multi-wall carbon nanotubes were observed. The diameter, density, morphology and structure of carbon nanotubes changed with the plasma power and pretreatment time.

Under our experimental conditions, we believe the effects of NH3 plasma pretreatment for the nanotube growth by controlling the NH3 plasma power and pretreatment time in CVD method. CNTs grown on the substrate showed fairly good morphology. However, during pretreatment, using NH3 only without plasma resulted in worm-like carbon fibers. The NH3 plasma resulted in melting and roughening of the substrate surface, and this enhanced the formation of metal particles. It is confirmed that NH3 plasma plays an important role in promoting the formation of uniformly separated particles and reducing Fe. The ion bombardment energy in NH3 plasma leads to the thick catalyst film to particles, yielding the nanotube-growth enhancement. The results show that NH3 plasma density was found to be the primary factor in synthesizing CNTs during the pretreatment. NH3 plasma power and pretreatment time have to be optimized in order to grow uniform and density controlled nanotubes.

REFERENCES

[1] S. Iijima, Helical microtubules of graphitic carbon, Nature 354, 56 (1991)
[2] Chris Bower et al，Plasma-induced alignment of carbon nanotubes，Appl. Phys. Lett., 77,No.6,830 (2000)
[3] A. Thess, R. Lee, P. Nikolaev et al, Crystalline ropes of metallic carbon nanotubes, Science 273, 483 (1996)
[4] Z.F. Ren, Z.P. Huang, J.W. Xu et al, Synthesis of Large Arrays of Well-Aligned Carbon Nanotubes on Glass, Science 282, 1105 (1998)
[5] L.C. Qin, D. Zhou, A.R. Krauss et al, Growing carbon nanotubes by microwave plasma-enhanced chemical vapor deposition, Appl. Phys. Lett. 72, 3437(1998)
[6] S. Fan, M.G. Chapline,H. Dai et al, Self-Oriented Regular Arrays of Carbon Nanotubes and Their Field Emission Properties, Science 283, 512 (1999)

[7] C.J. Lee, D.W. Kim, T.J. Lee et al, Synthesis of aligned carbon nanotubes using thermal chemical vapor deposition, Chem. Phys. Lett. 312, 461 (1999)
[8]B. Kleinsorge, V. B. Golovko et al, Growth of aligned carbon nanofibres over large areas using colloidal catalysts at low temperatures C h e m . C o m m u n . , 1416(2 0 0 4)
[9] Delzeit L, Chen B, Cassell A M et al,Multilayered metal catalysts for controlling the density of single-walled carbon nanotube growth, Chem. Phys. Lett., 348, 368(2001)
[10]Ji-Beom Yoo, NH3 effect on the growth of carbon nanotubes on glass substrate in plasma enhanced chemical vapor deposition, Thin Solid Films 409, 120(2002)

STRUCTURE AND ELECTRONIC PROPERTIES OF NOVEL UNCONVENTIONAL CARBON ALLOTROPES AND BN POLYMORPHES

V.V. Pokropivny, V.L. Bekenev

Frantsevich Institute for Problems of Materials Science of NASU, 03142 Kiev, Ukraine

Keywords: Allotrop, polymorph, carbon, BN, structure, electron, novel phase

Unconventional allotropic modifications of carbon and polymorphic phases of boron nitride known in the literature are survived, including amorphic and metallic carbon, carbon C8, carbynes, nanotubular crystals, "cubic graphite", chaoites, E-phase, etc. Their structures predicted theoretically and found experimentally are collected, and analyzed critically.

Full set of fullerene clusters (molecules) as building units of close packed crystals was predicted theoretically. Elementary cells of face centered, body centered cubic, hexagonal, diamond and other lattices were designed.

Energy band structure, the equation of states, the densities of electronic states. and the electronic density map of novel allotropic modifications of carbon and polymorphes of BN have been calculated in first time by ab-initio FLAPW method.

Electronic structure of simple cubic fullerites SCF-C24 and fulborenite SCF-B12N12 shown in figure 1 have been calculated. The equilibrium interatomic distance aCC=0.1550 nm and aBN=0.1537 nm is intermediate between diamond (sphalerite) and graphite (h-BN). Band structure consists of 4 (6) filled bands with gap ~1.9 eV and ~0.1 eV respectively. The SCF-C24 was shown to be the diamond-like molecular semiconductor combining the nonpolarisability and porosity with the mechanical strength (bulk module B=308 GPa), chemical inertness, thermal stability and high thermal conductivity. All of these point on the SCF-C24 as the perspective low-dielectric material ($\varepsilon < 5.7$) for interconnectors and substrates for integrated circuits. The SCF-B12N12 was shown to be the diamond-like molecular semimetal.

Electronic structure of fulborenite SCF-B24N24 (fig.1) have been calculated. Its building units clusters B24N24 have been discovered recently in mass-spectra of arc-melting BN. Calculated parameters are: the equilibrium lattice parameter A=0.73458 nm, length of B-N bond aBN=0.1521 nm, number of atoms per unit cell Z=48, density ρ=2.495 g/sm3, bulk module B0= 367 GPa, band gap ΔEg=3.76 eV. It was concluded to be the heteropolar semiconductor or dielectric with specific bulk module higher then for cubic boron nitride.

Electronic structure of hyperdiamond fulborenite HDF-B12N12 (fig.1) have been calculated. Bulk module of HDF-B12N12 B=590 GPa is greater then for diamond (B=540 GPa). This novel boron nitride faujasite type polymorphe is expected to become an extremely super-hard semiconductor.

This research was made possible in part by Award UE2-2456-KV-02 of U.S. CRDF.

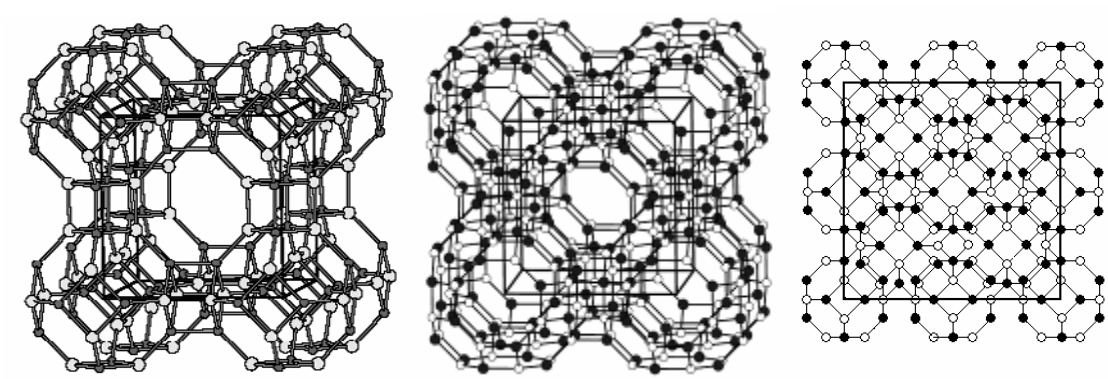

Fig. 1. Elementary cells of the simple cubic fulborenites SCF- $B_{12}N_{12}$ in which molecules $B_{12}N_{12}$ are covalently bonded by square faces, the SCF-$B_{24}N_{24}$ with molecules $B_{24}N_{24}$ bonded by octahedral faces, and hyperdiamonf fulborenite HDF-$B_{12}N_{12}$ with molecules $B_{12}N_{12}$ copolymerized by hexagonal faces.

DIRECT GROWTH OF BORON NITRIDE NANOTUBES ON SUBSTRATES

Yoke Khin Yap,* Jiesheng Wang, Vijaya Kayatha

Department of Physics, Michigan Technological University, 1400 Townsend Dr., Houghton, MI 49931, USA.

*ykyap@mtu.edu

Keywords: Boron nitride nanotubes, boron nitride, nanotubes, plasma, nanotechnology.

Abstract

We report here the first success of growing boron nitride nanotubes (BNNTs) on substrates. BNNTs have stable electronic properties (band gap of ~5.5 eV), which is independent of the tube diameter, number of walls, and chirality. Furthermore, this band gap can be tuned by substitution of carbon. Thus BNNTs are prospective for applications in nanoscale photonics and electronics devices. Previously, powder form BNNTs have been synthesized at temperatures >1100 °C. These products are mixed of various impurities including catalyst and BN particles. In this report, we describe the growth of BNNTs on substrates at 600 °C by a plasma-enhanced pulsed-laser deposition technique. Furthermore, these BNNTs are vertically-aligned on the substrate surface and can be grown at desired patterns and locations. We have demonstrated the growth of BNNTs in a series of matrix arrays (500 x 500 micrometers). This indicates that their growth is fully controllable by catalyst like the growth of carbon nanotubes. The growth of BNNTs is sensitive to the types of catalysts used, plasma density, and growth temperatures. At optimum condition, a well-defined growth region of BNNTs has been identified and explained. According to high-resolution field-emission scanning electron microscopy (FESEM), these BNNTs are grown in a base growth mode. This has been confirmed by high-resolution transmission electron microscopy (HRTEM). Furthermore, HRTEM indicates that these BNNTs are constructed of well-defined, multiwalled tubular structures with highly parallel tubular channels.

RESULTS AND DISCUSSION

Boron nitride nanotubes (BNNTs) were predicted after the discovery of carbon nanotubes (CNTs) [1]. They are expected to have a wide energy band gap of ~5.5 eV. This band gap is nearly independent of the tube diameter, number of walls, and chirality [2]. This means the electronic properties of BNNTs are uniform. Furthermore, it is possible to tune the band gap of BNNTs by substitution of carbon to make boron-carbon nitride (BCN) nanotubes. It is predicted that BC_2N nanotubes could have a band gap of about ~1.3 eV [3]. Thus BNNTs, and BCN nanotubes could be used for high-power electronic and photonic devices. Promising applications include the nanoscale laser, and light emitting devices (LED) with wavelengths tunable across the visible range into the ultraviolet. BN and BCN nanotubes are expected to accomplish the usage of CNTs as the building blocks for nanoscale devices in the new century.

Both BNNTs, and BCN nanotubes have received far less research attention than CNTs, probably because a high yield synthesis route has not been identified. BNNTs have been synthesized by catalytic arc discharge [4, 5], laser ablation [6, 7], a substitution reaction from CNTs [8], and chemical pyrolysis [9], typically at growth temperatures of 1100 to 3000 °C. Similar difficulty occurred on the growth of BCN nanotubes.

We think that effective growth of BNNTs is important and will lead toward systematic doping of BNNTs by carbon for achieving BCN nanotubes with tunable band gap. Besides a reasonably low growth temperature, accurate positioning of BNNTs and BCN nanotubes on are desired for the fabrication of most nanoscale devices. Here, we describe the first success of growing BNNTs on substrates at 600 °C by a plasma-enhanced pulsed laser deposition technique [10-12].

In Figure 1, images of vertically-aligned BNNTs are shown as detected by a high-resolution FESEM. As shown, these BNNTs can be grown as carbon nanotubes in most chemical vapor deposition technique. We think that this result will lead toward large-scale synthesis of BNNTs by various vapor phase deposition approaches. Details of these results will be discussed in the conference.

ACKNOWLEDGEMENT

Y.K.Y. acknowledges supports from the Michigan Tech Research Excellence Fund and the Army Research Office (W911NF-04-1-0029, through the City College of New York).

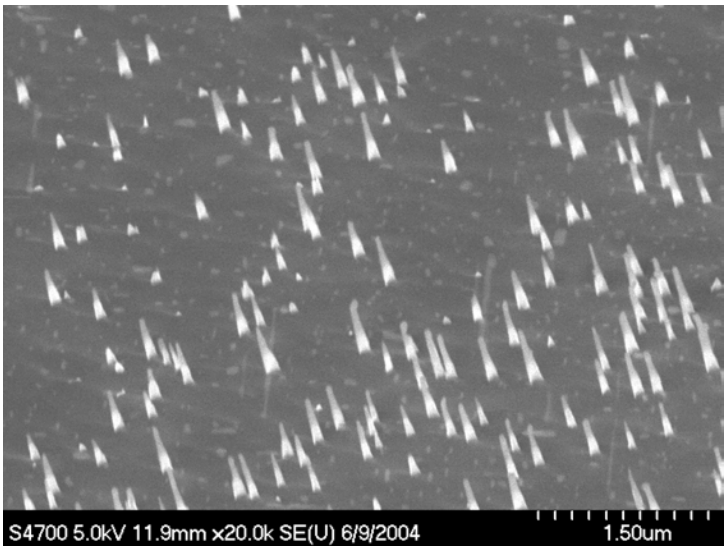

Figure 1. FESEM images of vertically-aligned BNNTs.

REFERENCES

1. Iijima, S., "Helical microtubules of graphitic carbon," Nature 354, 56 (1991).
2. Blasé X., et al, "Stability and band gap constancy of boron nitride nanotubes," Europhys. Letts. 28, 335 (1994).
3. Miyamoto, Y., et al., "Chiral tubules of hexagonal BC_2N," Phys. Rev. B. 50, 4976 (1994).
4. Chopra, N. G., et al., "Boron nitride nanotubes," Science 269, 966 (1995).
5. Loiseau, A., et al., "Boron nitride nanotubes with reduced number of layers synthesized by arc discharge," Phys. Rev. Lett. 76, 4737 (1996).
6. Golberg, D., et al., "Nanotubes in boron nitride laser heated at high pressure," Appl. Phys. Lett. 69 2046 (1996).
7. Yu, D. P. , et al., "Synthesis of boron nitride nanotubes by means of excimer laser ablation at high temperature," Appl. Phys. Lett. 72, 1966 (1998).
8. Han, W., et al., "Synthesis of boron nitride nanotubes from carbon nanotubes by a substitution reaction," Appl. Phys. Lett. 73, 3085 (1998).
9. Tang, C.; Bando, Y.; and Sato, T.: "Catalytic growth of boron nitride nanotubes," Chem. Phys. Lett. 362 185 (2002).
10. Yap, Y. K., et al., "Influence of negative dc bias voltage on structural transformation of carbon nitride at 600 °C," Appl. Phys. Lett. 73, 915 (1998).
11. Yap, Y. K., et al., "Hybridized boron-carbon nitride fibrous nanostructures on Ni substrates," Appl. Phys. Lett. 80, 2559 (2002).
12. Yap, Y. K., et al., "Formation of aligned-carbon nanotubes by RF-plasma-assisted pulsed-laser deposition, " *Special Issue for Tsukuba Symp. on Carbon Nanotubes in Commemoration of the 10th Anniversary of Its Discovery*; S. Ijima et al. Eds., Physica B 323, 341 (2002).

THERMODYNAMIC CONDITIONS OF ta-C FORMATION AT IMPLANTATION OF NOBLE-GAS IONS IN CARBON

A.I. Kalinichenko, S.S. Perepelkin, V.E. Strel'nitskij

National Science Center «Kharkov Institute of Physics and Technology»,

Akademicheskaya Str., 1, 61108, Kharkov, Ukraine. E-mail: strelnitskij@kipt.kharkov.ua

Keywords: ion implantation, diamondlike carbon, thermoelasticity, *P,T*-phase diagram, kinetic processes.

Abstract

Tetrahedral amorphous carbon (ta-C) formation at implantation of noble gas ions with energy from 25 to 1000 eV in carbon target is investigated in the model of thermoelastic peak (TEP). The dependences of radius, temperature and pressure in TEP on the ion energy were obtained. The *P,T* - trajectories of the points corresponding to the matter state in ion TEPs during acoustic and thermal relaxation were set on the phase *P,T*- diagram of carbon. The possibility of ta-C formation in TEP was qualitatively investigated from location of trajectory relative to boundary line "diamond - graphite". The effectiveness of «$sp^2 \rightarrow sp^3$» rearrangements in TEP was determined depending on sort and energy of the ion.

INTRODUCTION

As is known, the treatment of carbon by low-energy ions can promote its transformation to tetrahedral amorphous carbon (ta-C) [1]. There was intensive investigation of ta-C formation at $^{12}C^+$ ion implantation in carbon target (see, e.g. [1] and references there). The thermodynamic conditions of ta-c formation at implantation of C^+ ion in carbon were investigated theoretically in [2]. By hypothesis, these conditions are realized due to high temperature and pressure in thermoelastic peaks (TEPs) – nanometer-scale regions of matter where thermalized energy and volume of implanted ion are localized. The main features of this approach are taking into account the finiteness of initial dimension and origin time of TEP, as well as a combined action of temperature and all components of pressure in TEP on the rearrangement process.

In this paper, in the framework of the TEP concept [2], we perform a comparative analysis of conditions of ta-C formation at implantation of Ne^+ Ar^+, Kr^+ and Xe^+ ions with energy from 25 eV to 1000 eV in carbon. The effectiveness of ta-C formation in TEPs of noble gas ions was calculated.

RESULTS AND CONCLUSIONS

According to results of TRIM simulation, one can approximate TEPs of considered ions by spherical regions containing from 40 to 2000 atoms. It justifies correctness of the suggested thermodynamic approach. The radius, energy and lifetime of TEPs caused by noble gas ions were determined on the basis of TRIM simulation of ion-to-matter energy transfer and taking into account relaxation processes. Temperature in TEP was determined from phonon component of ion energy loss in TEP's volume. Thermoelastic, deformation and residual components of pressure in TEP have been found using radiation acoustic equations. Calculation has shown that temperature and all components of pressure in TEPs depend considerably on sort and energy of the ion.

The initial positions and trajectories of points corresponding to TEPs matter state on *P,T* phase diagram of carbon were determined (see Figure 1). Here dash-dot lines separate stability regions of different phases whereas dotted lines show initial locations of TEPs of specific ions. The sharp pressure decay on initial stage of the peak evolution corresponds to the acoustic wave escape almost without cooling. After that, pressure achieves the quasi-static level and decreases in accordance with increase of TEP volume. Analysis shows that trajectories of TEPs generated by ions with energy $E<E_1$ ($E>E_2$) lie entirely in the region of diamond (graphite) stability. Hence, ions with energies $E<E_1$ produce high concentration of ta-C whereas the ones with $E>E_2$ do not produce ta-C at all. Here $E_1 \approx 75$, 150, 150, 200 eV and $E_2 \approx 450$, 900, 750, 600 eV for ions Ne^+, Ar^+, Kr^+, Xe^+, correspondingly. The ions with energies $E_1 < E < E_2$ also produce ta-C but its concentration decreases with increase of the ion energy.

The total number W(E) of sp^2 to sp^3 transitions in ion TEP under combined action of temperature and pressure was used as a factor of effectiveness of ta-C formation. As one can see from Figure 2 the effectiveness of ta-C formation

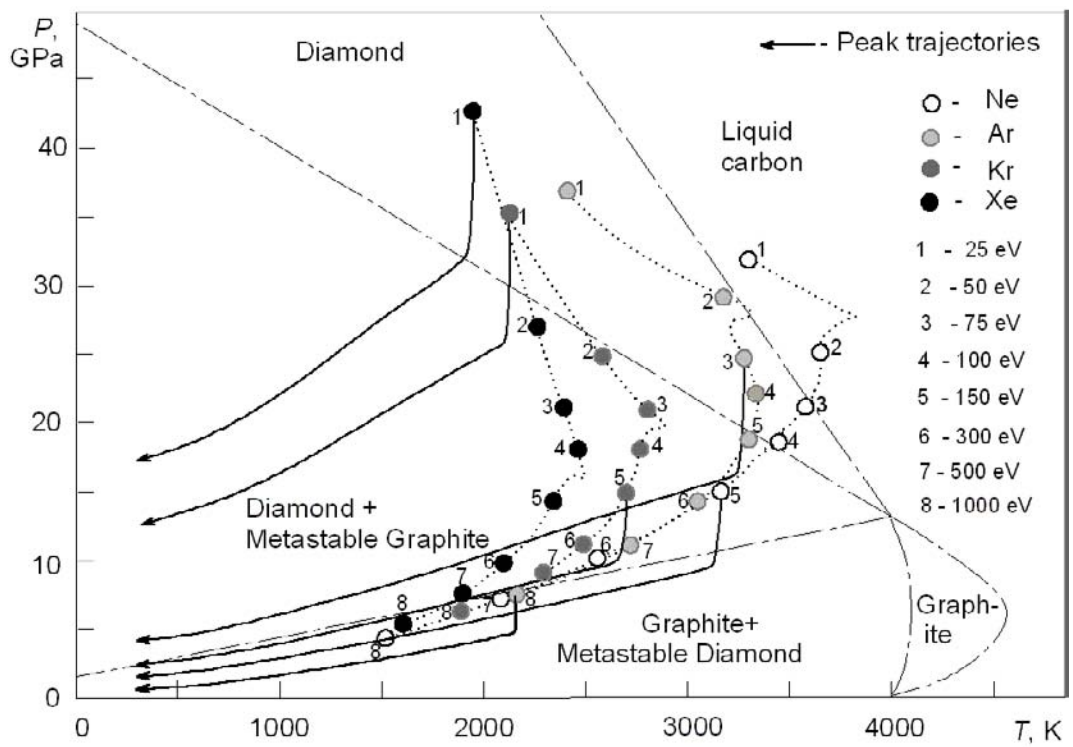

Figure 1. Location of P,T-trajectories (solid lines) of TEPs of noble gas ions on phase diagram of carbon.

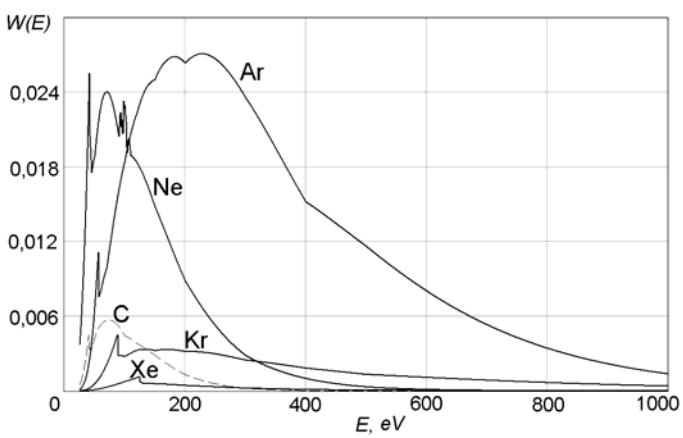

Figure 2. Energetic dependence of number of rearrangements $sp^2 \rightarrow sp^3$ in TEPs of C^+ and noble gas ions in carbon.

depends considerably on the ion sort. The maximal effectiveness is observed for Ar^+ and Ne^+, the minimal one is for Xe^+. The maxima of effectiveness for different ions are observed at different energies. Moreover, there are several peaks on the curves of effectiveness of ta-C formation for different ions: at 40, 60 and 90 eV for Ne^+ , at 56 and 200 eV for Ar^+, at 90 and 150 eV for Kr^+. The presence of two peaks in sp^3 content of carbon target after Ar^+ ion treatment is experimentally justified [3]. The dense phase formation in TEPs of Ar^+ and Kr^+ ions with energy $\leq$1000 eV occurs with an appreciable rate whereas the rates of the structural rearrangement to sp^3 state in TEPs of C^+, Ne^+ and Xe^+ of such energies are negligible.

REFERENCES

1. Hofsäss, H., et al. “Cylindrical spike model for the formation of diamondlike thin films by ion deposition,” *Appl. Phys. A: Materials Science and Processing*, Vol. 8, pp.1351-1363 (1998).
2. Kalinichenko A.I., Strelnytskiy V.E. “Role of thermoelastic stress in formation of diamond-like coating at irradiation of amorphous carbon by low-energy C^+ ions,” *Physics and Chemistry of Material Processing*, No 2, pp. 5-10 (2003). (In Russian.)
3. Patsalas P., et al. “Surface-activation processes and ion-solid interactions during the nucleation and growth of ultra-thin amorphous carbon films,” *Thin Solid Films*, Vol. 428 pp.211-215 (2003).

ACTION OF ACOUSTIC EFFECTS AT ION IMPLANTATION ON KINETIC PROCESSES IN CARBON FILMS

A.I. Kalinichenko, V.E. Strel'nitskij

National Science Center «Kharkov Institute of Physics and Technology»,

Akademicheskaya Str., 1, 61108, Kharkov, Ukraine. E-mail: strelnitskij@kipt.kharkov.ua

Keywords: ion implantation, thermoelasticity, impact, acoustic waves, kinetic processes.

Abstract

Variable stresses originating due to energy, impulse and volume transfer at low-energy C^+, Ar^+ ions implantation in carbon films are theoretically investigated. A spatial dependence of generated pulse is analyzed taking into account the sound absorption. The influence of the elastic waves on kinetic processes in irradiated matter is discussed.

INTRODUCTION

Experiments show a remote action of low-energy ions on properties of deposited film on depths considerably exceeding the ion ranges. The thermodynamic conditions in thermoelastic peaks (TEPs) – nanometer regions around ion trajectories containing thermalized ion energy were investigated in [1]. It was shown that a powerful acoustic pulse is generated in TEP due to energy E and volume V_1 introduced by ion. The stress pulse is a spherical bipolar wave diverging with the longitudinal sound velocity s. Its amplitude in the wave zone can be represented as

$$\sigma(r_0,t)=\frac{1}{2}\frac{st}{r_0}\cdot\frac{\Gamma E\eta+KV_1}{V}\left[H\left(t-\frac{r_0-R}{s}\right)-H\left(t-\frac{r_0+R}{s}\right)\right],\qquad (r_0\gg R) \tag{1}$$

where t is time counting from the moment of TEP origination, $\vec{r}$ - radius-vector from TEP center to the observation point, $H(t)$ - the Heaviside's unit, $\eta=\eta(E)$ – a part of ion energy transferred to the phonon excitations, $R=R(E)$ and $V=V(E)$ – radius and volume of TEP, K – the compression modulus and Γ - the Gruneisen parameter of a target material. Taking from [1] data concerning $\eta(E)$, $R(E)$ and $V(E)$ we get estimate $\sigma(R)\sim 10$ GPa. Such stresses can stimulate rearrangement of carbon to sp^3 bonds, result in change of rate of kinetic processes in irradiated material (i.e., creep, diffusion of impurities and interstitials, etc.) To right estimate the acoustic effect action on radiation – stimulated processes one need to take into account all basic mechanisms of elastic wave generation. Particularly, the generation of high pressure pulses also takes place due to transfer of the ion momentum $P=\sqrt{2ME}$ to the target material during the time of ion-ion relaxation τ. Such impact pressure $p_D\sim\sqrt{2ME}/(\pi R^2\tau)$ in front of TEP exceeds the material yield stress and is able to cause structural rearrangements (the radiation cold hardening), to move the surface atoms in depth of the material, etc. In this paper by the example of C^+ и Ar^+ ions with energy from 25 to 1000 eV bombarding carbon target the contributions of different mechanisms of elastic wave generation are determined and compared. A spatial dependence of the pulse amplitude including a sound absorption is investigated. The action of variable stresses from ion TEPs on kinetic processes in irradiated material is discussed.

RESULTS AND CONCLUSIONS

The acoustic stress generated due to transfer of impulse $\vec{P}$ from incident ion to TEP material was estimated in the hydrodynamic approximation:

$$\sigma_D(\vec{r}_0,t)=-2s\frac{\sqrt{ME}}{V}\frac{R}{r_0}\cos\theta\; e^{-(st-r_0+R)/R}\sin\left(\frac{st-r_0+R}{R}-\frac{\pi}{4}\right) \tag{2}$$

Here θ is the angle between the direction on the observation point and vector $\vec{P}$. Note that the impact stress depends on θ in accordance with the law of dipole radiation: $\sigma_D\sim\cos\theta$.

The energetic dependence of ratio σ_D/σ for C^+ и Ar^+ ions at $\theta = 0$ is shown in Figure 1. One can see that the impact stress is comparable or exceeds the thermoelastic and deformation ones.

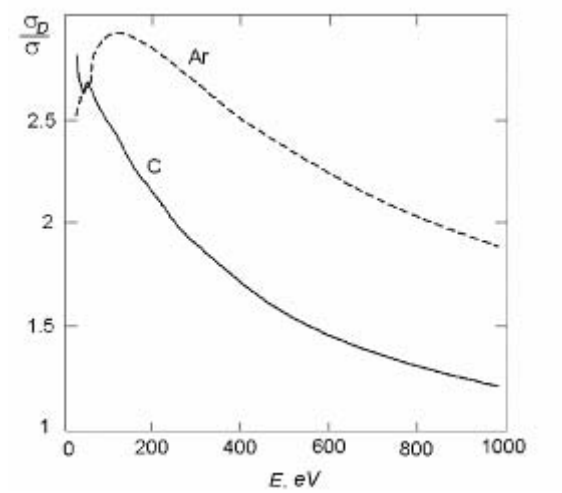

Figure 1. Energetic dependence of ratio σ_D/σ for C^+ and Ar^+ ions in carbon

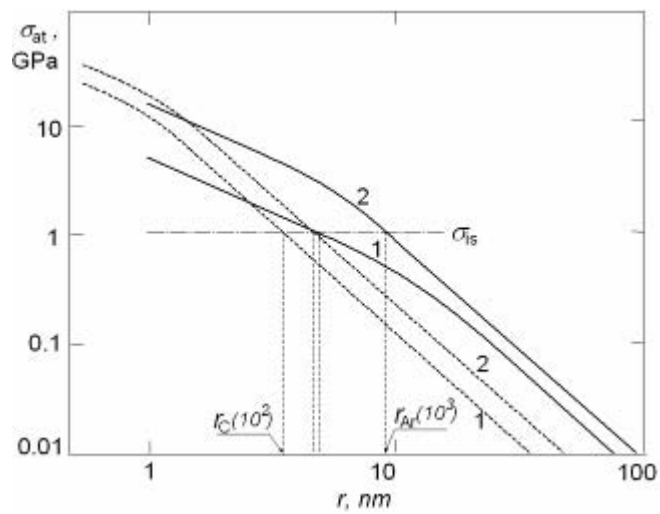

Figure 2. Spatial dependence of total acoustic stress, generated by C^+ (curves 1) and Ar^+ (curves 2) with energies 100 eV (dashed) and 1 KeV (solid) in carbon

The equations (1), (2) are correct only for distances $r_0 << r_{at} = (R/s)^2/\beta$ when one can neglect the sound absorption on the boundary frequency *s/R*. So, taking for the index of absorption β=2 м$^{-1}$·ГГц$^{-2}$ (the typical value for hard dielectric materials like sapphire) we get r_{at} = 3 nm (r_{at} = 20 nm) in case of C^+ ion with energy 100 eV (1000 eV). For maximum of total acoustic stress the following estimate is correct:

$$\sigma_{at}(\vec{r}_0) \approx \begin{cases} \dfrac{R}{2r_0}\dfrac{\Gamma E\eta + KV_1 + 2s\sqrt{2ME}\cos\theta}{V}, & r_0 << r_{at}, \\ \dfrac{\Gamma E\eta + KV_1 + 2s\sqrt{2ME}\cos\theta}{\sqrt{2\pi e}\beta s^2 r_0^{\,2}}, & r_0 >> r_{at}. \end{cases} \tag{3}$$

The spatial dependence of total acoustic stresses from C^+ and Ar^+ TEPs (curves 1 and 2, respectively) with energies 1 KeV (solid lines) and 100eV (dashed lines) is shown in Figure 2. The point of observation lies in axis $\theta = 0$. When the stress exceeds a threshold of activation then corresponding kinetic process is stimulated in the irradiated matter. So, the displacement of interstitials from stoppers goes everywhere in the neighborhood of TEP where the acoustic pulse amplitude $\sigma_{at}(\vec{r})$ exceeds the value of the activation energy $\sigma_{is} = U_{is}/\Omega_{is}$ ~ 1 GPa of the displacement (see Figure 2). Here U_{is} ~ 0.1 eV is the energy of migration of the interstitial, Ω_{is} ~ 2·10^{-23} cm^3 is the interstitial volume in carbon. As one can see from Figure 2, the radiuses $r_C(E)$ and $r_{Ar}(E)$ of the activation zones around TEPs of C^+ and Ar^+ where the over-barrier movement of diffusants occurs depends considerably on sort and energy of the ion.

REFERENCES

1. Kalinichenko A.I., Strel'nitskij V.E. "Thermoelastic peak effect at ion implantation and its role in diamondlike coating formation," *The Journal of Kharkiv National University*, No 2/18/, pp. 72-84 (2003). (In Russian.)

THE EFFECTS OF METHANE GAS PRESSURE ON OPTICAL AND ELECTRICAL PROPERTIES OF NITROGENATED CAMPHORIC CARBON THIN FILMS GROWN BY SURFACE WAVE MICROWAVE PLASMA CHEMICAL VAPOR DEPOSITION

M. Rusop, T. Soga and T. Jimbo

Department of Environmental Technology and Urban Planning,

Nagoya Institute of Technology, Gokiso-cho, Showa-ku, Nagoya 466-8555, Japan

S. Adhikari, A.M.M. Omer, S. Adhikary, H. Uchida and M. Umeno

Department of Electronic Engineering, Faculty of Engineering,

Chubu University, Matsumoto-cho1200, Kasugai 487-8501, Japan

Keywords: a-C:N; camphoric carbon; optical gap; surface wave; microwave CVD.

Abstract

We have studied the influence of the methane gas (CH_4) pressure on the bonding, structural, optical and electrical properties of the nitrogen doped amorphous carbon nitride (a-C:N) thin films grown by newly developed Surface Wave Microwave Plasma Chemical Vapor Deposition (SWMP-CVD) on quartz and silicon (100) substrates. The a-C:N films are deposited with varying CH_4 partial gas pressure in range from 5 to 20 ml/min. To incorporate nitrogen in the a-C:N film, we have introduced nitrogen gas (N) at 5 ml/min partial gas pressure in the chamber. The effects of the CH_4 gas pressure on the surface morphology, composition, structure, optical and electrical properties of the N incorporated camphoric carbon thin films have been investigated using Scanning electron microscopy (SEM), Atomic force microscopy (AFM), Auger electron spectroscopy (AES), UV-Visible spectroscopy and Four-point probe resistance measurement. We have succeeded to grow a-C:N thin films using SWMP-CVD at room temperature and found that the amorphous structure of a-C:N films can be changed and is strongly dependent on the CH_4 gas source.

RESULTS AND DISCUSSIONS

Recently, a new deposition method (Fig. 1), namely Surface Wave Microwave Plasma Chemical Vapor Deposition (SWMP-CVD) has been developed [1,2]. This deposition technique is a new deposition method of carbon thin films without corroding ions on substrate. It is also noticed as one of promising plasma sources for the large area thin film deposition. Since structural, physical and optical properties of a-C thin films grown by SWP-CVD for solar cell application are not yet understood, in this paper, we report our latest result on the properties of nitrogen doped amorphous carbon nitride (a-C:N) thin films.

The optical properties was characterized by studying the optical transmittance and reflectance spectra of the films using UV|VIS|NIR spectrometer - Jasco V570. The optical absorption spectra of the films were obtained from optical transmittance and reflectance measurements in the range of 200 to 2500 nm.

From the measurements of optical transmittance and reflectance in range of 300 to 1150 nm wavelength (about 1 to 4 eV photon energy), an optical absorption coefficient (α) on the order of $10^3 – 10^4$ cm^{-1} is obtained for the undoped a-C. The α has increase with increased up to $10^3 – 10^4$ cm-1 for a-C:N films grown at 5 ml/min of CH_4 gas. The α is almost unchanged with higher CH_4 gas up to 20 ml/min. The high absorption in the power-law (Tauc) and exponential (Urbach) region is ascribed to the presence of more graphitic component (sp^2- bonds) in the carbon film. The optical absorption spectra in this experiment have a similar shape to the absorption spectra reported by Puretzky et al. [3].

As shown in figure 2, the optical gap (E_g) is obtained from the extrapolation of the linear part of the curve at the absorption coefficient $\alpha = 0$ using the Tauc relation [4], $(\alpha hv)^{1/2} = B(E_g\text{-}hv)$, where, B is the Tauc parameter. The estimated E_g for undoped a-C films A is approximately 2.3 eV and decreased up to approximately 2.1 eV with

increased of CH_4 gas at 5 ml/min. Our result shows the E_g is almost constant at 2.1 eV, indicates there is no micro-structural disorder with higher CH_4 gas up to 20 ml/min.

The electrical resistivity (ρ) was measured at RT by a 4-point probe resistance measurement method, the usual way for high resistance measurement. The ρ values for each film were the average of measurements made at different positions on the film surface. The ρ values of Sample A was measured to be around 6.2 x 10^5 (Ω -cm), is higher compared with the ρ = 5 x 10^4 (Ω-cm) values of a-C:N film grown at 5 ml/min CH_4 gas. The ρ of a-C:N films decrease with higher CH_4 gas up to 8 x 10^3 (Ω-cm), 4 x 10^3 (Ω-cm) and 1 x 10^3 (Ω-cm) respectively.

Details of the experimental results and discussions will be presented during the conference presentation.

Conclusions

We have successfully grown nitrogen doped amorphous carbon (a-C:N) thin films by newly developed surface wave microwave chemical vapor deposition (SWP-CVD) at 5 ml/min N_2 gas ambient with the CH_4 precursor gas from 5 to 20 ml/min. The dependence of the CH_4 gas ambient on the surface morphology, composition, structure, optical and electrical properties of the films was investigated. It is found that the amorphous structure of a-C:N films can be changed by CH_4 gas and the a-C:N films grown at higher CH_4 gas have relatively high electrical conductivity.

REFERENCES

1. M. Nagatsu, T. Sane, N. Takada, W.X. Guang, T. Hirao and H. Sugai, Jpn. J. Appl. Phys. Vol. 39, pages 929 (2000).
2. M. Nagatsu, T. Sano, N. Takada, N. Toyoda, M. Tanga and H. Sugai, Diamond Relat. Mater. Vol. 11, pages 976 (2002).
3. A.A. Puretzky, D.B. Geohegan, G.E. Jellison Jr. and M.M. Mc Gibbon in: H.A. Atwater, J.T. Dickinson, D.H. Lowndes and A. Polman (Eds.), Film Synthesis and Growth Using Energetic Beams, San Francisco, U.S.A., April 17-21, 1995, Materials Research Society Symposium Proceeding Vol. 388 pages 145 (1995).
4. J. Tauc: Amorphous and Liquid Semiconductors (Plenum Press, London, New York, 1974) Chap. 4.

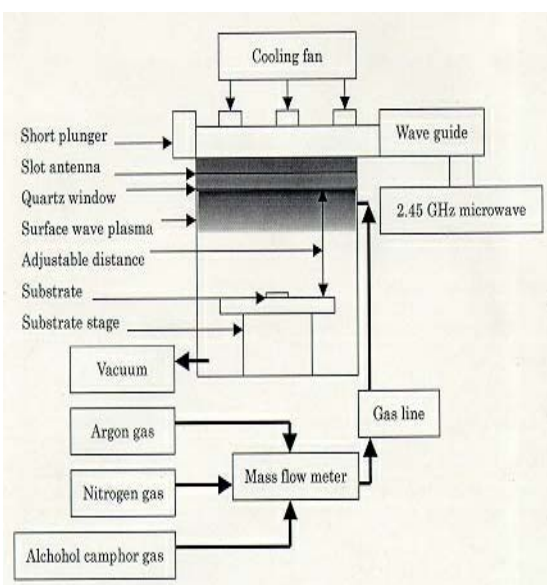

Figure 1: Image of newly developed Surface Wave Microwave Plasma Chemical Vapor Deposition (SWMP-CVD) System.

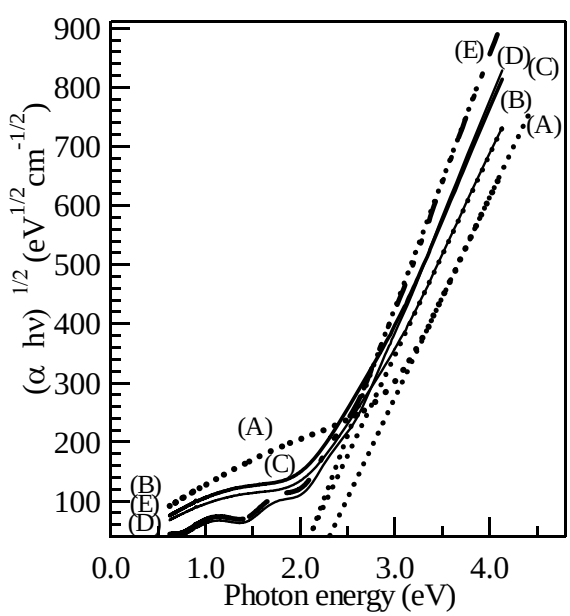

Figure 2: Tauc plot of $(\alpha h\nu)^{1/2}$ as a function of photon energy (hv), for (A) undoped a-C, and a-C:N films grown at (B) 5, (C) 10, (D) 15, and (E) 20 ml/min of CH_4 gas source.

Diamond Growth on an Array of Seeds: The Revolution of Diamond Production

James C. Sung

Address: KINIK Company, 64, Chung-San Rd., Ying-Kuo, Taipei Hsien 239, Taiwan, R.O.C.
Tel: 886-2-2677-5490 ext.1150
Fax: 886-2-8677-2171
e-mail: sung@kinik.com.tw

[1] KINIK Company, 64, Chung-San Rd., Ying-Kuo, Taipei Hsien 239, Taiwan, R.O.C.
[2] National Taiwan University, Taipei 106, Taiwan, R.O.C.
[3] National Taipei University of Technology, Taipei 106, Taiwan, R.O.C.

Key Words: Diamond Synthesis, High Pressure, Diamond Seed, Diamond Grit, De Beers

Abstract

Industrial diamond production was pioneered by General Electric Company of U. S. in 1957 and followed by De Beers of S. Africa in 1961. The two companies optimized the production of diamond grits by heating alternative layers of graphite disks and metal catalyst (Fe, Ni, Co) under high pressure. Although there have been 20 countries attempting to duplicate the success of GE and DB, only Iljin Diamond of S. Korea is able to join the lucrative business starting with a technology provided by the author in 1989. In 1970s Winter of Germany developed a powdered mixture of graphite and metal and demonstrated that this assembly can greatly improve the diamond yield and quality. This technology has since been applied to make high grade saw diamond by the above "big three."

China start commercial production of diamond grits in 1966, since then, their diamond output has been growing at a much faster pace than that of the "big three." Today, Chinese makes 2/3 of diamond grits of the world consumption of about 600 tons. However, Chinese cannot make saw diamond larger than about 45 mesh (0.36 mm). Even so, the "big three" has felt the pressure of "yellow fever." As a consequence, De Beers reorganized their industrial diamond group in 2000 and renamed it Element Six, GE Superabrasives was sold to Little John in 2003, and Iljin Diamond suffered the first loss in 2003.

The world high pressure diamond synthesis is due for another technology advancement, this time, the random nucleation of diamond in the reaction cell is planted with a matrix of diamond seeds that will do away with the erratic growth of diamond. The result would be doubling of the diamond yield and quadrupling of the sales value.

POSTER SESSION 1

ELECTROCHEMISTRY

Probing Electrical Conductivity Homogeneity Across a Boron-Doped Nanocrystalline Diamond Film Using Conductive Probe-Atomic Force Microscopy

Shihua Wang and Greg M. Swain

Department of Chemistry
Michigan State University
East Lansing, MI 48824-1322

In recent years, boron-doped diamond thin film, grown using chemical vapor deposition (CVD) techniques, has been characterized and employed as an electrode material for electrochemistry. Much has been learned from electrochemical measurements about factors influencing their electrochemical activity, but they still possess some characteristics that are not fully understood. One property not fully understood is the electrical conductivity and what properties influence electron transfer across the diamond/solution electrified interface. Conductive probe-atomic force microscopy (CP-AFM) was used to map the topography and electrical conductivity of boron-doped diamond films, in particular, nanocrystalline films. The dependence of electrical conductivity on the boron doping level and bias voltage polarity were studied. Discontinuous conductive regions were observed on all films, with the fraction of conductive area increasing with the boron doping level. At the higher doping levels, the conductive regions exhibited metallic electronic properties. The results clearly show that diamond films are not uniformly conducting. They possess regions of high electrical conductivity isolated by regions of low conductivity. The results have important implications for the application of diamond in such fields as electrochemistry and field emission.

References:

[1] Swain, G.M., et al., "Electrochemical performance of diamond thin-film electrodes from different commercial sources", *Anal. Chem.*, **76**, 2553(2004).

[2] Holt, K.B., et al., "Scanning electrochemical microscopy and conductive probe atomic force microscopy studies of hydrogen-terminated boron-doped diamond electrodes with different doping levels", *J. Phys. Chem. B*, **108**, 15117(2004).

The Analysis of Chlorinated Phenols Pollutants Using Diamond Microelectrodes

Grace W. Muna, Veronika Quaiserova-Mocko, and Greg M. Swain
Department of Chemistry
Michigan State University
East Lansing, MI 48824-1322

Abstract

A boron-doped diamond microelectrode was employed for the amperometric detection of chlorinated phenols in capillary electrophoresis (CE-EC). Detection was made in both the direct and indirect modes. The microelectrode was prepared by (i) coating a thin film of boron-doped polycrystalline diamond on a sharpened platinum wire (76-μm diameter) and (ii) sealing the coated wires in a polypropylene pipette tip. The diamond microelectrode, in the end-column format, exhibited a low and stable background current with low peak-to-peak noise. The electrode performance was evaluated in terms of the linear dynamic range, sensitivity, limit of quantitation, and response precision for the detection of several important chlorinated phenols (2-chlorophenol, 3-chlorophenol, 4-chlorophenol, 2,4-dichlorophenol, 2,4,6-trichlorophenol, and pentachlorophenol). The diamond microelectrode exhibited outstanding detection figures of merit for these contaminants in the direct amperometry. For example, the mass limit of detection for 2-chlorophenol in the direct amperometric mode was 14 fg (12 ppb S/N = 4) and the relative standard deviation of the peak height for 9 injections was 4.7 % (1.1 nL inj.). The separation efficiency was greater than 100,000 plates/m for all seven analytes. Water from a local river was spiked with chlorinated phenols and analysed. The first step in the analysis was extraction of the phenols by solid phase extraction prior to analysis. The preconcentrated phenol solution was then analyzed using CE-EC. The preconcentration by solid phase extraction lowered the limit of quantitation to low ppb to high ppt level.

A diamond microelectrode was also employed for the indirect amperometric detection detection of these pollutants in CE. In this approach, ferrocene carboxylic acid was added to the run buffer as the electrophore. Good reproducibility was observed for the separation and detection of 2-chlorophenol, 3-chlorophenol, and 2,4-dichlorophenol. The mass limit of detection for these analytes was in the pg (low ppm) range. Data for both direct and indirect amperometry will be presented.

MONITORING ARSENIC (III) IN WATER SUPPLIES USING ANODIC STRIPPING VOLTAMMETRY AND A DIAMOND ELECTRODE

Yang Song and Greg M. Swain

Department of Chemistry, Michigan State University, East Lansing, MI, 48824-1322

Keywords: Arsenic, Anodic Stripping Voltammetry, Diamond electrode, water monitoring

Abstract

Arsenic contamination in drinking water can cause not only short term poisoning but also chronic medical effects such as keratosis, dyspigmentation, skin lesions, and skin and internal cancers even at low part-per-billion (ppb) levels.[1] The inorganic trivalent form is the most toxic.[2] Current methods of analysis such as atomic absorption spectrometry and inductively coupled plasma mass spectrometry are expensive, time consuming and unsuitable for on-site detection.[1] Electrochemical methods, like anodic stripping voltammetry (ASV) are easy to operate, sensitive, fast, portable, and a less expensive alternative for arsenic detection.[3] However, electrode materials currently used are limited by toxicity, stability and sensitivity issues.[4]

Boron doped diamond (BDD) is a relatively new alternate electrode material for ASV. Its low background current, large potential window and long term stability distinguish BDD from conventional electrode materials.[5] Some preliminary results of arsenic (III) detection in 1 M HCl with a diamond thin-film electrode modified by co-deposited gold particles will be presented. Detection of arsenic on diamond was characterized by cyclic voltammetry (CV) and atomic force microscopy (AFM). Factors affecting the ASV detection such as deposition potential, deposition time, and gold (III) concentration were optimized. The LOD with a gold (III) concentration of 100 ppb at the optimized conditions was determined to be 0.005 ppb, the linear dynamic range under these conditions was 0.005 ppb-40 ppb. A sensitivity of ca. 0.01 μA/ppb was achieved. The RSD was ca. 5% with 10 consecutive runs.

REFERENCES

1. Dai, X., Nekrassova, O., Hyde, M. E., Compton, R. G., “Anodic Stripping Voltammetry of Arsenic (III) Using Gold Nanoparticle-Modified Electrodes,”*Anal. Chem*. Vol. 76, 5924 (2004).
2. Mandal,B.K., Suzuki, K.T., “Arsenic Round the Word: a Review,” *Talanta*, Vol. 58, 201 (2002).
3. Feeney, R., Kounaves, S. P., “On-Site Analysis of Arsenic in Groundwater Using a Microfabricated Gold Ultramicroelectrode Array,” *Anal. Chem*. Vol. 72, 2222 (2002).
4. Cavicchioli, A., La-Scalea, M. A., Gutz, I. G. R., “Analysis and Speciation of Traces of Arsenic in Environmental, Food and Industrial Samples by Voltammetry: a Review,” *Electroanalysis*, Vol. 16, 697 (2004).
5. Granger, M. C., Xu, J., Strojek, J. W., Swain, G. M., “Polycrystalline Diamond Electrodes: Basic Properties and Applications as Amperometric Detectors in Flow Injection Analysis and Liquid Chromatography,” *Anal. Chim. Acta*, Vol. 397, 145 (1999).

DIAMOND MICROELECTRODES FOR THE *IN VITRO* MEASUREMENT OF NOREPINEPHRINE RELEASE FROM SYMPATHETIC NERVES IN RATS

Jinwoo Park , James J. Galligan, Gregory D. Fink* and Greg M. Swain*

Michigan State University, East Lansing, Michigan 48824

Keywords: Polycrystalline boron-doped diamond microelectrode, Norepinephrine (NE)

Abstract

Polycrystalline boron-doped diamond microelectrode is an advanced electrode material that possesses attractive properties for electroanalytical measurements in biological environments (e.g., low limit of detection, response precision, wide working potential window, and pH independence). The diamond surface is non-polar with a low surface oxygen content and this results in weak adsorption of polar molecules and contaminants. Therefore, the response stability and fouling resistance of diamond are superior to that of carbon fiber microelectrode - a common electrode material used for the electrochemical detection of catecholamine neurotransmitters.

Norepinephrine (NE) is the primary neurotransmitter in the sympathetic nervous system and controls vasomotor tone. We report presently on the use of diamond microelectrodes and video imaging techniques to monitor local NE release and mesenteric arterial constriction using *in vitro* preparations from laboratory test rats. NE release was elicited by focal electrical stimulation (1-20 Hz) of periarterial nerves. The diamond response sensitivity and stability for this *in vitro* measurement will be compared with that of a carbon fiber. Data will also be presented showing the correlation of NE release with vasoconstriction.

Electrochemical Tuning and Investigations on Actuator Mechanism of Single-Wall Carbon Nanotubes

S. Gupta

Department of Physics and Materials Science, Missouri State University, Springfield, MO 65804-0027. E-mail address: sxg535f@smsu.edu

Keywords: Single-wall carbon nanotube mat, Raman spectroscopy, electrochemistry, actuator mechanism

Abstract

The isothermal conversion of chemical energy into mechanical work underlies the motility of all living systems - *natural muscles*. In this presentation, actuators built from a macro scale sheets of single-wall carbon nanotubes (*bucky paper*), which is among the growing list of several actuator materials since its pioneer demonstration, will be investigated. They are therefore dubbed as *artificial muscles* lying under the category of electro-chemo-mechanical devices, whereby the transformation of chemical energy into mechanical energy is triggered by electrical signal or dc bias [1]. They operate as a result of double-layer (*i.e.* electrochemical double layer; ECDL) charge injection in electrodes having very high gravimetric surface area and gravimetric/specific capacitance and the output of the actuator may be a mechanical displacement that can be used to accomplish mechanical work. Despite several benefits (low operating voltages, conducting nature, high temperature performance, and unusual electro-mechanical coupling), some open questions concerning the actuation principle/mechanism remain. They stretch if they are electrically charged and stretching is due to the elongation of C-C bond (*i.e.* tangential displacement mode) - if bonding states are depopulated or if anti-bonding states are populated.

This study addresses and presents these issues and aim to comprehend the various contributions by investigating the charge transfer dynamics on the surface of single-wall carbon nanotubes using *in situ* resonance Raman spectroscopy (RRS) and to determine the associated parameters include microscopic strain, fractional charge transfer and the corresponding shift in Fermi level through modeling [2, 3]. We found the in-plane compressive strain (~ -0.25%) and the charge transfer per carbon atom (f_c ~ -0.005) as an upper bound for the electrolytes used *i.e.* $CaCl_2$ (see Fig. 1). These results can be quantitatively understood in terms of the changes in the energy gaps between the one-dimensional van Hove singularities in the electron density of states arising possibly due to the alterations in the overlap integral of π bonds between the p orbitals of the adjacent carbon atoms. Moreover, the extent of variation of the absolute potential of the Fermi level or alternatively modification of band gap is estimated from modeling Raman intensity to be around 0.1 eV as an upper bound for $CaCl_2$. The cyclic voltammetry (see Fig. 2) and ac electrochemical impedance spectroscopy results will be discussed briefly which help to demonstrate well-developed capacitive behavior of single-wall carbon nanotubes sheet and to estimate the gravimetric/specific capacitances as well.

References

1. Baughman R. *et. al.* “Carbon Nanotube Actuators”, Science, **284**, 1340 (1999).

2. S. Gupta, M. Hughes, A. H. Windle, and J. Robertson, “Charge transfer in carbon nanotube actuators investigated using *in situ* Raman spectroscopy”, J. Appl. Phys. **95**, 2038 (2004) and

references therein. **[Selected for Virtual Journal of Nanoscale Science & Technology June Issue (2004)].**

3. Gupta S. *et. al.* "*In situ* Raman spectro-electrochemistry study of single-wall carbon nanotube mat", Diam. and Relat. Mater. **13**, 1314 (2004).

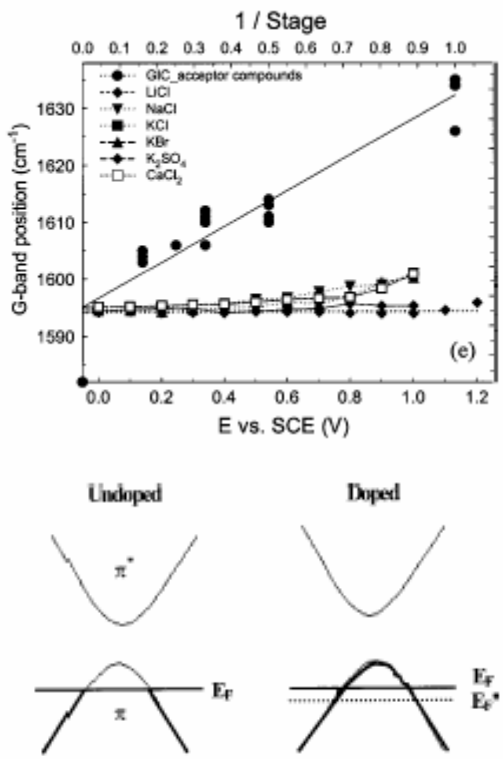

Figure 1. (top) Variation of *G* band vs. electrochemical potential relative to reference electrode (SCE) for all of the aqueous electrolytes: LiCl, NaCl, KCl, KBr, K_2SO_4 , and $CaCl_2$. The variation of *G* band for several GIC-acceptor compounds from is also provided for comparison. (bottom) Schematic of suggested energy-level band diagram corresponding to (top) demonstrating the tuning of electronic structure of SWNTs due to electrochemical charge transfer.

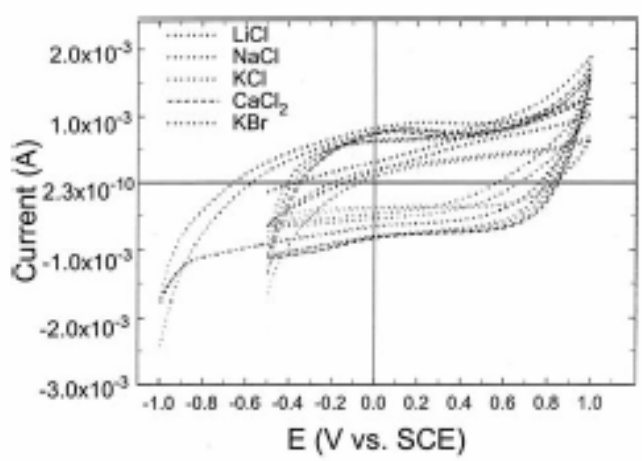

Figure 2. Shown are the cyclic voltammograms for all of the aqueous electrolytes scan rate, 50 mV/s from -0.5 to 0.1 V vs. SCE. The CV curve for one of the electrolytes; LiCl for a full potential cycle from -1.0 to 1.0V is also provided. All of the electrolytes are of 0.1 M concentrations.

POSTER SESSION 1

THEORY

2005 ADC meeting

Argonne, IL

Electronic structure calculations of Nitrogen and Hydrogen in diamond twist grain boundaries

Michael Sternberg[1], *Peter Zapol*,[1,2] *Larry A. Curtiss*,[1,2]

[1] Materials Science Div., Argonne National Laboratory, Argonne, IL, USA.
[2] Chemistry Div., Argonne National Laboratory, Argonne, IL, USA.

Films of ultrananoctrystalline diamond grown in methane/argon plasmas have grain sizes of 3 to 10 nm and show an increase of several orders of magnitude in *n*-type conductivity upon nitrogen addition to the plasma [Bhattacharyya *et al.*, Appl. Phys. Lett. **79**, 1441 (2001)]. Our computational studies have shown that nitrogen impurities are more stable in the grain boundaries than in the bulk. Using a density-functional-based tight-binding method, we have investigated the atomic and electronic structure of $\Sigma 13$ and $\Sigma 65 - (100)$ diamond twist grain boundaries containing hydrogen and nitrogen at the same time. We have studied the formation of N–H complexes and associated changes in the electronic structure of the films for different hydrogen to nitrogen concentration ratios. We have also calculated participation ratios in order to find mobility edges in these systems and investigate the formation of defect sub-bands in the forbidden gap of diamond. These studies are being used to understand the experimentally observed changes in the electronic properties of the films associated with changes in the plasma composition during the growth process.

* Work supported by the U.S. Department of Energy, BES-Materials Sciences, under Contract W-31-109-ENG-38.

Keywords

diamond, grain boundaries, electronic structure.

THERMODYNAMIC STABILITY OF NANODIAMONDS: A NANOTHERMODYNAMIC APPROACH

H. Cui, C. X. Wang, P. Liu, G. W. Yang

State key laboratory of optoelectronic materials and technologies, School of Physics Science & Engineering, Zhongshan University, Guangzhou 510275, P. R. China

Keywords: nanodiamond, thermodynamics, nucleation, Gibbs free energy, stability

Abstract

Since Lewis et al. found nanometer-scaled diamonds from primitive meteorites in 1987, a lot of researchers have also detected nanodiamonds in protoplanetary nebulae, interplanetary dust originating from comets and asteroids, and some circumstellar disks. All extraterrestrial nanodiamonds have similar size distribution, i.e., 3-5 nm, so far. On the Earth, nanodiamonds synthesize by detonation, chemical vapor deposition (CVD), and hydrothermal synthesis and reduction of carbide (HSRC). Pure TNT detonation synthesizes nanodiamonds with diameters about 10 nm. However, Chen *et al.* synthesized mostly spheroidal diamond nanoparticles with sizes of 3-6 nm by detonating TNT in the inert gases atmosphere. Similarly, nanodiamonds have been produced using CVD techniques. Lee *et al.* found diamond nanoparticles with diameter of 2-6 nm (small enough to identify the nucleation sites) in CVD diamond films. Furthermore, Gruen *et al.*, by partially or outright replacing the hydrogen with argon in the CVD process, deposited the smooth films of nanoparticles only a few nanometers in size. Recently, the important progress of micron-sized diamond synthesis was developed by HSRC with hydrogen or without hydrogen under conditions of pressure less than 200 MPa and temperature not exceeding 1300 K. Importantly, Gogotsi *et al.* realized the conversion of silicon carbide to diamonds with diameter of about 5 nm in the noble gas atmosphere under ambient pressure and temperature less than 1300 K conditions. Thus, both extraterrestrial and Earth's nanodiamonds are not only stable, not also have the nearly equal size distribution. These important data imply that there would be a common underlying factor in the formation of nanocrystalline diamonds. To our best knowledge, a few studies are involved in the stability of nanodiamonds. However, in all these calculations and experiments mentioned above, we hardly find the reasonable and satisfying explanation for the two fundamental issues: which physical origin causes the nanodiamond stability and why the nearly equal size distribution of nanodiamonds produced in space and on the Earth under very different temperature-pressure conditions is in the range of 3-5 nm. To gain a better understanding of the physical origin of the two fundamental issues mentioned above from the point of view of thermodynamics, in this study, we therefore perform the phase stability analysis of nanodiamonds and calculations of the critical nuclei sizes of diamonds upon CVD and HSRC systems. Interestingly, our theoretical results show that the radiuses of critical nuclei of diamonds upon CVD and HSRC are less than 2.5 and 3.0 nm, respectively. Furthermore, our analysis indicate that at atmospheric pressure and temperature not exceeding 1300 K, nanodiamonds less than 6 nm in diameter are thermodynamic stable phase. Additionally, we provide a reasonable explain for the diamond nucleation upon the hydrogen-free CVD.

A COMPARISON STUDY OF HYDROGEN INCORPORATION IN DIAMOND: EFFECT OF CRYSTALLINE STATE AND ORIGIN OF DIAMOND

C.J. Tang, A.J. Neves, L. Rino

Department of Physics, University of Aveiro, Aveiro, 3810-193, Portugal

Keywords: Hydrogen incorporation, Diamond, CH stretching vibration, Infrared absorption

Abstract

Hydrogen is a very important impurity for semiconductor science and technology. It is well known that hydrogen is unevitablly incorporated into CVD diamond during the growth process [1,2], due to rich hydrogen in the growth atmosphere. By controlling the growth conditions, diamond of different crystalline state ranging from single crystalline, polycrystalline through microcrystalline to nanocrystalline have been obtained, and correspondingly the size of the grains which compose these films decreases rapidly. In order to identify the origin and forms of hydrogen incorporated in CVD diamond, we present this review-like work. In this work a comparison study of hydrogen incorporation in diamond is primarily performed by three ways, i.e. in terms of crystalline state of diamond, origin of diamond and type of carbon. Among different types of CVD diamond films in terms of crystalline state, the effect of grain size on hydrogen incorporation is also discussed. Considering the origin and growth technique of diamond, hydrogen incorporation among natural diamond, high-pressure high-temperature (HPHT) synthetic diamond and CVD diamond is investigated. In terms of type of carbon, hydrogen incorporation in diamond and non-diamond such as diamond-like carbon (DLC) film and hydrogen terminated amorphous carbon (α–C:H) film is briefly discussed. In the end, based on our work and those in the literature, a summary including concluding remarks on hydrogen incorporation in diamond is presented.

REFERENCES

1. Dischler B., et al., Hydrogen in polycrystalline diamond: An infrared analysis, Physica B, Vol. 185, No. 1-4, 217-221 (1993).
2. McNamara K.M., et al., Identification of defects and impurities in chemical-vapor-deposited diamond through infrared spectroscopy, J. Appl. Phys., Vol. 76, No. 4, 2466-2472 (1994).
3. Tang C.J., et al., Investigation of hydrogen incorporation in CVD diamond films using infrared reflection spectroscopy, Diamond Relat. Mater., Vol. 13, No.4-8, 769-775 (2004).

POSTER SESSION 2

CHARACTERIZATION

SURFACE PLASMON RESONANCE STUDY OF SINGLE-WALLED NANOTUBE POLYMER FILM

V.I. Chegel,

Lashkarev Institute of Physics of Semiconductors of NASU, pr. Nauki, 41, 03028, Kyiv, Ukraine

L.V. Poperenko, Y.V.Chegel , V.V. Pokropivny*,

Physics Department, T. Shevchenko National Kyiv University, 6 Acad. Glushkov Ave., 03022 Kyiv, Ukraine

*Frantsevich Institute for Problem of Material Science of NASU, 03142 Kyiv

Keywords: **SPR, nanotube, plasmon, polymer, matrix**

Abstract

Surface plasmon resonance (SPR) in a first time was applied to experimental study and modeling of the single walled nanotubes (SWNT)-polymer films. Several types of SWNT, including carbon and bornitride shows unexpected optical properties for matrix film consisting of nananotubes and polyethilenimine, placed on the surface of evaporated SPR-supported gold film. Modelling of obtained reflectance dependencies, using Fresnel reflection coefficients for cases of simple SPR multylayers structure and possible waveguide was performed. Another possible explanations of observed phenomena are discussed..

Introduction

Surface plasmon resonance (SPR) method is power tool for real-time study of a optical properties and geometry of nanofilms and intensively applied into practice [1-2]. Single walled nanotube (SWNT) have been the subject of extensive investigations last years [3-4] due to they unique mechanical and electronic properties. The basic objective of presented work is a first observation of changes in behaviors of conventional SPR in a gold film covered by single walled nanotube (SWNT)-polyethilenimine layer. The technique of use of SPR assumes an irradiation of the interface between a glass prism, covered by thin (~45nm) gold layer (optically more dense medium) and the researched material (optically less dense medium) from the side of more dense medium by p-polarized laser beam and measurement of the reflected intensity under conditions of attenuated total reflection. The dependence of the intensity of the reflected irradiation vs. an angle of incidence (the surface plasmon resonance-curve) has a minimum at the characteristic angle of incidence, that reveals involving of energy of laser irradiation for oscillation of plasma of free electrons at the surface of gold film (surface plasmon). The form of the SPR-curve and, in particular, the angle position of the minimum, depends on the optical constants and thickness of all substances with which the electromagnetic wave of plasmon cooperates. In presented work we have studied a different types of SWNT- polyethilenimine films, using SPR method. Experiment was carried out with use of SPR-device Biosuplar-2 (www.biosuplarusa.com), where open optical circuit includes the gold film on which nanotubes in a mix with polymer is represented. The measurements was performed for several types of polymer matrix-SWNT nanotubes, placed on an surface of Au film by dropping. The samples of nanotubes were differed between itself with concentration of nanotubes. To compare the results, pure polymer films and film for polymer, mixed with soot was measured also.

Result and discussion

For all SWNT containing samples as well as for bare Au angular reflection spectra for air conditions were measured (Fig.1). It is seen, that surface plasmon resonance is observed on all samples, containing SWNT and on a bare gold. The resonant minimum for the comparison sample (pure polymer) as well as for sample with soot was not observed. This result is surprising, because of strong dependence of SPR angular position on mass of material, involved in electric field of surface plasmon. It was noted also, that depth of SPR minimum directly depend on the homogeneity of film and increase with more dense packing of nanotube layer. With another words, we observe a trend, that is not in agreement with a classical approach in SPR measurements.

The possible explanations of the observed phenomena will be discussed. An appearance of reflective dipping with such angular position in presence of high refractive layer on the surface of metal is possible, if consider the layer SWNT-polymer, as waveguide. In previews work [5] we show, using Fresnel modeling, that for SPR structures it is possible, when thickness of waveguide exceed 640 nm. AFM measurements shows the thickness of

pure polymer layer, close to 2 μm, that is quite enough for occurring of waveguide modes, if refractive index of layer is close to n=2.2+0.2i. To obtain the effective value of the refraction index of a layer of a polymeric matrix with nanotubes modeling with use of calculation of integrated Fresnel coefficient of the reflection for the system of investigated layers was carried out. The experimental SPR curves were mathematically treated, using procedure of fitting with theoretical SPR-curve. A minimal value of objective function at the end of processing reveals the optical parameters (refractive index and thickness of investigated layer), that is close to real. Calculation for usual multilayers model was performed also. The modeling without waveguide reveals another explanation of observed phenomena, where refractive index of SWNT polymer matrix on the surface of gold is close to refraction of air. This result could be explain by observed high adsorption activity of SWNT, which do not allows a close contact of polymer molecules to gold surface. We will also discuss the relation between the evanescent wave and possibility for tunneling of electrons from nanotubes to surface of gold.

The observed phenomena of nanotube-induced angular shift of SPR opens a new possibility for the revealing of nanotube fractions existing in material as well as to real-time registration of nanotubes interactions with another objects of study, including biological.

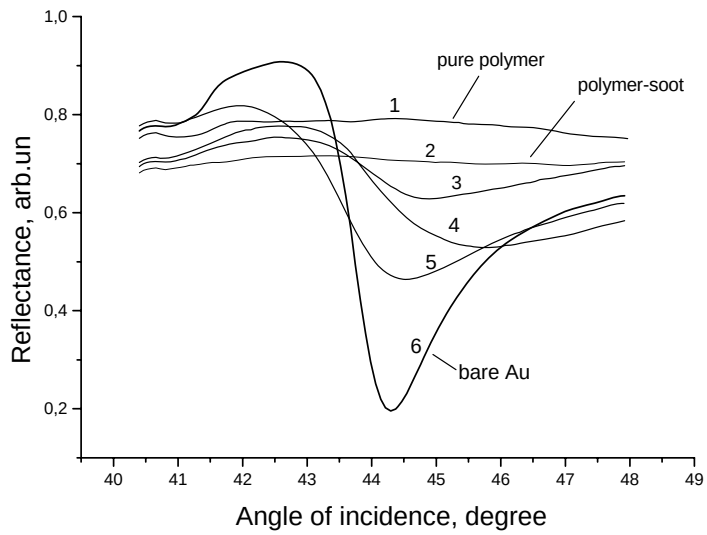

Figure 1. Surface plasmon resonance curves for gold film with different covering. 1 - pure polymer film, 2 - matrix polymer-soot, 3 - 5 matrix SWNT-polymer (3 - 20% SWNT, 4 - 40% SWNT, 5 –60% SWNT). 6 - bare gold film.

REFERENCES

1. Mulchan N.M, Rodriguez M, O'Shea K, et al. "Application of a high-resolution SPR technique for monitoring real-time metal/dielectric interactions", *Sensors and Actuators B: Chemical*, Vol. 88, Issue 2, Pages 132-137, 2003.

2. Lioubashevsky, O. , Chegel, V., Patolsky, F et al., "Enzyme-Catalyzed Bio-Pumping of Electrons into Au-Nanoparticles: A Surface Plasmon Resonance and Electrochemical Study", *JACS*, 2004, p.7133-7143, 2004.

3. Terrones, M., Jorio, A., Endo, M., et al., " New direction in nanotube science", *Materials Today,* , Vol. 7, Issue 10, Pages 30-45, 2004.

4. Raffaelle, R.P., Landi, B.J., Harris, J.D., et al., " Carbon nanotubes for power applications", *Materials Science and Engineering B*, In Press, 2004.

5. Chegel, V.I.; Poperenko, L.V.; Pokropivny, V.V, et al.: "Modification of the surface plasmon resonance in the gold film covered by nanotube BN", Proceedings of IV International Conference "Problems of Optics and High Technology Material Science" SPO 2004, page 73-74, Kyiv, 2004.

FTIR STUDIES OF NITROGEN-DOPED CARBON NANOTUBES

Abha Misra, Pawan K. Tyagi, M. K. Singh and D. S. Misra[@]

Department of Physics, Indian Institute of Technology Bombay, Mumbai-400 076

Abstract

Purified and defect free carbon nanotubes have great potential of applications in electronic, polymer composites and biological sciences. The removal of impurities (carbon nanoparticles and amorphous carbon) is an important step before the CNT applications have been realized[1,2]. In this paper we report the results of FTIR and TGA studies of the impurities present in the carbon nanotubes. The multiwalled CNTs were grown using Microwave Plasma Chemical Vapor Deposition (MPCVD) technique. Fourier transform infrared (FTIR) studies were carried out in the range 400-4000 cm^{-1} to study the attachment of the impuriteis on carbon nanotubes. FTIR spectra of as-grown MWCNTs shows dominant peaks at 614, 1026, 1372, 1445, 1736, 2362, 2851, 2925cm^{-1} which are identified as Si-O, Si, C-N, N-CH_3, CNT , C-O, C-H_x respectively. The peaks are sharp and highly intense showing the chemical adsorption nature of the dipole bond. The intensity of the peaks due to N-CH_3, C-N and C-H reduces after annealing. It is interesting to note that these peaks vanish on annealing at high temperature (900^0C). The presence of C-N peak may imply the doping of the CNTs with N in substitution mode, TGA measurements, carried out under argon flow, show that the dominant weight loss of the sample occurs in the temperature range 400-600 ^{o}C corresponding to the removal of the impurities and amorphous carbon.

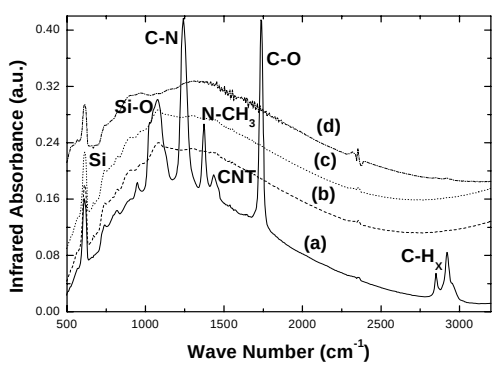

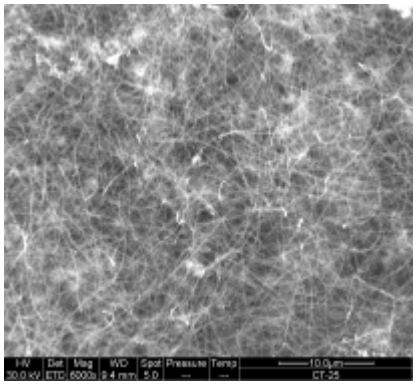

Figure 1(a): FTIR spectra of carbon nanotubes. (b) SEM image of carbon nanotubes grown on Cu foil.

References

1. S. Chopra, A. Pham, J. Gaillard, A. Parker, A. M. Rao, Appl. Phys. Lett**. 24**, 4632 (2002).
2. O.K. Varghese, P.D. Kichambre, D. Gong, C.A. Grimes, Sensors and Actuators **B 81**, 32 (2001).

Characterization of single-crystal diamonds grown by high-growth-rate chemical vapor deposition methods

Yu-Chun Chen, Chih-Shiue Yan, Ho-kwang Mao and Russell J. Hemley

Geophysical Laboratory, Carnegie Institution of Washington,

5251 Broad Branch Road NW, Washington, DC 20015

Marcus Origlieri

Department of Geosciences, University of Arizona, Tucson, AZ 85721-0077

Szczesny Krasnicki

Experimental Facilities Division, Argonne National Laboratory,

9700 South Cass Avenue, Argonne, IL 60439

Yonhua Tzeng

Department of Electrical and Computer Engineering, 200 Broun Hall,

Auburn University, Auburn, AL 36849-5201

Keywords: single crystal diamond, annealing, ultrahard

High-quality single crystal diamonds have been obtained by microwave plasma chemical vapor deposition (CVD) with a very high growth rate, in excess of 100 μm/hr. These diamond crystals, with thickness in the millimeter range, were found to have outstanding mechanical properties before and after HPHT annealing (ref. 1). Characterization was accomplished using scanning electron microscopy (SEM), atomic force microscopy (AFM), Raman and photoluminescence spectroscopy, and X-ray diffraction. As-grown diamond crystal surfaces show feature rich surfaces with undulating waves consisting of planar slopes and rough terraces using SEM (Fig. 1) and AFM. These parallel stacking steps have a uniform separation. Analysis of rocking curves obtained by X-ray diffraction provides a comparison of the crystal qualities of the seed substrates, CVD layers (Fig. 2), and the differences of annealed superhard and ultrahard CVD diamonds.

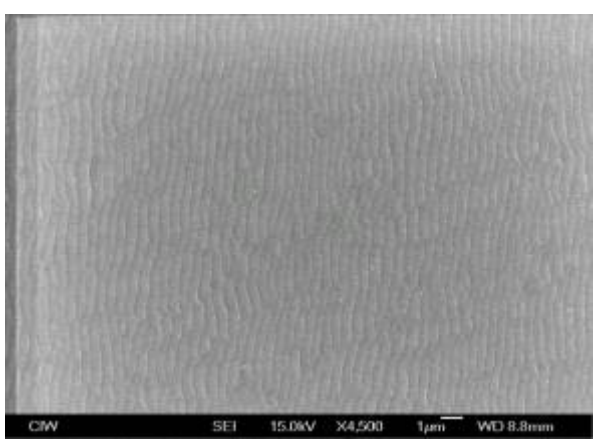

Figure 1. SEM image of typical surface morphology of an as-grown diamond single crystal

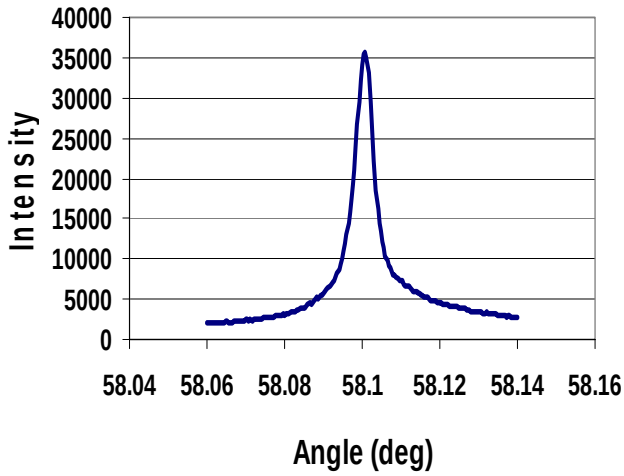

Figure 2. Rocking curve measurement of a CVD layer. A full width at half-maximum (FWHM) of 0.006° was measured, while the seed had a FWHM of 0.005°.

Reference

1. Yan, C-S., et al., "Ultrahard diamond single crystals from chemical vapor deposition," *Physica Status Solidi*, (a) Vol. 201, No. 4, R25-R27 (2004).

SPECTROSCOPY APPLICATION FOR CHARACTERIZATION AND IDENTIFICATION OF THE ARTIFICIALLY COLOURED DIAMONDS

M. A. Viktorov, M.B. Kopchikov

Moscow State University, Department of Geology, 119992 Moscow, Russia, viktorov@pisem.net

Keywords: diamond, irradiation, annealing, color-treatment, spectroscopy.

Abstract

There are still some concern about mechanisms of defects transformations and structure of some lattice defects in diamonds. This work is performed for better understanding the processes which take place in diamond lattice during irradiation and annealing.

Samples of artificially colored natural and synthetic diamonds were investigated by the means of standard gemological equipment (e.g. UV-lamp, microscope) and also VIS-range absorption spectroscopy (at room temperature), spectral (at room and liquid nitrogen temperatures) and color cathodoluminescence, and laser induced photoluminescence (lasers with wavelengths of 488 nm at the room temperature). Among studied samples there are several octahedral natural diamond crystals, synthetic diamond crystals, flat plates cut from natural and synthetic diamonds. Several samples (natural octahedral diamond crystal) have undergone annealing at the temperatures of 1700-1800 degrees C under high pressure (6 GPa) during 5 hours and some samples (octahedral natural diamond crystals, natural and synthetic diamond flat plates) were irradiated by protons. Irradiated samples then were annealed at the different temperatures in the range of 800-900 degrees C. At every stage spectroscopic data was acquired.

The color of the annealed samples has changed from brownish to yellow-green. In the absorption spectra of the annealed samples there were viewed increasing of 415 nm line (N3-center) and appearing of 503 nm line (H3-center). In the laser photoluminescence spectra of the annealed diamonds there were viewed appearing of intense H3-center line at 503 nm. Images of the color cathodoluminescence of the annealed samples revealed changing of color (from blue to green) in the luminescence.

The color of the irradiated samples has changed to green for natural diamonds and to greenish-yellow for synthetic diamonds. In the absorption spectra of the irradiated samples there were viewed appearing of 503 nm line (H3-center). Images of the color cathodoluminescence of the irradiated natural diamond samples revealed no changing of color and distribution of luminescence (remain blue). Images of the color cathodoluminescence of the irradiated synthetic diamond samples revealed changing of the intensity of luminescence: weakening of red cathodoluminescence.

Acquired data provide a useful information on causes of diamond color, mechanism of the transformation and stability of lattice defects in diamonds and can be useful for gemologists in the identification of annealed and irradiated diamonds.

EXTENDING THE 3-OMEGA METHOD TO THE MEGAHERTZ RANGE FOR MEASURING THE THERMAL CONDUCTIVITY OF DIAMOND THIN FILMS

Romy Liske, Thomas Wunderer, Michael Leonhardt, Timothy Grotjohn, Jes Asmussen, Thomas Schuelke

Michigan State University / Fraunhofer USA Inc., Center for Coatings and Laser Applications,
B100 Eng. Research Complex,
Michigan State University, MI 48824-1226

Keywords: 3-omega method, thermal conductivity, diamond thin films

Abstract

Knowing the thermal conductivity of a material is important for the successful design and implementation of any thermal management application. A special challenge however is the experimental determination of the thermal conductivity of highly thermal conductive materials such as diamond, which are synthesized in the form of thin films. Not only may the thin film's thermal conductivity significantly differ from well-established literature values for the bulk material. It may also strongly depend on the particular synthesis conditions. For example, chemical vapor deposited diamond thin films exhibit a wide process depending range of microstructures with crystal dimensions from a few nanometers to several hundreds of micrometers. The grain boundary density and therefore potential sites for thermal wave scattering vary accordingly.

With diamond thin films becoming increasingly important for high-power and high-speed electronics applications we are developing an experimental technique to measure the thermal conductivity of these films. One such technology is the so-called 3-Omega method [1]. This method can be applied to measure the thermal conductivity of dielectric materials and requires depositing a conductive pattern to the surface of the film, which may be accomplished via a lithographic process. For example, in our case we use a 5 nm chromium interface to promote the adhesion of a 200 nm silver layer. Applying a lift-off masking process, structures were generated as shown in Fig.1.

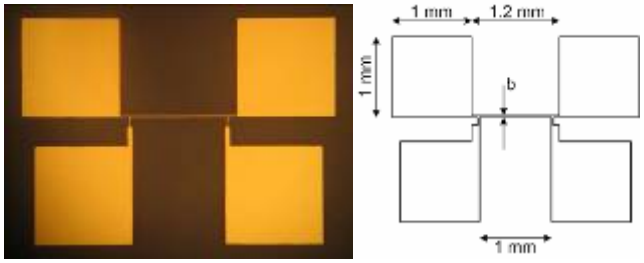

Fig.1 Heater / thermometer electrode structures

The metal pattern consist of a thin line (5 – 20 µm, depending on lithographic capabilities) functioning as heater/thermometer, whereas the 1 mm^2 large squares serve as contact pads.. The, for the analysis necessary, dR/dT curves of the heater/thermometer structures are measured by applying a 2.5ºC/min temperature ramp up to 150ºC. The values are recorded during rising and falling temperatures and the procedure is repeated twice for each sample to ensure that the samples are properly annealed.

A current at the angular frequency ω is applied to the thin line, which generates a temperature oscillation ΔT at a frequency of 3ω. The driving frequency dependence of this temperature oscillation can be determined by measuring the first and third harmonic voltages, the dR/dT curve and the average resistance of the heater/thermometer. The thermal conductivity of the dielectric material can then be determined by fitting the solution of the appropriate heat conduction equation to the experimental data. For the particular geometry of a thin heater/thermometer line Cahill [1] developed an efficient method to allow for a straight forward linear approximation.

However, this linear approximation is limited to the lower frequency range (up to kHz, depending on material), where the penetration depth of the thermal wave is significantly larger than the width of the heater/thermometer. Simultaneously the penetration depth of the thermal wave, which is proportional to the square root of the thermal

conductivity, has to be smaller than the film thickness to avoid substrate effects. These conditions can be summarized as follows:

$$\text{line width} << s = \sqrt{\frac{\lambda}{i\omega\rho C}} << \text{film thickness} \quad (1)$$

Expression (1) illustrates the difficulties that arise for measuring thin and highly thermal conductive films. Keeping the thermal penetration depth *s* smaller than the film thickness requires using higher frequencies ω, which in return requires an even smaller line width. For example, a 5 µm diamond film would require more than 8 MHz to keep the thermal penetration depth just under 5 µm, and the heater/thermometer should be much narrower than 5 µm, which makes it more difficult to produce.

In this paper we address the specific challenges of the method for measuring highly conductive thin films by extending the applied frequency into the MHz range as well as analyzing the measured data beyond the low frequency limit by fitting to the complete solution of the thermal conductivity equation rather than to the linear fraction of it. Fig. 2 demonstrates the capability of the setup for SiO_2 measurements.

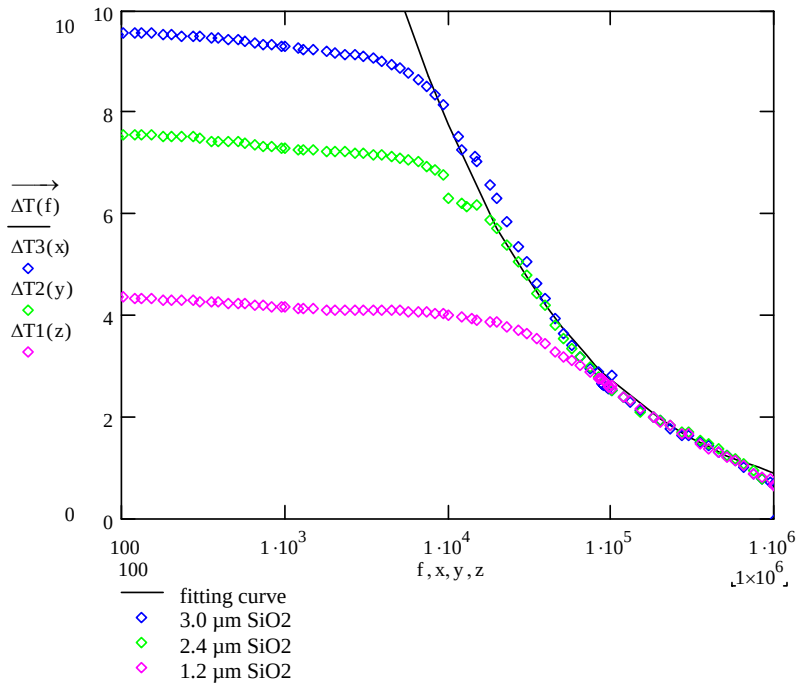

Fig. 2 Temperature versus frequency for SiO2 films on silicon

The SiO2 layers shown above demonstrate the capability of our set-up to measure up to 1 MHz driving frequency. The three SiO2 films of different thicknesses (1.2 µm, 2.4 µm and 3.0 µm) indicate that the thermal conductivity (λ = 1 W/(m K)) is independent of film thickness.

Our current driving frequency limit of 1 MHz is determined by the cable length between the probes and the compensating measurement circuitry. Currently we are measuring diamond films as thin as ≈ 15 µm. A redesigned probing head is under development and will enable to apply this 3-Omega technique to even thinner diamond films.

REFERENCES

1. D. G. Cahill, Thermal *conductivity measurement from 30 to 750 K: the 3w method*, Ref. Sci. Instrum. 61(2), 802 (1990).

OBSERVATION OF STRUCTURAL CHANGES IN CARBON FILMS UNDER EXTERNAL INFLUENCES

Zh.R. Panosyan, A.V. Meliksetyan, A.S. Voskanyan,
Y.V. Yengibaryan, A.A. Sahakyan, A.T. Darbasyan
State Engineering University of Armenia, RA

The carbon films obtained by the method of plasma chemical deposition from the multicomponent stream of ionized particles on the various substrates surface are investigated. The photographs obtained with the help of electron microscope evidenced rising on the film surface the structural formations looks like direct parallel lines. The charge accumulation takes place apparently along these lines. When the film is exposed to the local thermal impact the micro tube-like structural peculiarities are formed along these lines. Observed peculiarities possess by the periodic structure with the well-defined constant period for both along the formations and between the formations itself.

The analysis of obtained results evidenced the possibility of coincidence of lines of charge accumulation with the micro tube-like formations. It is important to emphasize that the parameters of micro tube-like formations, that is their period and linear dimensions are controlled only by operating practices details and are independent on the type of external influence Fig.1.

The investigation of volt-ampere characteristics of sandwich-like structures on the base of Metal -carbon film-Si reveals the availability of irreversible breakdowns (Fig 2) connected apparently with structural changes. These changes are observed with the help of microscope and conditioned apparently by the strong electric field (~10^5-10^6 V/sm) influence.

Thus the the possibility to obtain the controlled micro and nano formation both on the surface and in the bulk of carbon films at the their deposition from multi component ion stream is established.

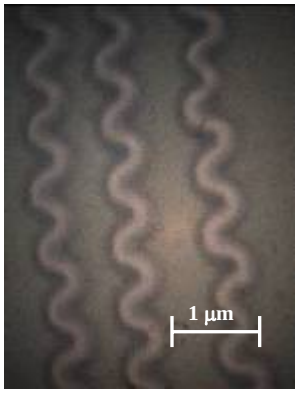

Fig.1

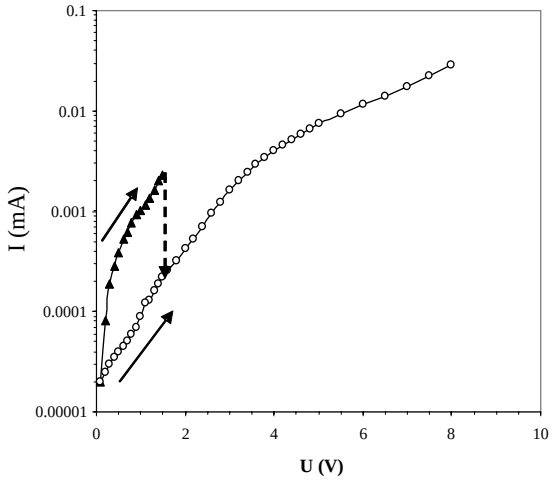

Fig.2

POSTER SESSION 2

MEMS

POLYCRYSTALLINE DIAMOND MEMS RESONATOR TECHNOLOGY FOR SENSOR APPLICATIONS

Nelson Sepúlveda and Dean M. Aslam

Electrical and Computer Engineering Department, Michigan State University, E. Lansing, MI, USA
sepulve6@msu.edu

D. A. Czaplewski, J. P. Sullivan, T. A. Friedmann

Sandia National Laboratories, Albuquerque, NM, USA

Keywords: Diamond, MEMS Resonators

Abstract

MEMS resonators, currently made out of poly-Si [1], have potential applications in the areas of RFMEMS, resonant sensors and MEMS oscillators. However, due to material limitations of poly-Si resonators, new materials such as polycrystalline diamond (poly-C) offer an excellent alternate [2,3]. The goal of this work is to develop a reliable and reproducible poly-C resonator technology for possible applications in resonant sensors and MEMS oscillators, benefiting from carbon based micro and nano technologies developed at Michigan State University [4]. The poly-C resonators, fabricated at MSU are tested using electrostatic (MSU) and piezoelectric (Sandia National Laboratories) actuation methods.

FABRICATION TECHNOLOGY

Continuous poly-C films with low surface roughness and high quality (indicated by high sp3/sp2 ratios) affect the resonator performance. A better control of nucleation density along with deposition parameters can help produce high quality poly-C films [4]. An earlier study [3] showed the influence of growth temperature and diamond powder size on the poly-C film quality. Higher growth temperatures typically lead to better film quality but rough surface. The seeding was provided by nanodiamond particles (10 - 50 nm) leading to a nucleation density of 1×10^{11} cm^{-2}. The poly-C films, with surface roughness in the range of 18-23 nm, were patterned using dry etching. This work includes the comparison between poly-C films grown in different environments. One set of samples were grown in MPCVD in the temperature range of 600-650 °C using 1.5% CH_4 in hydrogen, and the other were grown in the same temperature range but using a gas mixture of $Ar/H_2/CH_4$ (100:2:1) .

Sidewall Roughness

Another important point is the sidewall roughness resulting from dry etching, which depends on the grain size of the poly-C film. It has been reported that the optimum diamond grain size can be controlled by adjusting the flow rate of Ar/H_2 in the MPCVD reaction chamber [5,6]. Poly-C films were grown in a gas mixture using $Ar/H_2/CH_4$ plasma. The sidewall smoothness of the fabricated resonator structures using the new films are compared to that of earlier results (poly-C films grown in H_2 plasma) as shown in figure 1. The results show a smoother film sidewall for poly-C films grown in $Ar/H_2/CH_4$ plasma. These results are reported for the first time.

TESTING

The previous studies of poly-C resonator technology [3] with minimum feature sizes in the range of 1 - 2 μm led to an excellent quality of released structures. These structures have now been excited using electrostatic actuation and the initial results are shown in figure 2. Bridges and comb-drive structures have been tested. The frequencies and quality factors are in the range of 0.303 – 2.09 MHz and 1,000 - 1,500, respectively. Currently, the samples are being measured at Sandia National Laboratories using piezoelectric actuation. The results from these measurements will be compared with the results obtained by using electrostatic actuation.

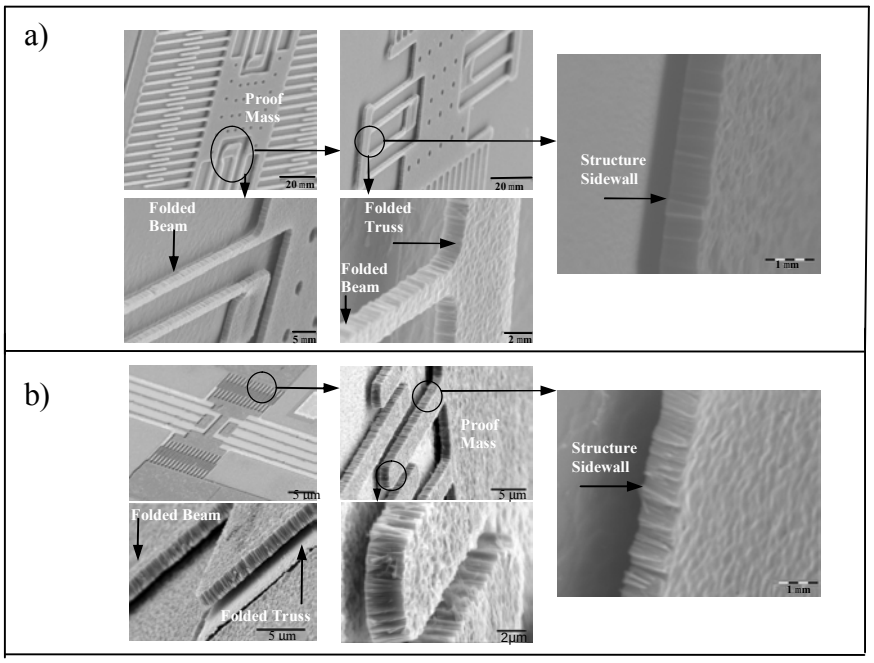

Figure 1 Poly-C structures grown in different environments (a)Ar H_2/CH_4, (b) H_2/CH_4

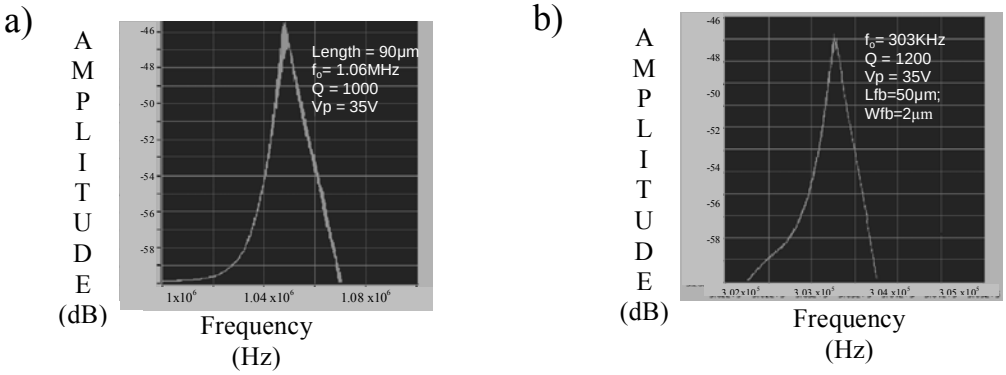

Figure 2 Testing results for a poly-C bridge (a), and a comb-drive resonator (b).

REFERENCES

1. C. T.-C. Nguyen, *Proceedings*, 1998 IEEE International Micro Electro Mechanical Systems Workshop, Heidelberg, Germany, Jan. 25-29, 1998, pp. 1-7

2. Jing Wang; Butler, J.E.; Feygelson, T.; Nguyen, C.T.-C. "1.51-GHz nanocrystalline diamond micromechanical disk resonator with material-mismatched isolating support" Micro Electro Mechanical Systems, 2004. 17th IEEE International Conference on. (MEMS) , 2004 pp.641-644

3. N. Sepulveda, and Dean M. Aslam "Polycrystalline diamond technology for RFMEMS resonators" J. of Microelectronic Engineering 73-74 (2004) 435-440

4. G.S.Yang and M. Aslam, Appl. Phys. Lett., 66 (3), (1995) 311-313; Hong D, Aslam DM, IEE Transactions on Electron Devices 46 (4): 787-791 APR 1999.

5. Haitao Ye, Chang Q Sun and Peter Hing, J. Appl. Phys Lett., 33 (2000) L148-L152

6. D. Zhou, T.G. McCauley, L.C. Qin, A.R. Krauss, and D.M. Gruen. J. App Phys 83 (1) (1998) 540-543

CARBON NANOTUBE TECHNOLOGY FOR MICRO GAS CHROMATOGRAPH AND CHEMICAL NANOSENSORS

Y. Lu and D. M. Aslam

Department of Electrical and Computer Engineering, Michigan State University, East Lansing, MI 48824

E. T. Zellers

Department of Environmental Health Sciences, University of Michigan, Ann Arbor, MI 48109

Keywords: Carbon Nanotube; Nanosensor; Micro gas chromatograph.

Abstract

Multiwall carbon nanotubes (MWCNT), with number of wall layers in range of 5 - 30 and lengths up to 500 micrometers are synthesized by microwave plasma enhanced chemical vapor deposition (MPCVD) using evaporated multi-layer Fe catalyst. The growth of MWCNT inside a deep reactive ion etched (DRIE) Si channel of the pre-concentrator focuser (PCF) section of an on-chip micro gas chromatograph (µGC) is reported for the first time by applying the catalyst selectively in the channels. A MWCNT based chemical nanosensor has also been fabricated using the same technology and initial test results are reported.

CARBON NANOTUBE TECHNOLOGY FOR µGC CHANNELS

An intensive study of tube density, diameter and catalyst application led to the selection of Fe/Ti (10 nm/10nm) double layer, evaporated on p-type Si wafers, for growth of high quality multiwall carbon nanotubes (MWCNT). While Fe serves a catalyst, the Ti layer provides a diffusion barrier. The samples were treated in hydrogen plasma for 10 minutes at 40 torr using H_2 flow rate of 20 sccm before increasing the microwave power to 1800 W. After the hydrogen plasma treatment, the MWCNT were grown at 650 ^oC by introducing CH_4 at a flow rate of 10 sccm into the growth chamber. The growth rate was approximately 10 micro-meters per minute [3].

The preconcentrator channels were fabricated in Si by deep reactive ion etching (DRIE) as shown in Figure 1(a) followed by evaporation of Fe/Ti (10 nm/10nm) double layer at $5x10^{-6}$ torr. Photoresist, left at the top of the channels after DRIE, was used to lift off the unwanted metal layers on the top surface of Si channels. After a MWCNT growth time of 15 minutes in the channels the sample was cooled down to room temperature in vacuum [1] [2]. Figure 1(b-d) shows the sample after the growth. The tube length and density are approximately 50 µm and $4.2x10^9$ cm^{-2}, respectively. The TEM pictures (JEOL 2010F field emission TEM), indicating number of wall layers in the range of 5 – 10 and shown in Fig. 1(e-f), were taken on a separate set of samples.

CARBON NANOTUBE NANOSENSOR TECHNOLOGY

The sensor structure was fabricated on a quartz substrate using growth conditions described above. The Fe/Ti metal layer was patterned to form the electrodes separated by 200 µm. As the tubes are 400 µm tall, the tubes from the neighboring electrodes overlap to form the sensor structure as shown in Figure 2(a).

Sensor Testing

The fabricated sensor was placed on a temperature-controlled stage inside a high vacuum chamber kept at $2x10^{-7}$ torr. The surface temperature of the sensor structure was measured by a K type thermocouple. A Keithley 2010 multimeter was used to monitor the resistance change of the sensor and a HP 4140B pA meter/ DC voltage source was used to characterize the current-voltage (I-V) characteristics. Figure 2(b) shows the response of the sensor after exposure to acetone in air at room temperature, indicating shorter response times than those reported in the literature [4]. The resistance of the exposed sample decreases below that of the control sample. Figure 2(c) shows the I-V characteristics of the sensor structure in vacuum at 25 ^oC. The structure shows a linear current-voltage response which indicates there is no junction between the MWCNT and the metal electrode [5]. Figure 2(d) shows the resistance- temperature response of the sensor structure in vacuum. When the sample was heated up, the pressure inside the vacuum chamber increased from $2x10^{-7}$ torr to $1x10^{-6}$ torr. A resistance hysteresis was also observed during the temperature cycle. This phenomenon appeared even after 48 hours inside the vacuum chamber and two temperature cycles.

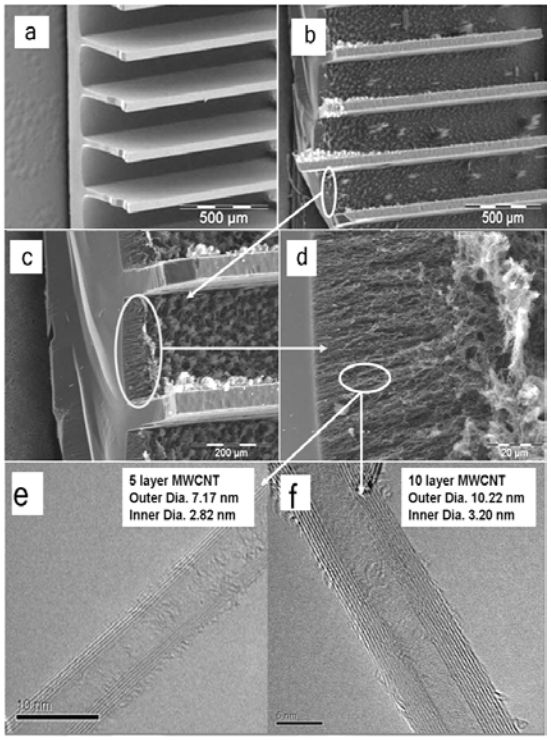

Figure* 1 *(a) - (d) SEM of the PCF; (e),(f) TEM of the MWCNT.

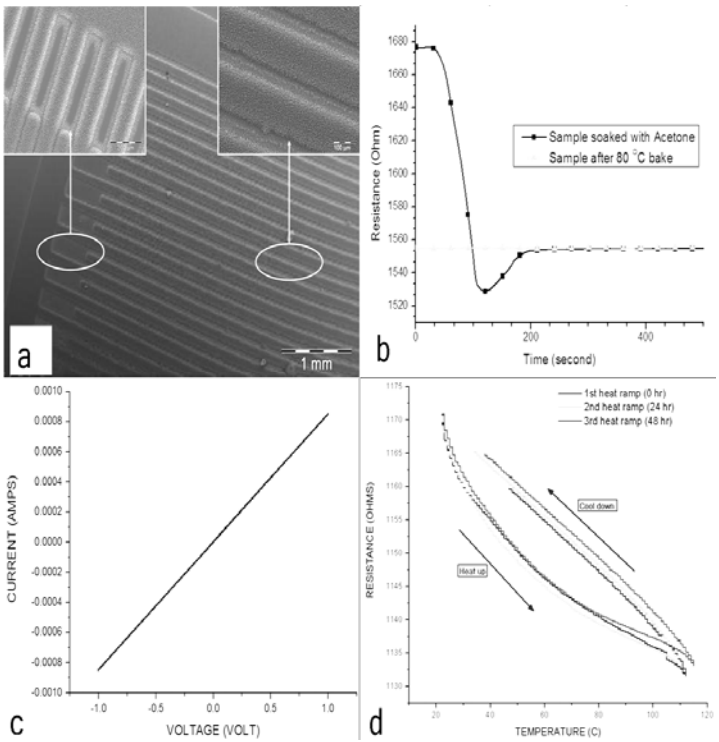

Figure* 2 *(a) SEM of the sensor; (b) Resistance measurement in air, (c) I-V characteristic, (d) Resistance-Temperature response of the sensor in vacuum.

REFERENCES

1. W. C. Tian, S. W. Pang, C. J. Lu, and E. T. Zellers "Microfabricated preconcentrator/focuser for a micro-scale gas chromatograph," J. MEMS 12(3), 264-272, (2003).
2. D.M. Aslam, K. Najafi, K.D. Wise and T. Zellers, "Poly-Carbon Nano- And Micro-Technologies For Wireless Integrated Micro-Systems", COMS 2002, Ypsilanti, MI 2002.
3. U. Kim, R. Pcionek, D.M. Aslam and D. Tománek, ”Synthesis of high-density carbon nanotube films by microwave plasma chemical vapor deposition”, Diamond & Related Materials (10)11 pp. 1947-1951 (2001).
4. L. Valentini, I. Armentano, J. M. Kenny，C. Cantalini，L. Lozzi and S. Santucci，” Sensors for sub-ppm NO2 gas detection based on carbon nanotube thin films”, Applied Physics Letters (82)6 pp. 961-963 (2003).
5. Jing Kong, Nathan R. Franklin, Chongwu Zhou, Michael G. Chapline, Shu Peng, Kyeongjae Cho, Hongjie Dai, “Nanotube Molecular Wires as Chemical Sensors”, Science (287) pp. 622-625 (2000).

Growth Of High-Quality AlN on Diamond Using Ti Buffer Layer

Cheng-Hsien Chou, Yung-Chen Lin, Jin-Hua Huang, Nyan Hwa Tai,

Department of Material Science and Engineering, National Tsing-Hua University,
Hsin-Chu 300, Taiwan, R. O. C.

I-Nan Lin

Department of Physics, Tamkang University, Tamsui 251, Taiwan, R. O. C.

Keywords: MPECVD, UNCD, AlN, buffer layer ,

Abstract

A high performance piezoelectric film, such as Aluminum nitride (AlN), combined with high acoustic wave velocity substrate, such as diamond, is a promising for applications as high frequency SAW devices. However, the growth of high quality AlN on diamond is a great challenge. The diamonds by microwave plasma enhanced chemical vapor deposition (MPECVD) technique usually possess faceted grains with very rough surface, which is not suitable for growing the piezoelectric AlN thin films. Polishing the diamond films is extremely difficult due to their hardness. Diamond films with smoother surface are thus urgently needed. In this work, we first grow diamond films using CH4/Ar plasma to result in a diamond film with very small grain size (< 10 nm), the ultra-nano-crystalline films (UNCD). Then we grow high quality AlN thin films on UNCD, using Ti-buffer layer (10 nm to 200 nm) for enhancing the adhesion of the AlN on UNCD. By tunning the Ti-buffer layer and AlN deposition parameters, c-axis oriented AlN with a thickness of 1 μm were obtained by reactive RF-sputtering technique. The column structured AlN grains were grown, with c-axis oriented almost perpendicular to the diamond surface. AFM showed the average surface roughness (Ra) was less than 20 nm. The AlN/Ti/UNCD materials show good potential for SAW device applications.

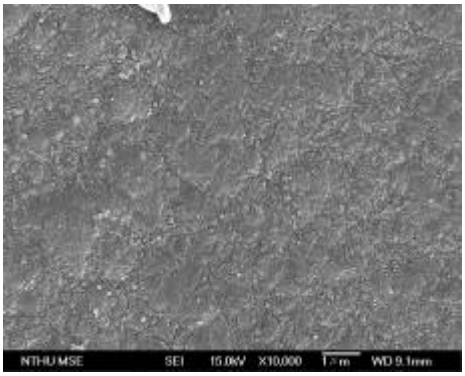

Figure 1. Diamond surface after polishing by diamond polishing paper.

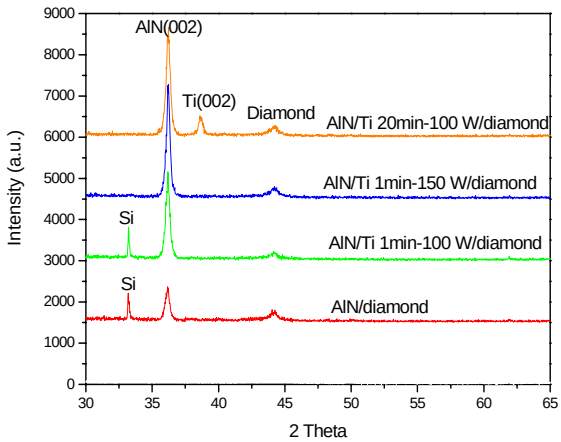

Figure 2. XRD of AlN on diamond and different Ti buffer layer.

REFERENCES

1.M.Ishihara, T.Manabe and T. Mukagai et al., “Synthesis and Surface Acoustic Wave Property of Aluminum NitrideThin Films Fabricated on Si licon and Diamond Substrates Using the Sputtering Method” ,Jpn. J. Appl. Phys. 40, 5065-5068,(2001)

2. J. Wan, R. Q.Zhang and H. F. Cheung, “Energetics of Ti atom diffusion into diamond film” ,Computational Materials Science, 23,. 73-79, (2002).

3. P. E. Viljoen, E. S. Lambers and P. H. Holloway, “Reaction between diamond and titanium for ohmic contact and metallization adhesion layers” J. Vac. Sci. Technol. B, 12, 2997-3005, (1994).

4. Y. Zhu, W. Yao, B. Zheng and L. Cao, “Application of AES Line Shape Analysis for the Identification of Interface Species During the Metallization of Diamond Particles ” SURFACE AND INTERFACE ANALYSIS, 28, 254-257, (1999).

POSTER SESSION 2

TRIBOLOGY & INTERFACES

DEVELOPMENT OF A MEMS PLATFORM FOR THE ASSESMENT OF REINFORCEMENT MECHANISMS OF CARBON NANOTUBES IN A POLYMER MATRIX

Eric Zimney, Jayhyun Chung, and Rodney S. Ruoff

Department of Mechanical Engineering, Northwestern University, 2145 Sheridan Road, Evanston, IL 60208-3111

Keywords: Carbon Nanotube, Polymer Composite, Atomic Force Microscope, Crack Propagation, Thermal Stress

Abstract

We present the design and fabrication of a MEMS platform that enables observation of fracture events, a propagating crack, in a model multi-walled carbon nanotube (MWCNT)-PMMA composite system. Preliminary results indicate that cracks can be driven large distances (~1 µm) in a 200 nm thick PMMA thin film.

INTRODUCTION

The exceptional mechanical properties of carbon nanotubes (CNTs) make them excellent candidates for use as a reinforcing phase in polymer composite systems. However, in order to realize the true potential of these polymer composites a better understanding of the CNT-polymer interaction and load transfer characteristics needs to be developed. Previous attempts to characterize the reinforcement mechanisms of CNTs in polymer matrices have studied CNTs protruding from composite fracture surfaces created by local heating from a focused TEM electron beam. [1],[2] However, this method is limited because one can not image the fracture event while simultaneously driving the crack with the focused electron beam. Here, we present the design and fabrication of a MEMS platform that enables the simultaneous imaging and driving of a crack in a MWCNT-PMMA composite sample.

Device Design

The MEMS platform, Figure 1, consists of two major components: the MWCNT-PMMA composite sample and a micromachined heater fabricated on a silicon nitride membrane. The composite sample was assembled on top of the MEMS heater using the composite electric field guided assembly method (CEGA) developed by Chung *et al*.[3] This method allows for the fabrication of an aligned MWCNT array whose spacing is readily controlled by changing the ratio of a *dc* to *ac* electric field components. Once the MWCNT array is deposited, a thin PMMA layer is spun on the device, thereby forming a composite sample whose structure is well defined.

The MEMS platform also contains a micro-heater that is integrated into the substrate supporting the composite sample. The micro-heater locally heats the sample causing a steep temperature gradient, which supplies the necessary thermal stress to drive crack propagation. The micro-heater is fabricated out of a thin metal film and uses Joule heating. The heater has a serpentine layout, Figure 1, to maximize the surface area in contact with the polymer film. Finite element modeling (FEMLAB; Comsol, Inc.) of the micro-heater shows that a local temperature of 350ºC (a temperature that is sufficient to degrade the structure of the polymer) can be achieved with an applied potential of 50 V. The low profile, planar design of the MEMS platform allows for observation of fracture events in either a transmission electron microscope (TEM) or an atomic force microscope (AFM).

Fabrication

The fabrication of the MEMS platform is a multi-step process that makes use of conventional surface micromachining techniques. The MEMS platform uses a 200µm thick single crystal silicon (p-type with <100> orientation) as a substrate. First a 200 nm thick thermal silicon dioxide film, and then a 50 nm thick LPCVD low stress silicon nitride film, is grown on the silicon substrate. These films in combination serve as a masking layer during the KOH anisotropic etch process and as a membrane to support the PMMA during the fabrication of the composite sample. Optical lithography is used to define the specimen window on the backside of the silicon substrate, and the pattern is transferred into the wafer using reactive ion etching (RIE). A through wafer window is formed by anisotropic etching of the silicon substrate using 45% (by volume) KOH solution at 95ºC for approximately 3 hours. The specimen window is necessary to allow for observation of the composite sample in the TEM and improves the efficiency of the micro-heater. Optical lithography with backside alignment is then used to define two sets of electrodes: one set is used by the micro-heater and the other is used in the deposition of the

MWCNT array. A thin chromium/gold (10/20nm) metal film is then deposited by electron-beam evaporation, and lift-off of the photoresist layer using acetone leaves the desired metal electrodes. Electron-beam lithography of a bi-layer resist (PMMA - Microchem Nano 495/Copolymer – Microchem MMA 8.5) is then used to form the serpentine shape of the micro-heater. A 30 nm thick chromium film is then deposited, and the heater is defined by lifting off the resist layer using acetone.

The composite sample is fabricated on top of the nanoscale heater by first depositing MWCNTs (previously grown by an arc-discharge method [4]) across opposing electrodes using the CEGA method. Once the MWCNTs are deposited, a PMMA polymer layer (Molecular Weight of 495k) is spin coated on the device, forming the composite sample. The final step is to pattern a pre-notch into the PMMA film using electron beam lithography. The pre-notch provides an initial crack where the thermal stress is maximized and provides a marker for the observation of crack propagation.

Conclusion

The observation of a propagating crack in this MWCNT-PMMA composite sample provides qualitative information about the reinforcement mechanisms of carbon nanotubes in polymer matrices. This approach may be useful in the future for developing a deeper understanding of the composite at the local (nanoscale) level. Preliminary results indicate that cracks can be driven large distances (~1 μm) in a 200 nm thick PMMA film using this device.

Acknowledgements

This work was funded by NIRT: Synthesis, Characterization and Modeling of Aligned Nanotube Arrays for Nanoscale Devices and Composites (NSF #030450) and the NASA University Research, Engineering and Technology Institute on Bio Inspired Materials (BIMat) under award No. NCC-1-02037.

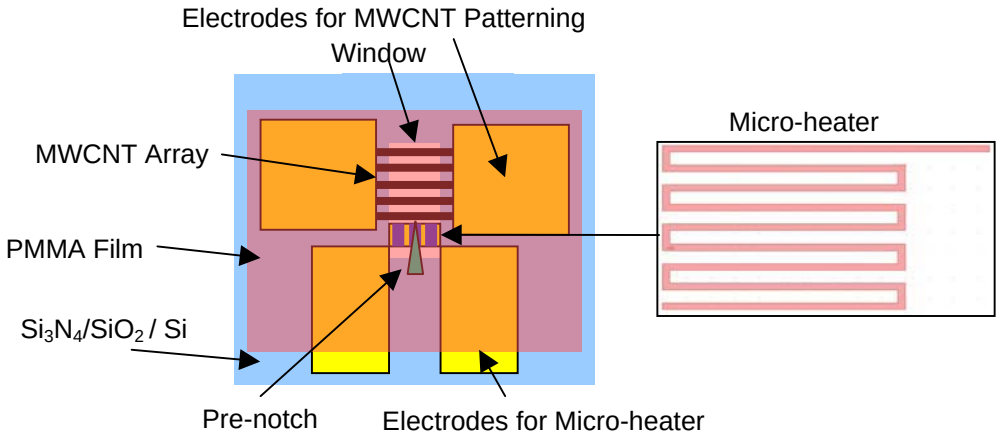

Figure 1. Schematic of the fabricated MEMS platform.

REFERENCES

1. Quain, D., et al., "Load transfer and deformation mechanisms in carbon nanotube-polystyrene composites," *App. Phys. Let.*, **76**, 20, 2868-2870 (2000).
2. Thostenson, E.T. and Chou, T.W., "Aligned multiwalled carbon nanotube-reinforced composites: processing and mechanical characterization," *J. Phys. D: Appl. Phys.*, **35**, L77-L80 (2002).
3. Chung, J., et al., "Toward Large-Scale integration of Carbon Nanotubes," *Langmuir*., **20**, 3011-3017 (2004).
4. Setlur, A., et al., "A promising pathway to make multiwalled carbon nanotubes," *Appl. Phys. Lett.*, **76**, 3008-3010 (2001).

SILICON CARBIDE SAMPLES FOR CVD DIAMOND FILM DEPOSITION WITH APPLICATION ON RASTILHO FOR MUSICAL INSTRUMENTS OF CHORD AND WAVES ANALYSIS TRANSMITTED BY THE SAMPLES

Teófilo M. de Souza[a], Leonardo N. Kawakami[a], Samuel E. Lucena[a], Paulo R. Alves[a]

a) Laboratório de Pesquisa e Desenvolvimento de Dispositivos com Diamante CVD e Novos Materiais – Unesp - Campus de Guaratinguetá (teofilo@feg.unesp.br)

Keywords: CVD Diamond, Spanish Guitar, Sound Speed in Film, SiC

Abstract

The diamond obtained by CVD (chemical vapor deposition) presents a high capacity of transmission of the sound. The sound speed in the diamond film is of the order of 18.000 m/s, while, by example, the sound speed in the aluminum is 6.420 m/s [1]. That proprierty permits the application of in "rastilhos"* of musical instruments of chord for the transmission of sound. For so much to first phase of preparation of the substrate was the cut of the SiC bulks, followed by the preparation of the surfaces by means of scratch and scouring in order to a good adhesion of the film. The CVD diamond film was deposited, on the substrates, utilizing hot filament reactor doing use of a hidrogênio and methane mixture. Parallel it was carried out a study about the capture of the sound and an exit wave analysis. In this phase, was utilized a spanish guitar which had his sonorous waves grasped by a microphone, these were visualized in an oscilloscope. The waves presented a very irregular form compared with a sinusidal wave. For it improve the viewing of the wave, was necessary the use electronic screens, that permitted the isolation of the fundamental harmonic one that interested.

* Piece that transmits the vibration of the spanish guitar chords for the acoustic box.

Support: FAPESP, FUNDUNESP, Ao Rei dos Violões (tonante@tonante.com.br), PROPP-UNESP, CNPQ,

REFERENCES

1. Davis, R.F. – Diamond Film and Coating – Development, Properties and Applications – Noyes Publications – edited North Carolina State University Department of Materials Science and Engineering Raleigh, North Carolina – 1993.

STRESS AND PURITY CRISTALLINITY OF CVD DIAMOND FILMS GROWTH IN HOT FILAMENT REACTOR ON TI6AL4V ALLOY WITH VARIOUS METHANE CONCENTRATION

Teófilo M. de Souza[a], Joanisa Possato[a], Joelma de Oliveira[a,b], J.E.Bueno[a]
a) Laboratório de Pesquisa e Desenvolvimento de Dispositivos com Diamante CVD e Novos Materiais – Unesp - Campus Guaratinguetá (teofilo@feg.unesp.br)
b) FAMINAS- Bairro Universitário-Muriaé-MG(joelmaoliveira@imicro.com.br)

V. J. Trava-Airoldi[c]

INPE- São José dos Campos-SP- Brazil

Keywords: Methane Concentration, Hot Filament Reactor, CVD Diamond, Stress, Ti6A14V.

Abstract

CVD diamond film on the surface of Ti6Al4V alloy will increase its lifetime. The diamond films were deposited in hot filament reactor with various methane and hydrogen concentration, in order to study the adherence between film and substrate. Raman Scattering Spectroscopy evaluated film quality, purity cristallinity and total stress. Thermal stress was evaluated from the calculus of thermal expansion coefficient of the film and of the alloy from room temperature to growth temperature. Intrinsic stress was calculated considering the difference between the total and the thermal stresses. Adherence tests were done with indentation technique and studied by Scanning Electron Microscopy. Its can observe a strong dependence with the sample preparation technique. Best results in terms of the film quality are obtained for a methane concentration ranging from 0.5% vol. to 1.0% vol. in hydrogen. The diamond films obtained have compressive stress and good adherence.

Financial support: FAPESP, FUNDUNESP, PROPP-UNESP, CNPQ

DENTAL IMPLANTS RECOVERED WITH CVD DIAMOND FILM

Joanisa. Possato[a], Teófilo M. de Souza[a]

a) Laboratório de Pesquisa e Desenvolvimento de Dispositivos com Diamante CVD e Novos Materiais – Unesp - Campus Guaratinguetá (teofilo@feg.unesp.br; mec03256@feg.unesp.br)

Keywords: Dental Implants, Ti, Biocompatible, Hemocompatible

Abstract

Utilizing Chemical Vapor Deposition(CVD) is possible deposit a film of diamond on the surface of dental implants. The diamond by be an organic material, him confers the states of biocompatible and hemocompatible, being these of extreme importance you dental implant, deeds of titanium and its alloys, enabling diminish the symptoms of rejection. On the samples of dental implants with titanium they were deeds cleaning from the surface with oxalic acid and afterwards with ultra-sound, and determination from the morphology from the surface of the body of test with observations by scanning electronic microscope and optic. The surface of the prepared substrate had its composition analyzed by X-Rays diffraction and Energy Dispersive X-Rays(EDX). CVD diamond film was deposited by hot filament reactor assisted technique. After deposition, analysis were carried out using Scanning Electronic Microscope, X-rays diffraction and Scattering Raman Spectroscopy. The results showed a good adhesion of the CVD diamond film on the surface of dental implants.

Financial support: FAPESP, FUNDUNESP, PROPP-UNESP, CNPQ.

Human micro-vascular endothelial cell attachment and tube formation on balloon expanded stainless steel Stents coated with DLC and Si-DLC thin solid films

*Okpalugo TIT, PD Maguire, J McLaughlin
N. Ireland Biomedical Eng. Centre (NIBEC) & Nanotechnology Research Institute (NRI)
School of Electrical & Mechanical Engineering; University of Ulster
Shore Road, BT37 0QB, Northern Ireland, UK

Stainless steel stents commonly used for surgical percutaneous transluminal coronary angioplasty have been coated with diamond like carbon (DLC), DLC with Si-sub-layer and with Si-doped DLC; and have been examined after balloon expansion for material coating durability, haemocompatibility and endothelialisation potential. The surface energy of the coatings, the thin solid film coating adhesion to SS, crack propagation based on Weibull-like analysis of these coatings show changes under tensile forces of clinical balloon expansion. The haemocompatibility was examined by assessing the growth, adhesion and proliferation of human micro-vascular endothelial cells (HMECs) on the stents standing in 3-dimensional geometry inside test tubes containing HMECs in suspension for ~ 6 hrs ('upper limit time scale' for cell attachment). It seems that HMECs attach to the stents mesh at certain distances apart following expansion (Fig. 1) in order to successfully form tubes necessary for re-vascularisation, endothelialisation and for preventing re-stenosis. Endothelialisation of the stent's 2/3-dimensional side walls is desirable but at same time any 'cross bridges' or tissue tending to form across the stent tubulule (central/long axis or diameter) is unwanted since this could encourage tissue hyperplasia, narrowing and in-stent restenosis. Both the tubular diameter/cross-section of the non-expanded and expanded stents if wide enough should not encourage this process. The mechanical and micro-structural properties of the stent material and/ or the coating are important consideration. It is desirable that the stent materials and/ or coating materials are malleable enough (and that the coating has good substrate adhesion and minimal intrinsic stress) such that on balloon expansion the surface properties are not greatly altered and the micro-cracks forming on the thin solid film coatings are minimal.

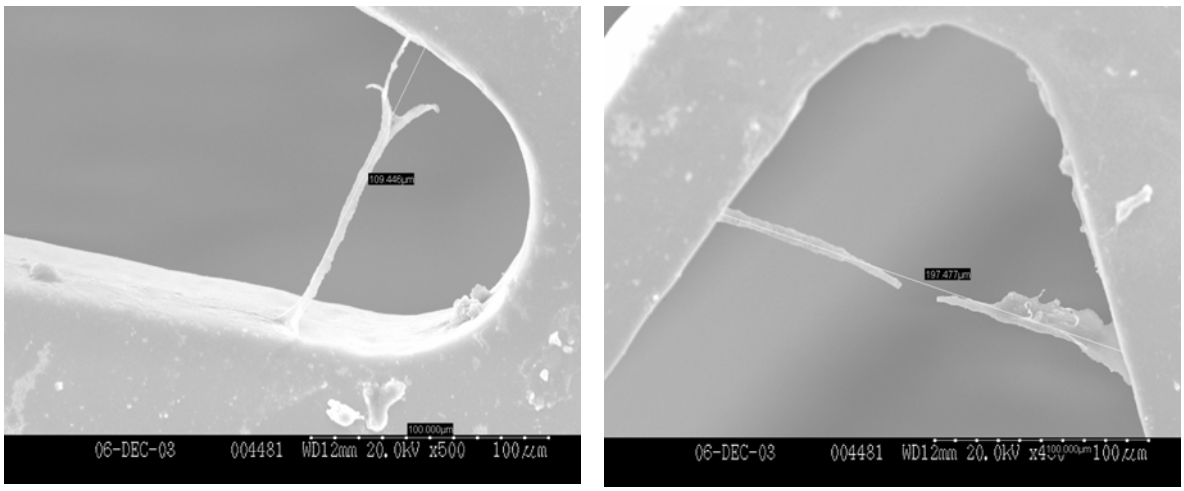

Fig. 1: SEM image of HMEC tube formation on SS-Stent coated with Si-sub-layer-DLC thin solid films.

The thin solid film coatings were done under RF 13.56MHz PECVD system with acetylene, Argon and Tetramethylsilane feed gases. XPS, Raman, SEM, contact angle and statistical analysis were done.

Keywords: DLC, Stents, endothelial cells, adhesion, micro-vessels/tube formation

*Correspondence: tit_okpalugo@yahoo.com; thomas@nibec-s1.nibec.ulst.ac.uk

Nanocarbon Thin Films: The Link between Surface Chemistry and Nanotribology

V. Sumant, D. S. Grierson, R. W. Carpick
Department of Engineering Physics, University of Wisconsin-Madison, WI

J. E. Gerbi[*], J. Birrell[#], J. A. Carlisle, O. Auciello
Materials Science Division, Argonne National Laboratory, Argonne, IL
Center for Nanoscale Materials, Argonne National Laboratory, Argonne, IL

T. A. Friedmann, J. P. Sullivan
Sandia National Laboratory, Albuquerque, NM

[*]Presently at Department of Materials Science, University of Illinois at Urbana-Champaign, IL
[#]Presently at Advanced Diamond Technologies, Inc, Chicago, IL

Keywords: Ultrananocrystalline diamond, ta-C, NEXAFS, Nanotribology

ABSTRACT

Fundamental understanding of the chemistry and bonding configuration of materials at or near surfaces, particularly at tribological interfaces, is absolutely essential to build reliable MEMS and NEMS devices that involve rolling and/or sliding contacts. Ultrananocrystalline diamond (UNCD) and tetrahedral amorphous carbon (ta-C) thin films have exceptional physical, chemical and tribological properties at the macroscale, nearly equivalent to those of single crystal diamond, and are promising materials for high performance MEMS and NEMS devices[1,2]. However, little is known about the surface chemistry of these materials, and how it changes with different processing conditions. In our previous studies on UNCD thin films, we have devised methods to control the surface chemistry at the tribological interface through hydrogen termination, which significantly improves its nanotribological properties[3]. We will review these results and discuss the effect of other chemical termination schemes such as fluorine and hydroxyl groups. We will also report the first comprehensive study of the surface chemistry and nanotribology for as-deposited, furnace-annealed, and laser-annealed ta-C. This is particularly of interest because it is known that as-deposited ta-C possesses high residual stress, and full stress relief is achieved by post-annealing at approximately 650°C. However, no detailed experimental studies have been performed to understand the surface chemistry and bonding configuration of these ta-C films after annealing, which most likely will affect the nanotrbological properties as well. We present our approach using a combination of synchrotron-based near-edge X-ray absorption fine structure (NEXAFS) spectroscopy, X-ray photoelectron spectroscopy (XPS), and atomic force microscopy (AFM) techniques to understand surface chemistry, bonding configuration and nanotribological properties of these materials. We show that there are subtle and correlated changes in the surface chemistry, the ratio of sp^2- and sp^3-bonded carbon, and the local and long-range order on the surface and in the sub-surface region of ta-C. We also show how it changes with different annealing methods used (Figure 1(a) and (b)). The nanoscale friction and adhesion also changes as these materials undergo different processing conditions.

Part of this work was funded by Sandia. Sandia is a multiprogram laboratory operated by Sandia Corporation, a Lockheed Martin Company, for the United States Department of Energy's National Nuclear Security Administration under contract DE-AC04-94AL85000. Part of this work was also supported by the US Department of Energy, BES-Materials Sciences, under Contracts DE-FG02-02ER46016 and W-13-109-ENG-38.

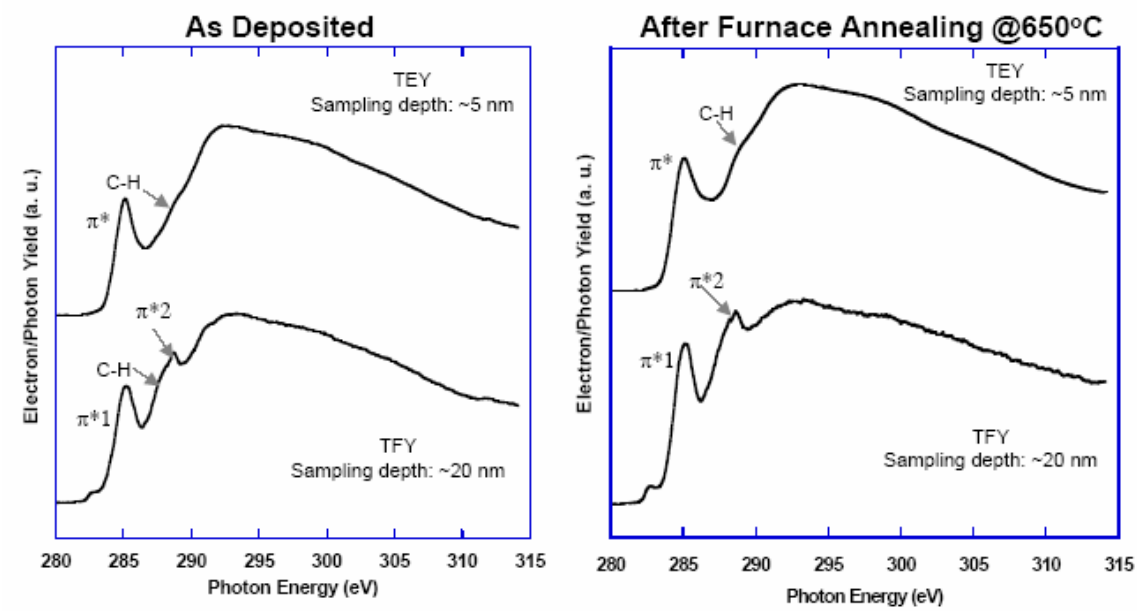

Figure 1: NEXAFS spectra of ta-C at C 1s absorption edge (a)as-deposited and (b) after furnace annealing treatment recorded in electron yield and florescence yield mode.

References:

1. A. Krauss, O.Auciello D. Gruen, A. Jayatissa, A. Sumant, J. Tucek, D. Macini, M. Molodvan, A. Erdemir, D. Ersoy, M. Gardos, H. Busmann, E. Meyer, M Ding, Ultrananocrystalline diamond thin films for MEMS and moving mechanical assembly devices, ***Diamond and Related Materials***, Vol. 10, Issue 11, 1952 (2001).
2. T. A. Friedmann, J. P. Sullivan, J. A. Knapp, D. R. Tallant, D. M. Follstaedt, D. L. Medlin, and P. B. Mirkarimi, Thick stress-free amorphous-tetrahedral carbon films with hardness near that of diamond***, Appl. Phys. Lett***. 71, p. 3820 (1997).
3. A.V. Sumant, D.S. Grierson, J.E. Gerbi, J. Birrell, U.D. Lanke, O. Auciello, J.A. Carlisle, and R.W. Carpick, Toward the Ultimate Tribological Interface: Surface Chemistry and Nanotribology of Ultrananocrystalline Diamond, ***Advanced Materials***, in press (2004).

IN SITU NANOINDENTATION OF ULTRANANOCRYSTALLINE DIAMOND AND AMORPHOUS DIAMOND THIN FILM COATINGS

E.A. Stach, A.M. Minor, D. Ge, J.W. Morris, Jr., T.A. Friedmann, X. Xiao, O. Auciello, J.A. Carlisle

Ultrananocystalline diamond (UNCD) and amorphous diamond (a-D) thin films have great potential to be used as surface coatings and as structural layers to fabricate microelectromechanical systems (MEMS) devices in general and biodevices in particular due to their superior mechanical properties, biocompatibility and excellent conformality in the case of UNCD films. Nanoindentation is accepted as the most useful technique to study localized mechanical phenomena in materials of thin film form. However, the mechanisms of deformation can only be inferred from the load-displacement data obtained during a typical instrumented nanoindentation test.

In order to elucidate the underlying physics of the mechanical deformation process in these materials, we have utilized the technique of in-situ nanoindentation in a transmission electron microscope (TEM). With this technique, a voltage-actuated piezoceramic tube is used to position a sharp diamond in-plane with the edge of an electron transparent sample. The tip is driven into the material in order to induce deformation and the corresponding response is observed in real time and at high spatial resolution.

In this presentation, we will discuss our observations of the indentation of both UNCD and a-D thin films deposited onto bulk micromachined silicon substrates. The use of micromachined substrates to provide electron-transparent samples is critically necessary for the evaluation of these diamond films, since ion-milling converts sp^3-bonded carbon to sp^2-bonded. Both thin films show an ideal combination of strength and compliance during elastic loading. In each case, we find that the high stresses induced by the indenter are effectively transferred to the substrate, resulting in room temperature dislocation plasiticity in the underlying silicon substrate (Figure 1). Figure 2 presents data from instrumented indentation tests of these same films. A pop-in event is observed at a displacement of approximately 50 – 60 nm indentation depth, corresponding to the depth at which dislocation plasticity is induced.). Upon removal of the indenter, no permanent deformation or large-scale fracture of the films is observed, indicating that both a-D and UNCD are particularly effective as ‘hard’ coatings.

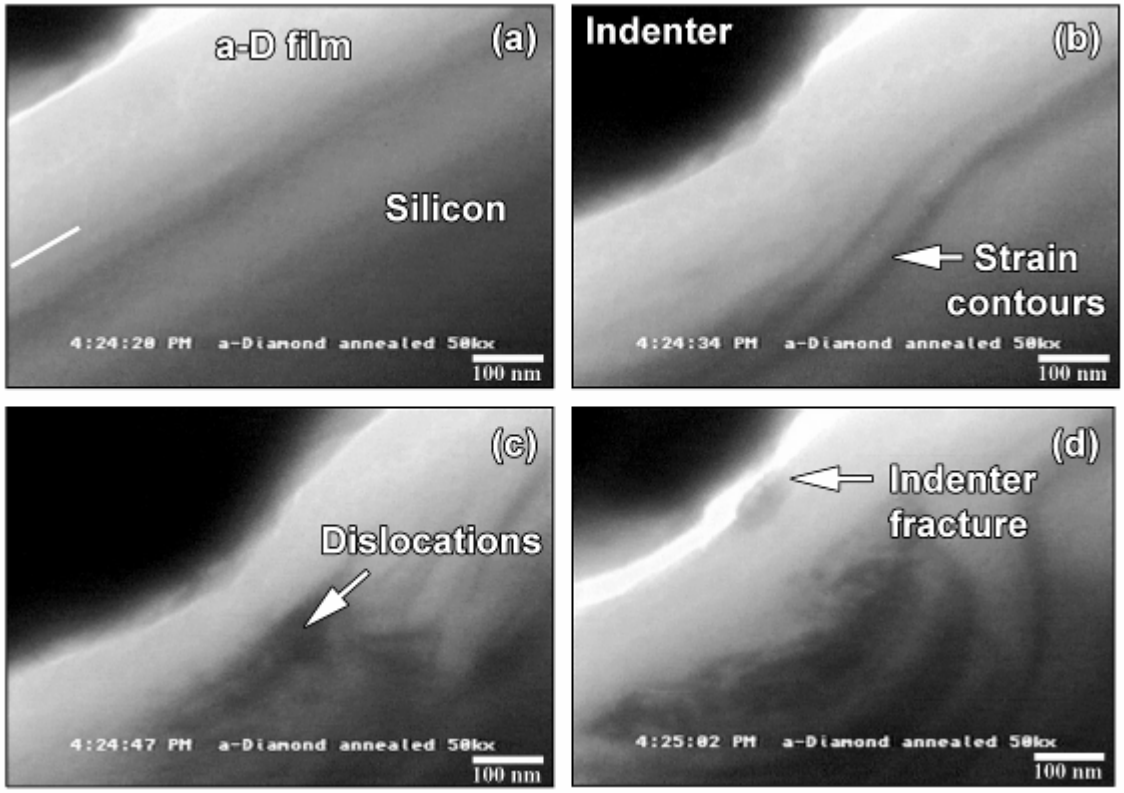

Figure* 1. *(a) Cross section TEM image of an amorphous diamond thin film coating on silicon, prior to indentation (b) initial elastic indentation (c) dislocation plasticity induced in the underlying silicon substrate (d) permanent deformation in the substrate following removal of the indenter tip.

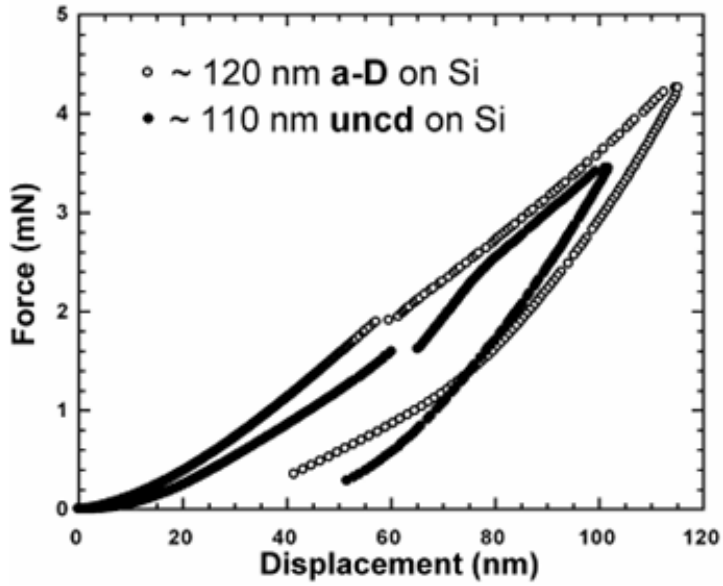

Figure* 2. *Load-displacement data from instrumented indetation tests of both a-D and UNCD films on silicon

STRUCTURAL CHANGES DURING THE WEAR OF DIAMONDLIKE CARBON FILMS AT LOW TEMPERATURE

JB Woodford & JA Johnson

Tribology Section, Energy Technology Division, Argonne National Laboratory

G Helen Xu

Department of Mechanical Engineering, University of Alaska-Fairbanks

H Liang

Department of Mechanical Engineering, Texas A&M University

Keywords: Diamondlike carbon, Raman, wear

Abstract

Visible Raman spectroscopy was used to investigate structural changes in diamondlike carbon films worn against steel and diamondlike carbon-coated counterfaces at temperatures ranging from -40°C to +20°C. The shape of the D and G peaks remained approximately constant in the worn areas of the film, but once the film had worn away the peak shapes in the wear debris spectra were much sharper. This indicates little or no change in crystallinity with wear until the film is removed, when it becomes more crystalline. The ratio of D to G peak height and area in the worn areas remained approximately constant as well, indicating little change in overall structure (Figure 1). These phenomena were independent of wear test temperature or counterface material. This was not expected, since the predominant wear mechanism changed markedly with temperature and counterface material, as shown by changes in wear rate, friction coefficient, and wear track morphology [1]. However, changes in photoluminescent background may indicate more subtle structural or compositional changes taking place during the wear process [2]. These bear directly on the functionality of these and similar films for low-temperature unlubricated tribological applications.

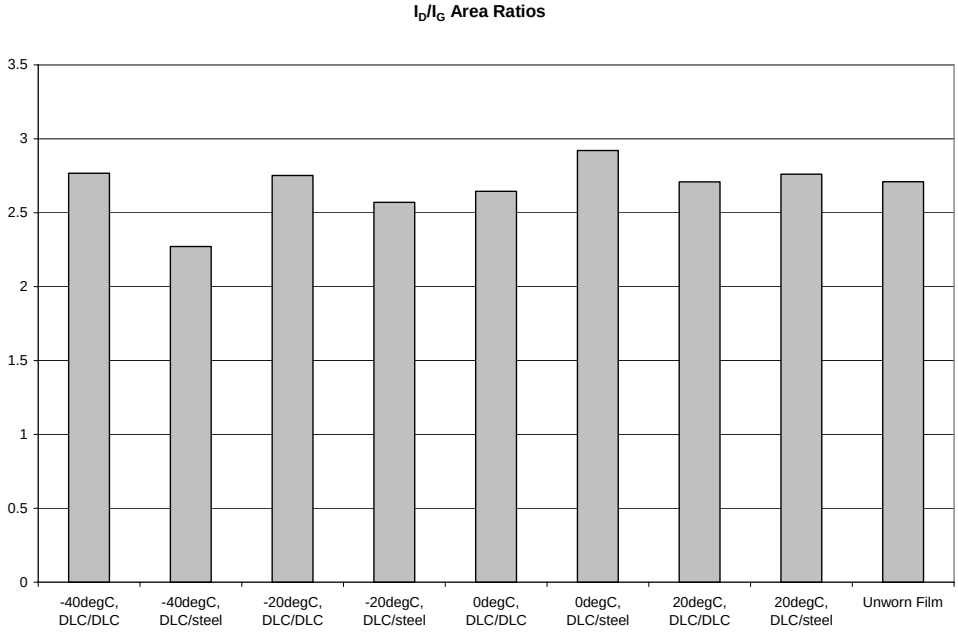

Figure 1. Raman D/G peak area ratios for DLC film worn with different counterfaces and temperatures, compared to unworn film.

REFERENCES

1. Xu, G. Helen, et al., “Temperature Dependence of DLC Film Tribological Characteristics,” *J. Amer. Ceram. Soc*, in press.
2. Marchon, B., et al.: “Photoluminescence and Raman Spectroscopy in Hydrogenated Carbon Films,” *IEEE Trans. Magnetics*, Vol. 33, No. 5, pages 3149-3150 (1997).

POSTER SESSION 2

ELECTRONIC DEVICES

ANALYSIS OF P-TYPE CVD DIAMOND FOR HIGH-POWER AND HIGH-TEMPERATURE APPLICATIONS

Susan L. Heidger

Air Force Research Laboratory

AFRL/PRPE, 1950 Fifth St., Wright-Patterson AFB, OH 45433

(937) 255-6932, Fax: (937) 255-3211, Susan.Heidger@wpafb.af.mil

Jacob K. Matthews

UES, Inc.

4401 Dayton-Xenia Rd., Dayton, OH 45432

(937) 255-4132, Fax: (937) 255-3211, Jacob.Matthews@wpafb.af.mil

Howard E. Smith

University of Dayton Research Institute

300 College Park, Dayton, OH 45469

(937) 255-6366, Howard.Smith@wpafb.af.mil

Keywords: CVD diamond, high temperature, ohmic contacts, doping, passivation

Abstract

Conductive polycrystalline diamond films are desirable for a variety of high temperature and high power applications due to their high thermal conductivities, approaching the 20 W/cm-ºK of natural diamond. P-type diamond films may be produced by introducing boron as a dopant during growth by chemical vapor deposition (CVD). These films have properties which make them ideal for both passivation layers and ohmic contacts when a thin layer of p-type diamond is grown on top of non-conductive diamond. Applications in electronic devices that benefit from these films include passives, electromechanical devices, switches, integrated circuits, sensors and diamond heat spreaders [1].

Diamond films were produced in a 1.5 kW ASTEX system by Microwave Plasma Enhanced Chemical Vapor Deposition (MWCVD). Microwave power was 900 W and methane concentration in hydrogen was approximately 0.25%. Pressure was 25 mtorr and the substrate was heated to approximately 670 ºC. Boric acid dissolved in methanol was used as a dopant source and was delivered by bubbling hydrogen through a system of two bubblers in series. The head pressure of the bubblers was regulated at approximately 150 torr. The hydrogen flow rate was varied from 2.5 to 15 sccm to adjust the dopant concentration. Boron concentration was measured by Secondary Ion Mass Spectroscopy. Film thicknesses of approximately 15,000 Å were measured using a Dektak^{3}ST surface profiler. Film morphology was examined using scanning electron microscopy. Resistivity measurements were performed using the transmission line technique where the resistance is measured between two patterned contacts.

REFERENCES

1. Heidger, S.L., et al.: "High Power and High Temperature Applications for CVD Diamond," *Proc. Int'l High Temp. Elect. Conf. (HiTEC)*, IMAPS, 18-20 May, pages (2004).

Neutron Transmutation of ^{10}B doped Diamond

K. Jagannadham, M. L. Reed
Materials Science and Engineering, North Carolina State University, Raleigh, NC 27695
M. J. Lance, T. R. Watkins
High Temperature Materials Laboratory, Oak Ridge National Laboratory, Oak Ridge, TN 37831
K. Verghese
Nuclear Engineering, North Carolina State University, Raleigh, NC 27695
J. E. Butler
Code 6174, Naval Research Laboratory, Washington DC 20375

Keywords: n-type diamond, transmutation, spectroscopy, conductivity, boron

Abstract

Free standing ^{10}B isotope doped diamond films deposited by chemical vapor deposition in a microwave chamber were irradiated to thermal neutron fluence values of $0.32x10^{19}$, $0.65x10^{19}$, $1.3x10^{19}$, and $2.6x10^{19}$ n/cm^2. Cooling of the diamond films was maintained during irradiation. Neutron irradiation to a fluence of 10^{20} n/cm^2 of fast and thermal neutrons was also performed on a diamond epilayer without cooling. The films were characterized by Raman, FTIR, and photoluminescence spectroscopy for defect generation and non-diamond phase formation. The crystalline quality of diamond was characterized by X-ray diffraction. Electrical characterization was performed by measuring conductivity over the temperature range of 150 to 630 K using Van der Pauw set up. It is concluded that transmutation of ^{10}B to ^{7}Li can be carried out without the formation of irrecoverable damage by irradiation with low fast neutron and high thermal flux and continuous cooling of diamond films.

Characterization by spectroscopy

It was found that defect configurations in diamond responsible for increase in continuum back ground in the one-phonon region of Raman spectrum were absent in the films that have been cooled during irradiation, as shown in figure 1. Absence of characteristic infrared absorption peaks that were observed only upon annealing neutron-irradiated diamond is used to conclude that the temperature of the samples during irradiation was well below that needed for mobility of defects and accumulation of stable unrecoverable damage. On the other hand, results from diamond epilayer subjected to equal thermal and fast neutron fluence close to 10^{20} n/cm^2 and without cooling showed that defects formed from displaced carbon atoms become mobile and form complex configurations of irrecoverable damage. The temperature rise in the neutron-irradiated sample from transmutation was modeled and found to reach high values in the absence of cooling and as a result of reduced thermal conductivity of diamond.

Electrical characterization

From the measurement of electrical conductance of the unirradiated and 400 hr and 800 hr irradiated diamond samples, a decrease in conductance with lower value of activation energy was observed in the irradiated samples compared to that in the unirradiated, as shown in figure 2 [1]. The electrical conductivity could not be associated with a single activation process and it is thought to arise from different mechanisms. Further detailed characterization and annealing of the irradiated sample is continued.

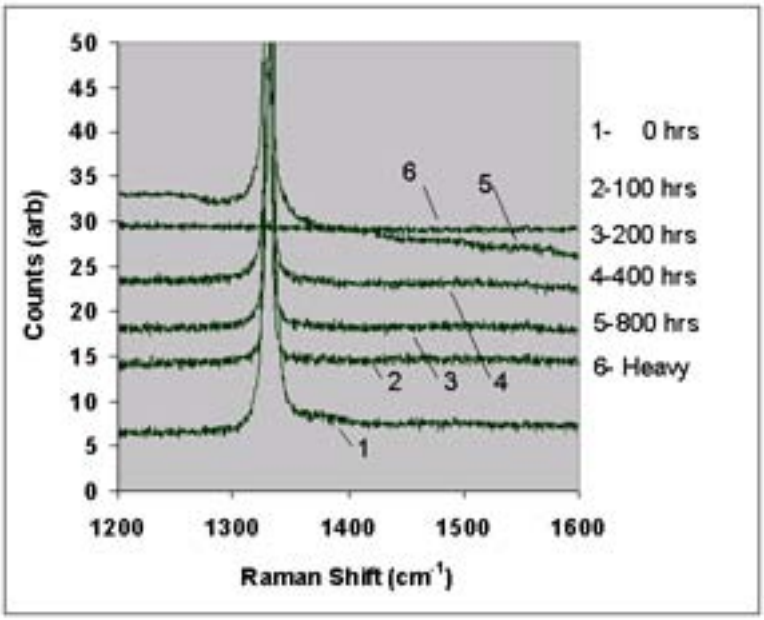

Figure 1. Raman spectrum from the unirrdiated and neutron irradiated samples with a thermal flux of 9.0×10^{12} $n.cm^{-2}s^{-1}$ and different irradiation periods is shown. Fluence values are given in the text.

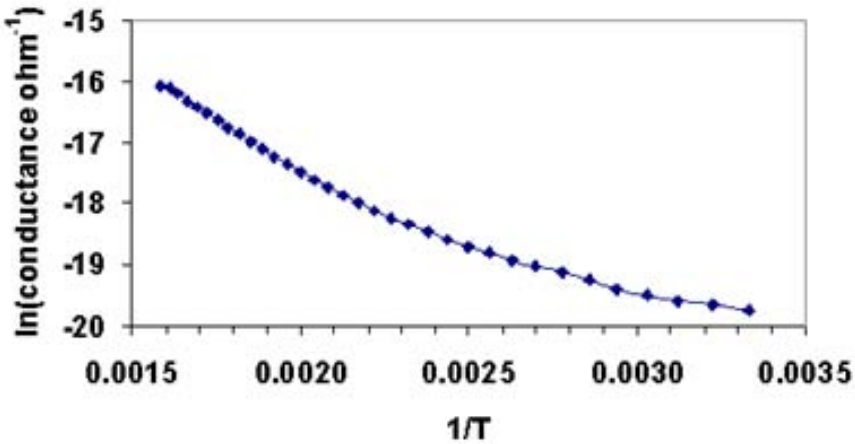

Figure 2. Electrical conductance of 800 hr neutron irradiated sample of ^{10}B isotope doped diamond sample.

References

[1]. M. L. Reed et al., J. Vac. Sci. Technol., 2004, v. 22A, p. 1191.

CVD SINGLE CRYSTAL DIAMOND FOR EXTREME UV PHOTODETECTION

A. Balducci, Marco Marinelli, E. Milani, M.E. Morgada, G. Pucella, A. Tucciarone, G. Verona-Rinati

INFN – Dip. di Ingegneria Meccanica, Università di Roma "Tor Vergata", Via del Politecnico 1, 00133 Roma, Italy

E. Pace, A. De Sio

Dip. Astronomia e Scienza dello Spazio, Università di Firenze, L.go E. Fermi 2, 50125 Firenze, Italy

Keywords: Single crystal diamond, VUV spectroscopy, Extreme UV, Photodetectors

Abstract

The fabrication and the characterization of a high quality CVD single crystal diamond UV/VUV photodetector is reported. Such a device was tested over a very wide spectral range, from the extreme UV (20 nm) up to the near IR region (2400 nm).

Different experimental setup were adopted. An Optical Parametric Oscillator (OPO) tunable laser was used to investigate the 210-2400 nm region in pulse mode. In this region the spectral response shows an UV to visible contrast of about 6 order of magnitude. A fast time response of at least 5 ns, i.e. the laser pulse duration, was observed.

A vacuum monochromator with a deuterium lamp was used to measure the device responsivity in the 120-250 nm spectral range in a continuous mode. DC gas discharge sources in the extreme UV region and a toroidal grating vacuum monochromator were used to measure the device response down to 20 nm. In both cases, device time response lower then 0.2 s was measured, which is the minimum acquisition time allowed by the used electronics.

In all measurements neither persistent photoconductivity nor undesirable pumping effects were observed so that extremely good stability and reproducibility of the device response were obtained.

INTRODUCTION

Due to its outstanding physical properties, diamond is an ideal candidate for a number of technological and commercial applications, in which extreme operating conditions are required. Indeed, diamond based devices have been shown to withstand harsh environments, high temperatures, high ionizing particle fluxes as well as intense X-Rays and Vacuum Ultraviolet (VUV) irradiation [1,2]. In particular a radiation hard and visible blind detector with a good responsivity in the VUV region is a relevant issue in both astrophysics and nuclear fusion experiments. At present, such practical applications are prevented either by the relative poor quality of polycrystalline diamond films or the very high cost and rareness of detector grade natural diamonds. This is why a great effort is now being devoted from a number of research groups in order to produce high quality single crystal CVD diamond films.

EXPERIMENTAL AND RESULT

A 150 μm thick single crystal diamond film was deposited by Microwave CVD on a $5\times4\times0.3$ mm^3 (100) oriented (HPHT) diamond substrate. A UV photodetector was then realized by depositing interdigitated Al contacts on the CVD diamond surface by a standard photolithographic process.

The obtained device was than tested in the 210-2400 nm spectral range using an Optical Parametric Oscillator (OPO) tunable laser as light source (Opolette by Opotek), producing 5 ns pulses. In the 120-250 nm spectral range the device responsivity was measured in continuous mode (DC) by using a deuterium lamp and a 0.5 m vacuum monochromator (McPherson 280). In the extreme UV region a He DC gas discharge source and a toroidal grating vacuum monochromator (Jobin Yvon LHT-30) with 5Å wavelength resolution were used.

In Fig. 1 the normalized responsivity is reported as a function of the incident laser radiation wavelength in the case of 100 V applied bias voltage. The detector shows more than five order of magnitude visible/UV rejection ratio and a very sharp drop of about 10^4 is observed in correspondence of the 225 nm diamond energy gap. At wavelengths

greater than 1300 nm the responsivity becomes lower than our detectable limit. It should be pointed out that the detector response is stable and highly reproducible, so that undesirable effect such as pumping or memory effects under irradiation could be excluded.

The vacuum UV and extreme UV spectral ranges were then extensively investigated using the above described experimental setup. As an example, the emission spectrum of a DC discharge He lamp is reported in Fig. 2, as measured by our single crystal diamond photodetector in the 20-65 nm interval. The He^{+} 25.6 nm and 30.4 nm as well as the He^{++} 58.4 nm emission lines are clearly detected, assessing a very good detection capability of the device even in this extreme UV spectral region.

In the inset of Fig. 2 the response to t=20 s irradiation intervals, at the wavelength of the 58.4 nm He^{++} emission line, are reported using four different detector bias voltages. It's worth noting that a very good signal to noise ratio is obtained even at bias voltages as low as 1 V. The rise time, which was estimated to be about 4 s, and the decay time, about 5 s, are completely ascribed to the electrometer preamplifier time constants. By properly choosing the instrument current scale, an upper limit of about 0.2 s can be derived for the diamond device time response, even though the real value is expected to be considerably lower.

CONCLUSIONS

A CVD single crystal diamond UV/VUV photodetector was fabricated and tested over a very wide spectral range, from the extreme UV (20 nm) up to the near IR region (2400 nm).

In pulsed mode, a fast time response of at least 5 ns, i.e. the laser pulse duration, was observed. A time response lower then 0.2 s was measured in continuous mode, which is the minimum acquisition time allowed by the used electronics. In particular, a He lamp spectrum in the 20-65 nm range was clearly detected with a very good signal to noise ratio.

In all measurements no persistent photoconductivity nor undesirable pumping or memory effects were observed, so that extremely good stability and reproducibility of the device response were obtained.

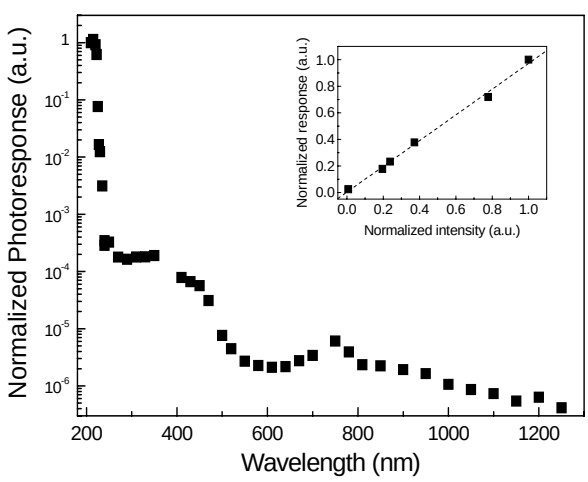

Figure* 1 *Normalized responsivity in pulsed mode as a function of the incident wavelength (full plot). Responsivity of the detector as a function intensity at 220 nm (inset).

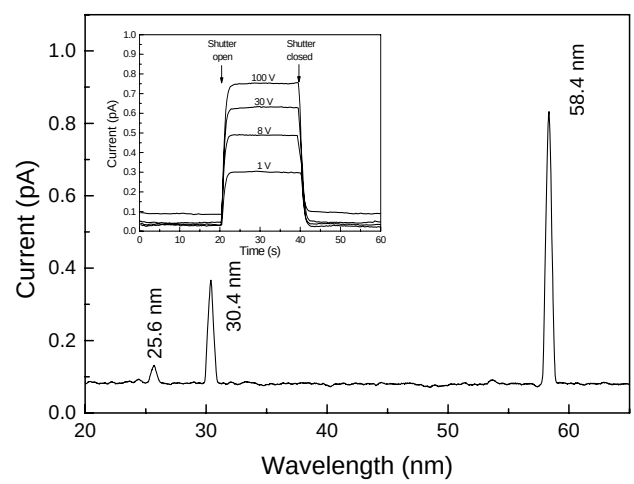

Figure* 2 *He spectrum in the 20-65 nm range as measured by the CVD single crystal detector (full plot). Photocurrent at 58.4nm for different bias voltages (inset). The rise and decay time are completely ascribed to the electrometer time constants.

REFERENCES

1. McKeag, R. D et al. "Photoconductive properties of thin film diamond" *Diam. Relat. Mater.*, Vol. 6, 374-380 (1997)
2. Brescia, R. et al. "Photoconductive properties of single-crystal CVD diamond" *Phys. Stat. Sol.* , Vol. 199, 113-118 (2003).

TAILORING THE PROPERTIES OF CVD DIAMOND FOR PASSIVE AND ACTIVE RADIATION APPLICATIONS

P. Ascarelli, E. Cappelli, D.M. Trucchi

CNR-ISC, Via Salaria km 29.300, 00016 - Monterotondo Scalo (RM), Italy

G. Conte

University of "Roma Tre", Dept. of Electronic Engineering, Via Vasca Navale, 84 - 00146 Rome, Italy

Keywords: CVD Diamond, conductivity, dosimeters, active applications.

Abstract

Diamond represents a paramount material for applications involving the use of radiations and electron beams of high-energy. In fact, due to a high radiation damage resistance and to the tissue-equivalent properties, coherently with wide band-gap properties, diamond is considered one of the most suitable material for the realization of x-ray detectors, especially for dosimetry in radiotherapy applications.

CVD diamond shows a polycrystalline structure in which the material quality largely influences the photoconductive response of the resulting detectors. The control of the material properties during the growth process and the optimal design of the final detector is the basis of the tailoring operation we performed.

The control of the initial nucleation density allows an actual engineering of the electrical properties of the diamond films. We developed a method to fix the device optimal leakage conductivity[1] as a function of the peculiar application. In fact, we found precise conditions about the electrical conductivity in order to contemporarily avoid space charge formation and to have sufficient discrimination of the signal.

At present, we realized x-ray linear dosimeters and tested them in DC and AC conditions using a beam produced by a standard Cu-target tube (CuKα at 8.05 keV). The analysis of the collection efficiency of the generated charge carriers and of the density of shallow states in the band-gap in proximity of the valence band, affecting the response time and intensity, were correlated with structural parameters as the crystal grain quality and the grain boundary presence. The necessary condition to provide a linear response to the radiation dose-rate absorbed by the detector is correspondent to the condition of high collection efficiency. Once obtained such a condition, the deviation from a correct response can be attributed to space charge effects and to electron-hole recombination mechanisms.

Moreover, some experimental evidences seem to indicate new possible applications of CVD diamond for the realization of *active devices* (conversion of high energy radiation into electrical power) making use of the charging induced by secondary electron emission.

REFERENCES

1. D.M. Trucchi, P. Ascarelli, E.Cappelli, et al., "The Influence of Grain-Boundaries on the Electronic Performance of CVD Diamond Films" *Diam.Relat. Mater.*, accepted for publication (2005).

Morphology, optical properties and single-electron spectrum of 'detector-quality' DLC layers, prepared by MW CVD

V. Ligatchev[1], B. Gan[2]
[1]*School of Electrical and Electronic Engineering,*
Nanyang Technological University, Nanyang Avenue, 639798 *Singapore*
[2] *Agilent Technologies, Singapore*
abstract.presenting-evaleri@ntu.edu.sg, ligatchev@hotmail.com

So-called 'charge collection distance' rises apparently at the increment in the film thickness and average grain size in 'detector-quality' polycrystalline DLC films [1]. This effect was mainly attributed to diminishment in density of inter-granular defects in thicker DLC films with bigger average grain sizes, whereas density N(E) of the 'in-grain' states was supposed to be independent on the film thickness and morphology. In our study we are intend to demonstrate, that the N(E) distribution for the intra-granular electron states could also be influenced considerably by sizes of the DLC grains. Dependencies of spectrum of coefficient of optical absorptions, $\alpha(h\nu)$, 'indirect' gap width E_G and Urbach tail slope E_U of freestanding polycrystalline diamond-like carbon (DLC) films on their thickness and morphology have been studied. Two series of the <100>- and <110>-oriented DLC samples with different thickness were initially grown on the <100>-oriented silicon substrates by microwave plasma chemical vapour deposition (MW CVD) at fixed (within each series) deposition conditions, and thereafter separated from the silicon substrates. Main deposition and morphological parameters of the studied films are given in the Table.

Sample series	T_s, °C	Gas mixture	Dominant crystalline orientation	Thickness range, μm	Average grain size, μm
'a'	670	H_2:CH_4:O_2 400:8:2	<100>	2.0 – 20.0	0.4 – 4.0
'b'	670	H_2:CH_4:CO 400:5:10	<110>	3.0 – 12.0	0.8 – 3.1

Alteration in crystalline orientation of the DLC layers has been achieved via changes in composition of a gas mixture employed at the samples depositions (see the Table) as well as by implementing of a short period of pure hydrogen plasma etching immediately after the nucleation process.

An increment in the film thickness from 2 to 20 μm for <100>-oriented samples and from 3 to 12 μm for the <110>-oriented ones cause almost linear enlargement in the average transverse size of the surface morphology (from 0.4 to 4.0 μm for the <100>-oriented samples and from 0.8 to 3.1 μm at the <110>-oriented ones), see the Table. At the same time, significant lowering in the $\alpha(h\nu)$ (Fig.1, symbols) and E_U values (the E_U drops from 615±15 to 299±4 meV) is observed as thickness of the DLC samples rises, while the E_G quantity remains almost constant and equals to 5.40±0.05 eV for the all studied samples. Such abnormal $\alpha(h\nu)$ and E_U dependencies on the film thickness are attributed to significant influence of average sizes of DLC grains on the N(E) parameters within and just beyond the band gap of the material. A simulation of the influences of the granular morphology on the $\alpha(h\nu)$ and N(E) spectra of the DLC has been fulfilled within a framework of semi-empirical adiabatic Generalized Skettrup Model, GSM [2-4]. The GSM is essentially based on statistical description of behaviour of multiple acoustic phonons, confined within volumes of the DLC grains. It also employs assumptions on linear relationship in between single-electron energy E and reduced elastic energy of this material as well as on absence of momentum conservation for all optically activated carrier transitions. The N(E) distribution within framework of the GSM is predetermined by formulas:

$$N_c(E) = \frac{ZD}{B_c} W_c\left[E_G(0,0) - E\right], \quad (1a); \qquad N_v(E) = \frac{ZD}{B_v} W_v(E), \quad (1b).$$

$$W_{c,v}(E) \cong \exp\left(-\frac{E}{k_B T B_{c,v}}\right) \int_{M0}^{\infty} \frac{1}{Z_M [\Gamma(M)]^{r1}} \left[\frac{2 L_x L_y F(L_x, L_y, L_z) E^2}{M^{r2} (B_{c,v} hc_s)^2}\right]^M dM, \quad (2)$$

where D is an average atomic density, Z is the atomic valency, B_v and B_c are dimensionless constants which characterize the intensity of interactions of the confined acoustic phonons with charge carriers on bonding (within the VB) and anti-bonding (within the CB) electron levels, respectively; ZQE/B is an instant value of aggregate

energy of *all* longitudinal acoustic phonons, confined at the given moment in time in a rectangular coherency cell with orthogonal edges of the lengths L_x, L_y, L_z, Q is the number of atoms (of a single sort) in the confinement volume ($Q \equiv D * L_x * L_y * L_z$), M = N/ZQ and M0 = N0/ZQ, N0 is the integer *ceil* of the $ZQE/Bk_B\theta_D$ ratio (here *ceil* denotes the smallest integer greater than or equal to the rational quantity in the brackets), T and θ_D are the absolute and Debye temperatures (respectively), k_B is the Boltzmann constant, $\Gamma(M)$ is the Euler gamma-function, c_s is a velocity of longitudinal sound waves, Z_M is a statistical sum, and *r1* and *r2* are model parameters ($1 \le r1 \le 0.5$; $2 \le r2 \le 0.5$) [4]. The function $F(L_x, L_y, L_z)$ in Eq.(2) depends only on the ratios of the edge lengths [4]. The $E_G(0, 0)$ = 7.216 eV, and N(E) equal to $N(E)_v + N(E)_c$.

This model reproduces experimentally observed changes in the parameters of both 'algebraic' and exponential parts on the optical absorption spectrum, which occur at alterations of the thickness and average grain sizes of the studied DLC samples (Fig. 1, lines). All $\alpha(h\nu)$ curves in this figure have been simulated at varied lengths L_x, L_y, L_z of the phonon confinement, but almost constant values of other simulation parameters (c_s, B_c, B_v, D, $E_G(0)$, T, Z and θ_D). In particular, each of the L_x, L_y, L_z dimension is assumed to be exactly equal to the average transverse size of the DLC grains, deduced from the SEM image of the given sample. The model parameters r1 and r2 have also been slightly varied in the $0.820 \le r1 \le 0.845$ and $0.710 < r2 < 0.740$ ranges in order to obtain the best approximation of the simulation curves for the experimental data. The GSM allows us to explain as well an existence of Urbach tail with relatively large E_U values in high-quality polycrystalline DLC films and diamond powder with ordered atomic structure within DLC/powder grains. Fig. 2 reveal the N(E) curves, simulated for the films from the 'b' series at the above-listed values of the GSM parameters. These simulation results are in reasonable quantitative agreement with the experimental data on the defect states density in the <110>-oriented films, obtained with the space-charge-limited-current technique [5], see insertion in Fig. 2.

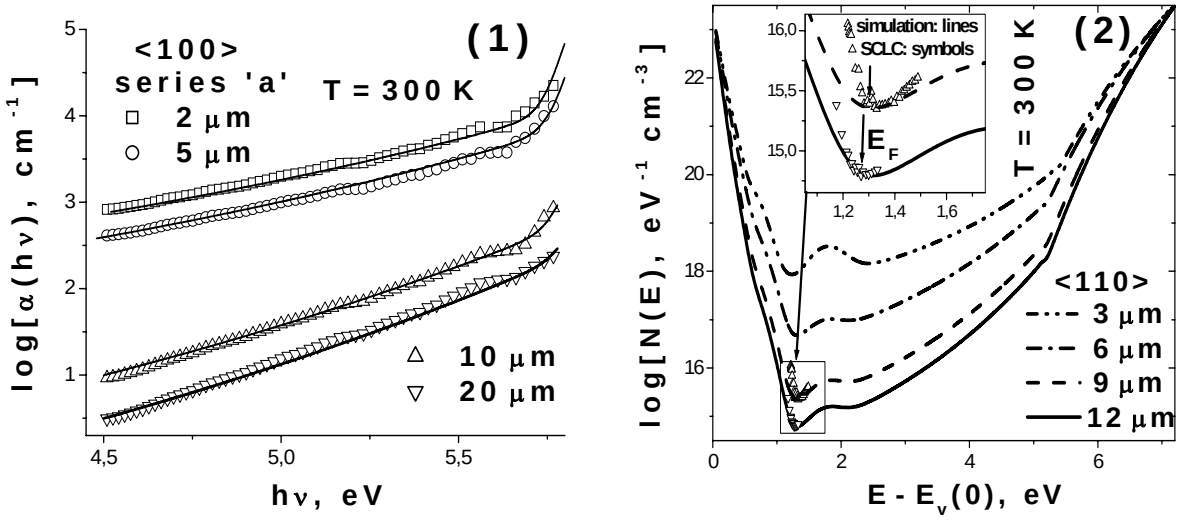

Figs. 1, 2. Typical experimental (symbols) and simulated (lines) (1) α(hν) and (2) N(E) spectra of the DLC.

References

1. Marinelli, M.; Milani, E.; Paoletti, A. *et al.*, "High-quality diamond grown by chemical-vapor deposition: improved collection efficiency in α-particle detection" *Appl. Phys. Lett.* **75**, 3216 (1999).
2. Ligachev, V.A. "Phonons fluctuation and the pseudodoping effect in in-homogeneous amorphous media. II. Quantitative analysis of the probability of states of a multiphonon system" *Physics of Solid State*, **37**, 1879 (1995).
3. Ligatchev, V. "Phonon Confinement and Properties of a-Si:H Films" *Mat. Res. Soc. Proc.* **664**, A9.8.1 (2001).
4. Ligatchev, V. "The long-range ordering, electron spectrum, and properties of amorphous silicon films I. The generalized Skettrup model" *Physica B* **337,** 333 (2003).
5. Bo Gan; Ahn, J.; Rusli *et al.* "Thickness dependence of density of gap states in diamond films studied using space-charge-limited current." *J. Appl. Phys.*, **89,** 5747 (2001).

POSTER SESSION 2

FIELD EMISSON

Syntheses of boron-doped polycrystalline diamond on molybdenum substrate for cold discharge cathode

Hiroaki Yoshida, Isamu Yanase, Naoshi Sakuma, Tomio Ono and Tadashi Sakai

Corporate Research and Development Center, Toshiba Corporation

Keywords: polycrystalline diamond, cold discharge cathode, trimethyl borate, microwave plasma CVD

Abstract

Diamond is considered as a promising candidate for the cold discharge cathode material due to large ion-induced secondary electron yield and good resistance to sputtering. In this paper, we report growth condition of boron-doped polycrystalline diamond film on molybdenum substrate and fundamental discharge characteristics of the film.

We have proposed to apply diamond as a cold cathode material to reduce the electric power consumption of cold cathode discharge lamps (CCFL). For the CCFL application, it is important to grow diamond films controlling conductivity on an applicable cathode substrate material. In this research, we selected molybdenum (Mo) as the substrate, and tried to grow boron-doped polycrystalline diamond films on that by microwave plasma CVD.

The Mo substrate was pretreated by inorganic acid, and then the bias-enhanced nucleation (BEN) was performed in the CVD chamber. To grow diamond layer, we used acetone and trimethyl borate mixed solution as carbon (C) and dopant boron (B) sources. B/C ratio was easily varied by mixing ratio of solution, and vapor of the solution was carried into the chamber with hydrogen. Growth time was 2 hours, microwave power was 1.5kW, and substrate temperature was 850 ℃ approximately. The resulted film thickness was about 4 μm, and B concentrations in the layers was found to between 1017 and 1020 /cm3 from SIMS measurements.

Grow discharge characteristics of the film were evaluated in argon (Ar) ambient gas with open-cell resume. Cathode fall voltages (Vc) were measured both for hydrogen-plasma and acid treated surface conditions. The corresponding Vc were 70 V and 90 V, respectively. These values were significantly low compared to that of conventional metal cathodes (140V). It was confirmed that B-doped CVD poly-diamond films could be a new cold cathode material candidate for discharge lamps.

This work has been performed as a part of the Advanced Diamond Device (ADD) project, which is supported by METI through NEDO.

EFFECT OF GRANULAR STRUCTURE ON THE ELECTRON FIELD EMISSION PROPERTIES OF NANODIAMOND FILMS

Hsiu-Fung Cheng

Department of Physics, National Taiwan Normal University, Taiwan 106, R.O.C.

Yen-Chih Lee, Su-Jien Lin

Department of Materials Science and Engineering, National Tsing-Hua University, Hsinchu, Taiwan 300, R.O.C.

I-Nan Lin

Department of Physics, Tamkang University, Tamsui, Taiwan 251, R.O.C.

Abstract

Diamond films have attracted considerable scientific attention as electron field emission materials due to hardness to withstand ion bombardment, and good thermal and electrical conductivity to handle high current[1-2]. Another advantage of diamond films, in term of field emission applications, is that these films can be synthesized easily by using microwave plasma enhanced chemical vapor deposition (MPECVD) process with consistent electron field emission properties. To further improve the electron field emission capacity of diamond films, reducing the grain size for the diamond films so as to increase the proportion of grain boundary region is required, as it has been proposed that the grain boundaries contain sp^2-bond[3] and provide conduction path for electron, facilitating the electron field emission process. In this present work, we adopted the bias enhanced technique for promoting the nucleation of nano-diamonds and suppressing the growth of grains. The electron field emission behavior of the nanodiamond films was observed to be pronouncedly superior to that of the diamond films with micron- or submicron-sized grains, which is ascribed to the presence of abundant grains boundaries with sp^2-bonds. Incorporation of boron species into the nanodiamond films further improves the electron field emission properties for the films. The best electron field emission properties achieved are turn-on field E_0=18 V/μm with electron field emission capacity J=0.7 mA/cm^2 at around 30 V/μm applied field. However, boron doping into the nanodiamond films does not result in consistent boron-content dependence of the electron field emission properties for the films as those in conventional micron-sized diamonds. The complication is explained by the fact that the small size of the diamond grains (~ 20 nm) may not be able to accommodate the boron species into the lattices to effectively act as acceptor dopants. Moreover, the formation of aggregates of the nano-sized diamond grains may alter the local field enhancement factor, which further complicates the correlation of the field emission behavior with the boron doping concentration for the nanodiamond films.

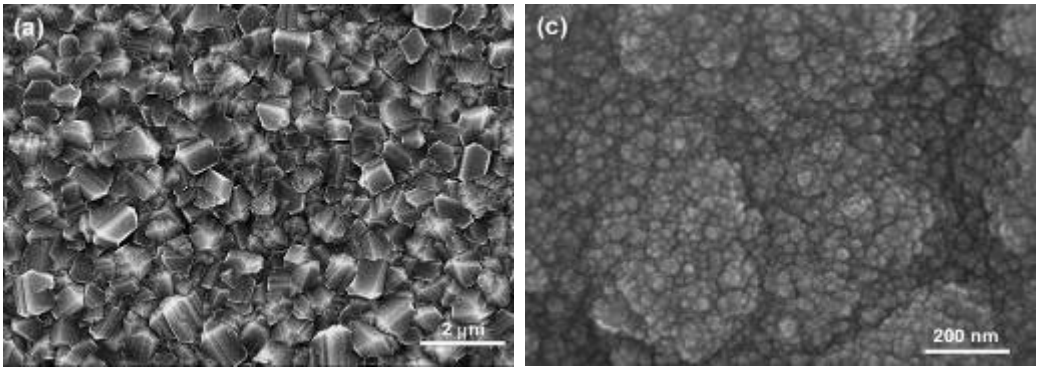

Fig. 1 SEM microstructure for the diamond films with (a) micron-sized grains and (c) nano-sized grains.

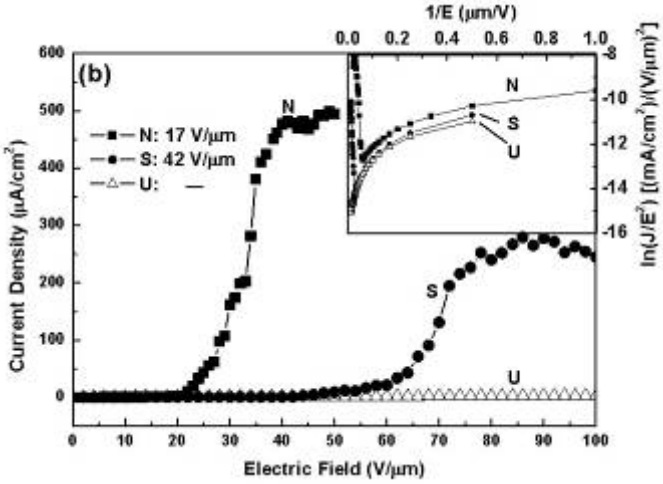

Fig. 2 The electron field emission properties for the diamond films with micron-sized grains (U), submicron-sized grains (S) and nano-sized grains (N).

REFERENCES

1. C.A. Spindt, I. Brodie, C. E. Holland, P. R. Schwoebel, in Vacuum Microelectronics, Wiley, 105 (2001); “Spindt Field Emitter Arrays”.

2. W. Zhu, P. K. Baumann, C. A. Bower, in Vacuum Microelectronics, Wiley, 247 (2001); “Novel Cold Cathode Materials”.

3. D. M. Gruen, Rev. Mater. Sci. 29, 211 (1999).

GEOMETRICAL FIELD ENHANCEMENT ON MICROPATTERNED NANODIAMOND FILM FOR ELECTRON EMISSIONS

K. Subramanian, W. P. Kang, J. L. Davidson, W. H. Hofmeister, B. K. Choi, and M. Howell

Department of Electrical Engineering and Computer Science, Vanderbilt University, TN 37235, USA

Keywords: nanodiamond, chemical vapor deposition, geometrical field enhancement, electron field emission.

Abstract

Introduction: Chemical vapor deposited (CVD) diamond has unique material properties suitable for electron emission such as low electron affinity, hardness to withstand ion bombardment, and good thermal and electrical conductivity to handle high current. In particular, nanocrystalline diamond, apart from excellent chemical, mechanical and thermal characteristics, possesses properties distinct from the conventional CVD microcrystalline diamond including smaller grain size (1 nm-100 nm), higher volume density of grain boundaries, more sp^2-bonded carbon content, uniform surface morphology, and a wider latitude for materials integration [1]. In this paper, we report a robust and reliable technique to micropattern nanodiamond films using reactive ion etching (RIE) process and thereby study the effect of the geometrical field enhancement for electron emissions.

Nanodiamond for field emission: "Cauliflower-like" nanodiamond films with grain size as small as 5-10 nm have been achieved by employing an effective growth-rate control technique through the process of $CH_4/H_2/N_2$ microwave plasma enhanced chemical vapor deposition (MPECVD). We observe that a means to grow nanodiamond films is to increase the nucleation rate and decrease the growth rate by adjusting the CVD process parameters, viz., microwave power, reactant pressure and gas flow rate [1]. Raman spectroscopic analysis of the nanodiamond film indicates that the degree of sp^2-bonded carbon content in the diamond film increases as the grain size decreases. The sp^2/sp^3 peak ratio of the 5-10 nm grain-sized nanodiamond film is found to be ~0.97. The favorable properties of the nanodiamond film, namely, 5 nm grain size, smoother surface morphology, and increased sp^2-carbon content can be utilized in the development of enhanced field emission devices.

Micropatterned nanodiamond emitter with enhanced field emission geometry: The single-mask fabrication process begins with the growth of a 2-μm thick nanodiamond film on a silicon-on-insulator (SOI) wafer by $CH_4/H_2/N_2$ MPECVD. Next, a 0.5 μm-thick layer of aluminum is deposited on the nanodiamond film to form the masking layer. Conventional photolithography is performed to pattern the emitter structures on the aluminum. The exposed Aluminum is etched away by wet chemical etching and the photoresist removed. With aluminum as mask, the exposed nanodiamond is etched with high selectivity by reactive ion etching (RIE) in pure oxygen plasma. The patterned diamond emitters on the silicon layer are then used as a mask for silicon etching to yield the isolation between the emitters. The final structure consists of patterned nanodiamond emitters, supported by a silicon layer underneath, sitting on the SiO_2 layer on the silicon substrate. Figure 1 displays the SEM micrographs of the micropatterned nanodiamond 6-finger, 4-finger, and edge emitters. The aspect ratio of each emitter finger is ~46 and ~52 in specific cases.

Field emission characterization: The as-deposited nanodiamond film and the micropatterned nanodiamond emitter structures were characterized for field emission in a vacuum of ~10^{-6} Torr. Electron emission from the as-deposited nanodiamond film surface was measured using a heavily doped silicon sample as the anode and an insulating spacer of 40 μm, which defined the anode-cathode spacing. The micropatterned nanodiamond finger and edge emitters were tested for field emission laterally with an integrated adjacent anode structure. The field emission characteristics of the three different emitters are presented in Figure 2. The highly linear F-N plots clearly confirm that the current is attributed to field emission. The as-deposited nanodiamond film demonstrated a high turn-on field of 18 V/μm and 3 μA emission current at an electric field of ~30 V/μm. The 6-fingered nanodiamond emitter exhibited a very low turn-on electric field of 1.9 V/μm and a high emission current of ~104 μA at 20 V/μm, while the edge emitter, with a 6.5 V/μm turn-on field, showed 4.6 μA emission current at the same electric field of 20 V/μm. The effect of the geometry of the high aspect-ratio fingers and the edge emitters on field emission from the nanodiamond film was studied. The emission data of the different emitters was correlated to the modified Fowler-Nordheim equation:

$$\ln(I/E_0^2)=\ln(A*K_1*\beta^2/\Phi)-(K_2*\Phi^{1.5}/\beta)(1/E_0) \qquad (1)$$

where K_1 and K_2 are constants, I is the emission current, Φ is the work function of the emitting surface (eV), β is the total field enhancement factor, A is the emitting area, and E_0 is the macroscopic applied electric field (V/cm). Furthermore, the total field enhancement factor β can be expressed in terms of the product of each field enhancement factor as $\beta=\beta_g\ \beta_{sp2}\ \beta_n$, where β_g, β_{sp2}, β_n are the field enhancement factor due to the geometry, sp^2-carbon content, and nitrogen doping, respectively. The slope of the linear F-N plot $\{\ln(I/E^2)$ vs. $1/E\}$ is given by $-K_2\Phi^{1.5}/\beta$. The observed field emission enhancement of the micropatterned nanodiamond emitters can be explained by an increase in the geometrical enhancement factor. This can be deduced from the observation that the F-N slope decreases significantly for the fingered and edge emitters (see figure 2 (b)). The reduction of the F-N slope should mainly arise from the geometric effect because the as-deposited nanodiamond film and the nanodiamond emitters have the same sp^2-carbon and nitrogen concentration and thus should have the same Φ, β_{sp2}, and β_n. Considering that Φ, β_{sp2}, and β_n are the same for the nanodiamond films and the micropatterned emitters, β_g can be found from the F-N slopes of emission data. It was found that β_g of the 6-fingered nanodiamond emitter is ~198 times that of the as-deposited nanodiamond film and ~35 times that of the nanodiamond edge emitter. It was also deduced that the β_g of the edge emitter was ~6 times that of the as-deposited nanodiamond film. In order to utilize the excellent geometrical field enhancement offered by the fingered emitters for electron emission, nanodiamond lateral diode has been fabricated employing the process schema outlined in this paper, with the high aspect-ratio fingers serving as the cathode, and the edge structure as the anode, isolated by the SiO_2 layer (see figure 1).

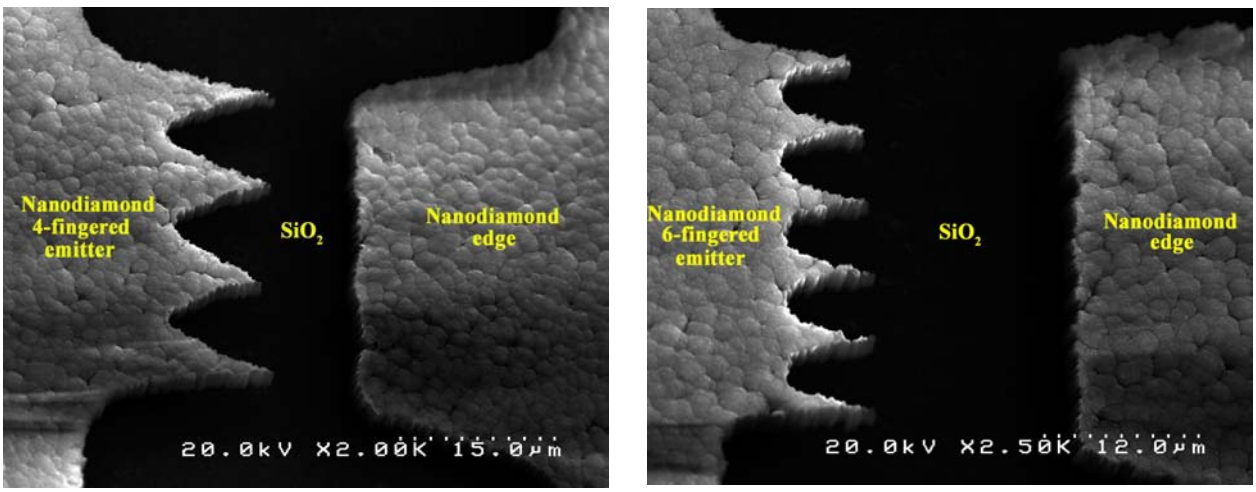

Figure 1. SEM micrographs of the micropatterned nanodiamond lateral field emitters

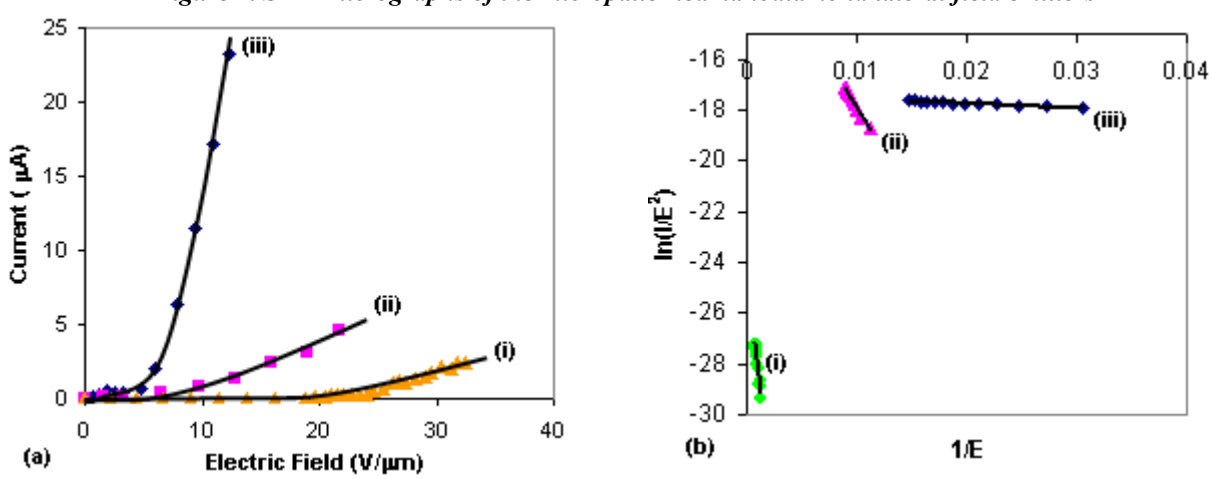

Figure 2. (a) Field emission characteristics of nanodiamond and (b) Corresponding F-N plots: (i) as-deposited nanodiamond film; (ii) nanodiamond edge emitter; (iii) nanodiamond 6-finger lateral emitter

References: [1] K.Subramanian, W.P. Kang, J.L. Davidson, et al., *Proceedings of the 17th IVNC*, pg. 82-83 (2004).

[2] T.D. Corrigan, D.M. Gruen, et al., *Diamond and Related Materials 11,* pp. 43-48, 2002.

FIELD EMISSION PROPERTIES OF SELECTED SINGLE WALL CARBON NANOTUBE SAMPLES

A.Fiori [(*)], S.Orlanducci [(*)], V.Sessa[(*)], E.Tamburri[(*)], M.L.Terranova[(*)]

Dipartimento di Scienze e Tecnologie Chimiche, Università di Roma Tor Vergata, via della Ricerca Scientifica, 00133 Roma; E-mail: marialetizia.terranova@roma2.infn.it

A. Di Carlo[(*)], A. Reale[(*)], F. Brunetti[(*)], P. Regoliosi[(*)], R. Riccitelli[(*)]

Dipartimento di Ingegneria Elettronica, Università di Roma Tor Vergata, via del Politecnico, 00133 Roma

[(*)] Micro and Nano Structured System Laboratory (MINAS)

A. Ciorba, M. Rossi

Dipartimento di Energetica, Università di Roma La Sapienza via Scarpa 16, 00162 Roma

Keywords: nanotubes, field emission

Carbon based nanostructures have proven very attractive materials and their properties are very widely investigated.
Our synthesis approach, based on a Hot Filament Chemical Vapor Deposition (HFCVD) system coupled to a powder mixing cell, has proved to be particularly versatile in obtaining a variety of nanostructures. Carbon nanopowders obtained by laser pyrolisis of ethylene/acetylene mixtures are used as carbon source; the reaction with a filament-activated atomic hydrogen plasma allows us to obtain good quality Single Wall Carbon Nanotubes (SWCNT) [1].
We successfully exploited controlled variations of synthesis parameters such as time, powder flux orientation and intensity of hydrogen flux and managed to control tubes' orientations and bundles' dimensions.

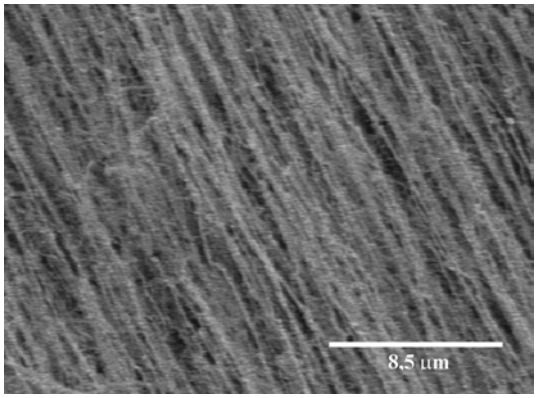

Fig. 1 SEM image of a SWCNT sample showing a very good alignment of the bundles

The influence of different morphologies on field emission behavior constitutes a non secondary key point, both for a deeper understanding of emission phenomenon and for a more precise tuning of the future devices' performances.
Moreover, our synthesis process proved to be substrate selective, so that we are able to obtain selected area growth of SWCNTs [2]: field emission properties of such ordered arrays of emitters constitutes a hot technological spot in view of the wide number of applications [3].
Finally, we are investigating the field emission behavior of a newly synthesized kind of carbonaceous nanostructures made up of SWCNTs covered by a nanocristalline phase identified with diamond [4] whose properties promise to be very interesting.

We set up and tested a home made field emission measurement apparatus: cathode-anode system resembles the plan to sphere set up; their distance can be adjusted by means of a high resolution linear actuator driven by PC and measured by a capacimetric approach; two micrometric knobs allows us to scan over the sample.
We demonstrate the possibility of obtaining very promising results: our actual interest is particularly concerned with reproducibility (i.e. the reliability of the future field emission device) and durability of our samples' performances.

Field emission measures have been carried out on a series of morphologically well defined samples. Our cathodes required a prolonged conditioning period before reaching a reasonably reproducibility of I-V emission curves. Training

of samples has been undertaken both by successive potential scans and prolonged application of high fields: as a result of both processes, the maximum current undergoes a slight decrease, I-V curves gets smoother and smoother, Fowler-Nordheim plots gets linear in a wider potential range. The non reproducible features which initially affect emission measures has been interpreted as irreversible modification of samples' surfaces during potential scans such as the field evaporation of absorbed gaseous species [5]: once the cathode gets clean, its emission performances get stable. By keeping our cathodes under high emission current conditions, we verified the durability of the nanotube samples as well: they survived long (up to three full days) to extreme conditions such as high current (at μA level) and low vacuum level (10^{-6} mbar) thus demonstrating the real possibility of using SWCNTs as field emitter in a variety of electronic devices.

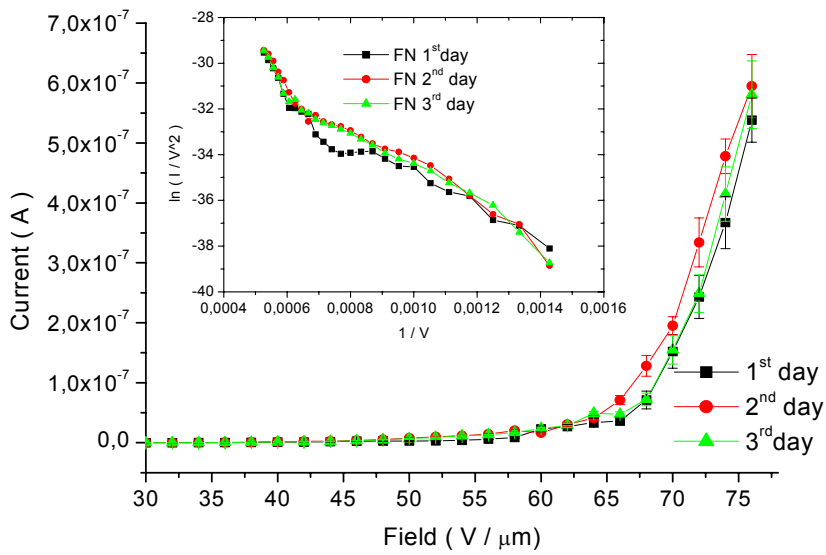

Fig. 2 Field-Current curves showing reproducibility of performances in different measurement days. The inset shows the corresponding Fowler Nordheim plots.

REFERENCES

[1] M.L. Terranova, S. Piccirillo, V. Sessa, P. Sbornicchia, M. Rossi, S. Botti, D. Manno *Chem. Phys. Lett.* 327 (2000) 284

[2] S. Orlanducci, V. Sessa, M.L. Terranova, M. Rossi, D. Manno *Chem. Phys. Lett.* 367 (2003) 109

[3] Y. Saito, S. Uemura *Carbon* 38 (2000) 169

[4] M. L. Terranova, S. Orlanducci, A. Fiori, E. Tamburri, V. Sessa, M. Rossi, A. S. Barnard *Chem. Mat.* submitted

[5] S. T. Purcell, P. Vincent, C. Journet, V. T. Binh *Phys. Rev. Lett.* 88 (2002) 105502

COLD CATHODES FOR APPLICATIONS IN POOR VACUUM AND LOW-PRESSURE GAS ENVIRONMENTS: CARBON NANOTUBES VERSUS ZINC OXIDE NANONEEDLES

A-J. Cheng[1], D. Wang[2], H. W. Seo[2], C. Liu[1], M. Park[2], and Y. Tzeng[1]

[1] Alabama Microelectronics Science and Technology Center, Department of Electrical and Computer Engineering, Auburn University, Auburn, Alabama 36849 USA

[2] Department of Physics, Auburn University, Auburn, Alabama 36849 USA

Keywords: Electron Field Emission, Zone, Carbon Nanotubes

Carbon nanotubes and ZnO nano-needles were grown on silicon substrates and used as cold cathodes. These cold cathodes exhibit excellent electron field emission characteristics in high vacuum with turn-on electric field near 1 V/µm and below. Long-term stability of electron field emission for cold cathodes coated with carbon nanotubes and ZnO are compared. The effects of gas pressure on the characteristics of electron field emission are reported and discussed. Electron field emission current for both cold cathodes coated with carbon nanotubes and ZnO decreases with air pressure that is intentionally leaked into the experimental chamber. For the same air pressures up to tens of mTorr, ZnO nano-needle coated cold cathodes exhibit percentage-wise less decrease in electron field emission current as compared to carbon nanotube coated cold cathodes. ZnO nano-needles appear to be more favorable for cold-cathode applications in poor vacuum environments and for low-pressure gas-filled electron devices.

The extremely high aspect ratios and/or small radius of curvature of nanoscale materials such as nanotubes, nanowires, nanoneedles, nanoparticles, and nanocrystalline grains have been explored and reported to promote the field emission of electrons at low applied electric fields in vacuum. Among these nano-scale materials, carbon nanotube is the most well studied material for cold cathode applications because of both its high aspect ratio and the small radius of curvature at its tip. Numerous publications have reported the effects of diameter, length, spacing between carbon nanotubes, tip geometry and composition, placing and patterning, and post-deposition processing on the electron field emission characteristics of carbon nanotubes. Effects of residual gases that are adsorbed on the surfaces of carbon nanotubes have also been studied.

For some practical applications, the electron field emission must operate in a poor vacuum or at a low gas pressure with an intentionally filled gas. Energetic oxygen molecules, atoms and ions are known to react with carbon nanotubes causing defect formation and etching of the exposed carbon nanotubes resulting in the degradation of the electron field emission characteristics.

Oxide nanowires or nano-needles are expected to be more resistance to environments containing oxidizing species. In this paper, ZnO is chosen as the oxide cold cathode material for a comparison with non-oxide carbon based cold cathodes that are coated with carbon nanotubes.

Both carbon nanotubes and ZnO nano-needles are deposited on silicon substrates by means of thermal chemical vapor deposition methods. ZnO nano-needles are grown on silicon using gold nanoparticles as a catalyst in the presence of Zn vapor. Carbon nanotubes were grown by means of thermal chemical vapor deposition using iron as a catalyst in the gas mixture of acetylene and argon.

Electron field emission measurement is done in a vacuum chamber with base pressure of 10^{-6} Torr. An air leak valve can be turned on to allow controlled amount of ambient air to enter the chamber for a desired air pressure. Cold cathode is place at a distance from the anode of 3 mm^2 in surface area by means of spacers. The anode is inserted in an electrical insulating block. Spacers are placed between the cathode and the electrically insulating block so that in case the side walls of the spacers are coated with conducting materials, the measurement of electron field emission current will not be affected.

A TEM photograph of carbon nanotubes and a SEM photograph of ZnO nanoneedles are shown in Figure 1 (i) and (ii), respectively. Electron field emission current as a function of the applied electric fields using the air pressure as a parameter is measured using a tungsten anode of 3 mm^2 in area. Both cold cathodes allow electron field emission to be detected at an applied electric field around 1 V/µm or below (not shown in this figure of linear scale). The electron field emission current measured from the carbon nanotube coated cathode is higher than that measured from the ZnO nanoneedle coated cathode because the number density and concentration of electron emission sites of ZnO nanoneedles used for this experiment are not as high as that of carbon nanotubes. Figure 2 shows that as the air pressure increases, the electron field emission currents for both cathodes decrease with the carbon nanotube coated

cathode showing more dramatic decrease than the ZnO nanoneedle coated cathode. Electron field emission current measurement is repeated in vacuum after exposing both cold cathodes to electron field emission at a gas pressure of 60 mTorr. ZnO nanoneedles recover most of the original electron field emission characteristics; but, carbon nanotubes exhibit electron field emission current several orders of magnitude less than the original field emission current before being subjected to electron field emission at 60 mTorr as shown in Figure 2.

In summary, both carbon nanotubes and ZnO nanoneedles serve as excellent electron field emission cold cathode coatings with low turn-on electric fields in high vaccum. The electron field emission current decreases with increasing air pressure. ZnO nanoneedles is more favorable for cold cathode applications in poor vacuum and in low pressure environments filled with oxidizing gases.

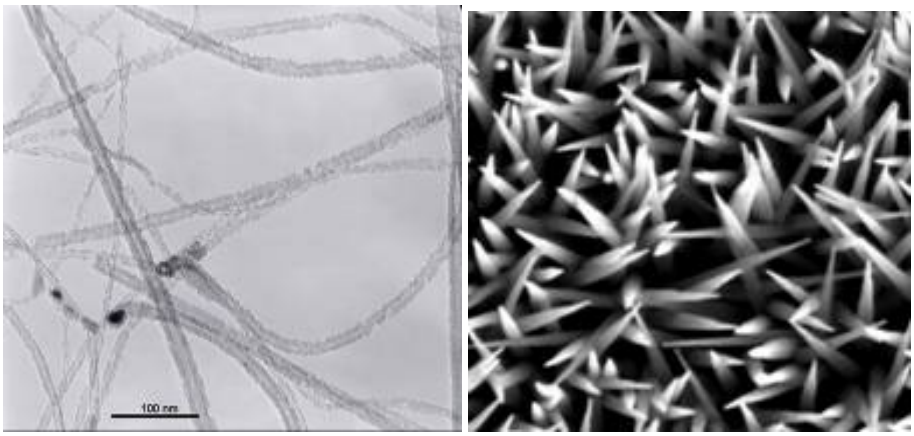

Figure 1. (i) TEM photograph of carbon nanotubes. (ii) SEM photograph (9x9 μ) of ZnO nano-needles.

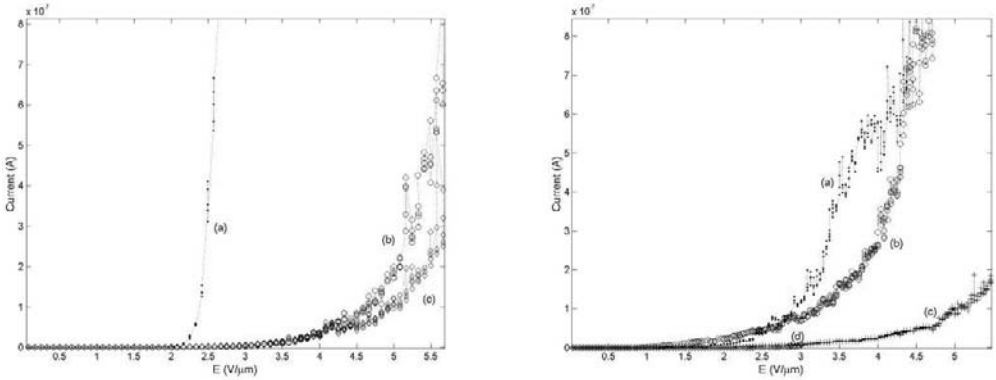

Figure 2. (i) I-E curves for carbon nanotubes. (ii) I-E curves for ZnO nano-needles.

For both sets of curves the electron field emission current was measured for (a) the as-grown samples at 10^{-6}Torr and (b) the same samples at the same pressure of 10^{-6}Torr after being subjected to the environments in which electron field emission in ambient air at a pressure of 60 mTorr was measured . Curve (i-c) and (ii-d) are for measurements at 60 mTorr. Curve (ii-c) is for measurement at 30 mTorr.

Nitrogen Doping and Graphitization of Nanocrystalline Diamond Films for Enhanced Field Electron Emission

A.V. Karabutov[1], V.I. Konov[1], E.N. Loubnin[2], V.V. Pereverzev[1], I.I. Vlasov[1], E.V. Zavedeev[1], and S.M. Pimenov[1]

[1)] General Physics Institute, 38 Vavilova street, 119991 Moscow, Russia

[2)] Institute of Physical Chemistry, 31 Leninsky prospect, 117915 Moscow, Russia

Nitrogen-doped nanocrystalline diamond films were grown by d.c. arc plasma CVD on Si substrates from $CH_4/Ar/N_2$, $CH_4/H_2/N_2$, and $CH_4/Ar/H_2/N_2$ gas mixtures. Different nitrogen content in the gas mixtures and different substrate temperatures were used to grow the films with different nitrogen content and microstructure. A nitrogen incorporation is promising for field electron emission from diamond films due to formation of electrical conductivity channels inside the films and changing the electron affinity on the film surface (n-doping and/or additional surface energy levels). In addition, higher growth temperature leads to partial graphitisation of the diamond films that can also improve the emission. So a set of the films with and without nitrogen was grown at high temperatures as well.

The film surface and microstructure was studied using AFM, SEM, Raman spectroscopy, X-ray Photoelectron Spectroscopy, Auger Electron Spectroscopy, and EELS to find correlations between the field emission and other film properties. The field electron emission was studied using both a macroscopic phosphor screen setup and a microprobe setup with tungsten probes of 10 μm in radius. Emission I-V dependences as well as emission sites distribution were measured and then analyzed depending on nitrogen and/or sp^2-carbon content in the films.

It was found that nitrogenated nanocrystalline CVD diamond films show different microstructure than the films prepared without nitrogen, and the field electron emission for the nitrogenated films was typically better than for the films grown without nitrogen at the same the rest conditions. On the other hand, partially graphitized films grown at higher temperatures (with or without nitrogen in the gas mixtures) typically show the best field emission properties with emission threshold fields of as low as 1-1.5 V/μm, much higher density of emission sites, and higher working limit of the emission current. A competition of the nitrogen incorporation and graphitization for the field emission from the diamond films is discussed in dependence on the microstructure. Possible field emission mechanism are considered basing on the grain boundary effect.

POSTER SESSION 2

SURFACES & SENSORS

ELECTROCHEMICAL DETECTION OF IODOPHENOLS AT BORON-DOPED DIAMOND THIN-FILM ELECTRODES

Audrey N. Martin and Greg M. Swain

Department of Chemistry, Michigan State University, East Lansing, MI 48824

Keywords: iodophenol, water disinfection, boron-doped diamond

Abstract

Currently there is little on-line monitoring capability onboard the International Space Station (ISS) for water quality management. Water quality is presently monitored by periodically returning samples to earth; consequently, there is no way to promptly respond to a contamination outbreak. In the past, water samples were regularly returned for analysis by the Space Shuttle, however, since the Columbia accident, water samples have not been regularly brought back for analysis. Therefore, water quality monitoring has become a major concern for the National Aeronautic Space Administration (NASA). Water disinfection can be accomplished by introducing iodine (I_2), taking advantage of its biocidal and virucidal properties to purify the water supply. Concerns have been raised about the possibility that I_2 could react with aromatic contaminants reclaimed from the shuttle condensate to form iodinated aromatics.[1] Although the toxicity of iodinated aromatics is unknown, it is hypothesized that they possess toxicity similar to that of their chlorinated counterparts, such as chlorophenol.

This research is focused on development of an electrochemical detection scheme for iodinated phenols using boron-doped diamond (BDD) electrodes. Electrochemical detection of waterborne contaminants is relatively simple, inexpensive, and utilizes small and easy to operate instrumentation. The most important component of any electrochemical detection system is the electrode material. BDD thin-film electrodes are appealing because of their (i) wide potential window, (ii) minimal pretreatment for activation, (iii) stable morphology and microstructure in harsh chemical environments, (iv) stable and low background current, (v) and weak adsorption of polar molecules on the hydrogen-terminated surface (i.e., resistance to fouling). These qualities are especially appealing to the detection of phenolic compounds because their oxidation potentials approach that of oxygen evolution on many electrode materials and phenolic reaction by-products can polymerize and adsorb on (foul) the electrode surface. Boron-doped diamond electrodes have previously been used for the detection of chlorinated phenols and have been shown to be an ideal electrode material in terms of electrochemical activity and response stability.[2]

The feasibility of BDD electrodes for the oxidative detection of iodinated phenols was investigated. 2-iodophenol (2-IP), and 4-iodophenol (4-IP) in phosphate buffer (pH 3.5), and 2,4,6-triiodophenol (TIP) in acetonitrile/phosphate buffer (pH 7.1) were characterized with microcrystalline boron-doped diamond thin-film electrodes using cyclic voltammetry and flow injection analysis (FIA) with amperometric detection. The decreased solubility of TIP necessitated the use of the mixed buffer solution. Characteristics, such as the electrode response, reaction products, and fouling resistance, were investigated. The mechanism for phenol oxidation has been extensively studied[3] and it is hypothesized that the iodophenol oxidation follows the same mechanism. Figure 1 shows the typical cyclic voltammetric i-E curve for 2-iodophenol at a BDD microcrystalline electrode. During the first scan, only the oxidation peak is observed for the oxidation of 2-IP to the iodophenoxy radical (peak A). The radical can then either (i) polymerize or (ii) be further oxidized to form quinone-like compounds, which are then reduced on the reverse sweep (peaks B and C). The shoulder on peak C is assumed to be associated with the reduction of a dissolved quinone-like species. Subsequent scans show two additional oxidation peaks, D and E, which are associated with the species formed during the reduction at peaks B and C. The oxidation current near 0.9 V (peak A) decreases to a point with cycling, while the reduction currents near 0.15 V and 0.5 V increase (peaks B and C). This leads to the hypothesis that oxidation reaction products adsorb on the electrode surface and block some electrochemically-active sites. Similar phenomena were seen during the electrochemical detection of chlorinated phenols.[2] 4-IP and TIP show similar electrochemical behavior to 2-IP at microcrystalline diamond.

FIA was used to study the electrochemical response of iodophenols on BDD. FIA allows for an on-line method of detection that serves as a very basic prototype for a constant monitoring system. It is hypothesized that the constant movement of solution through the flow-cell will reduce the rate of electrode fouling. Preliminary studies with 2-IP show the ideal detection potential for FIA of 2-IP is 950 mV vs. Ag/AgCl. After stabilization, a current of 8.5nA was measured. The analytical figures of merit of 4-IP and TIP will also be presented.

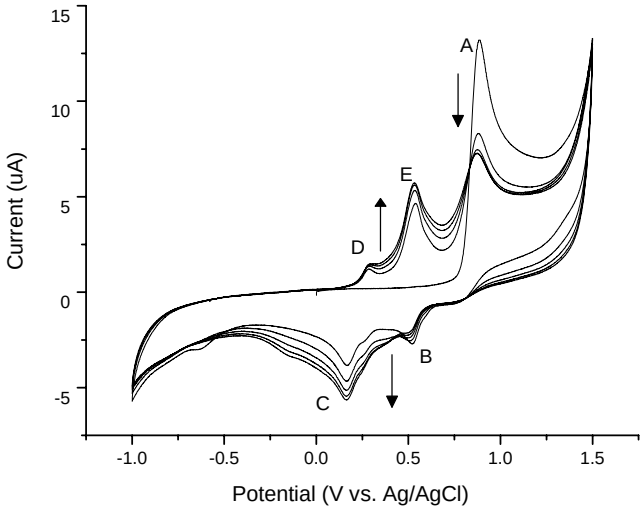

Figure 1. Cyclic voltammetric i-E curve for 0.1mM 2-iodophenol in 0.1M phosphate buffer, pH 3.5 at a microcrystalline BDD thin-film electrode. Scan rate: 100mV/s, Electrode area: 0.2cm^2.

REFERENCES

1. Dietrich, A.M., et al.: "Flavor Profile Analysis and GC/MS Detection of Phenolic Iodinated Disinfection Byproducts in Drinking Water for the USA Space Program," *Wat. Sci. Tech.*, Vol. 40, No. 6, 45-51 (1999).
2. Muna, G.W.; Tasheva, N.; and Swain, G.M.: "Electro-oxidation and Amperometric Detection of Chlorinated Phenols at Boron-Doped Diamond Electrodes: A Comparison of Microcrystalline and Nanocrystalline Thin Films," *Environ. Sci. Technol.*, Vol. 38, No. 13, 3674-3682 (2004).
3. Gattrell, M. and Kirk, D.W.: "A Study of the Oxidation of Phenol at Platinum and Preoxidized Platinum Surfaces," *J. Electrochem. Soc.*, Vol. 140, No. 6, 1534-1540 (1993).

ELECTRICAL CHARACTERIZATION AND BIOSENSING APPLICATION OF MODIFIED CARBON NANOFIBERS AND NANOCRYSTALLINE DIAMOND

Kiu-Yuen Tse, Sarah E. Baker, Beth M. Nichols, Wensha Yang, and Robert J. Hamers

Department of Chemistry, University of Wisconsin-Madison, 1101 University Avenue, Madison, WI-53706

Keywords: Biosensing, nanocrystalline diamond, carbon nanofibers, electrical.

Abstract

Carbon-based materials, such as carbon nanofibers and nanocrystalline diamond, are attractive candidates for use in chemical and biological sensor applications. Recent studies have shown that when these materials are functionalized with biomolecules such as DNA, the biomolecules retain their activity and specificity. Furthermore these modified materials show very good stability and biocompatibility. Nanocrystalline diamond provides semiconducting properties while carbon nanofibers provide very high surface area, which can be used for new ways of detecting biological binding events, such as DNA hybridization, through electrical measurements.

We have been investigating the electrical properties of carbon nanofibers and nanocrystalline diamond. Measurements of the electrical impedance between 0.1 Hz and 1MHz were performed. The spectra show that the low frequency response is dominated by the capacitance of the system. Unlike simple planar surfaces, nanofibers arrays show a more complex dependence on frequency, which reflects the penetration of ions into the interstices between the nanofibers. The equivalent capacitance of these nanofibers is much higher than the capacitance of an equivalent planar surface, suggesting they may be useful as high density capacitors.

We have also examined nanofibers arrays in which the nanofibers have been covalently linked to biomolecules such as DNA and have investigated how the electrical properties change in response to biological binding events. Our initial results show that biomolecular recognition events can be detected using electrical measurements. The results of these data will be presented and the potential use of nanofiber arrays for biosensing will be described.

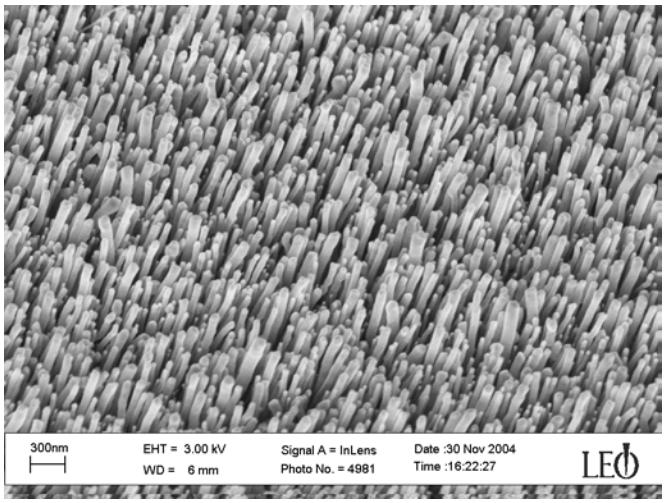

Figure 1: A scanning electron micrograph of carbon nanofibers

REFERENCES

1. Tse, K.Y. et al., "Electrical properties of diamond surfaces functionalized with molecular monolayers", *J. Phys. Chem.*, submitted for publication

FABRICATION AND ADDRESSABLE FUNCTIONALIZATION OF VERTICALLY-ALIGNED CARBON NANOFIBERS

Sarah E. Baker, Kiu Yuen Tse, Chang-Soo Lee, Robert J. Hamers

Department of Chemistry, University of Wisconsin-Madison

1101 University Avenue, Madison, Wisconsin 53705

Matthew S. Marcus, Mark Eriksson

Department of Physics, University of Wisconsin-Madison

1150 University Avenue, Madison, Wisconsin 5705

Keywords: carbon nanofibers, electrically addressable functionalization

Abstract

Recent studies have shown that carbon-based materials are extremely stable substrates for biosensing applications.[1] We are exploring vertically-aligned carbon nanofibers (VACNFs) as high-stability electrode materials for biosensing arrays. In addition to having very high chemical stability, it is likely that VACNFs also have additional interesting and useful properties due to their nanoscale width. For example, the extremely high surface area that can be obtained when carbon nanofibers are grown in the "forest" geometry may amplify the electrochemical signal that indicates biological binding to their surfaces. Additionally, VACNFs can be used as individual nanoscale sensing elements because single VACNFs can be patterned by a several methods and grown in the desired locations onto microelectrodes.

VACNFs are grown by DC plasma-enhanced chemical vapor deposition using an acetylene/ammonia mixture, catalyzed by a nickel thin film on the surface. By patterning this catalyst using electron-beam lithography, it is possible to grow small bundles of VACNFs or even individual carbon nanofibers that are electrically connected to an underlying substrate. When desired, it is also possible to deposite SiO_2 onto the VACNFs substrate so that the entire underlying electrical contact system is insulated. Additionally, using a reactive ion etch process we can expose the very end of the nanofiber so that it remains accessible for electrical measurement and/or chemical functionalization (Figure 1).[2]

We are exploring methods for functionalizing VACNFs for biological recognition. We have developed a photochemical method for terminating VACNFs forests with amines. This chemistry is very similar to that shown to form stable covalent attachment of amines to diamond, where in this case the VACNF forest sample is exposed to an N-Boc protected amino alkene in the presence of UV light. After attachment of the alkene to the surface of the nanofibers, the protecting group is subsequently removed to form amine-terminated nanofibers. The amine termination is an excellent starting point for covalent attachment of a variety of biological molecules to the surface. We have further functionalized these surfaces with DNA by reacting the amine-terminated VACNFs with a heterobifunctional cross-linker sulfosuccinimidyl 4- [N-maleimidomethyl]-cyclohexane-1-carboxylate (SSMCC), terminating the VACNFs with maleimide functionality. We then react these surfaces with 5' thiol-terminated oligonucleotides, and have shown that these oligo functionalized surfaces retain their biological recognition. The oligonucleotide tethered to the surface is specific for its complement and does not bind appreciably to a mismatched strand. Additionally, the surface is stable and can be re-hybridized after stringent denaturation conditions.

Toward the goal of using individual and small bundles of VACNFs as discrete nanoscale sensing elements, we have developed chemistry that can enable the selective functionalization of closely spaced sub-micron sized VACNF bundles with different biological molecules on the same chip.[3] The patterned, electrically addressable VACNF substrate is exposed to p-nitro benzene diazonium tetrafluoroborate in the presence of surfactant. This step terminates the nanofibers with nitrophenyl moieties. We can selectively convert individual bundles of nitrophenyl terminated nanofibers to more reactive aminophenyl terminated nanofibers using an electrochemical reduction step. This step enables the addressability of the chemistry; the fiber bundles that were *not* reduced remain terminated with nitrophenyl groups. The aminophenyl terminated bundles can then be reacted with thiol-terminated DNA and

SSMCC similarly to the method described above. After this step, another nanofiber bundle on the same chip can be reduced, and reacted with a *different* sequence of DNA, and so on. This work has implications toward the fabrication of high-density VACNF biosensor arrays.

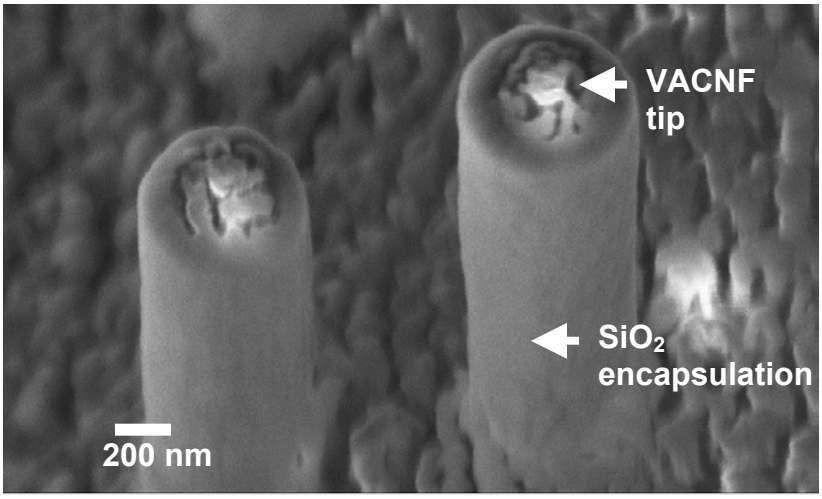

Figure 1: Electrically-addressable VACNFs with insulated sidewalls and underlying substrate, but with electrochemically active VACNF tip.

REFERENCES

1. Yang, W., et al. "DNA-modified Nancrystalline Diamond Thin Films as Stable, Biologically Active Substrates," *Nat. Mater,* 1, 253-257 (2002).
2. Guillorn, M.A. et al. "Individually Addressable Vertically-Aligned Carbon Nanofiber-based Electrochemical Probes," *J. App. Phys* ,91, 6, 3824-3828 (2002).
3. Lee, C.-S. et al. "Electrically-Addressable Biomolecular Functionalization of Carbon Nanotube and Carbon Nanofiber Electrodes," *Nanolett*, 4, 9, 1713-1716 (2004).

POSTER SESSION 2

GROWTH

SCALE-UP OF DIAMOND DEPOSITION WITH MICROWAVE PLASMA CVD

Ralf Spitzl, Hildegard Sung-Spitzl

iplas innovative plasma systems gmbh, Langbaurghstr. 10 – 53842 Troisdorf, info@cyrannus.com

Keywords: Microwave plasma, PACVD, high pressure, diamond film, ultra-nano-crystalline diamond

Abstract

The scale-up of diamond CVD pocesses for economic production is related to growth speed and desposition area. By introducing the CYRANNUS concept (cylindrical resonator with annular slots) a new device for generation of uniform microwave plasma at higher pressure became available. That type of plasma sources combine a resonator structure (which enables high pressure operation) with a multi-antenna microwave feeding (which enables high power transfer).

SIZE VARIATION

Several sizes of plasma sources have been used for deposition of diamond and will be compared:

- A plasma source with 150mm diameter chamber size was excited with 2.45GHz microwave and has successfully been used for deposition of diamond at medium pressure. The plasma shows the shape of a sphere. Deposited <100> films showed thickness uniformity better than ±3% at 50mm diameter. The possible deposition diameter is larger than 100mm. High pressure deposition at 300mbar increased the growth rate up to 50µm/h.
- An antenna scaled system with 250mm diameter chamber size was also operated at 2.45GHz and shows a discus-like shape of the plasma.
- Scaling the plasma source to a microwave frequency of 915Mhz increased the diameter of the chamber to 350mm. Such system has been used for deposition of diamond at a pressure of 60mbar hydrogen. The process and deposition temperature was controlled by the pressure of the plasma gas. The results of a 200mm wafer coating will be presented.

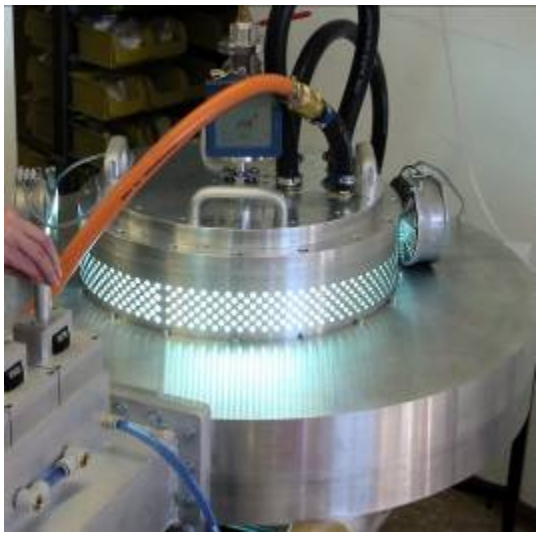

Figure* 1. *Diamond deposition with PACVD in 915MHz CYRANNUS system

INVESTIGATING THE ROLE OF HYDROGEN IN ULTRANANOCRYSTALLINE DIAMOND THIN FILM GROWTH

J. Birrell

Advanced Diamond Technologies, Champaign, IL

J.E. Gerbi

Dept. of Materials Science, University of Illinois at Urbana-Champaign, Urbana, IL

O. Auciello, J.A. Carlisle

Materials Science Division, Argonne National Laboratory, Argonne, IL

Center for Nanoscale Materials, Argonne National Laboratory, Argonne, IL

Keywords: diamond growth, nanocrystalline, hydrogen, transmission electron microscopy

Abstract

A great deal of recent experimental studies and computer simulations have been performed to try to understand the surface stability of diamond nanocrystals. These results have yielded a number of striking conclusions that can help explain the transition of diamond thin film structure from microcrystalline to nanocrystalline with the reduction of hydrogen in the gas phase during microwave plasma enhanced chemical vapor deposition; namely, that the stability of the surface of the diamond nanoparticle is a strong function of both the hydrogen coverage and the size of the crystallite. This study investigates the role of hydrogen in the growth of ultrananocrystalline diamond (UNCD) thin films in two different regimes. First, we add hydrogen to the Ar/CH_4 gas phase during growth, and observe that rather than a monotonic increase in the grain size from the nanocrystalline to the microcrystalline regime, there is an apparent competitive growth process occurring between the two regimes, with the microcrystalline diamond grains becoming much more prominent with added hydrogen. Second, we remove hydrogen from the plasma by changing the hydrocarbon precursor for methane to acetylene and observe that there does seem to be some sort of lower limit to the amount of hydrogen that can sustain ultrananocrystalline diamond growth, below which a significant amount of graphite is nucleated. We speculate the reasons for these observed changes is that large amounts of hydrogen in the plasma favor the rapid growth of diamond microcrystals, while low concentrations of hydrogen result in unstable diamond nanocrystals and the nucleation of graphitic material. This work was supported by the DOE-Office of science-Materials Science under Contract No. W-31-109-ENG-38.

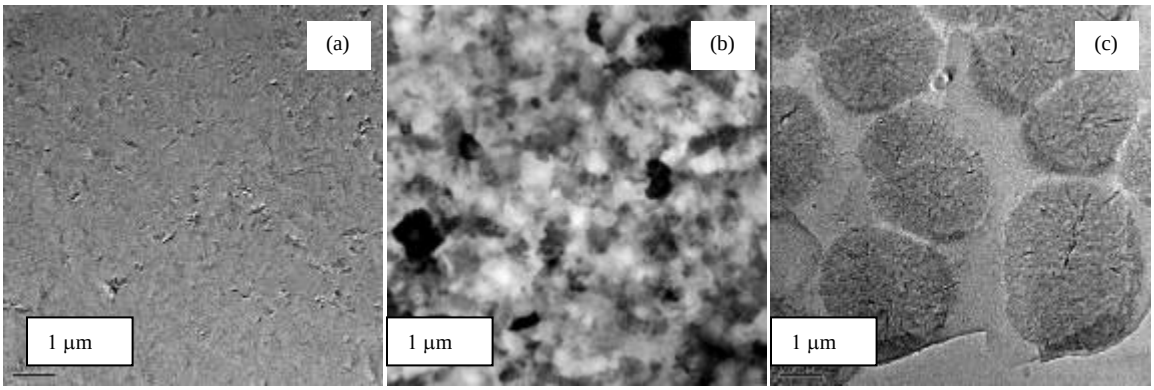

Figure 1: TEM images of UNCD grown using (a) methane and 0% added hydrogen and (b) methane and 20% added hydrogen (c) acetylene and 0.5% added hydrogen.

EFFECT OF NUCLEATION METHODS ON CHARACTERISTICS OF LOW-TEMPERATURE DEPOSITED ULTRANANOCRYSTALLINE DIAMOND

Li-Ju Chen, Yen-Chih Lee, Nyan-Hwa Tai, Chi-Young Lee, Su-Jien Lin

Department of Material Science and Engineering, National Tsing-Hua University, Hsin-Chu 300, Taiwan R. O. C.

I-Nan Lin

Department of Physics, Tamkang University, Tamsui 251, Taiwan R. O. C.

Keywords: UNCD, nucleation methods, low temperature, MPECVD

Abstract

Ultra-nano-crystalline diamond (UNCD) thin films possess very fine grains and very smooth surface. These films are very promising for the applications in a device requiring smooth surface, such as surface acoustic wave (SAW) devices. UNCD films can be grown using CH_4/Ar plasma at relatively lower substrate temperature, which renders the formation of UNCD on a glass substrate possible and increases tremendously the potential for device applications. However, in order to deposit the diamond films at low substrate temperature, creation of nucleation sites is necessary. In this study, various kinds of nucleation methods were used for enhancing the formation of ultra-nano-crystalline diamond (UNCD) films. The surface morphologies and other properties of these UNCD films were observed to correlate intimately with nucleation methods.

UNCD films were grown in a 2.45 GHz microwave plasma enhanced chemical vapor deposition (MPECVD) system on mirror polished Si (100) substrates. The substrate assembly was immersed in 1200 W CH_4/Ar plasma with 1 % CH_4, 99 % gas mixture at total pressure of 150 Torr. The substrates were pretreated either by (1) scratching with submicron (0.1 μm) or nano-sized (~ 3 nm) diamond powders; (2) ultrasonically polished with submicron (0.1 μm) or nano-sized diamond (~3 nm) powders; (3) spin coating slurry containing nano-sized diamond powder as seeds; or (4) by bias enhanced nucleation (BEN) method. The results showed that the growth rate and surface morphologies of UNCD films are significantly affected by nucleation methods, although all the UNCD films showed similar grain size and Raman spectra.

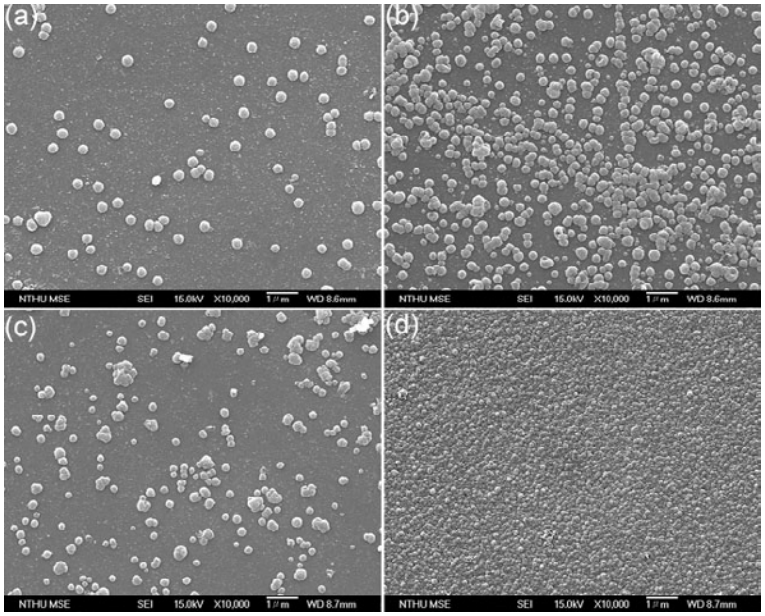

Figure* 1. *SEM surface morphology of UNCD grown under 400°C, 3 hr on different nucleation substrate a) scratched by0.1 mm diamond powder; b) scratched by nano-sized powder; c) ultrasonic by nano-sized powder; d) bias enhanced nucleation substrate .

REFERENCES

1. D. M. Gruen., A. R. Krauss, and C. D. Zuiker et al., "Characterization of nanocrystalline diamond films by core-level photoabsorption", ***Appl. Phys. Lett.* 68 (12)**, 1640 (1996).
2. X. Xiao, J. Birrell, and J. E. Gerbi et al., "Low temperature growth of ultrananocrystalline diamond", ***J. Appl. Phys.* 96 (4)**, 2232 (2004).
3. H. Liu, D. S. Dandy, "Studies on nucleation process in diamond CVD: an overview of recent developments", **Diamond Relat. Mater. 4**, 1173 (1995).
4. H. Makita, K. Nishimura, and N. Jiang, "Ultrahigh particle density seeding with nanocrystal diamond particles", **Thin Solid Film 281-282**, 279 (1996).
5. S. Yugo, T. Kanai, and T. Kimura et al., "Generation of diamond nuclei by electric field in plasma chemical vapor deposition", ***Appl. Phys. Lett.* 58**, 1036 (1991).

EFFECTS OF NANO- AND MICRO-CRYSTALLINE SEEDS ON THE GROWTH OF NANO- AND MICRO-CRYSTALLINE DIAMOND THIN FILMS

F. Piazza, R. Velázquez and J. De Jesús

Department of Physics, University of Puerto Rico, San Juan, P.O. Box 23343, Puerto Rico 00931

G. Morell

Department of Physical Sciences, University of Puerto Rico, San Juan, P.O. Box 23323, Puerto Rico 00931

Keywords: diamond, CVD, growth, seeding, nucleation

Abstract

The early growth stages are critical for the adhesion and final structure of diamond films synthesized by chemical vapor deposition (CVD). We report on the effect of molybdenum substrate seeding with ultra dispersed nano-crystalline diamond and micro-crystalline diamond powders on the nucleation process, growth and structure of hot filament chemical vapor deposited nano- and micro-crystalline diamond, n-D and μ-D, respectively. For each powder used as seeds, diamond thin films were grown for 1, 5, 10 and 20 hours using the same process parameters. Raman spectroscopy (RS), X-ray diffraction analysis (XRD), X-ray photoelectron spectroscopy (XPS), scanning electron microscopy (SEM), and atomic force microscopy (AFM) were performed to study the nucleation process, film nano-structure and diamond quality.

The results show that the nucleation increases as the seed particle size decreases (Figure 1). When nano-crystalline powder is used as seeds, the resulting diamond film is densely clustered, showing both micro and submicro crystallites, whereas when micro-crystalline powder is employed, the resulting film is micro-crystalline and well faceted (Figure 2). All types of seeds lead to high quality (>97%) diamond films growth according to the Raman spectra, although quantitative analysis shows a slightly lower (by ~3 %) diamond film quality when nanocrystalline seeds are employed (Figure 3). Moreover, X-ray diffraction patterns indicate that the seed particle type also affects the film texture. Microcrystalline diamond seeds yield high (111) texture, while the nanocrystalline diamond seeds yield high (400) texture (Figure 4).

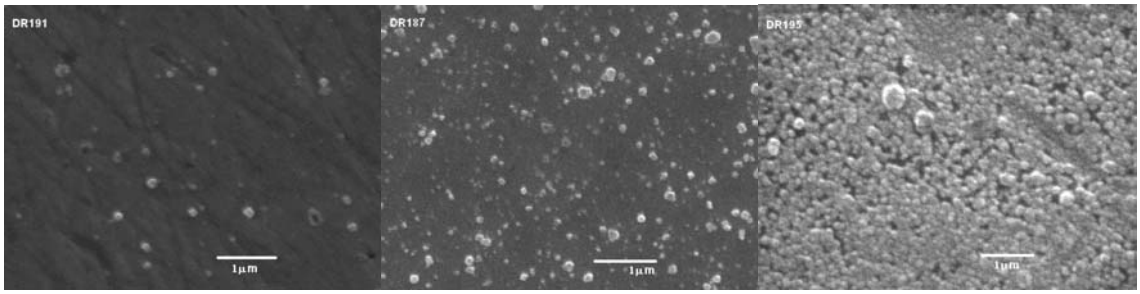

Figure 1. SEM pictures of films deposited after 1 hour using different powders as seeds: (left) high-quality micro-crystalline diamond (from Dr. P. Feng, China); (middle) sub micro-crystalline diamond (from Alfa Aesar); (right) detonation ultra-dispersed nano-crystalline diamond (UDD from Nanodiamond).

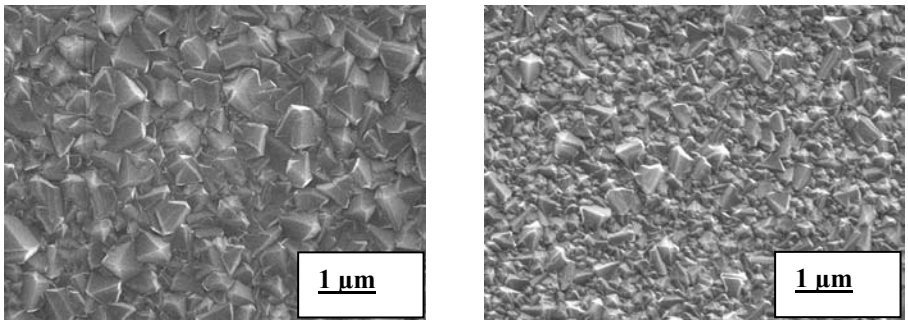

Figure 2. SEM of films deposited after 10 hour using different powders as seeds: (a) high-quality micro-crystalline diamond;(b) detonation ultra-dispersed nano-crystalline diamond).

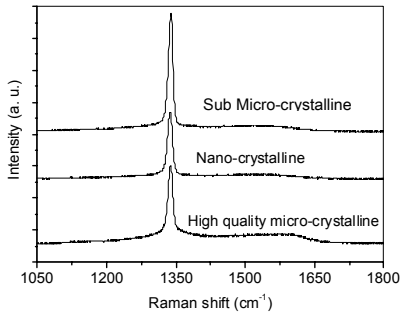

Figure 3. Visible Raman spectra of films deposited after 20 hours using different powders as seeds (sub micro-crystalline, nano-crystalline and high-quality micro-crystalline).

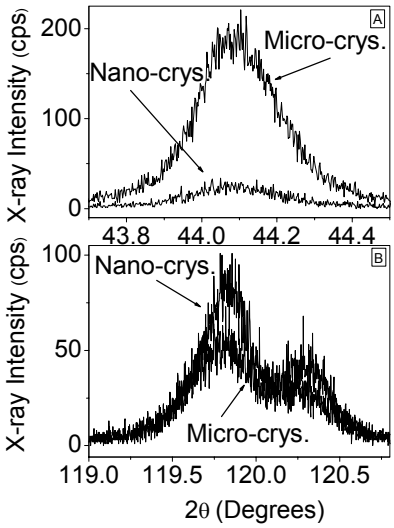

Figure 4. X-ray diffractograms of films deposited after 20 hours using different powders as seeds (micro-crystalline from Alfa Aesar, and nano-crystalline from NanoDiamond), depicting the characteristic diamond peaks corresponding to the (111) (A) and (400) (B) diamond reflections.

Acknowledgements: Research supported by NASA (Grants NCC3-1034 and NGT5-40091; Cooperative Agreement NCC5-595), Department of Energy (Grant DE-FG02-01ER45868), and the UPR-Río Piedras FIPI (Grant 8-80-514).

DEPOSITION AND POST-PROCESSING OF POLYCRYSTALLINE DIAMOND FOR FREESTANDING FILMS AND SUBSTRATES

S. Zuo, T. Grotjohn, D. Reinhard, and J. Asmussen[1]

Michigan State University, 2120 Engineering Building, Electrical & Computer Engineering Department, East Lansing, MI 48824

R. Ziervogel

[1]Fraunhofer USA, Center for Coatings and Laser Applications, B100 Engineering Research Complex, Michigan State University, East Lansing, Michigan 48826-1226

Keywords: Diamond deposition; Microwave plasma CVD; Stripping Foil; Polishing: Intrinsic stress.

Abstract

High quality freestanding films and substrates of polycrystalline diamond with greater than 25 microns thickness have applications for windows, thermal heat sinks and stripping foils for high energy ion beams. Such applications of thick films or substrates require both deposition and post processing steps. In this paper we report on the synthesis of high quality diamond and the fabrication of optical quality windows and uniform thickness ion beam stripping foils. Both of these applications require the deposition of high quality diamond, the laser cutting of the diamond to a desired shape, the post processing of the diamond by etching, lapping and polishing steps to produce smooth, flat and uniformly thick films or substrates. The thickness of the diamond films needed for the ion beam stripping foils are up to 40 μm.

The polycrystalline diamond films are grown in a microwave plasma-assisted CVD reactor using hydrogen/methane chemistry. The methane percentage is nominally 1 %. The deposition reactor is a microwave cavity applicator with the plasma confined inside a 12 cm diameter quartz dome [1]. The substrates utilized are 1 and 2 inch silicon wafers with thickness in the range of 1-2 mm. The substrate is actively cooled with a water cooled substrate holder to achieve a substrate temperature of 850-950 C. The pressure utilized is 120-180 Torr and the microwave power is 3.5-5 kW. The substrate holder is designed to achieve a reasonable uniform substrate temperature distribution. The silicon substrates are prepared using mechanical polishing with diamond powder for nucleation. The growth rate of the polycrystalline diamond is approximately 1 μm/hr at 120 Torr. Influence of the deposition chemistry and reactor configuration on substrate temperature and deposited film uniformity will be presented. Additionally, initial modeling studies to understand the substrate temperature uniformity and control will be shown.

Once the diamond is deposited on the silicon substrate a number of post processing steps are performed to fabricate smooth, flat and uniformly thick films or substrates. These processing steps typically include laser cutting, lapping and polishing of the growth side of the diamond, removal of the silicon substrate, and plasma etching to remove a thin layer on the nucleation side of the diamond film. Laser cutting is performed with a pulsed Nd-YAG laser operating with the third harmonic. Lapping and polishing is performed with a Logitech LP 50. The polishing system has been used to achieve surface roughness values of 3 nm. During the post processing of the diamond film the bowing (stress) of the film is characterized at various steps. The diamond films/substrates are also characterized at the end of the post-processing a number of ways including Raman spectroscopy, photoluminescence spectroscopy, and optical absorption.

A challenge to the fabrication of flat and uniform films/substrates is dealing with the intrinsic stress of the diamond film. When the film is deposited on a silicon wafer a bowing of the wafer and diamond film occurs due to the thermal expansion mismatch of at the diamond-silicon interface and due to intrinsic stress in the diamond film itself [2, 3]. Once the diamond is removed from the silicon substrate by etching the silicon away, the diamond film bowing is due to stresses within the diamond film itself. A gradient in the stress within the diamond film in the direction of growth leads to a bending of the freestanding film. Techniques to compensate for this bowing that include removal of a layer of the film on the nucleation side are explored.

REFERENCES

1. K.-P. Kuo and J. Asmussen, “An experimental study of high pressure synthesis of diamond films using a microwave cavity plasma reactor,” *Diamond and Related Materials*, 6, 9, 1097-1105 (1997).

2. S. Kamiya, M. Sato, M. Saka, and H. Abe, “Residual stress distribution in the direction of the film normal in thin diamond films,” *J. Appl. Phys*., 86, 1, 224-229 (1999).

3. D. Roy, Z. H. Barber, and T. W. Clyne, “Strain gradients along the growth direction in thin diamond film deposited on silicon wafer,” *J. Appl. Phys.*, 94, 1, 136-139 (2003).

REACTIVE ION ETCHING OF MULTIPHASE STRUCTURES FOR CARBON-DERIVED CARBON SYNTHESIS

P. Gupta, M. Tlustochowicz, R. Zhu, C. White, M. McNallan, A. Erdemir, B. Prorok, Y. Gogotsi

University of Illinois at Chicago

Abstract

Carbide Derived Carbon (CDC) is produced by selective removal of metals from metal carbides by high temperature etching in halogen containing gases at atmospheric pressure. In a multi-phase structure, the relative affinity of the metal for the halogen will determine which phase is selectively etched and which phase is relatively unaffected by the presence of the halogen. In some practical cases, this selective attack can be a hindrance to the formation of useful CDC layers. For example, most WC components are cemented carbide materials containing Co or Ni binders. At elevated temperatures, selective attack of the metal binder occurs more rapidly than conversion of WC to CDC, leading to damage of the surface before a CDC layer can form. In the context of SiC based MEMS devices fabricated on Si wafer substrates, high temperature chlorine gases etch the elemental Si more rapidly than they convert SiC to CDC, so that it is difficult to produce CDC layers on these devices.

As an alternative to high temperature treatment, the materials can be etched at lower temperatures in a reactive halogen ion plasma at reduced pressure. Rather than reaching local equilibrium on a microscale resulting in selective attack of the more reactive component of the structure, the halogen radicals tend to react immediately upon encountering the surface and the metal halide species are removed producing a more uniform reaction front. Reactive ion etching has been used to produce carbon layers on multiphase carbide materials containing silicon, titanium, and tungsten. The resulting carbon layers have been characterized using a variety of techniques.

CHARACTERIZATION OF HIGH TEMPERATURE-TREATED NANOSTRUCTURED CARBONS FROM SELF-ASSEMBLED BLOCK COPOLYMER PRECURSORS

Kevin Kohlhaas, Xinqi Chen, Rodney S. Ruoff

Department of Mechanical Engineering, Northwestern University, Evanston, IL 60208

Michal Kruk, Bruno Dufour, Krzysztof Matyjaszewski, Tomasz Kowalewski

Department of Chemistry, Carnegie Mellon University, Pittsburgh, PA 15213

Ewa B. Celer, Mietek Jaroniec

Department of Chemistry, Kent State University, Kent, OH 44240

Keywords: pyrolysis, block copolymer, mesoporous carbon, polyacrylonitrile

Abstract

Nanostructured carbons with controlled morphology (nanocarbons) are promising materials for use in a number of devices. Arrays of carbon dots and vertical cylinders would be ideal for use in field-emission arrays [1], and highly porous nanoscale carbon materials are promising candidates for supercapacitor electrodes [2]. Recent findings have shown that it is possible to stabilize nanoscale thin-film morphology of phase-separated block copolymers with polyacrylonitrile (PAN) blocks, and to convert these materials, by pyrolysis, into carbons with well-defined nanostructure [3,4]. This presentation will describe the effects of further high-temperature treatment of nanocarbons aimed at their graphitization.

Nanocarbon samples were obtained from PAN homopolymers or PAN-containing block copolymers which were assembled inside the channels of ordered nanoporous silica templates [4]. PAN was then converted to carbon via stabilization under air and subsequent pyrolysis under inert atmosphere at 800°C. The resulting materials exhibited well defined nanoscale morphology, replicating the channels within the silica template (Figure 1) [4]. Further graphitization was carried out by heating in a graphite furnace (Centorr/Vacuum Industries Inc., Model HP-2058) at 2200 °C in a 5 psi argon atmosphere for 1 hour. Gas adsorption analysis revealed that the graphitized samples retained appreciable specific surface area and pore volume, whereas x-ray diffraction and preliminary TEM analysis provided the indications of the improved atomic scale ordering.

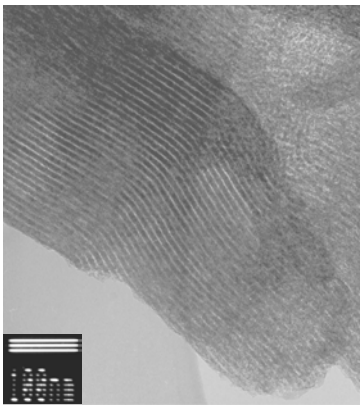

Figure 1. TEM image of ordered nanocarbon obtained by stabilization and 800 ^{o}C pyrolysis of PAN assembled inside the channels of ordered nanoporous silica template.

ACKNOWLEDGEMENTS

The support from NSF grant DMR-0304508 is gratefully acknowledged. Noel T. Nuhfer (Carnegie Mellon University) is acknowledged for assistance in TEM analysis.

REFERENCES

1. Talin, A.A.; Dean, K.A.; and Jaskie, J.E.: "Field emission displays: a critical review," *Solid-State Electronics*, **45**(6), 963-976 (2001).
2. Conway, B.E., *Electrochemical Supercapacitors: Scientific Fundamentals and Technological Applications*, Kluwer Academic/Plenum Publishers, New York, NY (1999).
3. Kowalewski, T.; Tsarevsky, N.V.; and Matyjaszewski, K.: "Nanostructured Carbon Arrays from Block Copolymers of Polyacrylonitrile," *J. Am. Chem. Soc.*, **124**(36), 10632-10633 (2002).
4. Kruk, M.; Dufour, B.; Celer, E. B.; Kowalewski, T.; Jaroniec, M.; Matyjaszewski, K.: "Synthesis of Mesoporous Carbons Using Ordered and Disordered Mesoporous Silica Templates and Polyacrylonitrile as Carbon Precursor", *J. Phys. Chem. B*, submitted for publication.

SYTHESIS OF ALIGNED CARBON NANOTUBES BY MICROWAVE PLASMA CHEMICAL VAPOR DEPOSITION

Shuangjie Zhou[1], Liming Zong, Nikki Sgriccia, Martin C. Hawley

Department of Chemical Engineering and Materials Science, Michigan State University, East Lansing, MI 48824

Shengxi Zuo, Jes Asmussen

The Fraunhofer Center for Coatings and Laser Applications, Department of Electrical and Computer Engineering, Michigan State University, East Lansing, MI 48824,

Keywords: Carbon Nanotubes, Microwave Plasma, Chemical Vapor Deposition, Scanning Electron Microscopy (SEM), Transmission Electron Microscopy (TEM)

Abstract

Aligned carbon nanotubes (CNTs) were synthesized on flat graphite substrates and silicon wafers by microwave plasma chemical vapor deposition (MPCVD) of a gas mixture of methane and hydrogen. Nickel catalyst was not directly deposited on the substrates, but migrated from a small piece of catalyst supplier to the substrate surface during microwave plasma pretreatment. SEM and TEM were used to characterize the morphologies of the CNTs.

INTRODUCTION

CNTs have many potential applications due to their superior mechanical, thermal, and electrical properties. Currently CNT synthesis methods include arc discharge, laser ablation, and chemical vapor deposition (CVD). The CVD method is used for rapid synthesis of nanotubes with high purity at lower temperatures and is easy to scale up for commercial production. Microwave plasma chemical vapor deposition (MPCVD) has been used to synthesize aligned nanotubes. These nanotubes are aligned either vertically to the substrate [1-2], or parallel to the substrate [3]. The alignment was affected by catalyst grain sizes, temperature, gas composition, etc. The CNTs produced in a batch MPCVD process was usually several tens of micrometers long with aspect ratio in the range of 300 to 1500. In this paper, we report the synthesis of high aspect ratio, up to 4500, and well-aligned CNTs with MPCVD method.

EXPERIMENTAL

The CNTs were prepared by MPCVD at a growth temperature range of 680 to 700°C, with a pressure range of 4.7-4.9 kPa, and under the microwave power of 2.2 kW. The hydrogen flow rate was 80 sccm (Standard Cubic Centimeter per Minute) while the methane flow rate was 20 sccm. The growth time was 20 minutes. The silicon wafers were pretreated with diamond carbon. The nickel catalyst was not deposited onto the substrates or wafers, but migrated from a small piece of catalyst supplier onto the substrates during microwave plasma pretreatment. The catalyst supplier on the graphite substrate was silicon sputter deposited with a 30nm nickel layer. The detailed process is described in our patent application [4]. After synthesis, a piece of nanotube film was collected from the substrates and was examined with SEM and TEM

PRELIMINARY RESULTS AND DISCUSSIONS

Figure 1 shows 45° tilted SEM image of the synthesized CNTs on graphite substrate, which are 200-250 micrometer long and aligned vertically to the substrate surface, though slightly curly. The vertical alignment of nanotubes synthesized with plasma enhanced CVD was speculated to result from the electrical self-bias field generated on the substrate surface in plasma environment [1]. The plasma sheath may also influence the alignment of the nanotubes synthesized in these experiments. Figure 2 shows a typical TEM image of the CNTs. The diameters of the nanotubes are in the range of 40 to 70nm. They are not completely hollow and seem to be separated into many nano-compartments by curved platelets. The platelets were much thinner than the nanotube walls. Similar structures were observed in other studies [2, 5, 6]. The morphologies might be related with the nanotube growth mechanism. The nanotubes can grow from its root, and/or tip, depending on the positions of the catalyst particles. In this study, nickel was detected at the top of nanotubes with Energy Dispersive x-ray Spectrometer (EDS), indicating a tip growth route. The most widely accepted growth model of carbon nanotubes was adapted from the catalytic synthesis

---

[1] Now with Freescale Semiconductor, Inc., Mail Drop: TX32/PL51, 7700 W. Parmer Lane, Austin, Texas 78729

of carbon fibers. The hydrocarbon, first, decomposes into carbon and hydrogen at the front (exposed) face of the catalyst particle. Then, the carbon dissolves in the catalyst, diffuses through the particle, and precipitates at the trailing face to form the nanotube [7, 8]. The morphology results of the CNTs on silicon wafers are under characterization.

PRELIMINARY CONCLUSIONS

A MPCVD method can be used to synthesize CNTs on graphite substrates and silicon wafers. The nanotubes growth was catalyzed by nickel, which migrated onto the substrates and silicon wafers during microwave plasma pretreatment. For the CNTs on graphite substrates, SEM study showed that the CNTs were aligned vertically to the substrate surface and were up to 250 micrometers long; TEM results showed that the nanotubes had diameters in the range of 40 to 70 nanometers; The nanotubes were not completely hollow and were separated into many nano-compartments by curved platelets.

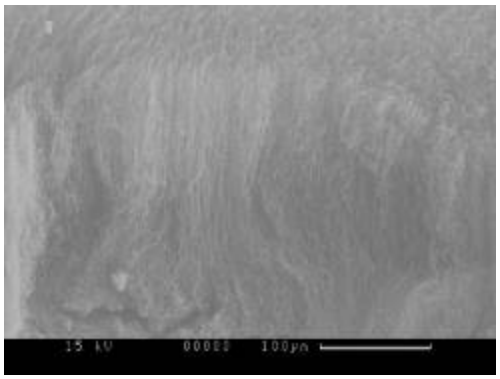

Figure 1. SEM image (tilted 45º) of the CNTs grown on a graphite substrate. The Scale bar is 100 micrometers.

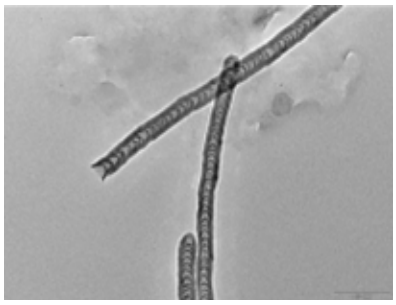

Figure 2. TEM image of the CNTs on a graphite substrate. The scale bar is 200nm.

REFERENCES

1. Bower, C., et al. *Appl Phys Lett*, **77**, 830 (2000).
2. Cui, H., et al. *J Appl Phys*, 88, 6072 (2000).
3. Singh, M. K., et al. *Chem Phys Lett*, 354, 331 (2002)
4. Hawley, M. C.; Asmussen, J.; Zhou, S.; and Zuo, S. "An integrated catalyst deposition and nanotube growth process with microwave plasma chemical vapor deposition," Patent application in process (Michigan State University).
5. Zhang, Q., et al. *J Phys Chem Solids*, 61, 1179 (2000).
6. Wang, E.G., et al. *Carbon*, 41, 1827 (2003)
7. Harris, P. J. F. *Carbon Nanotubes and Related Structures*, Cambridge University Press, 30-33 (1999).
8. Daenen, M. J. M., et al. http://www.pa.msu.edu/cmp/csc/nanotube.html

The Fe Catalyst on Copper Substrates: A Way Forward for Production of Carbon Nanotube Bundles, Ropes and Other Self Assembled Structures

Pawan K. Tyagi[1], Abha Misra[1], Manoj K.Singh[1], Pradip Das[1], D. S. Misra[1@], Jay Ghatak[2], P.V. Satyam[2], F. Le Normand[3]

[1]Deaprtment of Physics, Indian Institute of Technology, Bombay, Mumbai-400076, India
[2]Institute of Physics, Bhubaneswar-751005, India
[3]Groupe Surfaces-Interfaces, IPCMS, UMR 7504, CNRS, BP 43, 67038, Strasbourg Cedex, France

Abstract

Self assembled foams and other structures of carbon nanotubes have recently been the center of interest for the scientific community[1]. These will be assembled as the new applications of the carbon nanotubes appear on the horizon. For instance, a nano-size mat of carbon nanotubes may prove to be an excellent stopper of high-energy particles. Carbon nanocages may have good application as selective filters for the proteins and other biological molecules. Self-assembled carbon tubes were grown onto iron electroplated copper foil substrates. The iron layers were treated in the plasma of ammonia (NH_3) gas for 1-3 minutes in the temperature range 250 ^{0}C – 500 ^{0}C at pressure 10 torr for the formation of nano-sized iron catalyst, which became nuclei for subsequent growth of CNTs. Methane (CH_4) and hydrogen (H_2) were used as pressure gases at 40 torr in a temperature range 700 ^{0}C-900 ^{0}C and deposition time was 3-5 minutes. The aligned multiwalled nanotube bundles, of very high purity, could be easily grown in our system[2]. For certain parameter window the nanotubes self assembled in the form of a rope bundles. Also the length of nanatubes in our case is very long with the tubes arranging to form cage like structure. The TEM, SEM, Raman and XRD studies on these structures will be presented.

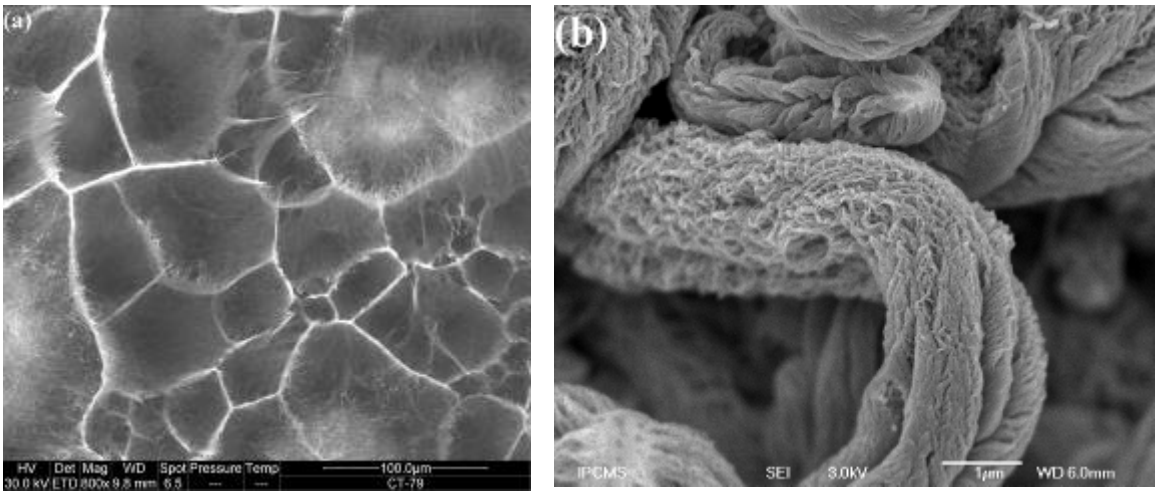

Figure1: (a) SEM (Scanning electron microscope) image of the self assemble of the carbon nanotubes (b) carbon nanotubes in the form of ropes.

Reference:

1.Nirupama Chakrapani, Bingqing Wei, Alvaro Carrillo, Pulickel M. Ajayan, and Ravi S. Kane. PNAS,**101**,4009 (2004)

2. Pawan K. Tyagi, M. K. Singh, Abha Misra, N. Kumar, D. S. Misra, E. Titus, N. Ali, J. Gracio, M. Roy and A. K. Dua. Thin Solid Films, Volumes 469-470, 127.(2004),

Purification of nano-crystalline ultra-dispersed diamond to be employed as nanoprobes for cellular imaging

R. Acosta, J. De Jesús, F. Piazza, G. Morell

Dept. of Physics, University of Puerto Rico, San Juan, Puerto Rico

E. R. Fachini

Dept. of Chemistry, University of Puerto Rico, San Juan, Puerto Rico

Keywords: nanocrystalline, diamond, UDD, nanoprobe, imaging

Abstract

The development of novel nanoparticles for imaging living cells in vivo without harming or disrupting their intracellular molecular dynamics is an important area of nanotechnology that intersects Materials Science, Physics, Chemistry, and Biology. Nano-crystalline ultra-dispersed diamond (UDD) particles are photo stable, biocompatible, and can be tailored for a range of excitation and emission wavelengths. Purification of the powder is necessary in order to remove the non-diamond carbon components and other impurities surrounding the nano-diamond crystals. The effects of UV exposure in air and of heat treatment in H_2 and H atmosphere on the structure and properties of detonation UDD are investigated. The variation in the powder structure and properties after the exposure at different temperatures for variable periods is studied by TEM, X-ray photoelectron spectroscopy, visible and UV Raman spectroscopy, and Fourier transform infrared spectroscopy. The results show that it is possible to significantly increase the purity of the UDD powder by UV irradiation in air (Fig. 1 and Fig. 2). The role of oxygen and hydrogen radicals is discussed. A strong luminescence background is excited with the 514 nm laser line (Ar ion laser) during Raman spectroscopy experiments (Fig. 3). We aim to learn how to tailor the nanoparticle size, composition, and surface termination, particularly targeting for long-lived yellow-green-blue luminescence states, in preparation for subsequent in vivo studies.

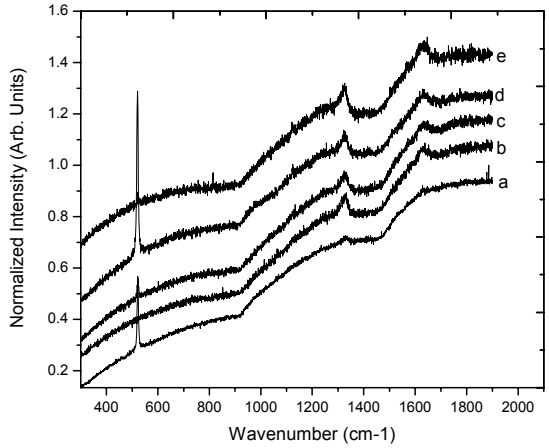

Figure 1. Visible Raman spectroscopy of the UDD that were treated with UVO, at naked eyes we can see how the diamond peak growths as the time of exposure increases. Here (a) is the powder not exposed, (b) after 1 hour of treatment, (c) after 5 hours, (d) after 15 hours and (e) after 45 hours.

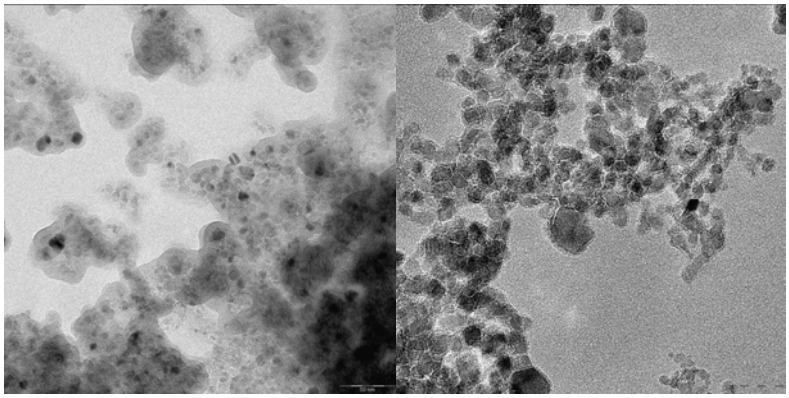

50 nm ---------- 20 nm ----------

a. Original UDD powder b. Purified UDD powder

Figure 2. TEM image of diamond nanoparticles (UDD), before and after purification, showing their rounded shape and nanoscale size.

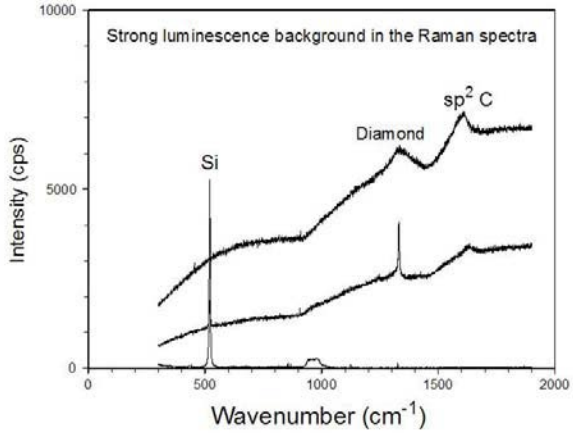

Figure 3. Strong luminescence background excited with the 514 nm laser line (Ar ion laser) during Raman spectroscopy experiments of different nanocrystalline diamond powders. The luminescence becomes stronger as the n-D particle size decreases, as indicated by the diamond band broadening. The dips in the spectra are artifacts of the CCD detector employed due to the fact that three spectral regions were collected and joined. Collecting the data with a PMT will give a smooth broad band with the Raman peaks on top. The Si spectrum taken under identical conditions is shown as reference.

Acknowledgements: Research supported by NASA (Grants NCC3-1034 and NGT5-40091; Cooperative Agreement NCC5-595), Department of Energy (Grant DE-FG02-01ER45868), and the UPR-Río Piedras FIPI (Grant 8-80-514).

REFERENCES

1. Diamonds in detonation soot, N. R. Greiner, D. S. Phillips, and J. D. Johnson, F. Volk. *Nature*, 333, 440 (1988).
2. Ultradisperse diamond cluster aggregation studied by atomic force microscopy, Aleksenskii AE, Osipov VY, Dideikin AT, Vul' AY, Adriaenssens GJ, Afanas'ev VV, Technical Physics Letters 26, 819 (2000).

FLUID SYNTHESIS AND STRUCTURE OF NOVEL BORON NITRIDE POLYMORPHE - HYPERDIAMOND FULBORENITE HDF-B12N12 (E-PHASE)

V. Pokropivny[1], A. Smolyar[1], A. Pokropivny[1], V. Kuts[2], R. Partch[3]

1Frantsevich Institute for Problems of Materials Science of NASU, Kiev, 03142, Ukraine

2Institute of Magnetizm of NASU, Kiev, 03142, Ukraine

3Clarkson University, Potsdam, NY, 13699-5814, USA

Keywords: BN, polymorph, E-phase, fulboren, fluid synthesis

Introduction

For boron nitride as being the isomorphic analog of carbon several polymorph phases, intermediate in density between graphite-like g-BN and cubic c-BN, have been discovered [1-7].Batsanov was the first who have synthesized a novel BN polymorph named E(Explosion)-phase by shock compression of turbostratic t-BN [1-3] . Its elementary cell was proposed to be rhombohedral with the parameters a=0.72 nm, b=0.81 nm, c=1.89 nm [2]. Akashi have obtained a novel BN phase by multiple shock compression identifying its unit cell as face centered lattice with parameter a=0.8405 nm [4]. Sokolovski, Olszyna et al. have synthesized the E-phase by different techniques notably at normal pressure [5,6]. Wang et al. have obtained E-phase nanocrystals at g-BN/acetone interface by pulsed laser irradiation [7].

In this work a novel BN polymorph for a first time was obtained by supercritical fluid synthesis, the XRD pattern and IR spectra of which are close to E-phase. Its structure was suggested to be hyperdiamond fulborenite HDF-$B_{12}N_{12}$ that confirmed by XRD analysis. It is novel faujasite on base of BN.

Results

Synthesis was carried out on high pressure gazostat at intermediate pressure (P~200MPa) and temperature (T<1000C) in different atmospheres (He, H_2O, N_2, Ar). At the conditions the gaze transforms in a supercritical fluid becoming an effective catalyst which easy penetrates in crystalline lattice due to its low viscosity. Samples were characterized by SEM, TEM, XRD, IR, Raman, and EPR techniques. In table 1 XRD results are presented.

In spite of some discrepancy one can to conclude that: 1) number of lines in our samples relate to unconventional BN polymorph; 2) this lines are in satisfactory correlation with the lines distinguishing for E-phase; 3) number of lines calculated for HDF-$B_{12}N_{12}$ are in good agreement with experimental ones for E-phase.

The IR spectra of our samples in spite of some discrepancy are closed to the lines peculiar for both the E-phase, namely, (450, 550, 700, 800, 940, 1030, 1110, 1200, 1260, 1400, 1650 cm^{-1}) [1] and the nanocrystalline BN (649, 699, 783, 883, 927, 1026, 1104, 1195, 1252, 2260, 3217, 3376 cm^{-1}) [7] . Two common lines 927 cm^{-1} (960 cm^{-1}) and 1250 cm^{-1} are the most peculiar for E-phase [1,7].

Raman and EPR spectra confirm the presence of novel phase in turn.

To resolve unknown so far E-phase structure we have considered the number of potential sc, fcc, bcc, hcp, sphalerite and wurtzite lattices , named as fulborenites [8], with fulborene molecules B12N12 and B24N24 in it vertexes. Among them only the diamond type lattice called us as hyperdiamond fulborenite HDF-B12N12 [8] (fig.1) gives the satisfactory agreement between experimental (A=1.114 nm, ρ=2.5- 2.6 g/cm3) [3] and calculated (A=1.152 nm, ρ=2.59 g/cm3) values of lattice parameter and density under a bond length aBN=0.145 nm.

Table 1. Some XRD interplane distances for E-phase [3,4,5,7] in comparison with our experimental samples (1-4)) and suggested HDF-B12N12 structure.

[3]	[5]	[7]	[4]	1	2	3	4	HDF-$B_{12}N_{12}$
-	-	-	-	8.04	8.84	12.20	10.40	10.88
6.28	-	6.146	-	6.03	6.03	5.95	5.98	6.280
4.85	5.03	-	4.854	5.19	-	4.58		4.864
4.25	4.27	-	4.330	-	4.58		4.53	4.441
3.85	3.86	3.86	-	3.95	3.90		4.14	3.846
3.54	3.56		-	3.51	3.51	3.49	3.52	3.626
3.04	3.20	3.189	-	3.19	3.18	3.18	3.16	3.140
2.983	-	2.981	2.973	3.03	3.01			3.017
2.784	2.97	-	-	2.91	2.92	2.91	2.93	2.907
2.686	2.64	2.689	-	2.72	2.70			2.719
2.567	-	2.57	2.536	2.54	2.53	2.54		2.564
2.430	2.41	2.428	-	-	-			2.432
2.298		-	-	2.29	-	2.28		2.374
2.201	2.21	2.239	-	2.24	-	2.24	2.23	2.220
2.076	2.04	-	-	2.08	2.09	2.09	2.10	2.093
1.955	1.99	-	-	1.933	-			1.923
1.901	-	-	-	-	1.907	1.903	1.845	1.893
1.769	-	-	-	1.752	-			1.764
1.696	1.68	-	1.716	1.685	-	1.681		1.720

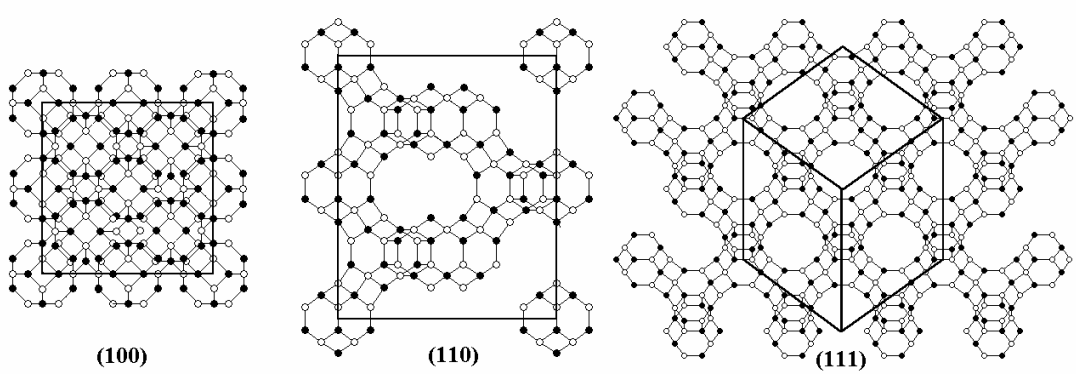

Fig.1. Fragments of elementary cell in (100), (110), and (111) planes of hyperdiamond fulborenite HDF-$B_{12}N_{12}$ suggested as E-phase. It is diamond type lattice with fulborene $B_{12}N_{12}$ in its vertexes copolymerized by hexagonal faces with alternated B-N atoms.

Acknowledgement

This research was made possible in part by Award UE2-2456-KV-02 of U.S. CRDF.

References

1. Batsanov S.S., Blochin G.E., and Deribas A.A. J.Struct. Chem. 6, 227 (1965).

2. Batsanov S.S., *Zh. Neorg. Khim*. 28, 2723 (1983).

3. Batsanov S.S., Kopaneva L.J., and Lazareva E.V. *Propellants, Explosives, Pyrotechnics* 18, 352 (1993).

4. Akashi T., Pak H.R., and Sawaoka A. B. *J. Mater. Sci*. 21, 4060 (1986).

5. Rusek A., Sokolovski M., and Sokolovska A. *J.Mater.Sci*. 16, 2021 (1981).

6. Olszyna A., Konwerska J., Lisicki M. *Diamond and Related Mater*. 6, 617 (1997)

7. Wang J.B., Zhong X.L., Zhang C.Y., et al. J.Mater.Res. 18, 2774 (2003)

Pokropivny V.V., Skorokhod V.V., Oleinik G.S., et al. J.Solid State Chem. 154, 214(2000).

GROWTH OF ADHESIVE CUBIC PHASE BORON NITRIDE FILMS WITHOUT ARGON ION BOMBARDMENT

Jiesheng Wang and Yoke Khin Yap *

Department of Physics, Michigan Technological University, 1400 Townsend Dr., Houghton, MI 49931, USA.

*ykyap@mtu.edu

Keywords: cubic boron nitride, PLD, plasma, ion bombardment.

Abstract

We show that adhesive cubic phase boron nitride (c-BN) films can be grown without the use of Ar ion bombardment. c-BN has several attractive properties such as extreme hardness, high thermal conductivity, and wide band gap (6eV). c-BN is also chemically inert to oxidation and ferrous metals. Previously, i*n-situ* bombardment of massive ions (Ar^+, Kr^+, etc.) was considered to be necessary for the formation of c-BN films. Bombardment of massive ions has lead to c-BN films with poor adhesion to the substrates due to the accumulated stress. We found that while ion bombardment is still required for the formation of c-BN films, it can be achieved without involving massive ions. We have succeeded to growth adhesive c-BN films by two approaches: 1) plasma-assisted pulsed-laser deposition (PLD) in pure N_2 plasma, and 2) PLD in high vacuum (~10^{-5} mbar during growth).

INTRODUCTION

Cubic phase boron nitride (c-BN) films have attracted much attention due to its desirable properties such as extreme hardness comparable to diamond, high thermal conductivity, wide band gap (6eV) and chemically more inert than diamond to oxidation and ferrous metals, etc [1]. In the past decade, it was found that ion bombardment is necessary for growth of cubic phase boron nitride, especially with heavy ions, i.e., Ar or Kr ions [2, 3]. However, as an adverse effect of that, poor adhesion of cubic phase boron nitride is observed which hindered the actual application of c-BN films [4]. We have conducted a series of experiments in order to reduce the adverse effect of ion bombardment for the formation of adhesive c-BN films. It appears that adhesive c-BN films can be formed by pure N_2 plasma with reduced ionic flux at reduced deposition rate. Furthermore, energetic BN growth species generated by pulsed-laser deposition (PLD) could possibly sufficient for the growth of c-BN without the assistant of auxiliary ion bombardment. We have tested and verified these possibilities by using a PLD technique.

EXPERIMENTS

In the first approach, c-BN films were prepared at 600 °C by RF (13.56MHz) plasma-enhanced PLD [5-7]. A fourth harmonics generation of Nd:YAG laser (λ = 266nm) was used for the ablation of a hot-pressed h-BN target. The RF power was capacitively applied on a Si (100) substrate to generate a plasma in pure N_2 ambient at a pressure of 2 x 10^{-2} mbar. A negative dc bias voltage was induced by this plasma on the substrate for enhancing bombardment of positive ions during the deposition of BN films.

In the second approach, similar experimental setup was used for the growth of c-BN film in vacuum. RF plasma was not used in this case.

RESULTS AND DISCUSSION

In the first approach, all c-BN films were deposited within 4 h, with a constant substrate bias voltage of -500V. Different pulsed laser energies were applied in order to deposit BN films at different deposition rates. The BN films are characterized by Fourier transform infrared (FTIR) transmission spectroscopy. The IR absorption due to the entire BN film can be detected as shown in Fig. 1. Two absorption bands at 1390 and 780 cm^{-1}, represents the in-plane (B–N) and out-of-plane (B–N–B) stretching modes of the sp^2-bonded BN phase. The c-BN band appeared at 1080 cm^{-1} [5, 8]. c-BN films with massive ion bombardment were easily peeled off. However, c-BN films synthesized in pure N2 plasma is much more adhesive [5].

In the second approach, all c-BN films are deposited within 6h in vacuum. Different pulsed laser energies were applied in order to search for an optimum deposition rates for the formation of c-BN films. By using FTIR, the IR absorption due to the entire BN film can be detected for samples deposited at pulsed laser energy of 2.66mJ, 4mJ, 5mJ and 8mJ.

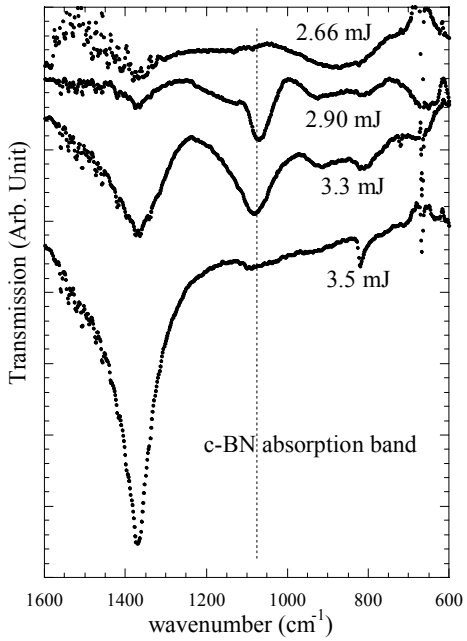

Fig. 1. FTIR spectra of c-BN films prepared at a substrate biasing of −500V in pure N_2 plasma at various pulsed laser energies.

REFERENCES

1. Holleck, H., "Material Selection for Hard Coatings", J. Vac. Sci. Technol. A4, 2661 (1986).
2. Yoshida, T.: "vapor phase deposition of cubic boron nitride", Diamond Relat. Mater. 5, 501 (1996).
3. Kester, D. J.; and Messier, R.: "phase control of cubic boron nitride thin films", J. Appl. Phys. 72, 504 (1992).
4. Kester, D. J., et al., "growth and characterization of cubic boron-nitride thin-films", J. Vac. Sci. Techno. A. 12, 3074 (1994).
5. Yap, Y. K., et al, "Synthesis of adhesive c-BN films in pure nitrogen radio-frequency plasma", Diamond and Relat. Mater. 8, 382 (1999).
6. Yap, Y. K., et al., "Influence of negative dc bias voltage on structural transformation of carbon nitride at 600 °C," Appl. Phys. Lett. 73, 915 (1998).
7. Yap, Y. K., et al., "Hybridized boron-carbon nitride fibrous nanostructures on Ni substrates," Appl. Phys. Lett. 80, 2559 (2002).
8. Ichiki, T.; Momose, T.; and Yoshida, T.: "effects of the substrate bias on the formation of cubic boron nitride by inductively coupled plasma enhanced chemical vapor deposition", J. Appl. Phys. 75, 1330 (1994).

FEATURES OF DC CATHODIC VACUUM-ARC PLASMA SOURCES FOR DLC FILMS DEPOSITION

I.I. Aksenov, V.E. Strel'nitskij

NSC Kharkov Institute of Physics and Technology, Akademicheskaya Str. 1, 61108 Kharkov, Ukraine

Keywords: diamond-like films, vacuum-arc, plasma source, macroparticles, filtering, system productivity.

Vacuum-arc methods of diamond-like carbon (DLC) or amorphous carbon (a-C) films deposition have gained wide recognition in recent decades for use in laboratory and industrial practice. The method is based on a growing of the films through condensation of high ionized carbon plasma flows generated by the cathodic vacuum-arc discharge with a cold graphite cathode. The DLC films synthesized by this method have the highest physical characteristics near to those of natural diamond. However, in early experiments the films comprised a great many macrodefects in view of the fact that in condensed plasma there were many graphite macroparticles (MP's). The cardinal solution of the issue associated with MPs became possible with the advent of magnetic plasma filters. Application of this filters has given results that eliminated the basic restriction on the use of vacuum-arc discharge to form high quality a-C films [1]. Nevertheless, there are some difficulties in the vacuum-arc technological process of the DLC films deposition so far. The problems appear when igniting dc vacuum arc discharge and maintaining its stable arcing in plasma sources with graphite cathode. These difficulties are conditioned by specificity of a cathode spots (CS) behavior on the graphite cathode. The velocity of the CS motion through graphite is essentially (on 2-3 orders of magnitude) less than on metal. The averaged lifetime of CS strongly depends on the sort of graphite. As a rule it results in strongly non-uniform erosion of the working surface of the cathode, that in turn is the reason of unpredictable change of plasma stream parameters, raise of an arc exiting frequency and loss of serviceability of the apparatus. Efficient plasma transport through magnetic filters as well as cleaning MPs from plasma are the features of merit that should be improved vastly too.

This article is a brief review of results from investigations and developments performed by the authors an coworkers to solve the said problems.

It has been established experimentally, that in plasma source with so called "antostabilization" of CS, described in ref. [2], the uniform erosion of the graphite cathode can be ensured by appropriate selection of stabilizing magnetic field configuration around the cathode. At the presence of argon the arc stability vastly rises. At $p \gtrsim 1{,}5$ mTorr the arc burns practically without extinctions.

At use of graphite characterized by low arc stability, the multicathode triggering device is recommended to be used.

The additional anode disposed around the cathode should be covered by a layer or plate of graphite. Such measure allows to prevent contamination of DLC condensate by metal impurities, which could be appeared from sputtered surface of uncovered additional anode.

In the plasma source considered the CS is ignited in immediate vicinity of the cathode working surface. It excludes a delay between triggering and working stage of the arc, caused be travel of CS from triggering point to the working surface of the cathode. It is a fact of great importance in case of short deposition time when forming ultrathin DLC films (of nanometre range of thickness).

The dependence of an arc extinction frequency on argon pressure for cathodes made from different graphite materials is shown in the Fig.1. It was established [3] that discharge stabilyty decreases with increasing of porocity and graphite crystals dimensions. The best arc discharge stability was observed when cathodes were made from graphites MG and MPGA with pores sizes not more than about 70 micrometres.

The burning of an arc in plasma source considered, at presence of focusing and transporting magnetic fields is hindered because current transmission between the cathode and anode occurs predominantly crosswise to the magnetic field. Besides a high-resistive carbon layer deposits on the water-cooled walls of the anode. As the layer thickness increase the arc voltage rises that inevitably leads either to discharge extinction, or to breakdown of the layer and consequent melting of the anode wall in the place of the breakdown. To prevent such wreck situation a ring-shaped graphite insert inside the anode was used.

Analysis of data on efficiency of plasma transport along magnetic filters shows that the highest results are attained for the systems with wide-aperture curvilinear plasma duct. The main results of experimental studies of the source with L- and T-shaped plasma filter can be formulated as follows. An increase in the linear dimensions of the cross

section of the plasma duct (up to about 200 – 300 mm in the case under consideration) with a low aspect ratio $R/a \approx$ 1,3 is favorable for significant improvement in the efficiency of the system (R and α are radius of curvature and inner radius of the duct respectively). The main losses of plasma during its travel along the duct are due to ions diffusion across the magnetic field. Besides, a significant part of the plasma flow drifts to the walls due to unhomogeneity and curvature of the magnetic field (so called gradient and centrifugal drifts). The drift losses can be appreciably reduced by local correction of the magnetic fields using correcting coils (Fig. 2) [5]. The losses decreased with rise in the positive bias potential of the plasma duct (up to 25-35 volt). The problem of MPs suppression in the filter was solved using appreciable set of intercepting screens and baffles. Selection of the intercepting elements was performed by resorting to computation of MPs motion [6].

The achievements in development of the system with axial-to-radial transformation of two plasma flows are noted. The index of plasma transport efficiency for this system makes up to 90% [7]. This results can be used for development of a new generation of high-efficient filtered vacuum-arc plasma sources.

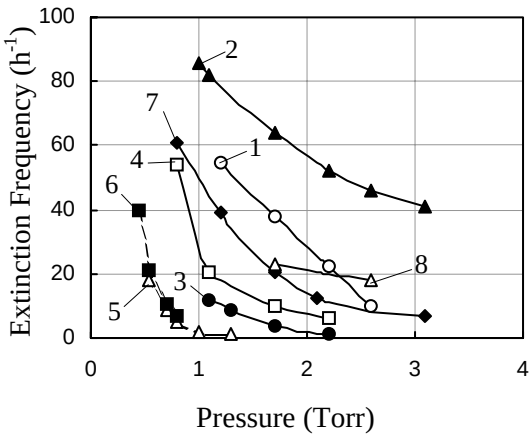

Figure1. Dependence of an arc discharge frequency extinction on Ar pressure for cathodes manufactured from different sorts of graphite: GIP (1), EG–0 (2), GSP (3), GIP (4), MPGA (5), MG (6), impregnated by pyrocarbon (7).

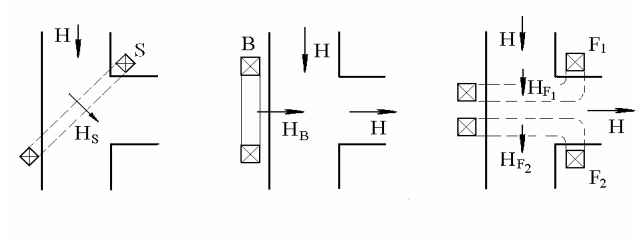

Figure 2. Arrangement of the correcting coils S,B,F_1, and F_2 around T-shaped plasma duct. H - transporting magnetic field; H_S, H_B, H_{F1}, and H_{F2} - magnetic fields created by coils S, B, F_1, and F_2, respectively.

REFERENCES

1. I.I. Aksenov, S.I. Vakula, V.G. Padalka, V.E. Strel'nitskij. *Sov. Phys. Tech. Phys.* 25 (1980) 1164.
2. I.I. Aksenov, V.A. Belous. *Pribory i Technika Eksnerimenta*, No. 3 (1979) 160 (in Rus.)
3. V.E. Strel'nitskij, I.I. Aksenov. *Proc. of the XXIth Int. Symp. on Discharges and Electrical Insulation in Vacuum, 2004, Yalta, Ukraine.* V.2, p. 461.
4. I.I. Aksenov, V.V. Vasilyev, A.A. Luchaninov, V.E. Strel'nitskij, D. Yu. Zaleskij, J.S. Zabinski, A.A. Voevodin. *Proc. of the XXIth Int. Symp. on Discharges and Electrical Insulation in Vacuum, 2004, Yalta., Ukraine.* V.2, p.491.

5. I.I. Aksenov, D. Yu. Zaleskij, V.E. Strel'nitskij. *1st Int. Congress on Radiation Physics. High Current Electronics and Modification of Materials*. *Tomsk, Russia*, 2000. Proc. vol.3, p.133.

6. I.I. Aksenov. *Proc. of the XXIth Int. Symp. on Discharges and Electrical Insulation in Vacuum, 2004, Yalta, Ukraine.* V.2, p.467.

Structural studies of graphite-like CNx films deposited on silicon by chemical vapor deposition of 1 H-1,2,3-triazole

Md. Nizam Uddin and Masamitsu Nagano
Department of Chemistry and Applied Chemistry, Faculty of Science and Engineering, Saga University, 1 Honjo-machi, Saga, 840-8502, Japan

M. Jahurul Islam
Department of Chemistry, Shah Jalal University of Science and Technology, Sylhet-3114, Bangladesh

Keywords: X-ray diffraction; Chemical vapor deposition (CVD); Nitrides.

Abstract

In 1989, Liu and Cohen[1] presented firstly theoretical calculation for C_3N_4, a new hypothetical material and suggested that it should be metastable and possesses extreme hardness, wide band gape, high velocity of sound, large thermal conductivity, low dielectric constant, and low friction coefficient. They also predicted its outstanding mechanical properties. Graphite like carbon nitride composed of only sp^2 hybrids has recently attracted much attention. However, there have been few works so far which show the synthesis of graphite-like carbon nitride. In this paper, we report on the synthesis of graphite-like CN_x by micro-wave plasma enhanced chemical vapor deposition (CVD) method. 1 *H*-1,2,3-triazole + N_2 and Si (100) were used as precursor and substrate, respectively. The details of the experimental procedures are described elsewhere[2]. Substrate temperature during the deposition was recorded to be 850 °C. The deposited films were characterized with respect to crystal structure and states of chemical bonding by x-ray diffraction (XRD) and x-ray photo-electron spectroscopy (XPS) analyses, respectively. XRD observation (Figure 1) strongly suggests that the films consist of graphitic (Gr.) C_3N_4 (002), (200) and (004) with small contribution of Gr. carbon (101)[3]. Narrow scans of C(1s) and N(1s) photoelectron peaks are depicted in Figure 2(a) and 2(b), respectively. Four deconvoluted peaks of C(1s) (Fig. 2(a)) at 284.8 (peak 1), 285.8 (peak 2), 286.8 (peak 3), and 288.3 eV (peak 4) are attributed to adventitious carbon, sp^2C-N, sp^3C-N, and C-O bonding structures, respectively[2]. On the other hand, five deconvoluted peaks of N(1s) (Fig. 2(b)) at 397.9 (peak 1), 398.9 (peak 2), 399.8 (peak 3), 400.5 (peak 4), and 402.0 eV (peak 5) are attributed to N (1s)-Si, N-sp^3C, N-sp^2C, N-N and N-C bond in a variable stoichiometry, and N-O bonding structures, respectively[2]. CN_x with sp^2 hybrid structure is dominant in the deposited films which are shown in Figs. 2(a) and 2(b). These observations support that 1 *H*-1,2,3-triazole favors the formation of graphite-like CN_x films and thus is in good agreement with XRD results. We do propose that 1 *H*-1,2,3-triazole can be used as an important promising precursor for CVD to deposit graphite-like CN_x films.

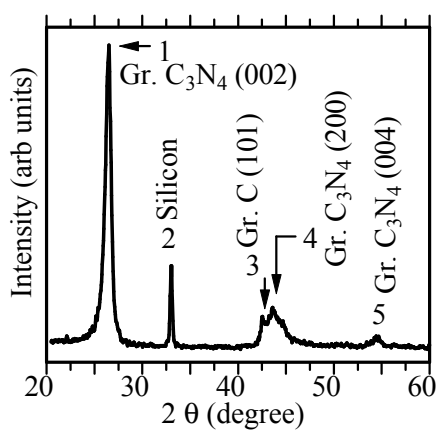

Figure 1 XRD spectra of CN_x films deposited on Si (100).

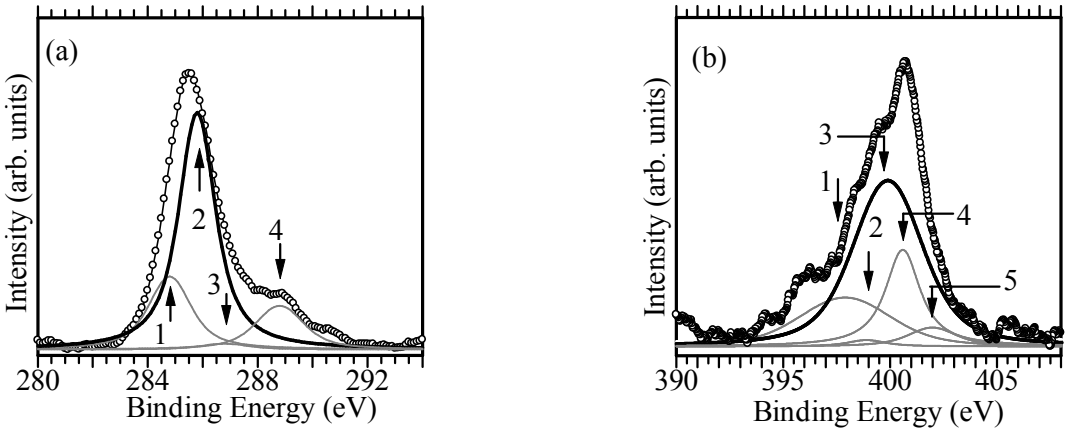

Figure 2 XPS scans of (a) C (1s) and (b) N (1s) for the CN_x films deposited from 1 H-1,2,3-triazole+N_2 on Si (100).

REFERENCES

1. A. Y. Liu and M. L. Cohen, "Prediction of new low compressibility solids", Science 245 (1989) 841; A. Y. Liu and M. L. Cohen, "Structural properties and electronic structure of low-compressibility materials: beta-Si_3N_4 and hypothetical beta-C_3N_4",*Phys. Rev. B* 41, 10727 (1990).
2. M. N. Uddin et al., "Deposition and characterization of carbon nitride films from hexamethylenetetramine / N_2 by microwave plasma enhanced chemical vapor deposition", *Appl. Surf. Sc.* 240, 120 (2005).
3. S. Matsumoto, E. –Q. Xie, and F. Izumi, "On the validity of the formation of crystalline carbon nitrides, C_3N_4", *Diamond Rel. Mater.* 8, 1175 (1999).

THE PROPERTIES OF AMORPHOUS CARBON NITRIDE FILMS GROWN BY NEWLY DEVELOPED SURFACE WAVE MICROWAVE PLASMA CVD AFTER HEAT-TREATED AT VARIOUS ANNEALING TEMPERATURES

M. Rusop, T. Soga and T. Jimbo

Department of Environmental Technology and Urban Planning,

Nagoya Institute of Technology, Gokiso-cho, Showa-ku, Nagoya 466-8555, Japan

S. Adhikari, A.M.M. Omer, S. Adhikary, H. Uchida and M. Umeno

Department of Electronic Engineering, Faculty of Engineering,

Chubu University, Matsumoto-cho1200, Kasugai 487-8501, Japan

Keywords: amorphous carbon nitride; a-CN_x; heat treated; annealing temperature; surface wave.

Abstract

We have studied the effects of annealing temperature (AT) on the properties of amorphous carbon nitride (a-CN_x) thin films grown at room temperature (RT) on quartz substrates by surface wave microwave plasma chemical vapor deposition (SWMP-CVD) using camphor alcohol gas as carbon plasma sources. The thickness, optical, bonding, structural and electrical properties of the as-grown (RT) and heat-treated in range from 100 to 500 ^{o}C of a-CN_x films were measured and compared. The film thickness is decreased rapidly with increasing AT above 350 ^{o}C. The wide range of optical absorption coefficient characteristics is observed depending on the AT. The optical band gap of as-grown a-CN_x films is found to be approximately 2.8 eV, after which it gradually decreased down to 2.5 eV for the films heat-treated at 300 ^{o}C and beyond that it decreased rapidly down to 0.9 eV at 500 ºC of AT. Visible-Raman Spectroscopy (Raman) has revealed the amorphous structure of as-grown a-CN_x films and, the growth of nanocrystallinity of a-CN_x films upon increase of AT. Raman and Fourier transform infrared spectroscopy (FTIR) analyses respectively shown the structural and composition of the films can be tuned by optimizing the AT. The change of optical, bonding, structural and electrical properties of SWMP-CVD grown a-C:N films with higher AT was attributed due to the fundamental changes in the bonding and band structure of the a-C:N films. All of the measurements were carried out using standard measurement techniques.

RESULTS AND DISCUSSIONS

Figure 1 displays the evolution of the RS in the range 1000 to 1800 cm^{-1} of as-grown and heat-treated a-CN_x films. The shape and position of the spectra are almost unchanged up to 150 ^{o}C, after which it gradually grows splitter in to sub band with higher AT. The G peak shifts to higher wave number and become narrower with increase of AT higher than 300 ^{o}C. The experimental data were best fitted with the accuracy factor is about 0.95 by two peaks considering 2 Gaussian line shapes into two Raman bands of D and G peaks, and the linear background and the plot of this kind of RS for the as-grown and heat-treated a-CN_x films. It is clear that the broad band resulted from the a-C:N film (grown at 25 ^{o}C) gradually splitted into two peaks (commonly known as D and G peaks) with the increase of AT, may be due to the progressive crystallization upon increase of AT. The RS shows a similar trend to those observed by Dillon et al. [1] and Mominuzzaman et al. [2] in their heat treatment experimental of C films. This indicates that these films consisted of a disordered graphite matrix with some sp^3- hybridized C states [3].

The electrical resistivity (ρ) was measured at room temperature (RT) by a 4-point probe resistance measurement method, the usual way for high resistance measurement. The ρ values for each film were the average of measurements made at different positions on the film surface. Figure 2 shows the ρ values of as-grown a-C:N film measured to be around 7.5 x 10^5 (Ω-cm) gradually decreases with higher AT to 6.1 x 10^5 (Ω-cm) at 100 ^{o}C. As AT increases, the ρ decreases up to 3.5 x 10^5 (Ω-cm) at 200 ^{o}C. At higher AT, as can be seen in figure 6 and figure 10, both of the E_g and ρ are gradually decreases up to 2.3 eV and 2.3 x 10^5 (Ω-cm) at 300 ^{o}C, respectively. The variation of the optical and electrical properties can be related to interstitial doping of N in a-C films through modifications of C-N bonding configurations by rearranging of N atoms upon increase of AT. However with further

increase of AT above 300 ^{o}C, both E_g and ρ are drastically decreases up to 0.9 eV and 1.5 x 10^4 (Ω-cm) at 500 ^{o}C, respectively. This is probably due to the graphitization of the a-C:N films. Perhaps the doping of N accompanied by increase of AT above 300 ^{o}C increases crystallinity and subsitutional doping of N thereby sharply decreases resistivity. These phenomena also supported by the Raman and FTIR spectroscopy measurements.

Details of the experimental results and discussions will be presented during the conference presentation.

Conclusions

We have grown nitrogenated amorphous carbon (a-CN_x) films by surface wave microwave plasma chemical vapor deposition (SWMP-CVD) method and the effects of annealing temperature (AT) in range from 100 to 500 ^{o}C has been studied in details. The thickness, optical, structural and bonding properties of the as-grown and heat-treated a-CN_x films were measured and compared. The film thickness is decreased rapidly with increasing AT above 300 ^{o}C. The optical band gap of the as-grown a-CN_x films was found to be approximately 2.8 eV, remained almost constant until 300 ^{o}C, and beyond that it decreased monotonically up to 0.9 eV at 500 ^{o}C. Visible-Raman scattering analyses revealed the amorphous structure of as-grown a-CN_x films and, the growth of nanocrystallinity of a-CN_x films upon increase of AT. We found that, both the sp^2 and sp^3- hybridized C atoms can be bound to the N atoms in the a-CN_x films. The FTIR spectroscopy measurements also have shown that the structural and composition of the films can be tuned by optimizing the AT. The change of bonding, structural, optical and electrical properties of SWMP-CVD grown a-CN_x films with higher AT was attributed due to the fundamental changes in the bonding and band structure of the films. The result shows it is possible to control the bonding, structural, optical band gap and electrical properties of SWMP-CVD grown a-C:N films by the annealing process for its possible application in various electronic devices.

REFERENCES

1. R.O. Dillon, J.A. Woollam, V. Katkanant, Phys. Rev. B Vol. 29, pages 3482 (1984).
2. S.M. Mominuzzaman, K.M. Krishna, T. Soga, T. Jimbo, M. Umeno, Carbon Vol. 38, pages 127 (2000).
3. Y.K. Yap, S. Kida, T. Aoyama, Y. Mori, T. Sasaki, Appl. Phys. Lett. Vol. 73, pages 7 (1998).

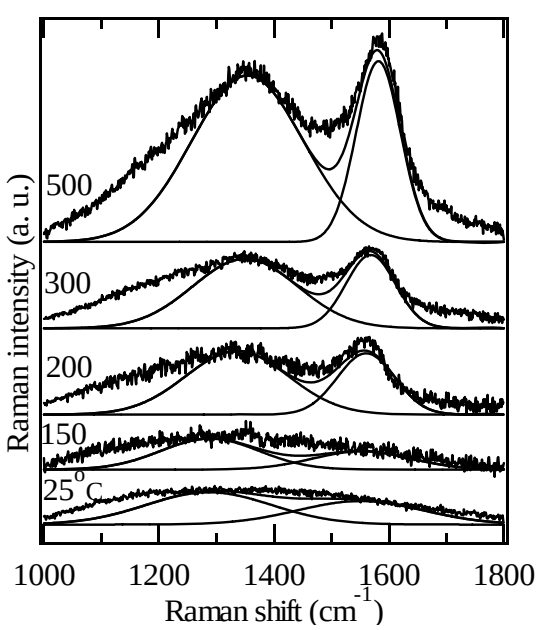

Figure 1: The Raman spectra of as-grown and a-C:N films heat-treated at various temperatures, and their images of deconvolution of Raman D and G peaks using 2 peaks of Gaussian lines. (Substrate: Quartz).

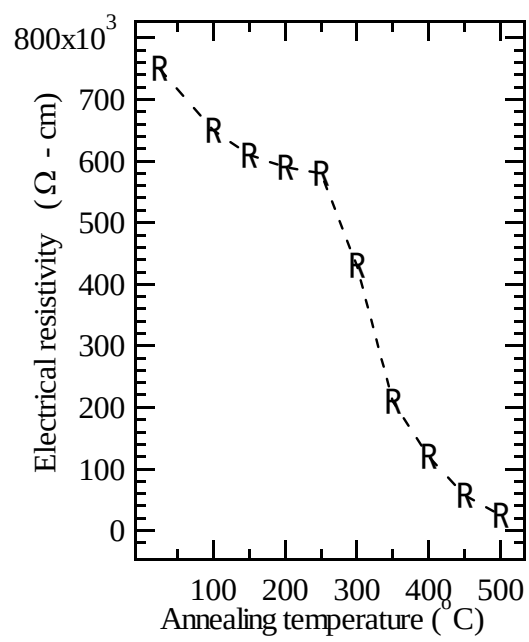

Figure 2: The variation of electrical resistivity of as-grown (25 ^{o}C) a-C:N film, and a-C:N films anneal-treated at various temperatures. (Substrate: Quartz).

Cermet Ceramic Coating on Diamond Dresser for In-Situ Dressing of Chemical Mechanical Planarization

James C. Sung[*,1,2,3], Kevin Kan[1]

Address: KINIK Company, 64, Chung-San Rd., Ying-Kuo, Taipei Hsien 239, Taiwan, R.O.C.

Tel: 886-2-2677-5490 ext.1150

Fax: 886-2-8677-2171

e-mail: sung@kinik.com.tw

[1] KINIK Company, 64, Chung-San Rd., Ying-Kuo, Taipei Hsien 239, Taiwan, R.O.C.

[2] National Taiwan University, Taipei 106, Taiwan, R.O.C.

[3] National Taipei University of Technology, Taipei 106, Taiwan, R.O.C.

Key Words: DLC, Cermet, CMP, Coating

Abstract

In recent years, copper circuitry has been replacing aluminum wires and tungsten via as the dominant interconnections. The polishing of copper circuitry requires using highly acidic solution (e.g. pH = 4) and with strong oxidizing agent (e.g. hydrogen peroxide). In order to withstand the corrosive reactions, the bonding metal of the CMP pad conditioners must be corrosion resistant. Otherwise, it will be dissolved in the acidic slurry that may contaminate the delicate circuitry. Ideally, the diamond pad conditioner is best shielded from contacting with the acidic slurry. The chemical shield must be made of a hard substance so it can withstand the polishing action of the slurry. In addition, this hard substance ought to be highly inert so it will not react with the chemicals in the slurry.

The best chemical shield is diamond-like carbon (DLC) and the second best is ceramic coating. Kinik Company pioneered diamond pad conditioners protected by DLC barrier (DiaShield® Coating) back in 1999 (Sung & Lin, US Patent 6,368,198)[1] and there has been no follower since then. Kinik's offered two varieties of DiaShield® Coatings: ultrahard amorphous diamond and superhard hydrogenated DLC. Recently, Kink also evaluated Cermet Composite Coating (CCC or C^3, patent pending). C^3 is unique that the coating composition grades from a metallic (e.g. stainless steel) under layer to a ceramic (e.g. Al_2O_3 or SiC) exterior. The metallic under layer can form metallurgical bond with metallic matrix on the diamond pad conditioner. The ceramic exterior is both wear and corrosion resistant. The gradational design of C^3 coating will assure its strong adherence to the substrate because there is no weak boundary between coating and substrate.

By dipping diamond pad conditioners of various designs in acidic solution (e.g. copper cleaning solution) for extended period of time (e.g. 50 hours) the chemical inertness of various matrix materials are determined with the decreasing ranking as: hydrogenated DLC > C^3 coating > amorphous diamond > sintered nichrome > brazed alloy > electroplated nickel.

POSTER SESSION 2

ELECTROCHEMISTRY

EFFECTS OF GRAIN SIZE REDUCTION ON THE ELECTROANALYTICAL PERFORMANCE OF CONDUCTIVE DIAMOND ELECTRODE DEPOSITED IN CH_4/H_2 GAS MIXTURE

K. L. Soh, W. P. Kang, J. L. Davidson, Y. M. Wong, B. K. Choi
Department of Electrical and Computer Engineering, Vanderbilt University, Nashville, TN 37235, USA.

D. E. Cliffel
Department of Chemistry, Vanderbilt University, Nashville, TN 37235, USA.

Keywords: Conductive diamond electrode, electroanalytical performance, nanocrystalline diamond, grain boundary, ferrocyanide.

Abstract

Diamond is one of the most recent carbon allotropes to find utility in electrochemical analysis. Boron-doped polycrystalline diamond planar electrodes synthesized by chemical vapor deposition (CVD) methods exhibit many properties of an excellent electrode such as low non-Faradaic current over a wide working potential window, quasireversible to reversible kinetics and large signal-to-background ratio for several redox system without need for surface pretreatment, excellent morphological and structural stability at extreme potentials and current densities, and long-term stability [1]. In addition, its resistance to surface fouling and chemical inertness also make it well suited for application in harsh environments and *in vivo* conditions.

The electrochemical behavior of the diamond electrode is governed by its physicochemical properties, which in turn is largely influenced by the CVD deposition process. Variation of deposition parameters and types of plasma used can be manipulated to affect the morphology of the diamond crystallites and thus cause a modification of the surface chemistry which will determine the course of application. This work reports on the effects of grain size reduction on the electroanalytical performance of conductive diamond electrode deposited in CH_4/H_2 gas mixture. Grain size reduction was achieved by decreasing the CH_4 flow rate while keeping other fabrication parameters constant. The diamond deposition was performed at microwave power 5 kW, temperature 800º C, pressure 120 torr, H_2 flow rate 478 sccm, and varying CH_4 flow rate 15, 10, 5 and 1 sccm. Boron doping was achieved using a p-type gaseous dopant; trimethylboron (TMB) = 20 sccm. Diamond deposition duration was two hours.

Figure 1 (a) shows the SEM micrographs of diamond electrodes deposited using 15, 10, 5 and 1 sccm CH_4. Diamond crystallites transitioned from microcrystalline to nanocrystalline when CH_4 flow rates were decreased. Nanocrystallinity of diamond electrode was achieved at CH_4 = 1 sccm as supported by Raman spectroscopy. Figure 1 (b) shows the Raman spectra of the four diamond electrodes. As CH_4 flow rate was decreased, the diamond peak at 1332 cm^{-1} broadened due to reduction in grain size and increase in defects [2]. The peak intensity at ~1615 cm^{-1} results from graphitic sp^2 bonds at the grain boundary [2]. As microcrystalline diamond (MCD) transitioned into nanocrystalline diamond (NCD), the fraction of grain boundary increased thus causing the ratio of I_{1332}/I_{1615} to fall. At CH_4 = 1 sccm, the diamond peak was less resolved. Additional peaks were also observed and two of importance are the shoulders at ~1160 cm^{-1} and ~1450 cm^{-1} which were characteristic of NCD [3].

Figure 2 (a)(i) shows the cyclic voltammograms for the redox reaction of 1 mM $Fe(CN)_6^{4-}$ in 0.1 M KNO_3 at a scan rate of 10 mV/s for the four electrodes. A plot of oxidation peak current, $i_{p,ox}$ vs. square root of scan rate, $\nu^{1/2}$ is linear (not shown), indicative of linear diffusion-controlled process. Table 1 shows that the diamond electrodes displayed higher resistance (R), lower oxidation peak current ($i_{p,ox}$) and larger peak separation (ΔE_p) for oxidation of ferrocyanide, $Fe(CN)_6^{4-}$ with decreasing grain size. The electroanalytical performance of the diamond electrode for this redox species deteriorated with decreasing grain size. This shows that the properties of NCD electrodes fabricated in this manner does not support redox reaction of ferrocyanide. However, as the NCD electrode has different surface chemistry from that of MCD, it may find utility in sensing other analytes whose electrochemical reaction is usually not favored on MCD. Figure 2 (b) shows the cyclic voltammogram for 1 mM dopamine (DA) in PBS buffer, pH = 7.2 at a scan rate of 100 mV/s using an independent high-quality, hydrogen-terminated MCD electrode. As expected, it's redox reaction at the MCD electrode is very sluggish with ΔE_p = 350 mV while the kinetics of $Fe(CN)_6^{4-}$ at the same electrode was reversible with ΔE_p ~ 60 mV (figure 2 (a)(ii)). Detailed comparison of the electroanalytical performance of the four electrodes for sensing of DA will also be presented.

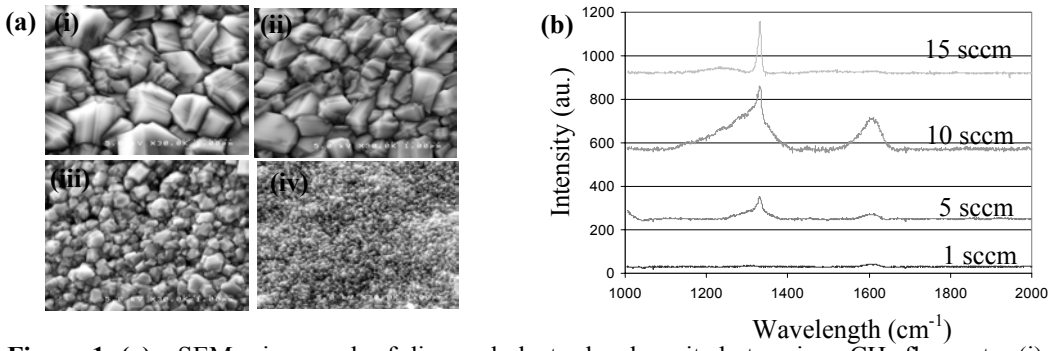

Figure 1. (a): SEM micrograph of diamond electrodes deposited at various CH_4 flow rate: (i) 15 sccm, (ii) 10 sccm, (iii) 5 sccm, and (iv) 1 sccm. TMB = 20 sccm, H_2 = 478 sccm, microwave power = 5 kW, pressure = 120 torr, temperature = 800 °C; **(b)** Raman spectra of diamond electrodes deposited with various CH_4 flow rate.

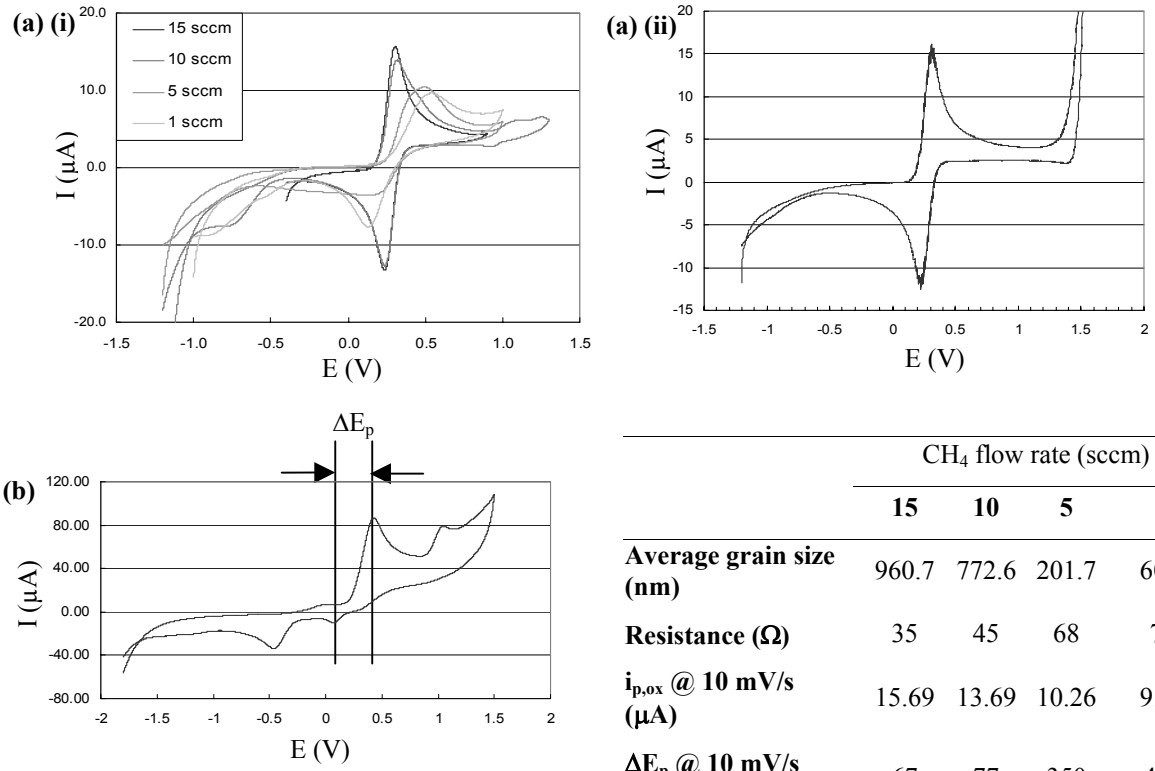

Figure 2. Cyclic voltammogram of **(a):** 1 mM $Fe(CN)_6^{4-}$ in 0.1 M KNO_3 at scan rate = 10 mV/s for **(i):** diamond electrodes with various CH_4 flow rate, and **(ii)**: an independent MCD electrode; **(b):** 1mM DA in PBS, pH = 7.2 at scan rate = 100 mV/s for independent MCD.

	CH_4 flow rate (sccm)			
	15	**10**	**5**	**1**
Average grain size (nm)	960.7	772.6	201.7	60.5
Resistance (Ω)	35	45	68	74
$i_{p,ox}$ @ 10 mV/s (μA)	15.69	13.69	10.26	9.34
ΔE_p @ 10 mV/s (mV)	67	77	350	406

Table 1. Effect of methane flow rate on grain size, film resistance, oxidation peak current, $i_{p,ox}$ and peak separation, ΔE_p.

REFERENCES

1. Granger, M.C., et al., "Standard Electrochemical Behavior of High-Quality, Boron-Doped Polycrystalline Diamond Thin Film Electrode," *Anal. Chem.*, 72, 3793-3804 (2000).
2. Yarbrough, W.A.; and Messier, R., "Current Issues and Problems in the Chemical Vapor Deposition of Diamond," *Science*, Vol. 247, No. 4943, 688-696 (1990).
3. Birrell, J., et al., "Interpretation of the Raman Spectra of Ultrananocrytalline Diamond," *Diam. Relat. Mater.*, 14, 86-92 (2005).

Electrochemical Detection of Nitroaromatics using the Boron-Doped Diamond Electrode

Jesse C. Seegmiller, Veronika Quaiserova-Mocko, Jason M. Stotter and Greg M. Swain

Department of Chemistry
Michigan State University
320 Chemistry Building
East Lansing, MI 48824

Keywords: microcrystalline diamond, nitroaromatic reduction

Due to growing environmental concerns, nitroaromatic compounds have been targeted for monitoring because of their inherent biological toxicity. There is significant motivation for the development of rapid, stable, inexpensive and robust sample analysis protocols for this class of analytes in both the military and civilian sectors. The use of capillary electrophoresis (CE) systems coupled with electrochemical detection provides many attractive features toward achieving the above goal. The electrochemical reduction mechanism of the nitro group on these compounds has been described by Rubinstein.[1] Boron-doped diamond electrodes have been shown to offer robust electrochemical properties with respect to the fouling associated with electrochemical organic reactions[2,3] and provide an obvious choice for the present task at hand. Our long-term goal is to develop a microchip separation method for these contaminants that uses diamond electrodes and amperometric detection.

One complication for the analysis of nitroaromatics, such as nitrotoluenes, is the absence of a formal net charge. Therefore, separation of nitrotoluenes cannot be achieved through capillary zone electrophoresis (CZE) and requires the use of micellar electrokinetic capillary chromatography (MEKC). It has been shown that micelles can have a profound influence the reduction mechanism, specifically for the hanging mercury drop electrode.[4] Thus, a study of the electrode response for nitrotoluene in the presence of micelles is of great importance in order to achieve optimum signal-to-noise for such systems.

In this contribution, the electrochemical reduction of 2,4-dinitrotoluene (DNT) at microcrystalline boron-doped diamond will be reported on. The electrode response was evaluated in the presence and absence of micelles. It was found that the micelles had a significant influence on the oxygen reduction reaction at the boron-doped diamond electrode. Oxygen reduction is problematic in microchip separations as it leads to large background currents at the detection electrode. Figure 1 is 10 consecutive cyclic voltammetric scans in 25 ppm DNT in 15mM borate buffer and 15mM sodium dodecyl sulfate (SDS) at pH of 9.2. Current attenuation is observed with the increasing scan number. The sites labeled 1, 2 and 3 refer to the 2e- reduction of the nitroso to the hydroxylamine, the 4e- reduction of the nitro to the hydroxylamine and the 2e- oxidation of the hydroxylamine to the nitroso analogs respectively.

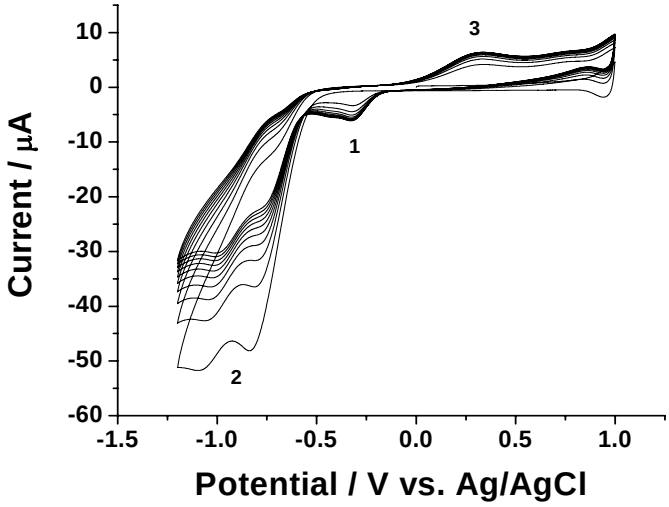

Figure 1.

References

1. Rubinstein, I., "Voltammetric Study of Nitrobenzene and Related Compounds on Solid Electrodes in Aqueous Solution"*J. Electroanal. Chem.* **183,** 379-386, (1985).

2. Pedrosa, V.A., et al., "Is the boron-doped diamond electrode a suitable substitute for mercury in pesticide analyses? A comparative study of 4-nitrophenol quantification in pure and natural waters", *J. Electroanal. Chem.* **573,** 11-18, (2004).

3. Muna, G.W., Tasheva, N., and Swain, G.M., "Electro-oxidation and Amperometric Detection of Chlorinated Phenols at Boron-Doped Diamond Electrodes: A Comparison of Microcrystalline and Nanocrystalline Thin Films", *Environ. Sci. Technol.* **38,** 3674-3682, (2004).

4. McIntire, G.L., et al., "Electrochemistry in Ordered Systems. 2. Electrochemical and Spectroscopic Examination of the Interactions between Nitrobenzene and Anionic, Cationic and Nonionic Micelles", *J. Phys. Chem.* **86,** 2632-2640, (1982).

WATER QUALITY MONITORING ON BORON-DOPED DIAMOND ELECTRODES

Elizabeth A. McGaw, Prerna Sonthalia, and Greg M. Swain

Department of Chemistry, Michigan State University, East Lansing, MI 48824-1322

Keywords: Electroanalysis, Boron-Doped Diamond, Stripping Voltammetry, Metal

Abstract

On-board the International Space Station (ISS), potable water is used for drinking, food preparation, and hygiene. There are several potential sources of contamination, both organic as well as inorganic, that are potentially toxic to the crew. Several heavy metal ion contaminants have been recently detected in the ISS water (e.g. Ag(I), Pb(II), and Cd(II))[1]. The latter two were found at concentrations much higher than the EPA action levels. On-board monitoring of these contaminants is essential for crew health and safety. However, there is currently no system used for on-board water quality monitoring (organic and/or inorganic contaminants).

Electrochemical methods are attractive for use in environmental monitoring in space as they are versatile, energy efficient, easy to be automated, environmentally compatible, and cost effective. Traditionally, anodic stripping voltammetry (ASV) with a Hg electrode has been employed for trace metal ion analysis. Alternate electrodes, however, are being investigated because of the stability, toxicity, and volatility of Hg. Boron-doped diamond electrode has many advantageous properties, such as a wide working potential window, a low background current, and a reusable surface, that make it well suited as an alternative to Hg. Our group has shown that boron-doped diamond is a viable alternate electrode and can be used successfully for terrestrial ASV analysis of heavy metals found in water, sludge, and soil samples.[2]

Specifications for water quality monitoring on-board ISS will require additional modifications and optimization to the current assay. In this presentation, the effect of solution pH, dissolved oxygen, and salt content on the diamond electrode response (e.g., Ag(I), Cu(II), Pb(II), Cd(II) and Zn(II))will be presented. The results for diamond will be compared with the results for the state-of-the-art electrode, Hg.

References

1. Plumlee, D., Mudget, P.D., Schultz, J.R., "Chemical Sampling and Analysis of ISS Potable Water: Expeditions 1-3", *32nd International Conference on Environmental Systems*, San Antonio, TX, SAE Technical Paper, #2002-01-2537 (2002)
2. Sonthalia, P., McGaw, E., Swain, G.M., "Metal Ion Analysis in Contaminated Water Samples Using Anodic Stripping Voltammetry and a Nanocrystalline Diamond Thin-film Electrode", *Anal. Chim. Acta*, 522, 35 – 44 (2004)

DIAMOND NANOPARTICLES AS A SUPPORT MATERIAL FOR FUEL CELL ELECTROCATALYSTS

Donald A. Tryk, Lyda La Torre, Ileana González González, Carlos R. Cabrera

Department of Chemistry, University of Puerto Rico, Río Piedras Campus, San Juan, PR 00931-3346

Keywords: nanodiamond, electrocatalyst support

Abstract

The conventional support material for fuel cell electrocatalysts is high area carbon black. This material can undergo slow oxidation at the potentials existing at a fuel cell oxygen cathode [0.7–0.9 V vs. reversible hydrogen electrode (RHE)]. Conductive diamond in a high area form might be an attractive substitute for carbon black. Preliminary characterization and electrochemical results will be presented.

INTRODUCTION

As fuel cell technology matures and approaches the point at which it will see widespread implementation, there is a continuing need to to make improvements in the characteristics of the electrodes, particularly, the electrocatalytic activity and lifetime. One of the major problems with the fuel cell oxygen cathode is that the conventional electrocatalyst support material is carbon black, which can undergo slow oxidation at the potentials that typically exist at this electrode (0.7–0.9 V vs. RHE). At the fuel cell anode, whether hydrogen or methanol, the potentials are much lower, and there is significantly less oxidation of the support, but even in this case, the potential under heavy load or short circuit conditions could accelerate the oxidation process. In addition, there is the possibility that the catalyst nanoparticles could have mobility on the carbon surface and slowly agglomerate, particularly at elevated temperatures.

Conductive diamond, typically boron-doped, has been used recently extensively for electrochemical measurements due to its wide potential operating range. It is intriguing to consider diamond as a replacement for carbon black in the fuel cell. Diamond is usually considered to be prohibitively expensive, but detonation diamond nanoparticles are relatively low in cost. These nanoparticles have been shown theoretically to have a preferred size range of 2-5 nm due to the special stability of the bare (non-hydrogenated) surface in this size range (1).

We are in the process of characterizing a series of diamond powders, including several detonation samples, from various sources. The techniques being used include x-ray diffraction, x-ray photoelectron spectroscopy, Raman, Fourier transform infrared spectroscopy, transmission electron microscopy and electron energy loss spectroscopy. We are also studying methods for introducing dopants into these particles, as well as methods for modifying their surface chemistry as a means of attaching metallic nanoparticles more firmly, so that they will not tend to agglomerate. The diamond surface, particularly for the nanodiamond particles, is eminently suited for surface modification, because the surfaces appear to be extremely well-defined.

RESULTS AND DISCUSSION

We have examined thus far a total of four diamond powders, two of which are detonation samples, one from Russia and the other from the Ukraine (Alit). The others, from Alfa-Aesar and from China, consist of larger particles, on the order of hundreds of nanometers and micrometers, respectively. The problems we are addressing include how to purify the nanodiamonds and how to prevent their agglomeration. The purified sample received from Alit is relatively pure, according to the measurements we have carried out, including TEM (Fig. 1). This shows that the particles have predominantly the shape predicted theoretically, i.e., a truncated triangular (nearly hexagonal) shape in a two-dimensional projection, which would be expected if the view were from a vector perpendicular to the (111) plane. There are also some cubic particles, which would be expected if (100) planes were exposed only. Now that we are confident that the nanoparticles appear to be rather perfect single crystals, we can proceed to employ the techniques that have been developed in previous work at the University of Tokyo (2), as well as techniques that have been developed by a number of other groups to functionalize diamond surfaces.

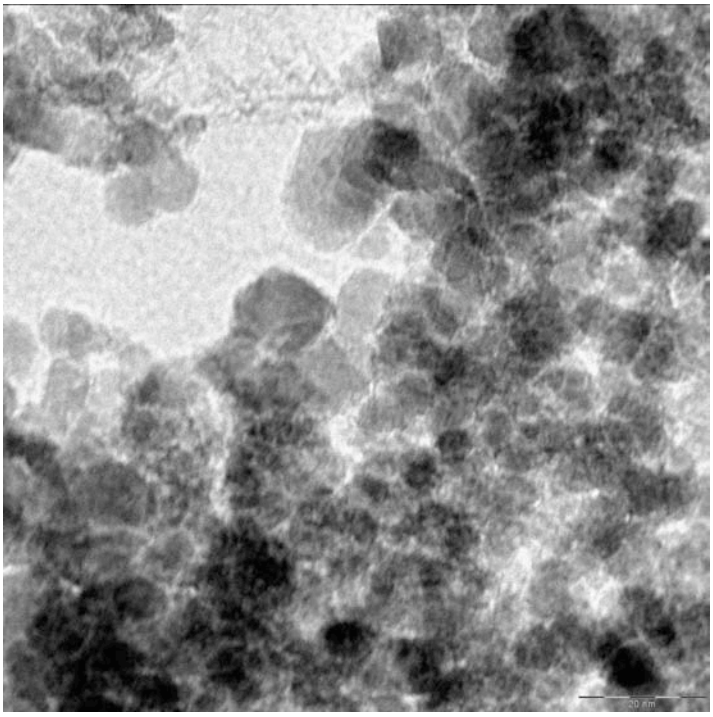

Figure 1. TEM image of the detonation nanodiamond sample from Alit (as-received, high purity), taken on a Zeiss 200 kV microscope. The scale bar is 20 nm.

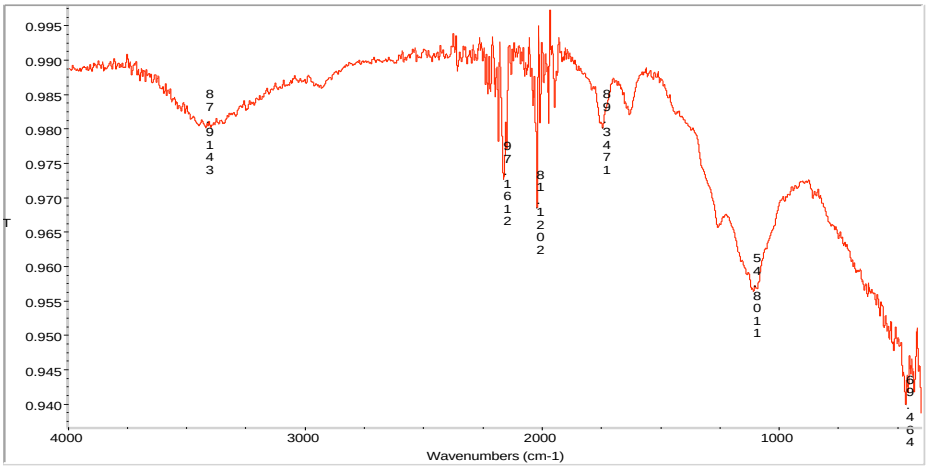

Figure 2. FTIR spectrum for the Alit nanodiamond sample, showing the presence of carbonyl groups (ca. 1700 cm^{-1}), which are expected for the oxidized (100) surface.

REFERENCES

1. Raty, J.-Y. and Galli, G., "Ultradispersity of diamond at the nanoscale," *Nature Mater.*, 3, 792-794 (2003).
2. Kondo, T., Honda, K., Tryk, D. A., and Fujishima, A., "Covalent modification of single crystal diamond electrode surfaces, *J. Electrochem. Soc.*, 152, E18-E23 (2005).

BENTONITE CARBON COMPOSITE POLYVINYL-COATED WIRE ELECTRODE FOR LEAD DETECTION AS AN ENVIRONMENTAL SENSOR

Anahita Izadyar

Chemistry Department, Shiraz University, Faculty of Science ,Hafezieh Shiraz. 71454,Iran

Keywords:C-PVC,CWE,bentonite lead ,wastewater

Abstract

The composite carbon –polyvinyl chloride (C-PVC) with bentonite (natural zeolite) as an ionophore in a selective and sensitive coated wire electrode (CWE) for lead determination by potentiometric method is demonstrated. The sensor shows a good Nernstian slope of 29.42 ± 0.5 mV per decade in wide linear range concentration from 1.0×10^{-7} to 1.0×10^{-3} M for $Pb(NO_3)_2$.The detection limit of this electrode 5.0×10^{-8} M of $Pb(NO_3)_2$, and was found to be very selective, and usable in pH range of 3.0 – 6.7.Selectivity was obtained over 19 various metal ions. The electrode is reproducible and stable for a period of three months. The proposed electrode has been used as an indicator electrode in potentiometric titration with EDTA .This kind of CWE was successfully applied in determination of lead in industrial wastewater and river's water as real sample.

REFERENCES

1. A. Abbaspour, A. Izadyar,et al ,"Carbon composition PVC based membrane in highly selective and sensitive coated wire electrode for silver ion"525,91-96(2004)
2. A.J.King ,G.C. Lillie, et al, Analyst, 129,157-160(2004)

POSTER SESSION 2

THEORY

DIAMOND NANOWIRES GROWN INSIDE CARBON NANOTUBES UPON CHEMICAL VAPOR DEPOSITION: THERMODYNAMIC AND KINETIC APPROACH

C. X. Wang, P. Liu, H. Cui, G. W. Yang

State key laboratory of optoelectronic materials and technologies, School of Physics Science & Engineering, Zhongshan University, Guangzhou 510275, P. R. China

Keywords: diamond nanowire, thermodynamics, kinetics, nucleation, growth

Abstract

One-dimensional nanostructures such as wires, rods, belts, and tubes have become the focus of intensive research owing to their unique applications in mesoscopis physics and fabrication of nanoscale devices. Due to several unique properties including extreme high hardness, very high thermal conductivity, large band gap, and chemical inertness, etc., diamonds are expected to be an important semiconductor material for high-temperature and high-power microelectronics device, and UV-light emitting optoelectronics. Very recently, one-dimensional nanostructures of diamond have received increasing interesting in theoretical. For example, due to stronger than fullerene nanotubes, diamond nanorods are expected to be an important and viable target structure for synthesis. Barnar's studies indicate that the energy band gap of diamond nanowires (DNWs) is significantly reduced, due to the contributions from occupied and unoccupied surface states. However, up to date, any successful syntheses of diamond nanowires have not been found in the literature yet, to our best knowledge. On the other hand, carbon nanotubes (CNTs) have many potential applications as molecular sieves, membranes, and "nanopipes" for precise delivery of gases or liquid. Furthermore, some studies focused their attentions on transport, adsorbed, and condensed phases of gases inside CNTs. Especially, the transport rates of CH_4 and H_2 gases in CNTs were suggested to be exceptionally high. Interestingly, CH_4 and H_2 gases are just two typical reactive gases that are employed to deposit diamond films upon chemical vapor deposition (CVD). These studies mentioned above naturally imply that CNTs could be expected to be a possible path to fabricate DNWs by CVD. In this study, we propose a nano-scaled thermodynamic nucleation and growth kinetic approach in theoretical, with respect to the effect of nanosize-induced surface tension, for the formation of DNWs inside CNTs upon CVD. Thermodynamic analyses show that the diamond nucleation inside a CNT would be preferable to that on the flat surface of silicon substrate due to the effect of surface tension induced by the nanosize curvature of CNTs. Meanwhile, the capillary effect of the nanosize curvature of diamond nuclei could drive the metastable phase region of diamond nucleation into a new stable phase region in the carbon thermodynamic equilibrium phase diagram. Kinetic analyses indicate that the growing rate of DNWs would go to much high once nuclei formed inside CNTs, due to the same nanosize-induced effect. Eventually, we predict that CNTs could be an effective route to grow DNWs by CVD.

THERMODYNAMICAL PREDICTIONS OF NANODIAMONDS SYNTHESIZED BY PULSED LASER ABLATION IN LIQUID

P. Liu, C. X. Wang, H. Cui, G. W. Yang

State key laboratory of optoelectronic materials and technologies, School of Physics Science & Engineering, Zhongshan University, Guangzhou 510275, P. R. China

Keywords: nanodiamond, thermodynamics, nucleation, Gibbs free energy, stability

Abstract

3-5 nm ultrananocrystalline diamonds have emerged as potentially revolution materials for various applications. As with all nanomaterials, the nanodiamond synthesis has a large impact on the usefulness of these materials. For instance, control of the size of nanodiamonds and a high transition probability from graphite to diamond has been pursued in nanodiamonds syntheses both theoretically and experimentally in recent years. Recently, a novel method of pulsed- laser ablation in liquid, so-called pulsed-laser induced liquid-solid interfacial reaction (PLIIR), has been intensively studied aimed at the synthesis of the metastable nanocrystals. By using PLIIR, a series of nanocrystals including diamond with cubic and hexagonal structure, cubic C_3N_4, and boron nitride with cubic and other metastable structures were prepared. More recently, PLIIR was extended to synthesize metastable one-dimensional nanostructures and ultrananocrystals. Accordingly, PLIIR is expected to be advantageous in the preparation of metastable nanocrystals that prefer a state of high pressure and high temperature. More importantly, PLIIR is a relatively new laser-based material processing method, and the mechanisms involved in the nucleation and phase transition of nanocrystals upon PLIIR are not well understood. It is therefore important to provide theoretical tools to investigate the physical and chemical phenomena involved in this processing method. Based on the nanothermodynamical approach, we performed the thermodynamical predictions of nanodiamonds synthesized by pulsed laser ablation in liquid. The nanothermodynamical analyses showed that the formation of nanodiamonds with sizes of 3-5 nm would be preferable to that of large nanodiamonds in the pressure-temperature region of 10-15 GPa and 4000-5000 K created by pulsed laser ablation of a graphite target in water in the carbon phase diagram. Meanwhile, the probabilities of the phase transition from graphite to diamond are calculated to be rather high, up to 10^{-3}-10^{-2} in the same pressure-temperature region. These theoretical results indicated that pulsed laser ablation in liquid is expected to be an effective industrial route to synthesize ultrananocrystalline diamonds.

ATTENDEE LIST

Ibrahim Abdel-Motaleb
Dept of Electrical Engineering
Northern Illinois University
Engineering College
Engineering Building
DeKalb, IL 60115 USA
Phone: 815.753.8570
Fax: 815.753.1289
E-mail: ibrahim@ceet.niu.edu

Roberto I. Acosta
Dept of Physics
University of Puerto Rico-Rio Piedras
P.O. Box 23343
San Juan, PR 00931
Phone: 787.645.0685
Fax: 787.756.7717
E-mail: physicupr@yahoo.com

Sudip Adhikari
Dept of Electrical & Electronic Engineering
Chubu University
1200 Matsumoto-cho
Kasugai, Aichi 487-8501 JAPAN
Phone: 81.568.51.9244
Fax: 81.568.51.1478
E-mail: sudipchubu@yahoo.com

Aleksandar Aleksov
Dept of Material Science & Engineering
North Carolina State University
1001 Capability Drive, RB1, Rm. #240
Raleigh, NC 27695-7919 USA
Phone: 919.515.7083
Fax: 919.515.3419
E-mail: aaleksov@ncsu.edu

Joakim Andersson
Dept of Physics II
Uppsala University
The Angstrom Laboratory
Box 503
SE-751 21 Uppsala SWEDEN
Phone: 46.18.471.35.33
Fax: 46.18.471.35.24
E-mail: joakim.andersson@angstrom.uu.se

Maki A. Angadi
Materials Science Division
Argonne National Laboratory
Building 200
9700 South Cass Avenue
Argonne, IL 60439 USA
Phone: 630.252.8922
Fax: 630.252.9555
E-mail: angadi@anl.gov

John C. Angus
Dept of Chemical Engineering
Case Western Reserve University
10900 Euclid Avenue
Cleveland, OH 44106-7217 USA
Phone: 216.368.4133
Fax: 216.368.3016
E-mail: john.angus@case.edu

Dean M. Aslam
Dept of Electrical & Computer Engineering
Michigan State University
3211 Engineering Building
East Lansing, MI 48824 USA
Phone: 517.353.6329
E-mail: aslam@egr.msu.edu

Orlando Auciello
Materials Science Division
Argonne National Laboratory
Building 212
9700 South Cass Avenue
Argonne, IL 60439 USA
Phone: 630.252.1685
Fax: 630.252.4289
E-mail: auciello@anl.gov

Sarah E. Baker
Dept of Chemistry
University of Wisconsin-Madison
1101 University Avenue
Madison, WI 53706 USA
Phone: 608.262.9081
Fax: 608.262.0453
E-mail: baker@chem.wisc.edu

Amanda S. Barnard
Center for Nanoscale Materials
Argonne National Laboratory
Building 200
9700 South Cass Avenue
Argonne, IL 60439 USA
Phone: 630.252.8377
Fax: 630.252.9555
E-mail: amanda.barnard@anl.gov

Shubham Basu
Dept of Materials Science
Vanderbilt University
5622 SRC
Nashville, TN 37232 USA
Phone: 615.343.6712
E-mail: shubham.basu@vanderbilt.edu

Fabien Bénédic
LIMHP
CNRS
Université Paris 13
99 avenue J. B. Clément
93430 Villetaneuse FRANCE
Phone: 1.49.40.34.39
Fax: 1.49.40.34.14
E-mail: benedic@limhp.univ-paris13.fr

Patricia Bianconi
Dept of Chemistry
University of Massachusetts
701 Lederle Tower Ave.
710 North Pleasant Street
Amherst, MA 01003 USA
Phone: 413.545.3119
Fax: 413.545.4490
E-mail: bianconi@chem.umass.edu

Branislav Brajuskovic
Advanced Photon Source/XFD
Argonne National Laboratory
Building 401
9700 South Cass Avenue
Argonne, IL 60439 USA
Phone: 630.252.5039
Fax: 630.252.9350
E-mail: bran@aps.anl.gov

Paola Bruno
Science Division
Argonne National Laboratory
Building 200
9700 South Cass Avenue
Argonne, IL 60439 USA
Phone: 630.252.8471
Fax: 630.252.9555
E-mail: bruno@anl.gov

Jeannette M. Bursee
Dept of Chemical Engineering
Case Western Reserve University
1615 Ridgefield Road
Cleveland Heights, OH 44118 USA
Phone: 216.288.4501
E-mail: jeannette.bursee@gmail.com

James E. Butler
Gas/Surface Dynamics Section
Naval Research Laboratory
Code 6174
Washington, DC 20375 USA
Phone: 202.767.1115
Fax : 202.767.3321
E-mail: butler@ccf.nrl.navy.mil

Madalina D. Buzaianu
Dept of Physics
University of Puerto Rico-Rio Piedras
Ave. de Diego #368
P.O. Box 23343
San Juan, PR 00923
Phone: 787.349.7636
Fax: 787.756.7717
E-mail: bmdora@hotmail.com

Carlos T. Cabrera
Dept of Chemistry
University of Puerto Rico-Rio Piedras
P.O. Box 23346
San Juan, PR 00931-3346
Phone: 787.764.0000 ext. 4807
Phone: 787.756.8242
E-mail: ccabrera@cnnet.clu.edu

Emilia Cappelli
Dept of Materials & Devices
CNR-Institute of Complex Systems
via Salaria Km. 29.3
00016 Monterotondo, Rome ITALY
Phone: 39.069.067.2230
Fax: 39.069.067.2238
E-mail: emilia.cappelli@isc.cnr.it

John A. Carlisle
Materials Science Division/CNM
Argonne National Laboratory
Building 200
9700 South Cass Avenue
Argonne, IL 60439 USA
Phone: 630.252.3431
Fax: 630.252.9555
E-mail: carlisle@anl.gov

Robert W. Carpick
Dept of Engineering Physics
University of Wisconsin-Madison
1500 Engineering Drive
Madison, WI 53706 USA
Phone: 608.263.4891
Fax: 608.263.7451
E-mail: carpick@engr.wisc.edu

Vidhya Chakrapani
Dept of Chemical Engineering
Case Western Reserve University
A. W. Smith Building, Rm. 223
Cleveland, OH 44106 USA
Phone: 216.368.2648
Fax: 216.368.3016
E-mail: vxc19@case.edu

Vladimir I. Chegel
Dept of Functional Optoelectronic
Institute of Semiconductor Physic NAS Ukraine
43, pr. Nauki
03028 Kiev UKRAINE
Phone: 380.44.525.56.36
Fax: 380.44.265.18.27
E-mail: vche111@yahoo.com

Kuei-Hsien Chen
Institute of Atomic & Molecular Sciences
Academia Sinica
P.O. Box 23-166
Taipei 106 Taiwan, ROC
Phone: 886.2.2366.8232
Fax: 886.2.2362.0200
E-mail: chenkh@po.iams.sinica.edu.tw

Xinqi Chen
Dept of Mechanical Engineering
Northwestern University
2145 Sheridan Road
Evanston, IL 60208 USA
Phone: 847.467.5298
Fax: 847.491.3915
E-mail: xchen@northwestern.edu

Ying-Chieh Chen
Dept of Material Science & Eng
National Tsing Hua University
101, Section 2 Kuang Fu Road
Hsinchu 30013 Taiwan, ROC
Phone: 886.3.5715131
E-mail: d923549@oz.nthu.edu.tw

Yu-Chun Chen
Dept of Electrical & Computer Eng
Auburn University
200 Broun Hall
Auburn, AL 36849 USA
Phone: 334.524.7770
Fax: 334.844.1809
E-mail: chenyuc@auburn.edu

An Jen Cheng
Dept of Electrical & Computer Eng
Auburn University
200 Broun Hall
Auburn, AL 36849 USA
Phone: 334.524.8073
E-mail: chenga1@auburn.edu

Hsiu-Fung Cheng
Physics Dept
National Taiwan Normal University
88, Section 4 Ting-Chou Road
Taipei 116 Taiwan, ROC
Phone: 886.2.2933.1075
Fax: 886.2.2932.6408
E-mail: hfcheng@phy03.phy.ntnu.edu.tw

Jaewu Choi
Dept of Electrical & Computer Engineering
Wayne State University
5050 Anthony Wayne Drive, #3100
Detroit, MI 48202 USA
Phone: 313.577.3990
Fax: 313.577.1101
E-mail: jchoi@ece.eng.wayne.edu

Cheng-Hsien Chou
Dept of Materials Science & Engineering
National Tsing Hua University-Taiwan
101, Section 2 Kuang Fu Road
Hsinchu 300 Taiwan, ROC
Phone: 886.3.5742575
Fax: 886.3.5716977
E-mail: d907515@oz.nthu.edu.tw

Shih-Feng Chou
Dept. of Mechanical Eng & Energy Processes
Southern Illinois University
1630 Logan Drive, Apt. 6
Carbondale, IL 62901 USA
Phone: 618.201.0600
E-mail: chou@siu.edu

Brian L. Cline
Cline Innovations, LLC
23 Boutelle Road
Sterling, MA 01564 USA
Phone: 978.422.2901
Fax: 978.422.2907
E-mail: brian@clineinnovations.com

Heather S. Cline
Cline Innovations, LLC
23 Boutelle Road
Sterling, MA 01564 USA
Phone: 978.422.2901
Fax: 978.422.2907
E-mail: heather@clineinnovations.com

Simon H. Connell
Dept of Physics
University of Witwatersrand
Jan Smuts Avenue
Braamfontein, Johannesburg,
Gauteng 2050 SOUTH AFRICA
Phone: 27.11.717.6928
Fax: 27.11.717.6932
E-mail: connell@src.wits.ac.za

Larry A. Curtiss
Materials Science Division
Argonne National Laboratory
Building 200
9700 South Cass Avenue
Argonne, IL 60439 USA
Phone: 630.252.7380
Fax: 630.252.9555
E-mail: curtiss@anl.gov

David A. Czaplewski
Dept of Nanostructure & Semiconductor Physics
Sandia National Laboratories
M/S: 1415 Dept 01112
Albuquerque, NM 87185 USA
Phone: 505.844.2338
Fax: 505.844.1197
E-mail: daczapl@sandia.gov

Jim L. Davidson
Dept of Electrical Engineering
Vanderbilt University
VU Station B-350099
Nashville, TN 37235-0099 USA
Phone: 615.343.7886
Fax: 615.343.6614
E-mail: jim.davidson@vanderbilt.edu

Filip De Weerdt
HRD Research
Hoveniersstraat 22
2018 Antwerp BELGIUM
Phone: 32.322.20511
Fax: 32.322.20605
E-mail: fdw@hrd.be

Dmitriy A. Dikin
Dept of Mechanical Engineering
Northwestern University
2145 Sheridan Road
Evanston, IL 60208 USA
Phone: 847.467.2024
Fax: 847.491.3915
E-mail: d-dikin@northwestern.edu

Weiqiang Ding
Dept of Mechanical Engineerimg
Northwestern University
2145 Sheridan Road
Evanston, IL 60208 USA
Phone: 847.491.4231
Fax: 847.467.5298
E-mail: w-ding@northwestern.edu

Morinobu Endo
Dept of Electrical & Electronic Engineering
Shinshu University
4-17-1 Wakasato
Nagano 380-8553 JAPAN
Phone: 81.26.269.5201
Fax: 81.26.269.5208
E-mail: endo@endomoribu.shinshu-u.ac.jp

Charlee Fansler
Dept of Electrical Engineering
Michigan State University
B100 Research Complex - Engineering
East Lansing, MI 48824 USA
E-mail: fanslerc@egr.msu.edu

Susan A. Farhat
Dept of Chemical Engineering
Michigan State University
2527 Engineering Building
East Lansing, MI 48824 USA
Phone: 517.353.9946
E-mail: farhats1@egr.msu.edu

Naoji Fujimori
Diamond Research Center
NAIST
Central 2
1-1-1 Umezono Tsukuba,
Ibaraki 305-8568 JAPAN
Phone: 81.29.861.5417
Fax: 81.29.861.2771
E-mail: fujimori-naoji@aist.go.jp

Jacob M. Garguilo
Dept of Physics
North Carolina State University
Partners III, Rm. 163
851 Main Campus Drive
Raleigh, NC 27695-0001 USA
Phone: 919.515.2474
Fax: 919.513.0670
E-mail: jmgargui@ncsu.edu

Jose A. Garrido
Walter Schottky Institute
Technical University of Munich
Am Coulombwall 3
85748 Garching GERMANY
Phone: 49.89.289.12766
Fax: 49.89.289.12737
E-mail: garrido@wsi.tum.de

J. Murray Gibson
Scientific User Facilities/PA - APS
Argonne National Laboratory
Building 401
9700 South Cass Avenue
Argonne, IL 60439 USA
Phone: 630.252.7990
Fax: 630.252.4599
E-mail: jmgibson@aps.anl.gov

Ileana Gonzalez-Gonzalez
Chemistry Dept
University of Puerto Rico-Rio Piedras
Villa Carolina 192-35 calle 522
Carolina, PR 00985
Phone: 737.604.4800
Fax: 787.756.8242
E-mail: gonzalez.ileana@gmail.com

David S. Grierson
Dept of Engineering Physics
University of Wisconsin-Madison
1500 Engineering Drive
Madison, WI 53706 USA
Phone: 608.263.1622
E-mail: dsgrierson@wisc.edu

Dieter M. Gruen
Materials Science Division
Argonne National Laboratory
Building 200
9700 South Cass Avenue
Argonne, IL 60439 USA
Phone: 630.252.3513
Fax: 630.252.9555
E-mail: dmgruen@anl.gov

Prateek Gupta
Dept of Civil & Material Engineering
University of Illinois
1841 Morgan Circle
Naperville, IL 60565 USA
Phone: 630.355.8823
Fax: 630.355.8823
E-mail: teektok@hotmail.com

Sanju Gupta
Dept of Physics & Materials Science
Southwest Missouri State University
901 South National Avenue
Kemper Hall, PAMS
Springfield, MO 65804 USA
Phone: 417.836.8565
Fax: 417.836.6226
E-mail: sxg535f@smsu.edu

Jeffrey M. Halpern
Dept of Chemical Engineering
Case Western Reserve University
AW Smith #223
10900 Euclid Avenue
Cleveland Heights, OH 44118 USA
Phone: 216.368.2648
E-mail: jmh12@case.edu

Robert J. Hamers
Dept of Chemistry
University of Wisconsin-Madison
1101 University Avenue
Madison, WI 53706 USA
Phone: 608.262.6371
Fax: 608.262.0453
E-mail: rjhamer@wisc.edu

Kadek W. Hemawan
Dept of Electrical & Computer Engineering
Michigan State University
2120 Engineering Building
East Lansing, MI 48824 USA
Phone: 517.355.5066
Fax: 517.353.1980
E-mail: hemawank@egr.msu.edu

Russell J. Hemley
Geophysical Laboratory
Carnegie Institution of Washington
5251 Broad Branch Road, NW
Washington, DC 20015 USA
Phone: 202.478.8951
Fax: 202.478.8464
E-mail: r.hemley@gl.ciw.edu

Philip R. Hemmer
Dept of Electrical Engineering
Texas A&M University
3128 TAMU
College Station, TX 77843 USA
Phone: 979.845.8932
E-mail: prhemmer@ee.tamu.edu

Kazuyuki Hirama
Waseda University of Science & Eng
Kawarada Laboratory
School of Science & Engineering
Building 61-504
3-4-1 Okubo
Shunjiku-ku 169-0072 JAPAN
Phone: 81.3.5286.3391
Fax: 81.3.5286.3391
E-mail: hirama@kaw.comm.waseda.ac.jp

Atsushi Hirata
Dept. of Mechanical Sciences & Engineering
Tokyo Institute of Technology
2-12-1 O-okayama, Meguro-ku
Tokyo 152-8550 JAPAN
Phone: 81.3.5734.2163
Fax: 81.3.5734.2893
E-mail: ahirata@ctrl.titech.ac.jp

Shih-Shian Ho
Geophysical Laboratory
Carnegie Institution of Washington
5251 Broad Branch Road, NW
Washington DC, 20015 USA
Phone: 202.478.8817
Fax: 202.478.8901
E-mail: s.ho@gl.ciw.edu

David S. Hsu
Code 6174 Chemistry
Naval Research Laboratory
Building 207
4555 Overlook Avenue, SW
Washington, DC 20375 USA
Phone: 202.767.2742
Fax: 202.767.3321
E-mail: dhsu@ccs.nrl.navy.mil

Chialing Huang
Dept of Engineering Science
Southern Illinois University-Carbondale
500 North Westridge Drive, Apt. #E1
Carbondale, IL 62901 USA
Phone: 618.713.5532
E-mail: jialing@siu.edu

Eric D. Isaacs
Center for Nanoscale Materials
Argonne National Laboratory
Building 200
9700 S. Cass Avenue
Argonne, IL 60439 USA
Phone: 630.252.5749
Fax: 630-252-6866
E-mail: isaacs@anl.gov

Sathyaharish Jeedigunta
Dept of Electrical Engineering
University of South Florida
4202 East Fowler Avenue
Tampa, FL 33620 USA
Phone: 813.396.9351
Fax: 813.974.3610
E-mail: jeedigun@eng.usf.edu

Xiaogang Jian
School of Mechanical Engineering
Tong Ji University
Si Ping Road No. 1239
Shanghai 200092 PRC
Phone: 86.21.65119587
Fax: 86.21.64036018
E-mail: jianxgg@tongji.edu.cn

Ming-Chi Kan
Diamond Technology Center
Kinik Company
No. 64, Chung San Road, Ying-Kuo
Taipei County 239 Taiwan, ROC
Phone: 886.2.2679.1931 ext. 5210
Fax: 886.2.8677.1671
E-mail: mck@kinik.com.tw

Neil D. Kane
Advanced Diamond Technologies, Inc.
60 Hazelwood Drive, Ste. 224
Champaign, IL 61820 USA
Phone: 217.265.9824
Fax: 217.265.9823
E-mail: kane@thindiamond.com

Chan Hyoung Kang
Dept of Advanced Materials Engineering
Korea Polytechnic University
2121 Jungwang-Dong
Shihung City, Kyonggi-Do 429-793 SOUTH KOREA
Phone: 82.31.496.8307
Fax: 82.31.496.8319
E-mail: chkang@kpu.ac.kr

Hiroshi Kawarada
Dept of Electrical Eng & Bioscience
Waseda University
Ohkubo 3-4-1, Shinjuku-ku
Tokyo 169-8555 JAPAN
Phone: 81.3.5286.3391
Fax: 81.3.5286.3391
E-mail: kawarada@waseda.jp

Vijaya K. Kayastha
Dept of Engineering Physics
Michigan Technological University
1812 E Woodmar Drive
Daniell Heights
Houghton, MI 49931 USA
Phone: 906.483.8233
E-mail: vkkayast@mtu.edu

Changhong Ke
Dept of Mechanical Engineering
Northwestern University
2145 Sheridan Road
Evanston, IL 60208 USA
Phone: 847.467.7673
Fax: 847.491.3915
E-mail: c-ke@northwestern.edu

Hyungwook Kim
Dept of Electrical & Computer Engineering
Auburn University
200 Broun Hall
Auburn, AL 36849 USA
Phone: 334.559.9880
E-mail: kimhyun@auburn.edu

Keun-Ho Kim
Dept of Mechanical Engineering
Northwestern University
2145 Sheridan Road
Evanston, IL 60208 USA
Phone: 847.467.7673
Fax: 847.491.3915
E-mail: kkim@northwestern.edu

Franz A. Koeck
Dept of Physics
North Carolina State University
Centennial Campus - Partners III - Rm. 158
851 Main Campus Drive
Raleigh, NC 27695 USA
Phone: 919.515.3417
Fax: 919.513.0670
E-mail: fakoeck@unity.ncsu.edu

Kevin M. Kohlhaas
Dept of Mechanical Engineering
Northwestern University
2145 Sheridan Road
Evanston, IL 60208 USA
Phone: 847.491.4866
E-mail: k-kohlhaas@northwestern.edu

Erhard Kohn
Dept of Electron Devices & Circuits
University of Ulm
Albert-Einstein-Allee 45
89081 Ulm GERMANY
Phone: 49.731.50.26150
Fax: 49.731.50.26155
E-mail: kohn@ebs.e-technik.uni-ulm.de

Xianhua Kong
Dept of Physics
North Carolina State University
Campus Box 7518
851 Main Campus Drive, Partners III
Raleigh, NC 27695 USA
Phone: 919.515.2474
Fax: 919.513.0670
E-mail: xkong@ncsu.edu

Ralph Korenstein
IDS Dept
Raytheon
350 Lowell Street
Andover, MA 01810-4400 USA
Phone: 978.470.9491
Fax: 978.470.9003
E-mail: ralph_korenstein@raytheon.com

Tomasz P. Kowalewski
Dept of Chemistry
Carnegie Mellon University
4400 Fifth Avenue
Pittsburgh, PA 15213 USA
Phone: 412.268.5927
Fax: 412.268.1061
E-mail: tomek@andrew.cmu.edu

Felix Krasnicki
Advanced Photon Source/XFD
Argonne National Laboratory
Building 401
9700 South Cass Avenue
Argonne, IL 60439 USA
Phone: 630.252.9186
Fax: 630.252.9303
E-mail: krasnick@aps.anl.gov

Michal Kruk
Dept of Chemistry
Carnegie Mellon University
4400 Fifth Avenue
Pittsburgh, PA 15213 USA
Phone: 412.268.9175
Fax: 412.268.1061
E-mail: mkruk@andrew.cmu.edu

Ashok Kumar
Dept of Mechanical Engineering
University of South Florida
Nanomaterials Research Center
4202 East Fowler Avenue, ENB 252
Tampa, FL 33647 USA
Phone: 813.974.2395
Fax: 813.974.3610
E-mail: akumar@eng.usf.edu

Aaron G. Kusne
Dept of Electrical & Computer Engineering
Carnegie Mellon University
328 REH
5000 Forbes Avenue
Pittsburgh, PA 15213 USA
Phone: 412.915.1433
E-mail: agiladk@yahoo.com

William C. Lanter
Innovative Scientific Solutions, Inc.
2766 Indian Ripple Road
Dayton, OH 45440 USA
Phone: 937.252.2706 ext. 215
Fax: 937.656.4095
E-mail: william.lanter@wpafb.af.mil

Allen K. Lee
Dept of Civil & Materials Engineering
University of Illinois-Chicago
842 West Taylor Street
Chicago, IL 60607-7021 USA
Phone: 312.413.7588
E-mail: alee17@uic.edu

Yen-Chih Lee
Dept of Material Science & Engineering
National Tsing Hua University
101, Section 2 Kuang Fu Road
Hsinchu 30013 Taiwan, ROC
Phone: 886.3.5742575
Fax: 886.3.5716977
E-mail: d907514@oz.nthu.edu.tw

Leonid C. Lev
MPL Dept
General Motors R&D
MC: 480-106-185
30500 Mound Road, RAB, Rm. 1-169
Warren, MI 48090 USA
Phone: 586.986.7450
Fax: 586.986.8697
E-mail: leo.lev@gm.com

Chao Yang Li
Dept of Electronic & Photonic Systems Engineering
Kochi University of Technology
185 Miyanokuchi, Tosayamada-cho, Kami-gun
Kochi 782-8502 JAPAN
Phone: 81.887.57.2274
Fax: 81.887.57.2005
E-mail: 076025w@gs.kochi-tech.ac.jp

Joseph A. Libera
Energy Systems Division
Argonne National Laboratory
Building 200
9700 South Cass Avenue
Argonne, IL 60439 USA
Phone: 630.252.2852
Fax: 630.252.1342
E-mail: jlibera@anl.gov

Valeri Ligatchev
School of Electrical & Electronic Engineering
Nanyang Technological University
169 Jalan Jurong Kechil #07-03
Singapore 598669 SINGAPORE
Phone: 65.6790.5129
Fax: 65.6793.3318
E-mail: evaleri@ntu.edu.sg

I-Nan Lin
Physics Dept
Tamkang University
151 Ying-Chuan Road, Tamsui
Taiwan 251 Taiwan, ROC
Phone: 886.2.2626.8907
Fax: 886.2.2626.9917
E-mail: inanlin@mail.tku.edu.tw

Yu-Ming Lin
T. J. Watson Research Center
IBM
P.O. Box 218, Rt. 134
Yorktown Heights, NY 10598 USA
Phone: 914.945.1461
E-mail: yming@us.ibm.com

Reginald B. Little
National High Magnetic Field Laboratory
308 Great Lakes Street
Tallahassee, FL 32305 USA
Phone: 850.339.5592
E-mail: redge_little@yahoo.com

Chao Liu
Materials Science Division
Argonne National Laboratory
Building 200
9700 South Cass Avenue
Argonne, IL 60439 USA
Phone: 630.252.7520
Fax: 630.252.9555
E-mail: chaoliu@anl.gov

Jie Liu
Dept of Chemistry
Duke University
Box 90346
Durham, NC 27708 USA
Phone: 919.660.1549
Fax: 919.660.1605
E-mail: j.liu@duke.edu

Yenkang Liu
Dept of Power Mechanical Engineering
National Tsing Hua University
101, Section 2 Kuang Fu Road
Hsinchu 30013 Taiwan, ROC
Phone: 886.968724766
Fax: 334.4448.772
E-mail: d897710@oz.nthu.edu.tw

Yung Y. Liu
Energy Technology Division
Argonne National Laboratory
Building 308
9700 South Cass Avenue
Argonne, IL 60439 USA
Phone: 630.252.5127
Fax: 630.252.3250
E-mail: yyliu@anl.gov

Chun Loong
Intense Pulsed Neutron Source Division
Argonne National Laboratory
Building 360
9700 South Cass Avenue
Argonne, IL 60439 USA
Phone: 630.252.5596
Fax: 630.252.4163
E-mail: ckloong@anl.gov

Shaoning Lu
Dept of Mechanical Engineering
Northwestern University
2145 Sheridan Road
Evanston, IL 60208 USA
Phone: 847.491.4231
Fax: 847.491.3915
E-mail: slu@northwestern.edu

Yang Lu
Dept of Electrical & Computer Engineering
Michigan State University
2120 Engineering Building
East Lansing, MI 48824-1226 USA
Phone: 517.355.5066
Fax: 517.353.1980
E-mail: luyang@msu.edu

Albert T. Macrander
Advanced Photon Source/XFD
Argonne National Laboratory
Building 401
9700 South Cass Avenue
Argonne, IL 60439 USA
Phone: 630.252.5672
Fax: 630.252.9303
E-mail: atm@aps.anl.gov

Audrey N. Martin
Dept of Chemistry
Michigan State University
312 Chemistry Building
East Lansing, MI 48824 USA
Phone: 517.355.9715 ext. 231
Fax: 517.353.1793
E-mail: martin@chemistry.msu.edu

Heidi B. Martin
Dept of Chemical Engineering
Case Western Reserve University
10900 Euclid Avenue
Cleveland, OH 44106-7217 USA
Phone: 216.368.3810
Fax: 216.368.3016
E-mail: hbm@case.edu

Jeffrey H. Matsuura
Alliance Law Group
7700 Leesburg Pike, Ste. 410
Falls Church, VA 22043 USA
Phone: 703.848.8349
E-mail: jmatsuura@alliancelawgroup.com

Jacob K. Matthews
UES, Inc.
5691 Chimney Circle, Apt. 2B
Kettering, OH 45440 USA
Phone: 937.255.4132
Fax: 937.255.3211
E-mail: jacob.matthews@wpafb.af.mil

Paul W. May
School of Chemistry
University of Bristol
Cantock's Close
Bristol BS8 1TS UNITED KINGDOM
Phone: 44.0.117.9389927
Fax: 44.0.117.9251295
E-mail: paul.may@bris.ac.uk

Elizabeth A. McGaw
Dept of Chemistry
Michigan State University
306 Chemistry
East Lansing, MI 48824 USA
Phone: 517.355.9715 ext. 230
E-mail: emcgaw@chemistry.msu.edu

Michael J. McNallan
CME Dept
University of Illinois-Chicago
M/C: 246
842 West Taylor Street
Chicago, IL 60607 USA
Phone: 312.996.2436
Fax: 312.996.2426
E-mail: mcnallan@uic.edu

Areg V. Meliksetyan
Dept of Physics
State Engineering University of Armenia
105 Teryan Street
375009 Yerevan
ARMENIA
Phone: 3741.56.16.48
Fax: 3741.58.12.11
E-mail: vachikm@ysu.am

John W. Mintmire
Dept of Physics
Oklahoma State University
145 Physical Sciences
Stillwater, OK 74078 USA
Phone: 405.744.5663
Fax: 405.744.1769
E-mail: john.mintmire@okstate.edu

Ericka A. Mujica
Dept of Physics
University of Puerto Rico-Rio Piedras
Rio Piedras Campus
P.O. Box 23343
San Juan, PR 00931
Phone: 787.645.0685
Fax: 787.756.7717
E-mail: ea_mujica@yahoo.com

Grace W. Muna
Dept of Chemistry
Michigan State University
Chemistry Building 320
East Lansing, MI 48824 USA
Phone: 517.355.9715 ext. 231
E-mail: mutaagag@msu.edu

Nevin N. Naguib
Materials Science Division
Argonne National Laboratory
Building 200
9700 South Cass Avenue
Argonne, IL 60439 USA
Phone: 630.252.7979
Fax: 630.252.9555
E-mail: nevin.naguib@anl.gov

Christoph E. Nebel
Surface Functionalized Device Team
Diamond Research Center/AIST
Central 2
1-1-1 Umezono
Tsukuba, Ibaraki 305-8568 JAPAN
Phone: 81.29.861.4836
Fax: 81.29.861.2773
E-mail: christoph.nebel@aist.go.jp

Mary L. Nemanich
Editorial Office
Diamond & Related Materials
Cox Hall
Raleigh, NC 27695-8202 USA
Phone: 919.513.4806
Fax: 919.515.7331
E-mail: mary_nemanich@ncsu.edu

Robert J. Nemanich
Dept of Physics
North Carolina State University
Cox Hall
Raleigh, NC 27695-8202 USA
Phone: 919.515.3225
Fax: 919.513.0670
E-mail: robert_nemanich@ncsu.edu

Mark E. Newton
Dept of Physics
University of Warwick
Coventry, Warwickshire CV4 7AL UNITED KINGDOM
Phone: 44.2476.674358
Fax: 44.2476.692016
E-mail: m.e.newton@warwick.ac.uk

Clark T. Nguyen
MTO Dept
DARPA
3701 North Fairfax Drive
Arlington, VA 22203 USA
Phone: 571.218.4586
Fax: 703.696.2206
E-mail: cnguyen@darpa.mil

Beth M. Nichols
Dept of Chemistry
University of Wisconsin-Madison
1101 University Avenue
Madison, WI 53706 USA
Phone: 608.262.9081
E-mail: bmnichols@wisc.edu

Guoqing Ning
Dept of Engineering Physics
University of Wisconsin-Madison
Engineering Research Building, Rm. 202
1500 Engineering Drive
Madison, WI 53706-1687 USA
Phone: 608.263.5444
E-mail: gning@wisc.edu

Thomas Okpalugo
Nanotechnology Research Institute
University of Ulster
Shore Road
Newtownabbey
Belfast, Northern Ireland BT37 0QB UK
Phone: 44.289.036.8997
Fax: 44.289.036.6863
E-mail: thomas@nibec-s1.nibec.ulst.ac.uk

Silvia Orlanducci
Dept of Science & Chemical Technology
University of Tor Vergata of Rome
Via della Ricerca Scientifica
00133 Rome ITALY
Phone: 39.0672594402
Fax: 39.0672594328
E-mail: silvia.orlanducci@uniroma2.it

Zhozef R. Panosyan
Dept of Physics
State Engineering University of Armenia
105 Teryan Street
375009 Yerevan ARMENIA
Phone: 3749.41.27.18
Fax: 3741.58.12.11
E-mail: joseph@seua.am

Pagona Papakonstantinou
Nanotechnology Research Institute
University of Ulster
School of Electrical & Mechanical Engineering
Newtownabbey, N. Ireland BT37 0QB UK
Phone: 44.289.036.8932
E-mail: p.papakonstantinou@ulster.ac.uk

Jinwoo Park
Dept of Chemistry
Michigan State University
312 Chemistry
East Lansing, MI 48824 USA
Phone: 517.355.9715 ext. 231
E-mail: parkjinw@msu.edu

Mitchell D. Parr
Dept of Electrical & Computer Engineering
Michigan State University
551 Cornell Avenue
East Lansing, MI 48823 USA
Phone: 517.410.5043
E-mail: parrmitc@msu.edu

Simon R. Phillpot
Dept of Materials Science & Engineering
University of Florida
162 Rhines Hall
Gainesville, FL 32611 USA
Phone: 352.846.3782
Fax: 352.846.3355
E-mail: sphil@mse.ufl.edu

Fabrice Piazza
Dept of Physics
University of Puerto Rico-Rio Piedras
P.O. Box 23343
San Juan, PR 00931
Phone: 787.764.0000 ext. 2602
Fax: 787.756.7717
E-mail: fabrice@adam.uprr.pr

Vasily I. Polyakov
Dept of Microelectronics
Institute of Radio Engineering & Electronics, RAS
Mohovaya Str. 11
103907 Moscow RUSSIA
Phone: 7.095.3579383
Fax: 7.095.2038414
E-mail: pvi@aha.ru

Jeffrey E. Post
Dept. of Mineral Sciences
Smithsonian Institution
P.O. Box 37012
Washington, DC 20560-7012 USA
Phone: 202.633.1814
Fax: 202.357.2476
E-mail: postj@si.edu

Munish Puri
Dept of Physics
GND University
Near Custom Office
Mission Road
Pathankot, Punjab 91145001 INDIA
Phone: 911.862.225.145
E-mail: munish_puri@hotmail.com

Supil Raina
Dept of Materials Science
Vanderbilt University
511 Chesterfield Avenue, Apt. 7D
Nashville, TN 37212 USA
Phone: 615.343.6712
Fax: 615.343.6614
E-mail: supil.raina@vanderbilt.edu

Jeremy S. Rashid
Engineering Dept
University of Cambridge
Trumpington Street
Cambridge, Cambridgeshire CB21PZ UK
Phone: 44.01223.332766
Fax: 44.01223.332662
E-mail: sjr63@eng.cam.ac.uk

K. V. Ravi
Fab Materials Operation
Intel Corporation
2200 Mission College Boulevard
Santa Clara, CA 95054 USA
Phone: 408.765.5760
Fax: 408.765.4881
E-mail: k.v.ravi@intel.com

Donnie K. Reinhard
Dept of Electrical & Computer Engineering
Michigan State University
2120 Engineering Building
East Lansing, MI 48824 USA
Phone: 517.355.5214
Fax: 517.353.1980
E-mail: reinhard@egr.msu.edu

Robert Rosner
Laboratory Director
Argonne National Laboratory
Building 201
9700 South Cass Avenue
Argonne, IL 60439 USA
Phone: 630.252.2481
Fax: 630.252.7923
E-mail: r-rosner@anl.gov

Rodney S. Ruoff
Dept of Mechanical Engineering
Northwestern University
2145 Sheridan Road
Evanston, IL 60208 USA
Phone: 847.467.6596
Fax: 847.491.3915
E-mail: r-ruoff@northwestern.edu

Philippe Rychen
Management Dept
Adamant Technologies, Inc.
Jaquet-Droz-1
2000 Neuchâtel SWITZERLand
Phone: 41.32.720.55.54
Fax: 41.32.720.57.10
E-mail: philippe.rychen@adamantec.com

Kikuo Sakuma
Dept of Diamond Systems
Seki Technotron Corp.
5-6-30 Kiba, Koto-ku
Tokyo 135-0042 JAPAN
Phone: 81.3.3820.1712
Fax: 81.3.3820.1728
E-mail: ksakuma@stc.sekitech.co.jp

Lothar Schaefer
Dept of Diamond Technology
Fraunhofer IST
Bienroder Weg 54E
38108 Braunschweig GERMANY
Phone: 49.531.2155.520
Fax: 49.531.2155.900
E-mail: schaefer@ist.fraunhofer.de

John B. Schaeffer
Dept of Chemical Engineering
Case Western Reserve University
10900 Euclid Avenue
Cleveland, OH 44106 USA
Phone: 216.368.4237
E-mail: john.schaeffer@case.edu

Thomas Schuelke
Center for Coatings & Laser Applications
Fraunhofer USA
8100 Research Complex Engineering
East Lansing, MI 48824 USA
Phone: 517.432.8173
Fax: 517.432.8168
E-mail: tschuelke@fraunhofer.org

Jesse C. Seegmiller
Dept of Chemistry
Michigan State University
312 Chemistry
East Lansing, MI 48824 USA
Phone: 517.355.9715 ext. 231
Fax: 517.353.1793
E-mail: jseegmil@chemistry.msu.edu

Nikki A. Sgriccia
Dept of Chemical Eng. & Materials
Michigan State University
2527 Engineering Building
East Lansing, MI 48824 USA
Phone: 517.432.5488
E-mail: sgricci1@msu.edu

Andy Hsi-Tien Shen
Gemological Institute of America
5355 Armada Drive
Carlsbad, CA 92008 USA
Phone: 760.603.4523
E-mail: andy.shen@gia.edu

Robert K. Smither
Advanced Photon Source/XFD
Argonne National Laboratory
Building 401
9700 South Cass Avenue
Argonne, IL 60439 USA
Phone: 630.252.4959
Fax: 630.252.9303
E-mail: rks@aps.anl.gov

Ka L. Soh
Dept of Engineering
Vanderbilt University
5617 Stevenson Center
Nashville, TN 37232 USA
Phone: 615.343.6791
Fax: 615.343.6614
E-mail: ka.l.soh@vanderbilt.edu

Shin-Min Song
Dept of Mechanical Engineering
Northern Illinois University
DeKalb, IL 60115 USA
Phone: 815.753.9970
Fax: 815.753.0416
E-mail: smsong@ceet.niu.edu

Yang Song
Dept of Chemistry
Michigan State University
320 Chemistry Building
East Lansing, MI 48824 USA
Phone: 517.355.9715 ext. 231
E-mail: songyang@msu.edu

Youngsik Song
Dept of Electrical & Computer Eng
Wayne State University
3100 Engineering Building
5050 Anthony Wayne Drive
Detroit, MI 48202 USA
Phone: 313.577.5801
Fax: 313.577.1101
E-mail: song@wayne.edu

Boris V. Spitsyn
Diamond Film Crystallization Laboratory
Institute of Physical Chemistry RAS
Leninsky Pr. 31
119991 Moscow RUSSIA
Phone: 7.095.955.4475
Fax: 7.095.952.5308
E-mail: bspitsyn@yahoo.com

Eric Stach
School of Materials Engineering
Purdue University
501 Northwestern Avenue
West Lafayette, IN 47907 USA
Phone: 765.494.1466
Fax: 765.494.1204
E-mail: eastach@purdue.edu

Michael Sternberg
Materials Science Division
Argonne National Laboratory
Building 200
9700 South Cass Avenue
Argonne, IL 60439 USA
Phone: 630.252.7020
Fax: 630.252.9555
E-mail: sternberg@anl.gov

Volodymyr Strelnytskiy
National Science Centre
Kharkov Institute of Physics & Technology
Institute of Solid State Physics
Akademicheskaya, 1
61108 Kharkov UKRAINE
Phone: 38.057.3356561
Fax: 38.057.3350755
E-mail: strelnitskij@kipt.kharkov.ua

Karthik Subramanian
Dept of Electrical Engineering
Vanderbilt University
511 Chesterfield Avenue, 7-H
Nashville, TN 37212 USA
Phone: 615.945.2134
Fax: 615.343.6614
E-mail: karthik.subramanian@vanderbilt.edu

Anirudha V. Sumant
Dept of Engineering Physics
University of Wisconsin-Madison
CAE-258
1500 Engineering Drive
Madison, WI 53706 USA
Phone: 608.263.5444
Fax: 608.263.7451
E-mail: sumant@engr.wisc.edu

Bin Sun
Dept of Chemistry
University of Wisconsin-Madison
1101 University Avenue
Madison, WI 53706 USA
Phone: 608.262.9081
Fax: 608.262.0453
E-mail: binsun@wisc.edu

Chien-Min Sung
Kinik Company
64, Chung-San Road, Ying-Kuo
Taipei Hsien 239 Taiwan, ROC
Phone: 886.2.2677.5490 ext. 1150
Fax: 886.2.8677.2171
E-mail: sung@kinik.com.tw

In Ha Sung
Dept of Engineering Physics
University of Wisconsin-Madison
260 CAE Building
1410 Engineering Drive
Madison, WI 53706-1608 USA
Phone: 608.262.7476
E-mail: isung@wisc.edu

Mahendra K. Sunkara
Dept of Chemical Engineering
University of Louisville
Ernst Hall, Rm. 106
Louisville, KY 40292 USA
Phone: 502.852.1558
Fax: 502.852.6355
E-mail: mahendra@louisville.edu

Joseph W. Tabeling
Applied Diamond, Inc.
3825 Lancaster Pike
Wilmington, DE 19805 USA
Phone: 302.999.7476
Fax: 302.999.8320
E-mail: joe@ddk.com

Rohit S. Takalkar
Dept of Electrical Engineering
Vanderbilt University
5617 Stevenson Center
Nashville, TN 37232 USA
Phone: 615.500.2946
Fax: 615.343.6614
E-mail: rohit.takalkar@vanderbilt.edu

Chuanbing Tang
Dept of Chemistry
Carnegie Mellon University
4400 Fifth Avenue
Pittsburgh, PA 15213 USA
Phone: 412.268.9175
Fax: 412.268.6897
E-mail: ctang@cmu.edu

Yuxing Tang
Dept of Electrical & Computer Engineering
Michigan State University
2120 Engineering Building
East Lansing, MI 48824 USA
Phone: 517.432.5648
E-mail: tangyuxi@egr.msu.edu

Chien-Chung Teng
Dept of Research & Development
Kinik Company
No. 64, Chungsan Road, Yingge Town
Taipei County 239 Taiwan, ROC
Phone: 886.2.2679.1931 ext. 5140
Fax: 886.2.2678.8054
E-mail: shark@kinik.com.tw

Marcin Tlustochowicz
Dept of Civil & Materials Engineering
University of Illinois-Chicago
842 West Taylor Street
Chicago, IL 60607 USA
Phone: 312.413.7941
Fax: 312.413.7900
E-mail: marcin14@yahoo.com

Hiren V. Trada
Dept of Electrical Engineering
University of Louisville
Paul C. Lutz Hall, Rm. 428
Brook Street & Warnock Avenue
Louisville, KY 40292 USA
Phone: 502.767.8954
E-mail: email.trada@louisville.edu

Dzung T. Tran
Dept of Electrical Engineering
Michigan State University
3725 Calvin Drive
Lansing, MI 48911 USA
Phone: 517.331.2648
E-mail: trandung@msu.edu

Donald A. Tryk
Dept of Chemistry
University of Puerto Rico
P.O. Box 23346
San Juan, PR 00931-3346
Phone: 787.764.0000 ext. 17383
Fax: 787.756.8242
E-mail: dtryk@cnnet.upr.edu

Kiu Yuen Tse
Dept of Chemistry
University of Wisconsin-Madison
1101 University Avenue
Madison, WI 53706 USA
Phone: 608.262.9081
Fax: 608.262.0453
E-mail: kytse@wisc.edu

Pawan K. Tyagi
Dept of Physics
Indian Institute of Technology-Bombay
Mumbai 400076 INDIA
Phone: 91.022.25764571
Fax: 91.022.25767552
E-mail: tyagi@phy.iitb.ac.in

Yonhua Tzeng
Dept of Electrical & Computer Eng
Auburn University
200 Broun Hall
Auburn, AL 36849 USA
Phone: 334.844.1869
Fax: 334.844.1809
E-mail: tzengyo@eng.auburn.edu

Benjamin A. Ulmen
Dept of Physics
Michigan Technological University
205 Quincy Street
Houghton, MI 49931 USA
Phone: 906.482.1964
E-mail: baulmen@mtu.edu

Hitoshi Umezawa
Diamond Research Center , AIST
Umezono 1-1
Tsukuba, Ibaraki 305-8568 JAPAN
Phone: 81.29.861.3223
Fax: 81.29.861.2772
E-mail: hitoshi.umezawa@aist.go.jp

Kishore Uppireddi
Dept of Physics
University of Puerto Rico-Rio Piedras
P.O. Box 23343
San Juan, PR 00931-3343
Phone: 787.565.4162
Fax: 787.756.7717
E-mail: kishore_iitd@hotmail.com

Ashok K. Vaseashta
Dept of Physics
Marshall University
Graduate Program in Physical Sciences
One John Marshall Drive
Huntington, WV 25755-2570 USA
Phone: 304.696.2755
Fax: 304.696.2755
E-mail: vaseashta@marshall.edu

Gianluca Verona Rinati
Ingegneria Meccanica
Università di Roma "Tor Vergata"
Via del Politecnico 1
00133 Rome ITALY
Phone: 39.06.7259.7218
Fax: 39.06.7259.7217
E-mail: gianluca.verona.rinati@uniroma2.it

Chiu-Hui Wang
Dept of Mechanical Engineering & Energy Processes
Southern Illinois University-Carbondale
1630 Logan Drive, Apt. 6
Carbondale, IL 62901 USA
Phone: 618.303.5210
E-mail: chiuhui@siu.edu

Jian Wang
Materials Science Division
Argonne National Laboratory
Building 200
9700 South Cass Avenue
Argonne, IL 60439 USA
Phone: 630.252.8922
Fax: 630.252.9555
E-mail: jianwang@anl.gov

Jiesheng Wang
Dept of Physics
Michigan Technological University
604 Bridge Street
Fisher Hall
Houghton, MI 49931 USA
Phone: 906.483.2442
Fax: 906.483.2442
E-mail: jiewang@mtu.edu

Jing Wang
Dept of Electrical Engineering & Computer Science
University of Michigan
EECS Building, Rm. 1123
1301 Beal Avenue
Ann Arbor, MI 48109 USA
Phone: 734.764.3352
Fax: 734.763.9324
E-mail: jingw@engin.umich.edu

Shihua Wang
Dept of Chemistry
Michigan State University
320 Chemistry Building
East Lansing, MI 48823 USA
Phone: 517.355.9715 ext. 230
E-mail: wanshi7@msu.edu

Shuxia Wang
Dept of Physics & Astronomy
University of North Carolina-Chapel Hill
CB 3255, 238 Phillips Hall
Chapel Hill, NC 27599-3255 USA
Phone: 919.962.1384
Fax: 919.962.0480
E-mail: sxcqu@email.unc.edu

Wuyi Wang
Gemological Institute of America
580 Fifth Avenue
New York, NY 10036 USA
Phone: 212.221.5858 ext. 3507
Fax: 212.719.3134
E-mail: wuyi.wang@gia.edu

Taku Watanabe
Dept of Materials Science & Engineering
University of Florida
100 Rhines Hall
Gainesville, FL 32611-6400 USA
Phone: 352.846.3373
E-mail: taku@ufl.edu

Christopher L. White
Dept of Materials Engineering
University of Illinois-Chicago
Civil & Materials Engineering
842 West Taylor Street
Chicago, IL 60607-7023 USA
Phone: 708.535.9778
E-mail: cwhite3@uic.edu

Oliver A. Williams
Institute for Materials Research
Wetenschapspark 1
B-35590 Diepenbeek BELGIUM
Phone: 32.11268829
Fax: 32.11268899
E-mail: oliver.williams@luc.ac.be

Nicolas Woehrl
Dept of Physics
University Duisburg-Essen
Universitaetsstr. 3-5
45117 Essen, NRW GERMANY
Phone: 49.201.183.3026
Fax: 49.201.183.93.3026
E-mail: nicolas.woehrl@uni-essen.de

Yong M. Wong
Dept of Electrical Engineering & Computer Science
Vanderbilt University
5617 Stevenson Center
Nashville, TN 37232 USA
Phone: 615.343.6712
Fax: 615.343.6614
E-mail: yong.m.wong@vanderbilt.edu

John B. Woodford
Energy Technology Division
Argonne National Laboratory
Building 212
9700 South Cass Avenue
Argonne, IL 60439
Phone: 630.252.0910
Fax: 630.252.4798
E-mail: woodford@anl.gov

Xingcheng Xiao
Materials Science Division
Argonne National Laboratory
Building 200
9700 South Cass Avenue
Argonne, IL 60439 USA
Phone: 630.252.7520
Fax: 630.252.9555
E-mail: xxiao@anl.gov

Songtao Xie
Dept of Chemical Engineering
Case Western Reserve University
A.W. Smith Building, Rm. 219
10900 Euclid Avenue
Cleveland, OH 44106-7217 USA
Phone: 216.368.2648
E-mail: sxx5@cwru.edu

Zhenqing Xu
Dept of Mechanical Engineering
University of South Florida
ENG 118C
4202 East Fowler Avenue
Tampa, FL 33620 USA
Phone: 813.396.9351
Fax: 813.974.3610
E-mail: zxu3@eng.usf.edu

Chih-Shiue Yan
Geophysical Laboratory
Carnegie Institution of Washington
5251 Broad Branch Road, NW
Washington, DC 20015 USA
Phone: 202.478.8959
Fax: 202.478.8901E-mail: c.yan@gl.ciw.edu

Jie Yang
NOVA Research, Inc.
1900 Elkin Street, Ste. 230
Alexandria, VA 22308 USA
Phone: 202.767.2336
Fax: 202.767.3321
E-mail: : jyang@ccs.nrl.navy.mil

Hsao W. Yap
Dept of Engineering Physics
University of Wisconsin-Madison
202 ERB
1500 Engineering Drive
Madison, WI 53706 USA
Phone: 608.698.4794
E-mail: hwyap@wisc.edu

Yoke Khin Yap
Dept of Physics
Michigan Technological University
118 Fisher Hall
1400 Townsend Drive
Houghton, MI 49931 USA
Phone: 906.487.2900
Fax: 906.487.2933
E-mail: ykyap@mtu.edu

S. C. "Max" Yen
Materials Technology Center
Southern Illinois University-Carbondale
1230 Lincoln Drive
Carbondale, IL 62901 USA
Phone: 618.536.7525
Fax: 618.453.8216
E-mail: myen@siu.edu

Hiroaki Yoshida
Corporate Research & Development Center
Toshiba Corporation
1, Komukai-Toshiab-Cho, Saiwai-ku
Kawaskai, Kanagawa 212-8582 JAPAN
Phone: 81.44.549.2142
Fax: 81.44.520.1501
E-mail: hiroaki.yoshida@toshiba.co.jp

Peter Zapol
Materials Science & Chemistry Divisions
Argonne National Laboratory
Building 200
9700 South Cass Avenue
Argonne, IL 60439 USA
Phone: 630.252.6085
Fax: 630.252.9555
E-mail: zapol@anl.gov

Guangyu Zhang
Dept of Chemistry
Stanford University
P.O. Box #3
Stanford, CA 94305 USA
Phone: 650.725.9156
Fax: 650.725.0259
E-mail: gyzhang@stanford.edu

Longguang Zhou
Dept of Mechanical Engineering
Rensselaer Polytechnic Institute
110 8th Street
Troy, NY 12180 USA
Phone: 518.276.8136
E-mail: zhoul@rpi.edu

Ranyi Zhu
Dept of Civil & Materials Engineering
University of Illinois-Chicago
ERF 2095 (MC: 246)
842 West Taylor Street
Chicago, IL 60607 USA
Phone: 312.413.7941
E-mail: rzhu1@uic.edu

Xiangwei Zhu
Dept of Electrical & Computer Engineering
Michigan State University
2120 Engineering Building
East Lansing, MI 48824 USA
Phone: 517.432.5648
Fax: 517.353.0930
E-mail: zhuxiang@egr.msu.edu

Jerry W. Zimmer
sp3 Inc.
505 East Evelyn Avenue
Mountain View, CA 94041 USA
Phone: 650.966.0630
Fax: 650.966.0633
E-mail: jzimmer@sp3inc.com

Tom Zimmermann
Dept of Electron Devices & Circuits
University of Ulm
Albert-Einstin-Allee 45
89081 Ulm GERMANY
Phone: 49.731.502.6183
Fax: 49.731.502.6155
E-mail: tom.zimmermann@ebs.e-technik.uni-ulm.de

Eric J. Zimney
Dept of Mechanical Engineering
Northwestern University
2145 Sheridan Road
Evanston, IL 60201 USA
Phone: 847.491.4231
Fax: 847.491.3915
E-mail: e-zimney@northwestern.edu

Stanley S. Zuo
Dept of Electrical & Computer Engineering
Michigan State University
1642 Spartan Village, Apt. J
East Lansing, MI 48823 USA
Phone: 517.353.6875
E-mail: zuosheng@msu.edu

HeatWave Labs
www.cathode.com

Model 102436 8 inch diameter 1200C UHV heater.
Internal elements sealed from chamber atmosphere and differentially pumped/purged. Outer sice and rear shield package included (side shield removed for photo). Includes Type C thermocouples, 9 pairs.

Vacuum isolated, 200 mm wafer capable heater optimized for use in microwave plasma CVD of ultrananocrystalline diamond thin films.

See us at the Vendor Exhibit, Booth # 5